Mechanistic studies on the photodecomposition of caged *N*-hydroxysulfonamides incorporating the 2-nitrobenzyl, (2-nitrophenyl)ethyl and (6-bromo-7-hydroxycoumarin-4-yl)methyl chromophores

Vinay Bharadwaj Bangalore Shashidhar

A thesis submitted to Auckland University of Technology in fulfilment of the requirements for the degree of Doctor of Philosophy (PhD)

School of Science
Department of Chemistry
2021

Thesis Abstract

There is accumulating evidence that the redox cousin of nitric oxide (NO), nitroxyl (HNO), is a biologically important signaling molecule. HNO reacts rapidly with thiols and metal centres of metalloproteins. HNO prodrugs also show promise in treating congestive heart failure. Since HNO is highly unstable, several classes of molecules that decompose to release HNO, HNO donors, have been developed. The vast majority of these HNO donors release HNO slowly (minutes to hours).

Extremely reactive biological molecules such as HNO can be made inactive by binding a photoprotecting group (PPG) to the molecule of interest. Upon irradiation by light, the biological molecule (BM) will be rapidly released from the PPG-BM complex at the desired location in a highly controlled manner (Figure 1). This strategy has been utilized to generate various BM such as neurotransmitters, proteins, and nucleic acids, upon demand.

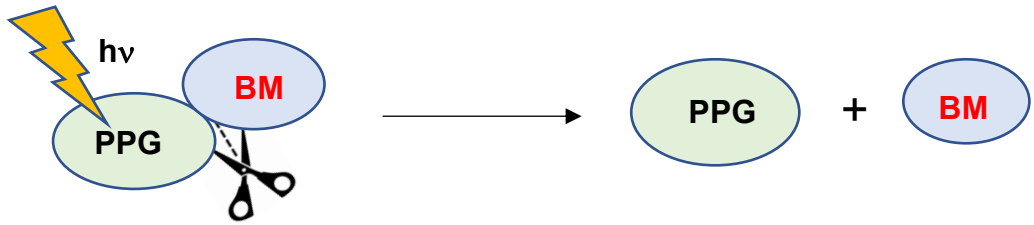

Figure 1. Release of a biomolecule (BM) from photocaged PPG-BM upon irradiation by light.

Our research team recently developed the first *N*-hydroxysulfonamides caged with the 3-hydroxynaphthalen-2-yl and 6-hydroxynaphthalen-2-yl chromophores, as potential photoactive HNO donors. The selectivity of the desired HNO generation pathway versus competing pathways involving C-O or O-N bond cleavage was found to be dependent on the *N*-hydroxysulfonamide, the chromophore and the solvent conditions.

In this thesis the mechanisms of photodecomposition of three new classes of photocaged *N*-hydroxysulfonamides have been investigated. In Chapter 2 the photodecomposition of *N*-hydroxysulfonamides caged with the well-established 2-nitrobenzyl moiety is presented. O-N bond cleavage to give the corresponding sulfonamide rather than the desired concerted C-O/N-S bond cleavage was the primary decomposition pathway. The results support a Norrish type II mechanism,

with the 1,5 hydrogen atom abstraction occurring in the excited state to give a *(Z)*-aci-nitro intermediate. The *(Z)*-aci-nitro intermediate either undergoes O-N bond cleavage to generate the sulfonamide and 2-nitrobenzaldehyde or instead isomerizes to the *(E)* isomer, ultimately undergoing C-O/N-S bond cleavage to release HNO and $CF_3SO_2^-$. The aci-nitro intermediate was detected by laser flash photolysis and decomposes on the microsecond timescale. For the related 2-NO_2Bn-OC(O)-ON(H)-SO_2CH_3 analogue, photodecomposition primarily occurred via C-O bond cleavage.

In Chapter 3 the photodecomposition of 2-(2-nitrophenyl)ethyl (2-NPE) photocaged *N*-hydroxysulfonamides is presented. The proposed mechanism of photodecomposition was also via a Norrish type II reaction. However in this case the *(Z)*-aci-nitro intermediate either undergoes C-O bond cleavage to release the parent sulfohydroxamic acid, concerted C-O/N S bond cleavage to generate a sulfinate and HNO, or isomerises to the *(E)* isomer and undergoes O-N bond cleavage. The pK_a of the N(H) of the *N*-hydroxysulfonamide plays a key role in determining whether C-O or concerted C-O/N-S bond cleavage occurs.

Finally, in Chapter 4 the mechanisms of photodecomposition were investigated for two (6-bromo-7-hydroxycoumarin-4-yl)methyl – caged N-hydroxysulfonamides. Heterolytic O-N, C-O and/or C-O/N-S bond cleavage are extremely rapid for these systems, occurring in the singlet excited state. Once again the pK_a of N(H) plays a key role in determining the mechanism of photodecomposition. Upon concerted heterolytic C-O/N-S bond cleavage a solvent-caged carbocation and $^1NO^-$ are released. The carbocation reacts rapidly with solvent, or with (H)NO to generate an oxime.

TABLE OF CONTENTS

LIST OF FIGURES

LIST OF SCHEMES

LIST OF TABLES

Attestation of Authorship

I hereby declare that this submission is my own work and that, to the best of my knowledge and belief, it contains no material previously published or written by another person (except where explicitly defined in the acknowledgements), nor material which to a substantial extent has been submitted for the award of any other degree or diploma of a university or other institution of higher learning

Vinay Bharadwaj
May 23, 2021

List of publications

1) Bharadwaj, V.; Rahman, M. S.; Sampson, P.; Seed, A. J.; Brasch, N. E., Exploring the Potential of 2-(2-Nitrophenyl)ethyl-Caged *N*-Hydroxysulfonamides for the Photoactivated Release of Nitroxyl (HNO). *The Journal of Organic Chemistry* **2021** (in press).
2) Adas, S. K.; Bharadwaj, V.; Zhou, Y.; Zhang, J.; Seed, A. J.; Brasch, N. E.; Sampson, P., Synthesis and HNO Donating Properties of the Piloty's Acid Analogue Trifluoromethanesulphonylhydroxamic Acid: Evidence for Quantitative Release of HNO at Neutral pH Conditions. *Chemistry–A European Journal* **2018,** *24* (29), 7330-7334.
3) Zhou, Y.; Bharadwaj, V.; Rahman, M. S.; Sampson, P.; Brasch, N. E.; Seed, A. J., Synthesis and photochemical studies of 2-nitrobenzyl-caged N-hydroxysulfonamides. *Journal of Photochemistry and Photobiology A: Chemistry* **2019,** *384*, 112033.

ACKNOWLEDGEMENTS

All thanks to Almighty for all his blessings.

Without the support of all the brilliant people around me, this PhD thesis completion would not have been possible. My earnest thanks to my mentor and primary supervisor, Prof. Nicola Brasch for her immense support throughout the PhD journey. From accepting my PhD proposal, guiding me with the project design and experiments to providing moral and financial support. Nicola, I am very grateful to you for helping me shape up my career and boosting my confidence. A special thanks to our collaborators Prof Paul Sampson and Prof Alexander Seed. I learnt a lot of concepts and nuances especially from group meetings which has helped a lot in my thesis writing. I am also thankful to my co-supervisors Prof Cather Simpson and Prof Allan Blackman for their support.

Thanks to our collaborator, Dr Mohammad Saifur Rahman, who synthesized most of the chemical molecules used for my experiments. I'm very grateful to Saif. Also, special thanks to Dr Yang Zhou and Dr Sonya K Adas for sharing your synthesized molecules with me for my experiments. Many thanks to colleague, Dr Ruth B Cink, who helped me in the initial days of my research.

A huge thanks to AUT for awarding me a doctoral scholarship and also thanks to the Dodd-Walls Centre for Photonic and Quantum Technologies for extending my scholarship and travel grants to visit conferences.

I'm also thankful to all the lab mates for their support: Dominique Rwizinkindi, Fouad Ismael, Marwa Omar, Lynn Lisboa, Jessica Fredericksen, Ema Maretic, Chloe Ren, Franko Schrumpf, Pablo Solis-Munana, Cameron Waghorn, Bronte Carr. Sincere thanks specially to all the lab technicians who helped me with the logistics during the experiments and support: Adrian Owens, Dr Tony Chen, Yan Wang, Tim Layt, Dr Sonya Popoff, Saeedeh Saraby. Thanks to other lecturers and professors at AUT, Dr Jack Chen and Dr Marcus Jones for their technical help.

I'm extremely grateful to have met my best friend, companion Dr Sridevi Ravi. Thanks for all wonderful things: friendship, never ending conversations, cooking dinner. I am very lucky to have a constant support and advice from you throughout my PhD journey.

A special thanks to Dr Frank Müller and Adrian Owens for helping me to sort out NMR

spectroscopy. Thanks also to Loretta White and Dr Lindsey White for introducing me to the cricket world.

I am very grateful to my family and friends back in India for their helpful advice. To my late grandfather, Suryanarayana Rao, who raised me and constantly support me financially, morally and emotionally so that I could pursue my dreams. To my aunt, A.S Savitha for her support, nurtured me as her own son and always lent an ear to all my woes. I'm also thankful to my high school science teacher Prakash M B for rekindling my interest in science. Finally, I am also thankful to my parents for allowing me to experience the cosmos.

Chapter 1: Introduction

HNO is an important biomolecule. In this chapter the fundamental chemistry of HNO, molecules that decompose to release HNO (HNO donors) and the decomposition mechanisms of HNO and HNO donors are discussed.

1.1 Fundamental chemistry of HNO

1.1.1 Structure and spectroscopy of HNO

HNO exhibits a bent type of structure (the H-N=O bond angle is 109°, Figure 1.1), like H_2O,[1] due to a lone pair of electrons on the nitrogen atom. The N-O bond distance is 1.21 A° and is larger than the N-O bond distance in NO due to one extra proton and electron.[1] HNO is a Raman and IR active molecule, with three stretching frequencies (ν), $\nu_{1\ \text{symmetric}} = 2717\ cm^{-1}$, $\nu_{2\ \text{(N-O) symmetric}} = 1563.3\ cm^{-1}$ and $\nu_{3\ \text{bent}} = 1500.4\ cm^{-1}$.[1]

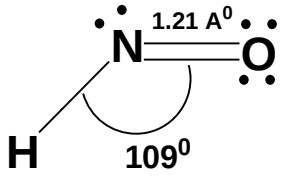

Figure 1.1. Lewis structure of HNO.

1.1.2 Spin states and pK_a

^{1}HNO exists in the singlet ground state. However, the anion, $^3NO^-$, has a triplet ground state and is isoelectronic with the ground state of $^3O_2$.[2] Loss of a proton from HNO is a spin-forbidden reaction and is therefore comparatively slow, with a rate constant, $k_f = 4.9 \times 10^4\ M^{-1}s^{-1}$, equation (1.1).[3, 4] Similarly, the protonation of $^3NO^-$ to ^{1}HNO is a slower reaction than usual in aqueous solution, with a rate constant, $k_r = 1.2 \times 10^2\ s^{-1}$.[2]

$$^1HNO + OH^- \underset{k_r}{\overset{k_f}{\rightleftharpoons}} {}^3NO^- + H_2O \qquad (1.1)$$

Thermodynamic calculations combined with laser flash photolysis studies (LFP) for the HNO donor Angeli's salt (AS) has revealed the pK_a of HNO to be 11.4.[2] A pK_a

value in this range is also supported by quantum mechanical calculations.[2] Therefore, at the physiological pH the species present is nitroxyl (HNO), not its anion.

1.1.3 Dimerization of HNO

HNO is not stable in aqueous conditions. It rapidly dimerizes to *cis*-$H_2N_2O_2^-$ with a second-order rate constant (k_1) of 8×10^6 $M^{-1}s^{-1}$.[5] The rapid decomposition of the *cis*-hyponitrate anion (*cis*-$N_2O_2H^-$) gives nitrous oxide and water with a first-order rate constant (k_2) = 5×10^{-4} s^{-1}, equation (1.2).[5] This irreversible reaction makes it challenging to stabilize HNO in solution. Therefore, biologically active HNO must be generated *in situ*.

$$2HNO \xrightarrow[k_1 = 8 \times 10^6\ M^{-1}s^{-1}]{-H^+} \textit{cis}\text{-}N_2O_2H^- \xrightarrow[k_2 = 5 \times 10^{-4}\ s^{-1}]{+H^+} N_2O + H_2O \quad (1.2)$$

1.1.4 Reaction with molecular oxygen

HNO reacts with molecular oxygen to give peroxynitrite with an estimated rate constant of 3×10^{-3} $M^{-1}s^{-1}$, equation (1.3). The reaction is slow due to the different spin states of ^1HNO and $^3O_2$.

$$^1HNO + O_2 \longrightarrow ONOO^- + H^+ \quad (1.3)$$

The pK_a of ONOOH is 6.8. At pH 7.0 $ONOO^-$ is therefore in equilibrium with its protonated form. Peroxynitrite acts as both an oxidizing and nitrating agent.[6] It also rapidly isomerises to form HNO_3 (70%) and undergoes O-N bond homolysis to give •OH and •NO_2 radicals (~30%).[6]

1.1.5 Differences between nitric oxide (NO) and HNO

HNO is a biological signaling molecule like its redox cousin NO.[7] Mechanisms for HNO generation include the conversion of L-arginine to HNO in a reaction catalysed by nitric oxide synthase in the absence of tetrahydrobiopterin or *N*-hydroxy-L-arginine oxidation.[8] Reduction of NO catalysed by ferrocytochrome c and superoxide dismutase also leads to HNO generation[9] and HNO is released from S-nitrosothiols when reacted with thiols.[10] Given the rich redox chemistry of nitrogen oxide species, it is of interest to know how easy it is to reduce or oxidize HNO. The reduction potentials (E^o ($NO/^3NO^-$ = -0.8 ± 0.2 V; E^o ($NO/^1NO^-$ = -1.7 ± 0.2 V (versus NHE)) are too negative to allow these reactions to occur by non-enzymatic biological reductants.[11]

HNO has been shown to have a different biochemical reactivity from the much more well-studied NO. Importantly, HNO and NO have distinct chemical reactivities.[12] For example HNO reacts directly with thiols while NO doesn't.[12] Indeed it has even been suggested that some of the physiological properties attributed to NO may actually be from HNO.[12] Furthermore, while the rate of the reaction between NO and superoxide to form peroxynitrite/peroxynitrous acid (ONOO(H)) is close to the rate of diffusion, HNO does not react appreciably with superoxide.[14]

1.1.6 Biological reactivity of HNO

HNO is a highly reactive biomolecule.[7] HNO is an electrophile and reacts with free thiols and thiol groups of proteins.[13-15] Nitroxylation of thiol residues of enzymes can potentially inactive enzymes.[16] Because HNO is unstable, HNO donors are required to release HNO rapidly for potential therapeutic applications.

The HNO prodrug cyanamide is used to discourage alcoholics from drinking alcohol.[17] Acetaldehyde is formed *in vivo* by the oxidation of ethanol in the presence of alcohol dehydrogenase.[18, 19] Aldehyde dehydrogenase catalyses the oxidation of acetaldehyde to acetic acid. Hydrogen peroxide oxidises cyanamide to hydroxycyanamide in a reaction catalysed by the enzyme catalase.[20] Hydroxycyanamide subsequently decomposes to give HNO and CN^- under physiological conditions. HNO acts as an inhibitor to the aldehyde dehydrogenase enzyme by modifying the thiol residue to the corresponding sulfonamide,[19, 21] resulting in a hangover.

HNO also shows considerable promise in treating cardiovascular disease and congestive heart failure. HNO reacts with the thiol residue of the myofilament protein to form disulfide and hydroxylamine. As a result, HNO increases positive inotropy and plasma levels of calcitonin gene-related peptide (CGRP).[22] HNO prodrugs CXL-1020 and CXL-1427 (Figure 1.2) were recently synthesised. [23] Phase IIa clinical trials are underway. Like NO, HNO is also a vasodilator.[23]

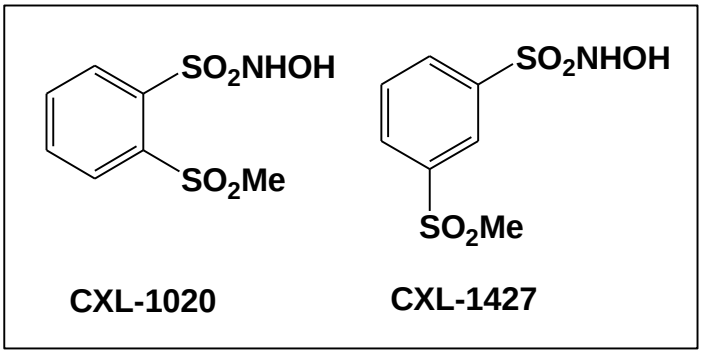

Figure 1.2. Structures of CXL-1020 and CXL-1427.

The metal centres of metalloproteins also react with HNO as HNO reduces redox active metal cations.[34] Porphyrin metal complexes (Mn(III)P, cobalt Co(III)P, P = porphyrin), react with HNO to form the corresponding nitrosyl complexes (NOMn(III)P and NOCo(III)P, respectively).[34] Also, HNO reacts with the Co(III) corrin complex aquacobalamin (H_2OCbl^+) to form nitrosylcobalamin (NOCbl),[24-26] equation (1.4(a) – (c)). The reaction of HNO with metal complexes is typically carried out under anaerobic conditions due to HNO rapidly reacting with atmospheric O_2.[6] Finally, metal complexes have been used to detect HNO in a range of studies, since a colour change is observed when NO^- binds to a metal centre.

$$\mathbf{Mn(III)P + HNO \longrightarrow NOMn(II)P \quad (a)}$$
$$\mathbf{Co(III)P + HNO \longrightarrow NOCo(II)P \quad (b)}$$
$$\mathbf{H_2OCbl^+(III) + HNO \longrightarrow NO^-Cbl(III) + H_3O^+ \quad (c)} \qquad (1.4)$$

1.2 Detection methods for HNO

Detection of HNO is challenging due its reactivity with molecular oxygen and the dimerization reaction (equation (1.2)). Several indirect detections of HNO have been reported. The qualitative or quantitative detection of HNO has been determined indirectly by GC-MS detection of its dimerized product N_2O.[5] This method has a disadvantage where the dimerization product N_2O is isoelectric with CO_2. Also, N_2O can be generated in other reactions in addition to the dimerization of HNO.[5]

1.2.1 Thiol traps of HNO

Although HNO does not react with H_2O or alcohols, it is very reactive with thiols.[3, 27-29] The rate of the reaction of HNO with thiols depends on the pH and the pK_a of the thiolate.[15] HNO react with thiophenol to give *N*-hydroxysulfonamide (RSNHOH)

(equation (1.5) (a) – (c)), an unstable intermediate. *N*-hydroxysulfonamide reacts further in the presence of thiol to form a disulfide ($RSSR^1$) and NH_2OH. In the absence of thiol, it isomerizes to a sulfonamide ($RS(O)NH_2$).[10] The reaction is rapid; for example the second-order rate constant for the reaction between glutathione and HNO is $2 \times 10^6\ M^{-1}s^{-1}$.[30]

$$\mathbf{RSH + HNO \longrightarrow RS\text{-}NHOH \quad (a)}$$
$$\mathbf{RSNHOH + R^1SH \longrightarrow RSSR^1 + NH_2OH \quad (b)}$$
$$\mathbf{RS\text{-}NHOH \longrightarrow RS(O)NH_2 \quad (c)} \qquad (1.5)$$

1.2.2 Phosphine traps of HNO

Phosphine trapping molecules (phosphine traps, R_3P, 2 equiv. required) reacts with HNO to produce an intermediate which decomposes to give an aza-ylide ($R_3P{=}NH$) and the corresponding phosphine oxide ($R_3P{=}O$), as shown in Scheme 1.1.[31]

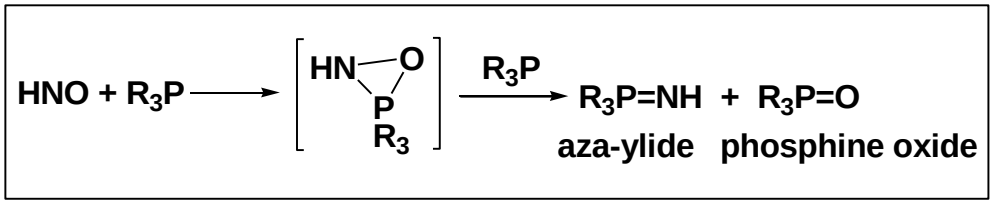

Scheme 1.1. The proposed mechanism for the reaction between HNO and phosphines.

The products of this reaction can be easily analyzed by ^{31}P NMR spectroscopy and mass spectrometry. The formation of the aza-ylide is an indicator of HNO generation. However, this reaction was found to be non-stoichiometric.[32] Various phosphine traps of HNO have been reported (Figure 1.6).[7, 32-36] The reaction between HNO generated from the HNO donor Angeli's salt with *tris*(2,4-dimethyl-5-sulphophenyl)phosphine (TXPTS) has been reported.[37] Nakagawa et al. has reported other phosphine trapping molecules synthesized using alkyl 2-(diphenylphosphino)benzoates where R = CH_3 and coumarin fluorophores.

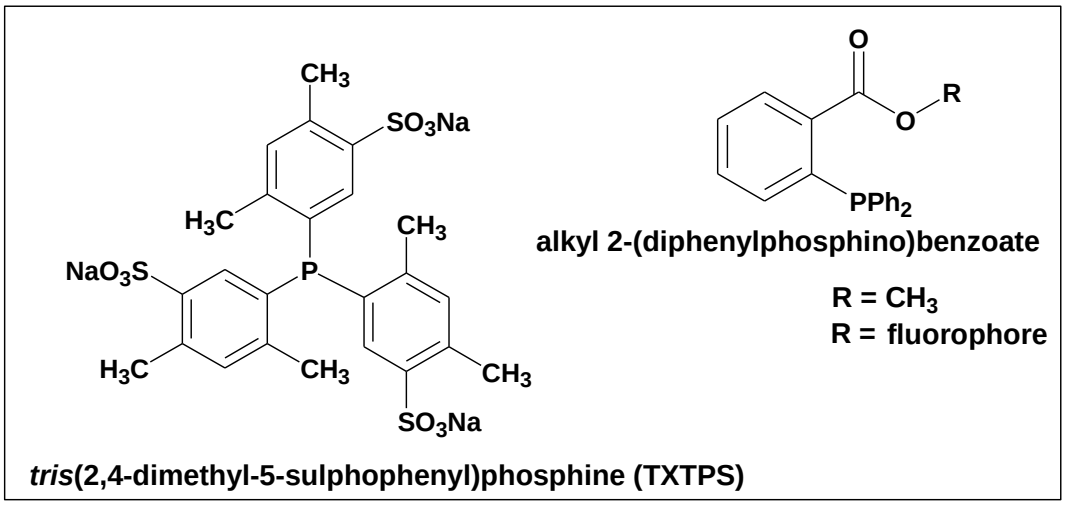

Figure 1.3. The structures of phosphine molecules which trap HNO.

1.3 HNO Donor Molecules

HNO donors (molecules that decompose to release HNO) are required to study the chemistry and biological activity of HNO, since HNO is unstable in aqueous solution. HNO donors can be classified based on the mechanism of HNO release. This includes protonation, deprotonation, thermolysis, enzymatic activation, oxidation, hydrolysis and activation by light, i.e. photolysis (Table 1.1).

Table 1.1. Classification of HNO donors based on their reactivity.

HNO donor	Structure	Mechanism of HNO release	Reference
Angeli's salt	$Na_2N_2O_3$	Protonation of $N_2O_3^{2-}$	38, 39
Piloty's acid and its derivatives (aromatic and aliphatic sulfo-hydroxamic acids)	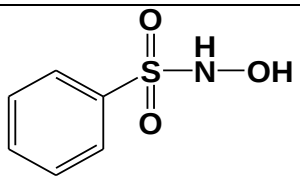	Deprotonation	40, 41
NONOates	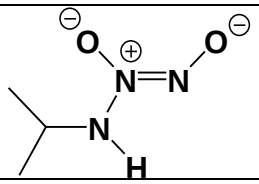	Heat	18, 42

N-substituted hydroxylamines of barbituric acid	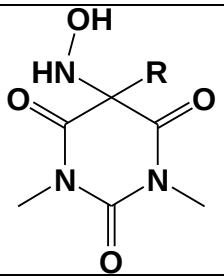	Deprotonation	59
Acyloxy nitroso compounds	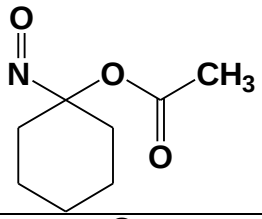	Hydrolysis	44
Hetero-Diels-Alder cycloadducts	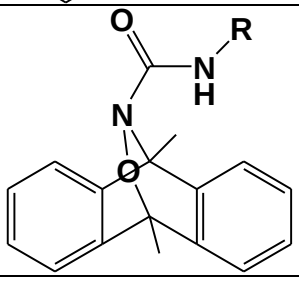	Photolysis	45, 46, 43
Transition metal complexes	{Co(CO)}^{9}	Protonation	47

1.3.1 Angeli's salt (AS)

To date AS is the most commonly used HNO donor in biological studies.[5] HNO is generated by protonation of $N_2O_3^{2-}$ to give $HN_2O_3^-$ in the pH 4-8 region ($pK_a(HN_2O_3^-)$ = 9.35),[48] which spontaneously decomposes. The mechanism is shown in equation (1.6).[4, 18] AS decomposition fits a first-order equation and can be directly measured by UV-Vis spectroscopy ($\varepsilon = 6.1 \times 10^3$ M^{-1} cm^{-1} at 237 nm).[5]

$$\mathbf{N_2O_3^{2-} + H^+ \rightleftharpoons HN_2O_3^{2-} \longrightarrow HNO + NO_2^-} \qquad (1.6)$$

At pH 7.4 the half-life for AS decomposition is ~17 min (25 °C).[49] At pH values below 4, $H_2N_2O_3$ is formed in solution (pK_a ($H_2N_2O_3$) = 2.39),[49] which decomposes to produce NO.[4, 38]

1.3.2 *N*-hydroxysulfonamides

Piloty's acid (PA) is the most commonly used *N*-hydroxysulfonamide. HNO is generated from PA (*N*-hydroxybenzenesulfonamide) upon deprotonation, equation (1.7) (R = C_6H_5).[40] Many *N*-hydroxysulfonamide derivatives of PA have been reported.

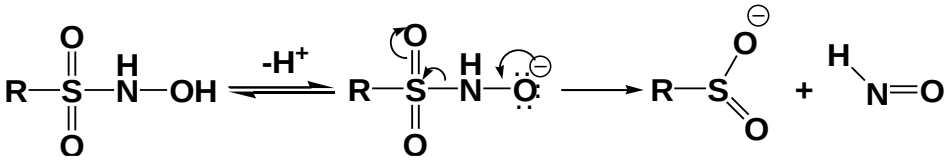

(1.7)

PA spontaneously produces HNO above pH 8 (pK_a(PA) = 9.29).[50] At pH 7.4 the rate of PA decomposition is slow ($t_{1/2}$ = 5500 min) and NO is produced.[49] The half-life of PA decomposition increases with increasing pH ($t_{1/2}$ = 33 min at pH 10). Several Piloty's acid derivatives incorporating substituents on the aromatic ring have been synthesized,[51] including *p*-methyl (toluene sulfohydroxamic acid), *p*-nitro, 2,4,6-triisopropyl and *p*-methoxy substituents.[51] The half-live for HNO release is significantly decreased by changing the substituent at the ortho position as shown in Figure 1.4.[52] Electron withdrawing substituents lower the pK_a values of *N*-hydroxysulfonamides and increase the rate of HNO release (Figure 1.4).[52] However, some of these pK_a values were not accurately determined.[52] Toscano et al have developed Piloty's acid-based HNO-releasing therapeutics for treating congestive heart failure, CXL-1020 and CX-1427 (Figure 1.2). These derivatives are in Phase IIa clinical trials.

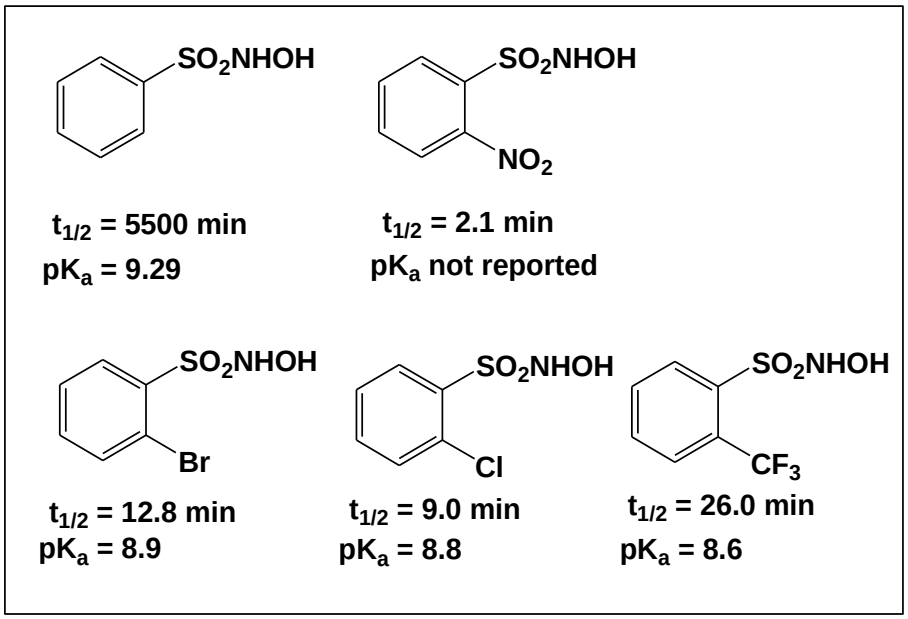

Figure 1.4. The structures of PA based HNO donors. The half-life ($t_{1/2}$) at physiological pH and the pK_a for spontaneous decomposition of the PA derivative are also given.

Aliphatic sulfohydroxamic acids are also well-known, in particular methane sulfohydroxamic acid (MSHA). HNO is again generated upon deprotonation of MSHA, equation (1.7) (pK_a of MSHA = 9.95).[53] At pH 11.5 the half-life for decomposition of MSHA is 25 min (25˚C).[54] Finally, CF_3SO_2NHOH has been synthesized recently by

our research team and also releases HNO, with a half-life of ~17 min at pH 7.0 (pK_a 5.89).[55]

1.3.3 NONOates

NONOates (diazonium diolates) are structurally similar to Angeli's salt and decompose to release HNO or NO.[42, 56] NONOates incorporating primary amines such as IPA-NONOate (IPA = isopropylamine) decompose to form HNO in alkaline solutions, equation (1.8, R = IPA), and a HNO/NO mixture under neutral pH conditions.[57] Secondary alkylamines are also useful as HNO donors in alkaline solution.[58]

$$[RNH\text{-}N(O)=NO]^- \rightleftharpoons [RH=N(O)\text{-}NHO]^- \longrightarrow HNO + RNNO^- \quad (1.8)$$

1.3.4 Other *N*-substituted hydroxylamine-based derivatives

N-substituted hydroxylamine-based derivatives with leaving groups which are not cyanamides have also been developed, equation (1.9) (X = leaving group).

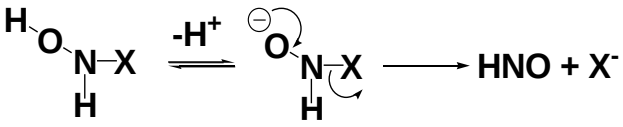

(1.9)

Having a good leaving group on the nitrogen is a convenient strategy to generate HNO, such as *N*-acylhydroxylamines.[43] Pyrazolone and barbiturate acid analogues of PA have been synthesized by Toscano's group.[59] These analogues release HNO with half-lives of 0.7 min and 9.75 min (phosphate buffer, pH 7). The structures are given in Figure 1.5.[59]

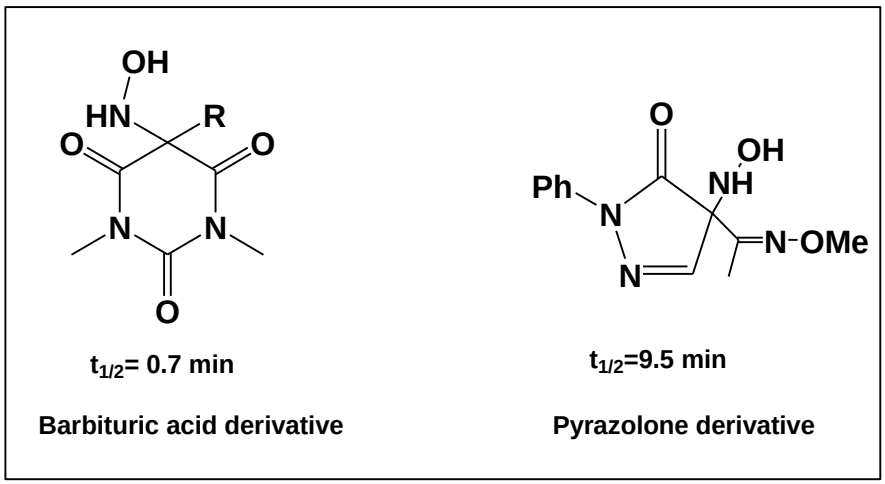

Figure 1.5. The structures of barbiturate acid (R = CH_3) and pyrazolone analogues of PA.

1.3.5 Acyloxy nitroso compounds

King and coworkers have developed acyloxy nitroso derivatives as HNO donors.[60, 61] Hydrolysis of the ester of acyloxy nitroso compounds produce HNO on treatment with base as shown in equation (1.10, X = -CH_2). At neutral pH a HNO/NO mixture can be formed.[44]

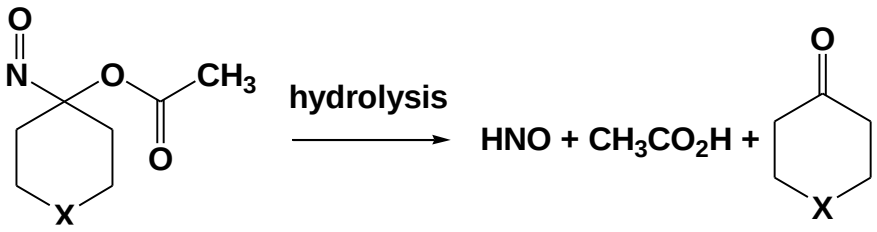

(1.10)

1.3.6 Transition metal-based HNO donors

Numerous transition metal complexes incorporating HNO ligands have been synthesized and some of these behave as HNO donors.[62] Metal-coordinated nitroxyl complexes {Co(CO)}^{9} have been shown to release HNO, equation (1.11) upon protonation by HBF_4•Et_2O and H_2O (10:1).[47, 63] {Fe $(NO)_2$}^{9} also acts as HNO donor.[64]

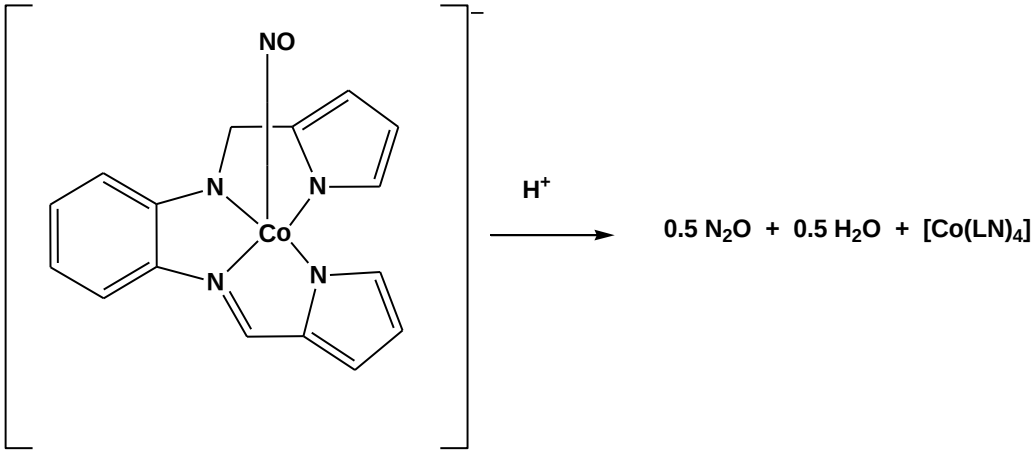

(1.11)

The Ru(II) complex $[Ru(bpy)_2(SO_3)(NO)]^+$ reacts with glutathione (2:1) at pH 7 to release HNO.[65] *Trans*-$[Ru(NO)(NH_3)_4P(OEt)_2](PF_6)_2$ releases NO/HNO with a half-life of 1.5 h (pH 7.5, 25˚C).[66] $[Fe(CN)_5HNO]^{3-}$ releases HNO spontaneously with $t_{1/2}$ ~14 h at pH 7.[67] Finally, LiNO has also been synthesized[68] but is only stable under anaerobic conditions.

1.3.7 Photoactivable HNO donors

Activation by light can result in rapid *in situ* generation of biologically important molecules.[69] Several classes of photoactive HNO donors have been developed. Light activation is a relatively new strategy to generate HNO. Photomediated methods for generation of HNO are advantageous because HNO generation is site-specific and can be initiated upon demand.

Toscano et al. have reported HNO release via an acyl nitroso intermediate upon irradiation of ethyl nitrodiazoacetate, equation (1.12).[70]

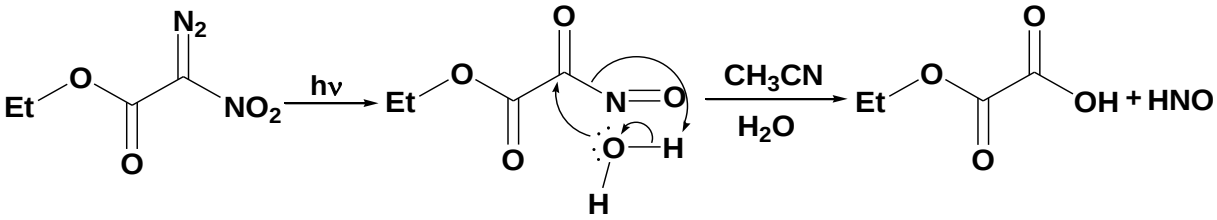

(1.12)

Nucleophilic attack on the acyl nitroso intermediate by H_2O is rapid ($k = 2\times10^7\ s^{-1}$).[71] The acyl nitroso intermediate can also react with other nucleophiles, such as amines, to release HNO.[71]

Nakagawa et al. have developed a photochemical hetero-Diels–Alder cycloadduct that undergoes a retro-hetero-Diels Alder reaction to generate an acyl nitroso intermediate and 9,10-dimethylanthracene, equation (1.13, R = CH_3). HNO is released upon hydrolysis of the acyl nitroso compound.[46, 72] By changing the solvent polarity, the amount of HNO and NO varies.[73,46] However, the half-life for HNO generation is long (minutes). HNO generation occurs via a non-radiative relaxation process and it is a contradiction of the Woodward-Hoffman rules. The hetero-Diels–Alder cycloadduct species also thermally decomposes to generate HNO.[45]

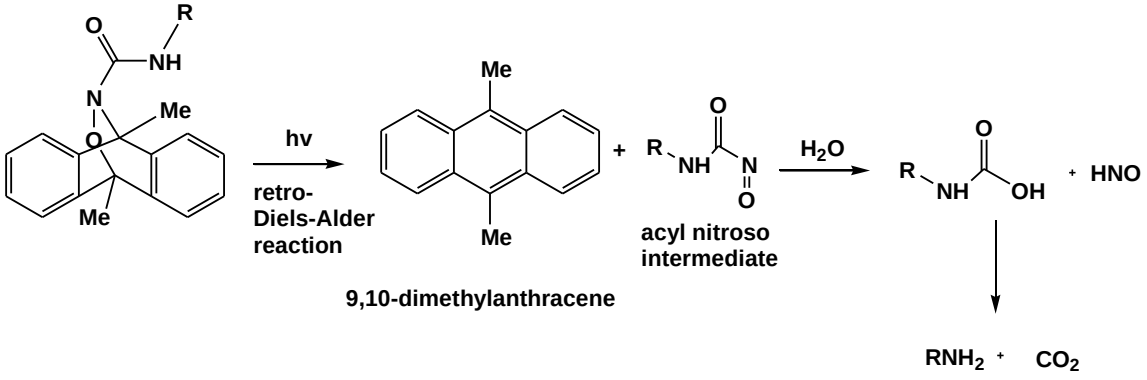

(1.13)

Irradiation of NONOates also results in HNO being generated. Diazen-1-ium-1,2,2-triolate (Angeli's salt anion) and *(Z)*-1[*N*-(3-aminopropyl)-*N*-(3-aminopropyl)amino]diazen-1-ium-1,2-diolate (DTPA NONOate) generates singlet ^{1}HNO and $^3NO^-$ at pH 7 after irradiation at 266 nm.[74]

Recently our research team developed a new class of HNO donors by caging *N*-hydroxysulfonamides with the established (3-hydroxynaphthalen-2-yl)methyl (3,2-HNM) and (6-hydroxynaphthalen-2-yl)methyl (6,2-HNM) photocages, Figure 1.6.[75-78]

A photocage is a chromophore which is bonded to a reactive molecule to prevent the molecule from reacting in the absence of light. Upon light exposure, the bond between the photocage and the molecule breaks, releasing the reactive molecule. The HNM group has a reasonable quantum yield and was expected to release HNO with a rate constant of ~10^5 s^{-1}.[79]

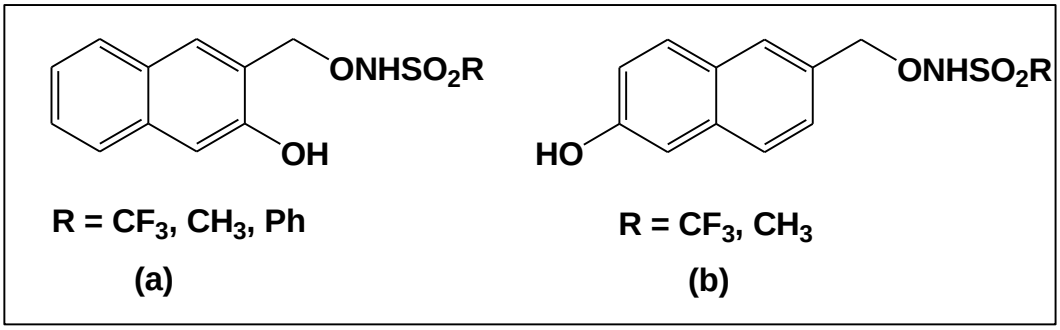

Figure 1.6. The structures of photocaged *N*-hydroxysulfonamides recently developed by our research team, incorporating the photocages (3-hydroxynaphthalen-2-yl)methyl (3,2-HNM) (**(a)**) and (6-hydroxynaphthalen-2-yl)methyl (6,2-HNM) (**(b)**).

Two other photodecomposition pathways occurred in addition to the desired HNO generating pathway, Scheme 1.2 (a). In Pathway 1 concerted C-O/N-S bond cleavage resulted in generation of a sulfinate (RSO_2^-), HNO and a diol. In Pathway 2 C-O bond cleavage generated the parent alkane sulfohydroxamic acid (RSO_2NHOH) and a diol. In Pathway 3 O-N bond cleavage resulted in formation of the sulfinamide (RSO_2NH_2) and an aldehyde. Whereas all three pathways occurred for R = CH_3 and Ph, C-O bond cleavage did not occur for both R = CF_3 systems.

For the 3,2-HNM photocaged molecules Pathway 1 was the preferred decomposition pathway for the CF_3 system (60% (R = CF_3) > 23% (R = Ph) > 9% R = CH_3, in mixtures of phosphate buffer (pH 7.0, 0.1 M) and CD_3CN (40:60 v/v)).[77] For the R = CF_3 system the percentage of the desired C-O/N-S generating pathway increased from 60 to 70% in 5:95 v/v phosphate buffer (pH 7.0, 0.1 M) and CD_3CN, whereas it was unchanged for the R = CH_3 system.[77] Since the parent alkane sulfohydroxamic acids

$MeSO_2NHOH$ and $PhSO_2NHOH$ are stable in acetonitrile and in aqueous solution, pH 7.0, the amount of each of these species directed reflected the amount of C-O bond cleavage. However CF_3SO_2NHOH is unstable in aqueous solution and decomposes rapidly to $CF_3SO_2^-$ and HNO ($t_{1/2}$ ~ 10 min at pH 7.0; $pK_a(CF_3SO_2NHOH)$ = 5.89.[55] There was, however, no evidence for the presence of $CF_3SO_2NHO(H)$ in any of the NMR spectra, providing support for concerted C-O/N-S bond cleavage in Pathway 1. Release of HNO was indirectly demonstrated by trapping HNO using the vitamin complex aquacobalamin and the phosphine trap.[76, 77]

More of the desired HNO-releasing pathway was observed for the 6,2-HNM system for R = CF_3 (98% in 80:20 v/v CD_3CN: phosphate buffer solution (5.0 mM, pH 7.0)), with less than 10% for the R = CH_3 system.[78] It was proposed that moving the hydroxy substituent from the 3 position (3,2-HNM) to the 6 position of the ring distal to the benzylic carbon (6,2-HNM) would limit excited-state intramolecular proton transfer from the OH to the N of the sulfonamidoxy group, which could result in undesired O−N bond cleavage. Importantly, the strongly electron-withdrawing trifluoromethanesulfonamidoxy leaving group is essential for quantitative HNO generation for the CF_3 system. Evidence for HNO release was again demonstrated using aquacobalamin and a phosphine trap, 3-(diphenylphosphino)-4-(methoxycarbonyl)benzoic acid.[78] It was also shown that in the absence of a molecule that reacts rapidly with HNO, an 6-[(*E*)-(hydroxyimino)methyl]-naphthalen-2-ol or 6,2-HNM-oxime species is observed in the photoproduct mixture (Scheme 1.2(b)).[76, 77]

A detailed mechanistic study was carried out for the 6,2-HNM photocaged derivative incorporating the trifluoromethanesulfonamidoxy group.[75] The protonation state of the N of the trifluoromethanesulfonamidoxy group (pK_a of N(H) = 4.4 ± 0.1 in aqueous solution, 25 °C) was found to play a key role in the mechanism of photodecomposition, with deprotonation at this site being essential for HNO generation. Deprotonation of this site could be achieved by adding a small amount of aqueous buffer to a solution of this compound in acetonitrile or adding a stoichiometric amount of carboxylate salt to the acetonitrile solution. Significant quenching of the singlet excited state fluorescence was observed under solvent conditions where the HNO generation pathway occurred. It was proposed from the results of femtosecond time-resolved transient absorption spectroscopy experiments that C-O/N-S bond heterolysis occurs directly from the singlet excited state of the N-deprotonated parent molecule on the

picosecond timescale, to generate a carbocation and $^{1}NO^{-}$. The carbocation subsequently reacts rapidly with nucleophiles including the solvent (H_2O or CH_3OH) or HNO in the absence of a molecule that reacts rapidly with HNO, to form an oxime, 6-[(*E*)-(hydroxyimino)methyl]-naphthalen-2-ol.

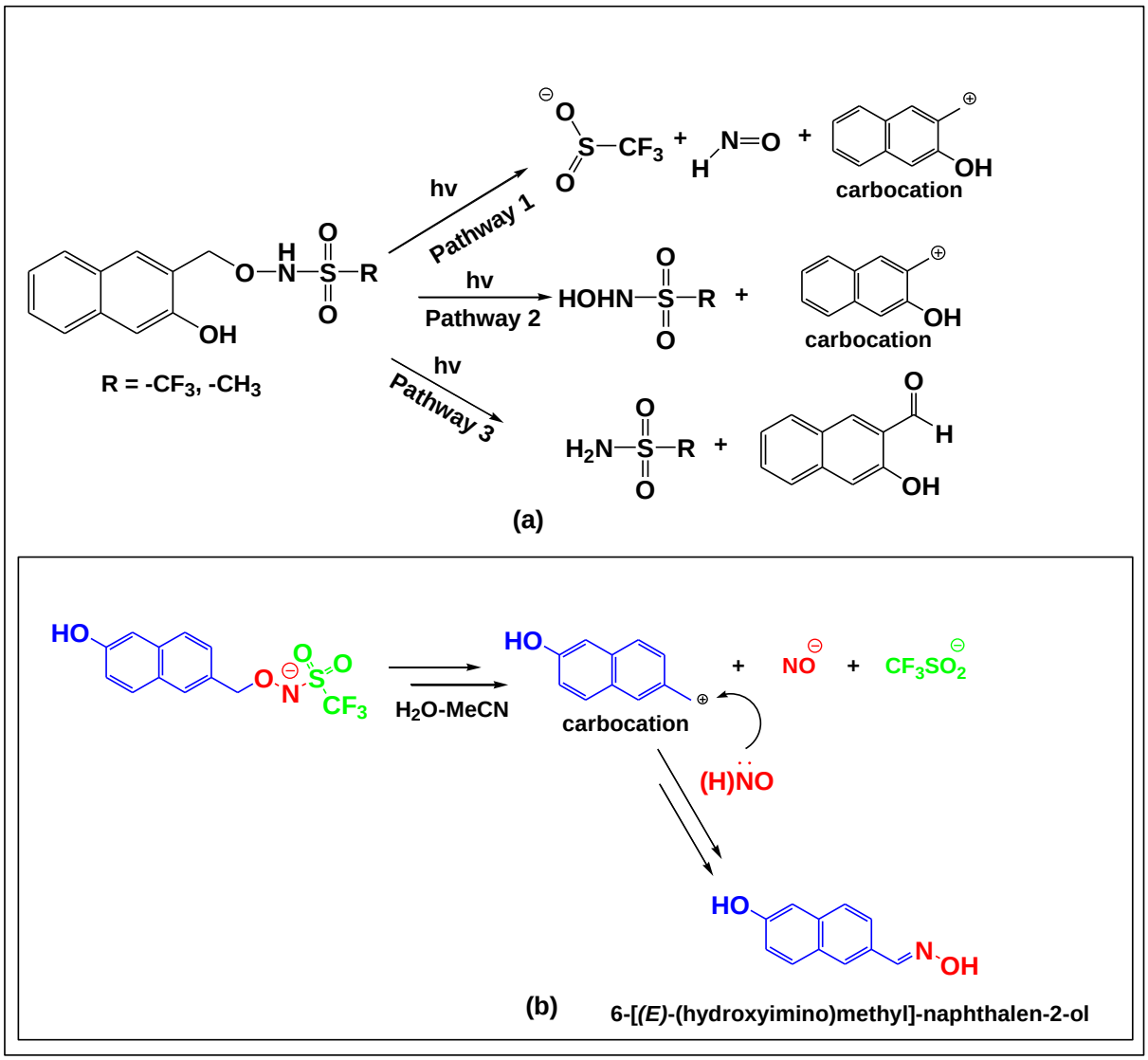

Scheme 1.2. (a) Proposed photolysis mechanisms of an HNO donor incorporating the (3-hydroxy-2-naphthalenyl)methyl (HNM) moiety (b) (6-hydroxy-2-naphthalenyl)methyl (HNM) moiety.

A photoactive HNO donor of the 2-nitro derivative of Piloty's acid has been recently developed tethered to the (7-diethylaminocoumarin-4-yl)methyl photocage.[80] The (7-diethylaminocoumarin-4-yl)methyl PPG chromophore absorbs in the visible region (400 nm). HNO generation was confirmed indirectly by monitoring the formation of N_2O (dimerization product of HNO) using GC-MS and observing the expected thiol derived products from the reaction of HNO with N-acetylcysteine. The corresponding

oxime compound was also observed upon irradiation of the photocaged 2-nitro derivative of Piloty's acid and the authors speculated that in addition to a minor amount of the desired pathway (~7%, Pathway 1, Scheme 1.3), subsequent nucleophilic attack of the nitrogen lone pair of the parent sulfohydroxamic acid on the carbocation intermediate results in generation of the sulfinic acid and a nitroso compound which tautomerises to give the oxime, Pathway 2, Scheme 1.3.

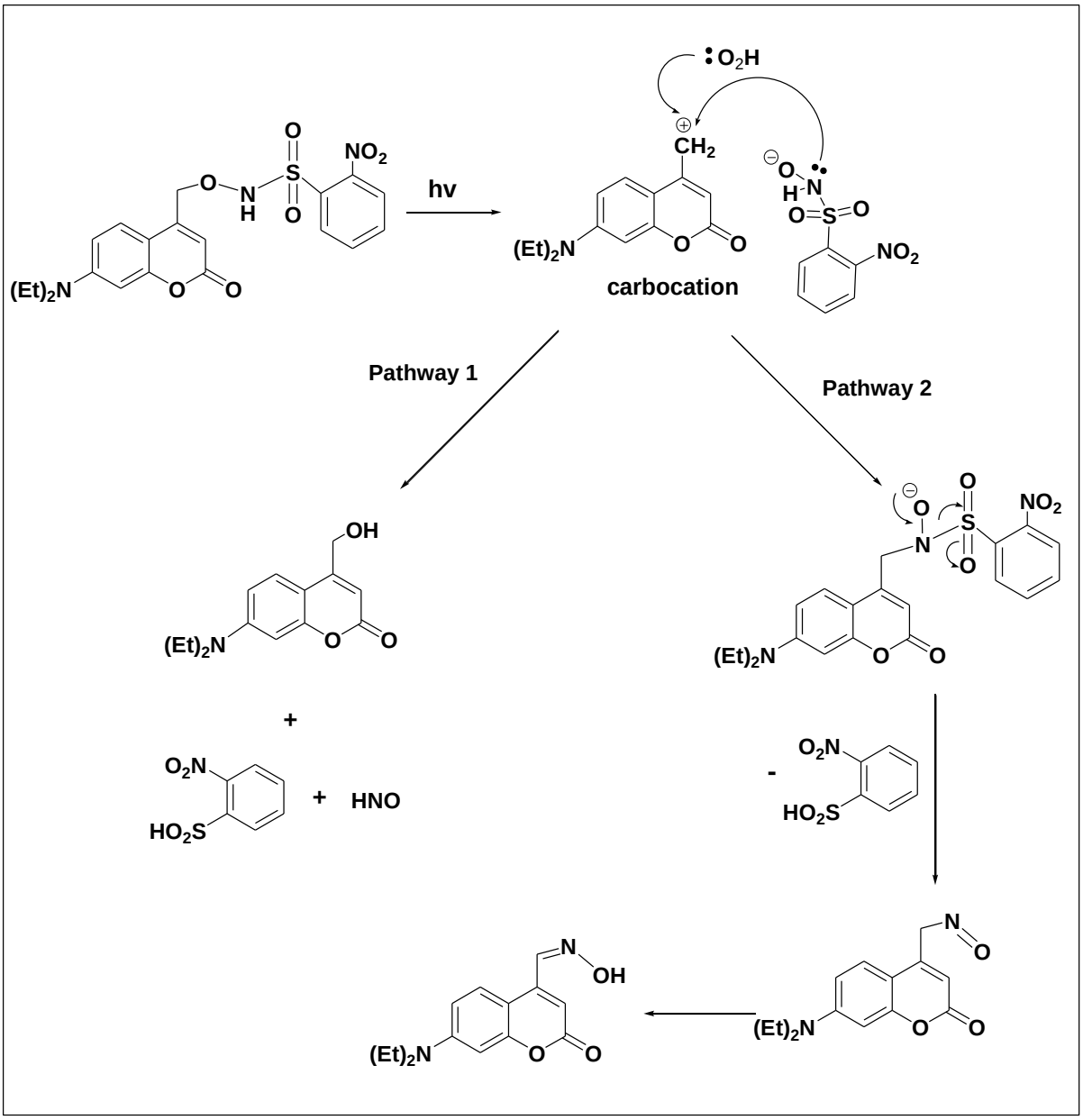

Scheme 1.3. Proposed mechanisms for photodecomposition upon visible light irradiation of (7-diethylaminocoumarin-4-yl)methyl photocaged 2-nitroPiloty's acid.

1.4 Photochemical reactions

The rate of chemical reactions is very well understood for reactions in the gas phase or in solution which require no external agent such as light or ionizing radiation. For

thermal reactions the activation energy is supplied by intermolecular collisions. The initial concentration of the reactants determine the order of the chemical reaction. Photochemistry is the study of chemical reactions initiated by light. Absorption of photons excites the molecule into one or more excited electronic states, which typically have a different reactivity compared with the electronic ground state of the molecule. In photochemical reactions, the activation energy is supplied by absorption of light.[81] The energy of a photon absorbed by a molecule obeys equation (1.14),

$$E = h\nu = hc/\lambda \quad (1.14)$$

where h = Planck's constant (Js), c = the velocity of light (ms^{-1}), ν = frequency (s^{-1}) and λ = wavelength (m). The energy of one mole of photons is $N_A h\nu$, where N_A = Avogadro's number.

Photochemical reactions are controlled by the rate of light absorption of the reactant in steady state experiments. Theoretically, all photochemical reactions are zero-order reactions with respect to the concentration of the reactant when the concentration of the reactant is low enough so that intermolecular interactions can be ignored.[82] The meaningful parameter used to denote photochemical conversion is the photoproduct quantum yield (φ).[82] Chemical actinometry has been widely employed in photochemistry as a relatively simple and accurate method to determine the quantum yield.

1.4.1 Photoproduct Quantum yield

The quantum yield (Φ) is the number of reactant molecules photolyzed to product(s) divided by the number of photons absorbed by the system. The rate of disappearance of the reactant, -dC/dt, is proportional to the quantum yield (Φ) and the concentration of the sample (c), equation (1.15).[83]

$$-\frac{dC}{dt} = \mathbf{k\Phi c} \quad (1.15)$$

A common method to determine the quantum yield is to use a chemical actinometer – a compound whose quantum yield is known. Useful chemical actinometers have been summarized by Khun and coworkers.[83] Examples of actinometers include the photoisomerisation of *trans*-azobenzene to *cis*-azobenzene, the photoisomerisation of 2-nitrobenzaldehyde to 2-nitrosobenzoic acid, the photochemical conversion of azoxybenzene to 2-hydroxyazobenzene, the reduction of potassium ferrioxalate and thymine dimerization.[83]

Potassium ferrioxalate is useful in the ultraviolet wavelength range,[83] and is reduced to Fe(II) upon irradiation by light, equations (1.16) and (1.17).

$$[Fe^{III}(C_2O_4)_3]^{3-} + hv \rightarrow Fe^{2+} + 2C_2O_4^{2-} + C_2O_4^{-} \quad (1.16)$$

$$[Fe^{III}(C_2O_4)_3]^{3-} + C_2O_4^{-} \rightarrow Fe^{2+} + 2C_2O_4^{-} + 2CO_2 \quad (1.17)$$

The overall reaction is

$$[Fe^{III}(C_2O_4)_3]^{3-} + hv \rightarrow Fe^{2+} + 2C_2O_4^{-} + CO_2 \quad (1.18)$$

After exposure of a ferrioxalate solution to UV light (313 nm), the Fe^{2+} generated can be analyzed by a colorimetric method. Fe^{2+} is complexed with 1,10-phenanthroline (phen) to form $[Fe(phen)_3]^{2+}$ ($\varepsilon_{510\ nm} = 1.11\times10^4\ M^{-1}\ cm^{-1}$).[83]

Trans-azobenzene is also often used as a chemical actinometer to determine quantum yields of molecules that absorb UV light. Upon light activation *trans*-azobenzene isomerises to *cis*-azobenzene, equation (1.19). The quantum yield is 0.14 in CH_3OH (313 nm irradiation)[84] and 0.21 (313 nm irradiation) in acetonitrile.[85]

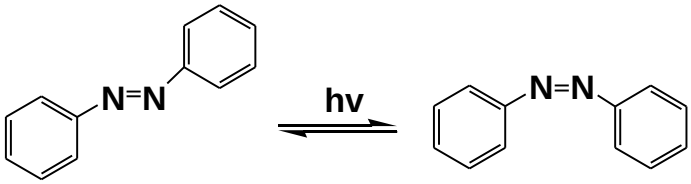

***trans*-azobenzene** ***cis*-azobenzene**

(1.19)

The value of the photoproduct quantum yield depends on the refractive index of the solvent.[83] If the experiment is conducted in different solvents, the refractive index should be taken into account as shown in equation (1.20).

$$\phi_X = \phi_{ST}\left(\frac{Grad_X}{Grad_{ST}}\right)\left(\frac{\eta_X^2}{\eta_{ST}^2}\right) \quad (1.20)$$

η_X and η_{ST} are the refractive indices of the two solvents, φ_X and φ_{ST} are the quantum yields of the compound in a solvent where the quantum yield has not yet been determined and a known quantum yield value reported for the compound in another solvent, respectively, and $Grad_X$ and $Grad_{ST}$ are the slopes of plots of the amount of photoproduct(s) versus irradiation time for the compound in the different solvent and the solvent in which the quantum yield has already been established, respectively.

1.4.2 Photophysical processes

A range of photophysical processes can occur upon excitation of a molecule. Photophysical changes do not involve bond cleavage or bond formation events. Figure 1.7 gives the well-known Jablonski diagram showing the various electronic excited states of molecules. According to the Franck-Condon principle, the time scales of events that occur for molecules in the excited state vary from 10^{-16}-10^{-1} s.[86, 87] The movement of electrons (10^{-16}-10^{-15} s) is rapid compared to vibrations of nuclei in a molecule.[92] After excitation rapid re-distribution of the electron density results in relaxation of the molecule to the lowest vibrational energy level (10^{-13}–10^{-14} s) of the electronic state. This process is called vibrational relaxation. Internal conversion (IC) occurs when the molecule relaxes to an excited state of lower energy as a result of vibrational coupling between the two states. This occurs within the 10^{-11}–10^{-13} s time frame. Each electronic excited state (S_1, S_2, S_3 etc) may relax via fluorescence (10^{-12}-10^{-6} s), intersystem crossing (ISC) to a triplet state (T_1, 10^{-12}-10^{-4} s), and phosphorescence (10^{-6}-10^{-1} s).[92] Non-radiative decay mechanisms may also occur, resulting in the return of the molecule to the electronic ground state. Photochemical reactions involving bond cleavage and bond formation events occur from excited state molecules. Ionization, dissociation, electron transfer, abstraction, isomerization and addition reactions can occur.[87]

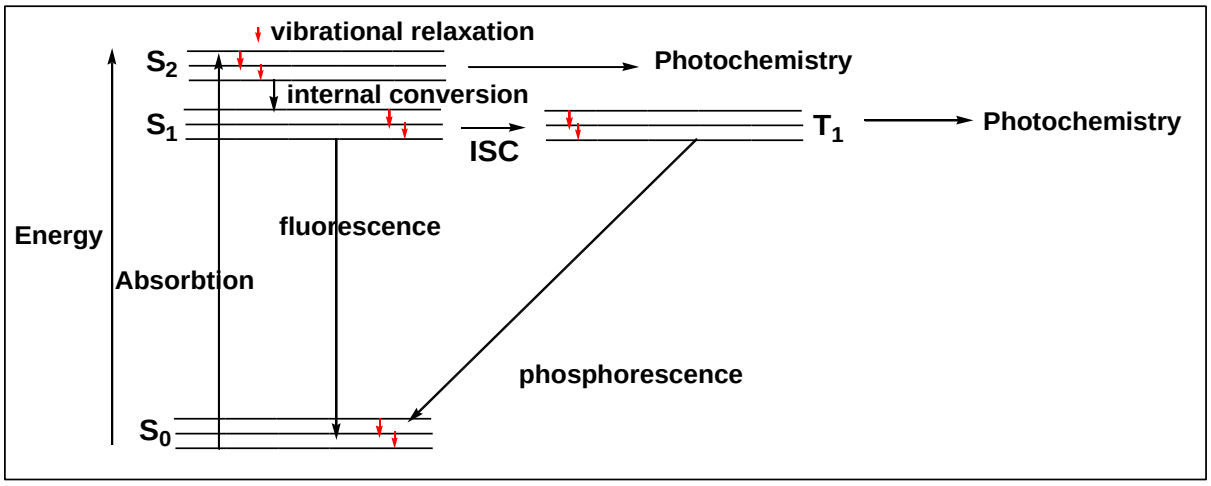

Figure 1.7. Jablonski diagram showing the ground and singlet excited states (S_0, S_1 etc). Vibrational relaxation occurs rapidly via radiationless transitions to the lowest excited vibrational state of each electronic state. Internal conversion results in the molecule returning to the lowest (S_1) excited state. Fluorescence occurs from the lowest excited singlet state. Intersystem crossing (ISC) may occur also occur via a triplet state (T_1) lead to phosphorescence.

1.5 Photoprotecting groups (PPGs)

Conjugation of molecules to PPGs is a widely used strategy used to generate molecules upon demand at a specific location. Light has been used to release molecules for a range of biological applications.[88, 89] In this case it is important that the PPG absorbs light at wavelengths above 330 nm, since the irradiation is otherwise absorbed by biological molecules.[89] The photoproducts generated from the PPG moiety are ideally unreactive and non-toxic, and the PPG-conjugated biomolecule should be stable prior to irradiation by an intense light source such as a laser. The PPG-biomolecule conjugate should also ideally be soluble in aqueous solution for biological applications,[89] the photochemistry clean (no side reactions) and the photochemistry occur with a high photoproduct quantum yield (φ). Finally, the photoproduct generated should not be reactive and absorb light at the same wavelength as the PPG-biomolecule conjugate to avoid inner filtering effects.

Many organic PPG's have been reported which absorb light in different regions of the light spectrum, Figure 1.8. For example, the *p*-hydroxyphenacyl,[90] 2-nitrobenzyl and 2-(nitrophenyl)ethyl PPG's absorb in the UV region whereas (coumarin-4-yl)methyl photocages absorb in the visible region.[89] The latter three chromophores are used as photocages for the molecules presented in this thesis. Time resolved absorption spectroscopy, time resolved FTIR (µs or faster), DFT calculations and characterization of the photoproducts obtained by steady state irradiation gives information on the mechanisms of photochemical reactions, including the rates of formation and decay of excited state species and ground state intermediates upon excitation of PPG-conjugated molecules.

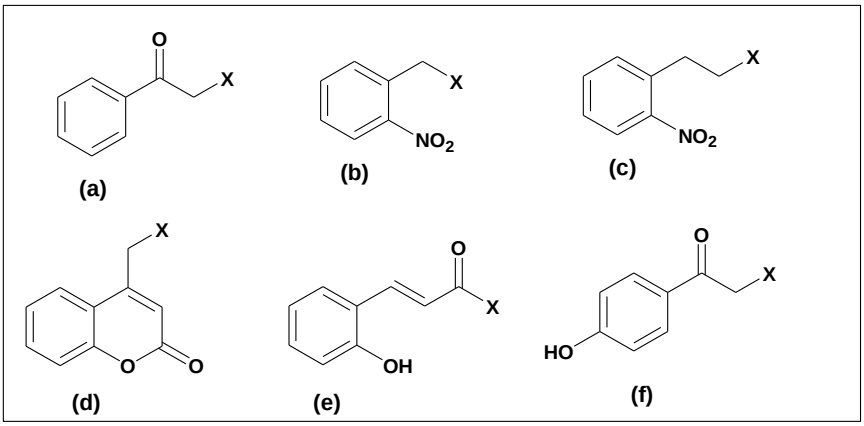

Figure 1.8. The structures of common PPGs. (a) phenacyl (b) 2-nitrobenzyl (2-NO_2Bn) (c) (2-nitrophenyl)ethyl (2-NPE) (d) (coumarin-4-yl)methyl (e) 2-hydroxycinnamyl and (f) *p*-hydroxyphenacyl.

1.5.1 Photoactive molecules incorporating the 2-NO_2Bn PPG

The 2-nitrobenzyl (2-NO_2Bn) chromophore is one of the most widely used and most well-understood PPG.[89, 91-93] This PPG has been used for numerous applications, including the rapid release of the signaling metal cation Ca^{2+},[94] for the *in situ* generation of nucleotides for automated nucleic acid synthesis,[95] and the release of 2,4-dinitrophenol in the mitochondria.[96] Molecules incorporating the 2-NO_2Bn PPG have also been used for photolithography.[97]

Figure 1.9 gives examples of systems incorporating the 2-NO_2Bn PPG that have been studied. Alcohols and esters including ATP are efficiently released from 2-NO_2Bn-caged ATP, Figure 1.9(a).[89] 2-Nitrobenzyloxycarbonyl derivatives decompose via a two-step process rapid process to ultimately generate CO_2 and release the leaving group, Figure 1.9(b).[98] 2-Nitrobenzaldehyde is photochemically isomerized to 2-nitrosobenzoic acid, Figure 1.9(c).[99, 100] The rate of release of the leaving group is dependent on the solvent, substituents on the chromophore and the leaving group.

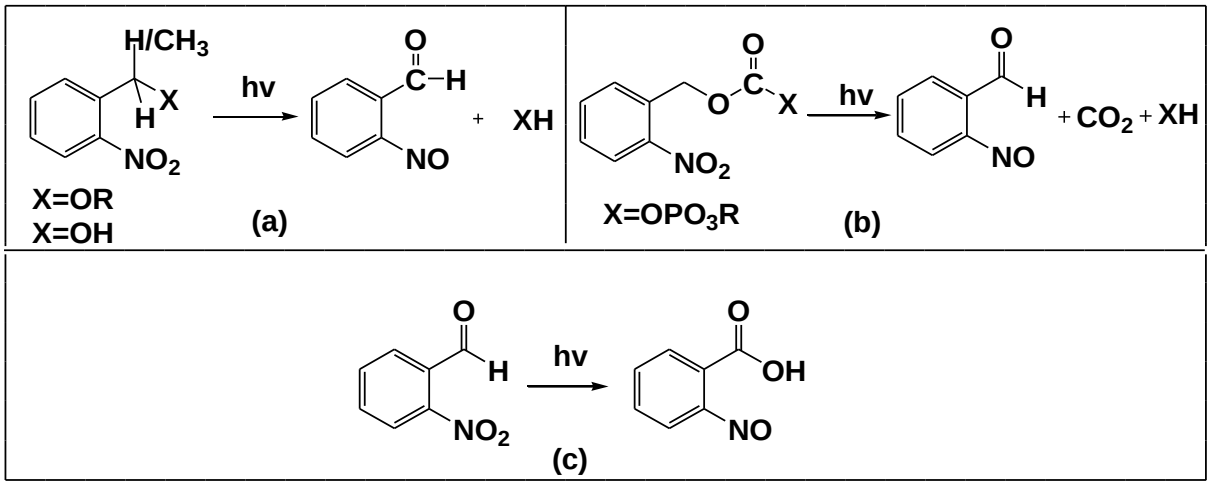

Figure 1.9. Photoactive molecules incorporating the 2-NO_2Bn group.

Scheme 1.4 shows the proposed mechanism for the photodecomposition of 1-(methoxymethyl)-2-nitrobenzene (species **a**).[89] Upon excitation to the singlet excited state (**a***), an intramolecular 1,5-hydrogen atom transfer occurs in the excited state via a Norrish type II reaction. This results in formation of a ground state quinonoid aci-nitro tautomer (**b**) within the duration of the pulse of a nanosecond laser flash photolysis instrument. The monoprotonated aci-nitro intermediate is in equilibrium with the deprotonated anionic form of this compound. The monoprotonated aci-nitro intermediate cyclizes to form a benzisoxazolidine species (**d**). A 1,3-hydrogen shift

results in ring opening to give the hemiacetal (**e**). Hydrolysis leads to the release of the leaving group (CH_3OH) and 2-nitrosobenzaldehyde. Multiple isomers exist for several of the intermediates, which can result in the observation of biexponential formation and decay processes.[89] Catalysis by buffers, and/or general acid and base catalysis can also occur.[101] For poor leaving groups such as CH_3OH, the last step is rate-determining and occurs on the seconds timescale ($k = 2.5 \times 10^{-2}$ s^{-1}).[101] The rate constant for the loss of the leaving group depends on the solvent, pH and the nature of the leaving group.[101-103]

The effect of aromatic substituents and substituents at the benzylic position of the 2-NO_2Bn PPG has been investigated.[89] Time resolved FTIR is an extremely valuable tool for characterizing the reaction intermediates for molecules caged with this PPG, with bands for C=O, N=O and C=N observed.[101, 102, 104] Possible excited state precursors include singlet and triplet state species and radical complexes for this system.[105-112] For the parent 2-nitrotoluene, a singlet excited state and a diradical excited state have been proposed to be precursors of the *(Z)*-aci-nitro intermediate using DFT calculations in combination with femtosecond transient absorption experiments and Raman spectroscopy.[105-112] For the *(E)*-aci-nitro intermediate an singlet excited state diradical precursor has been proposed.[106-112] One problem in these types of systems is that 2-nitrosoaldehyde also undergoes photodecomposition, producing brown decomposition products.[101] 2-Nitrosoaldehyde also undergoes acid and base-catalyzed decomposition in aqueous solution and is only stable in the pH 3-6 range.[101]

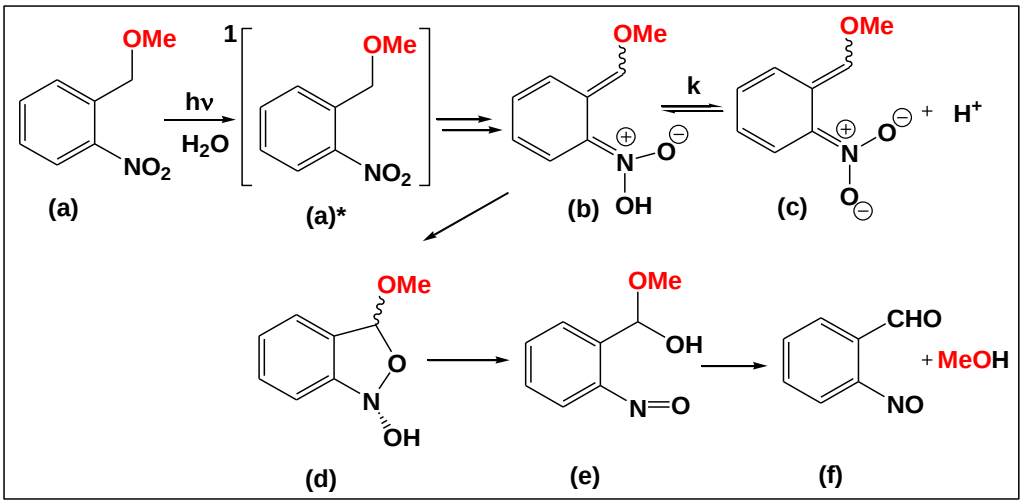

Scheme 1.4. Proposed mechanism for the photodecomposition of 1-(methoxymethyl)-2-nitrobenzene.

The 2-NO_2Bn phototrigger has been successfully used to photocage hydroxylamine derivatives. For example, McCulla et al. reported that 2-nitrobenzyl benzohydroxamate yields benzohydroxamic acid (75%) upon irradiation at 330 nm.[113] Photoprotected suberoylanilide hydroxamic acid and related analogues are released when caged with the 4,5-$(MeO)_2$-2-NO_2Bn PPG.[114, 115] Various hydroxylamine intermediates are photochemically generated (up to 95%) from caged analogs by use of the 2-NO_2Bn PPG.[116] McCune et al. successfully obtained several hydroxylamino acid compounds *via* photoprotection of the 2-NO_2Bn PPG.[117] Recently Qvortrup et al. reported the photolytic release of hydroxamic acids caged by 2-NO_2Bn in protic solvents via heterolytic C-O bond cleavage in high yield,[118, 119] while carboxamides were instead obtained in aprotic solvent from competing heterolytic O-N bond cleavage.[119] The mechanisms of photodecomposition proposed by Qvortrup et al. are shown in Scheme 1.5.[119] The reactant **a** undergoes a Norrish Type II reaction, with β-hydrogen abstraction to give the biradical intermediate **c**, which undergoes electron rearrangement to give **d**, a monoprotonated *(Z)*-aci-nitro intermediate. This species can either undergo O-N heterolytic bond cleavage to give **j** and an amide, or isomerises to give the monoprotonated *(E)*-aci-nitro intermediate **f** via the anion **e**. In an aprotic solvent only the former reaction occurs. Cyclisation of **f** followed by elimination of $RC(O)NHO^-$ gives the nitroso product **i** and a hydroxamic acid. The conversion of the monoprotonated (Z)-aci-nitro intermediate to the *(E)* isomer only occurred in the presence of H_2O. DFT calculations showed that the presence of the water molecule lowers the activation energy barrier and favors the formation of aci-nitro anion **e** in the presence of H_2O. The transient absorbance decay of aci-nitro intermediate **e** occurred within 5 ns.

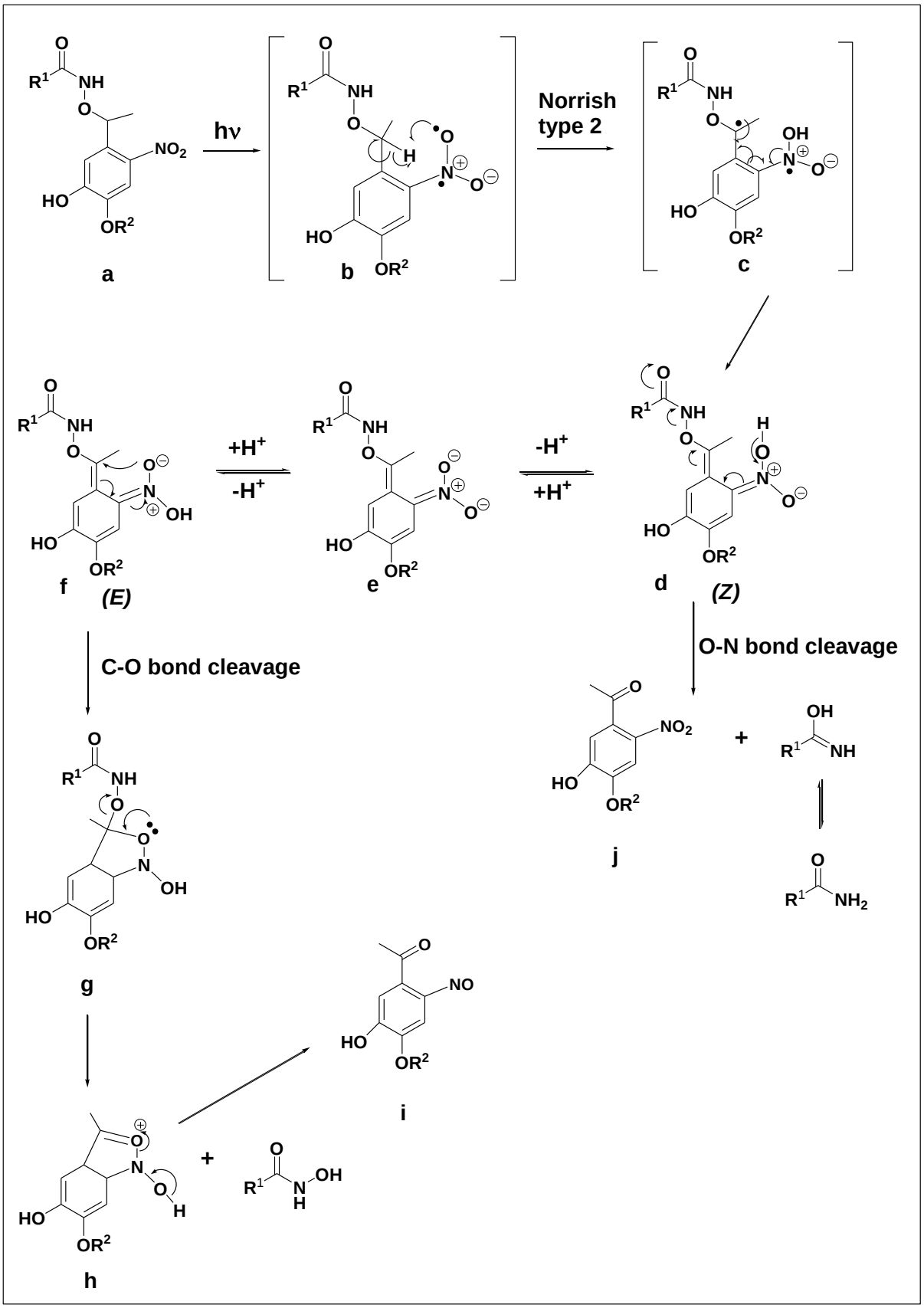

Scheme 1.5. Proposed mechanism for the photodecomposition of 2-NO_2Bn-caged hydroxamates.[119]

1.5.2 Photoactive molecules incorporating the 2-nitrobenzyloxycarbonyl (2-NBOC) PPG

Previous studies also show that carbonate and carbamate linkers can be inserted between the 2-NO_2Bn/4,5-$(MeO)_2$-2-NO_2Bn group and the molecule of interest.[120, 121] The 2-nitrobenzyloxycarbonyl (2-NO_2Bn-OC(O) has been utilized to prepare conjugates of amines, alcohols (Figure 1.10) and phosphates (Figures 1.11).[102, 122] The amines generated during the reaction undergo rapid condensation with the 2-nitrosobenzaldehyde product which results in an imine being formed. 2-Nitrosobenzaldehyde is also photosensitive.[101] 2-Nitrobenzyloxycarbonyl caged molecules photodecompose via a two-step process via an aci-nitro intermediate followed by a slower decarboxylation step and release of the leaving group.[98]

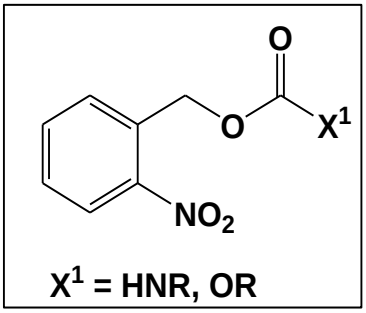

Figure 1.10. The structures of 2-nitrobenzyloxycarbonyl (2-NO_2Bn-OC(O)) conjugates of amines and alcohols.

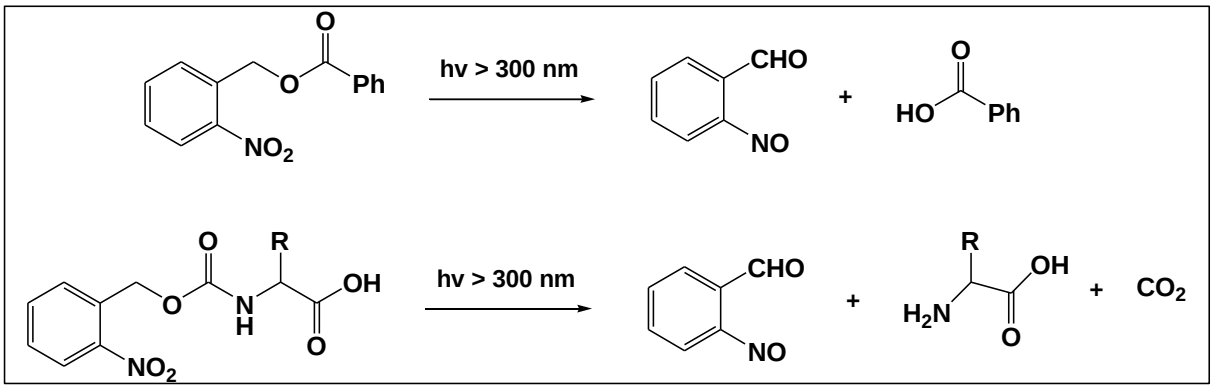

Figure 1.11. Photochemical decomposition of amine and alcohol conjugates of 2-nitrobenzyloxycarbonyl.

1.5.3 Photoactive molecules incorporating the (2-nitrophenyl)ethyl (2-NPE) PPG

More recently the 2-NO_2Bn photocage has been modified by the replacement of the methyl group for an ethyl group, to give (2-nitrophenyl)ethyl (2-NPE) caged systems. The 2-NPE moiety has been successfully used to photoprotect various biomolecules and releases molecules more efficiently (two times faster) compared with the **o-NO_2Bn**

photocage.[123, 89]The photochemistry of several 2-NPE-caged thymidine nucleosides has been studied by nanosecond laser flash photolysis. An aci-nitro intermediate was observed, and the decomposition of this species was found more rapid for these compounds, with lifetimes of 0.1 – 10 μs.[124]

The mechanisms of the photodecomposition of 2-NPE conjugated thymidine nucleosides were investigated in detail, Scheme 1.6.[124] The authors proposed that after excitation, the populated ^{1}(n-π*) state (**a***) undergoes 1,5-hydrogen atom transfer to ultimately form the (*E)*-aci-nitro intermediate (**c**) or intersystem crossing to form a triplet biradical (**b**) which decays to the (*E)*-aci-nitro intermediate. There was, however, no conclusive evidence that the aci-nitro species was generated directly from the singlet excited state and/or a triplet excited state species. The decay of the aci-nitro species was observed in the 0.1-10 μs time scale region and depends on the alkyl group R. The photoproducts were characterized in solvent mixtures of MeCN and H_2O. In pure MeCN the monoprotonated form of the (*E)*-aci-nitro species (**c**) was observed. This compound (**c**) decomposes via a cyclic intermediate (**d**) to ultimately generate the nitroso isomer of the reactant, product (**e**). Other uncharacterized products X and Y were also observed in the photoproduct mixture. In MeCN/H_2O mixtures, it was proposed that the monoprotonated (*E)*-aci-nitro species (**c**) deprotonated to give the aci-nitro anion (**f**). A subsequent elimination reaction (leading to heterolytic C-O bond cleavage) gives 2-nitrostyrene (**g**) and RO^-. A pK_a value of ~4 was reported for 2-quinonoid aci-nitro compounds.[124] Note that there are a number of minor problems associated with this proposed mechanism. Firstly, by analogy with 2-NO_2Bn caged molecules that also undergo 1,5-hydrogen atom transfer, it would be expected that the monoprotonated form of the (*Z)*-aci-nitro species would be directly formed from the singlet excited state, not the (*E)*-isomer as proposed in this scheme, and that both the (*E)* and (*Z)* isomers would be formed via the triplet pathway.[89] The monoprotonated (*E)* and (Z)-aci-nitro species would also be expected to be in equilibrium with each other via the aci-nitro anion.[119] Finally, the stereochemistry of the other alkene has also not been considered.

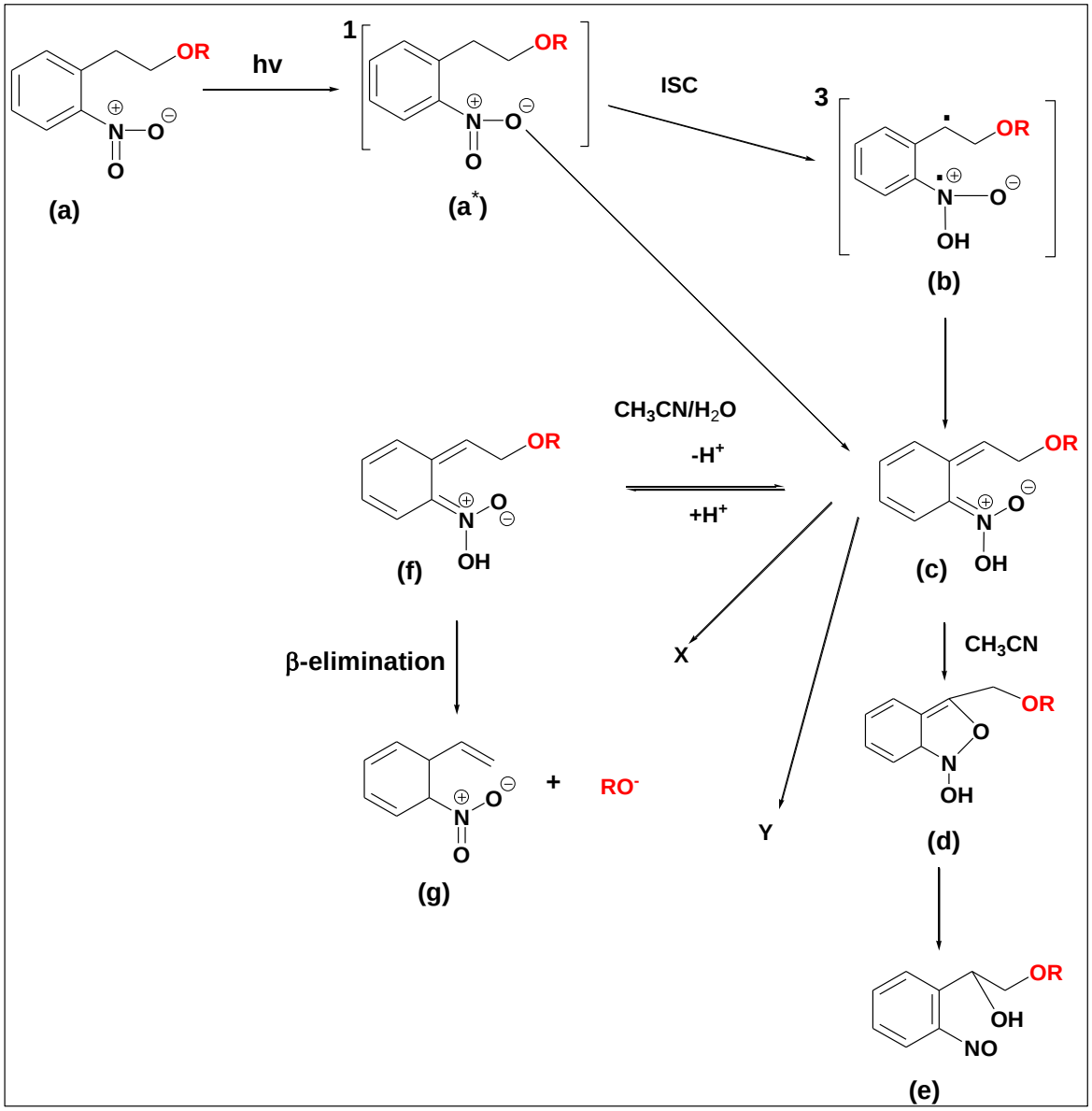

Scheme 1.6. Proposed mechanism for the photodecomposition of (2-nitrophenyl)ethyl caged nucleosides.[124]

1.5.4 Photoactive molecules incorporating the (coumarin-4-yl)methyl PPG

The (coumarin-4-yl)methyl PPG absorbs in the visible region and has a high molar extinction coefficient.[119] The absorbance region (380-480 nm) makes this PPG a perfect photocage for the controlled release of biomolecules.[71, 125-128] Biomolecules that have been successfully caged to the (coumarin-4-yl)methyl photocage include carbonates, phosphates, diols, sulfates, carbonyl compounds, pesticides (e.g. Fipronil) and sulfonates.[89, 126, 129, 130] Two photon uncaging for the coumarin PPG attached primary amines and sulfides in modified agarose gel (3D sites) has also been reported.[131, 132] The release of molecules from the (coumarin-4-yl)methyl PPG can be

orders of magnitude faster than molecules caged to 2-NO_2Bn or 2-NPE.[148] Quantum yields range from 0.21 to 0.28.[133,134]

The photodecomposition mechanism of (coumarin-4-yl)methyl esters and (7-methoxycoumarin-4-yl)methyl-caged phosphates, sulfonates and carboxylic acids are well-studied. After light excitation the (coumarin-4-yl)methyl ester relaxes to the $^1(\pi, \pi^*)$ state, Scheme 1.7.[135, 136] The $^1(\pi, \pi^*)$ state either undergoes C-O heterolytic bond cleavage leading to a solvent-caged contact ion pair or unproductive fluorescence and non-radiative decay back to the ground state (coumarin-4-yl)methyl ester. Spin crossover to the triplet excited has not been observed for these systems.[135] The solvent caged contact ion pair can recombine or escape from the solvent cage, resulting in a solvent separated ion pair (coumarin-4-yl)methyl cation and the conjugate base of the leaving group). The (coumarin-4-yl)methyl cation reacts rapidly with a nucleophile or solvent. Time resolved studies reveal that the rate of C-O heterolytic bond cleavage is very fast for the system shown in Scheme 1.7 with a rate constant of 2×10^{10} s^{-1}.[136] This is the highest rate constant reported for any PPG. However the contact ion pair recombination dominates and is 10 times faster than the addition of the nucleophile.[135, 136]

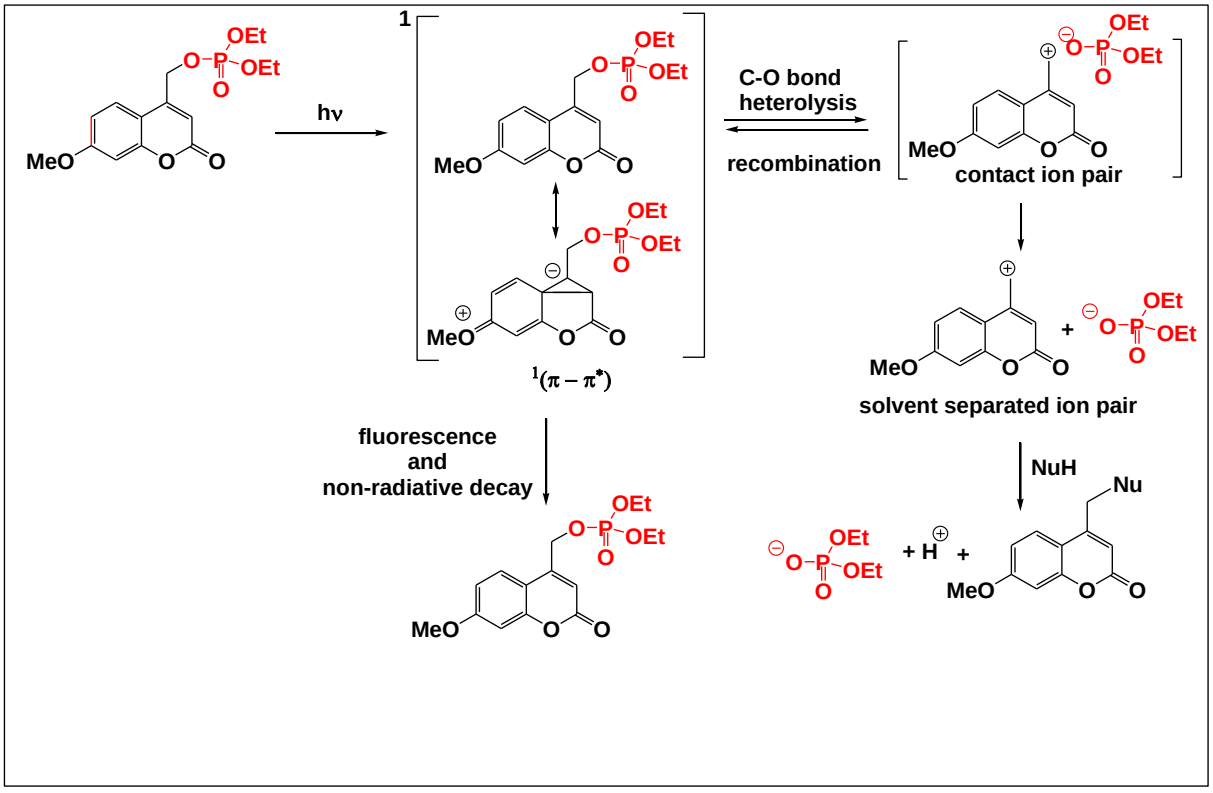

Scheme 1.7. Proposed mechanism for photodecomposition of (coumarin-4-yl)methyl phosphate esters.[135, 136]

^{18}O isotopic photolysis experiments of (coumarin-4-yl)methyl esters were carried out in a mixture of CH_3CN / $H_2{}^{18}O$ (30/70 v/v) to determine if the photodecomposition was occurring via solvent-assisted photoheterolytic bond cleavage to give a contact ion pair (Pathway **1**, Scheme 1.8, or via photosolvolysis (Pathway **2**, Scheme 1.8).[136] ^{18}O-enriched (coumarin-4-yl)methyl alcohol ((coumarin-4-yl)$CH_2{}^{18}OH$) was formed, supporting photodecomposition occurring via Pathway **1**. The photoproduct quantum yield of the (coumarin-4-yl)methyl ester of phosphate increases as the water content increased in CH_3CN/H_2O solvent mixtures, with a decrease in the fluorescence quantum yield.[136] This is consistent with the mechanism shown in Scheme 1.7 where fluorescence competes with the formation of the contact ion pair via C-O bond heterolysis.

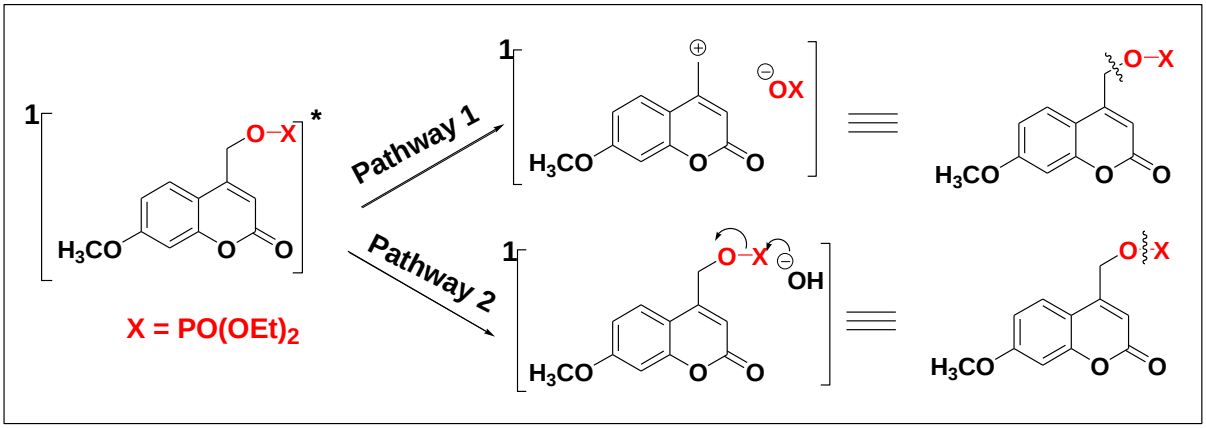

Scheme 1.8. Proposed pathways for photodecomposition of (coumarin-4-yl)methyl phosphate esters, via solvent-assisted photoheterolytic C-O bond cleavage to give a contact ion pair (Pathway **1**) and photosolvolysis (Pathway **2**).

Release of alcohols, phenols and thiols from (coumarin-4-yl)methyl caged molecules are not possible because they do not undergo heterolytic bond cleavage.[132] This problem can be successfully solved by the addition of the 6-bromo substituent, Scheme 1.9).[134, 137, 138] Photodecomposition again proceeds via heterolytic C-O bond cleavage to give a contact ion pair. The thiocarbonic acid or carbonic acid produced from the photoreaction undergoes decarboxylation to give a thiol or alcohol,[134, 137-139] with $k(co_2) = 10^{-3}\ s^{-1}$ (Scheme 1.9).[138, 140, 141] The rate of the reaction is significantly slower compared to (coumarin-4-yl)methyl esters because of the poorer leaving group.[142] The rate determining step is decarboxylation and is dependent on the pH and nature of the amino acid.[143]

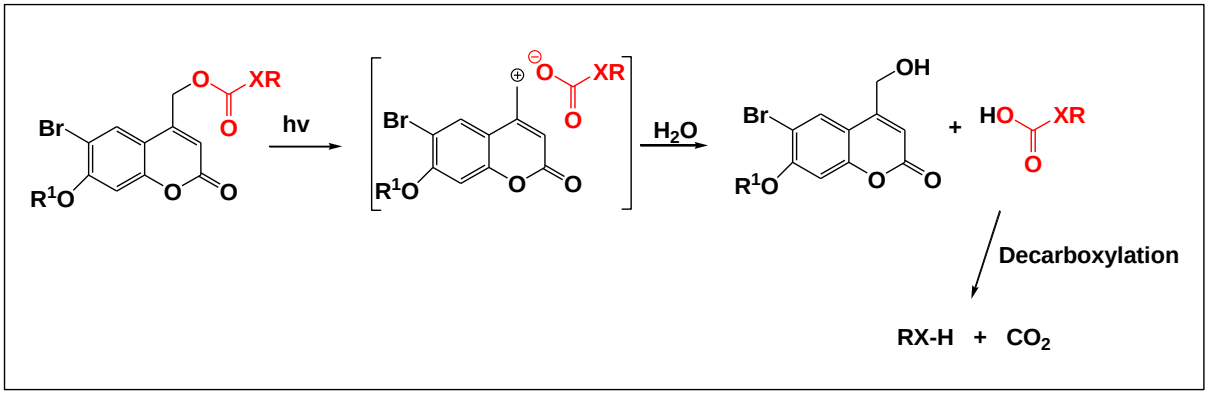

Scheme 1.9. Decarboxylative photorelease of alcohols, thiols, and amines.

Light-induced release of diols from cyclic (coumarin-4-yl)methyl acetals has also been reported. Once again C-C bond cleavage occurs to give a contact ion pair.[144] Single and two photon uncaging of (coumarin-4-yl)methyl-1,3-dioxalanes has also been reported under physiological conditions to release carbonyl compounds.[126, 145]

Finally, the ground and excited state properties have been studied in detail for coumarins. The labelling scheme is given in Figure 1.12.[146] These properties can be significantly altered by attaching an electron withdrawing or donating substituent to the coumarin moiety.[126, 147-149] The pK_a for the deprotonation of the OH of various hydroxycoumarins have been determined, Figure 1.12. This value pK_a follows the order 3-hydroxycoumarin (7.6) > 7-hydroxycoumarin (8.3) > 8-hydroxycoumarin (8.5).[146] These pK_a valyes are in the physiological pH range, therefore they are considered good for photocaging within the biological system. Coumarins are photoacids; that is, the excited state pK_a values can be much lower than the corresponding ground state values. Importantly, pK_a^* values follow a different order compared with the pK_a values, Figure 1.13, consistent with the location of the electron density being significantly different in the excited state coumarins.[126, 147-149]

In Chapter 4 of this thesis the photodecomposition of (6-bromo-7-hydroxycoumarin-4-yl)methyl – caged *N*-hydroxysulfinamides is investigated. The addition of the 6-bromo substituent to 7-hydroxycoumarin causes a significant bathochromic shift (λ_{max} ~330-380 nm for 6-bromo-7-hydroxycoumarin compared to ~320-330 nm for 7-hydroxy coumarin; 30 nm lower).[148] The pK_a of 6-bromo-7-hydroxycoumarin (pK_a ~6) is also lower compared to 7-hydroxycoumarin (pK_a ~8.5), by 2.5 pH units. The superior water solubility of 6-bromo-7-hydroxycoumarin is an advantage for biological studies.

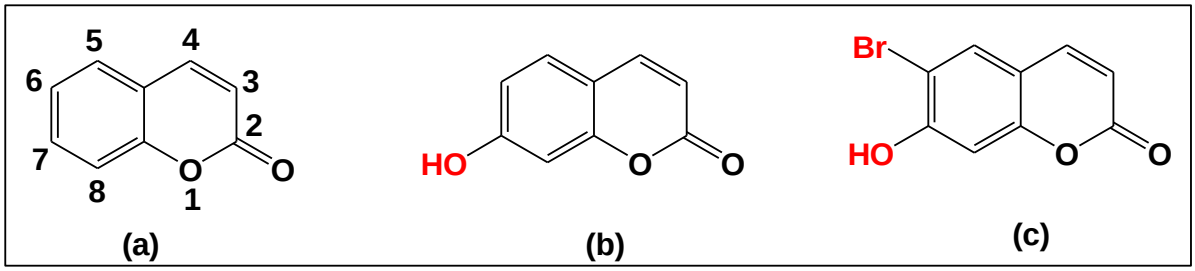

Figure 1.12. The structures of (a) coumarin showing the labelling of the positions on the aromatic ring (b) 7-hydroxycoumarin (c) 6-bromo-7-hydroxycoumarin.

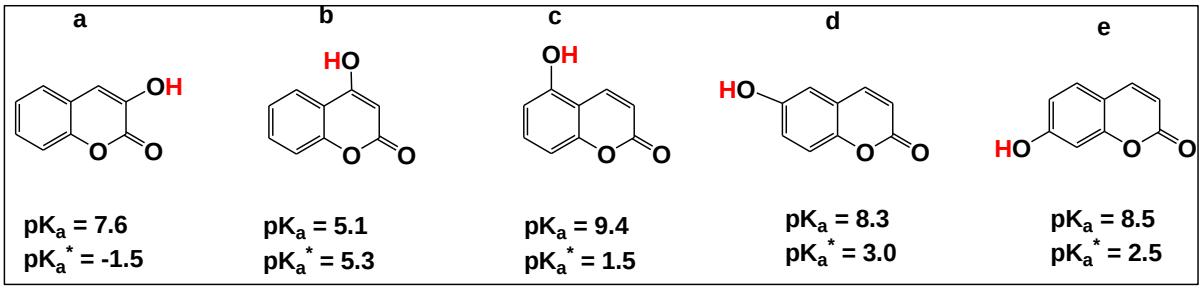

Figure 1.13. pK_a and pK_a^* values for the hydroxy group of various hydroxycoumarins.

1.6 Aims of this thesis

Photolysis is widely used to rapidly release molecules caged to chromophores with precise spatial and temporal control. Recently our research team developed a new class of *N*-hydroxysulphonamide-based HNO donors incorporating the photoactive (3-hydroxynaphthalen-2-yl) and 6-hydroxynaphthalen-2-yl) moieties, Figure 1.6.[75-78] This thesis focuses on elucidating the mechanisms of photodecomposition of a series of novel photoactive *N*-hydroxysulphonamide-based HNO donors incorporating the 2-nitrobenzyl (2-NO_2Bn) and 2-nitrobenzyloxycarbonyl (2-NO_2Bn-OC(O)) chromophores (Chapter 2), the 1-(2-nitrophenyl)ethyl (2-NPE) chromophore (Chapter 3) and the (6-bromo-7-hydroxycoumarin-4-yl)methyl (BHC) chromophore (Chapter 4). The structures of these molecule are shown in Figure 1.14. The compounds were synthesized in our collaborators' laboratories at Kent State University, USA, and are described in the PhD theses of Yang Zhou and Mohammad Saifur Rahman.[150] We hypothesized that upon excitation by light, these molecules would decompose to release HNO via concerted C-O/N-S bond cleavage and a leaving group (LG), with the latter molecule providing a convenient way to indirectly follow the release of HNO.[151] It was anticipated that the nature of the *N*-hydroxysulfonamide would play an important role in the release of HNO versus competing undesired photochemical reactions.

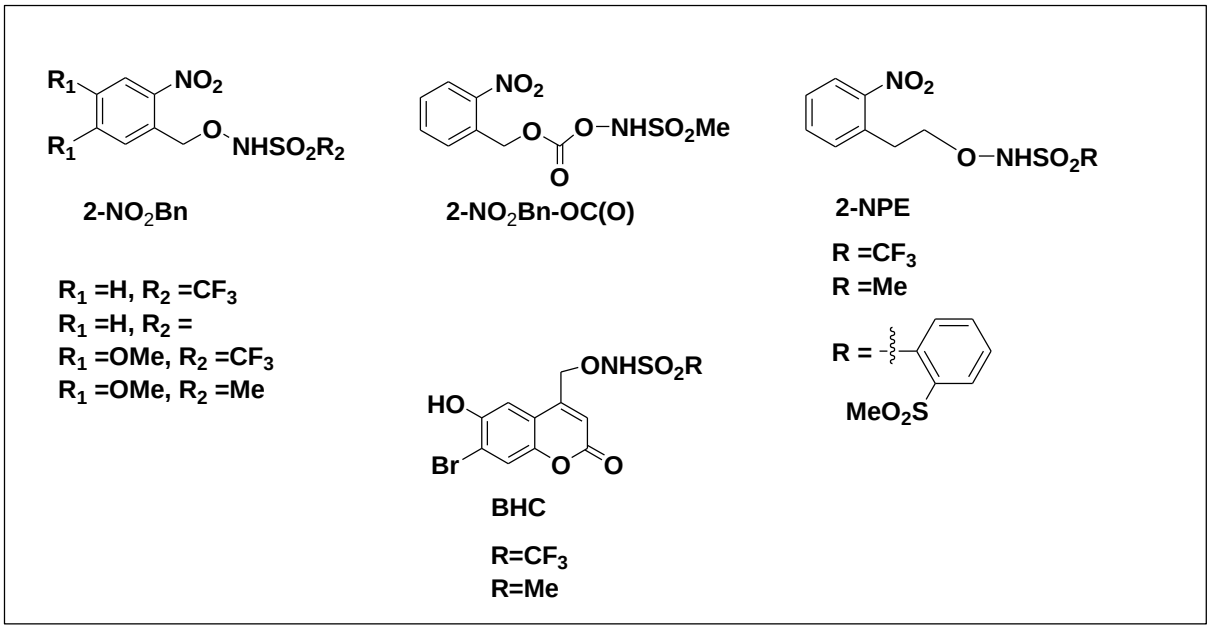

Figure 1.14. The structures of photoactive *N*-hydroxysulfonamide-based HNO donor molecules investigated in this thesis, caged with the 2-nitrobenzyl (**2-NO$_2$Bn**), *2*-nitrobenzyloxycarbonyl (**2-NO$_2$Bn-OC(O**)), 1-(2-nitrophenyl)ethyl (**2-NPE**) and (7-bromo-6-hydroxycoumarin-4-yl)methyl (**BHC**) chromophores.

Chapter 2: Studies of Photoactivatable *N*-Hydroxysulfonamide-caged HNO Donors incorporating the 2-(nitrobenzyl) (2-NO_2Bn) Phototrigger

2.1 Introduction

The 2-nitrobenzyl (**2-NO_2Bn**) chromophore is one of the most well-understood photoprotecting groups (PPG).[89, 91-93] Light excitation of the **2-NO_2Bn** chromophore leads to a short lived "aci-nitro" intermediate.[99, 121] The aci-nitro intermediate is observed on the µs to ms timescale,[121] with the lifetime of the aci-nitro species depending on the properties of the leaving group. The mechanisms concerning **2-NO_2Bn** are discussed in detail in Chapter 1, section 1.5.1.

Given the numerous successful examples of photoprotection using the **2-NO_2Bn** and **4,5-$(MeO)_2$-2-NO_2Bn** photoprotecting groups, this chapter investigates the potential of *N*-hydroxysulfonamides tethered to **2-NO_2Bn** and **4,5-$(MeO)_2$-2-NO_2Bn** in the absence and presence of an additional carbonate linker for photochemical HNO generation. The syntheses of **2-NO_2Bn-ON(H)-SO_2R**, **4,5-$(MeO)_2$-2-NO_2Bn-ON(H)-SO_2R** and **2-NO_2Bn-OC(O)-ON(H)-SO_2CH_3** (Figure 2.1) were carried out in our collaborators' laboratories at Kent State University, Ohio. Mechanistic studies have been carried out on the photodecomposition of these compounds using a range of experimental techniques.

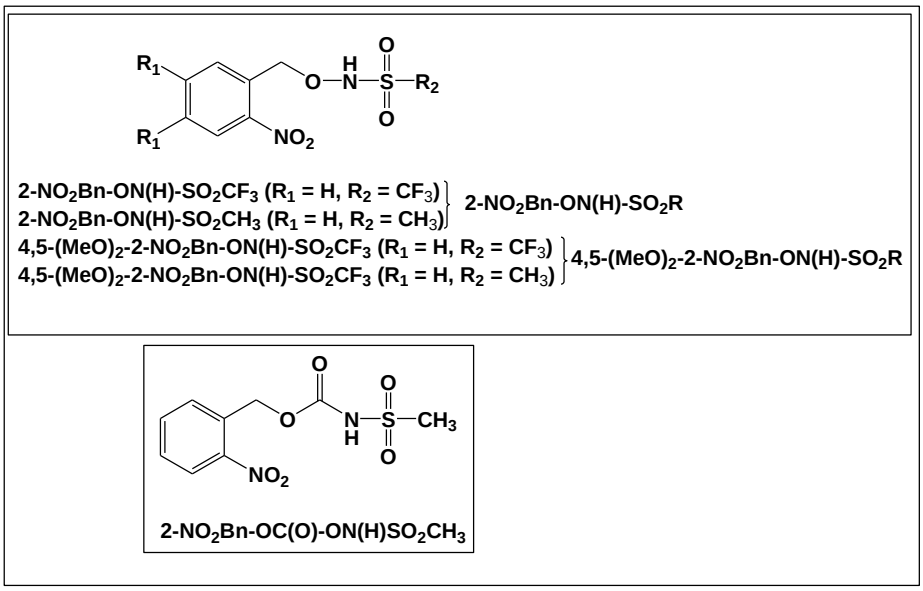

Figure 2.1. Structures of **2-NO_2Bn**, **4,5-$(MeO)_2$-2-NO_2Bn** and **2-NO_2Bn-OC(O)** photocaged *N*-hydroxysulfonamides investigated in this chapter.

2.2 Experimental section

2.2.1 Chemicals

2-NO_2Bn-ON(H)-SO_2R (R = CF_3 or CH_3) and **4,5-$(MeO)_2$-2-NO_2Bn-ON(H)-SO_2R** (R = CF_3 and CH_3), 3-(diphenylphosphino)-4-(methoxycarbonyl)benzoic acid (**Phosphine 1**), 3-(P,P-diphenylphosphorimidoyl)-4-(methoxycarbonyl)benzoic acid (**Phosphine 2**), 4-Carbamoyl-3-(diphenylphosphoryl)benzoic acid (**Phosphine 3**) and 3-(Diphenylphosphoryl)-4-(methoxycarbonyl)benzoic acid (**Phosphine 4**) were obtained from the laboratories of our collaborators, Prof. Paul Sampson and Dr Alexander Seed, at Kent State University USA. The synthesis and characterization of these compounds was presented in the PhD thesis of Dr Yang Zhou.[150] Trifluoromethanesulfonylhydroxamic acid (CF_3SO_2NHOH) was synthesized by Dr Sonya K. Adas.[53] **2-NO_2Bn-OC(O)-ON(H)-SO_2CH_3** was synthesized by Mohammad S. Rahman.[152]

2-NO_2Bn-ON(H)-SO_2CF_3 thermally decomposed during the transportation from the United States to New Zealand. Column chromatography was therefore carried out to purify **2-NO_2Bn-ON(H)-SO_2CF_3** before carrying out the photolysis experiments**.** Approximately 50% of the corresponding sulfinamide, $CF_3SO_2NH_2$, was observed in the product (δ = -80.2 ppm) which could be completely removed by column chromatography (30:70 v/v ethyl acetate-petroleum ether) with an excellent separation. ^{19}F and ^{1}H NMR spectra for the purified **2-NO_2Bn-ON(H)-SO_2CF_3** with the peak assignments are provided in Figure A2.1 (a and b), Appendix.

Sodium methanesulfinate ($Na^+CH_3SO_2^-$, 92%) and trifluoromethanesulfonic acid (CF_3SO_3H, 98%) were purchased from Sigma-Aldrich. Hydroxocobalamin hydrochloride (HOCbl.HCl, >95% purity) and *tris*(4,6-dimethyl-3-sulfonatophenyl)phosphine trisodium salt were purchased from Fluka. These chemicals were used as is without further purification. Water was purified using a Purite pure water 300 system.

2.2.2 Instrumentation

2.2.2.1 Glove box

Anaerobic solutions were prepared using a MBRAUN Labmaster 130 glovebox (1250/78, supplied with O_2 and H_2O sensors). The O_2 and H_2O levels were <0.3 ppm and <0.1 ppm, respectively.

2.2.2.2 pH measurements

pH measurements were carried using Orion Star A211 pH meter connected to Mettler-Toledo pH combination micro electrode. The micro electrode was filled with 3.0 M KCl solution and calibrated using commercially available pH 2.00, 4.00, 7.00, 10.00 and 12.00 buffers. Measurements were carried out at room temperature. The pH was adjusted using either NaOH (0.01M, 0.1 M) or HCl (0.01M, 0.1 M) solutions.

NMR spectroscopy

^{1}H, ^{13}C, ^{19}F and ^{31}P NMR spectra was recorded using a Bruker 400 MHz NMR spectrometer with a 5 mm probe at 25 ± 1 ^{o}C. The NMR data was analyzed using MestReNova version 5.3.1 software. Chemdraw 8.0 was used to draw the chemical structures of the molecules.

2.2.3 Determining the molar extinction coefficient of 2-NO_2Bn-ON(H)-SO_2R, 4,5-$(MeO)_2$-2-NO_2Bn-ON(H)-SO_2R and 2-NO_2Bn-OC(O)-ON(H)-SO_2CH_3

Standard solutions of **2-NO_2Bn-ON(H)-SO_2R**, **4,5-$(MeO)_2$-2-NO_2Bn-ON(H)-SO_2R** and **2-NO_2Bn-OC(O)-ON(H)-SO_2CH_3** (100, 150, 200, 250, 300, 350 and 400 µM) were prepared in a mixture of aerobic H_2O and CH_3CN (92:8 v/v). UV-Vis spectra were recorded at 25.0 ^{o}C. Molar extinction coefficients (slope, y = mx) were obtained from plots of absorbance versus concentration at 264 nm (**2-NO_2Bn-ON(H)-SO_2R, 2-NO_2Bn-OC(O)-ON(H)-SO_2CH_3**) or 351 nm (**4,5-$(MeO)_2$-2-NO_2Bn-ON(H)-SO_2R**). The plots are shown in Figure A2.2-A2.3, Appendix.

2.2.4 Steady state photolysis experiments

Samples were prepared in a quartz NMR tube fitted with a J-Young air-tight cap inside the glove box. Photolysis samples were irradiated using a Rayonet mini-photoreactor (RMR-600) with 300 nm bulbs (4 W, 8 lamps). The ^{1}H/ or ^{19}F NMR spectrum was recorded after each irradiation. Unless otherwise stated, all experiments were carried out under anaerobic conditions. 3-(Trimethylsilyl)propionic-2,2,3,3-*d*$_4$ acid, sodium salt (TSP) was used as an internal reference standard for ^{1}H NMR spectroscopy. α,α,α-Trifluorotoluene (Ph-CF_3) sealed in a capillary tube was used as an external reference standard for ^{19}F NMR spectroscopy.

The effect of the solvent mixtures in a CD_3CN and phosphate buffer (5.0 mM, pH 7.0) on the photoproducts and the observed rate of decomposition was determined under anaerobic conditions. The effect of the pH of the aqueous component of the solvent

(10% v/v CD_3CN in aqueous buffer (5.0 mM)), on the photoproducts and rate of decomposition was also determined. The aqueous component of the solution was phosphate, acetate or carbonate buffer in H_2O. The reported pH value is the pH of the aqueous component. After each irradiation, the sample was analyzed by ^{1}H and/or ^{19}F NMR spectroscopy.

2.2.5 Determination of Photoproduct quantum yield (Φ)

2.2.5.1 Synthesis of Ferrioxalate

The synthesis of potassium ferrioxalate was carried out using an established protocol.[153] The first step involved the synthesis of potassium oxalate ($K_2C_2O_4.H_2O$). Potassium oxalate (equation (2.1)) was formed by the addition of potassium hydroxide to oxalic acid. Ferric chloride hexahydrate ($FeCl_3.6H_2O$) was then added to form potassium ferrioxalate, $K_3[Fe(C_2O_4)_3]$ (equation (2.2)). Ferrioxalate ($K_2C_2O_4$) was prepared by mixing $H_2C_2O_4$ (1.17 g, 13 mmol) with KOH (1.35 g, 24 mmol).

$$H_2C_2O_4 + 2KOH \longrightarrow K_2C_2O_4 + H_2O \quad (2.1)$$

$$3K_2C_2O_4.H_2O + FeCl_3.6H_2O \longrightarrow K_3[Fe(C_2O_4)_3.3H_2O + 3KCl + 6H_2O \quad (2.2)$$

Distilled H_2O (7 mL) was then added and the mixture sonicated to ensure everything was dissolved. $FeCl_3.6H_2O$ (1.08 g, 4.0 mmol) was added to the mixture and the solution was filtered using a fritted sinter funnel. The flask containing the filtrate was wrapped with aluminum foil and placed in an ice bath for 30 min. The green crystals which formed were collected using a sinter filter and the weight was recorded. The yield of the potassium ferrioxalate was 56% (1.10 g). The product was characterized by recording the UV-vis spectrum in H_2O (Figure A2.4, Appendix section). A shoulder was observed at 265 nm which is in agreement with the literature (265 nm).[154]

2.2.5.2 Determining the molar extinction coefficient of *tris*(phenanthroline)iron (II), $[Fe(phen)_3]^{2+}$

A stock solution of $FeSO_4$ (0.4 mM) was prepared and aliquots (0, 0.25, 0.55, 0.75, 1 and 1.25 mL) were added to a series of 10 mL volumetric flasks containing a mixture of dilute H_2SO_4 (1 N, 0.25 mL) and NaOAc (0.1 M, 2.5 mL). The resulting solutions were diluted to 10.00 mL using H_2O. The concentrations varied from 0 to 10 µM. 1,10–Phenanthroline (5.50 mM, 1.00 mL) was added to each volumetric flask and the

solutions left for 30 min to allow complete formation of $[Fe(phen)_3]^{2+}$. The absorbances of the standard solutions (0, 10, 20, 30, 40 and 50 µM) were recorded at 510 nm in order to determine the molar extinction coefficient of $[Fe(phen)_3]^{2+}$. The plot of absorbance versus concentration at 510 nm was linear when the data was fitted to the equation y = mx. The molar extinction coefficient value was (1.03 ± 0.02) × 10^4 M^{-1} cm^{-1}; (Figure A2.5, see Appendix) similar to a previous reported value of 1.1 × 10^4 M^{-1} cm^{-1}.[154]

2.2.6 Laser Flash Photolysis experiments

Transient spectra were recorded using a LKS80 Applied Photophysics spectrophotometer operating with a Nd:YAG laser (Quantel Q-smart 450, ~60 mJ per pulse). The Nd:YAG laser was connected to 2nd and 4th harmonic generators (pulse width ~5 ns). To avoid photodegradation of the samples by the xenon lamp used for absorbance measurements, a second monochromator was connected between Xe lamp and the sample compartment. The slit widths of the monochromators were 1.0 and 2.5 mm for the first and second monochromator respectively.

Before starting the experiment, the power of the pulse was carried out using a pyroelectric joulemeter (Gentec, QE25LP-S-MB-QED) with a Maestro energy monitor. The energy of the laser at 266 nm was 60-70 mJ. When required, the power of the laser was decreased by increasing the laser sync delay (LSD).

In order to obtain transient absorption spectra, sample solutions were flowed through the sample cuvette from a round bottom flask (100 mL) containing 50 mL solution. A peristatic pump was used. The solution was circulated using a peristatic pump (0.8 mL/min) with stirring using Tygon MH pump tubing (152 mm). The inlet was placed in the corner at the bottom of the quartz cuvette and the outlet at the top to ensure fresh sample solutions were measured. 2-Napthol was used as a control sample to check that the instrument performance was acceptable. Data were collected with and without circulation of the solution using the peristatic pump at specific wavelengths and are shown in Figure A2.6, Appendix). The transient absorption spectra obtained is in good agreement with the literature.[75]

2.2.7 Synthesis of nitrosylcobalamin (NOCbl)

A previously reported procedure was used to synthesize **NOCbl**.[155] Angeli's salt (AS) (1.3 mol equivalent) in NaOH (10 mM, 0.1 mL) was added rapidly into an anaerobic

solution of HOCbl.HCl (50.3 mg) dissolved in TES buffer (0.1 M, 1.0 mL, pH 7.4). The resulting product was shaken frequently for 180 min at room temperature. Chilled acetone (20 mL, -20°C) was added dropwise to precipitate the product and the product filtered under vacuum. The entire synthesis was carried out three times with a yield of 75, 82 and 79%, respectively, under a nitrogen atmosphere in the glove box. The crystalized product **NOCbl** obtained was characterized using ^{1}H NMR spectroscopy (Figure A2.7, Appendix).

^{1}H NMR spectrum of **NOCbl** was recorded in TES buffer (0.010 M, pD 7.4) in D_2O: The aromatic chemical shifts were 7.42 (s), 7.21 (s) ,6.82 (s), 6.35 (s) and 6.26 (d) ppm. These ^{1}H NMR chemical shifts are in good agreement with literature values.[155] **NOCbl** is extremely air sensitive: in presence of air **NOCbl** is converted rapidly to H_2OCbl^+ and NO_2Cbl.[155]

2.2.8 Synthesis of Angeli's salt (AS)

The synthesis of AS was carried out using a previously published procedure.[49, 156] The synthesized AS was found to be 99% pure (molar extinction coefficient at 248 nm = 8.30 x 10^{-3} M^{-1} cm^{-1}) by UV-Vis spectroscopy.

2.3 Results

2.3.1 UV-Vis spectra of 2-NO_2Bn-ON(H)SO_2R, 4,5-$(MeO)_2$-2-NO_2Bn-ON(H)SO_2R and 2-NO_2Bn-OC(O)-ON(H)-SO_2CH_3

UV-Vis spectra of **2-NO_2Bn-ON(H)-SO_2R** (R = CF_3 and CH_3), **4,5-$(MeO)_2$-2-NO_2Bn-ON(H)-SO_2R** (R = CF_3 and CH_3) and **2-NO_2Bn-OC(O)-ON(H)-SO_2CH_3** are shown in Figure 2.2. The wavelength maximum of **2-NO_2Bn-ON(H)-SO_2R** and **2-NO_2Bn-OC(O)-ON(H)-SO_2CH_3** at 264 nm and **4,5-$(MeO)_2$-2-NO_2Bn-ON(H)-SO_2R** at 351 nm were assigned to a n-π^* transition.[157] UV-Vis spectra of **4,5-$(MeO)_2$-2-NO_2Bn-ON(H)-SO_2R** are shifted to lower energies compared to **2-NO_2Bn-ON(H)-SO_2R** and **2-NO_2Bn-OC(O)-ON(H)-SO_2CH_3** due to the presence of the electron donating methoxy substituents on the phenyl ring. The molar extinction coefficients of these molecules are summarized in Table 2.1. The experimental details are given in section 2.2.3 of the Experimental section, and the plots of absorbance versus concentration are given in the Appendix, Figures A2.2 and A2.3.

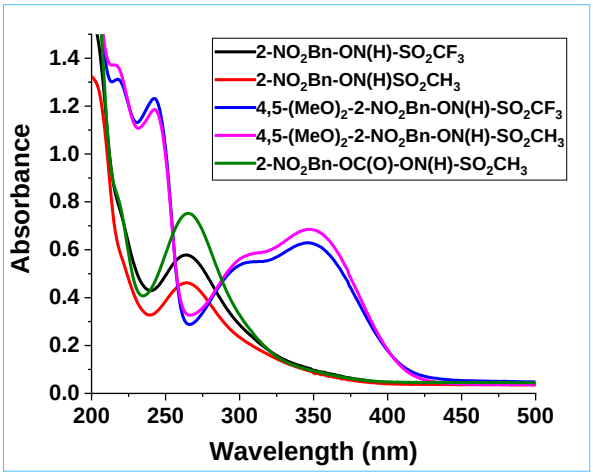

Figure 2.2. UV-Vis spectra of **2-NO_2Bn-ON(H)-SO_2R, 4,5-$(MeO)_2$-2-NO_2Bn-ON(H)-SO_2R** and **2-NO_2Bn-OC(O)-ON(H)-SO_2CH_3** (1.50×10^{-4} M) in a mixture of H_2O and CH_3CN (92:8, v/v) at 25 °C. R = CF_3 and CH_3.

Table 2.1. Molar extinction coefficients of **2-NO_2Bn-ON(H)-SO_2R, 4,5-$(MeO)_2$-2-NO_2Bn-ON(H)-SO_2R** and **2-NO_2Bn-OC(O)-ON(H)-SO_2CH_3** in a mixture of H_2O and CH_3CN (92:8, v/v; 25.0 °C).

Compound	Molar extinction coefficient (M^{-1} cm^{-1})
2-NO_2Bn-ON(H)-SO_2CF_3	$(3.68 \pm 0.02) \times 10^3$ (264 nm)
2-NO_2Bn-ON(H)-SO_2CH_3	$(2.95 \pm 0.02) \times 10^3$ (264 nm)
4,5-$(MeO)_2$-2-NO_2Bn-ON(H)-SO_2CF_3	$(3.99 \pm 0.02) \times 10^3$ (351 nm)
4,5-$(MeO)_2$-2-NO_2Bn-ON(H)-SO_2CH_3	$(4.44 \pm 0.04) \times 10^3$ (351 nm)
2-NO_2Bn-OC(O)-ON(H)-SO_2CH_3	$(4.86 \pm 0.03) \times 10^3$ (264 nm)

2.3.2 Thermal stability of 2-NO_2Bn-ON(H)-SO_2R, 4,5-$(MeO)_2$-2-NO_2Bn-ON(H)-SO_2R and 2-NO_2Bn-OC(O)-ON(H)-SO_2CH_3

The thermal stability of **2-NO_2Bn-ON(H)-SO_2R, 4,5-$(MeO)_2$-2-NO_2Bn-ON(H)SO_2R** and **2-NO_2Bn-OC(O)-ON(H)-SO_2CH_3** was checked by recording the $^{19}F/^{1}H$ NMR spectra immediately after preparing the sample and 12 h later. Figure 2.3 shows ^{19}F NMR spectra of **2-NO_2Bn-ON(H)SO_2CF_3** in a mixture of phosphate buffer (5.0 mM, pH 7.0) and CD_3CN (40:60, v/v) after 10 min and 12 h later after storage in the dark. No detectable decomposition was observed after 12 h.

2-NO_2Bn-ON(H)-SO_2R, **4,5-$(MeO)_2$-2-NO_2Bn-ON(H)SO_2R** and **2-NO_2Bn-OC(O)-ON(H)-SO_2CH_3** were also found to be thermally stable for 12 h in dark in the same solvent mixture (spectra not shown).

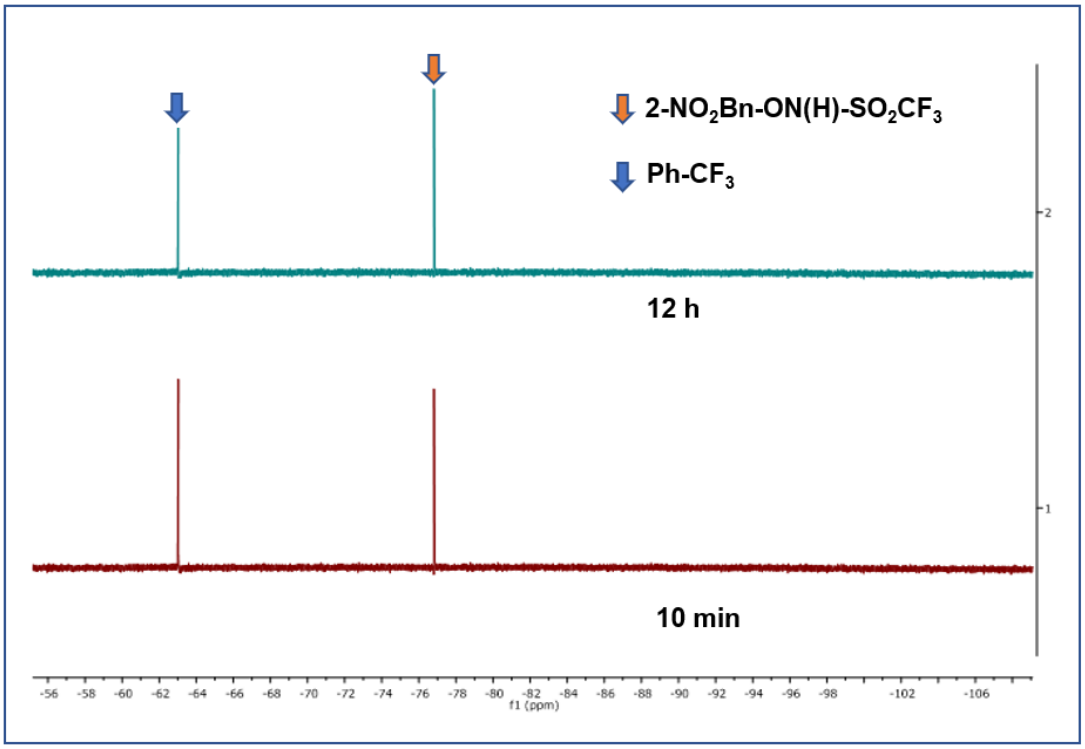

Figure 2.3. ^{19}F NMR spectra of **2-NO_2Bn-ON(H)-SO_2CF_3** (3.89 mM) in a mixture of phosphate buffer (5.0 mM, pH 7.0) and CD_3CN (40:60, v/v) after 10 min and 12 h. The sample was kept in the dark.

2.3.3 Photolysis studies of 2-NO_2Bn-ON(H)-SO_2CF_3, 2-NO_2Bn-ON(H)-SO_2CH_3, 4,5-$(MeO)_2$-2-NO_2Bn-ON(H)-SO_2CF_3 and 4,5-$(MeO)_2$-2-NO_2Bn-ON(H)-SO_2CH_3

2-NO_2Bn-ON(H)-SO_2CF_3 (3.89 mM) was photolyzed in an anaerobic mixture of phosphate buffer (5.0 mM, pH 7.0) and CD_3CN (40:60, v/v) using a sealed quartz NMR tube fitted with a J-Young air-tight cap. α,α,α-Trifluorotoluene (Ph-CF_3, -62.9 ppm) was used as an external reference. Anaerobic conditions were used to prevent any side reactions with O_2 occurring. The sample was irradiated using a Rayonet photoreactor (RMR-600, 300 nm). The steady state photolysis was monitored using ^{19}F NMR spectroscopy. Figure 2.4(a) shows ^{19}F NMR spectra of **2-NO_2Bn-ON(H)-SO_2CF_3** as a function of total irradiation time. The area of the CF_3 peak of the reactant decreases upon irradiation, decomposing to give $CF_3SO_2NH_2$ (-80.2 ppm, 91%) and $CF_3SO_2^-$ (-88.2 ppm, 9%). $CF_3SO_2^-$ is generated as a result of concerted C-O/N-S bond cleavage, whereas O-N bond cleavage results in $CF_3SO_2NH_2$ being produced (see later). The ^{19}F NMR spectra of authentic samples of $CF_3SO_2NH_2$ and $CF_3SO_2^-$ in the same solvent were recorded to confirm these chemical shift assignments. There was no evidence of CF_3SO_2NHOH (-74.1 ppm) in the product mixture. Separate control experiments showed that both $CF_3SO_2NH_2$ and $CF_3SO_2^-$ are photostable in the same solvent

mixture (2 h irradiation). The CF_3 peak of **2-NO_2Bn-ON(H)-SO_2CF_3** and the Ph-CF_3 peak were integrated and the ratios of the peak areas plotted as a function of irradiation time. The data was fitted to a first-order equation (Figure 2.4(b)) giving an observed first-order rate constant, k_{obs} = 0.30 ± 0.03 min^{-1} ($t_{1/2}$ ~2.3 min). The initial slope for decomposition under steady irradiation conditions indirectly reflects the quantum efficiency for the system in the wavelength region for excitation of the compound.

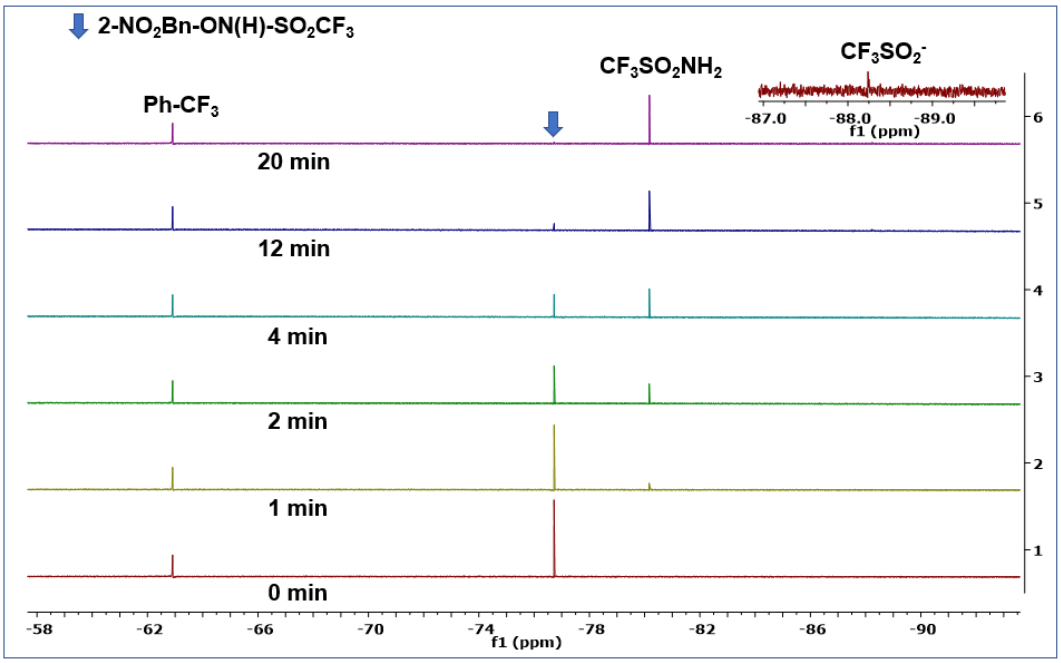

(a)

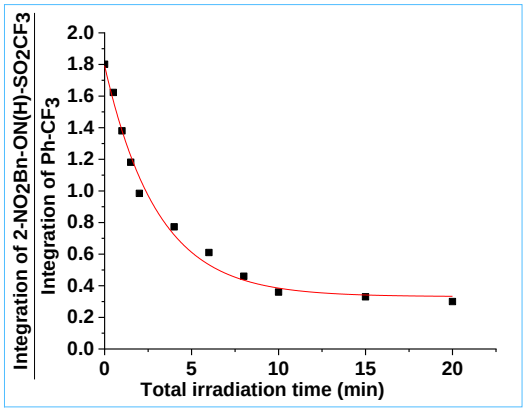

(b)

Figure 2.4. (a) ^{19}F NMR spectra as a function of the total irradiation time for the photolysis of **2-NO_2Bn-ON(H)-SO_2CF_3** (3.89 mM) in a mixture of phosphate buffer (5.0 mM, pH 7.0) and CD_3CN (40:60, v/v). (b) The ratio of the CF_3 signal of **2-NO_2Bn-ON(H)-SO_2CF_3** and the **Ph-CF_3** reference versus total irradiation time. The best fit of the data to a first-order rate equation gives k_{obs} = 0.30 ± 0.03 min^{-1}.

4,5-$(MeO)_2$-2-NO_2Bn-ON(H)-SO_2CF_3 (3.89 mM) was photolyzed under same conditions as **2-NO_2Bn-ON(H)-SO_2CF_3**. The ^{19}F NMR spectra as a function of total

irradiation time are shown in Figure 2.5(a). The percentages of $CF_3SO_2NH_2$ (-80.2 ppm) and $CF_3SO_2^-$ (-88.2 ppm) were 93% and 7%, respectively. The ratio of the area of the CF_3 peak of **4,5-(MeO)$_2$-2-NO$_2$Bn-ON(H)-SO$_2$CF$_3$** and **Ph-CF$_3$** was plotted as a function of total irradiation time (Figure 2.5(a)) and fitted to a first-order equation (Figure 2.5(b)), giving k_{obs} = 0.15 ± 0.02 min^{-1} ($t_{1/2}$ ~4.6 min).

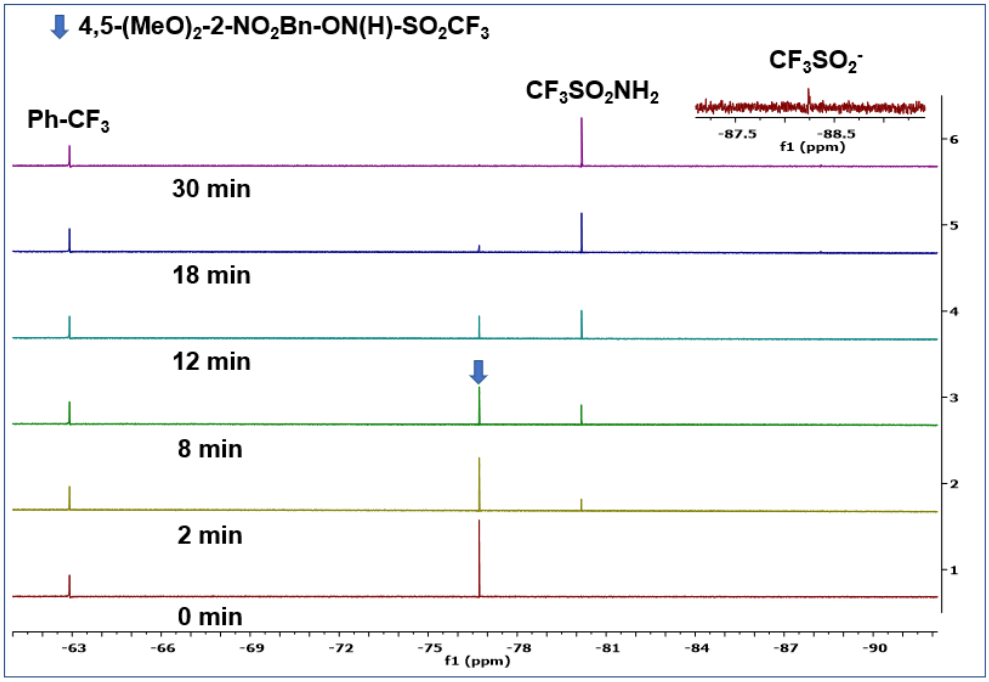

(a)

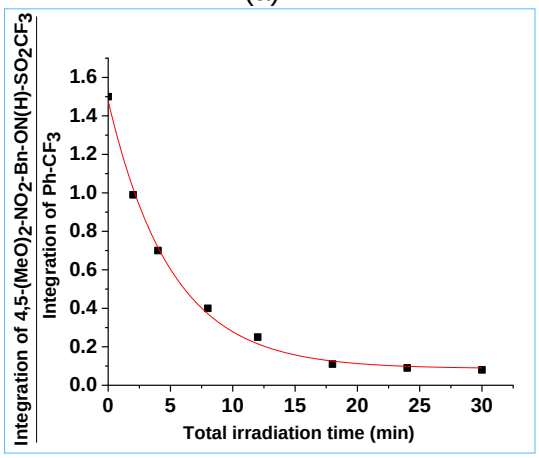

(b)

Figure 2.5. (a) ^{19}F NMR spectra as a function of total irradiation time for the photolysis of **4,5-(MeO)$_2$-2-NO$_2$Bn-ON(H)-SO$_2$CF$_3$** (3.89 mM) in a mixture of phosphate buffer (5.0 mM, pH 7.0) and CD_3CN (40:60, v/v). (b) Ratio of the CF_3 signal of **4,5-(MeO)$_2$-2-NO$_2$Bn-ON(H)-SO$_2$CF$_3$** and **Ph-CF$_3$** reference versus total irradiation time. The best fit of the data to a first-order rate equation gives k_{obs} = 0.15 ± 0.02 min^{-1}.

2-NO$_2$Bn-ON(H)-SO$_2$CH$_3$ and 4,5-(MeO)$_2$-2-NO$_2$Bn-ON(H)-SO$_2$CH$_3$ (3.89 mM) were photolyzed in a mixture of phosphate buffer (5.0 mM, pH 7.0) and CD_3CN (40:60, v/v) under anaerobic conditions. The photodecomposition was monitored using ^{1}H NMR spectroscopy. 3-(Trimethylsilyl)propionic-2,2,3,3-*d*$_4$ acid, sodium salt (TSP, 0.00 ppm)

was used as an internal reference. The solutions were irradiated using a Rayonet photoreactor (300 nm). ^{1}H NMR spectra of **2-NO_2Bn-ON(H)-SO_2CH_3** as a function of total irradiation time are shown in Figure 2.6(a). The peak area of the CH_3 signal was essentially unchanged after irradiation, whereas the peak area of the methylene protons and the aromatic protons decreased as a function of total irradiation time. The methyl peak of the $CH_3SO_2NH_2$ product at 3.03 ppm overlapped with the CH_3 peak of the **2-NO_2Bn-ON(H)-SO_2CH_3** reactant. Therefore, this peak was not useful to monitor the photodecomposition. The ^{1}H NMR spectrum of an authentic sample of $CH_3SO_2NH_2$ was recorded in the same solvent mixture to confirm this. The CH_2 peak at 5.28 ppm and TSP peak were integrated and the ratio of the peaks was plotted as a function of total irradiation time (Figure 2.6(b), giving k_{obs} = 0.21 ± 0.03 min^{-1}.

There was no evidence for $CH_3SO_2^-$ (2.20 ppm in this solvent mixture). However, a small amount of an unknown species (3.38 ppm) was observed which is most likely a secondary photoproduct. Control experiments showed that the unknown peak was not from methanesulfonate ($CH_3SO_3^-$, 2.68 ppm), CH_3OH (3.27 ppm) or CH_3SO_2NHOH (3.07 ppm; the photolysed sample was spiked with these species).

Finally, the photolysis experiments were also conducted in the absence of TSP to check if there was any effect on the photodecomposition. The percentage of the photoproducts (100% $CH_3SO_2NH_2$) were found to be unaffected.

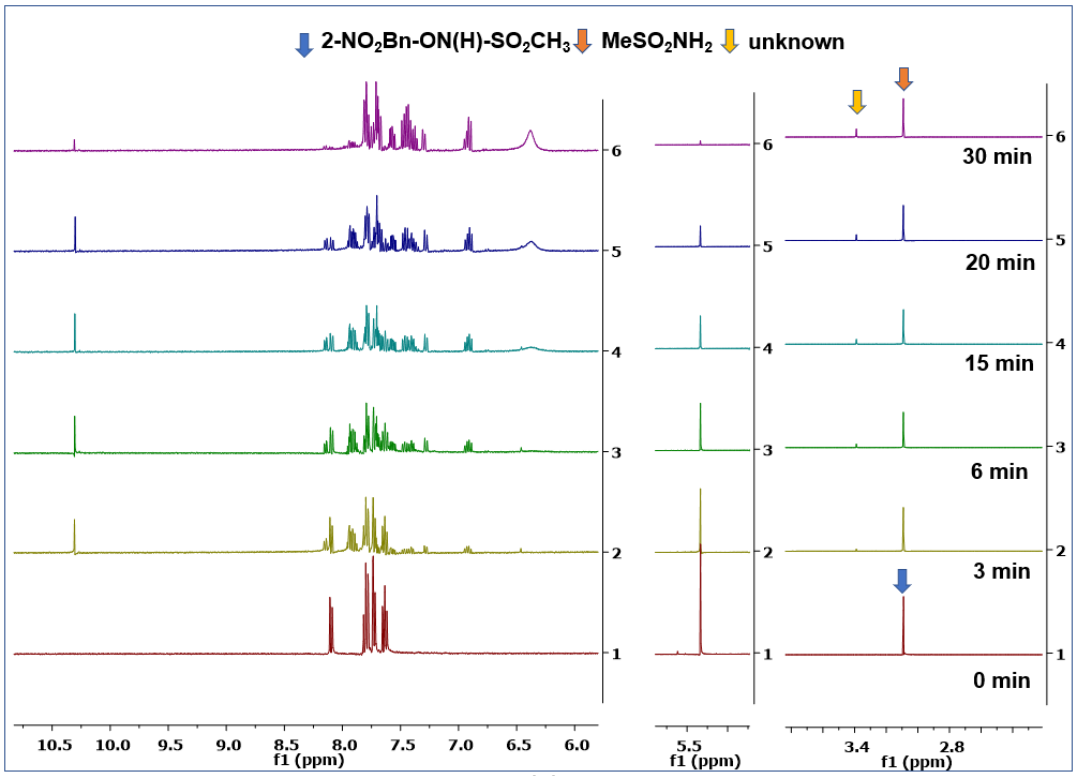

(a)

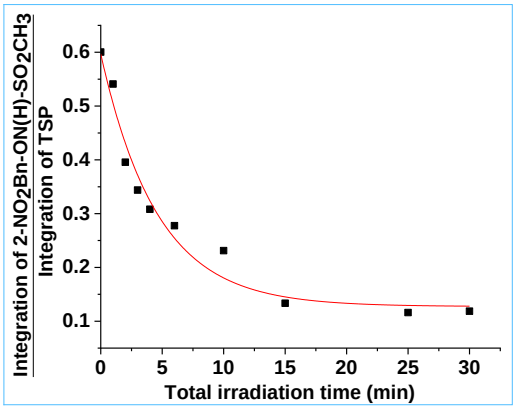

(b)

Figure 2.6. (a) ^{1}H NMR spectra as a function of total irradiation time for the photolysis of **2-NO_2Bn-ON(H)-SO_2CH_3** (3.89 mM) in a mixture of phosphate buffer (pH 7.0, 5.0 mM) and CD_3CN (40:60, v/v). (b) Plot of the ratio of the CH_2 peak at 5.28 ppm of **2-NO_2Bn-ON(H)-SO_2CH_3** and TSP versus total irradiation time. The best fit of the data to a first-order rate equation gives k_{obs} = 0.21 ± 0.03 min^{-1}.

^{1}H NMR spectra for **4,5-$(MeO)_2$-2-NO_2Bn-ON(H)-SO_2CH_3** as a function of total irradiation time are given in Figure 2.7(a). The peak at 3.03 ppm was assigned to $CH_3SO_2NH_2$ and no other products were observed. The ratio of the area of the methyl peak of **4,5-$(MeO)_2$-2-NO_2Bn-ON(H)-SO_2CH_3** at 3.10 ppm versus the peak area of TSP was plotted as a function of irradiation time. These data points were fitted to a first-order equation (Figure 2.7(b)), giving k_{obs} = 0.04 ± 0.01 min^{-1}. The photodecomposition results of **2-NO_2Bn-ON(H)-SO_2R** (R = CF_3 and CH_3) and **4,5-**

(MeO)$_2$-2-NO$_2$Bn-ON(H)SO$_2$R (R = CF_3 and CH_3) are in very good agreement with the Yang Zhou thesis.[150]

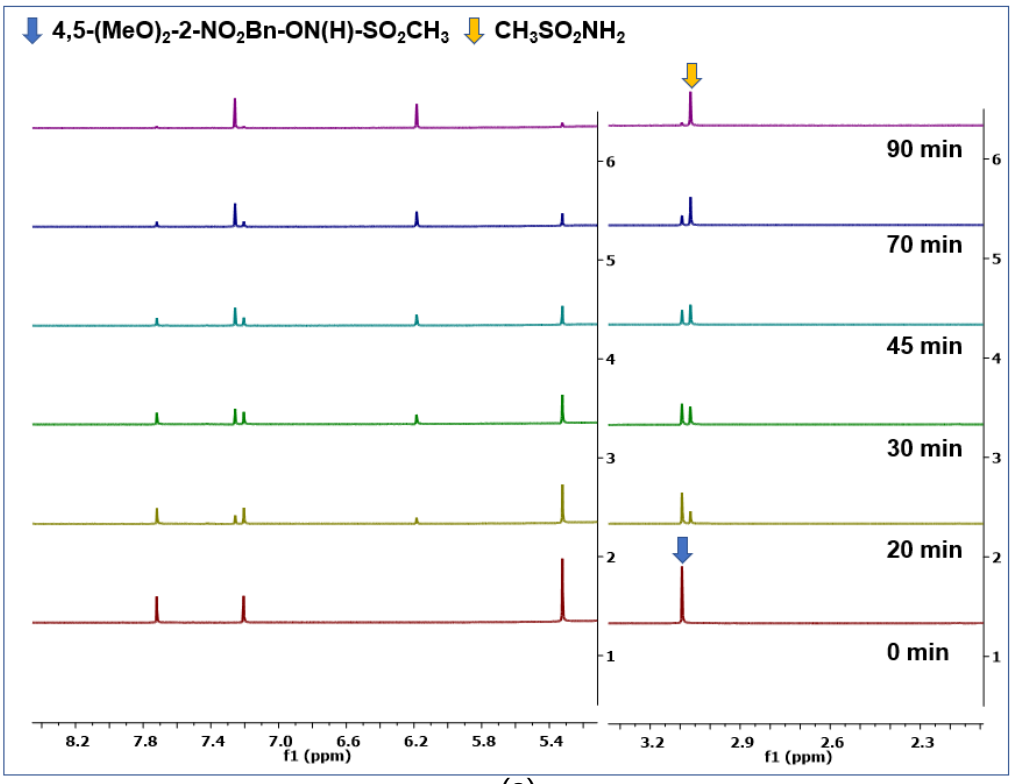

(a)

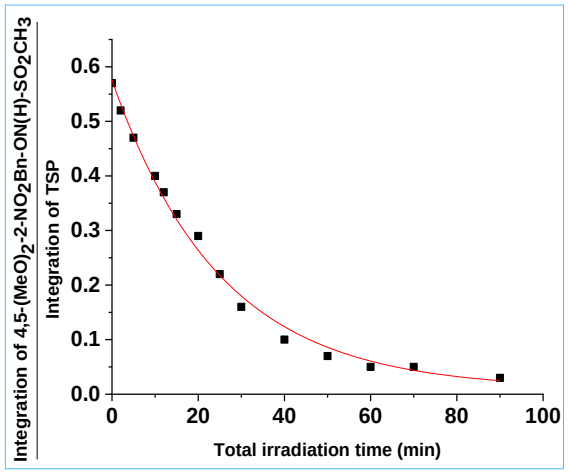

(b)

Figure 2.7. (a) ^{1}H NMR spectra as a function of total irradiation time for the photolysis of **4,5-(MeO)$_2$-2-NO$_2$Bn-ON(H)-SO$_2$CH$_3$** (3.89 mM) in a mixture of phosphate buffer (5.0 mM, pH 7.0) and CD_3CN (40:60, v/v). (b) Ratio of the CH_3 signal at 3.10 ppm of **4,5-(MeO)$_2$-2-NO$_2$Bn-ON(H)-SO$_2$CH$_3$** and the TSP reference versus total irradiation time. The best fit of the data to a first-order rate equation gives k_{obs} = 0.04 ± 0.01 min^{-1}.

2.3.4 Characterization of the aromatic photoproducts

Previous research by other students in our group for *N*-hydroxysulfonamides caged with the (3-hydroxy-2-napthalen-2-yl)methyl and (6-hydroxy-2-napthalen-2-yl)methyl photoprotecting groups showed that three major photodecomposition pathways can occur, involving concerted C-O/N-S bond cleavage, C-O bond cleavage or O-N bond cleavage.[78] These three decomposition pathways may also occur for 2-nitrobenzyl protected *N*-hydroxysulfonamides, Scheme 2.1. In Pathway 1 concerted C-O/N-S bond cleavage occurs to generate HNO, a sulfinate (RSO_2^-) and 2-nitrosobenzaldehyde (R_1 = H, R_2 = CF_3 or CH_3) or 4,5-dimethoxy-2-nitrosobenzaldehyde (R_1 = OMe, R_2 = CF_3 or CH_3). In Pathway 2 C-O bond cleavage would be expected to generate the parent alkanesulfohydroxamic acid $CF_3SO_2NHO(H)$ or $CH_3SO_2NHO(H)$ and 2-nitrobenzaldehyde or 4,5-dimethoxy-2-nitrosobenzaldehyde. In Pathway 3 O-N bond cleavage generates the corresponding sulfonamide (RSO_2NH_2), 2-nitrobenzaldehyde or 4,5-dimethoxy-2-nitrobenzaldehyde. For **2-NO_2Bn-ON(H)-SO_2CF_3** 91% $CF_3SO_2NH_2$ and 9% $CF_3SO_2^-$ were observed in the photoproduct solution using ^{19}F NMR spectroscopy. A similar result was observed for **4,5-$(MeO)_2$-2-NO_2Bn-ON(H)-SO_2CF_3** (93% $CF_3SO_2NH_2$ and 7% $CF_3SO_2^-$). There was no evidence for $CF_3SO_2NHO(H)$ being an intermediate in the reaction by ^{19}F NMR spectroscopy. Note that this species decomposes with a half-life of ~10 min in 60/40 v/v CD_3CN/phosphate buffer (5.0 mM, pH 7.0),[76] so if it was an intermediate it would have been observed by NMR spectroscopy. Hence C-O bond cleavage (Pathway 2, Scheme 2.1) does not occur.

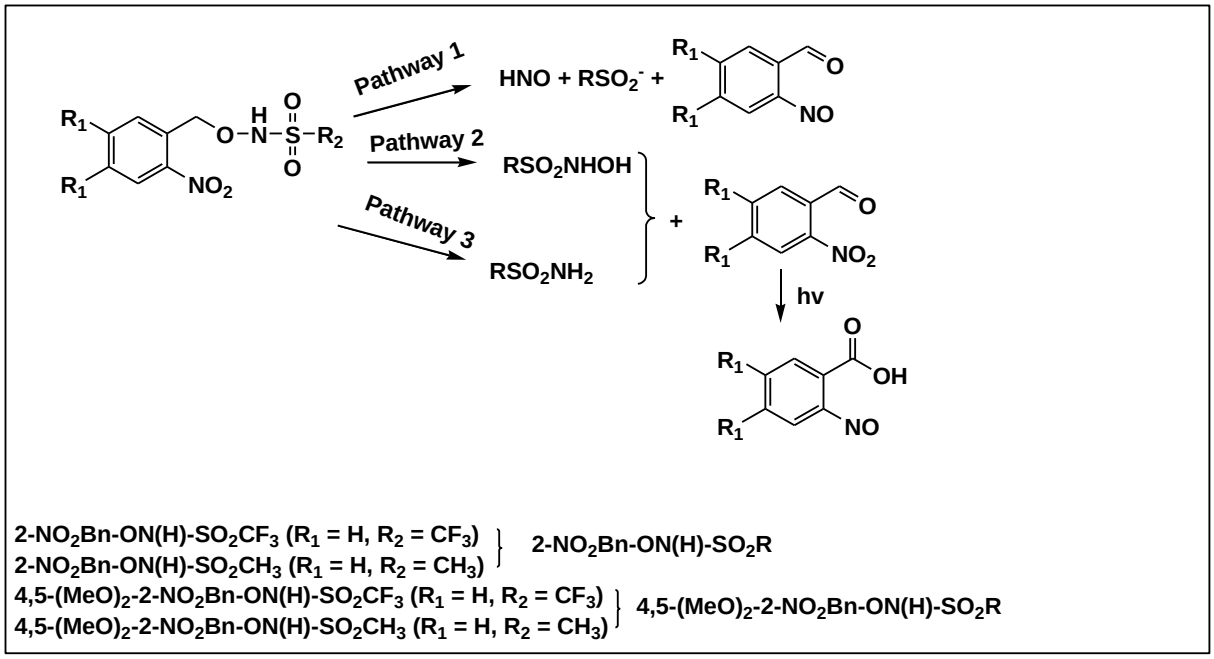

Scheme 2.1. Possible mechanisms of photodecomposition of **2-NO_2Bn-ON(H)-SO_2CF_3**, **2-NO_2Bn-ON(H)-SO_2CH_3**, **4,5-$(MeO)_2$-2-NO_2Bn-ON(H)-SO_2CF_3** and **4,5-$(MeO)_2$-2-NO_2Bn-ON(H)-SO_2CH_3**.

Upon O-N bond cleavage 2-nitrobenzaldehyde or 2-nitro-4,5-dimethoxynitrobenzaldehyde would be expected to be generated, Pathway 3, Scheme 2.1. Photolysis of **2-NO_2Bn-ON(H)-SO_2CH_3** resulted in only O-N bond cleavage (section 2.3.3). Figure 2.8 shows a comparison of the ^{1}H NMR spectra of a partially photolyzed sample of **2-NO_2Bn-ON(H)-SO_2CH_3** (3 min irradiation) with an authentic sample of **2-NO_2Bn-CHO** in a mixture of phosphate buffer (5.0 mM, pH 7.0) and CD_3CN (40:60, v/v). The peaks at 10.28, 8.14, 8.12, 7.84, 7.82 ppm were assigned to **2-NO_2Bn-CHO**. Numerous secondary photoproduct peaks were also observed at 7.50-7.53, 7.33-7.43, 7.22, 7.23, 7.67, 7.42 and 6.82-6.89 ppm. **2-NO_2Bn-CHO** was irradiated for 3.0 min (shown in the same Figure) to see if some of these peaks arise from the photodecomposition of this species. Some of the NMR peaks in the photoproduct mixture can be assigned to **2-NO_2Bn-CHO**.

Others have shown that **2-NO_2Bn-CHO** is photosensitive, decomposing to give 2-nitrosobenzoic acid.[99, 100] The 2-nitrosobenzoic acid product generated from the photolysis of **2-NO_2Bn-ON(H)-SO_2CH_3** was confirmed by high-resolution mass spectrometry (HRMS), appearing as [M+H$^+$] = 152.0341 (calculated m/z = 152.0342) (PhD thesis of our collaborator, Yang Zhou).[150]

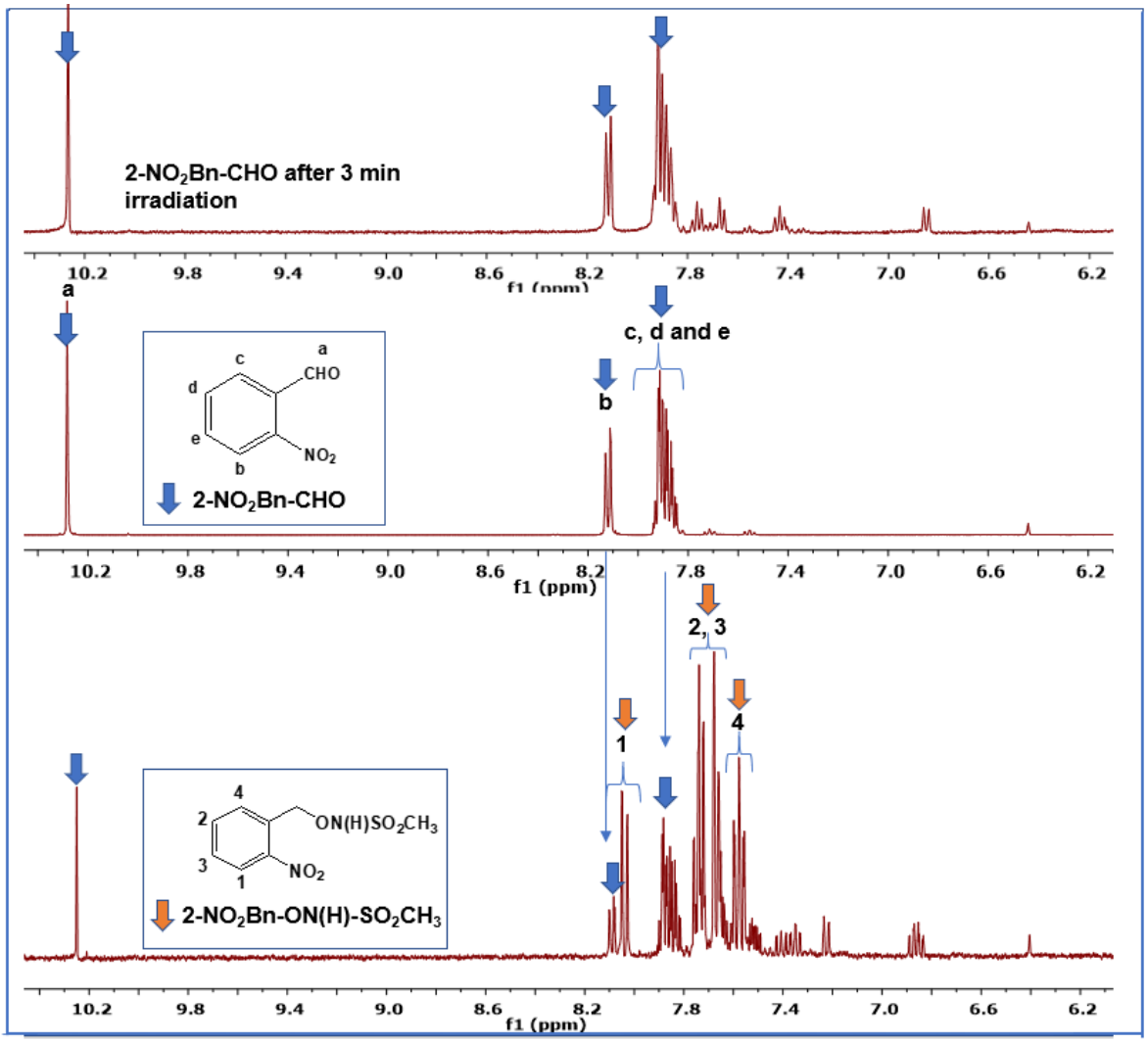

Figure 2.8. Comparison of ^{1}H NMR spectra of an irradiated sample (3.0 min) of **2-NO$_2$Bn-ON(H)-SO$_2$CH$_3$** with an authentic sample of **2-NO$_2$Bn-CHO** and an irradiated sample (3.0 min) of **2-NO$_2$Bn-CHO** in a mixture of phosphate buffer (5.0 mM, pH 7.0) and CD$_3$CN (40:60, v/v).

Upon photolysis of **2-NO$_2$Bn-ON(H)-SO$_2$CF$_3$**, both O-N and C-O/N-S bond cleavage occurs (section 2.3.3). Evidence for **2-NO$_2$Bn-CHO** in a partially photolyzed sample of **2-NO$_2$Bn-ON(H)-SO$_2$CF$_3$** (3.0 min) in a mixture of phosphate buffer (5.0 mM, pH 7.0) and CD$_3$CN (40:60, v/v) for this system is shown later, in Figure 2.28 (section 2.3.15). Figure 2.9 shows the ^{1}H NMR spectra of a partially photolyzed sample of **2-NO$_2$Bn-ON(H)-SO$_2$CF$_3$** (0.5 min irradiation) in a mixture of phosphate buffer (5 mM, pH 7.0) and CD$_3$CN (40:60, v/v). A singlet peak was observed at 10.21 ppm which would be expected for the 2-nitrosobenzaldehyde product arising from concerted C-O/N-S bond cleavage, Pathway 1, Scheme 2.1. Subsequent experiments with **2-NO$_2$Bn-OC(O)-ON(H)-SO$_2$CH$_3$** showed that 2-nitrosobenzaldehyde is indeed generated (see section 2.3.5).

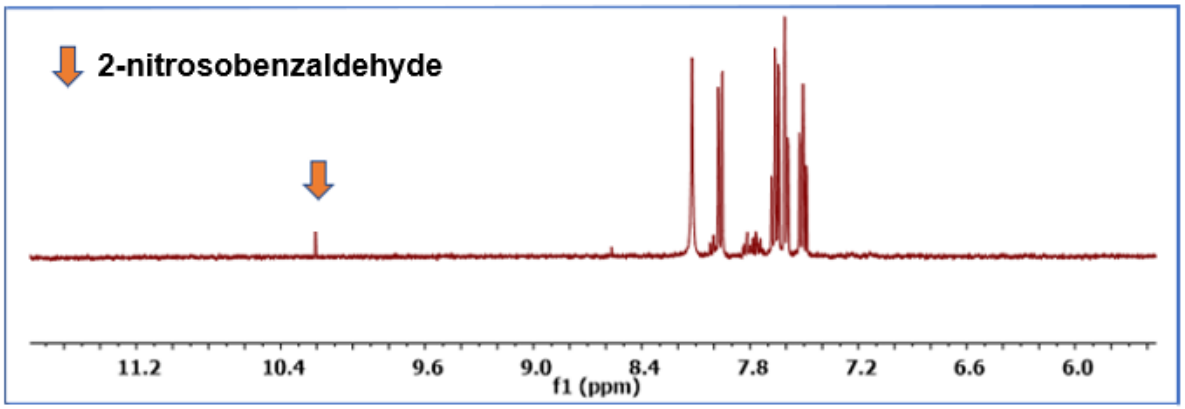

Figure 2.9. ^{1}H NMR spectra of a partially photolyzed sample of **o-NO_2Bn-ON(H)SO_2CF_3** (0.5 min irradiation) in a mixture of phosphate buffer (5.0 mM, pH 7.0) and CD_3CN (40:60, v/v).

Figure 2.10 shows the ^{1}H NMR spectra of a partially photolyzed **4,5-$(MeO)_2$-2-NO_2Bn-ON(H)-SO_2CF_3** (2.0 min irradiation) with an authentic sample of **4,5-$(MeO)_2$-2-NO_2Bn-CHO**. The photolyzed sample contained five peaks at 10.22, 7.67 7.37, 7.21 and 6.18 ppm. The peaks at 10.22, 7.67 and 7.37 ppm were assigned to **4,5-$(MeO)_2$-2-NO_2Bn-CHO.** Since **4,5-$(MeO)_2$-2-NO_2Bn-CHO** was photosensitive, **4,5-$(MeO)_2$-2-NO_2Bn-CHO** was photolyzed for 1.0 min to determine whether the remaining two unknown peaks at 7.21 and 6.18 ppm result from decomposition of this compound (Figure 2.10). These two peaks were assigned to 4,5-dimethoxy-2-nitrosobenzoic acid. The CH_3O peaks for the photoproducts could not be seen as these overlap with the HDO peak from the solvent.[150] The formation of 4,5-dimethoxy-2-nitrosobenzoic acid was also confirmed by HRMS, appearing as $[M+H^+]$ = 212.0551 (calculated m/z = 212.0553) in Yang Zhou's thesis.[150]

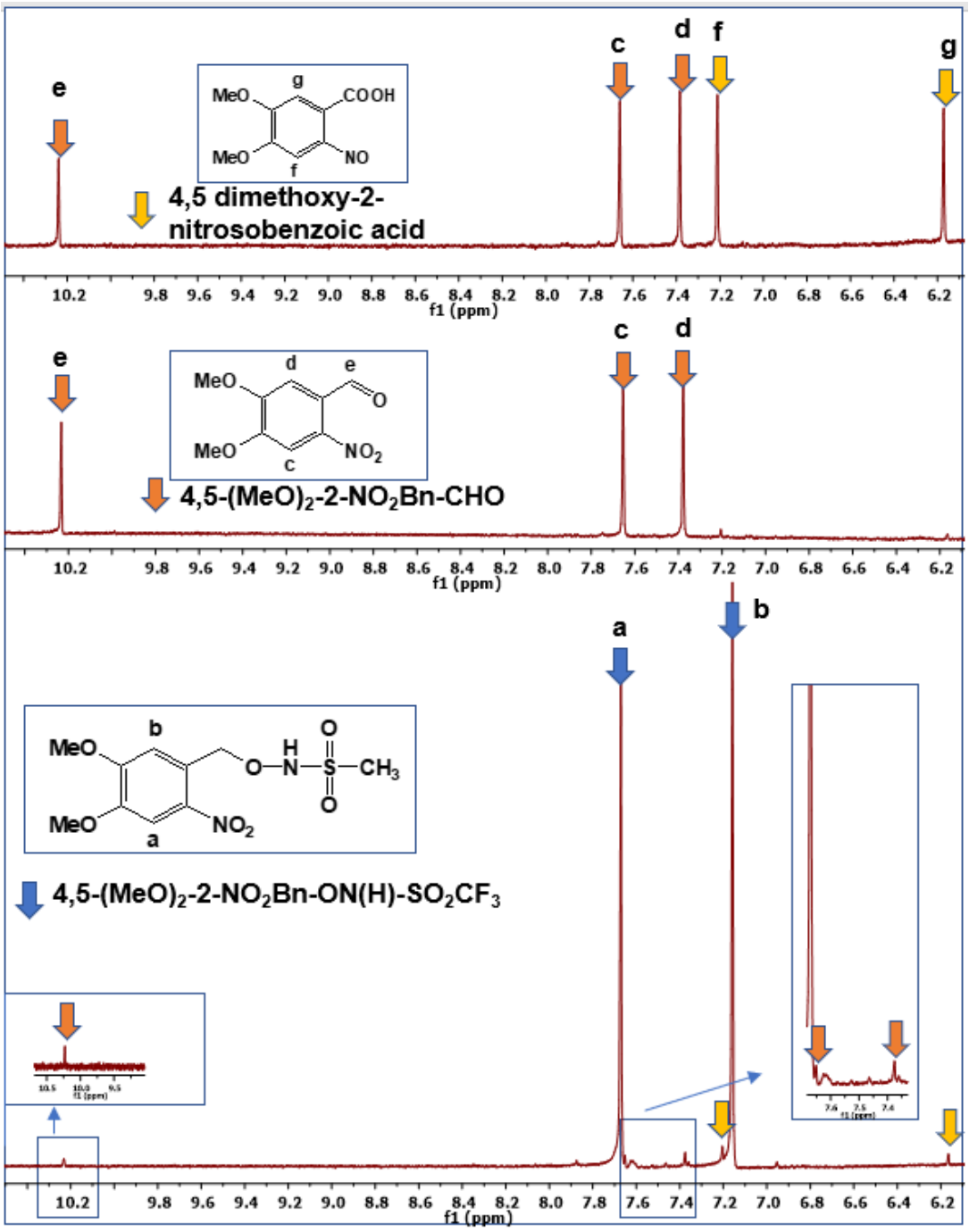

Figure 2.10. ^{1}H NMR spectra of a partially photolyzed sample (irradiated for 2.0 min) of **4,5-(MeO)$_2$-2-NO$_2$Bn-ON(H)-SO$_2$CF$_3$** (3.89 mM), **4,5-(MeO)$_2$-2-NO$_2$Bn-CHO** and a partially photolyzed sample (1.0 min) of **4,5-(MeO)$_2$-2-NO$_2$Bn-CHO** in a mixture of phosphate buffer (5 mM, pH 7.0) and CD_3CN (40:60, v/v) under anaerobic conditions.

Similarly, aromatic photoproducts were also investigated for **4,5-(MeO)$_2$-2-NO$_2$Bn-ON(H)SO$_2$CH$_3$**. Figure 2.11 shows the ^{1}H NMR spectra of partially photolyzed **4,5-(MeO)$_2$-2-NO$_2$Bn-ON(H)-SO$_2$CH$_3$** (2.0 min irradiation). Peaks at 10.22, 7.67 and 7.37

ppm can be assigned to **4,5-(MeO)$_2$-2-NO$_2$Bn-CHO** and peaks at 7.21 and 6.18 ppm to 4,5-dimethoxy-2-nitrosobenzoic acid**.**

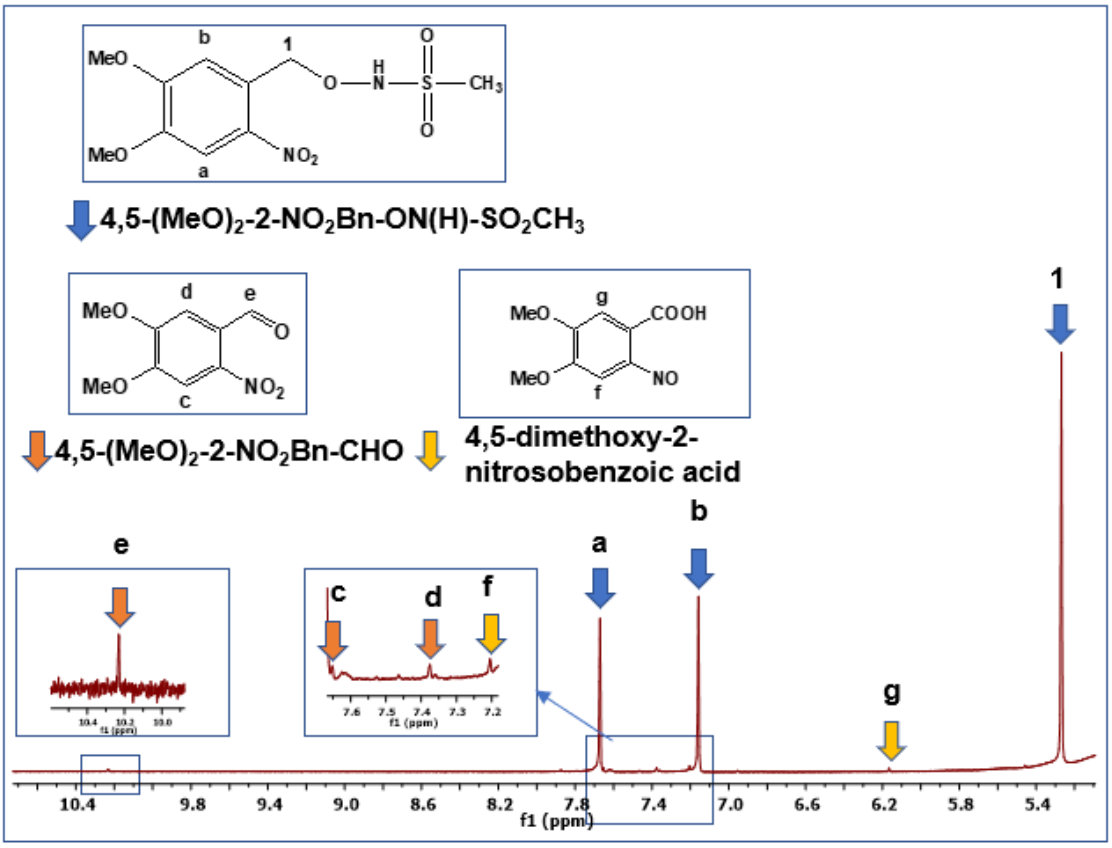

Figure 2.11. ^{1}H NMR spectrum of a partially photolyzed sample (2 min irradiation) of **4,5-(MeO)$_2$-2-NO$_2$Bn-ON(H)-SO$_2$CH$_3$** (3.89 mM) in a mixture of phosphate buffer (5 mM, pH 7) and CD_3CN (40:60, v/v) under anaerobic conditions.

2.3.5 Photolysis studies of 2-NO$_2$Bn-OC(O)-ON(H)-SO$_2$CH$_3$

The ^{1}H NMR spectra of **2-NO$_2$Bn-OC(O)-ON(H)-SO$_2$CH$_3$** as a function of total irradiation time are given Figure 2.12(a). The peak at 3.01 ppm was assigned to CH_3SO_2NHOH (71%), 3.04 ppm to $CH_3SO_2NH_2$ (12%), 2.64 ppm to $CH_3SO_2^-$ (10%) and 2.24 ppm to $CH_3SO_3^-$ (7%). The ^{1}H NMR spectra of authentic samples of $CH_3SO_2NH_2$, CH_3SO_2NHOH, $CH_3SO_2^-$ and $CH_3SO_3^-$ were recorded in the same solvent conditions to confirm this. The ratio of the CH_3 peak of the reactant at 2.96 ppm to the area of the TSP peak was plotted as a function of irradiation time and fitted to a first-order equation (Figure 2.12(b)), giving k_{obs} = 0.055 ± 0.0042 min^{-1}. The photodecomposition results are in good agreement with the PhD thesis of Mohammad Saifur Rahman.[152]

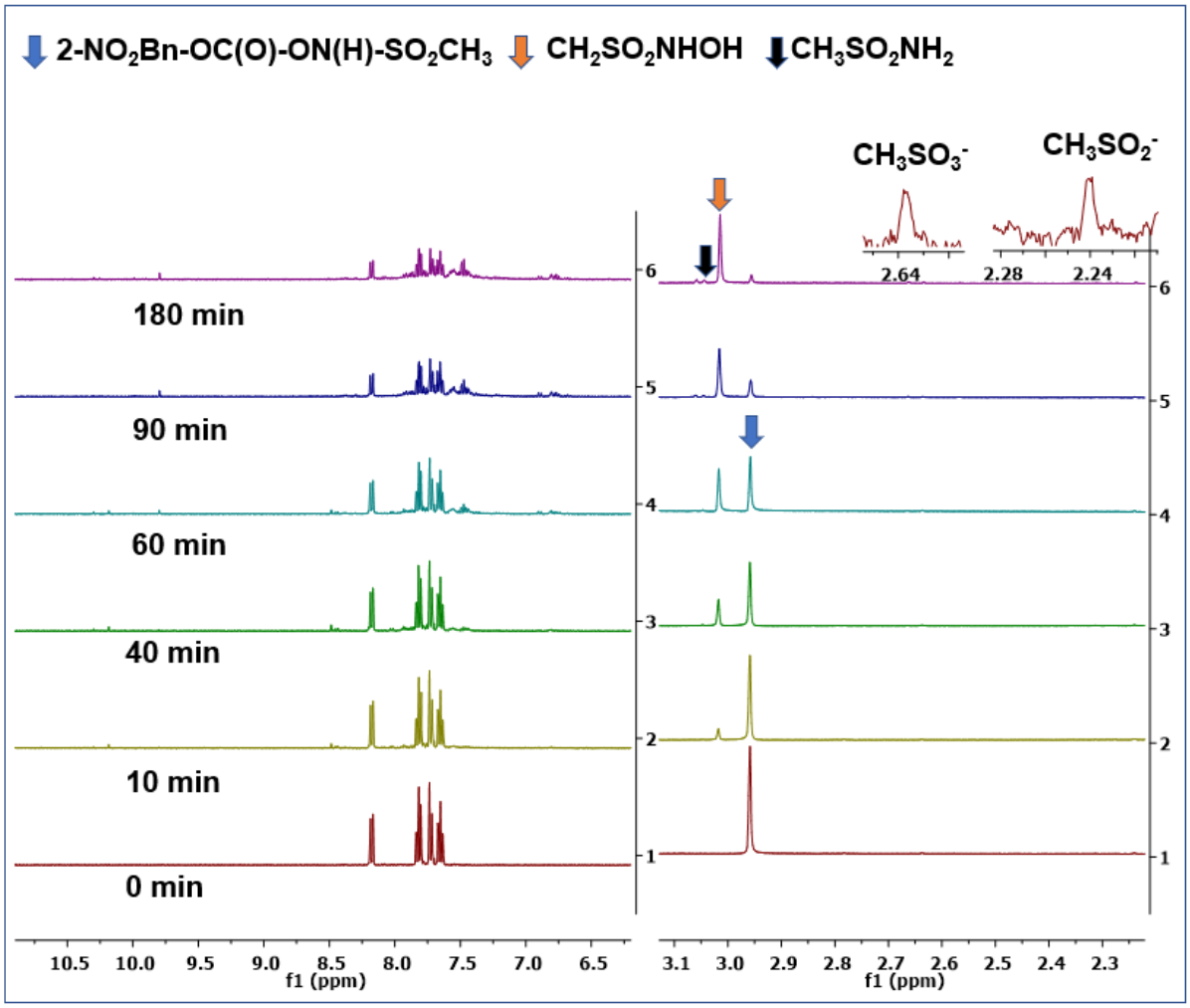

(a)

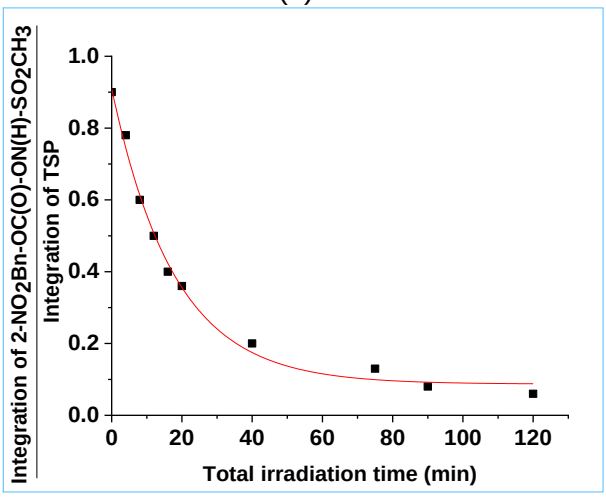

(b)

Figure 2.12. (a) ^{1}H NMR spectra as a function of total irradiation time for the photolysis of **2-NO_2Bn-OC(O)-ON(H)-SO_2CH_3** (3.89 mM) in a mixture of phosphate buffer (5.0 mM, pH 7.0) and CD_3CN (40:60, v/v). (b) The ratio of the CH_3 peak at 2.96 ppm of **2-NO_2Bn-OC(O)-ON(H)-SO_2CH_3** and the TSP reference peak versus total irradiation time. The best fit of the data to a first-order rate equation gives k_{obs} = 0.055 ± 0.0042 min^{-1}.

The possible photodecomposition pathways for **2-NO_2Bn-OC(O)-ON(H)-SO_2CH_3** are shown in Scheme 2.2. The presence of the methanesulfinate anion ($MeSO_2^-$) in the photoproduct mixture is diagnostic of HNO generation (Pathway 1). However, $MeSO_2^-$ was found to be unstable and can be easily oxidized to $MeSO_3^-$, with HNO, the methanesulfinate anion and the methanesulfonate anion arising as a result of C-O/N-S bond cleavage. One possibility is that trace amounts of the hydroxy radical produced upon photolysis of water reacts rapidly with $MeSO_2^-$ to give $MeSO_3^-$.[158] In addition, competing O-N and C-O bond cleavage may occur, leading to the generation of $CH_3SO_2NH_2$ (Pathway 3) and CH_3SO_2NHOH (Pathway 2) as shown in Scheme 2.2.

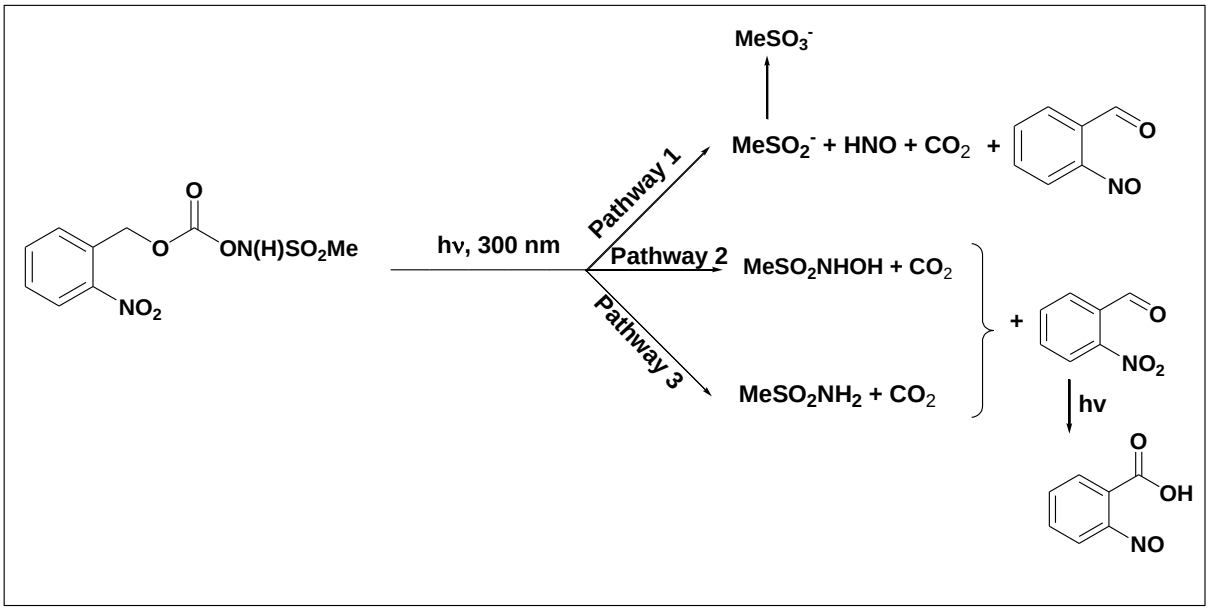

Scheme 2.2. Possible mechanisms of photodecomposition of **2-NO_2Bn-OC(O)-ON(H)-SO_2CH_3**.

Figure 2.13 shows the ^{1}H NMR spectra of a partially photolyzed sample of **2-NO_2Bn-OC(O)-ON(H)-SO_2CH_3** (0.5 min irradiation) in a mixture of phosphate buffer (5 mM, pH 7.0) and CD_3CN (40:60, v/v). A singlet peak was observed at 10.22 ppm which would be expected for the 2-nitrosobenzaldehyde product arising from concerted C-O/N-S bond cleavage, Pathway A, Scheme 2.2.

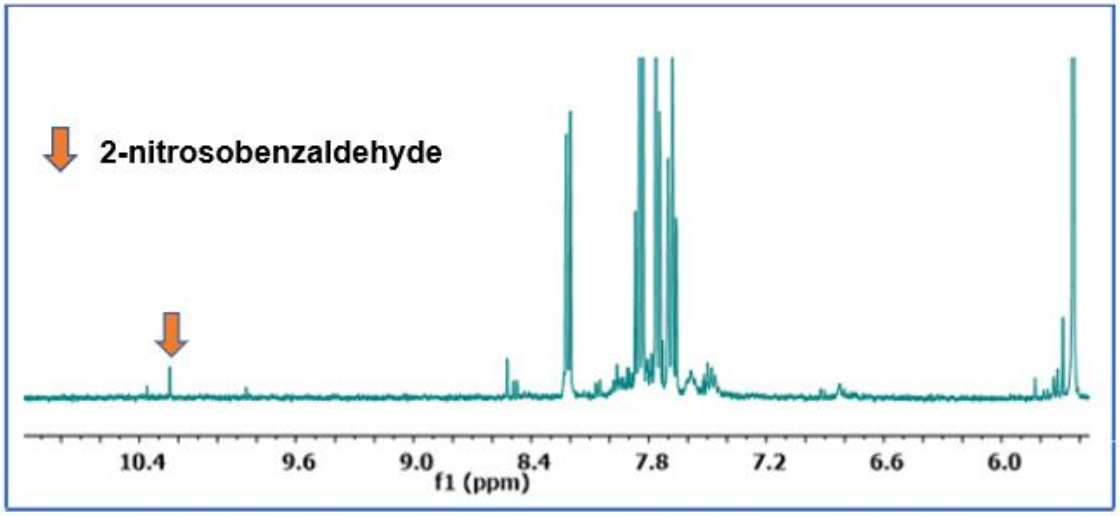

Figure 2.13. ^{1}H NMR spectra of a partially photolyzed sample of **2-NO_2Bn-OC(O)-ON(H)-SO_2CH_3** (3.0 min irradiation) in a mixture of phosphate buffer (pH 7.0, 5.0 mM) and CD_3CN (40:60, v/v).

After taking the photolyzed sample of **2-NO_2Bn-OC(O)-ON(H)-SO_2CH_3** to dryness, the ^{1}H NMR spectrum was recorded in $CDCl_3$. The chemical shifts of photolyzed sample were compared with the ^{1}H NMR spectrum of 2-nitrosobenzaldehyde, Table 2.2.[101] The chemical shifts are in excellent agreement with literature values, providing support for 2-nitrobenzaldehyde being a photoproduct. The formation of 2-nitrosobenzaldehyde was also confirmed by HRMS analysis, [M+H^+] = 136.0392 (calculated m/z = 136.0393) in Yang Zhou's thesis.

Table 2.2. Comparison of the chemical shifts (ppm) of 2-nitrosobenzaldehyde generated by the photolysis of **2-NO_2Bn-OC(O)-ON(H)-SO_2CH_3** in CD_3CN and literature values.

Chemical shifts (ppm) for 2-nitrosobenzaldehyde generated during the photolysis of **2-NO_2Bn-OC(O)-ON(H)-SO_2CH_3**	Chemical shifts (ppm) for 2-nitrosobenzaldehyde from the literature.[101]
6.43 (dd)	6.44 (dd)
7.68 (dt)	7.68 (dt)
7.89 (dt)	7.91 (dt)
8.19 (dd)	8.21 (dd)
12.08 (s)	12.1 (s)

2.3.6 Effect of excitation wavelength using a xenon lamp in conjunction with a monochromator

Although light-induced O-N bond cleavage has previously been observed for 2-NO_2Bn-O-N- systems,[113] little is known about the mechanism of this reaction. McCulla et al. studied the photoinduced release of benzohydroxamic acid from a nitrobenzyl photoprotected conjugate and postulated that O-N bond homolysis occurs.[113] Irradiation at a shorter wavelength favored O-N bond cleavage, whereas irradiation at a longer wavelength favored C-O bond cleavage. The photoproducts from irradiation of **2-NO_2Bn-ON(H)-SO_2R** and **4,5-$(MeO)_2$-2-NO_2Bn-ON(H)-SO_2R** (1.0 mM) in a mixture of phosphate buffer (5.0 mM, pH 7) and CD_3CN (40:60, v/v) at two different excitation wavelengths were therefore investigated, using a Xe lamp in conjunction with a monochromator. The results are summarized in Table 2.3. The excitation wavelength did not have any effect on the observed photoproducts.

Table 2.3. Effect of excitation wavelength on the percentage of O-N versus C-O bond cleavage of **2-NO_2Bn-ON(H)-SO_2R** and **4,5-$(MeO)_2$-2-NO_2Bn-ON(H)-SO_2R**(1.0 mM) in a mixture of phosphate buffer (5.0 mM, pH 7) and CD_3CN (40:60, v/v).

Compound	λ_{exc}	Photoproducts (percentage)
2-NO_2Bn-ON(H)-SO_2-CF_3	264	$CF_3SO_2NH_2$ (92) and $CF_3SO_2^-$(8)
2-NO_2Bn-ON(H)-SO_2-CF_3	330	$CF_3SO_2NH_2$ (92) and $CF_3SO_2^-$ (8)
2-NO_2Bn-ON(H)-SO_2-CH_3	264	$CH_3SO_2NH_2$ (100)
2-NO_2Bn-ON(H)-SO_2-CH_3	330	$CH_3SO_2NH_2$ (100)
4,5-$(MeO)_2$-2-NO_2Bn-ON(H)-SO_2CF_3	380	$CF_3SO_2NH_2$ (91) and $CF_3SO_2^-$ (9)
4,5-$(MeO)_2$-2-NO_2Bn-ON(H)-SO_2CF_3	330	$CF_3SO_2NH_2$ (91) and $CF_3SO_2^-$ (9)
4,5-$(MeO)_2$-2-NO_2Bn-ON(H)-SO_2CH_3	380	$CH_3SO_2NH_2$ (100)
4,5-$(MeO)_2$-2-NO_2Bn-ON(H)-SO_2CH_3	330	$CH_3SO_2NH_2$ (100)

2.3.7 Effect of solvent and pH

Studies were also carried out to determine whether the solvent ratio and/or the pH of the aqueous component of the solvent altered the amount of C-O versus O-N bond cleavage for **2-NO_2Bn-ON(H)-SO_2CH_3**. The selectivity for C-O versus O-N bond cleavage was highly dependent on the solvent ratio (CH_3CN : phosphate buffer) for related photocaged *N*-hydroxysulfonamides.[75-78] The rate of photolysis of **2-NO_2Bn-ON(H)-SO_2CH_3** was investigated at various CH_3CN : phosphate buffer (5.0 mM) solvent ratios (Figure 2.14). The results are summarized in Table 2.4. Only O-N, not C-O, bond cleavage was observed at all solvent ratios. The observed rate constant was independent of the solvent ratio.

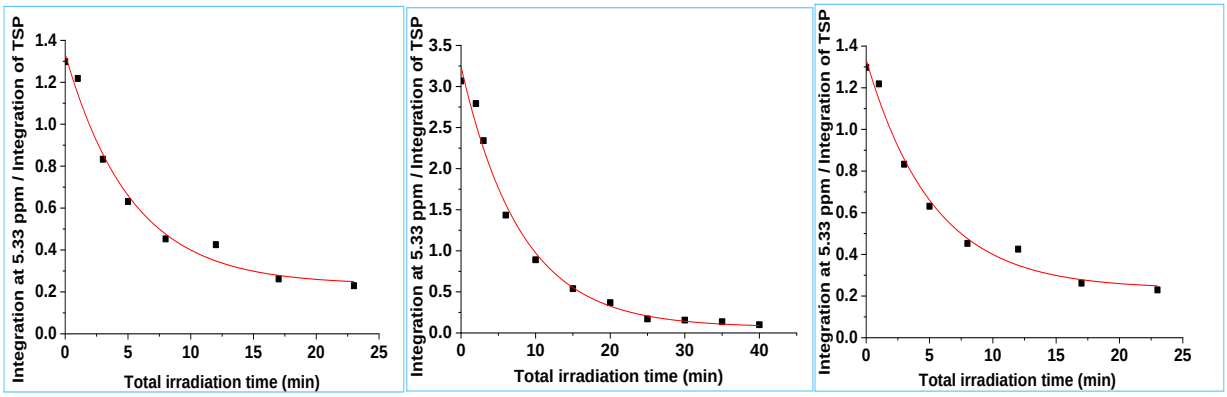

(a) (b) (c)

Figure 2.14. (a) Plot of the ratio of the CH_2 peak at 5.33 ppm for **2-NO_2Bn-ON(H)-SO_2CH_3** (3.89 mM) and TSP versus total irradiation time in CD_3CN. The best fit of the data to a first-order rate equation gives k_{obs} = 0.16 ± 0.03 min^{-1}. (b) Plot of the ratio of the CH_2 peak at 5.33 ppm for **2-NO_2Bn-ON(H)-SO_2CH_3** (3.89 mM) and TSP versus total irradiation time in a mixture of phosphate buffer (pH 7.0, 5.0 mM) and CD_3CN (20:80, v/v). The best fit of the data to a first-order rate equation gives k_{obs} = 0.18 ± 0.03 min^{-1}. (c) Plot of the ratio of the CH_2 peak at 5.33 ppm for **2-NO_2Bn-ON(H)-SO_2CH_3** (3.89 mM) and TSP versus total irradiation time in a mixture of phosphate buffer (pH 7.0, 5.0 mM) and CD_3CN (90:10, v/v). The best fit of the data to a first-order rate equation gives k_{obs} = 0.19 ± 0.02 min^{-1}.

Table 2. 4 Effect of solvent ratio on the percentage of O-N versus C-O bond cleavage and the observed rate constant for photodecomposition of **2-NO_2Bn-ON(H)-SO_2CH_3** (3.89 mM).

CD_3CN:PB solvent ratio[a]	k_{obs} (min^{-1})	% O-N bond cleavage
100:00	0.18 ± 0.03	100%
80:20	0.16 ± 0.01	100%
60:40	0.20 ± 0.03	100%
10:90	0.19 ± 0.02	100%

[a] PB = aqueous phosphate buffer (5.0 mM, pH 7.0).

The effect of the pH of the aqueous component in a mixture of 10:90 v/v CD_3CN: phosphate buffer (5.0 mM, pH 7.0) on the photodecomposition of **2-NO_2Bn-ON(H)-SO_2CH_3** (Figure 2.15) was investigated, to determine whether pH could influence the selectivity for C-O versus O-N bond cleavage. The results are summarized in Table 2.5. Varying the pH of the aqueous component has no effect on the observed rate constant for photodecomposition or the photoproducts obtained upon irradiating **2-NO_2Bn-ON(H)-SO_2CH_3**, with only O-N bond cleavage occurring.

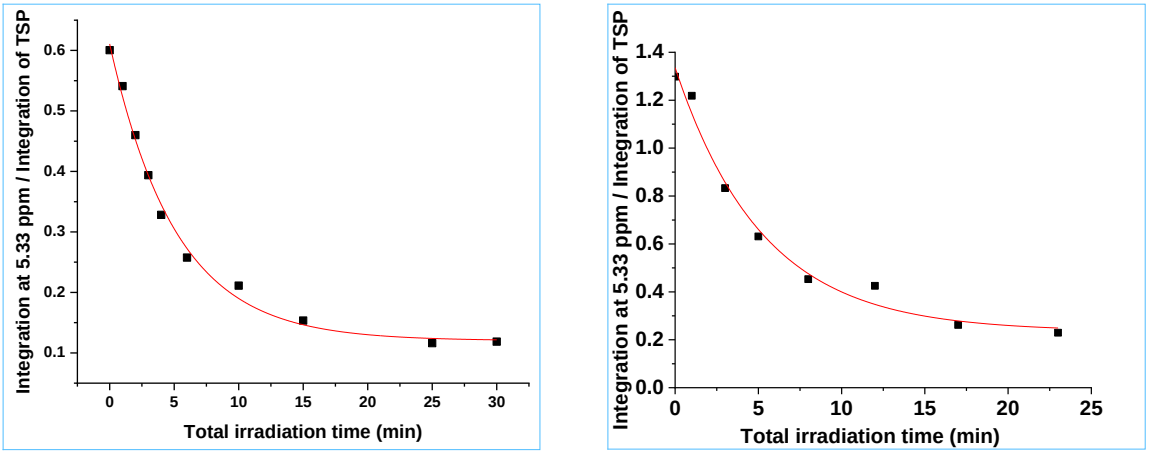

(a) (b)

Figure 2.15. (a) Plot of the ratio of the CH_2 peak at 5.33 ppm for **2-NO_2Bn-ON(H)-SO_2CH_3** (3.89 mM) and TSP versus total irradiation time in 0.10 M HCl (pH 1.0). The best fit of the data to a first-order rate equation gives k_{obs} = 0.21 ± 0.04 min^{-1}. (b) Plot of the ratio of the CH_2 peak at 5.33 ppm for **2-NO_2Bn-ON(H)-SO_2CH_3** (3.89 mM) and TSP versus total irradiation time in 0.10 M NaOH (pH 12.0). The best fit of the data to a first-order rate equation gives k_{obs} = 0.16 ± 0.04 min^{-1}.

Table 2.5. Effect of the pH of the aqueous component of the solvent on the photoproducts and the observed rate constant for photodecomposition for **2-NO_2Bn-ON(H)-SO_2CH_3** (3.89 mM) in 10:90 v/v CD_3CN: phosphate buffer (5.0 mM, pH 7.0).

pH	k_{obs} (min^{-1})	% N-O bond cleavage
1.0[a]	0.21 ± 0.02	100
7.0[b]	0.21 ± 0.04	100
12.0[c]	0.16 ± 0.03	100

Aqueous component of solution: [a] 0.10 M HCl; [b] 5.0 mM phosphate buffer; [c] 0.10 M NaOH.

2.3.8 Aerobic vs anaerobic steady state photolysis

The photolysis data reported thus far were all obtained under anaerobic conditions. To probe the effect of oxygen on the mechanism of the reaction, the photodecomposition of **2-NO_2Bn-ON(H)-SO_2CH_3** was also studied under aerobic conditions. The ^{1}H NMR spectrum of the photoproducts was identical to that observed under anaerobic conditions. The observed rate constant for photodecomposition, k_{obs}, was 0.20 ± 0.03 min^{-1} under aerobic conditions (Figure 2.16(a)), which is the same with that obtained under anaerobic conditions (Figure 2.16(b); 0.20 ± 0.03 min^{-1} ($t_{1/2}$ = 3.3 min). Given that oxygen efficiently quenches triplet excited states, this suggests that O-N bond cleavage involves excited state species in the singlet state.

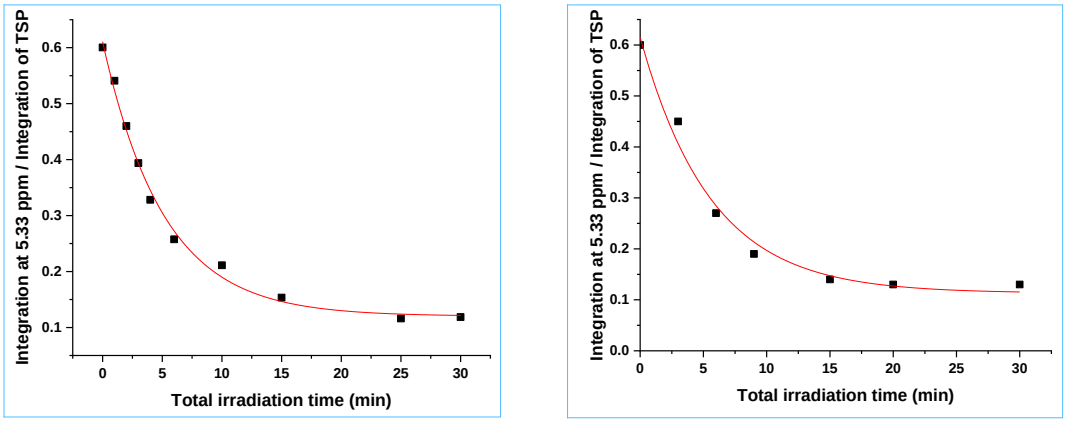

Figure 2.16. (a) Plot of the ratio of the CH_2 peak at 5.33 ppm for **2-NO_2Bn-ON(H)-SO_2CH_3** (3.89 mM) and TSP versus total irradiation time in a mixture of phosphate buffer (pH 7.0, 5.0 mM) and CD_3CN (40:60, v/v) under aerobic conditions. The best fit of the data to a first-order rate equation gives k_{obs} = 0.20 ± 0.03 min^{-1}. (b) Plot of the ratio of the CH_2 peak at 5.33 ppm for **2-NO_2Bn-ON(H)-SO_2CH_3** (3.89 mM) and TSP versus total irradiation time in a mixture of phosphate buffer (pH 7.0, 5.0 mM) and CD_3CN (40:60, v/v) under anaerobic conditions. The best fit of the data to a first-order rate equation gives k_{obs} = 0.20 ± 0.03 min^{-1}.

2.3.9 Evidence that the photolytic mechanism occurs via an aci-nitro intermediate

Laser flash studies were carried out to determine if the photodecomposition mechanism occurs via an aci-nitro intermediate. The structures of these species are shown in Figure 2.17. A short-lived aci-nitro intermediate (μs time scale) was reported to be a reaction intermediate for **2-NO_2Bn** systems by others.[98, 99, 101, 102, 159, 160] The lifetime of the aci-nitro species depends on the leaving group and the solvent conditions.

Figures 2.18(a) and (b) show a transient absorption spectrum for **2-NO_2Bn-ON(H)-SO_2CH_3** and **4,5-$(MeO)_2$-2-NO_2Bn-ON(H)-SO_2CH_3** in a mixture of phosphate buffer (pH 7.0, 5.0 mM) and CH_3CN (3 mL, 40:60, v/v). The absorbance maximum for the deprotonated aci-nitro species of **2-NO_2Bn-ON(H)-SO_2CH_3** was observed at 430 nm. This absorbance maximum value of aci-nitro anion is in excellent agreement with the reported value for 2-nitrobenzaldehyde (430 nm) by others.[124] The absorbance maximum for the aci-nitro anion species of **4,5-$(MeO)_2$-2-NO_2Bn-ON(H)-SO_2CH_3** was red shifted to ~490 nm.

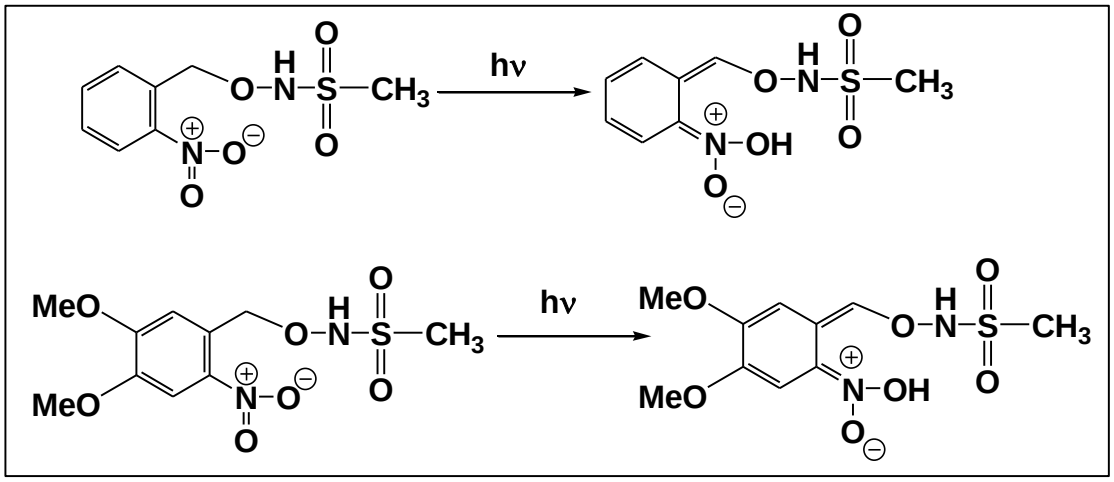

Figure 2.17. The structures of **2-NO$_2$Bn-ON(H)-SO$_2$CH$_3$** and **4,5-(MeO)$_2$-2-NO$_2$Bn-ON(H)-SO$_2$CH$_3$** and the corresponding *aci*-nitro anion species.

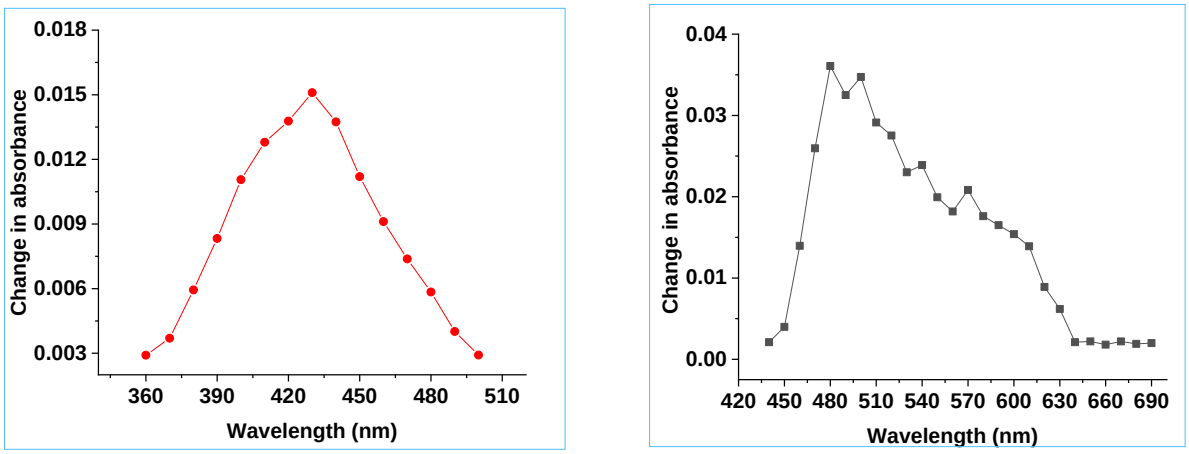

(a) (b)

Figure 2.18. (a) Transient absorption spectrum of **2-NO$_2$Bn-ON(H)-SO$_2$CH$_3$** (120 μM) at 3.5 × 10^{-5} s versus wavelength upon photolysis of **2-NO$_2$Bn-ON(H)-SO$_2$CH$_3$** in a mixture of phosphate buffer (pH 7.0, 5.0 mM) and CH_3CN (3 mL, 40:60, v/v, λ_{exc} = 266 nm) under anaerobic conditions. (b) Transient absorption spectrum of **4,5-(MeO)$_2$-2-NO$_2$Bn-ON(H)-SO$_2$CH$_3$** at 100 ns in anaerobic CH_3CN. Note that the reactant does not absorb in this wavelength region; hence the change in absorbance represents the absorbance of the aci-nitro species. A Nd:YAG laser fitted with 2nd and 4th harmonic generators operating at 62 mJ/pulse was used.

2.3.10 Photostability of *N*-Benzyloxy-*C,C,C*-trifluoromethanesulfonamide

The importance of the nitro group on photodecomposition for this family of molecules was also investigated by studying the steady state photodecomposition of the structurally related compound *N*-benzyloxy-1,1,1-trifluoromethanesulfonamide, **Bn-ON(H)-SO$_2$-CF$_3$**, which lacks the *o*-nitro substituent (Figure 2.19).

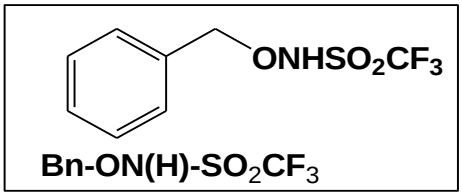

Figure 2.19. Structure of **Bn-ON(H)-SO_2CF_3**.

^{19}F NMR spectra of **Bn-ON(H)-SO_2CF_3** were recorded immediately after sample preparation and after 3 and 6 h irradiation in a mixture of phosphate buffer (pH 7.0, 5.0 mM) and CD_3CN (40:60, v/v) at 300 nm (Figure 2.20(a)). No detectable photodecomposition of **Bn-ON(H)-SO_2CF_3** was observed even after irradiation for 6 h. Therefore, the nitro functional group plays a key role in the photoactivity of the HNO-generating systems with all decomposition pathways being dependent on the presence of this group.

A similar photolysis experiment was carried out in CD_3CN. The ^{19}F NMR spectrum of **Bn-ON(H)-SO_2CF_3** (3.89 mM) was recorded immediately and after 6 h of irradiation at 300 nm (Figure 2.20(b)). A small percentage of decomposition occurred. $CF_3SO_2^-$ (-88.2 ppm, 8%), $CF_3SO_2NH_2$ (-80.7 ppm, 8%) and $CF_3SO_3^-$ (-79.4 ppm, 5%) were observed.

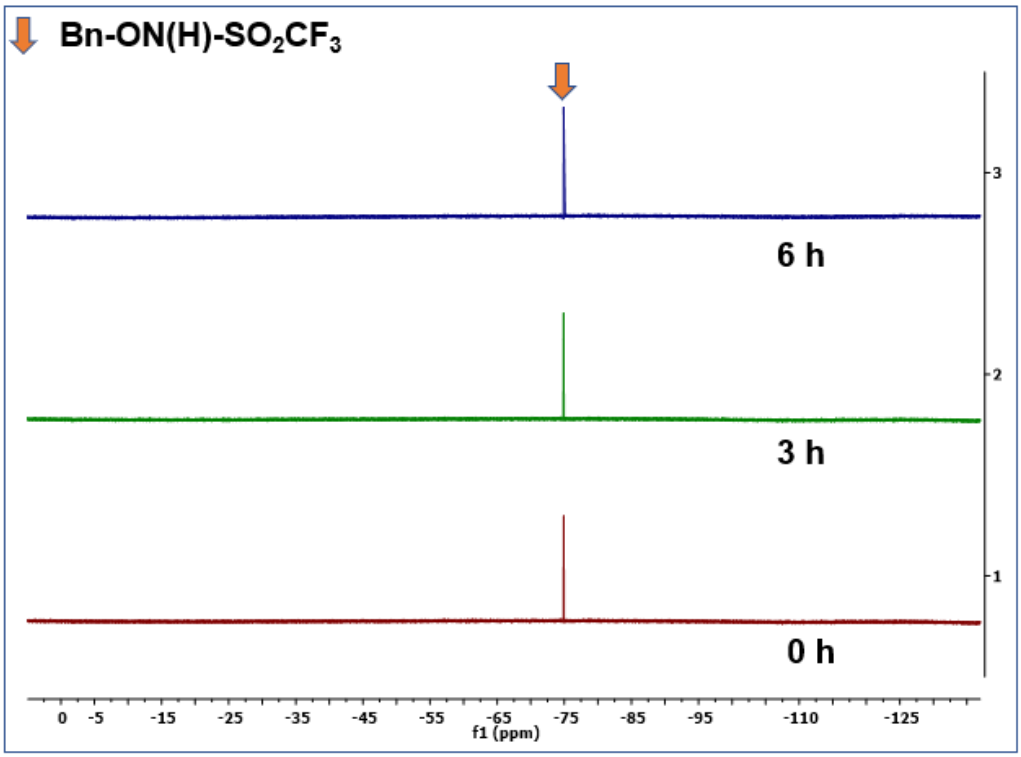

(a)

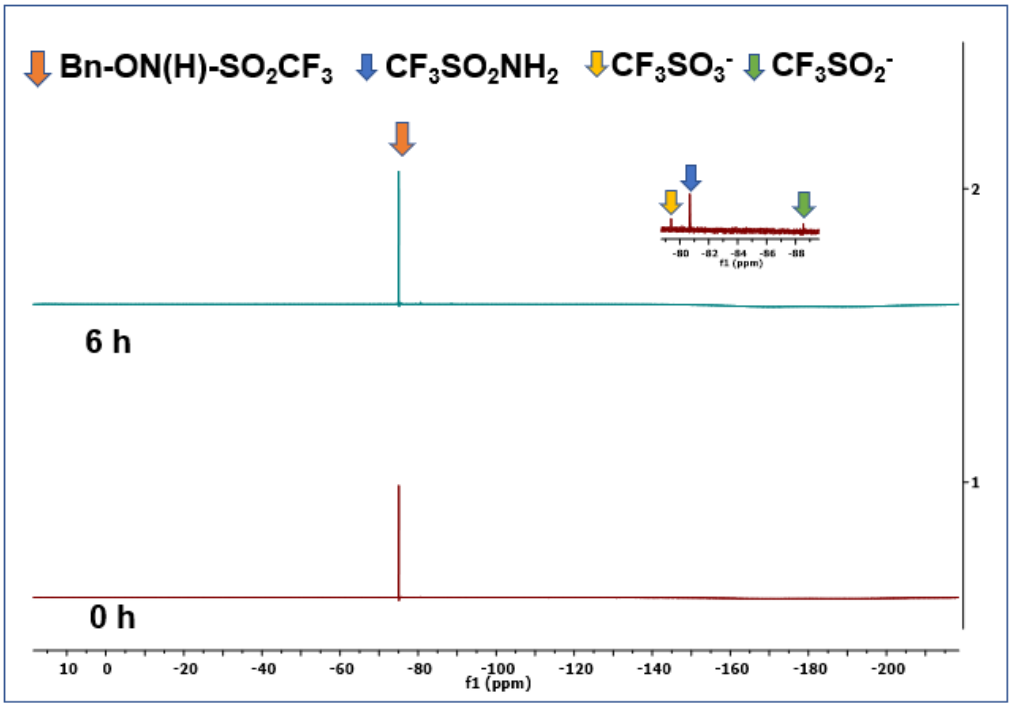

(b)

Figure 2.20. (a) Comparison of the ^{19}F NMR spectra of **Bn-ON(H)-SO$_2$CF$_3$** (-75.0 ppm) in a mixture of phosphate buffer (5.0 mM, pH 7.0) and CD_3CN (50:50, v/v) immediately after solution preparation (0 h), after 3 h irradiation and 6 h irradiation (300 nm). (b) Comparison of the ^{19}F NMR spectra of **Bn-ON(H)-SO$_2$CF$_3$** (-75.0 ppm) in CD_3CN: immediately after solution preparation (0 h) and after 6 h irradiation (300 nm). The photoproducts were $CF_3SO_2^-$ (-88.6 ppm), $CF_3SO_2^-$ (-78.2 ppm) and $CF_3SO_2NH_2$ (-80.7 ppm).

2.3.11 HNO detection using hydroxocobalamin (HOCbl) and a phosphine trap

Direct HNO detection is challenging as it rapidly dimerizes to $H_2N_2O_2$ and ultimately leads to H_2O and N_2O.[5] Indirectly, HNO can be detected using HOCbl and *tris*(4,6-dimethyl-3-sulfonatophenyl)phosphine trisodium salt (TXPTS).[55] Prior to determining if either HOCbl or TXPTS can trap HNO released from the photoactive HNO donors, control experiments were carried out using trifluoromethanesulfonylhydroxamic acid (CF_3SO_2NHOH). This molecule rapidly decomposes in aqueous solution (pH > 4) to release HNO and $CF_3SO_2^-$ (Scheme 2.3). The pK_a of the CF_3SO_2NHOH is 5.89 ± 0.05.[55] The structures of HOCbl and TXPTS are shown in Figure 2.21.

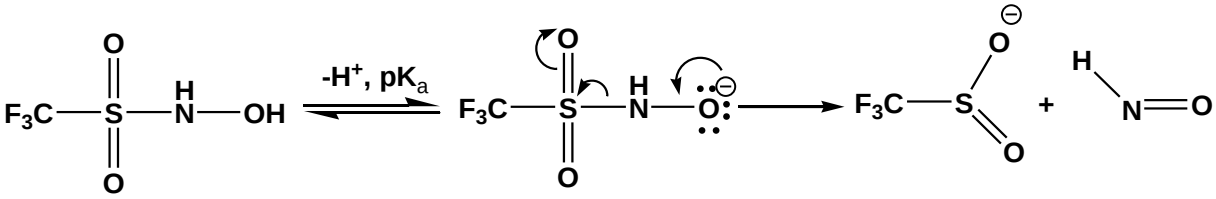

Scheme 2.3. The mechanism for HNO release from trifluoromethanesulphonylhydroxamic acid.

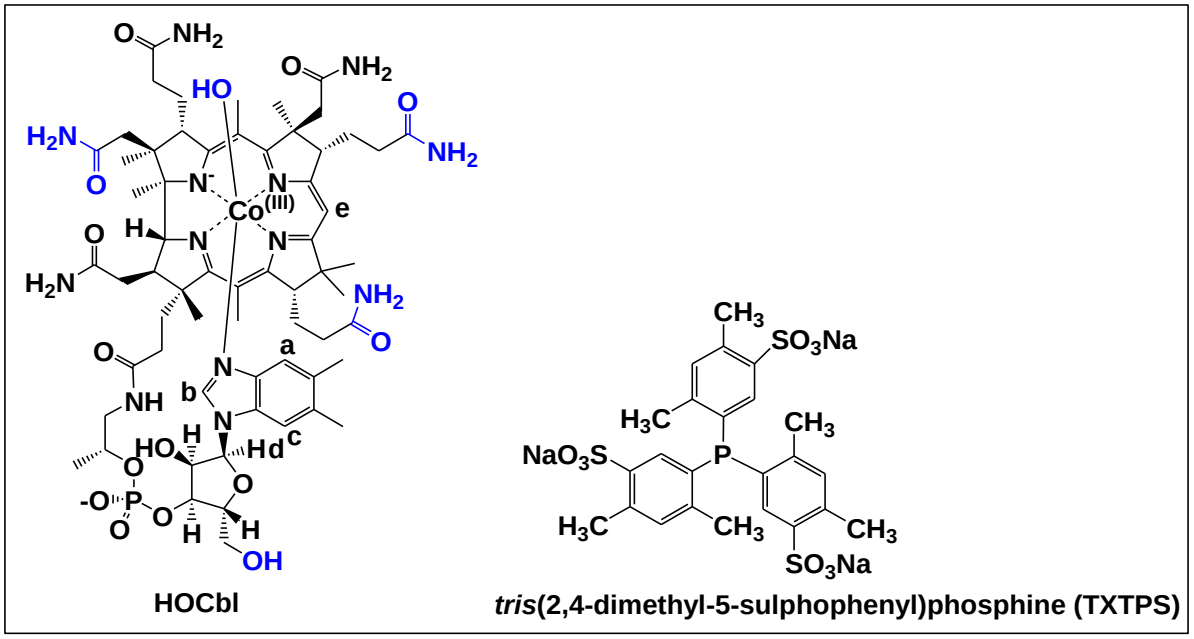

Figure 2.21. The structures of hydroxocobalamin (HOCbl) and TXPTS. The labelling scheme of the protons **a-e** that resonant in the aromatic region are shown for HOCbl.

2.3.12 Reaction between hydroxocobalamin and HNO released from CF_3SO_2NHOH

The concentration of hydroxocobalamin (HOCbl) and CF_3SO_2NHOH were determined accurately by UV-Vis and ^{19}F NMR spectroscopy (see Appendix section A1). The reaction between HOCbl and CF_3SO_2NHOH was investigated using UV−Vis spectroscopy. A series of vials were prepared in a glove box containing a fixed volume of anaerobic HOCbl•HCl solution (final concentration = 50.0 μM). Varying volumes of the anaerobic stock CF_3SO_2NHOH solution (0.95 mM) were added to the vials to achieve a range of mol equiv. CF_3SO_2NHOH (0, 0.20–2.0 mol-equiv.; 0.30 M carbonate buffer, pH 9.96) with 3.00 mL final solution volume. After the addition of CF_3SO_2NHOH, the vials were capped. The reactions were allowed to proceed to completion for at least 5 half-lives for the slowest reaction (HOCbl + 0.20 mol equiv. CF_3SO_2NHOH). The product solutions were subsequently transferred (anaerobic conditions) to a cuvette equipped with a J Young stopcock and the cuvette was equilibrated at 25.0 °C in the cell compartment of the spectrometer for at least for 15 min prior to recording the UV-Vis spectrum. HNO is released upon decomposition of CF_3SO_2NHOH in this buffer. Isosbestic points were observed at 340, 371 and 497 nm consistent with the reaction of HOCbl with HNO to give nitrosylcobalamin, NOCbl (Figure 2.22(a)).[161] The plot of absorbance at 357 nm versus mol equivalent of CF_3SO_2NHOH (Figure 2.22(b)) gives a stoichiometry of 1:0.9 ± 0.1 HOCbl :

CF_3SO_2NHOH at pH 9.96. These results demonstrate that HOCbl is an excellent trapping molecule for HNO, forming NOCbl as the product.

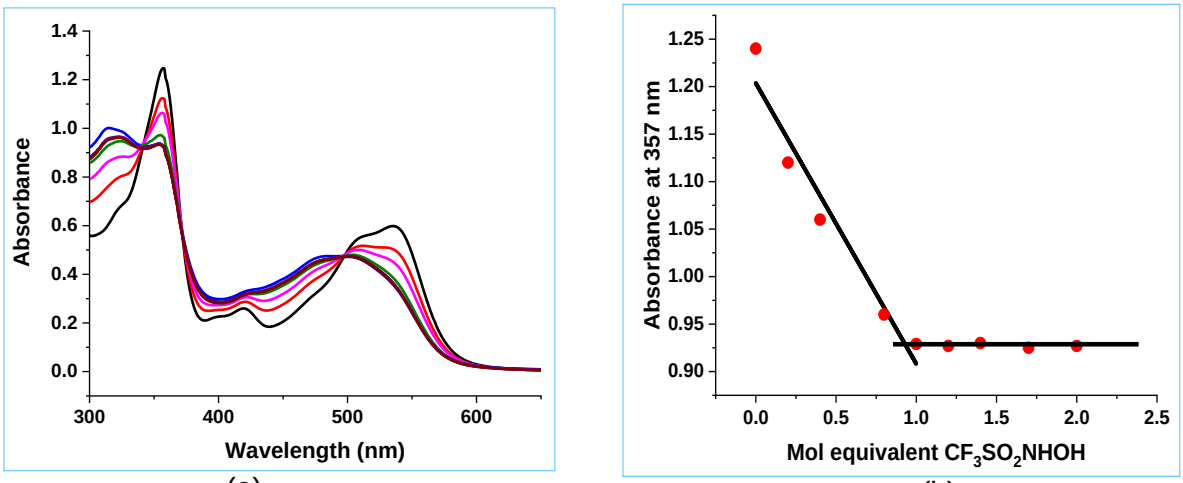

(a) (b)

Figure 2.22. (a) UV−Vis spectra of equilibrated solutions of HOCbl (5.00×10^{-5} M) with CF_3SO_2NHOH (0-2.0 mole equiv) at pH 9.96 under anaerobic conditions. (b) Plot of absorbance at 357 nm versus mol equivalent of CF_3SO_2NHOH at pH 9.00 (0.30 M carbonate buffer) for the data shown in (a).

2.3.13 Control experiment to determine if TXPTS can trap HNO released from CF_3SO_2NHOH

A control experiment was carried out to determine if the HNO released from CF_3SO_2NHOH reacts with the *tris*(2,4-dimethyl-5-sulphophenyl)phosphine anion (TXTPS), an established HNO trapping molecule. TXPTS reacts with HNO to produce the corresponding aza ylide and phosphine oxide, equation (2.3).

$$\mathbf{HNO + 2R_3P \longrightarrow \underset{\text{Aza ylide}}{R_3P{=}NH} + \underset{\text{Phosphine oxide}}{R_3P{=}O}} \qquad (2.3)$$

TXPTS (5.56 mM, 430 µL, 2.0 mol equiv.) in anaerobic carbonate buffer (pD 9.96, 0.3 M) was added to CF_3SO_2NHOH (60 mM, 20 µL) in anaerobic CH_3OH. The reaction was allowed to proceed for at least 5 half-lives and the ^{31}P NMR spectrum was subsequently recorded. H_3PO_4 was used as an external standard. Upon the addition of CF_3SO_2NHOH (2.66 mM) to an anaerobic solution of TXPTS (5.31 mM, 2.0 mol equivalent in carbonate buffer (0.30 mM, pD 9.96), aza ylide and phosphine oxide were produced (≈ 0.9:1.0 ratio) with no traces of unreacted TXPTS, Figure 2.23. Others have reported that this reaction is not stoichiometric.[32]

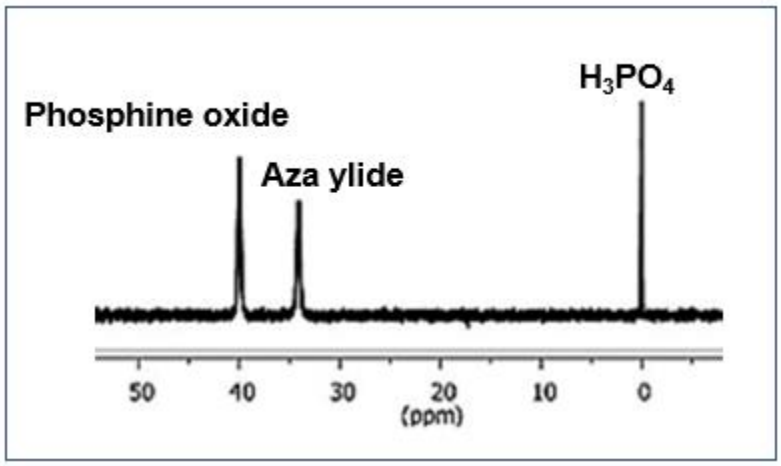

Figure 2.23. ^{31}P NMR spectrum of the products of the reaction between CF_3SO_2NHOH (2.66 mM) and TXPTS (5.31 mM) in carbonate buffer (0.30 M, pD 9.96). The peaks at 40.0 and 34.1 ppm can be attributed to the corresponding phosphine oxide and aza ylide of TXPTS, respectively. The spectrum is referenced externally to concentrated H_3PO_4 (0.0 ppm).

2.3.14 Studies on the reaction between 2-NO_2Bn-ON(H)-SO_2CF_3 and hydroxocobalamin

HNO release can be inferred by trapping with hydroxocobalamin (HOCbl).[78] The ^1H NMR spectrum of HOCbl (1.8 mM) was recorded in an anaerobic mixture of 40:60 v/v MeCN: 5 mM carbonate buffer (D_2O, pD 10.0), to check the stability of HOCbl in this solvent (Figure 2.24). The peaks at 7.72, 7.15, 7.02, 6.76 (d), 6.64 ppm can be assigned to the five peaks of HOCbl which resonate in the aromatic region (Figure 2.24). Additional unknown peaks are observed at 8.25, 8.20, 8.03, 7.75, 6.90, 6.80, 6.55 ppm which may be from the amide protons which have not fully exchanged with the D_2O to become deuterated.

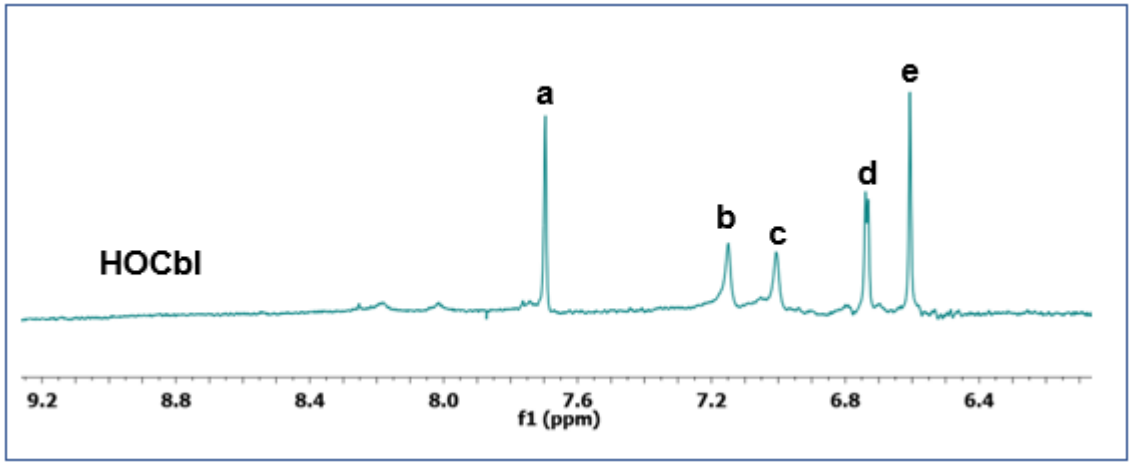

Figure 2.24. ^1H NMR spectrum of HOCbl (1.8 mM) in an anaerobic mixture of 40:60 v/v MeCN : 5 mM deuterated carbonate buffer (pD 10.0). The spectrum was recorded 2 h after solution preparation. The labelling scheme for the protons of HOCbl is shown in Figure 2.21.

A sample of **2-NO$_2$Bn-ON(H)-SO$_2$CF$_3$** (1.0 mM) and HOCbl (1.8 mM) was prepared in the same solvent mixture. The ^{1}H NMR spectrum was recorded immediately and after 12 h (Figure 2.25). In addition to HOCbl (7.72, 7.15, 7.02, 6.76 and 6.64 ppm) and **2-NO$_2$Bn-ON(H)-SO$_2$CF$_3$** (8.65 (dd), 8.35 (td) and 8.28 (m) ppm), a number of unknown peaks (7.40, 7.43, 7.68, 7.24, 6.90, 6.97, 6.47, 6.53 and 6.44 ppm) were observed immediately after sample preparation. The small unknown peaks may possibly have come from a complex formed between the HOCbl and **2-NO$_2$Bn-ON(H)-SO$_2$CF$_3$**.[162, 163] No further change in the ^{1}H NMR spectrum was observed after 12 h (Figure 2.25). The chemical shifts of the aromatic peaks of NOCbl in this solvent were observed at 7.50, 7.23, 6.87, 6.38 and 6.28 ppm (an authentic sample of this compound was used). The NOCbl peak at 7.23 overlaps with a peak of HOCbl; however, the remaining peaks of NOCbl are distinct from those of HOCbl.

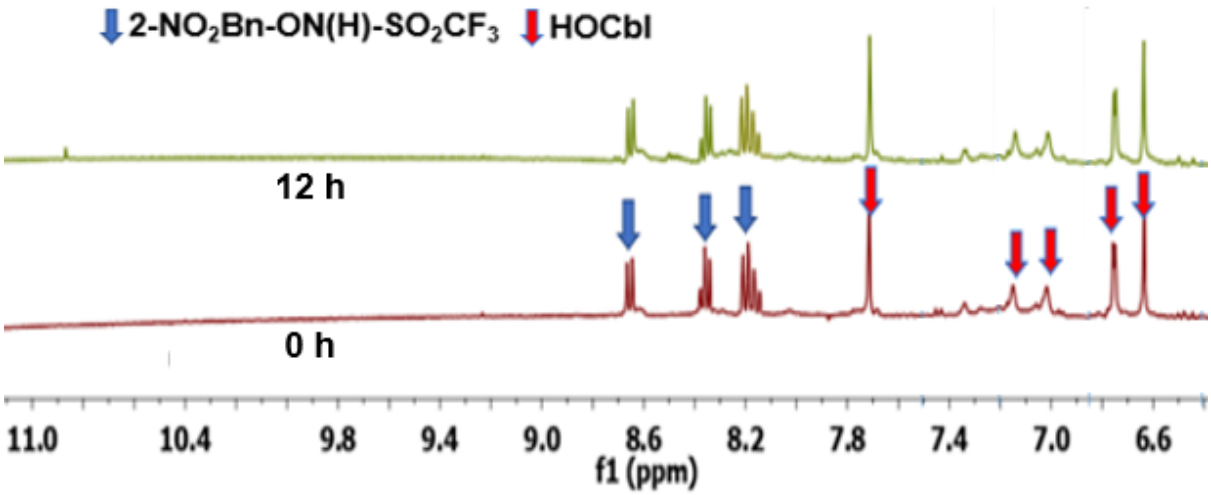

Figure 2.25. ^{1}H NMR spectra of **2-NO$_2$Bn-ON(H)-SO$_2$CF$_3$** (1.0 mM) and HOCbl (1.8 mM) in an anaerobic mixture of 40:60 v/v MeCN : 0.1 M deuterated carbonate buffer (pD 10.0) ~15 min and 12 h after the solution was prepared.

An anaerobic sample of **2-NO$_2$Bn-ON(H)-SO$_2$CF$_3$** (1.0 mM) and HOCbl (1.8 mM) was prepared in an anaerobic mixture of 40:60 v/v MeCN: 5 mM carbonate buffer (D_2O, pD 10.0). ^{1}H NMR spectra were recorded immediately after preparing the sample and after 2, 4 and 10 min total irradiation using 300 nm bulbs (Figure 2.26). The irradiated sample was then spiked with NOCbl and peaks from NOCbl were observed at 6.28, 6.38, 6.87, 7.23 and 7.50 ppm (Figure 2.26). The peaks at 6.87 and 7.23 ppm were present in the photolysed sample prior to the addition of NOCbl. However, the NOCbl peaks at 6.28, 6.38 and 7.50 ppm were not observed after photolysis, so appreciable amounts of NOCbl does not appear to be formed upon photolysis of **2-NO$_2$Bn-ON(H)-**

SO_2CF_3. The total peak area of the aromatic protons of the cobalamin decreased with increasing irradiation, suggesting that radical reactions may have occurred resulting in loss of aromaticity and/or the aromatic protons are exchanged with deuterons from the D_2O solvent.

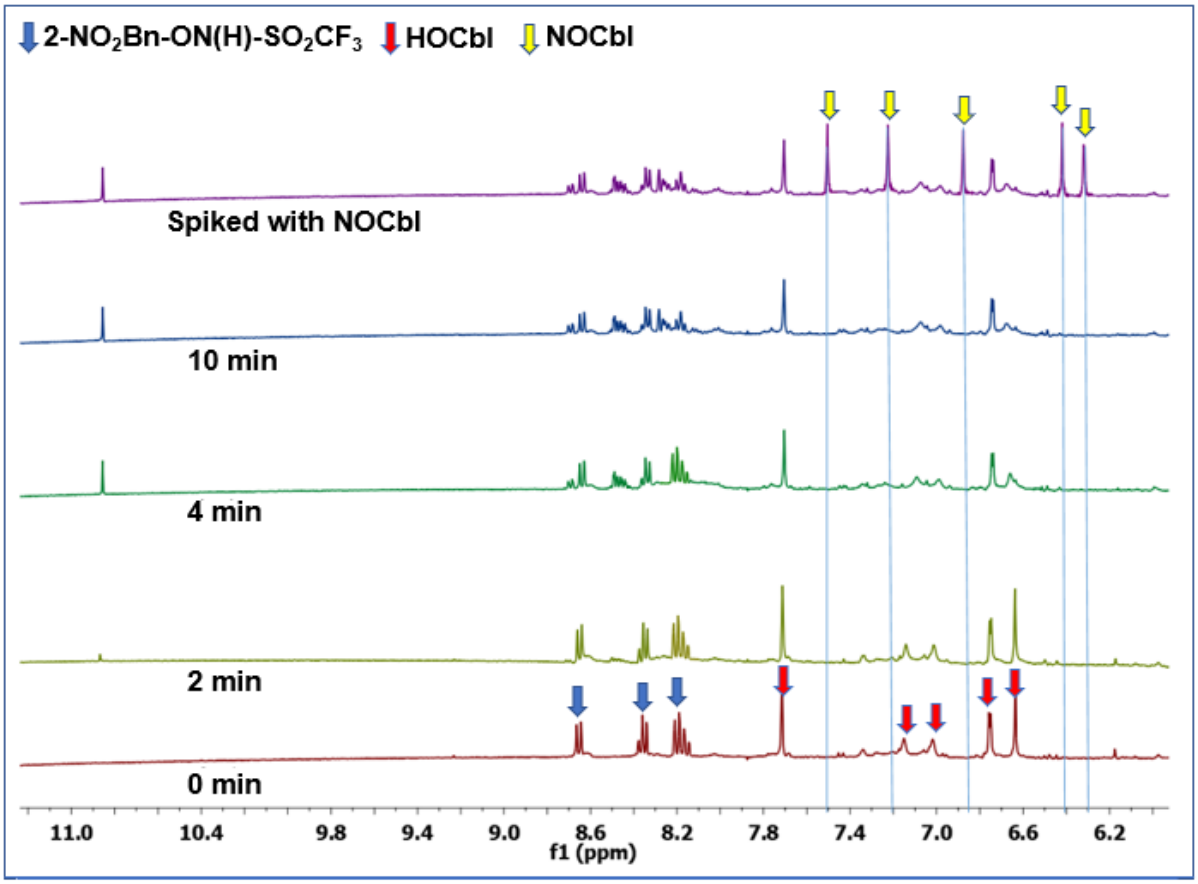

Figure 2.26. ^{1}H NMR spectra of **2-NO_2Bn-ON(H)-SO_2CF_3** (1.0 mM) and HOCbl (1.8 mM) in an anaerobic mixture of 40:60 v/v MeCN : 5 mM deuterated carbonate buffer (pD 10.0). The sample was photolysed for a total irradiation time of 0, 2, 4 and 10 min. The sample at 10 min irradiation time was spiked with NOCbl (upper NMR spectrum).

2.3.15 Reaction between Phosphine 1 and 2-NO_2Bn-ON(H)-SO_2CF_3

HNO generated from photolysis of a (6-hydroxy-2-naphthalen-2-yl)methyl photocaged *N*-hydroxysulfonamide was previously successfully trapped using **Phosphine 1**.[78] Importantly, **Phosphine 1** is photostable in the presence of UV light for 2 h.[78] TXPTS could not be used to trap HNO as it was light sensitive. When HNO reacts with 2 mol equiv. 3-(diphenylphosphino)-4-(methoxycarbonyl)benzoic acid (**Phosphine 1**), 3-(P,P-diphenylphosphorimidoyl)-4-(methoxycarbonyl)benzoic acid (**Phosphine 2)** and/or 4-Carbamoyl-3-(diphenylphosphoryl)benzoic acid (**Phosphine 3**) are formed, with **Phosphine 2** undergoing a Staudinger ligation reaction to give **Phosphine 3**.

(Scheme 2.4). However, hydrolysis of **Phosphine 2** also gives rise to 3-(Diphenylphosphoryl)-4-(methoxycarbonyl)benzoic acid (**Phosphine 4**).

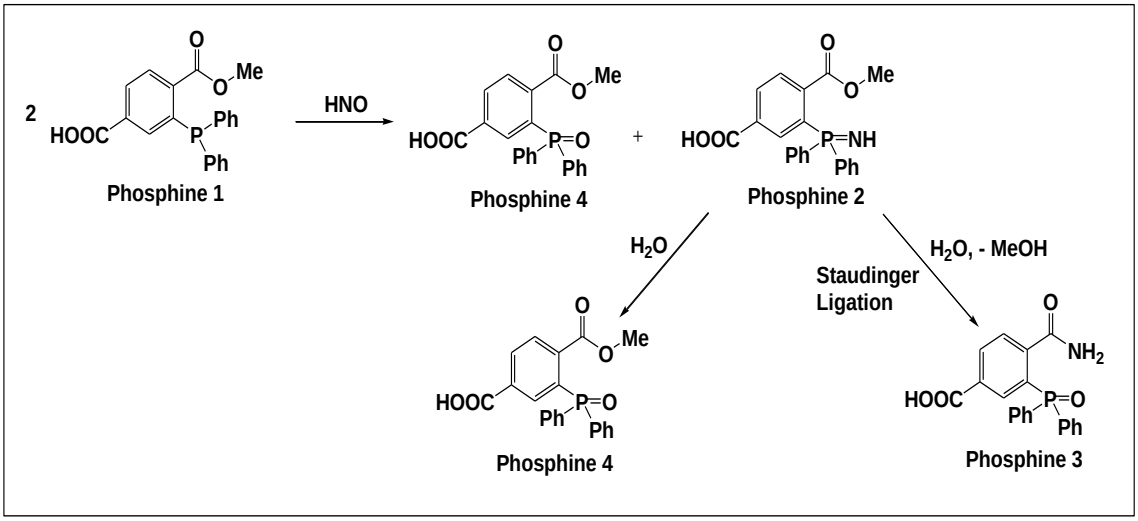

Scheme 2.4. Trapping of HNO using **Phosphine 1**.

As phosphines are well-known reducing agents and have been observed to reduce both nitro and nitroso compounds,[164, 165] a control experiment was conducted to check the reactivity of **Phosphine 1** (1.5 mM) and **2-NO_2Bn-ON(H)-SO_2CF_3** (15 mM) in an anaerobic mixture of carbonate buffer (0.1 M, pH 10) and CD_3CN (40:60, v/v). The ^1H NMR spectrum was recorded immediately and 10 min later (spectra not shown). There was no change in the ^1H NMR spectrum suggesting that **Phosphine 1** did not reduce **2-NO_2Bn-ON(H)-SO_2CF_3** in the absence of an intense light source. Therefore, **Phosphine 1** can be used as a potential HNO trapping agent.

The ^{31}P NMR spectra of **Phosphine 1** (1.5 mM) and **2-NO_2Bn-ON(H)-SO_2CF_3** (15 mM) in a mixture of carbonate buffer (0.1 M, pH 10) and CD_3CN (40:60, v/v) under anaerobic conditions were recorded immediately after preparing the sample and after irradiating the sample for 10 min (Figure 2.27). No **Phosphine 2** was observed in the ^{31}P NMR spectrum with only **Phosphine 4** (33.2 ppm) and an additional unknown peak at 23.7 ppm.

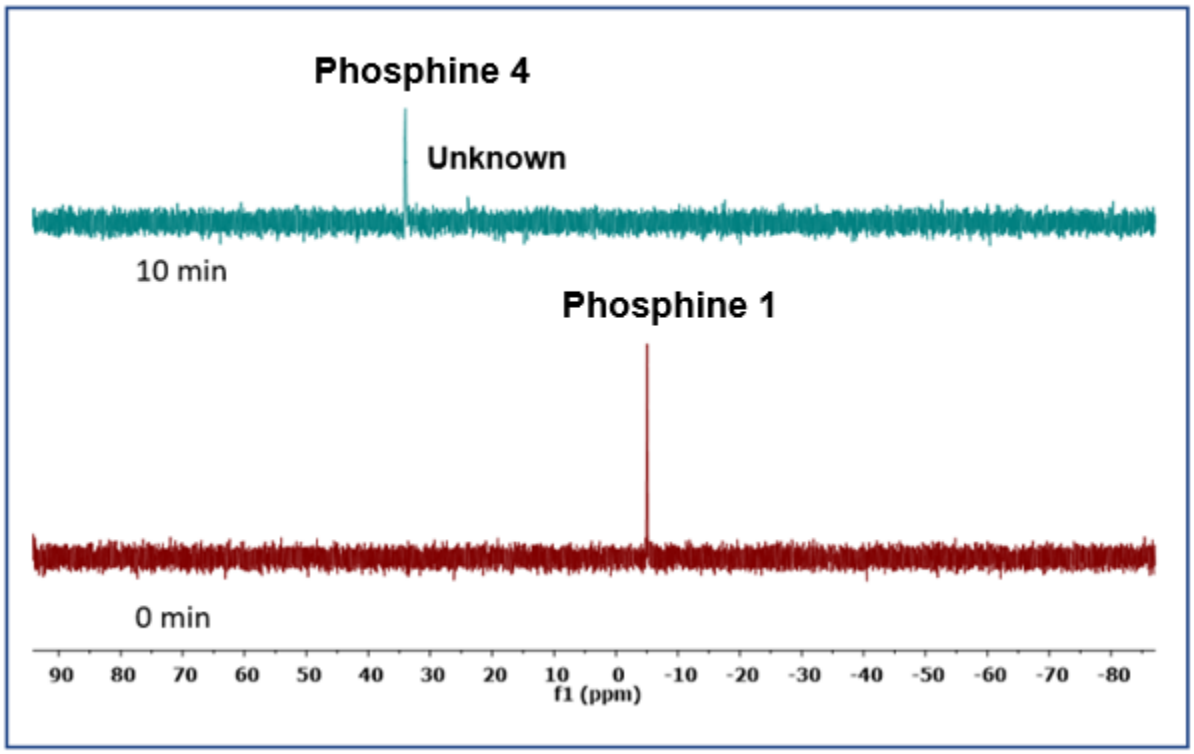

Figure 2.27. ^{31}P NMR spectra of **2-NO$_2$Bn-ON(H)-SO$_2$CF$_3$** (15 mM) and **Phosphine 1** (1.5 mM, -4.9 ppm) in a mixture of carbonate buffer (5 mM, pH 10.0) and CD$_3$CN (40:60, v/v) before after 10 min irradiation.

The ^{1}H NMR spectra of **Phosphine 1** (1.5 mM) and **2-NO$_2$Bn-ON(H)-SO$_2$CF$_3$** (15 mM) in a mixture of carbonate buffer (0.1 M, pH 10) and CD$_3$CN (40:60, v/v) under anaerobic conditions (Figure 2.28) were also recorded immediately after preparing the sample and after 10 min irradiation. After 10 min irradiation, mainly **2-NO$_2$Bn-CHO** (10.23, 8.05, 7.83, 7.37 ppm) was observed. Additionally, the peaks at 10.05 (s), 8.26 (d) ppm indicate the formation of a small amount of 2-nitrosobenzaldehyde. We speculate that a photoredox reaction between 2-nitrosobenzaldehyde and triphenylphosphine may have occurred, potentially leading to azoxybenzene and phosphine oxide products. This observation is consistent with previously reported results where **2-NO$_2$Bn-CHO** peaks mostly overlap with the reported azoxybenzenes peaks (for example benzofurazan).[164, 165]; ^{1}H NMR region: 7.90-7.80 and 7.45-7.33 ppm; Figure 2.28). The ^{1}H NMR spectrum analysis of the products was inconclusive due to overlapping of complex aromatic signals.[164, 165]

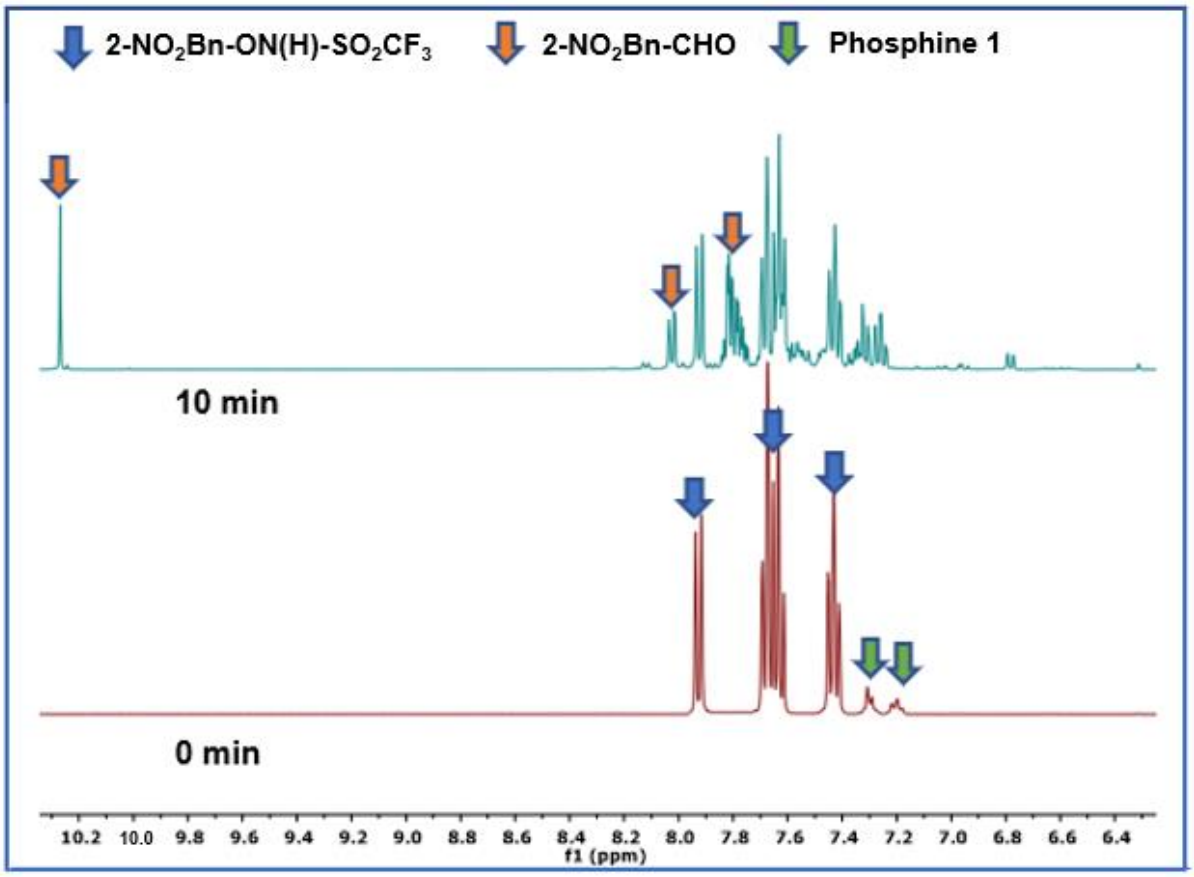

Figure 2.28. ^{1}H NMR spectra of **2-NO_2Bn-ON(H)-SO_2CF_3** (15 mM) and **Phosphine 1** (1.5 mM) in a mixture of carbonate buffer (5 mM, pH 7.0) and CD_3CN (40:60, v/v) before irradiation. The multiplet peaks centred at 7.27 and 7.37 ppm are assigned to **Phosphine 1** and the remaining peaks are assigned to **2-NO_2Bn-ON(H)-SO_2CF_3**. After 10 min irradiation peaks from **2-NO_2Bn-CHO** are observed as indicated on the spectrum.

2.3.16 Determination of the photoproduct quantum yield (Φ)

A control experiment was performed to assess the accuracy of actinometer experiments using two well-established actinometers, ferrioxalate and *trans*-azobenzene. The synthesis of ferrioxalate is described in the Experimental section, section 2.2.5.

2.3.17 Ferrioxalate and azobenzene actinometry

A control experiment was carried out to check that the actinometry procedure could be carried out satisfactorily. $[Fe(C_2O_4)_3]^{3-}$ solution (2.97 g, 6.00×10^{-3} M) was prepared by dissolving $K_3[Fe(C_2O_4)_3].3H_2O$ in H_2SO_4 (1N, 100 mL), followed by dilution to 1.00 L. An aliquot (3.00 mL) was transferred to a 10 mm pathlength quartz cuvette and irradiated for 3.0 min at 313 nm using a Xe lamp in conjunction with a monochromator (slit width 0.1 mm, 313 ± 3 nm). An aliquot (1.00 mL) of the irradiated solution was then transferred to a 10 mL volumetric flask containing aqueous phenanthroline (0.1

% m/v, 4.00 mL, stored in dark) and aqueous CH_3COONa (0.1 M, 0.5 mL). This solution was diluted with H_2O and the reaction was allowed to proceed in the dark for 15 min. The UV-Vis spectrum was recorded using a 10 mm quartz cuvette. The procedure was repeated multiple times after irradiating the $[Fe(C_2O_4)_3]^{3-}$ solution for 0, 3, 6, 9, 12 or 15 min. In this experiment, the conversion of $[Fe(C_2O_4)_3]^{3-}$ did not exceed 23%. $[Fe(C_2O_4)_3]^{2-}$ was obtained by the photochemical reduction of $[Fe(C_2O_4)_3]^{3-}$ to $[Fe(C_2O_4)_3]^{2-}$ which subsequently reacted with 1,10-phenanthroline to give $[Fe(phen)_3]^{2-}$ (Figure 2.29(a)). The number of moles of $[Fe(phen)_3]^{2+}$ was calculated using equation (2.4)

$$n = \frac{\Delta A * V_1 * 0.001 * V_3}{\varepsilon * V_2 * l} \qquad (2.4)$$

where V_1 (volume of solution) = 3 mL, V_2 (volume taken from the irradiated samples) = 1 mL, V_3 (volume after dilution for concentration determination) = 10 mL, ε_{510nm} (molar extinction coefficient) = 1.03 ± 0.02 × 10^4 M^{-1} cm^{-1}, l (pathlength) = 1 cm, ΔA=change in absorbance at 313 nm and n=number of moles of $[Fe(C_2O_4)_3]^{2+}$. Plots were drawn of the number of moles of $[Fe^{II}(C_2O_4)_3]^{2+}$ as a function of irradiation time (Figure 2.29(b)) and the data were fitted to a linear equation passing through the origin. The resulting slope was (2.56 ± 0.06) × 10^{-7} mol min^{-1}.

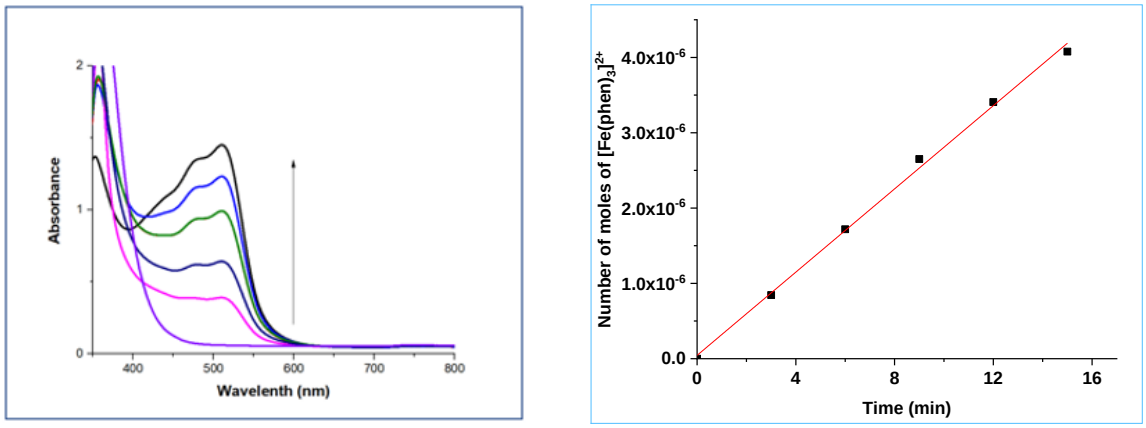

(a) (b)

Figure 2.29. (a) Plot of absorbance versus wavelength for irradiated solutions of ferrioxalate reacted with 1,10-phenanthroline. (b) The number of moles of $[Fe(phen)_3]^{2+}$ versus irradiation time (min). The slope is (2.56 ± 0.06) × 10^{-7} mol min^{-1}.

A plot of number of moles of *cis*-azobenzene versus total irradiation time was generated using the above experimental set up. Here, the photoreaction involves the photoisomerisation of *trans*-azobenzene to *cis*-azobenzene. In general, azobenzene in CH_3OH solution exists as the *trans* isomer, equation (1.19). A solution of *trans* azobenzene (6.71 x 10^{-5} M, $\varepsilon_{313\ nm}$= 22000 M^{-1} cm^{-1})[84] in CH_3OH was prepared and

stored in the dark. Azobenzene solution (3.00 mL) was transferred to a 10 mm quartz cuvette and irradiated for 0.66 min at 313 nm using a Xe lamp in conjunction with a monochromator (slit width 0.1 mm, 313 ± 3 nm). The absorbance was measured at 313 nm. The azobenzene solution was irradiated further at 0, 0.66, 1.33, 2.00, 2.66, 3.33 and 4 min and the absorbance were recorded after each irradiation.

A plot of absorbance vs irradiation time was obtained and in this experiment the conversion from *trans* to *cis* azobenzene did not exceed 8%. The $fraction_{cis}$ and the number of moles of the product *cis*-azobenzene was calculated using equations (2.5-2.6).

$$\boldsymbol{n_{cis} = fraction_{cis} * n_{reactant}} \quad (2.5)$$

$$\boldsymbol{fraction_{cis} = \frac{A_{trans} - A_{obs}}{A_{trans} - A_{cis}}} \quad (2.6)$$

where n_{cis} is the number of moles of *cis*-azobenzene product, $n_{reactant}$ is the number of moles of the *trans*-azobenzene reactant in the cuvette (= 1.98×10^{-7} mol), A_{trans} is the absorbance of *trans*-azobenzene reactant (1.47, $\varepsilon_{313\ nm}$ = 22337 M^{-1} cm^{-1} for *trans*-azobenzene)[84], A_{cis} is the absorbance of *cis*-azobenzene (0.147; ε_{313nm} = 2016 M^{-1} cm^{-1} for *cis*-azobenzene)[84] and A_{obs} is the observed absorbance at 313 nm. The number of moles of *cis*-azobenzene vs irradiation time were plotted (Figure 2.30) and the data were fitted to a linear equation. The slope for this experiment was (3.71 ± 0.08) × 10^{-8} mol min^{-1}.

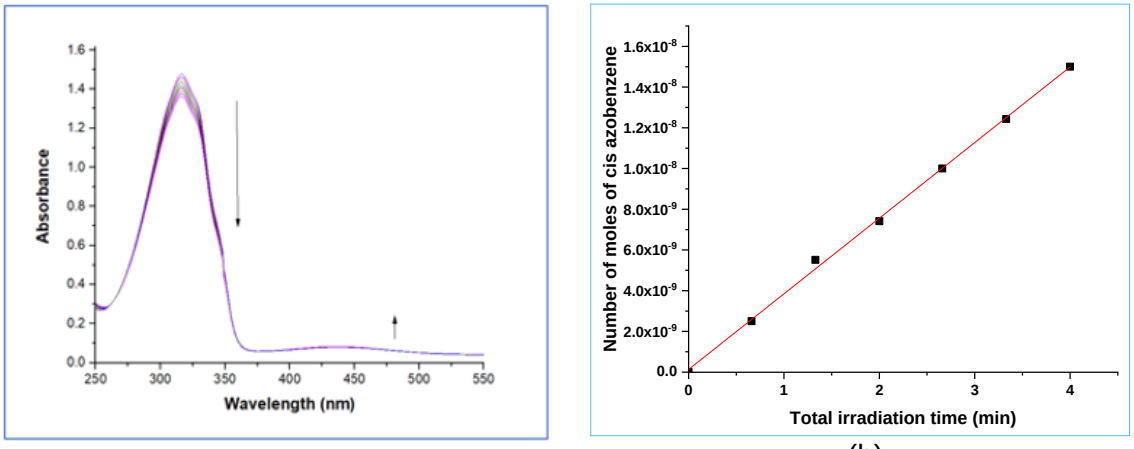

(a) (b)

Figure 2.30. (a) UV-Vis spectra for irradiated solutions of *trans*-azobenzene. (b) Plot of the number of moles of *cis*-azobenzene vs irradiation time (min). The slope is (3.71 ± 0.08) × 10^{-9} mol min^{-1}.

The photoproduct quantum yield (Φ) of the azobenzene can be calculated using equation (2.7).[157, 166]

$$\frac{\Phi\ (Azobenzene)}{\Phi\ (Ferrioxalate)} = \frac{\frac{slope\ (number\ of\ moles\ of\ cis-azobenzene\ vs\ irradiation\ time)}{Absorbance\ of\ trans\ azobenzene\ at\ 313\ nm}}{\frac{slope\ (\ number\ of\ moles\ of\ Fe(phen)2+\ vs\ irradiation\ time)}{Absorbance\ of\ Ferrioxalate\ at\ 313\ nm}} \quad (2.7)$$

The ratio of the slope (number of moles of *cis*-azobenzene vs total irradiation time) and absorbance of *trans*-azobenzene at 313 nm was (2.63 ± 0.08) × 10^{-9} mol min^{-1}. The ratio of the slope (number of moles of $[Fe(phen)_3]^{2+}$ vs irradiation time) and absorbance of ferrioxalate at 313 nm was (2.06 ± 0.08) × 10^{-8} mol min^{-1}. The absorbance of ferrioxalate was 13.35 (6.00×10^{-3} M, $\varepsilon_{313\ nm}$ = 2.22×10^3 M^{-1} cm^{-1}) and the absorbance of *trans*-azobenzene was 1.41 (6.71×10^{-5} M). The reported photoproduct quantum yield of ferrioxalate is 1.24 and the reported quantum yield of *trans*-azobenzene in CH_3OH is 0.14.[84] From the experimental data above, the ratio of Φ(azobenzene):Φ(ferrioxalate) was 1:(0.13 ± 0.01), which is in good agreement with the ratio calculated using the literature values of the quantum yields (1:0.11).[84]

2.3.18 Determination of photoproduct quantum yields of 2-NO_2Bn-ON(H)-SO_2R, 4,5-$(MeO)_2$-2-NO_2Bn-ON(H)-SO_2R and 2-NO_2Bn-OC(O)-ON(H)-SO_2CH_3

As described above, a control experiment was performed using another well-established actinometer, ferrioxalate. The ratio of the quantum yields for ferrioxalate (Φ = 1.24 in buffered acidic solution at 313 nm)[83] and *trans*-azobenzene (Φ = 0.14 in CH_3OH at 313 nm)[84] was experimentally determined at 313 (± 3) nm, using a Xe lamp equipped with a monochromator (slit width 0.1 mm) using literature procedures.[84] The ratio of Φ(azobenzene):Φ(ferrioxalate) was 1:(0.13 ± 0.01), which is in good agreement with the ratio calculated using literature values (1:0.11).

The photoproduct quantum yields of **2-NO_2Bn-ON(H)-SO_2R**, **4,5-$(MeO)_2$-2-NO_2Bn-ON(H)SO_2R** and **2-NO_2Bn-OC(O)O-N(H)-SO_2CH_3** were determined under aerobic conditions. Control experiments demonstrated that both the observed rate constants for decomposition and the photolytic products distribution from the photolysis of these compounds obtained in the mixture of CD_3OD/phosphate buffer (5 mM, pH 7.0) (60:40 v/v) are the same in the absence or presence of air. A stock solution of **2-NO_2Bn-ON(H)-SO_2R**, **4,5-$(MeO)_2$-2-NO_2Bn-ON(H)-SO_2R** and **2-NO_2Bn-OC(O)-ON(H)-SO_2CH_3** (10.0 mM) in CD_3OD was used to prepare a series of solutions of **2-NO_2Bn-**

ON(H)-SO_2R, **4,5-$(MeO)_2$-2-NO_2Bn-ON(H)-SO_2R** and **2-NO_2Bn-OC(O)-ON(H)-SO_2CH_3** (1.00 mM), with TSP and Ph-CF_3 as an internal reference for the ^{1}H and ^{19}F NMR experiments, respectively. For each compound the photolysis of a series of samples was carried out at 313 ± 3 nm (Xe lamp + monochromator) for a range of irradiation times. After irradiation, an aliquot of each sample was transferred into an NMR tube and the photoproducts characterized by NMR spectroscopy (**2-NO_2Bn-ON(H)-SO_2CF_3** and **4,5-$(MeO)_2$-2-NO_2Bn-ON(H)-SO_2CF_3** by ^{19}F NMR spectroscopy; **2-NO_2Bn-ON(H)-SO_2CH_3**, **4,5-$(MeO)_2$-2-NO_2Bn-ON(H)-SO_2CH_3** and **2-NO_2Bn-OC(O)-ON(H)-SO_2CH_3** by ^{1}H NMR spectroscopy).

The percentage decomposition of the starting material was less than 10% at the longest irradiation time. The moles of the photoproduct, RSO_2NH_2 (R = Me or CF_3) and RSO_2^-, determined from integration of a peak of the starting material, $CF_3SO_2NH_2$ and $CF_3SO_2^-$ and the initial concentration of **2-NO_2Bn-ON(H)-SO_2CF_3** and **4,5-$(MeO)_2$-2-NO_2Bn-ON(H)-SO_2CF_3** prior to irradiation. A similar calculation was performed to calculate the number of moles of photoproduct ($CH_3SO_2NH_2$) for **2-NO_2Bn-ON(H)-SO_2CH_3** and **4,5-$(MeO)_2$-2-NO_2Bn-ON(H)-SO_2CH_3**. The total number of moles of the photoproduct CH_3SO_2NHOH, $CH_3SO_2^-$ and $CH_3SO_3^-$ (determined from integration of the CH_3 peak of the starting material, CH_3SO_2NHOH, $CH_3SO_2^-$ and $CH_3SO_3^-$ and the initial concentration of **2-NO_2Bn-OC(O)-ON(H)-SO_2CH_3** prior to irradiation) was determined for each sample, and this value was plotted versus irradiation time (min). The slope of each plot of moles of photoproduct versus total irradiation time was determined (Figure 2.31).

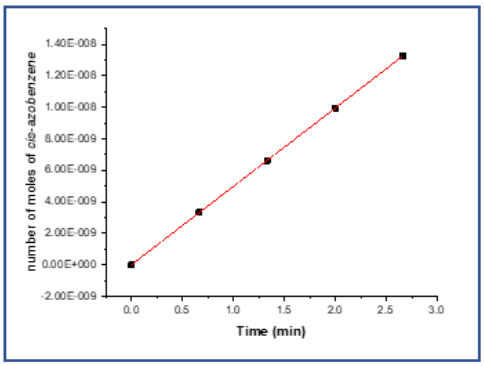

(a)

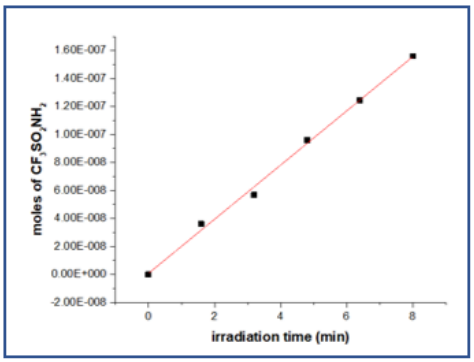

(b)

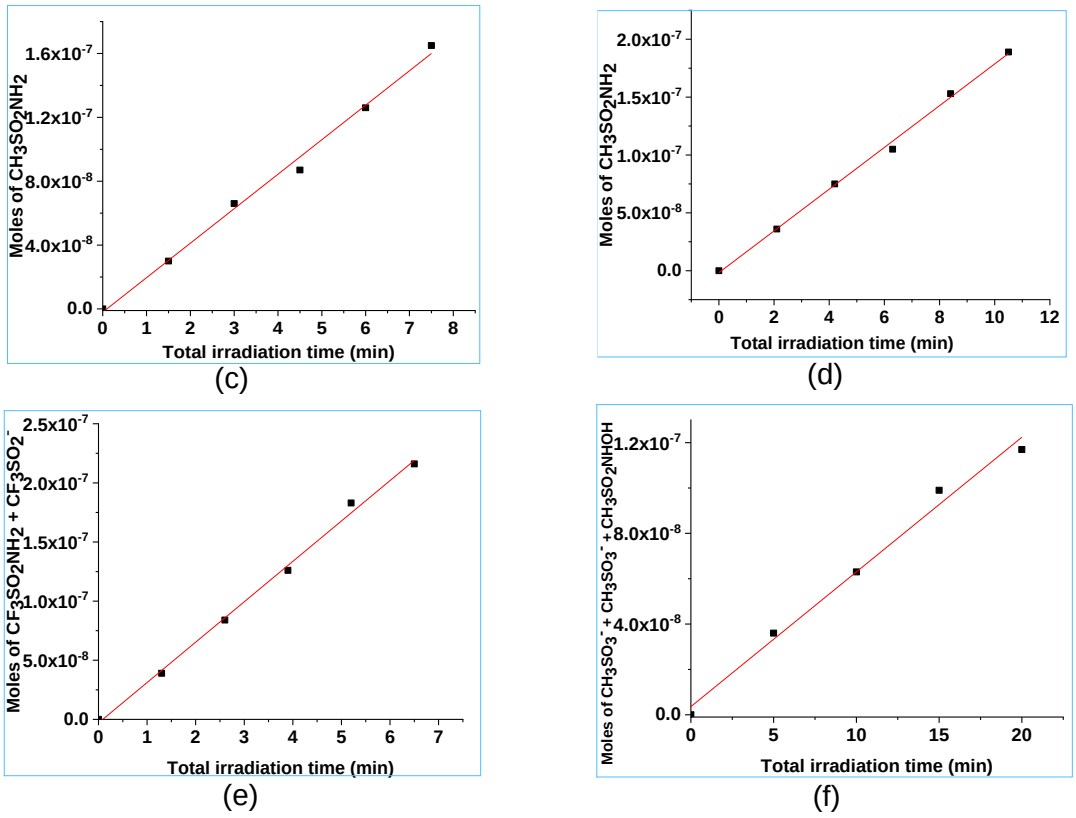

Figure 2.31. (a) Plot of the number of moles of *cis*-azobenzene versus total irradiation time (min). The best fit of the data to straight line gives a slope of (4.28 ± 0.03) × 10^{-9} mol min^{-1} (b) Plot of the number of moles of the photoproduct $CF_3SO_2NH_2$ and $CF_3SO_2^-$ versus total irradiation time (min) for **2-NO_2Bn-ON(H)-SO_2CF_3**. The best fit of the data to a straight line gives a slope of (1.95 ± 0.03) × 10^{-8} mol min^{-1}. (c) Plot of the number of moles of $CH_3SO_2NH_2$ versus total irradiation time (min) for **2-NO_2Bn-ON(H)-SO_2CH_3**. The best fit of the data to a straight line gives a slope of (1.78 ± 0.03) × 10^{-8} mol min^{-1}. (d) Plot of the number of moles of $CF_3SO_2NH_2$ and $CF_3SO_2^-$ vs total irradiation time (min) for **4,5-$(MeO)_2$-2-NO_2Bn-ON(H)-SO_2CF_3**. The best fit of the data to a straight line gives a slope of (3.35 ± 0.03) × 10^{-8} mol min^{-1}. (e) Plot of the number of moles of $CH_3SO_2NH_2$ versus total irradiation time (min) for **4,5-$(MeO)_2$-2-NO_2Bn-ON(H)-SO_2CH_3**. The best fit of the data to a straight line gives a slope of (2.12 ± 0.03) × 10^{-8} mol min^{-1}. (f) Plot of the total number of moles of $CH_3SO_3^-$, $CH_3SO_2^-$ and CH_3SO_2NHOH versus total irradiation time (min) for **2-NO_2Bn-OC(O)-ON(H)-SO_2CH_3**. The best fit of the data to a straight line gives a slope of (6.18 ± 0.03) × 10^{-9} mol min^{-1}.

Molar extinction coefficient values at 313 nm are also required to calculate the photoproduct quantum yields. Therefore, the absorbance of solutions of **2-NO_2Bn-ON(H)-SO_2R**, **4,5-$(MeO)_2$-2-NO_2Bn-ON(H)-SO_2R** and **2-NO_2Bn-OC(O)-ON(H)-SO_2CH_3** (1.00 mM) at the excitation wavelength was calculated using the molar extinction coefficient of each reactant at 313 nm. These values are listed in Table 2.6.

Table 2.6. Molar extinction coefficients of **2-NO_2Bn-ON(H)-SO_2R, 4,5-$(MeO)_2$-2-NO_2Bn-ON(H)-SO_2R** and **2-NO_2Bn-OC(O)-ON(H)-SO_2CH_3** in CD_3OD at 313 nm.

Compound	Molar extinction coefficients (M^{-1} cm^{-1})
2-NO_2Bn-ON(H)SO_2CF_3	(1.40 ± 0.02) × 10^3
2-NO_2Bn-ON(H)-SO_2CH3	(1.10 ± 0.03) × 10^3
4,5-$(MeO)_2$-2-NO_2Bn-ON(H)-SO_2CF_3	(3.50 ± 0.03) × 10^3
4,5-$(MeO)_2NO_2$-2-Bn-ON(H)-SO_2CH_3	(3.80 ± 0.04) × 10^3
2-NO_2Bn-OC(O)-ON(H)-SO_2CH_3	(1.35 ± 0.04) × 10^3

The quantum yield (Φ) for **2-NO_2Bn-ON(H)-SO_2R** were calculated using equation (2.8), with Φ(*trans*-azobenzene) = 0.14.[84] Similarly, the quantum yields (Φ) for **4,5-$(MeO)_2$-2-NO_2Bn-ON(H)-SO_2R** and **2-NO_2Bn-OC(O)-ON(H)-SO_2CH_3** were calculated.

$$\phi\,(\text{2-NO}_2\text{Bn-ON(H)-SO}_2\text{R}) = \frac{\text{slope (2-NO}_2\text{Bn-ON(H)-SO}_2\text{R) / Absorbance (2-NO}_2\text{Bn-ON(H)-SO}_2\text{R)}}{\text{Slope (Azobenzene) / Absorbance (azobenzene)}} \times \phi\,(\text{azobenzene}) \quad (2.8)$$

The photoproduct quantum yields were 0.67 ± 0.03 (**2-NO_2Bn-ON(H)-SO_2CF_3**), 0.77 ± 0.03 (**2-NO_2Bn-ON(H)-SO_2CH_3**), 0.46 ± 0.02 (**4,5-$(MeO)_2$-2-NO_2Bn-ON(H)SO_2CF_3**), 0.27 ± 0.01 (**4,5-$(MeO)_2$-2-NO_2Bn-ON(H)-SO_2CH_3**), and 0.23 ± 0.01 (**o-NO_2Bn-OC(O)ON(H)SO_2CH_3**), respectively. Photoproduct quantum yield values for **2-NO_2Bn-ON(H)-SO_2CF_3** (0.67 ± 0.03) and **2-NO_2Bn-ON(H)-SO_2CH_3** (0.77 ± 0.03) were higher in comparison to structurally related nitrobenzyl systems (Φ= 0.49 for 2-nitrobenzyl methyl ether[101]), with the leaving group affecting the photoproduct quantum yield.[89] The similarity in the quantum yield values for **2-NO_2Bn-ON(H)-SO_2CF_3** and **2-NO_2Bn-ON(H)-SO_2CH_3** was expected as these compounds are structurally similar. The photoproduct quantum yields of **4,5-$(MeO)_2$-2-NO_2Bn-ON(H)-SO_2CF_3** (0.46 ± 0.02) and **2-NO_2Bn-OC(O)-ON(H)-SO_2CH_3** (0.27 ± 0.01) were lower as a result of the electron-donating MeO substituents on the aromatic group, which significantly reduced the photoproduct quantum yields for nitrobenzyl-caged molecules.[157, 167]

2.4 Discussion

Numerous mechanistic studies have been carried out on the photodecomposition of molecules of the type **2-NO_2Bn-O-X**, where O-X bond cleavage occurs.[89, 113, 119] Although light-induced O-N bond cleavage has previously been observed for **2-NO_2Bn-O-N-** systems,[113] little is known about the mechanism of this reaction. McCulla et al. studied the photoinduced release of benzohydroxamic acid from a 2-nitrobenzyl photoprotected conjugate and observed that both C-O and O-N bond homolysis occurs.[113] Qvortrup et al. recently reported that the amount of C-O versus N-O bond cleavage was dependent on the solvent for 2-nitrobenzyl caged hydroxamates.[119] C-O bond cleavage occurred in protic solvents whereas release of a carboxamide occurred via O-N bond cleavage in aprotic solvents.[119] For our systems, concerted C-O/N-S bond cleavage (HNO generation, Pathway 1, Scheme 2.1) is only a minor photolysis pathway for **2-NO_2Bn-ON(H)SO_2CF_3** and **4,5-$(MeO)_2$-2-NO_2Bn-ON(H)-SO_2CF_3** in protic media and the competing O-N cleavage pathway dominates (>90%). The parent HNO donor ($CF_3SO_2NHO(H)$) was not observed by ^{19}F NMR spectroscopy during the photolysis of **2-NO_2Bn-ON(H)-SO_2CF_3** and **4,5-$(MeO)_2$-2-NO_2Bn-ON(H)-SO_2CF_3**. Given that the half-life for decomposition of CF_3SO_2NHOH is ~10 min,[55] the absence of $CF_3SO_2NHO(H)$ as a reaction intermediate in the ^{19}F NMR spectra suggests that the minor decomposition pathway involves concerted C-O/N-S bond cleavage to release $CF_3SO_2^-$ and HNO (Pathway 1, Scheme 2.1), rather than C-O bond cleavage followed by thermal decomposition of $CF_3SO_2N(H)O^-$ (Pathway 2, Scheme 2.1).

There was no HNO generating pathway operating for both **2-NO_2Bn-ON(H)-SO_2CH_3** and **4,5-$(MeO)_2$-2-NO_2Bn-ON(H)-SO_2CH_3**. Instead, 100% O-N bond cleavage occurred for these compounds. The reported pK_a values for CF_3SO_2H and CH_3SO_2H are -0.6 and 2.28, respectively.[77] $CF_3SO_2^-$ is therefore a much better leaving group than $CH_3SO_2^-$ and is responsible for the small differences in the photodecomposition mechanism for these compounds compared to the corresponding molecules with CF_3SO_2- leaving groups.

In studies of the photoinduced release of benzohydroxamic acid from a 2-nitrobenzyl photocaged conjugate, McCulla and coworkers found that irradiation at a shorter wavelength favored O-N bond cleavage, whereas irradiation at longer wavelengths favored C-O bond cleavage. The photoproducts from irradiation of **2-NO_2Bn-ON(H)-**

SO_2R (R = CF_3 and CH_3) and **4,5-$(MeO)_2$-2-NO_2Bn-ON(H)-SO_2R** (R = R = CF_3 and CH_3) at two different excitation wavelengths were therefore investigated, using a xenon lamp in conjunction with a monochromator. The excitation wavelength did not have any effect on the observed photoproducts. The importance of the nitro group on photodecomposition for this family of molecules was also investigated, by studying the steady state photodecomposition of the structurally related compound **Bn-ON(H)-SO_2CF_3** which lacks the 2-nitro substituent. There was essentially no photodecomposition, hence the 2-nitro functional group plays a key role in the photoactivity of molecules **2-NO_2Bn-ON(H)-SO_2R**, **4,5-$(MeO)_2$-2-NO_2Bn-ON(H)-SO_2R** and **2-NO_2Bn-OC(O)-ON(H)-SO_2CH_3**; that is, both the C-O and O-N bond cleavage pathways are dependent on the presence of this group.

Studies were carried out to determine whether the solvent ratio and/or the pH of the aqueous component of the solvent altered the amount of C-O versus O-N bond cleavage for **2-NO_2Bn-ON(H)-SO_2CH_3**. The selectivity for C-O versus O-N bond cleavage was highly dependent on the solvent ratio (CH_3CN: phosphate buffer) for *N*-hydroxysulfonamides caged with the (6-hydroxynapthalen-2-yl)methyl chromophore.[76-78] The rate and products of photolysis of **2-NO_2Bn-ON(H)-SO_2CH_3** were investigated at various CH_3CN:phosphate buffer (5.0 mM) solvent ratios. Only O-N, not C-O, bond cleavage was observed at all solvent ratios. The observed rate constant was independent of the solvent ratio, suggesting that photodecomposition occurs via a series of (solvent-independent) intramolecular reactions.

In previous studies, the pH of the solution was found to affect the observed rate of photodecomposition of 2-nitrobenzyl compounds which decompose via C-O bond cleavage.[101-103] Specifically, the rate of cyclization of the aci-nitro intermediate to the 1,3-dihydrobenz-[c]isoxazol-1-ol intermediate, the formation of hemiacetal intermediate via ring opening and the hydrolysis of the hemiacetal intermediate were pH-dependent processes.[101] The effect of the pH of the aqueous component in the solvent mixture was investigated on the photodecomposition of **2-NO_2Bn-ON(H)-SO_2CH_3**, to determine whether pH could influence the selectivity for C-O versus O-N bond cleavage. Varying the pH of the aqueous component had no effect on the observed rate constant for photodecomposition or the nature of the photolytic products derived from **2-NO_2Bn-ON(H)-SO_2CH_3**, with only O-N bond cleavage occurring.

The photolysis data discussed above were all obtained under anaerobic conditions. To probe the effect of oxygen on the mechanism of the reaction, the

photodecomposition of **2-NO_2Bn-ON(H)-SO_2CH_3** was also studied under aerobic conditions. The ^{1}H NMR spectrum of the photoproducts was identical to that observed under anerobic conditions; hence the presence of O_2 has no effect.

Laser flash photolysis experiments were carried out to determine whether the expected aci-nitro intermediate is observed for **2-NO_2Bn-ON(H)-SO_2CH_3** and **4,5-$(MeO)_2$-2-NO_2Bn-ON(H)-SO_2CH_3**. For both molecules the aci-nitro species were observed and decomposed on the μs time scale, which is in good agreement with the literature.[89, 101, 168]

Efficient trapping of HNO released upon the thermal decomposition of CF_3SO_2NHOH was demonstrated using the phosphine TXPTS and the vitamin B_{12} derivative HOCbl by ^{31}P NMR spectroscopy and UV-Vis spectroscopy, respectively, in an alkaline aqueous solution. The highly water soluble $CF_3SO_2NHO(H)$ decomposes rapidly at pH 10 to stoichiometrically release HNO. However release of HNO upon irradiation of **2-NO_2Bn-ON(H)-SO_2-CF_3** could not be confirmed using either the TXPTS and HOCbl trapping molecules. This is probably because the percentage of concerted C-O/N-S bond cleavage to release HNO versus O-N bond cleavage was so small (9%). It is also possible that NOCbl is photosensitive, releasing (H)NO upon irradiation.

Photochemical O-N bond scission is a commonly observed pathway in many hydroxamic acid and alkyl hydroxamate systems.[169, 170] However, as mentioned earlier, Qvortrup noted that the photolytic release of hydroxamic acids caged by the NB PPG was observed via C-O cleavage in protic solvents in high yield,[118, 119] while competing O-N bond cleavage leading to carboxamides was observed in aprotic solvents.[119] Th proposed photodecomposition pathways for **2-NO_2Bn-ON(H)-SO_2R** and **4,5-$(MeO)_2NO_2$Bn-ON(H)-SO_2R** are shown in Scheme 2.5. Based on an examination of the mechanistic insights for these competing C-O and O-N cleavage pathways proposed by Qvortrup, we hypothesize that the reversal in selectivity for C-O vs O-N bond cleavage in protic media with our substrates **2-NO_2Bn-ON(H)-SO_2R** and **4,5-$(MeO)_2NO_2$Bn-ON(H)-SO_2R** is due to the presence of the better sulfonamido leaving group in **2-NO_2Bn-ON(H)-SO_2R** and **4,5-$(MeO)_2$-2-NO_2Bn-ON(H)-SO_2R** compared with the carboxamido leaving group of the Qvortrup systems. The sulfonamido moieties are clearly better leaving groups as evidenced by their pK_a values. Reported pK_a values for $CF_3SO_2NH_2$ are 6.33 (H_2O)[171] and 9.7 (DMSO).[172] Reported pK_a values for $CH_3SO_2NH_2$ are 10.8 (H_2O)[171] and 17.5 (DMSO)[172] and the pK_a values for $CH_3C(O)NH_2$ are 15.1 (H_2O)[173] and 25.5 (DMSO).[172] Therefore,

depending on the solvent, the sulfonamide NH proton is approximately 10^4 to 10^8 times more acidic than the analogous carboxamide proton. With a weaker (amide) leaving group, Qvortrup observed protic solvent-mediated *(Z)-(E)* isomerization of the *aci*-nitro intermediate, leading to cyclization and then C-O cleavage as the dominant pathway. In our system, we hypothesize that rapid O-N cleavage with loss of a (better) sulfonamide leaving group occurs before there is an opportunity for the *(Z)-(E)* isomerization required for concerted C-O/N-S cleavage. This is consistent with this pathway exhibiting no dependence on either the solvent ratio or the pH of the aqueous component of the solvent mixture.

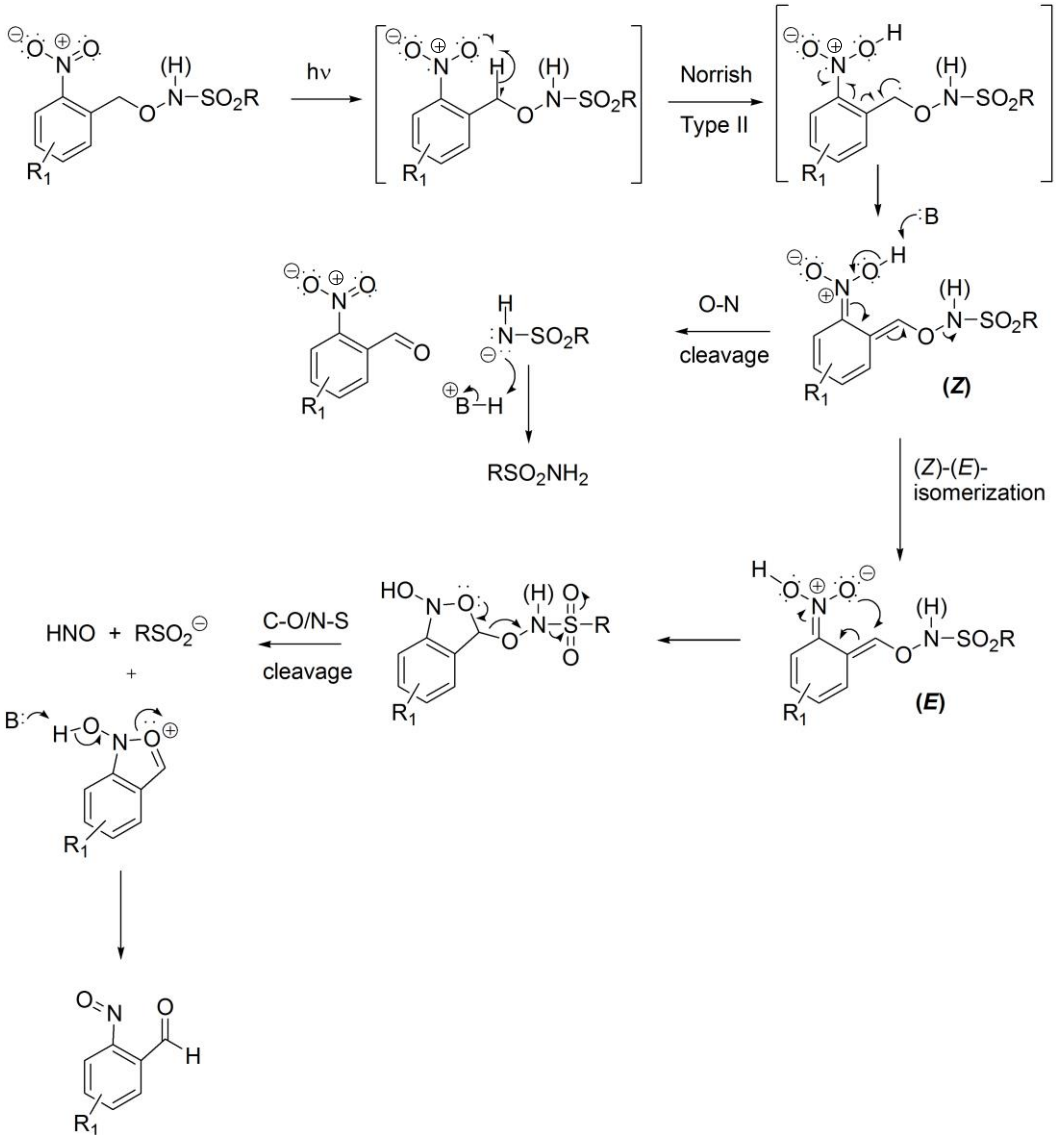

Scheme 2.5. Proposed mechanism for photolysis of **2-NO_2Bn** -caged HNO donors **2-NO_2Bn-ON(H)-SO_2R and 4,5-$(MeO)_2$-2-NO_2Bn-ON(H)-SO_2R (**R = CF_3 and CH_3). The C-O/N-S bond cleavage pathway via the *(E)*-aci-nitro intermediate was only observed for R = CF_3. Note that (*E)* and (*Z)* isomers are also possible with respect to the other alkene in the aci-nitro intermediate.

In contrast, the carbonate linked CH_3SO_2-derivative **2-NO_2Bn-OC(O)-ON(H)-SO_2CH_3** generated mostly the parent HNO donor CH_3SO_2NHOH (71%) *via* C-O bond cleavage, along with a small quantity of HNO (diagnosed by the presence $CH_3SO_2^-$, presumably formed *via* a concerted C-O/N-S bond cleavage mechanism) and $CH_3SO_2NH_2$, formed *via* direct O-N bond cleavage, Scheme 2.6. Control experiments demonstrated that CH_3SO_2NHOH is stable in the protic solvent mixture used for these studies due to its high pK_a value (9.95),[119] which precludes direct deprotonation and subsequent decomposition of CH_3SO_2NHOH to yield $CH_3SO_2^-$. Therefore, any $CH_3SO_2NHO^-$ formed from the photolysis of **2-NO_2Bn-OC(O)-ON(H)-SO_2CH_3** would be rapidly protonated to form CH_3SO_2NHOH under our photolytic conditions (pH 7.0). The small amount of $CH_3SO_2^-$ must therefore be formed via a minor competing C-O/N-S concerted decomposition pathway. The formation of small amounts of $CH_3SO_2NH_2$ results from competing O-N bond cleavage. The dramatic change in selectivity here vis-à-vis substrates **2-NO_2Bn-ON(H)-SO_2R** and **4,5-$(MeO)_2$-2-NO_2Bn-ON(H)-SO_2R** is likely due to the more enthalpically demanding bond cleavage requirements necessary for ultimate N-O cleavage. This presumably allows for competition from ***(Z)-(E)***-isomerization of the aci-nitro intermediate which permits the C-O cleavage pathway to dominate.

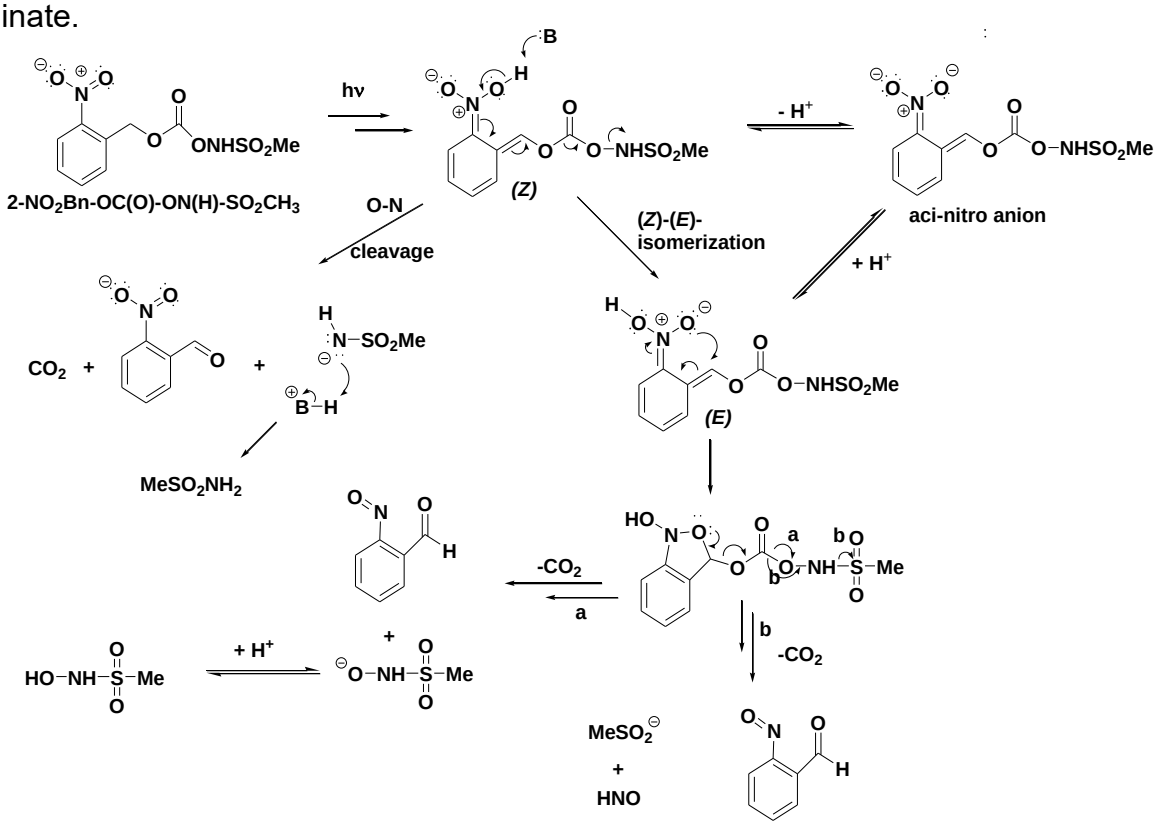

Scheme 2.6. Proposed mechanism for photolysis of carbonate linked **2-NO_2Bn-OC(O)-ON(H)-SO_2CH_3**.

In summary, the photodecomposition of **2-NO_2Bn-ON(H)-SO_2R** (R = CF_3 and CH_3), **4,5-$(MeO)_2$-2-NO_2Bn-ON(H)-SO_2R** (R = CF_3 and CH_3) and **2-NO_2Bn-OC(O)-ON(H)-SO_2CH_3** - photocaged *N*-hydroxysulfonamides has been investigated. Reasonable photoproduct quantum yields were obtained for all the systems, by actinometry. **2-NO_2Bn-ON(H)-SO_2CF_3** and **4,5-$(MeO)_2$-2-NO_2Bn-ON(H)-SO_2CF_3** release a small amount of HNO (9%) via concerted C-O/N-S bond cleavage, with 91% O-N bond cleavage. For **2-NO_2Bn-ON(H)-SO_2CH_3** and **4,5-$(MeO)_2$-2-NO_2Bn-ON(H)-SO_2CH_3**, only O-N bond cleavage occurs, to generate a sulfonamide. MeO substituents at the 4 and 5 positions of the aromatic ring do not affect the photoproduct percentages, whereas the 2-nitro substituent is essential for photodecomposition. For **4,5-$(MeO)_2$-2-NO_2Bn**, only O-N bond cleavage occurred regardless of the solvent ratio, the pH of the aqueous component and the absence or presence of oxygen. An aci-nitro intermediate was detected for **2-NO_2Bn-ON(H)-SO_2CH_3** and **4,5-$(MeO)_2$-2-NO_2Bn-ON(H)-SO_2CH_3** by laser flash photolysis. **2-NO_2Bn-OC(O)ON(H)SO_2CH_3** primarily undergoes C-O bond cleavage with the release of CH_3SO_2NHOH. A concerted C-O/N-S $MeSO_2$–releasing decomposition pathway and a pathway involving O-N bond cleavage were observed as minor pathways for this system. Mechanisms of photodecomposition have been proposed for both systems, with initial events involving 1,5-hydrogen atom abstraction to generate a *(Z)*-aci-nitro intermediate.

Chapter 3: Studies of Photoactivatable *N*-Hydroxysulfonamide-caged HNO Donors incorporating the (2-Nitrophenyl)ethyl (2-NPE) Phototrigger

3.1 Introduction

In Chapter 2 it was shown that 2-nitrobenzyl (2-NO_2Bn) tethered *N*-hydroxysulfonamides primarily undergo O-N bond cleavage. The desired C-O/N-S bond cleavage was a minor pathway, resulting in the production of a small amount of HNO. It was also shown that **2-NO_2Bn-OC(O)-ON(H)-SO_2CH_3** mainly underwent C-O bond cleavage to produce CH_3SO_2NHOH.[150] The 2-NO_2Bn moiety has been extensively used for photocaging molecules and its reaction mechanism has been investigated in detail.[101] Upon excitation an aci-nitro intermediate is formed.[101] The aci-nitro intermediate decays at a rate of roughly 10^2–10^4 s^{-1}, and is dependent on the substituents on the aromatic ring, pH and solvent conditions.[101]

This chapter explores the mechanisms of photodecomposition of three *N*-hydroxysulfonamides caged with the much-less well-studied (2-nitrophenyl)ethyl photocage, Figure 3.1. *N*-Hydroxy-2-methanesulfonyl benzenesulfonamide (CXL-1020) was used in addition to the $CH_3SO_2N(H)O^-$ and $CF_3SO_2N(H)O^-$ head groups. CXL-1020 is a most promising HNO donor which is currently in Phase IIa clinical trials for treating congestive failure.[23]

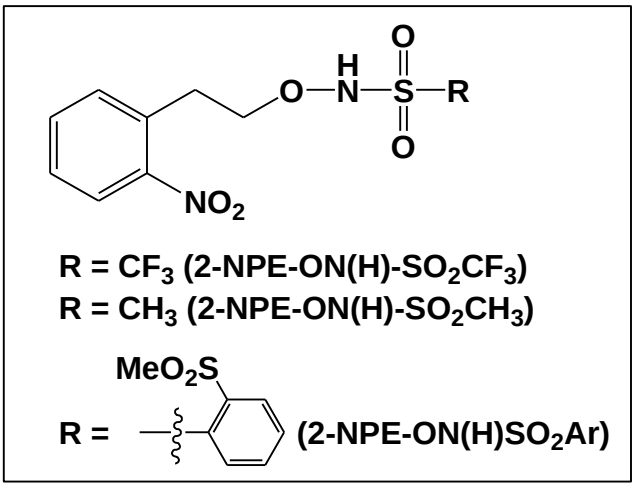

Figure 3.1. Structures of the **(2-nitrophenyl)ethyl (2-NPE)** photocaged *N*-hydroxysulfonamides investigated in this chapter.

3.2 Experimental section

3.2.1 Chemicals

2-NPE-ON(H)-SO_2CF_3, **2-NPE-ON(H)-SO_2CH_3**, **2-NPE-ON(H)-SO_2Ar** (Ar = 2-($MeSO_2$)Ph), 2-nitrostyrene, 2-nitrophenylacetaldehyde, 2-($MeSO_2$)$PhSO_2NH_2$ ($ArSO_2NH_2$), 2-($MeSO_2$)$PhSO_2^-$ ($ArSO_2^-$) and 2-($MeSO_2$)$PhSO_2NHOH$ ($ArSO_2NHOH$) were obtained from the lab of our collaborators at Kent State University, USA, Prof. Paul Sampson and Dr. Alexander Seed. The synthesis and characterization of these compounds was presented in the PhD thesis of Mohammad Saifur Rahman. [152] The purity of each compound was checked before conducting photolysis experiments using ^1H and/ or ^{19}F NMR spectroscopy. Methyl phenyl sulfone and 2-nitrophenethyl alcohol were purchased from AK Scientific Inc. Sodium trifluoromethanesulfinate ($NaCF_3SO_2$, 98%), sodium methanesulfinate ($NaCH_3SO_2$, 92%), trifluoromethanesulfonic acid (CF_3SO_3H, 98%), trifluromethanesulfonamide ($CF_3SO_2NH_2$) and methanesulfonamide ($CH_3SO_2NH_2$) were purchased from Sigma-Aldrich.

3.2.2 Determining the molar extinction coefficient of 2-NPE-ON(H)-SO_2R

Standard solutions of **2-NPE-ON(H)-SO_2R** (100, 150, 200, 250, 300, 350 and 400 µM) were prepared in a mixture of aerobic H_2O and CH_3CN (92:8 v/v) and UV-Vis spectra were recorded (25.0 ºC). The molar extinction coefficients were obtained from plots of absorbance versus concentration (Figure A3.1, Appendix), at 264 nm (**2-NPE-ON(H)-SO_2CF_3** and **2-NPE-ON(H)-SO_2CH_3**) or 272 nm (**2-NPE-ON(H)-SO_2Ar**).

3.2.3 Steady state photolysis experiments

Steady state photolysis experiments were carried out using the same procedure described in section 2.2.4 (Chapter 2). Unless otherwise stated, all experiments were carried out under anaerobic conditions. The concentration of the 2-NPE caged *N*-hydroxysulfonamide was ~1.0 mM.

The effect of the ratio of the solvent components for mixtures of CD_3CN and phosphate buffer (prepared in H_2O, pH 7.0, 30 mM) on the photoproducts and rate of photodecomposition was determined (~1.0 mM **2-NPE-ON(H)-SO_2R**). The samples were irradiated using a Rayonet photoreactor (RMR-600, 300 nm). After each irradiation, the sample was analyzed by ^1H and/or ^{19}F NMR spectroscopy. The effect

of the pH of the aqueous component of the solvent (10% v/v CD_3CN in aqueous buffer (30 mM)), on the photoproducts and the rate of decomposition was also investigated. The aqueous component of the solution was phosphate, acetate or carbonate buffer in H_2O. The reported pH value is the pH of the aqueous component.

3.2.4 Determination of pK_a by UV-Vis spectroscopy

2-NPE-ON(H)-SO_2CF_3 was dissolved in a mixture of aerobic CH_3CN and H_2O (8:92 v/v; CH_3CN:H_2O). The solution was circulated using a peristaltic pump through a 1 cm path length quartz flow-through cell at 25.0 °C. A small volume of acid (~1 M HCl; negligible change in total volume of the solution) was added to the solution (3.5×10^{-5} M, 30 mL). Absorbance spectra were recorded after the pH had stabilized in the reservoir flask. The absorbance as a function of pH was plotted to obtain the pK_a value.

3.2.5 Determination of pK_a by NMR spectroscopy

To determine the pK_a of **2-NPE-ON(H)-SO_2CF_3**, **2-NPE-ON(H)-SO_2CH_3** and **2-NPE-ON(H)-SO_2Ar**, the pH of an aqueous solution of D_2O was adjusted to the desired value (pD = pH + 0.4).[174] A small volume of **2-NPE-ON(H)-SO_2R** dissolved in CH_3CN was then added to the aerobic aqueous solution. The final solution was ~1.0 mM **2-NPE-ON(H)-SO_2-R** (total volume 0.45 mL) with 8% v/v CH_3CN in deuterated aqueous buffer. A constant ionic strength of 1.0 M was maintained, by the addition of $NaCF_3SO_3$. ^{19}F and ^{1}H NMR spectra were recorded for **2-NPE-ON(H)-SO_2CF_3**, whereas ^{1}H NMR spectra were recorded for **2-NPE-ON(H)-SO_2CH_3** and **2-NPE-ON(H)-SO_2Ar** as a function of pH. The following aqueous solutions were prepared in D_2O: 0.10 M HCl (pD 1.4), phosphate buffer (30 mM, pD 2.4-3.9 and 6.2-8.2), acetate buffer (30 mM, pD 4.0-6.0), borate buffer (30 mM, pD 8.9-9.9), carbonate buffer (30 mM, pD 9.6-11.0), and 0.010 M NaOH (pD 12.4).

3.2.6 Determination of the Photoproduct Quantum Yields (ϕ)

The photoproduct quantum yields were determined in CH_3OH using the same protocol as carried out for the 2-NO_2Bn compounds, under aerobic conditions (Section 2.3.15, Chapter 2).[150]

3.2.7 Synthesis of Piloty's acid ($PhSO_2NHOH$, PA)

The synthesis of PA was carried out using a literature procedure.[156, 175] The yield obtained was 39% and the purity of PA was checked by ^{1}H NMR spectroscopy and

was found to be 99%. ^{1}H NMR spectrum was recorded in d_6-acetone (7.94, 7.93, 7.92, 7.71, 7.69, 7.64, 7.62, 7.60 ppm) (Figure A3.2, Appendix). The chemical shifts of the product were in agreement with previously reported values.[156, 175]

3.2.8 Determining the pK_a for $PhSO_2NHOH$ and $Ph(2\text{-}MeSO_2)SO_2NHOH$ (CXL-1020, $ArSO_2NHOH$)

The spontaneous thermal decomposition of **$PhSO_2NHOH$** and **$Ph(2\text{-}MeSO_2)SO_2NHOH$ ($ArSO_2NHOH$**) was monitored by UV-Vis spectroscopy in a mixture of aqueous solution and a minimal volume of CH_3OH at a range of pH conditions (3-12, 30 mM). A stock solution of **$Ph(2\text{-}MeSO_2)SO_2NHOH$** (1.52 mg in 150 µL, 0.041 M) was prepared in CH_3OH. An aliquot of this solution (50 µL, 0.67 mM) was transferred to a cuvette containing 2.95 mL aqueous buffer solution (I= 1.0 M, $NaCF_3SO_3$) that had been thermostated in the cell holder of the Cary instrument for 15 min at 25.0 °C. The following buffers were used: phosphate buffer (30 mM, pH 2-3.5 and 5.8-7.8), acetate buffer (30 mM, pH 3.6-5.6), carbonate buffer (30 mM, pH 9.2-10.6), CAPS buffer (9.7-11.1), TAPS buffer (pH 7.1-9.1) and 0.010 M NaOH (pH 12.0). The final solution concentration was ~0.67 mM (total volume 3.00 mL) with 2% v/v CH_3CN in aqueous buffer. A similar procedure was used to determine the pK_a of **$PhSO_2NHOH$**. UV-Vis spectra were recorded in a mixture of 2% CH_3CN in aqueous buffer at different pH conditions.

3.2.9 Instruments and Methods

GC-MS analysis was carried out using an Agilent 7890A GC equipped with a 5977A mass spectrometer detector with an electron Impact ionization source. An Agilent DB-1701 column (3 mm x 0.25 mm x 0.25 µm) was used. The inlet temperature was set at 280 °C and the samples were injected in pulsed split mode with a split ratio of 10:1. The initial column temperature was held at 45 °C for 2 min and then ramped at 20 °C/min to 280 °C and held for 10 min. The total run time was 23.75 min. The MSD transfer line was held at 250 °C, ion source at 250 °C and the quad at 150 °C. The MSD was operated in scan mode with a mass range 38-650 Da and the solvent delay was 6.5 min.

Flow-injection ESI-MS analyses were conducted using an Agilent 6420 triple quadrupole MS system with electrospray ionization. The MS ionization source

conditions were as follows: capillary voltage of 4 kV, drying gas temperature of 300 °C, drying gas flow of 10 L/min, nebulizer pressure of 30 psi. The positive scan mode was performed with a scan range of 70-500 m/z. The mobile phase was 50% acetonitrile in milliQ H_2O with 0.1% formic acid and the injection volume was 5 µL.

3.2.10 Laser flash photolysis experiments

Details of the instrument used are given in Chapter 2, section 2.2.6.

3.3 Results

3.3.1 UV-Vis spectra of 2-NPE-ON(H)-SO_2CF_3, 2-NPE-ON(H)-SO_2CH_3, and 2-NPE-ON(H)-SO_2Ar

2-NPE-ON(H)-SO_2R was characterized by UV-Vis spectroscopy, Figure 3.2. The wavelength maximum of **2-NPE-ON(H)-SO_2CF_3** and **2-NPE-ON(H)-SO_2CH_3** at 264 nm can be assigned to an n-π^* transition.[157] The wavelength maximum of **2-NPE-ON(H)-SO_2Ar** (Ar = 2-($MeSO_2$)Ph) is slightly shifted to 272 nm due to the $ArSO_2$ chromophore. The molar extinction coefficients of **2-NPE-ON(H)-SO_2CF_3**, **2-NPE-ON(H)-SO_2CH_3** and **2-NPE-ON(H)-SO_2Ar** were (2.87 ± 0.01) × 10^3 M^{-1} cm^{-1} (264 nm), (4.17 ± 0.01) × 10^3 M^{-1} cm^{-1} (264 nm) and (6.06 ± 0.03) × 10^3 M^{-1} cm^{-1} (272 nm) respectively, in a mixture of H_2O and CH_3CN (92:8, v/v). The plots are shown in Figure A3.1, Appendix.

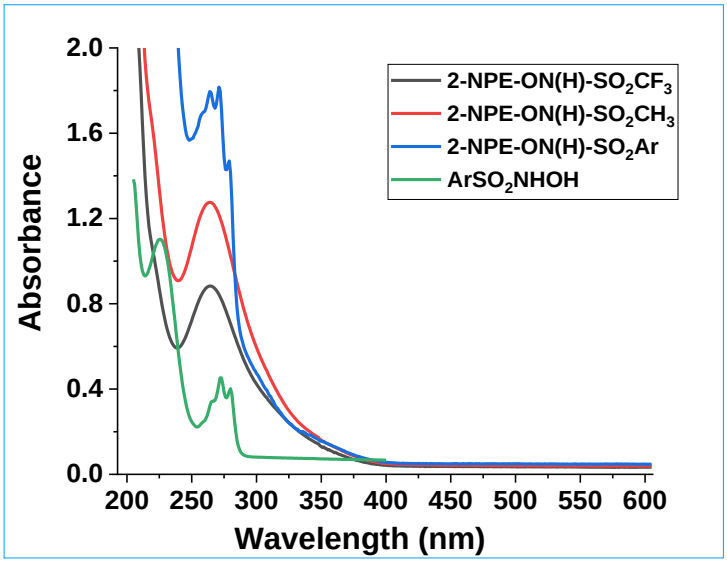

Figure 3.2. UV-Vis spectra of **2-NPE-ON(H)-SO_2CF_3**, **2-NPE-ON(H)-SO_2CH_3**, **2-NPE-ON(H)-SO_2Ar** and **$ArSO_2NHOH$** (-Ph(2-$MeSO_2$)SO_2NHOH) (3.00 × 10^{-4} M) in a mixture of H_2O and CH_3CN (92:8, v/v) at 25 °C.

3.3.2 Thermal stability of 2-NPE-ON(H)-SO_2CF_3, 2-NPE-ON(H)-SO_2CH_3 and 2-NPE-ON(H)-SO_2Ar

The thermal stability was checked for each compound prior to carrying out steady state irradiation experiments. The ^{19}F and/or ^{1}H NMR spectra of **2-NPE-ON(H)-SO_2CF_3**, **2-NPE-ON(H)-SO_2CH_3** and **2-NPE-ON(H)-SO_2Ar** were recorded ~10 min after dissolving each compound in a mixture of phosphate buffer (30 mM, pH 7.0) and CD_3CN (40:60, v/v) and 16 h later. No thermal decomposition was observed.

3.3.3 Determination of the ground state pK_a of 2-NPE-ON(H)-SO_2R

To understand better what factor(s) determine whether O-N bond cleavage or C-O or C-O/N-S bond cleavage occurs, the ground state pK_a for each 2-NPE-caged compound was determined. The previously reported pK_a value for the N(H) of the structurally similar 6-(hydroxynaphthalen-2-yl)methyl-photocaged *N*-hydroxysulfonamide (6,2-HNM-ON(H)-SO_2CF_3) is 4.4 ± 0.1.[78] Deprotonation of the N(H) of **2-NPE-ON(H)-SO_2R** (**R = CF_3, CH_3, Ar**) would also be expected to occur in aqueous solution, equation (3.1).

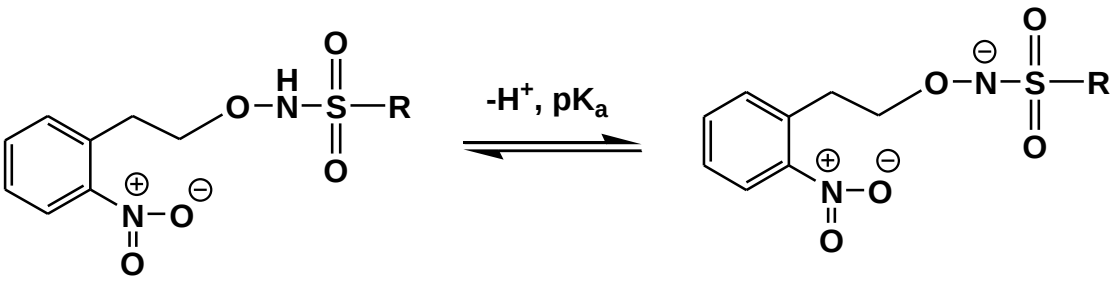

(3.1)

UV-Vis spectrophotometric titrations were conducted to obtain a pK_a value for deprotonation of the N(H) of **2-NPE-ON(H)-SO_2CF_3**. A small volume of acid (~1 M HCl; negligible change in total volume of the solution) was added to an aqueous solution of **2-NPE-ON(H)-SO_2CF_3** (3.5×10^{-5} M, 30 mL). The aqueous solution of **2-NPE-ON(H)-SO_2CF_3** was circulated using a peristaltic pump through a 1 cm path length quartz flow-through cell at 25.0 °C. UV-Vis spectra were recorded after the pH stabilized in the reservoir flask. There was, however, no significant change in the UV-Vis spectra since the deprotonation site is so far away from the aromatic part of the molecule.

^{19}F NMR spectra for **2-NPE-ON(H)-SO_2CF_3** were therefore recorded with the pD of the aqueous component of the D_2O/CH_3CN solvent mixture varying from pD ~1.9-10.2,

to obtain an estimate for the pK_a value. In this pD range **2-NPE-ON(H)-SO_2CF_3** is stable in the solvent. A small amount of CH_3CN (5% v/v CH_3CN) was required to ensure that the compound was fully dissolved. The chemical shift of the C*F*$_3$ signal progressively increased as the pD was increased from 1.93 to 5.44, since the CF_3 group is located close to the N(H) and experiences more electron density upon deprotonation (Figure 3.3(a) and Table 3.1). From pD 5.44 to 10.23 the chemical shift of **2-NPE-ON(H)-SO_2CF_3** (CF_3 signal) was unchanged (0.2 ± 0.1 ppm) as expected, since the protonation state of the molecule does not change in this pD region. Fitting the data to equation (3.2) (see equation A4.1 in the Appendix for a derivation for this equation) gave a pK_a value of 3.77 ± 0.03 (in D_2O with 5% v/v CH_3CN, I = 1.0 M, $NaCF_3SO_3$, Figure 3.3(b)).

$$\delta_{obs} = \frac{\delta_{HA} + \delta_{A^-}(10^{pD-pKa})}{1 + (10^{pD-pKa})} \qquad (3.2)$$

δ_{obs} = observed chemical shift (ppm), δ_{HA}= initial chemical shift (ppm) of the acid and δ_{A^-} = final initial chemical shift (ppm) of the conjugate base.

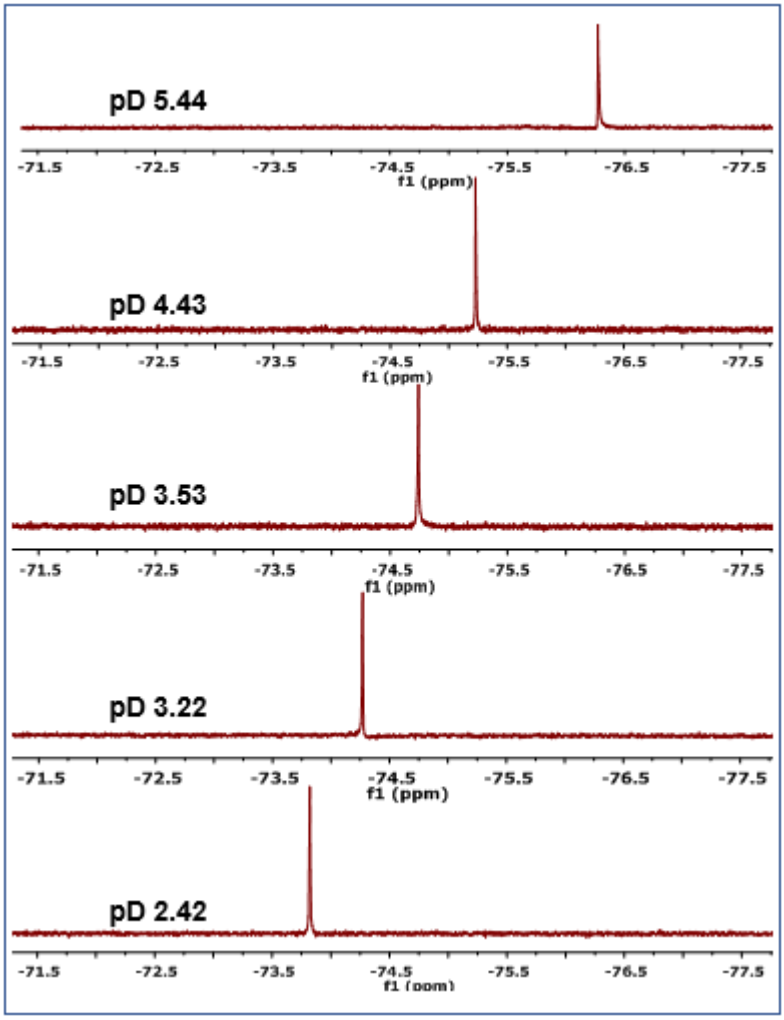

(a)

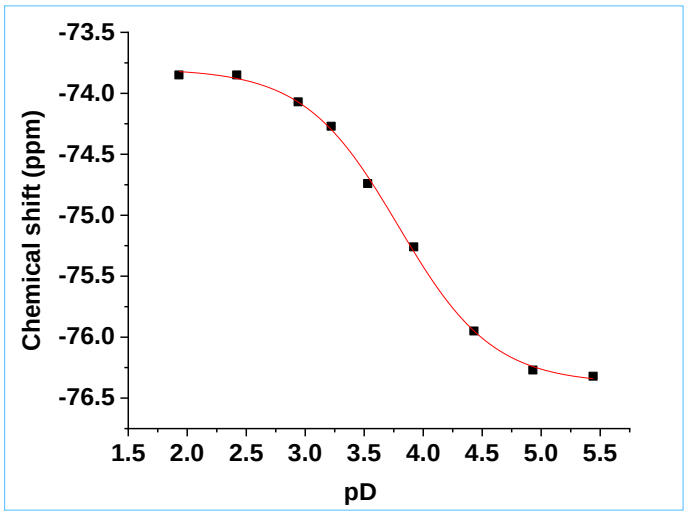

(b)

Figure 3.3. (a) Selected ^{19}F NMR spectra for **2-NPE-ON(H)-SO_2CF_3** as a function of pD, in D_2O with 5% v/v CH_3CN, I = 1.0 M, $NaCF_3SO_3$ at 25.0 °C. (b) Plot of chemical shift vs pD. Data were fitted to equation (3.2), giving pK_a = 3.77 ± 0.03, δ_{HA} = -73.8 ppm and δ_{A^-} = -76.6 ppm.

Control experiments were conducted to ensure that the changes in the chemical shifts with increasing pD is not a result of the decomposition of **2-NPE-ON(H)-SO_2CF_3**. For example, compound **2-NPE-ON(H)-SO_2CF_3** was dissolved in a mixture of CH_3CN and phosphate buffer (5:95 CH_3CN: phosphate buffer in D_2O), pD 1.93. The pD was then increased to pD 5.44 (adjusted by adding a small volume of NaOH in D_2O). The solution was then adjusted back to pD 1.98 (addition of a small volume of 40% v/v of D_2O in 0.01 M HCl). The ^{19}F NMR chemical shift of **2-NPE-ON(H)-SO_2CF_3** was identical within experimental error to its original value, and no decomposition was observed. Therefore, decomposition does not occur within the pD range used to determine the pK_a value for **2-NPE-ON(H)-SO_2CF_3**.

Finally, ^1H NMR spectra for **2-NPE-ON(H)-SO_2CF_3** were also recorded for the same solutions. The Ar-CH_2*<u>CH_2</u>* signals changed by 0.05 ppm. No changes in the chemical shifts were observed for the Ar-*<u>CH_2</u>* signals within experimental error (0.02 ppm; see Table 3.1), consistent with the site of deprotonation being some distance from the aromatic group.

Table 3.1. ^{19}F and ^1H NMR chemical shifts (in D_2O with 5% v/v CH_3CN, I = 1.0 M, $NaCF_3SO_3$) as a function of pD for **2-NPE-ON(H)-SO_2CF_3** (CF_3 signal) at 25.0 °C.

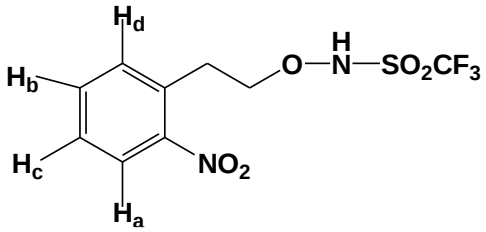

pD	Chemical shift (ppm) of -*CF_3* signal	Chemical shift (ppm) of *CH_3* signal				
		H_a (dd,1H)	H_b (dt, 1H)	$H_{c,d}$ (m, 2H)	Ar-*<u>CH_2</u>*	Ar-CH_2*<u>CH_2</u>*
1.93	-73.85	8.03	7.71	7.58-7.51	3.24	4.05
2.42	-73.85	8.03	7.71	7.58-7.51	3.24	4.05
2.94	-74.07	8.03	7.71	7.58-7.51	3.24	4.05
3.22	-74.27	8.05	7.72	7.60-7.53	3.25	4.02
3.53	-74.74	8.03	7.70	7.59-7.52	3.23	4.01
3.92	-75.26	8.05	7.72	7.61-7.54	3.25	4.00
4.43	-75.95	8.05	7.72	7.61-7.54	3.25	4.00
4.93	-76.27	8.05	7.72	7.61-7.54	3.25	4.00
5.44	-76.32	8.05	7.73	7.60-7.53	3.26	3.99
6.20	-76.30	8.03	7.72	7.61-7.54	3.25	3.99
7.42	-76.52	8.03	7.72	7.61-7.54	3.25	3.99
8.10	-76.48	8.03	7.72	7.61-7.54	3.25	3.99
9.5	-76.52	8.05	7.73	7.60-7.53	3.26	3.99
10.23	-76.38	8.05	7.73	7.60-7.53	3.26	3.99

To summarize, the pK_a of N(H) was investigated using ^{19}F NMR spectroscopy. A value of 3.77 ± 0.03 (in D_2O with 5% v/v CH_3CN, I = 1.0 M, $NaCF_3SO_3$) was obtained. ^1H NMR spectroscopy was not useful since only small change was observed in the Ar-CH_2-$\underline{CH_2}$ signal. The pK_a of **2-NPE-ON(H)-SO_2CF_3** (pK_a = 3.77 ± 0.03; in D_2O, 8% v/v CH_3CN) is similar to that reported for the structurally similar 6,2-HNM-ON(H)SO_2CF_3 (4.4 ± 0.1, in H_2O;[78] the pK_a value is 0.05–0.6 units higher in H_2O compared to the pK_a value in D_2O).[176-178]

^1H NMR spectroscopy was used to determine the pK_a for **2-NPE-ON(H)-SO_2CH_3**. For **2-NPE-ON(H)-SO_2CH_3** the chemical shift of the CH_3 signal decreased from 3.06 to 2.85 ppm in the pD range ~9.9-10.4 (Figure 3.4(a) and Table 3.2). The best fit of the data to equation 3.2 gave pK_a 10.06 ± 0.03 (in D_2O with 5% v/v CH_3CN, I = 1.0 M, $NaCF_3SO_3$, Figure 3.4(b)). A small change in the chemical shifts for the other signals was also observed (~0.09 ppm for Ar-$\underline{CH_2}$ and 0.14 ppm for Ar-$CH_2\underline{CH_2}$, Table 3.2). The magnitude of the changes in the chemical shifts are consistent with deprotonation occurring at the N(H) site. A control experiment demonstrated that **2-NPE-ON(H)-SO_2CH_3** does not decompose in the pD region used to determine the pK_a value.

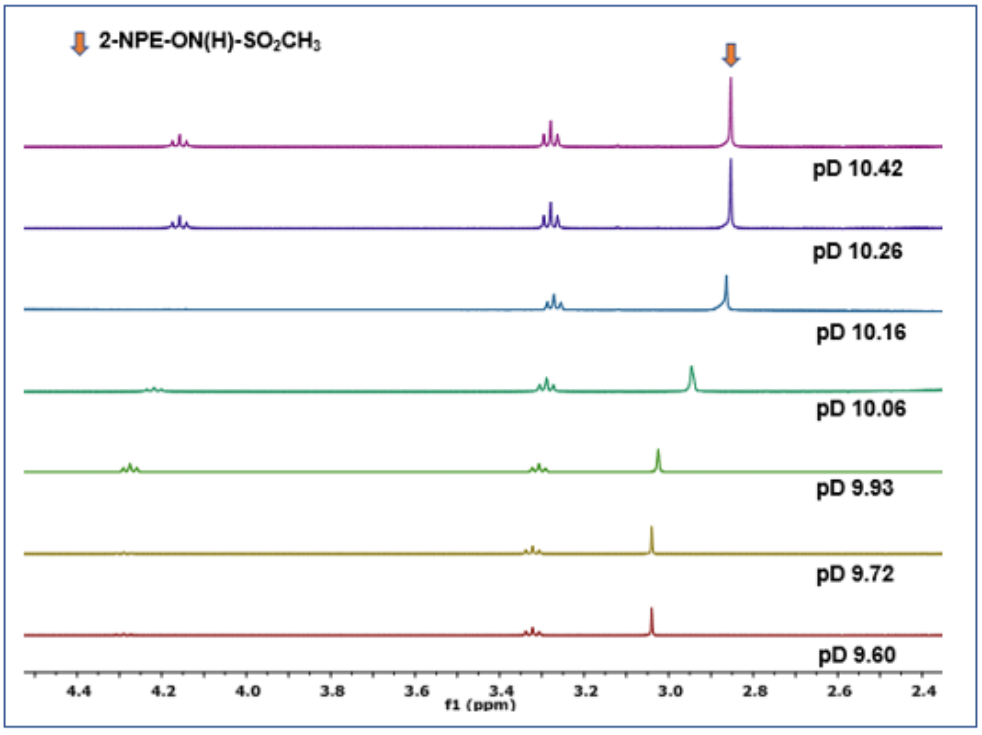

(a)

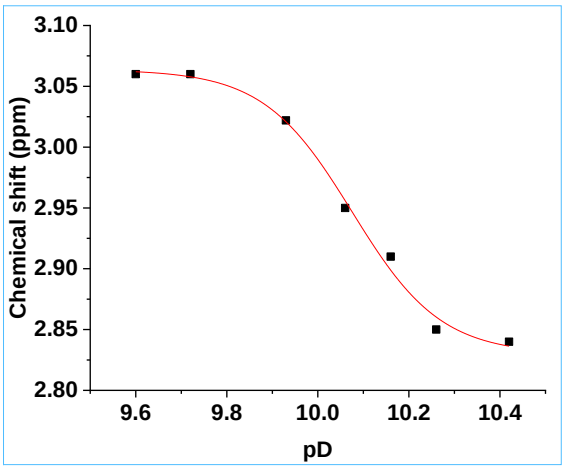

(b)

Figure 3.4. (a) ^{1}H NMR spectra for **2-NPE-ON(H)-SO_2CH_3** as a function of pD, in D_2O with 5% v/v CH_3CN, I = 1.0 M, $NaCF_3SO_3$ at 25.0 °C. (b) Plot of chemical shift vs pD. Data were fitted to equation (3.2), giving pK_a = 10.06 ± 0.03.

Table 3.2 ^{1}H NMR chemical shift as a function of pD for **2-NPE-ON(H)-SO_2CH_3** (in D_2O with 5% v/v CH_3CN, I = 1.0 M, $NaCF_3SO_3$) at 25.0 °C.

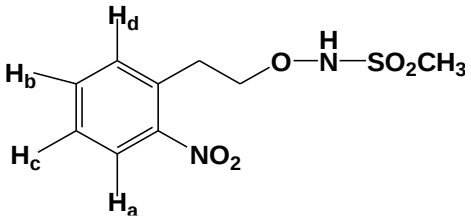

pD	H_a (dd, 1H)	H_b (dt, 1H)	$H_{c,d}$ (m, 2H)	Ar-$\underline{CH_2}$ (t, 2H)	Ar-$CH_2\underline{CH_2}$ (t, 2H)	$\underline{-CH_3}$ (s, 3H)
3.32	8.05	7.77	7.58-7.50	3.35	4.29	3.05
4.21	8.06	7.76	7.58-7.50	3.33	4.29	3.05
5.10	8.04	7.75	7.56-7.48	3.33	4.29	3.04
6.22	8.06	7.76	7.58-7.50	3.35	4.29	3.04
7.40	8.05	7.76	7.58-7.50	3.35	4.29	3.04
8.10	8.05	7.76	7.56-7.48	3.35	4.29	3.04
9.60	8.06	7.75	7.58-7.50	3.33	4.29	3.03
9.72	8.05	7.76	7.58-7.50	3.32	4.27	3.02
9.93	8.05	7.76	7.57-7.49	3.31	4.24	2.95
10.06	8.05	7.76	7.58-7.50	3.28	4.19	2.91
10.16	8.06	7.77	7.58-7.50	3.26	4.17	2.85
10.26	8.06	7.76	7.58-7.50	3.27	4.15	2.86
10.42	8.04	7.75	7.56-7.48	3.27	4.15	2.85
10.61	8.05	7.76	7.57-7.49	3.26	4.15	2.85
11.30	8.06	7.76	7.58-7.50	3.26	4.15	2.86
11.79	8.06	7.75	7.58-7.50	3.26	4.15	2.85

The considerably lower pK_a for **2-NPE-ON(H)-SO_2CF_3** compared with **2-NPE-ON(H)-SO_2CH_3** (pK_a = 10.06 ± 0.03) is in agreement with the much lower pK_a for the sulfonamide proton of $CF_3SO_2NH_2$ (pK_a 6.3) versus $CH_3SO_2NH_2$ (pK_a 10.8).[179]

The pK_a of **2-NPE-ON(H)-SO_2Ar** (Ar = 2-($MeSO_2$)Ph) was investigated by ^{1}H NMR spectroscopy. For **2-NPE-ON(H)-SO_2Ar,** the chemical shifts of the Ar-$CH_2\underline{CH_2}$ protons were plotted as a function of pD (Figure 3.5(a) and Table 3.3), giving pK_a 9.95 ± 0.03 (in D_2O with 5% v/v CH_3CN, I = 1.0 M, $NaCF_3SO_3$, Figure 3.5(b)). There was also a small change in chemical shift for the -$SO_2\underline{CH_3}$ protons, from 3.36 ppm (pD 3.52) to 3.41 (pD 10.38) (Table 3.3). Interestingly the Ar-$CH_2\underline{CH_2}$ peak broadens significantly at high pH, suggesting that a fast exchange process occurs, involving the solvent.

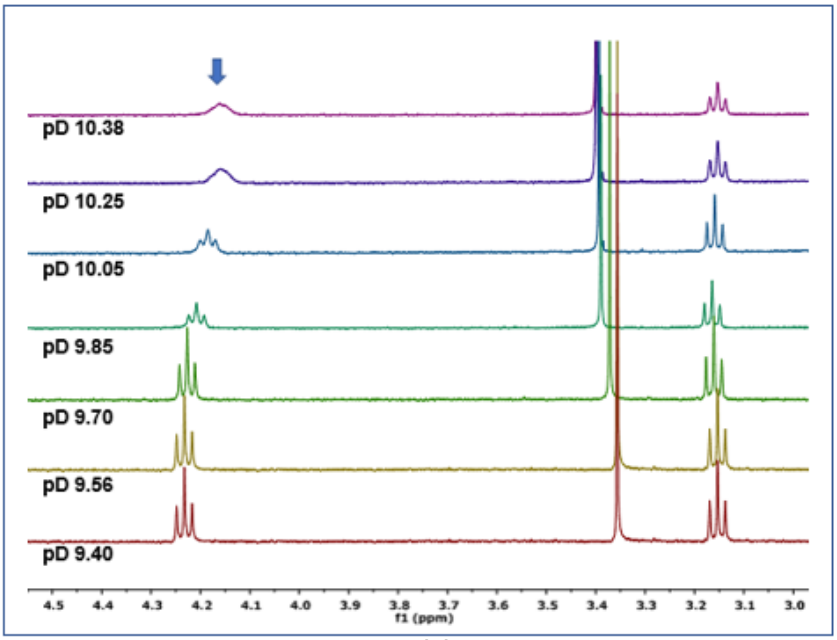

(a)

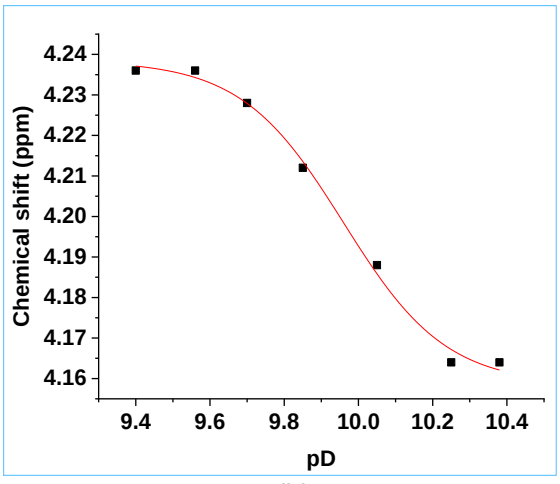

(b)

Figure 3.5. (a) ^{1}H NMR spectra for **2-NPE-ON(H)-SO_2Ar** as a function of pD, in D_2O with 5% v/v CH_3CN, I = 1.0 M, $NaCF_3SO_3$ at 25.0 °C. (b) Plot of chemical shift vs pD. Data was fitted to equation (3.2), giving pK_a = 9.95 ± 0.03.

Table 3.3. ^{1}H NMR chemical shift as a function of pD for **2-NPE-ON(H)-SO$_2$Ar** (in D_2O with 5% v/v CH_3CN, I = 1.0 M, $NaCF_3SO_3$) at 25.0 °C.

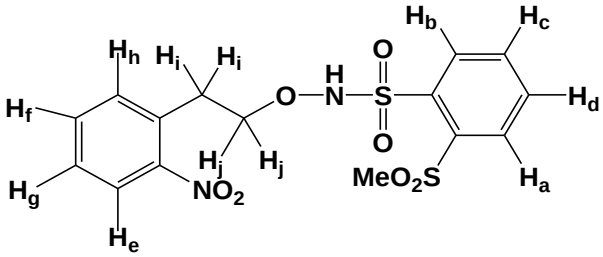

pD	H_a (m, 1H)	H_b (m, 1H)	H_c (m, 1H)	H_d (td, 1H)	H_e (dd, 1H)	H_f (td, 1H)	$H_{g,h}$ (m, 2H)	H_i (t, 2H)	-CH_3 (s, 3H)	H_j (t, 2H)
3.52	8.28-8.26	7.94-7.92	7.98	7.87	7.82	7.56	7.48-7.36	3.17	3.36	4.23
5.30	8.29-8.27	7.95-7.93	7.97	7.88	7.83	7.56	7.49-7.37	3.16	3.36	4.23
6.18	8.29-8.27	7.95-7.93	7.98	7.87	7.83	7.57	7.48-7.36	3.17	3.36	4.23
7.20	8.28-8.26	7.94-7.92	7.98	7.88	7.83	7.56	7.48-7.36	3.16	3.36	4.22
8.35	8.28-8.26	7.94-7.92	7.97	7.88	7.82	7.57	7.48-7.36	3.17	3.37	4.23
9.08	8.29-8.27	7.95-7.93	7.98	7.88	7.83	7.57	7.49-7.37	3.16	3.36	4.23
9.40	8.29-8.27	7.95-7.93	7.98	7.87	7.82	7.56	7.49-7.37	3.16	3.36	4.23
9.56	8.29-8.27	7.95-7.93	7.97	7.88	7.82	7.56	7.48-7.36	3.16	3.36	4.23
9.70	8.28-8.26	7.94-7.92	7.97	7.87	7.83	7.57	7.48-7.36	3.17	3.37	4.22
9.85	8.28-8.26	7.94-7.92	7.98	7.88	7.83	7.57	7.49-7.37	3.17	3.39	4.21
10.05	8.29-8.27	7.95-7.93	7.98	7.87	7.82	7.56	7.48-7.36	3.16	3.40	4.18
10.25	8.28-8.26	7.94-7.92	7.98	7.88	7.83	7.56	7.48-7.36	3.16	3.41	4.16
10.38	8.29-8.27	7.95-7.93	7.98	7.87	7.82	7.57	7.48-7.36	3.16	3.41	4.16

The pK_a of **2-NPE-ON(H)-SO$_2$Ar** was found to be 9.95 ± 0.03 (in D_2O with 5% v/v CH_3CN, I = 1.0 M, $NaCF_3SO_3$) by ^{1}H NMR spectroscopy titration.

3.3.4 Determination of the pK_a of $PhSO_2NHOH$ and 2-$(MeSO_2)PhSO_2NHOH$

It is well established that *N*-hydroxysulfonamide HNO donors spontaneously decompose, to give a sulfinate (RSO_2^-), equation (3.3). Experiments were therefore carried out to determine the pK_a for $PhSO_2NHOH$ and 2-$(MeSO_2)PhSO_2NHOH$.

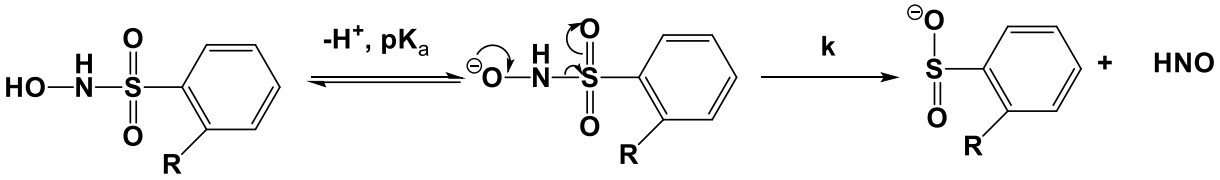

R = H ($PhSO_2NHOH$)
R = -SO_2Me 2-$(MeSO_2)PhSO_2NHOH$)

(3.3)

Rate data for the decomposition of $PhSO_2NHO(H)$ was collected as a function of pH, in 2% v/v CH_3CN in aqueous buffer. The rate of decay of the absorbance for $PhSO_2NHO(H)$ at 266 nm as a function of time was plotted at each pH condition. An example this of data is shown in Figure 3.6(a). Fitting the data to a first-order equation gave an observed rate constant, k_{obs} = (10.0 ± 0.1) × 10^{-2} min^{-1}. These values were then plotted as a function of pH (Figure 3.6(b)) and the data fitted equation (3.4), giving pK_a = 9.38 ± 0.04 (in 2% v/v CH_3CN in aqueous buffer). The pK_a of $PhSO_2NHOH$ was reported by others to be 9.29 ± 0.04 (in aqueous).[180] Our value is in good agreement with this value.

$$k_{obs} = \frac{k \times 10^{\,pH-pKa}}{1 + 10^{\,pH-pKa}}$$

(3.4)

The rate constants k_{obs} and k are the observed rate constant and the second-order rate constant, respectively.

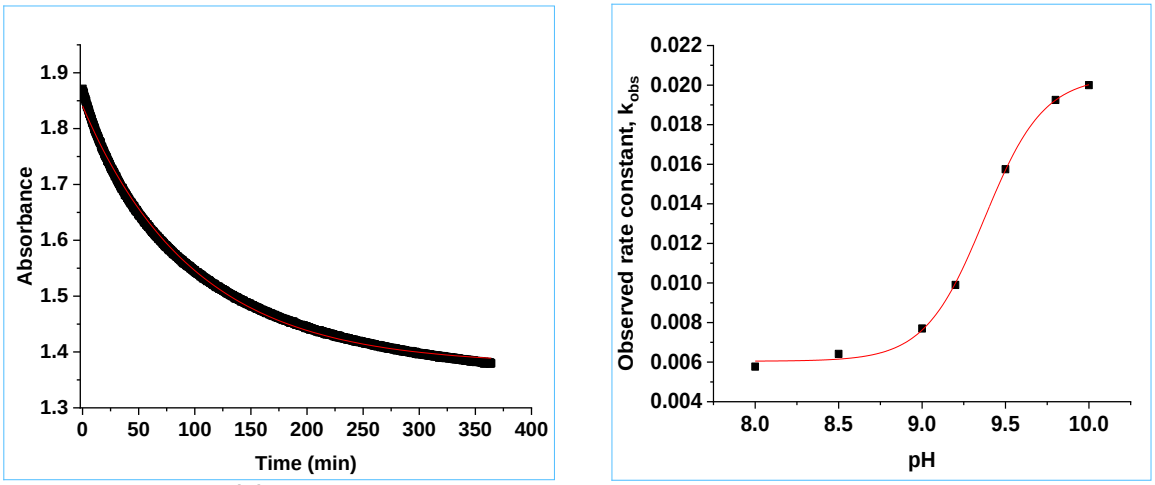

(a) (b)

Figure 3.6. (a) Plot of absorbance at 266 nm versus time for the spontaneous decomposition of $PhSO_2NHOH$ at pH 9.20 (in 2% v/v CH_3CN in aqueous buffer). The data were fitted to a first-order equation, giving $k_{obs} = (10.0 \pm 0.1) \times 10^{-2}$ min^{-1}. (b) Plot of observed rate constant, k_{obs}, as a function of pH (in 2% v/v CH_3CN in aqueous buffer) at 25.0 °C. The data were fitted to equation (3.4), giving $pK_a = 9.38 \pm 0.04$ and $k = 8.02 \pm 0.12$ min^{-1}.

The pK_a of 2-$(MeSO_2)PhSO_2NHOH$ has not been reported. A pK_a titration experiment was carried out (see section 3.2.8 for experimental details). The change in absorbance versus time was plotted at different pH conditions for 2-$(MeSO_2)PhSO_2NHOH$ and are provided in Figure A3.3, Appendix section. An example of this data is shown in Figure 3.7(a), which shows a plot of absorbance at 272 nm versus time for the spontaneous decomposition of 2-$(MeSO_2)PhSO_2NHOH$ at pH 10.01. Fitting the data to a first-order equation gives $k_{obs} = 3.62 \pm 0.05$. k_{obs} was then plotted as a function of pH and the data fitted to equation (3.4), giving $pK_a = 9.18 \pm 0.06$ (in 2% v/v CH_3CN in aqueous buffer).

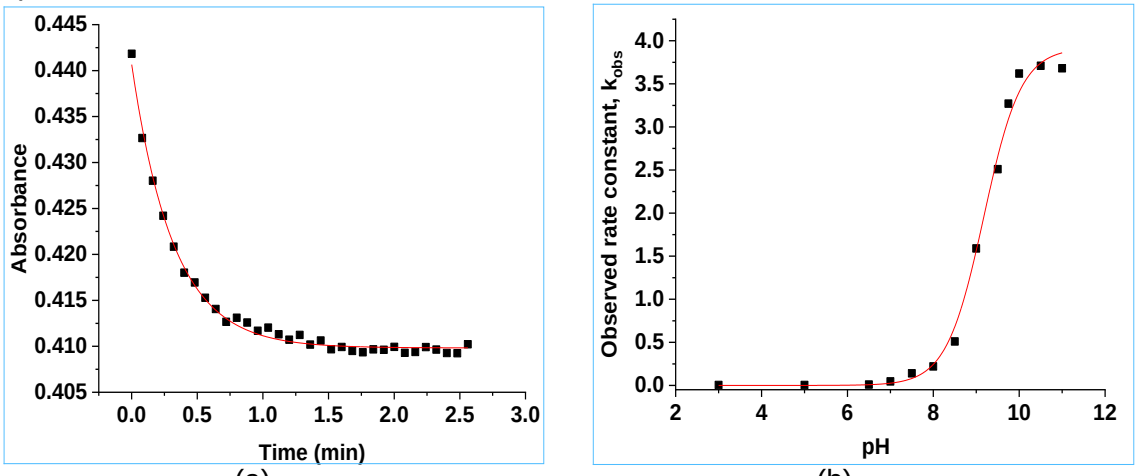

(a) (b)

Figure 3.7. (a) Plot of absorbance at 272 nm versus time for the spontaneous decomposition of 2-$(MeSO_2)PhSO_2NHOH$ at pH 10.01. The data were fitted to a first-order equation, giving $k_{obs} = 3.62 \pm 0.05$ min^{-1}. (b) Plot of observed rate constant, k_{obs}, as a function of pH (in 2% v/v CH_3CN in aqueous buffer). The data were fitted to equation (3.4), giving $pK_a = 9.18 \pm 0.06$ and $k = 3.91 \pm 0.12$ min^{-1}.

To summarize, the pK_a of $PhSO_2NHOH$ and 2-($MeSO_2$)$PhSO_2NHOH$ were found to be 9.38 ± 0.04 and 9.18 ± 0.06, respectively. The pK_a of 2-($MeSO_2$)$PhSO_2NHOH$ was lower than that for $PhSO_2NHOH$. The electron withdrawing group, 2-(SO_2Me), lowers the pK_a value.

3.3.5 Determination of the photoproducts

In Chapter 2 it was shown that **o-NO_2Bn** photocaged *N*-hydroxysulfonamides undergo O-N bond and C-O/N-S bond cleavage upon photolysis. However, **o-NO_2Bn-OC(O)ON(H)SO_2CH_3** decomposes via C-O bond cleavage in addition to O-N and C-O/N-S bond cleavage.[150] Hence for **2-NPE-ON(H)-SO_2R** three photodecomposition pathways are possible: O-N, C-O/N-S and C-O cleavage. C-O/N-S bond cleavage leads to release of HNO, RSO_2^- and 2-nitrostyrene (Pathway 1, Scheme 3.1). C-O bond cleavage generates $RSO_2NHO(H)$ and 2-nitrostyrene (Pathway 2, Scheme 3.1). Finally, in Pathway 3, O-N bond cleavage would result in the release of RSO_2NH_2 and 2-nitrophenylacetaldehyde.

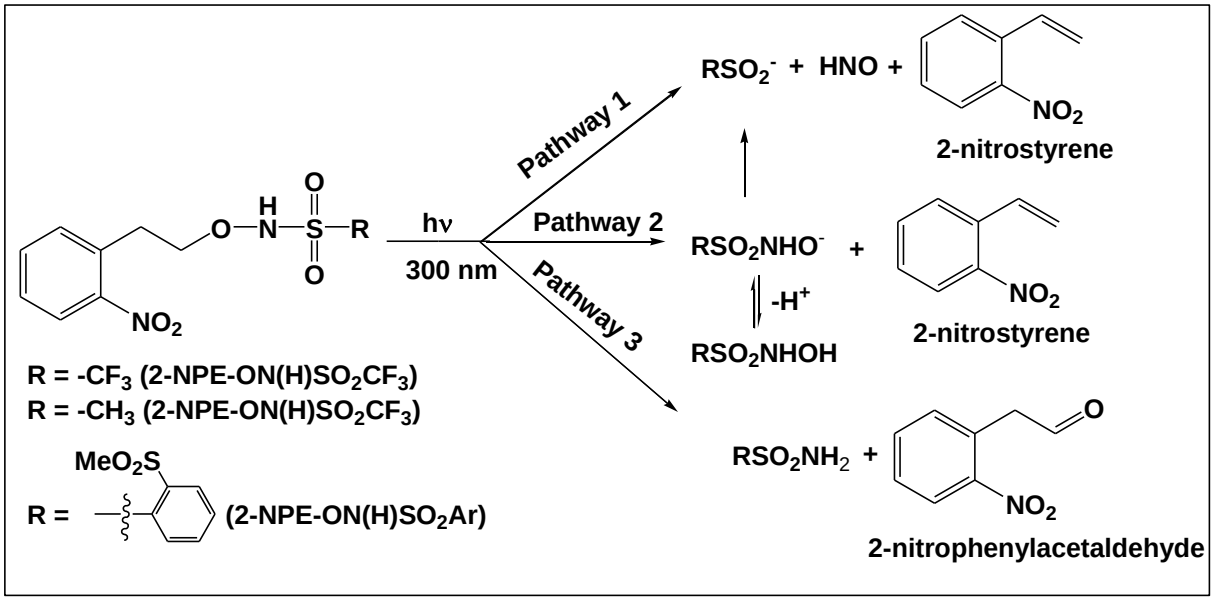

Scheme 3.1. Possible mechanisms for photodecomposition of the 2-NPE analogue of *N*-hydroxysulfonamides, via concomitant C-O/N-S bond cleavage (Pathway 1), C-O bond cleavage (Pathway 2), or O-N bond cleavage (Pathway 3).[76-78, 150]

Steady state photolysis experiments were conducted in a mixture of phosphate buffer (30.0 mM, pH 7.0) and CD_3CN (90:10, v/v) under anaerobic conditions to characterize the photoproducts for each system. Solutions were irradiated using a Rayonet mini-photoreactor (RMR-600) with 300 nm bulbs (4 W, 8 lamps). $^1H/^{19}F$ NMR spectra were recorded after each irradiation.

Figure 3.8(a) shows ^{19}F NMR spectra as a function of total irradiation time for a solution of **2-NPE-ON(H)SO_2CF_3** in a mixture of phosphate buffer (30.0 mM, pH 7.0) and CD_3CN (90:10, v/v) under anerobic conditions. The area of the CF_3 peak of the reactant decreases upon irradiation, decomposing to give $CF_3SO_2NH_2$ (72%) and $CF_3SO_2^-$ (28%) (see later). The CF_3 peak of **2-NPE-ON(H)SO_2CF_3** and trifluorotoluene (Ph-CF_3 external reference) peak were integrated and the ratios of the peak areas plotted as a function of irradiation time. Data were fitted to a first-order equation (Figure 3.8(b)) giving an observed first-order rate constant, k_{obs} = 0.139 ± 0.001 min^{-1} ($t_{1/2}$ ~ 4.9 min).

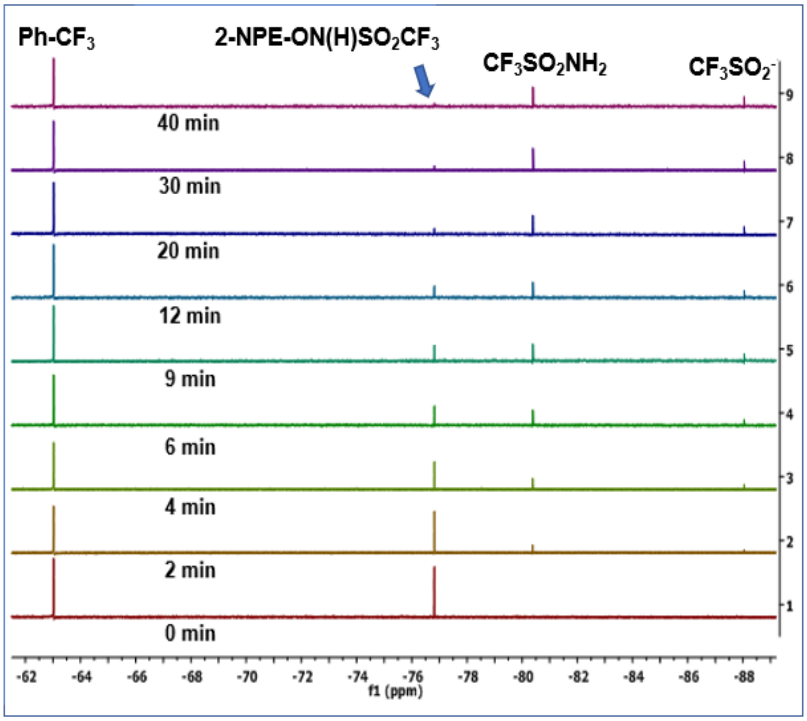

(a)

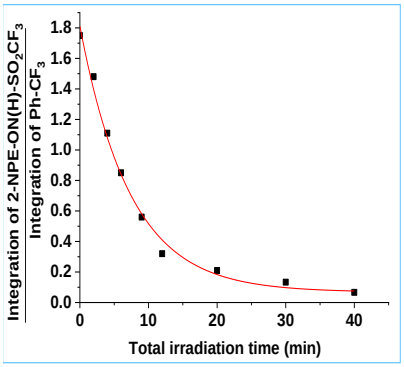

(b)

Figure 3.8. (a) ^{19}F NMR spectra as a function of total irradiation time for the photolysis of **2-NPE-ON(H)-SO_2CF_3** (1.0 mM) in a mixture of phosphate buffer (5.0 mM, pH 7.0) and CD_3CN (90:10, v/v). (b) Ratio of the area of the CF_3 signal of **2-NPE-ON(H)-SO_2CF_3** and the **Ph-CF_3** reference versus time. The best fit of the data to a first-order rate equation gives k_{obs} = 0.139 ± 0.001 min^{-1} ($t_{1/2}$ ~ 4.9 min).

The photoproducts derived from the *N*-hydroxysulfonamide upon bond cleavage were determined. The aliphatic photoproducts upon photolysis of **2-NPE-ON(H)-SO_2CF_3** were confirmed by comparing the ^{19}F NMR spectra of a partially photolyzed sample of **2-NPE-ON(H)-SO_2CF_3** (20 min) with authentic samples of $CF_3SO_2NH_2$ (-80.2 ppm) and $CF_3SO_2^-$ (-88.2 ppm) (Figure 3.9). There was no evidence for CF_3SO_2NHOH being

an intermediate or product upon irradiation of **2-NPE-ON(H)SO_2CF_3**. Photodecomposition of **2-NPE-ON(H)SO_2CF_3** therefore occurs via Pathway 1 (concomitant C-O/N-S bond cleavage to give $CF_3SO_2^-$ and HNO) and Pathway 3 (O-N bond cleavage to give $CF_3SO_2NH_2$), Scheme 3.1.

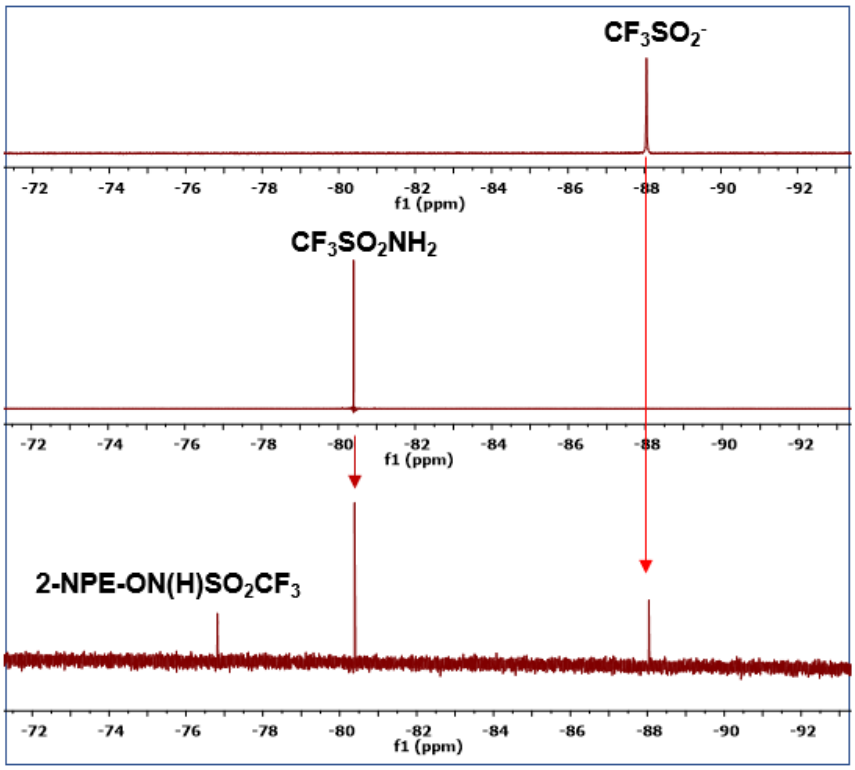

Figure 3.9. ^{19}F NMR spectra of a partially photolyzed sample of **2-NPE-ON(H)-SO_2CF_3** after 20 min irradiation and authentic samples of the aliphatic photoproducts $CF_3SO_2NH_2$ and $CF_3SO_2^-$ in a mixture of phosphate buffer (30.0 mM, pH 7.0) and CD_3CN (90:10, v/v).

The aromatic photoproduct formed upon C-O/N-S bond cleavage is 2-nitrostyrene, (Pathway 1, Scheme 3.1). Upon C-O bond cleavage, 2-nitrostyrene was anticipated (Pathway 2, Scheme 3.1). O-N bond cleavage would result in 2-nitrophenylacetaldehyde being observed in the photoproduct solution (Pathway 3, Scheme 3.1). ^1H NMR spectra of authentic samples of these compounds were compared with the photoproducts obtained for a partially photolyzed sample of **2-NPE-ON(H)-SO_2CF_3**. The photoproducts were determined from a partially photolyzed sample, because upon further photolysis secondary photoproducts were observed, with a substantial decrease in peak intensity in the aromatic region upon complete photodecomposition of the compound. From the partially photolyzed sample of **2-NPE-ON(H)-SO_2CF_3**, (Figure 3.10), the chemical shifts at 9.76, 8.09 and 7.72-7.70 ppm can be assigned to 2-nitrophenylacetaldehyde. Not all the peaks are clearly visible,

probably because of exchange of the aromatic protons for deuterium. The 2-nitrophenylacetaldehyde sample used in this experiment was not very pure. However, it was pure enough to whether or not this compound is a photoproduct. Peaks from 2-nitrostyrene were not observed. This species is photoactive and decomposes under the experimental conditions. The structures and assignments for the aromatic protons of 2-nitrostyrene and 2-nitrophenylacetaldehyde are shown in the Figure.

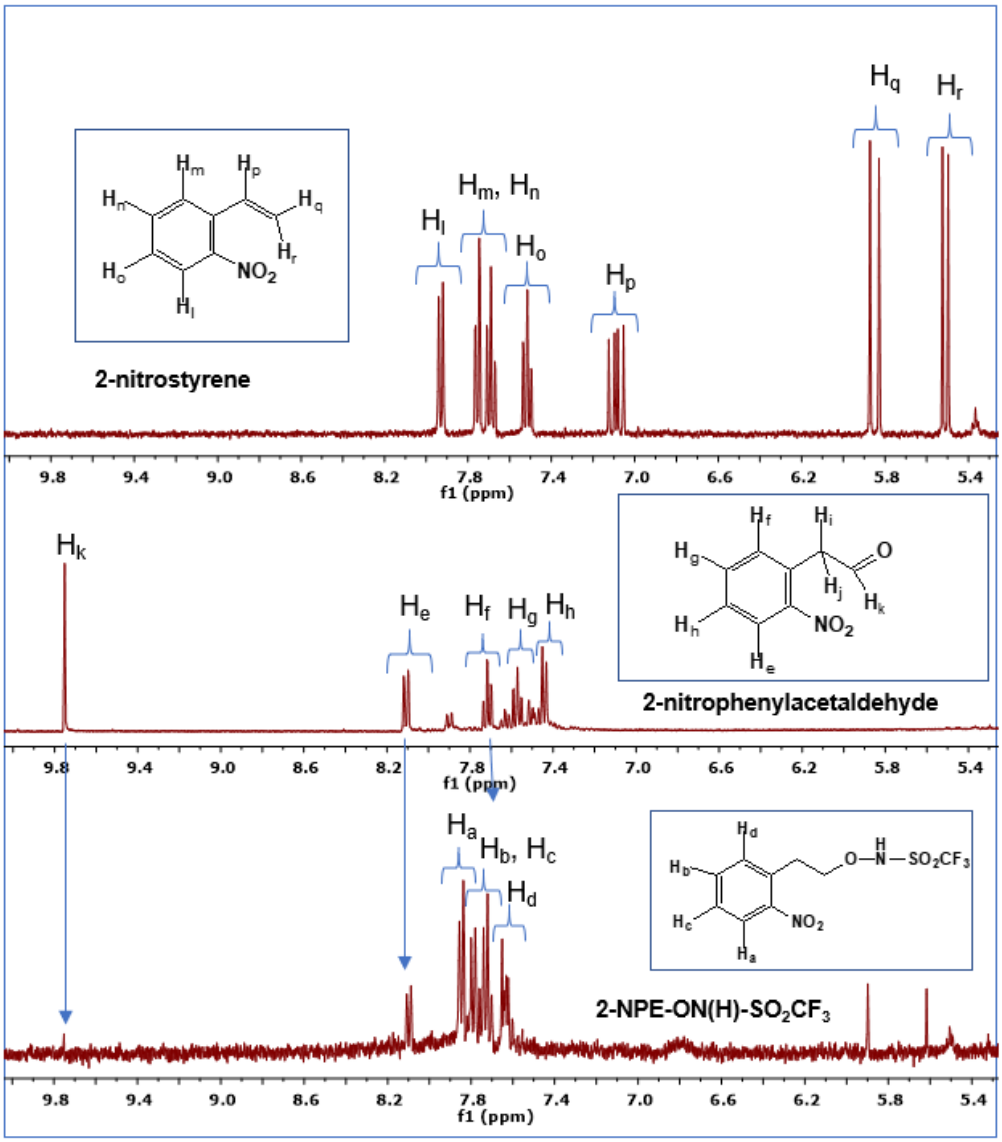

Figure 3.10. ^{1}H NMR spectra of a partially photolyzed sample (4.0 min irradiation) of **2-NPE-ON(H)-SO_2CF_3** and authentic samples of the possible aromatic photoproducts 2-nitrostyrene and 2-nitrophenylacetaldehyde in a mixture of phosphate buffer (30.0 mM, pH 7.0) and CD_3CN (90:10, v/v). 2-Nitrophenylacetaldehyde has impurities at 7.89, 7.63 and 7.48 ppm. Note: H_i and H_j peaks of 2-nitrophenylacetaldehyde overlap with the HDO peak of the solvent. An impurity from CD_3CN was observed at 5.37 ppm.

2-Nitrostyrene and 2-nitrophenylacetaldehyde were partially photolyzed, to determine if some of the peaks in the spectrum arose as secondary photoproducts from these

compounds (Figure 3.11 and Figure 3.12). The ^{1}H NMR spectra of partially photolyzed samples of both aromatic products contained a number of peaks in the 7-8 ppm region. Also, there was loss of signal intensity of the aromatic peaks. Others have reported that 2-nitrostyrene undergoes polymerization upon irradiation.[181] Further experiments were not carried out to characterize these complex species.

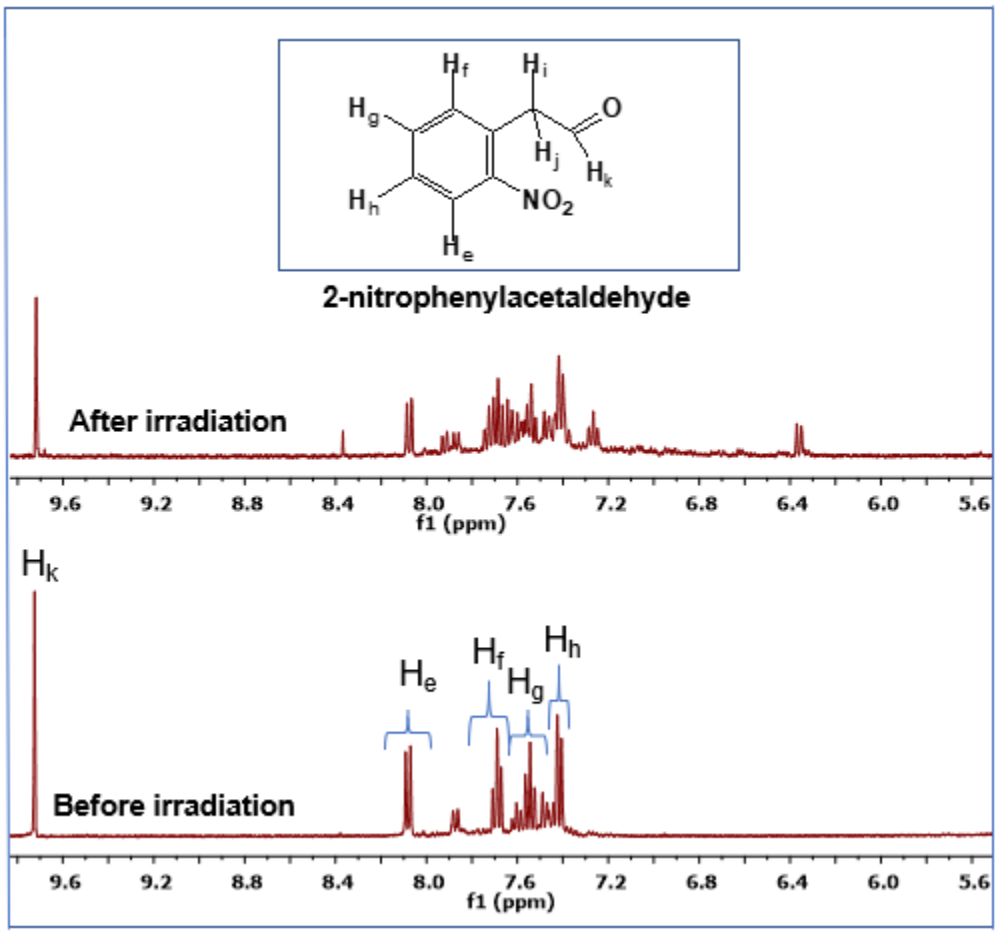

Figure 3.11. ^{1}H NMR spectra of 2-nitrophenylacetaldehyde before irradiation and after irradiation (2.0 min) in a mixture of phosphate buffer (30.0 mM, pH 7.0) and CD_3CN (90:10, v/v). The H_i and H_j peaks of 2-nitrophenylacetaldehyde overlap with the HDO peak of the solvent.

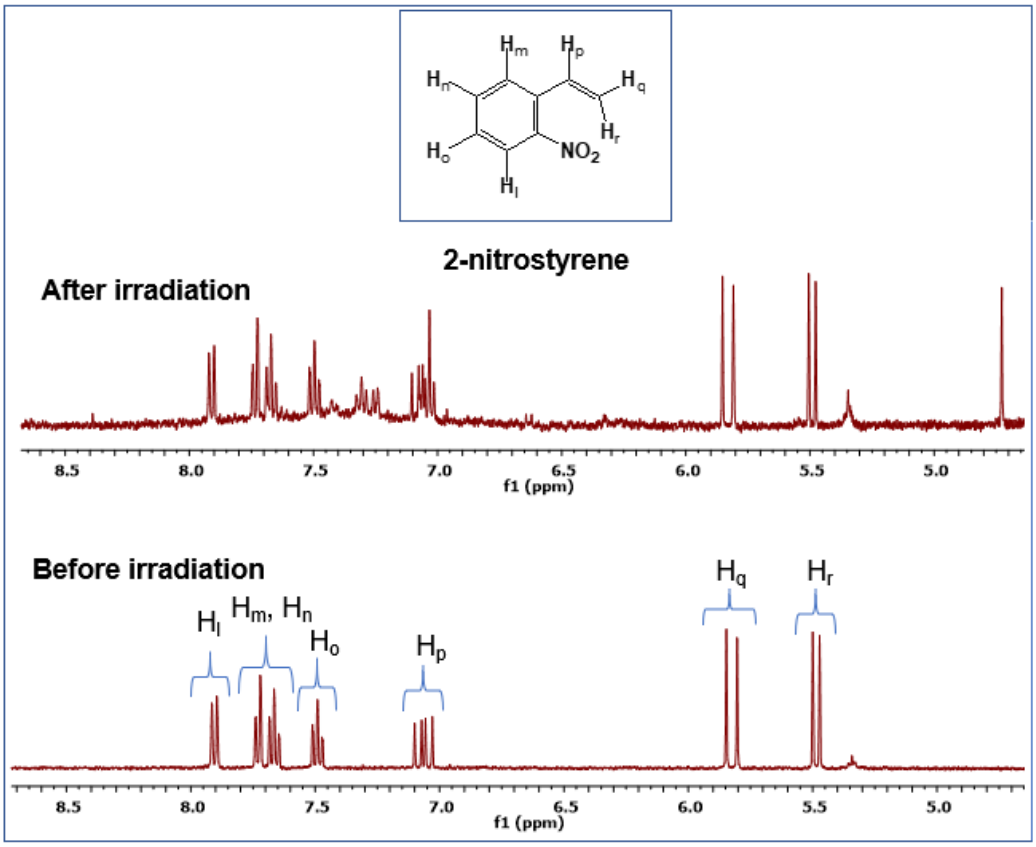

Figure 3.12. ^{1}H NMR spectra of 2-nitrostyrene before irradiation and after partial photolysis (2.0 min) in a mixture of phosphate buffer (30.0 mM, pH 7.0) and CD_3CN (90:10, v/v). The peak at 5.37 ppm is an impurity from CD_3CN.

Figure 3.13(a) shows ^{1}H NMR spectra as a function of total irradiation time for a solution of **2-NPE-ON(H)SO_2CH_3** in a mixture of phosphate buffer (30.0 mM, pH 7.0) and CD_3CN (90:10, v/v) under anaerobic conditions. The CH_3 peak of **2-NPE-ON(H)SO_2CH_3** and the CH_3 peak of TSP (internal reference) were integrated and the ratio of the peak areas plotted as a function of irradiation time. The data was fitted to a first-order equation (Figure 3.13(b)), giving an observed first-order rate constant, k_{obs} = 0.053 ± 0.005 min^{-1} ($t_{1/2}$ ~ 13 min). CH_3SO_2NHOH (3.02 ppm, 85%) appeared as the major photoproduct whereas $CH_3SO_2NH_2$ (3.06 ppm, 6%) and $CH_3SO_2^-$ (2.24 ppm, 9%) were minor photoproducts (see later).

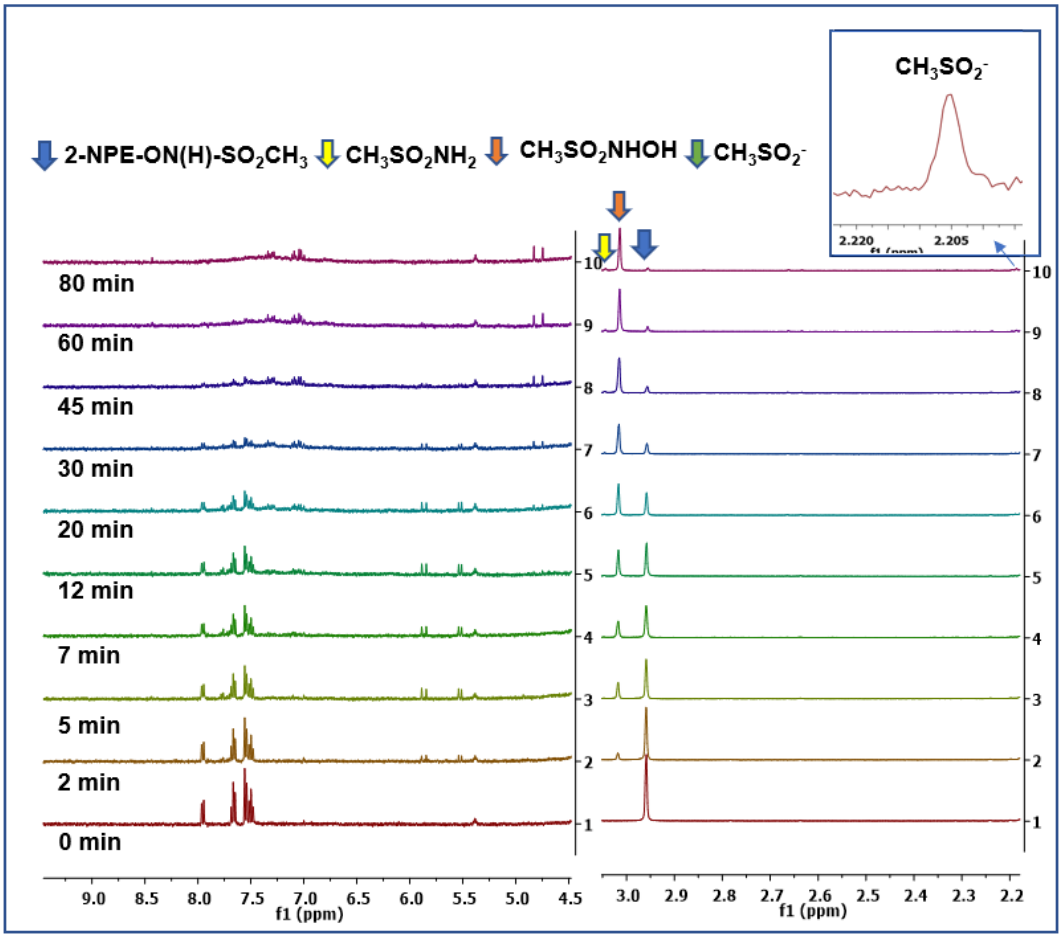

(a)

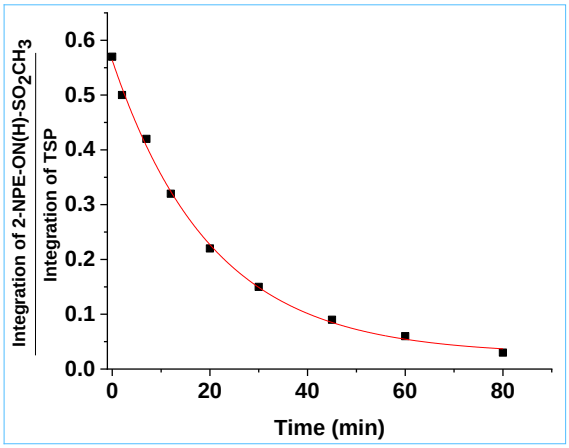

(b)

Figure 3.13. (a) ^{1}H NMR spectra as a function of total irradiation time for the photolysis of **2-NPE-ON(H)SO$_2$CH$_3$** (1.0 mM) in a mixture of phosphate buffer (30.0 mM, pH 7.0) and CD_3CN (90:10, v/v). (b) Ratio of the area of the CH_3 signal of **2-NPE-ON(H)-SO$_2$CH$_3$** and the **TSP** reference versus time. The best fit of the data to a first-order rate equation gives k_{obs} = 0.053 ± 0.005 min^{-1} ($t_{1/2}$ ~ 13 min).

The chemical shift assignments of the aliphatic photoproducts were confirmed by comparing the ^{1}H NMR spectrum of a partially photolyzed sample of **2-NPE-ON(H)-SO$_2$CH$_3$** with the ^{1}H NMR spectra of authentic samples of $CH_3SO_2NH_2$ (3.05 ppm), CH_3SO_2NHOH (3.02 ppm) and $CH_3SO_2^-$ (2.24 ppm) (Figure 3.14) in a mixture of

phosphate buffer (30.0 mM, pH 7.0) and CD_3CN (90:10, v/v). Note that the sample of CH_3SO_2Na was not pure. $CH_3SO_2^-$ is oxidized to $CH_3SO_3^-$ (2.73 ppm) in the presence of air.

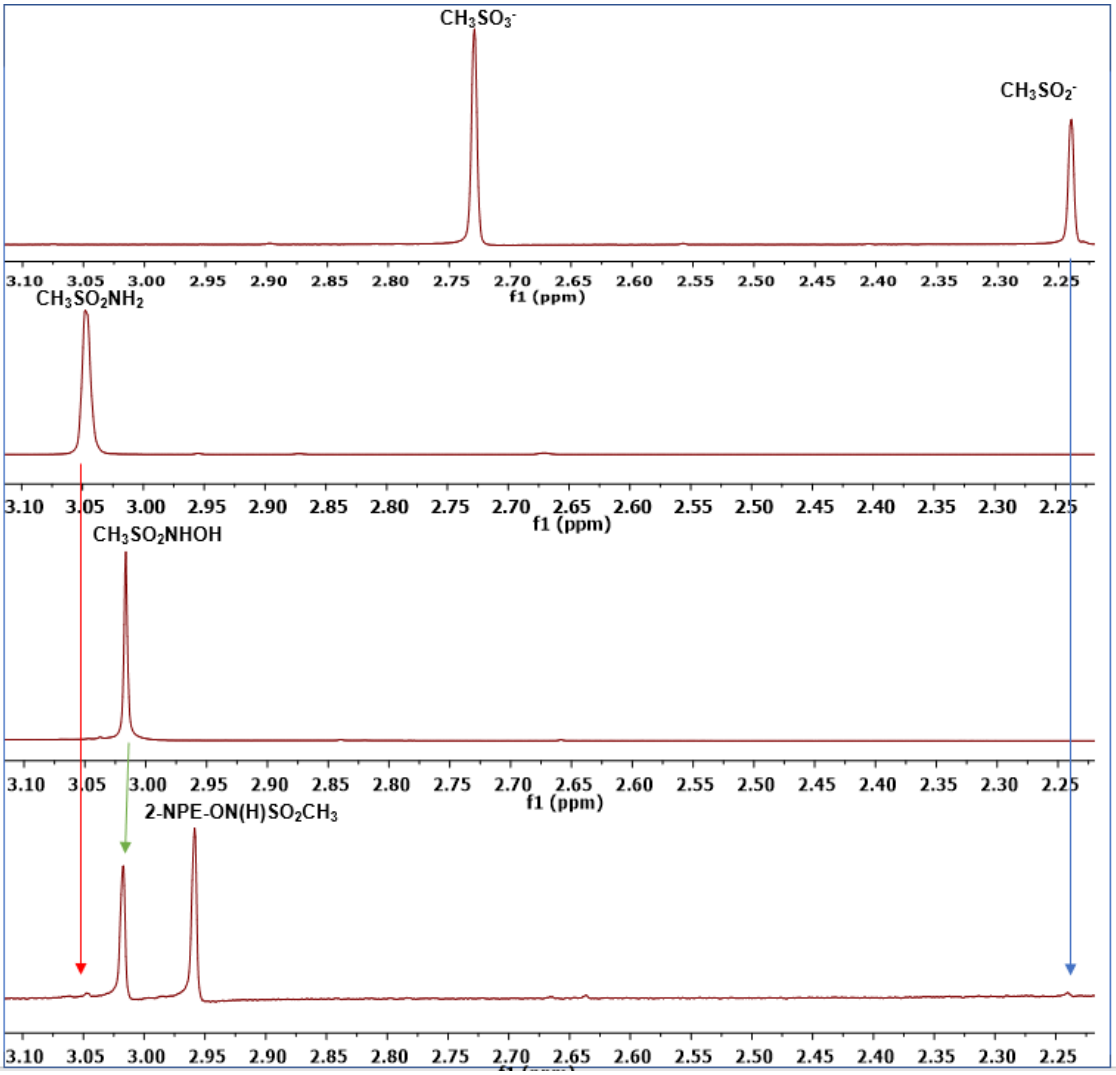

Figure 3.14. ^1H NMR spectra of a partially photolyzed sample (12 min irradiation) of **2-NPE-ON(H)SO_2CH_3** (1.0 mM) and authentic samples of $CH_3SO_2NH_2$, CH_3SO_2NHOH and $CH_3SO_2^-$, in a mixture of phosphate buffer (30.0 mM, pH 7.0) and CD_3CN (90:10, v/v).

The ^1H NMR spectra of authentic samples of 2-nitrostyrene and 2-nitrophenylacetaldehyde were compared with the ^1H NMR spectrum of the photoproducts obtained for a partially photolyzed sample of **2-NPE-ON(H)-SO_2CH_3** (Figure 3.15). Peaks from 2-nitrostyrene were observed in the partially photolyzed sample, consistent with the major product being CH_3SO_2NHOH in the completely

photolyzed sample (C-O bond cleavage, Pathway 2, Scheme 3.1), Figure 3.12.

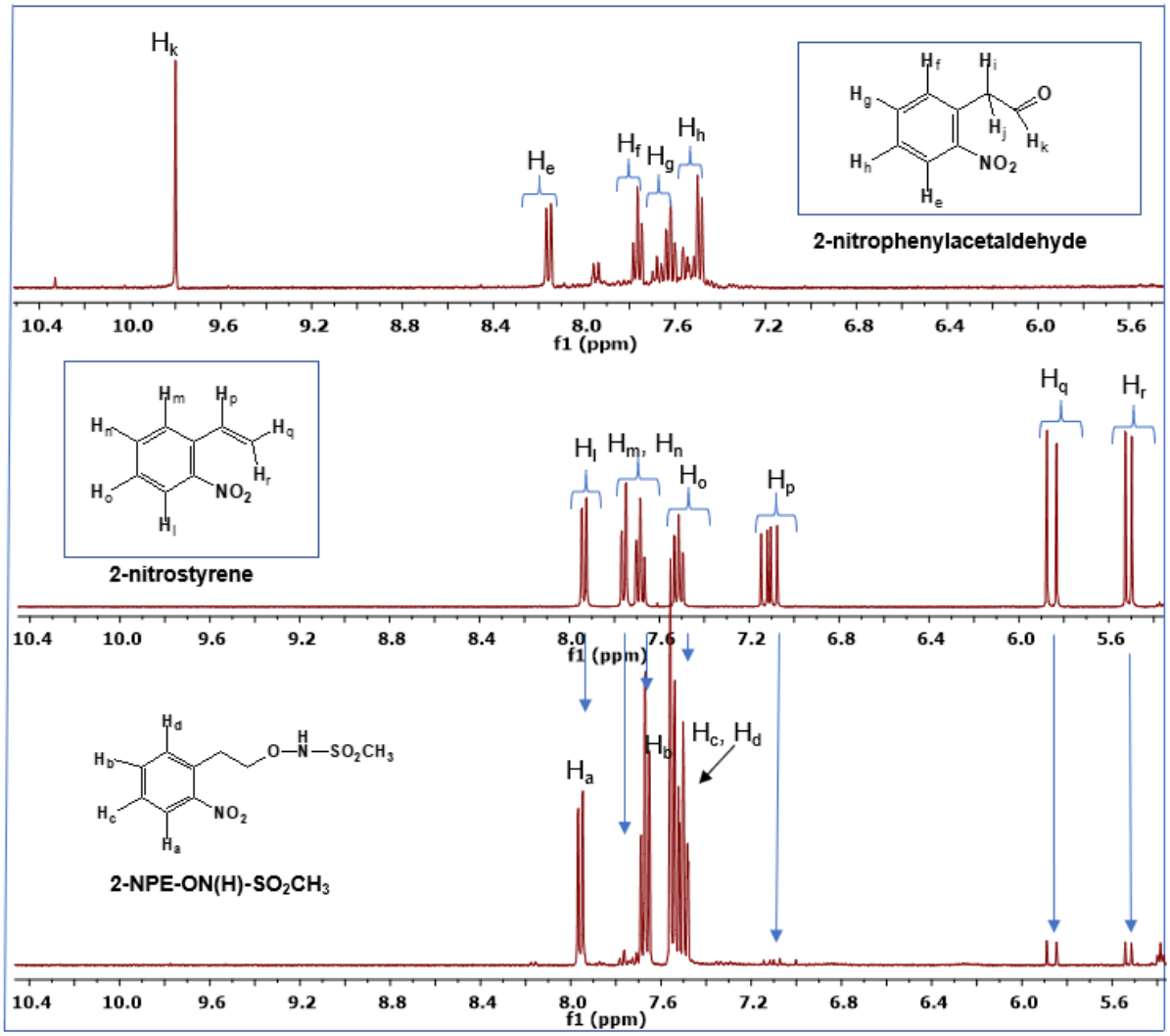

Figure 3.15. ^{1}H NMR spectra of a partially photolyzed sample (2.0 min irradiation) of **2-NPE-ON(H)-SO_2CH_3** and authentic samples of the possible aromatic photoproducts 2-nitrostyrene and 2-nitrophenylacetaldehyde, in a mixture of phosphate buffer (30.0 mM, pH 7.0) and CD_3CN (90:10, v/v). 2-Nitrophenylacetaldehyde has impurities at 7.89, 7.63 and 7.48 ppm. An impurity from CD_3CN was observed at 5.37 ppm.

2-NPE-ON(H)-SO_2Ar (Ar = (2-($MeSO_2$)Ph) found to contain ~2-3% of $ArSO_2NH_2$. Therefore, column chromatography was carried out to purify **2-NPE-ON(H)-SO_2Ar** before carrying out any photolysis experiments**.** Approximately 2-3% of the corresponding sulfinamide, $ArSO_2NH_2$, was observed in the product (δ = 3.41 ppm, 30:70 ethyl acetate-petroleum ether), which could not be removed by column chromatography despite the separation of this compound from **2-NPE-ON(H)-SO_2Ar** by TLC in the same solvent conditions (R_f (**2-NPE-ON(H)-SO_2Ar**) = 0.48 and R_f (**$ArSO_2NH_2$**) = 0.13). However, deliberate addition of a further 2% $ArSO_2NH_2$ to **2-NPE-ON(H)-SO_2Ar** resulted in no discernable change to the photoproducts in a

mixture of phosphate buffer (30.0 mM, pH 7.0) and CD_3CN (90:10, v/v), so the compound was used as it is.

Figure 3.16(a) shows ^1H NMR spectra as a function of total irradiation time for a solution of **2-NPE-ON(H)SO$_2$Ar** in a mixture of phosphate buffer (30.0 mM, pH 7.0) and CD_3CN (90:10, v/v) under anaerobic conditions. The integration of the CH_3 peak of **2-NPE-ON(H)SO$_2$Ar** versus the integration of TSP was plotted as a function of irradiation time and the data fitted to a first-order equation (Figure 3.16(b)), giving k_{obs} = 0.031 ± 0.005 min^{-1} ($t_{1/2}$ ~ 22 min). The photoproducts were assigned using authentic compounds and a partially photolyzed sample (see later). Ar_2SO_2NHOH (3.44 ppm) appeared as the major photoproduct and $ArSO_2NH_2$ (3.41 ppm) and $ArSO_2^-$ (3.35 ppm) as minor photoproducts. Importantly, $ArSO_2NHOH$ spontaneously (thermally) decomposed to give $ArSO_2^-$ and HNO in some of the solvent conditions, so the percentages of each of these species could not be considered individually. The percentages of photoproducts were ($ArSO_2NHOH$ + $ArSO_2^-$) (86%), $ArSO_2NH_2$ (10%) and an unknown species (4%).

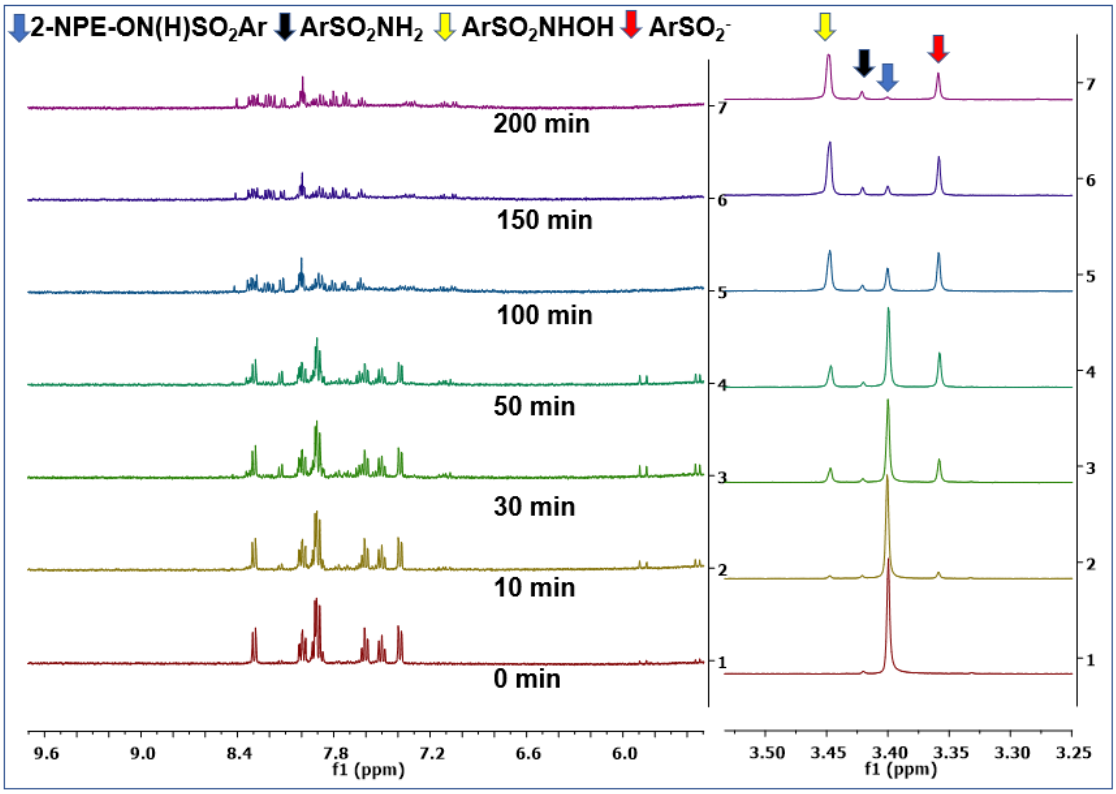

(a)

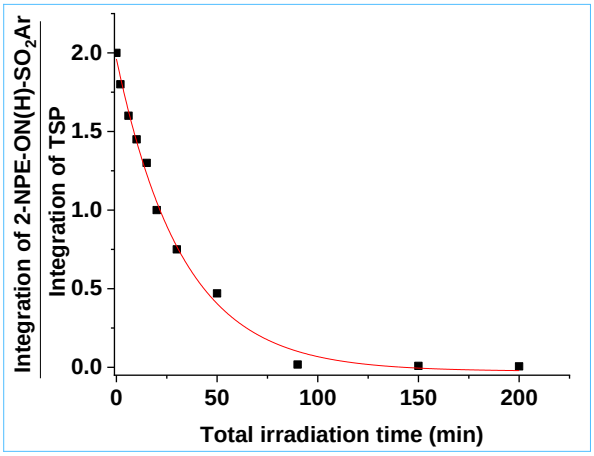

(b)

Figure 3.16. (a) ^{1}H NMR spectra as a function of total irradiation time for the photolysis of **2-NPE-ON(H)-SO$_2$Ar** (1.0 mM) in a mixture of phosphate buffer (30.0 mM, pH 7.0) and CD_3CN (90:10, v/v). (b) Ratio of the area of the CF_3 signal of **2-NPE-ON(H)-SO$_2$Ar** and the **TSP** reference versus time. The best fit of the data to a first-order rate equation gives k_{obs} = 0.031 ± 0.005 min^{-1} ($t_{1/2}$ ~ 22 min).

The photoproducts generated from **2-NPE-ON(H)-SO$_2$Ar** were confirmed by recording the ^{1}H NMR spectrum of a partially photolyzed sample of **2-NPE-ON(H)-SO$_2$Ar** and comparing this spectrum with the ^{1}H NMR spectra of authentic samples of $ArSO_2NH_2$ (3.41 ppm), $ArSO_2NHOH$ (3.44 ppm) and $ArSO_2^-$ (3.35 ppm) in the 3.29-3.45 ppm region of the ^{1}H NMR spectrum, Figure 3.17.

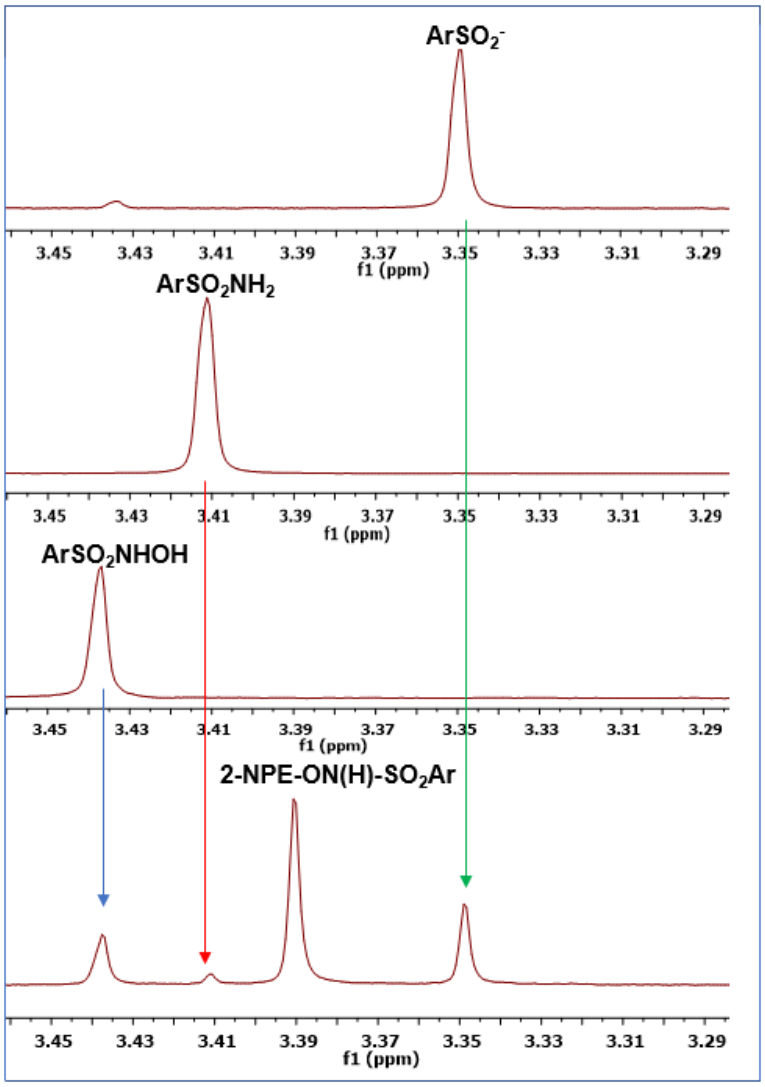

Figure 3.17. ^{1}H NMR spectra of a partially photolyzed sample (50 min irradiation) of **2-NPE-ON(H)-SO$_2$Ar** and authentic samples of the expected aliphatic photoproducts in a mixture of phosphate buffer (30.0 mM, pH 7.0) and CD_3CN (90:10, v/v).

The aromatic region of the ^{1}H NMR spectrum of the partially photolyzed sample was also closely examined. Peaks from $ArSO_2^-$ were observed. Peaks from $ArSO_2NH_2$ and $ArSO_2NHOH$ were not observed, Figure 3.18.

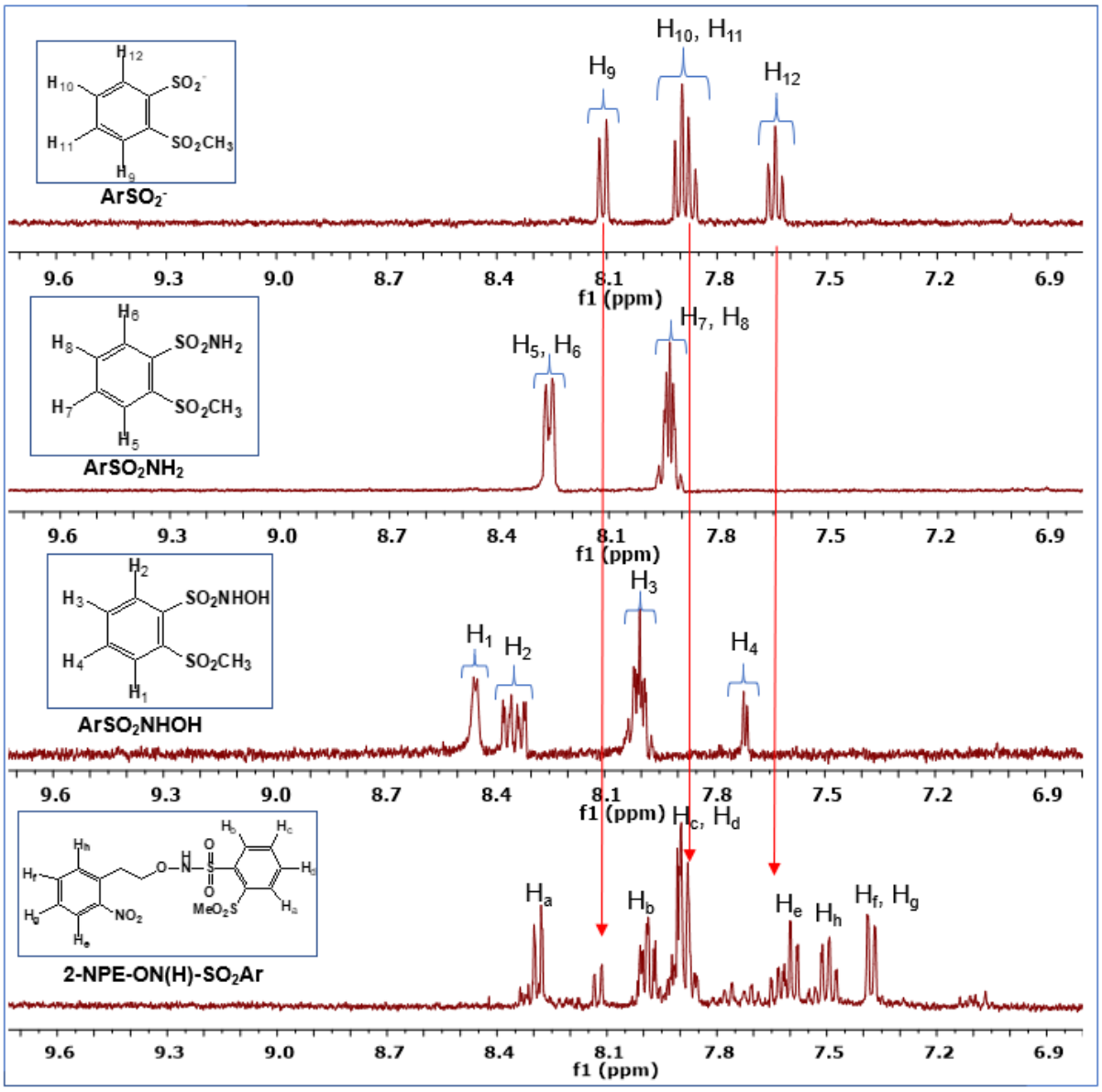

Figure 3.18. ^{1}H NMR spectra of a partially photolyzed sample (50 min irradiation) of **2-NPE-ON(H)-SO$_2$Ar** and authentic samples of the possible photoproducts $ArSO_2NHOH$, $ArSO_2NH_2$ and $ArSO_2^-$ in a mixture of phosphate buffer (30.0 mM, pH 7.0) and CD_3CN (90:10, v/v).

To establish the aromatic photoproducts arising from the 2-NPE photocage, the ^{1}H NMR spectra of authentic samples of 2-nitrostyrene and 2-nitrophenylacetaldehyde were compared with the ^{1}H NMR spectrum of the same partially photolyzed sample of **2-NPE-ON(H)-SO$_2$Ar** in the aromatic region of the spectrum, Figure 3.19. Since $ArSO_2^-$ (C-O/N-S bond cleavage, Pathway 1, Scheme 3.1) and $ArSO_2NHOH$ (C-O bond cleavage, Pathway 2, Scheme 3.1) are major products, 2-nitrostyrene would be expected and was observed.

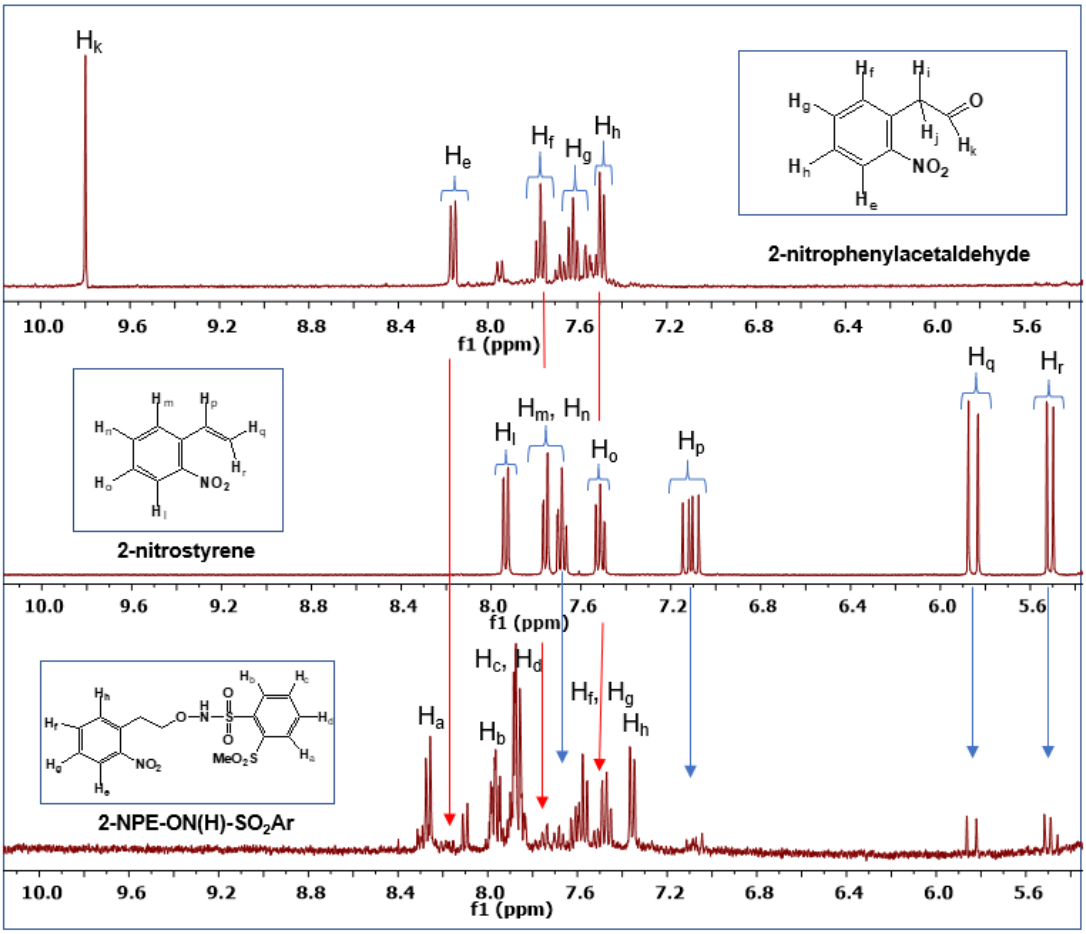

Figure 3.19. ^{1}H NMR spectra of a partially photolyzed sample (50 min irradiation) of **2-NPE-ON(H)-SO$_2$Ar** and authentic 2-nitrostyrene and 2-nitrophenylacetaldehyde in a mixture of phosphate buffer (30.0 mM, pH 7.0) and CD_3CN (90:10, v/v).

3.3.6 The effect of the solvent composition on photoproducts

To obtain more information on factors which affect the mechanism of photodecomposition, the effect of the solvent composition of the aqueous component of the buffer on the photoproducts was investigated. Walbert et al. reported that the solvent conditions have a significant effect on the mechanism of decomposition reaction pathways for (2-nitrophenyl)ethyl-caged molecules.[124] β-Elimination of the leaving group to give 2-nitrostyrene was found to occur with higher volumes of H_2O in a H_2O/CH_3CN solvent mixture, consistent with deprotonation of the monoprotonated aci-nitro intermediate to give the aci-nitro anion prior to β-elimination.[124] At low percent volumes of H_2O in the solvent mixture, cyclisation instead occurred to ultimately generate a nitrosobenzene derivative with no loss of the leaving group.

Steady state photolysis experiments were carried out in phosphate buffer (30.0 mM, pH 7.0) and CD_3CN. The samples were irradiated using a Rayonet photoreactor

(RMR-600, 300 nm). ^{19}F NMR spectra of **2-NPE-ON(H)-SO$_2$CF$_3$** were recorded at different irradiation times. The integration of the CF_3 peak as a function of total irradiation time was plotted to obtain the observed rate constant for photodecomposition, k_{obs}.

Intially a steady state photolysis experiment for **2-NPE-ON(H)-SO$_2$CF$_3$** was conducted in pure CD_3CN. Figure 3.20(a) shows ^{19}F NMR spectra as a function of total irradiation time for a solution of **2-NPE-ON(H)SO$_2$CF$_3$** in CD_3CN under anaerobic conditions. The area of the CF_3 peak of the reactant decreases upon irradiation. The photoproducts were $CF_3SO_2NH_2$ (72%) and $CF_3SO_2^-$ (28%). The CF_3 peak of **2-NPE-ON(H)SO$_2$CF$_3$** as a function of irradiation time was fitted to a first-order equation (Figure 3.20(b)), giving an observed rate constant, k_{obs} = 0.141 ± 0.001 min^{-1} ($t_{1/2}$ ~ 4.9 min).

A similar plot of ^{19}F NMR spectra as a function of total irradiation time for **2-NPE-ON(H)-SO$_2$CF$_3$** (1.0 mM) in a 60:40 mixture of CD_3CN and phosphate buffer (30.0 mM, pH 7.0) is given in Figure A3.4, Appendix. The percentage of the photoproducts and the observed rate constant are in reasonable agreement with values reported in the PhD thesis of our collaborator under the same conditions (67% $CF_3SO_2NH_2$ and 33% $CF_3SO_2^-$; 0.080 ± 0.002 min^{-1}).[157, 166]

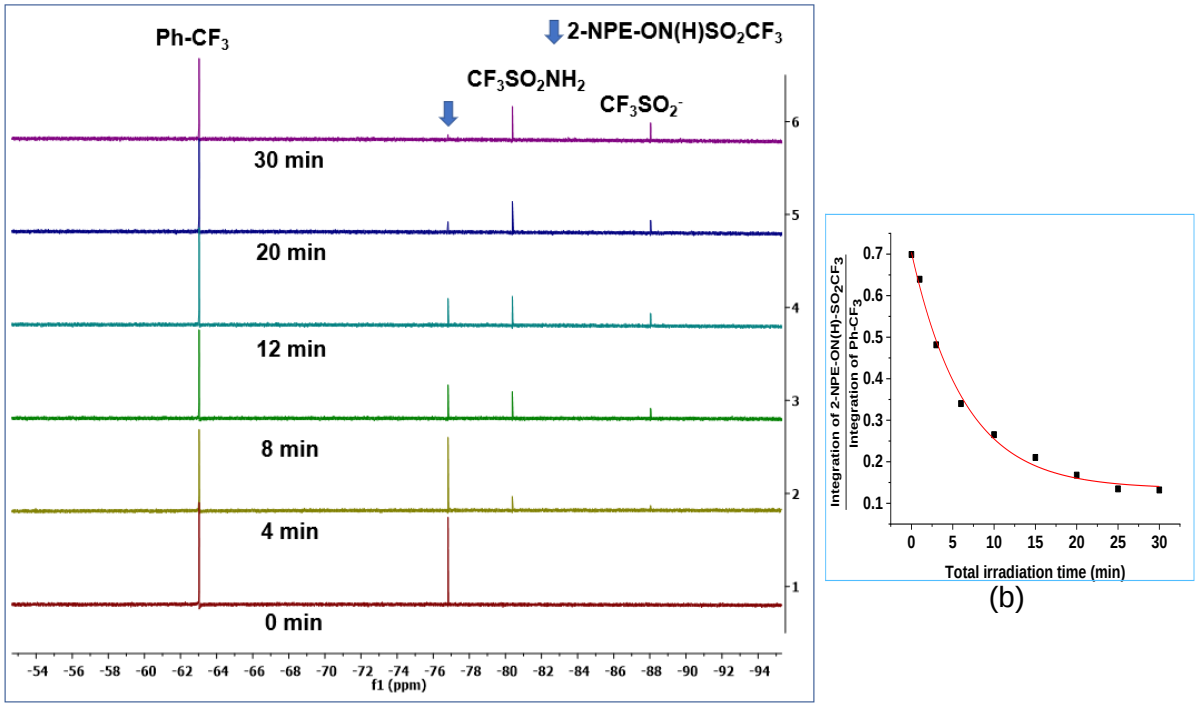

(a) (b)

Figure 3.20. (a) ^{19}F NMR spectra as a function of total irradiation time for the photolysis of **2-NPE-ON(H)-SO$_2$CF$_3$** (1.0 mM) in CD_3CN. (b) Ratio of the area of the CF_3 signal of **2-NPE-ON(H)-SO$_2$CF$_3$** and the **Ph-CF$_3$** reference versus time. The best fit of the data to a first-order rate equation is shown, giving k_{obs} = 0.141 ± 0.001 min^{-1} ($t_{1/2}$ ~ 4.9 min).

The effect of the solvent composition (CD_3CN and phosphate buffer (30 mM), pH 7.0) on the photoproducts obtained upon irradiating **2-NPE-ON(H)-SO_2CF_3** is summarized in Table 3.4. Duplicate data was collected, to obtain an estimate of the percentage error for each value, and establish how accurate the percentages of the photoproducts are from steady state irradiation experiments. The percentage of concerted C-O/N-S cleavage (observed photoproduct $CF_3SO_2^-$; ~30%) versus O-N bond cleavage (to give $CF_3SO_2NH_2$; ~70%) was independent of the solvent composition. CF_3SO_2NHOH was not observed in any of the NMR spectra; hence C-O bond cleavage is not an important photodecomposition mechanism for this system. $CF_3SO_2NHO(H)$ is stable in CD_3CN but decomposes in all the other solvent conditions (min).[53] If $CF_3SO_2NHO(H)$ had been a reaction intermediate, it would have been observed at shorter irradiation times in the NMR spectra. The observed rate constant for decomposition under steady state irradiation conditions was determined by monitoring the ^{19}F NMR signal of the reactant as a function of irradiation time. This was also independent of the solvent composition.

Table 3.4. Effect of solvent ratio on the photoproducts derived from the *N*-hydroxysulfonamide moiety and the observed rate constant for photodecomposition of **2-NPE-ON(H)-SO_2CF_3** (1.0 mM). The data are average values of two independent experiments (Table A3.1, Appendix).

Solvent ratio, % v/v (CD_3CN/30 mM phosphate buffer, pH 7.0)	Percentage of Photoproducts[a]		k_{obs} (min^{-1})[b]
	$CF_3SO_2NH_2$	$CF_3SO_2^-$	
100/00	72	28	0.141
80/20	70	30	0.137
60/40	67	33	0.134
40/60	70	30	0.136
10/90	72	28	0.139

[a] The percent of each photoproduct was determined upon complete photodecomposition of the compound. The absolute error of each value is estimated to be ± 3%.
[b] The percentage error is estimated to be ~ 5%.

Steady state photolysis experiments for **2-NPE-ON(H)-SO_2CH_3** were also carried out in different percentage volumes of CD_3CN and phosphate buffer (30.0 mM, pH 7.0). Once again samples were irradiated using a Rayonet photoreactor (RMR-600, 300 nm). The photodecomposition was followed using ^1H NMR spectroscopy. Initially photolysis studies were carried out in CD_3CN. Figure 3.21(a) shows ^1H NMR spectra

as a function of total irradiation. The area of the CH_3 peak of the reactant decreases as the total irradiation time increases. The area of the CH_3 peak was plotted as a function of total irradiation time, giving k_{obs} = 0.057 ± 0.003 min^{-1} (Figure 3.21(b)). The percentage of photoproducts was 85% CH_3SO_2NHOH, 7% $CH_3SO_2NH_2$ and 8% $CH_3SO_2^-$. The percentage of the photoproducts and the observed rate constant are in reasonable agreement with values obtained by our collaborator (82% CH_3SO_2NHOH, 10% $CH_3SO_2NH_2$ and 8% $CH_3SO_2^-$; 0.042 ± 0.002 min^{-1}).[152]

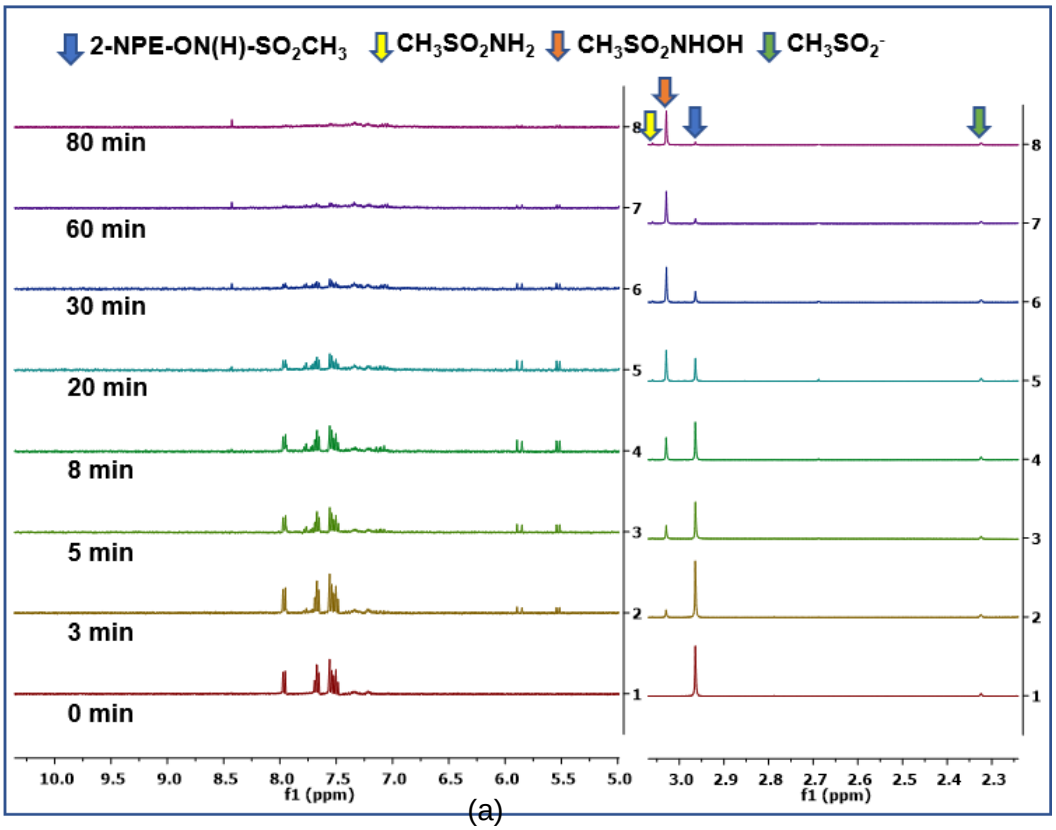

(a)

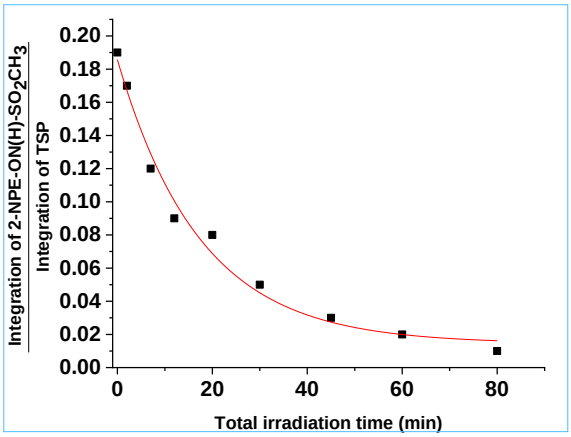

(b)

Figure 3.21. (a) ^{1}H NMR spectra as a function of total irradiation time for the photolysis of **2-NPE-ON(H)-SO_2CH_3** (1.0 mM) in CD_3CN. (b) Ratio of the area of the CH_3 signal of **2-NPE-ON(H)-SO_2CH_3** and the TSP reference versus time. The best fit of the data to a first-order rate equation gives k_{obs} = 0.057 ± 0.003 min^{-1} ($t_{1/2}$ ~ 12 min).

The aliphatic photoproducts generated during the photolysis were confirmed by comparing ^{1}H NMR spectra of a partially photolyzed sample of **2-NPE-ON(H)-SO_2CH_3** with authentic samples of $CH_3SO_2NH_2$ (3.09 ppm), CH_3SO_2NHOH (3.07 ppm) and $CH_3SO_2^-$ (2.22 ppm) in CD_3CN, Figure 3.22.

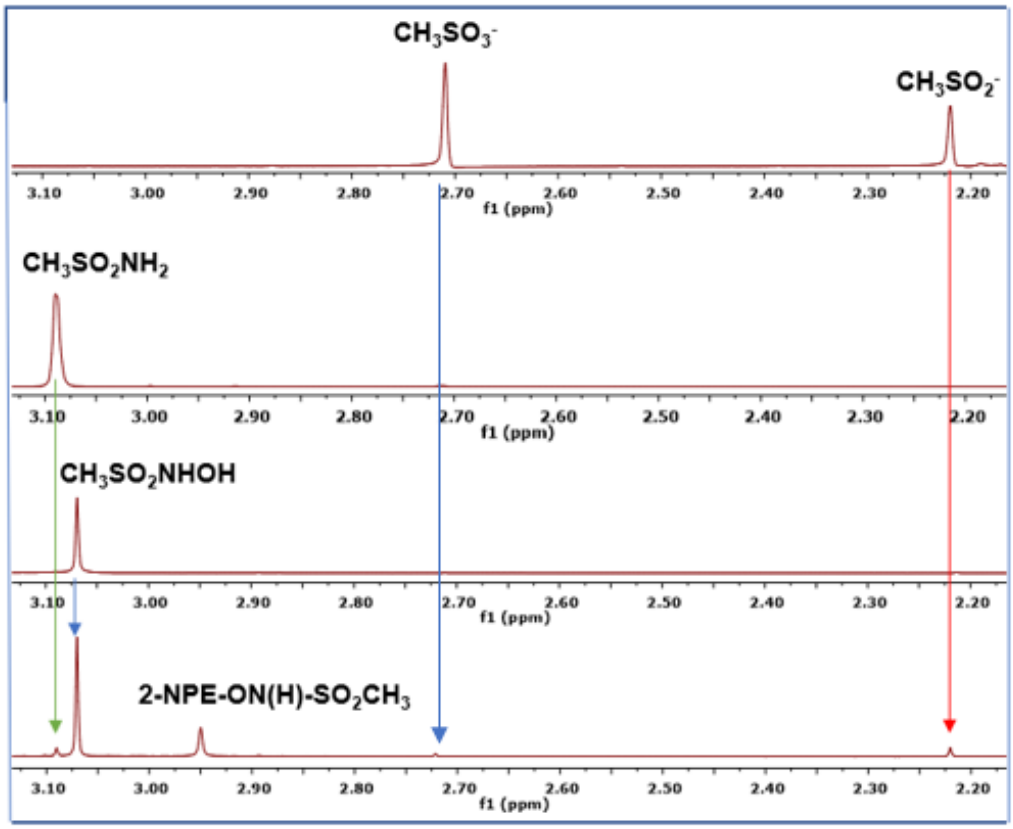

Figure 3.22. ^{1}H NMR spectra for a partially photolyzed sample (30 min irradiation) of **2-NPE-ON(H)SO_2CH_3** (1.0 mM) and authentic samples of $CH_3SO_2NH_2$, CH_3SO_2NHOH and $CH_3SO_2^-$ in CD_3CN.

^{1}H NMR spectra of authentic samples of 2-nitrostyrene and 2-nitrophenylacetaldehyde were also compared with the photoproducts obtained for a partially photolyzed sample of **2-NPE-ON(H)-SO_2CH_3** (Figure 3.23). Peaks attributable to 2-nitrostyrene were observed, consistent with CH_3SO_2NHOH being the major photoproduct (C-O bond cleavage, Pathway 2, Scheme 3.1).

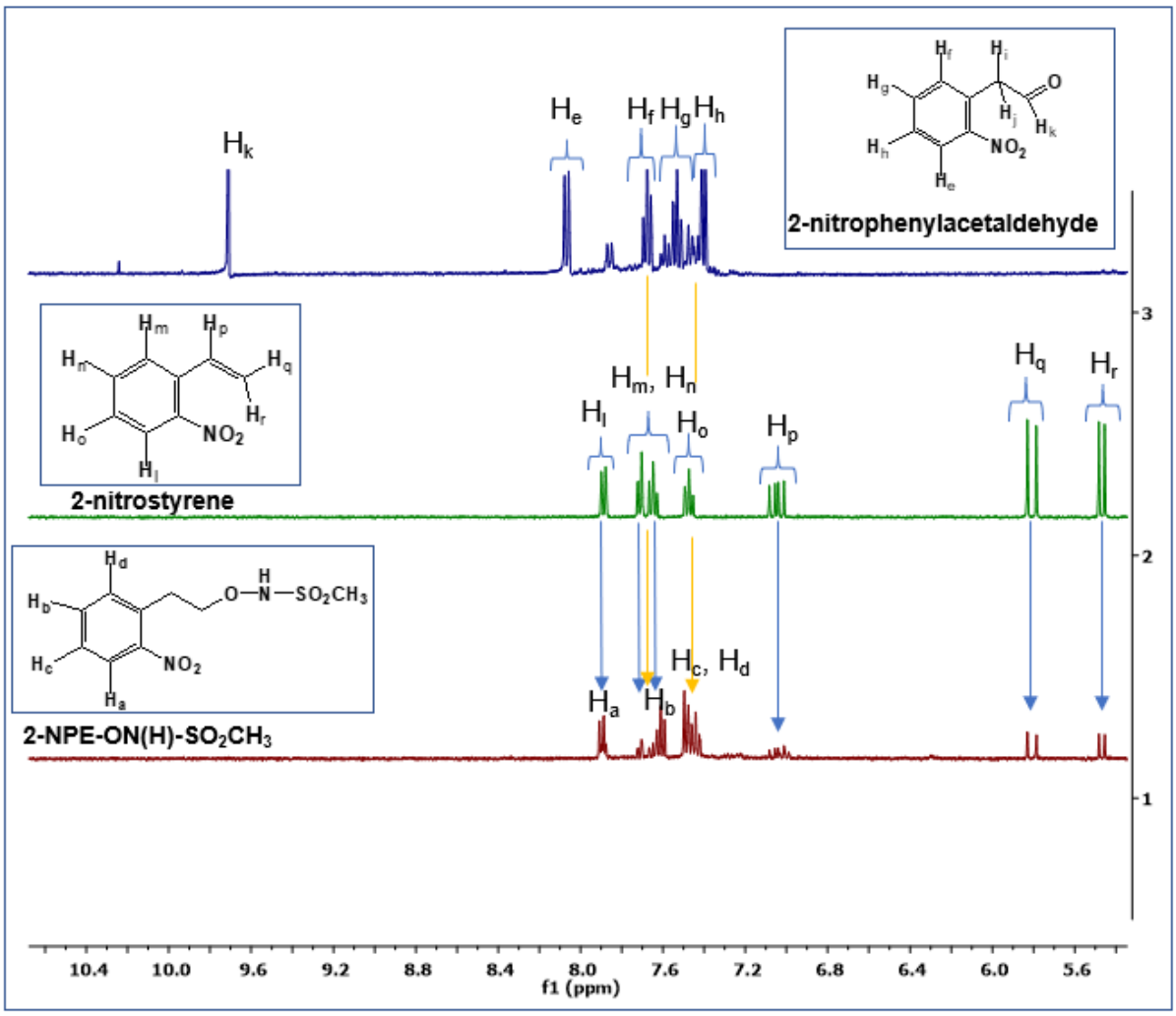

Figure 3.23. Comparison of ^{1}H NMR spectra of a partially photolyzed sample (5.0 min irradiation) of **2-NPE-ON(H)-SO_2CH_3** and authentic samples of the expected aromatic photoproducts 2-nitrostyrene and 2-nitrophenylacetaldehyde in CD_3CN.

^{1}H NMR spectra as a function of total irradiation time in a mixture of 60:40 phosphate buffer (30.0 mM, pH 7.0) and CD_3CN (v:v) are provided in Figure A3.5, Appendix section. The percentage of the photoproducts and the observed rate constant are in reasonable agreement with values reported in the PhD thesis of our collaborator under the same conditions (85% CF_3SO_2NHOH, 8% $CF_3SO_2NH_2$ and 7% $CH_3SO_2^-$; 0.056 ± 0.003 min^{-1} ($t_{1/2}$ ~ 12 min)).[152] The results for 90:10 v/v phosphate buffer (30.0 mM, pH

7.0) and CD_3CN (v:v) were presented earlier in section 3.3.5 of this chapter. The photoproducts were identified using authentic samples. The results are summarised in Table 3.5.

Table 3.5. Effect of solvent ratio on the photoproducts derived from the *N*-hydroxysulfonamide moiety and the observed rate constant for photodecomposition of **2-NPE-ON(H)-SO_2CH_3** (1.0 mM).

Solvent ratio, % v/v (CD_3CN/phosphate buffer (30 mM), pH 7.0)	Percentage of Photoproducts			k_{obs} (min^{-1})
	CH_3SO_2NHOH	$CH_3SO_2NH_2$	$CH_3SO_2^-$	
100/00	85	7	8	0.0572
80/20	85	7	8	0.0524
60/40	85	8	7	0.0563
40/60	85	7	8	0.0533
10/90	85	6	9	0.0554

Whereas ~30% of the desired concomitant C-O/N-S bond cleavage occurred to release $CF_3SO_2^-$ and HNO for **2-NPE-ON(H)-SO_2CF_3** (section 3.3.5), for **2-NPE-ON(H)-SO_2CH_3** only ~8% $CH_3SO_2^-$ is observed in the photoproduct solution with ~ 85% C-O bond cleavage occurring (observed photoproduct CH_3SO_2NHOH) and ~7% O-N bond cleavage (observed photoproduct $CH_3SO_2NH_2$). The thermal stability of CH_3SO_2NHOH was checked by recording the ^1H NMR spectrum of CH_3SO_2NHOH in CD_3CN (CH_3 peak at 3.02 ppm), 40/60 v/v phosphate buffer pH 7.0/CD_3CN (v/v) (CH_3 peak at 3.14 ppm) and 10/90 v/v phosphate buffer at pH 7.0/CD_3CN (CH_3 peak at 3.14 ppm) 3 h after preparing the sample. CH_3SO_2NHOH was found to be stable within this time frame. The $CH_3SO_2^-$ photoproduct therefore arises as a result of concomitant C-O/N-S bond cleavage, not from thermal decomposition of CH_3SO_2NHOH. Substituting the strong electron-withdrawing group of **2-NPE-ON(H)-SO_2CF_3** for the weaker electron-withdrawing group of **2-NPE-ON(H)-SO_2CH_3** significantly reduces the percentage of photoinduced O-N bond cleavage (from 70% to 7%). However the C-O bond cleavage pathway dominates instead of the desired concomitant C-O/N-S bond cleavage leading to HNO release.

Prior to doing steady state irradiation experiments for **2-NPE-ON(H)-SO_2Ar** (Ar = (2-SO_2Me)Ph), rate constants for the thermal decomposition of $ArSO_2NHO(H)$ (Ar = (2-SO_2Me)Ph) to $ArSO_2^-$ + HNO in CH_3CN/phosphate buffer, pH 7.0 solvent mixtures were determined by UV-Vis spectroscopy (Figure 3.24) and are given in the last

column of Table 3.7. The rate constant for thermal decomposition of $ArSO_2NHO(H)$ is independent of the components in the solvent mixture within experimental error. The half-life for decomposition of the parent $ArSO_2NHO(H)$ is 40 min in CD_3CN/phosphate buffer pH 7.0 solvent mixtures. As mentioned above, in pure CD_3CN, $ArSO_2NHOH$ is stable.

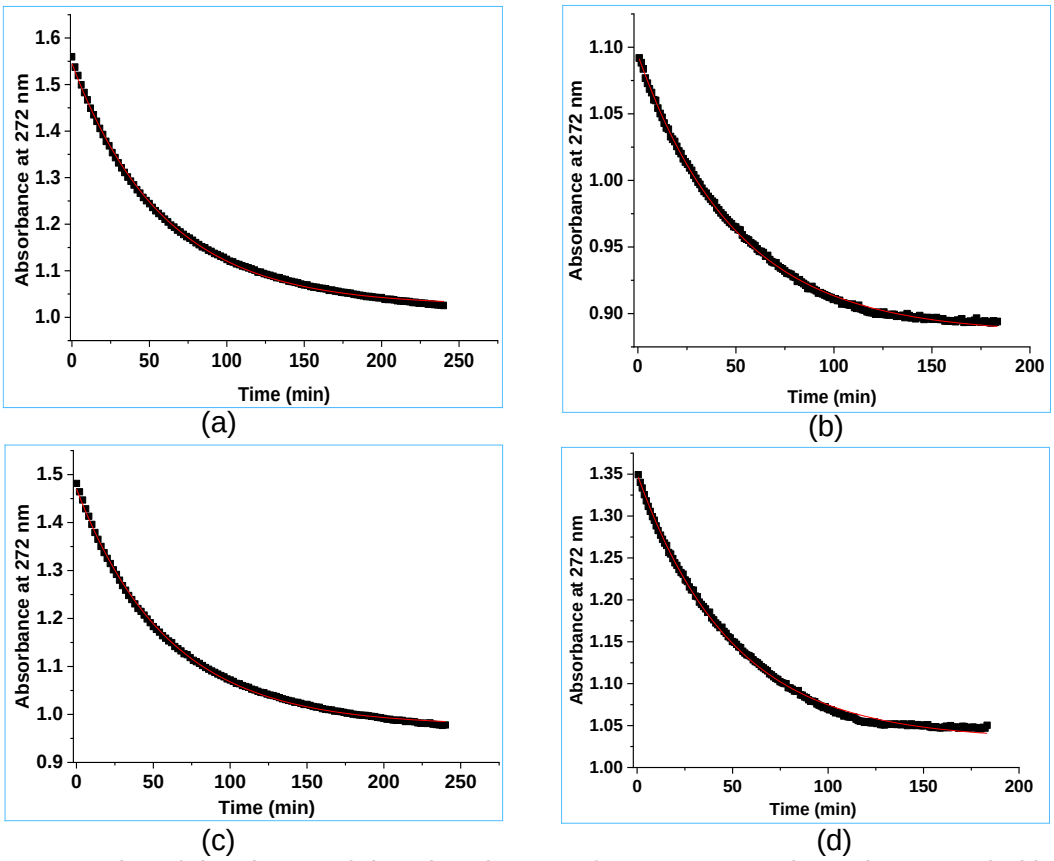

Figure 3.24. Plot of the decay of the absorbance of $ArSO_2NHOH$ (Ar = (2-SO_2Me)Ph) at 272 nm versus time at (a) 80:20, (b) 60:40, (c) 40:60 and (d) 10:90 v/v CH_3CN: phosphate buffer (30 mM, pH 7.0) (aerobic solution). The best fit of the data to a first-order rate equation gives the observed rate constants provided in the last column of Table 3.7.

The percentage of the photoproducts obtained upon steady state irradiation of **2-NPE-ON(H)-SO_2Ar** and the observed rate constant for decomposition were determined at different solvent ratios in mixtures of CD_3CN and phosphate buffer (pH 7.0, 30 mM) by ^1H NMR spectroscopy. Initially the steady state photolysis of **2-NPE-ON(H)-SO_2Ar** was conducted in CD_3CN. Figure 3.25(a) shows ^1H NMR spectra as a function of total irradiation time for a solution of **2-NPE-ON(H)-SO_2Ar** in CD_3CN under anaerobic conditions. The observed rate constant was determined by monitoring the CH_3 resonance of the reactant at 3.36 ppm in the ^1H NMR spectrum as a function of total irradiation time, giving $k_{obs} = 0.031 \pm 0.003$ min^{-1} (Figure 3.25(b)). O-N bond cleavage (43% $ArSO_2NH_2$) and concomitant C-O/N-S bond cleavage (45% $ArSO_2NHOH$ and

$ArSO_2^-$) occurs, with 12% of an unknown species observed in photoproduct mixture. The ^1H NMR spectrum of methyl phenyl sulfone was recorded to check the unknown species. The methyl peak of methyl phenyl sulfone appeared at 3.01 ppm. Therefore, the unknown species was not methyl phenyl sulfone. $ArSO_2NHOH$ was not stable in the presence of phosphate buffer, so the separate amounts of $ArSO_2^-$ and $ArSO_2NHOH$ could not be determined. The enlarged region of a fully irradiated ^1H NMR spectrum from an earlier experiment is shown in Figure 3.25(c). It took ~5-7 h to collect this data for each solvent condition, with the percentage of each photoproduct determined at the end of the experiment (almost complete photodecomposition of **2-NPE-ON(H)-SO_2Ar**).

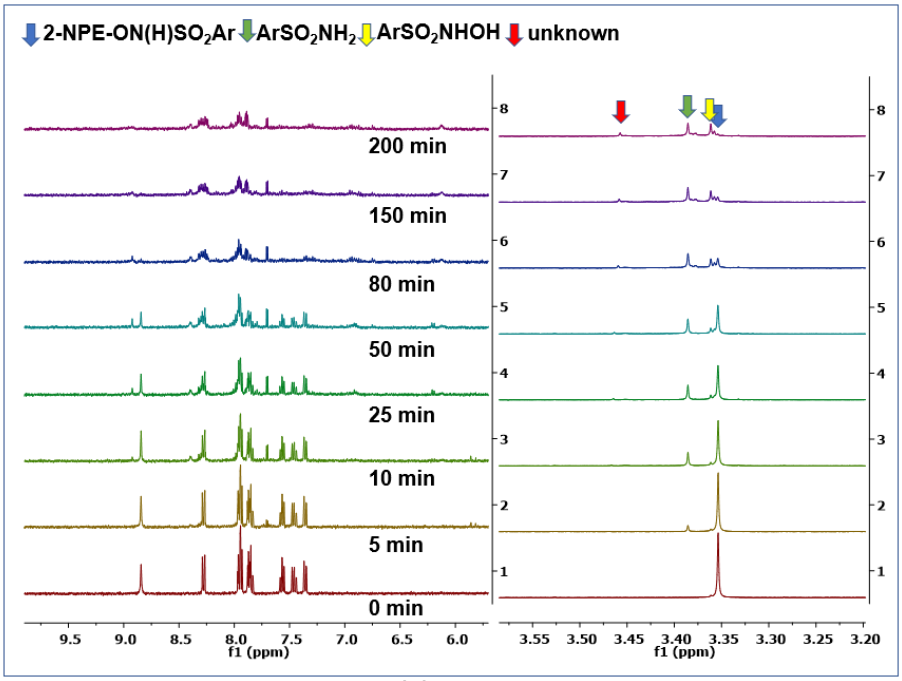

(a)

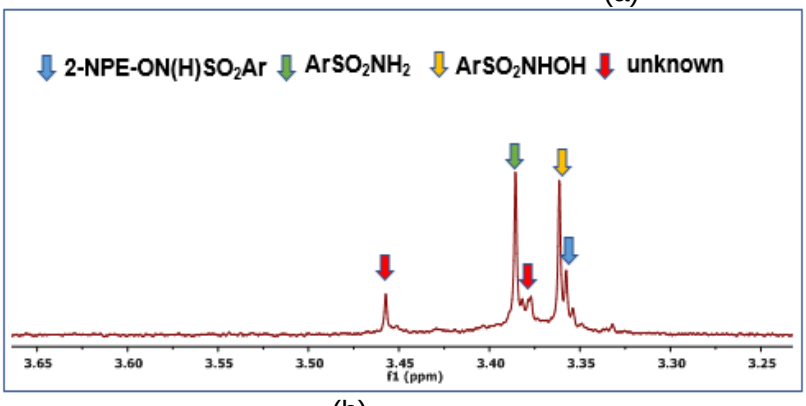

(b)

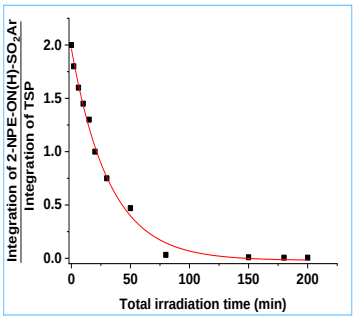

(c)

Figure 3.25. (a) ^1H NMR spectra as a function of total irradiation time for the photolysis of **2-NPE-ON(H)-SO_2Ar** (1.0 mM) in CD_3CN. (b) The final spectrum of the experiment shown in Figure 3.25(a), from 3.25 - 3.65 ppm. (c) Ratio of the area of the CH_3 signal of **2-NPE-ON(H)-SO_2Ar** and the TSP reference versus time. The best fit of the data to a first-order rate equation gives k_{obs} = 0.031 ± 0.003 min^{-1} ($t_{1/2}$ ~ 22 min).

The photoproducts generated from **2-NPE-ON(H)-SO_2Ar** were confirmed by comparing the ^{1}H NMR spectrum of a partially photolyzed sample of **2-NPE-ON(H)-SO_2Ar** (Figure 3.26) with ^{1}H NMR spectra of authentic samples of $ArSO_2NH_2$ (3.39 ppm), $ArSO_2NHOH$ (3.36 ppm) and $ArSO_2^-$ (3.35 ppm).

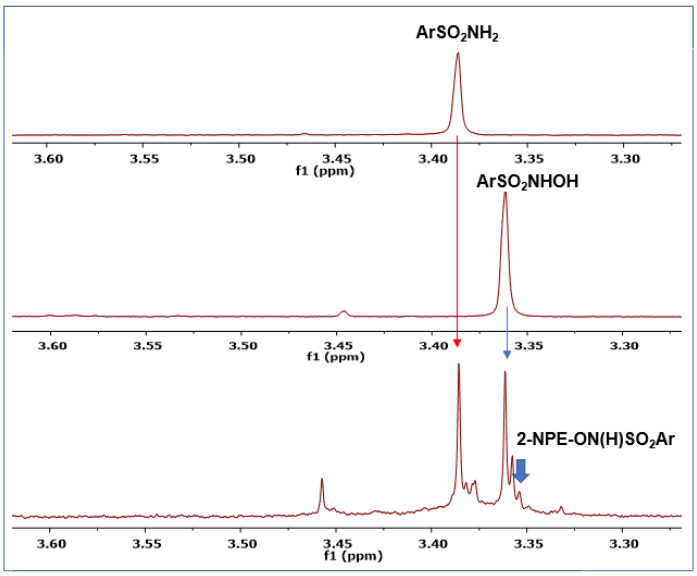

Figure 3.26. ^{1}H NMR spectra of a photolyzed sample (180 min irradiation) of **2-NPE-ON(H)-SO_2Ar** and authentic samples of $ArSO_2NH_2$ and $ArSO_2NHOH$ in CD_3CN from 3.65 ppm to 3.25 ppm.

Figure 3.27 shows a comparison of the aromatic region of the ^{1}H NMR spectrum of **2-NPE-ON(H)-SO_2Ar** and authentic sample of 2-nitrostyrene, 2-nitrophenylacetaldehyde, $ArSO_2NH_2$ and $ArSO_2NHOH$ in CD_3CN. Only peaks from 2-nitrostyrene were observed. Peaks from the other photoproduct peaks were not seen as they are photosensitive.

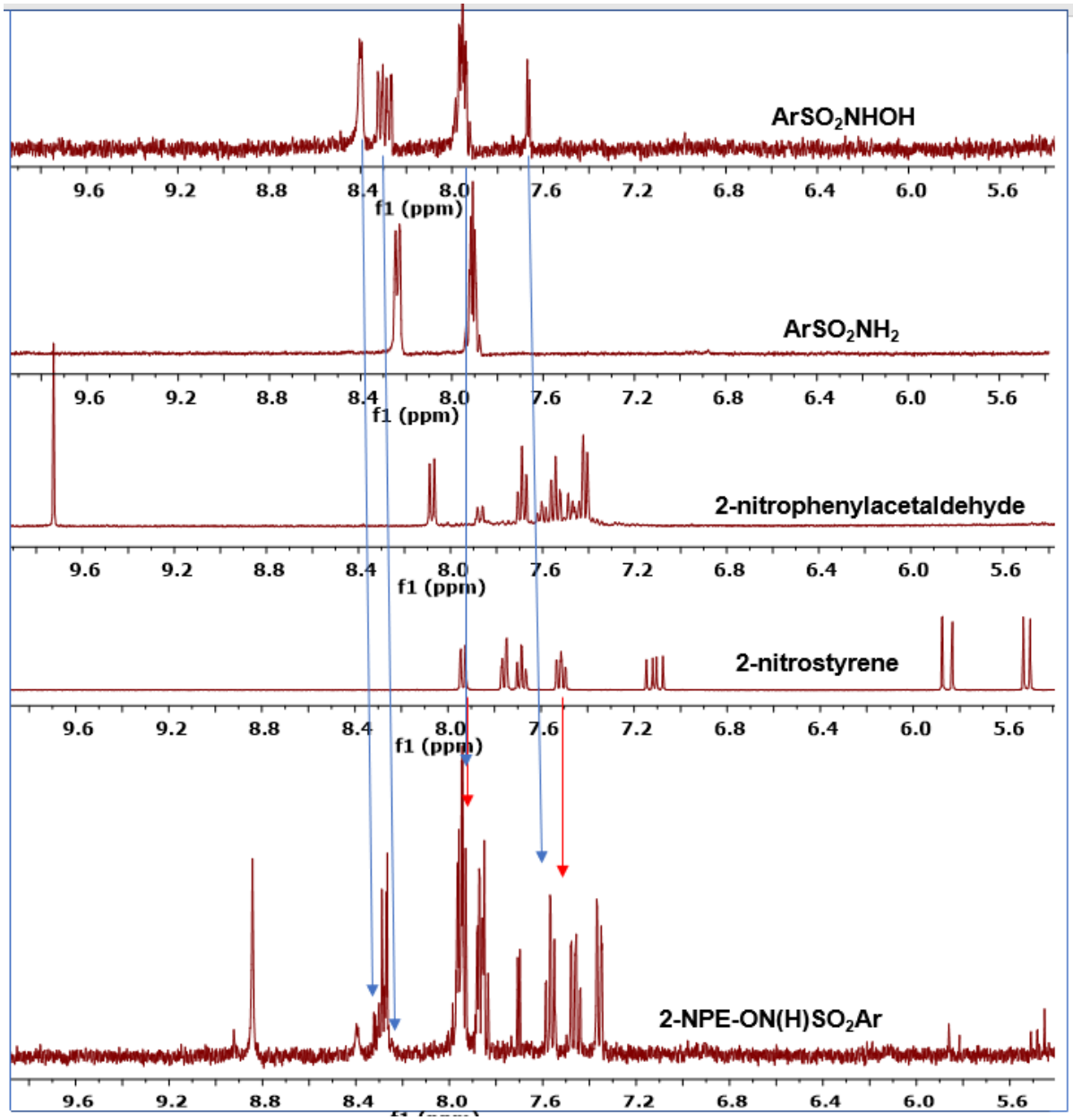

Figure 3.27. ^{1}H NMR spectra of a partially photolyzed sample (50 min irradiation) of **2-NPE-ON(H)-SO$_2$Ar** and authentic sample of 2-nitrostyrene, 2-nitrophenylacetaldehyde, $ArSO_2NH_2$ and $ArSO_2NHOH$ in CD_3CN.

The photoproduct solution was also analyzed using ES mass spectrometry (negative mode). Two species ($ArSO_2^-$ and $ArSO_3^-$) were identified by ES mass spectrometry in the photoproduct mixture. The observed and calculated *m/z* values of these compounds are given in Table.3.6.

Table 3.6. Observed and calculated *m/z* ratios for $ArSO_2^-$ and $ArSO_3$.

Compound	Calculated *m/z*	Observed *m/z*
$ArSO_2^-$	218.97	219.0
$ArSO_3^-$	234.97	235.0

GC-MS analysis on a partially photolyzed (20%) sample of **2-NPE-ON(H)-SO_2Ar** in CD_3CN showed four peaks in the chromatogram that could be assigned to 2-nitrostyrene (10.1 min), methyl phenyl sulfone (14.2 min), 2-nitrophenylacetaldehyde (13.6 min) and 2-nitrophenethyl alcohol (16.4 min) (Figures 3.28). The mass spectrum and the retention times of each species agreed with pure authentic standards of each compound. The methyl phenyl sulfone peak was not observed in the NMR spectrum of the photoproduct mixture (CH_3 peak of methyl phenyl sulfone peak was observed at 3.01 ppm). This species observed by mass spectrometry may therefore be produced during the mass spectrometry experiment. The parent sulfohydroxamic acid, $ArSO_2NHOH$ (Ar = 2-($MeSO_2$)Ph), which is stable in this solvent, was not observed, confirming that C-O bond cleavage does not occur in pure CD_3CN.

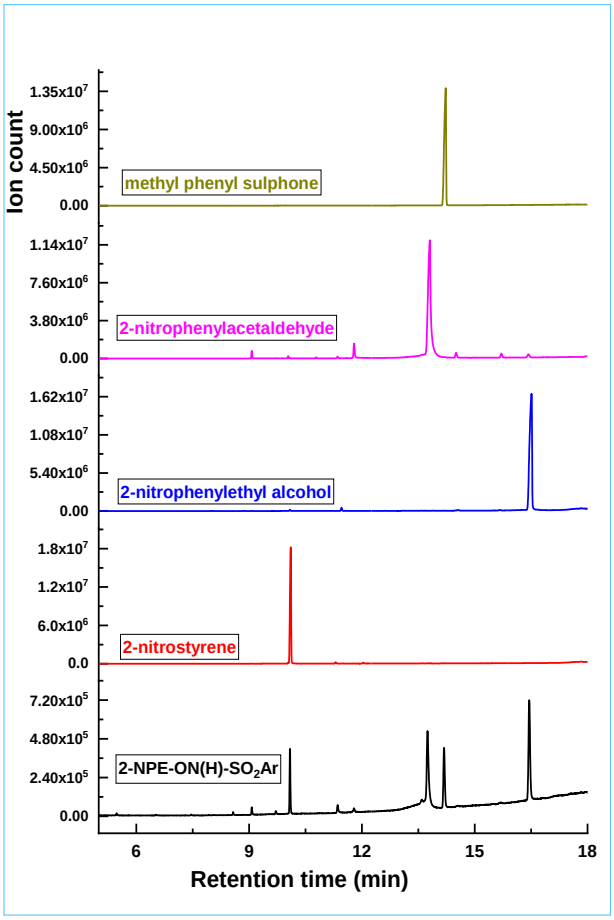

Figure 3.28. GC-MS chromatograms of a partially photolyzed sample (~20% decomposition) of **2-NPE-ON(H)-SO_2Ar** with the authentic standards of 2-nitrostyrene (10.1 min), methyl phenyl sulfone (14.2 min), 2-nitrophenylacetaldehyde (13.6 min) and 2-nitrophenethyl alcohol (16.4 min) in CD_3CN.

Steady state photolysis experiments for **2-NPE-ON(H)-SO_2Ar** were carried out in a mixture of phosphate buffer (30.0 mM, pH 7.0) and CD_3CN (20:80, v/v) to check the effect of solvent on the observed photoproducts. Figure 3.29(a) shows ^1H NMR

spectra as a function of total irradiation time for a solution of **2-NPE-ON(H)SO$_2$Ar** in CD_3CN under anaerobic conditions. Fitting the area of the CH_3 peak as a function of total irradiation time to a first-order equation gives k_{obs} = 0.032 ± 0.005 min^{-1} (Figure 3.29(b)). An enlarged ^{1}H NMR spectrum in the 3.00 to 3.70 ppm region is shown in Figure 3.25(c). The percentage of the photoproducts was 50% ($ArSO_2NHOH$ + $ArSO_2^-$), 40% $ArSO_2NH_2$ and 10% of unknown species (10%).

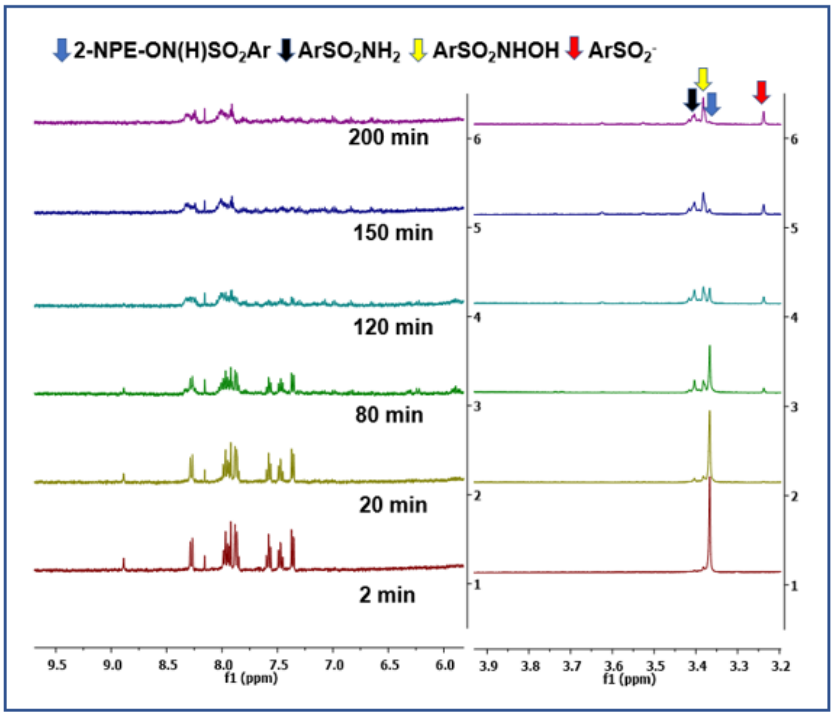

(a)

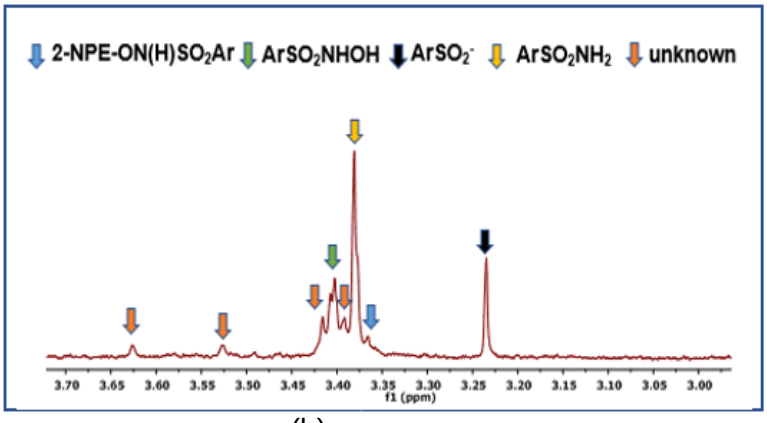

(b)

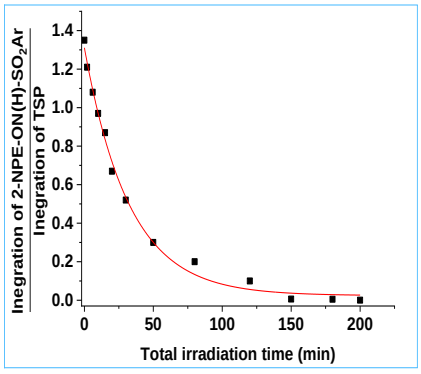

(c)

Figure 3.29. (a) ^{1}H NMR spectra as a function of total irradiation time for the photolysis of **2-NPE-ON(H)-SO$_2$Ar** (1.0 mM) in a mixture of phosphate buffer (30.0 mM, pH 7.0) and CD_3CN (20:80, v/v). (b) The final spectrum of the experiment shown in Figure 3.25(a), from 2.95 - 3.70 ppm. (c) Ratio of the area of the CH_3 signal of **2-NPE-ON(H)-SO$_2$Ar** and the TSP reference versus time. The best fit of the data to a first-order rate equation gives k_{obs} = 0.032 ± 0.005 min^{-1} ($t_{1/2}$ ~ 22 min).

The photoproducts were also determined in a mixture of phosphate buffer (30.0 mM, pH 7.0) and CD_3CN (40:60, v/v). Figure 3.30(a) shows ^1H NMR spectra as a function of total irradiation time for a solution of **2-NPE-ON(H)SO_2Ar** in this solvent mixture. The photoproducts were $ArSO_2NHOH$ + $ArSO_2^-$ (85%), $ArSO_2NH_2$ (10%) and an unknown species (4%). Fitting the area of the CH_3 peak as a function of irradiation time to a first-order reaction gives k_{obs} = 0.030 ± 0.006 min^{-1} (Figure 3.30(b)). The percentage of the photoproducts and the observed rate constant are in reasonable agreement with values reported by our collaborator (87% $ArSO_2NHOH$ + $ArSO_2^-$, 13% $ArSO_2NH_2$, k_{obs} = 0.032 ± 0.001 min^{-1}).[152]

The data for steady state photolysis in a mixture of phosphate buffer (30.0 mM, pH 7.0) and CD_3CN (90:10, v/v) has been discussed in section 3.3.5. ^1H NMR spectra as a function of total irradiation time in a mixture of 60:40 v/v phosphate buffer (30.0 mM, pH 7.0) and CD_3CN are provided in Figure A3.6, Appendix section.

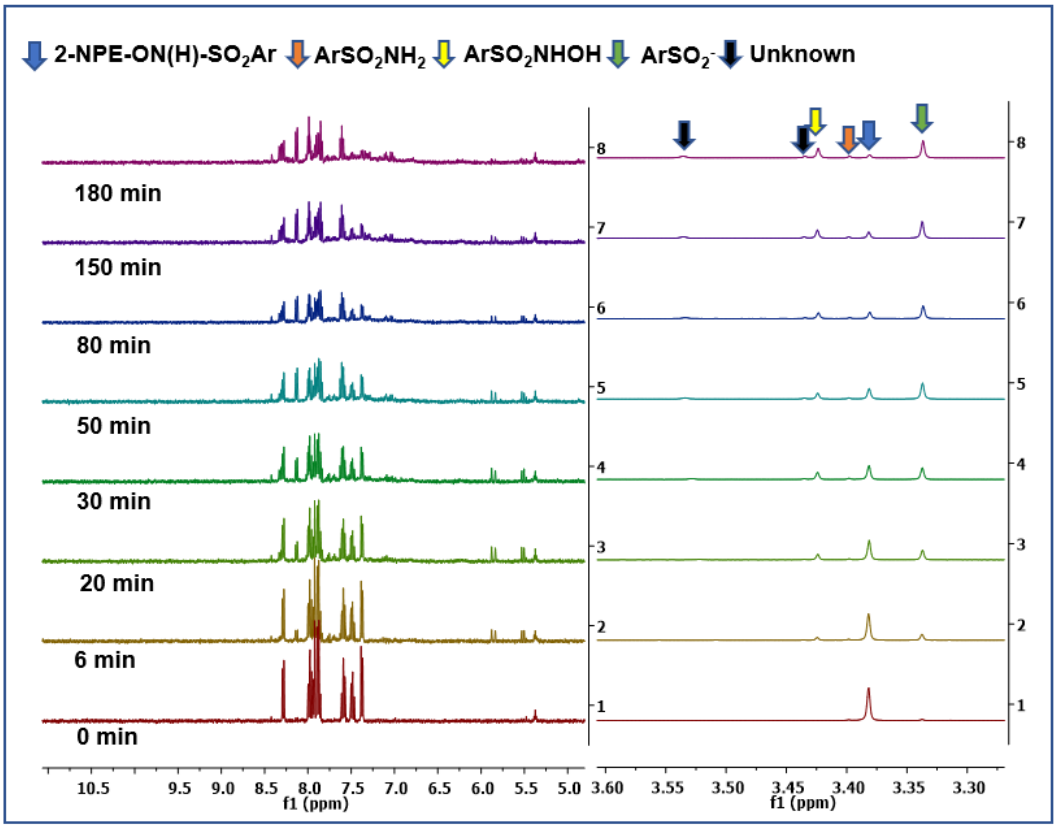

(a)

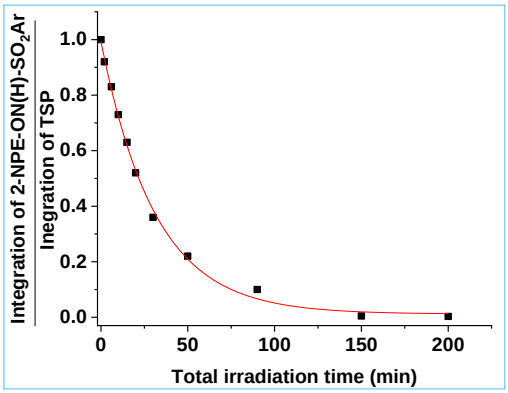

(b)

Figure 3.30. (a) ^{1}H NMR spectra as a function of total irradiation time for the photolysis of **2-NPE-ON(H)-SO$_2$Ar** (1.0 mM) in a mixture of phosphate buffer (30.0 mM, pH 7.0) and CD_3CN (40:60, v/v). (b) Ratio of the area of the CH_3 signal of **2-NPE-ON(H)-SO$_2$Ar** and the TSP reference versus time. The best fit of the data to a first-order rate equation gives k_{obs} = 0.030 ± 0.006 min^{-1} ($t_{1/2}$ ~ 23 min).

The effect of the solvent composition on the photoproducts for **2-NPE-ON(H)-SO$_2$Ar** is summarized in Table 3.7. Interestingly, for this compound the percentage of photoinduced O-N cleavage significantly decreases with the increasing volume percentage of phosphate buffer in the solvent mixture. As the aqueous component reaches 40%, more C-O (and/or C-O/N-S) bond cleavage occurs (up to 85% $ArSO_2NHO(H)$ + $ArSO_2^-$). However, since $ArSO_2NHO^-$ is not stable in the solvent mixture, observation of some or all of the $ArSO_2^-$ in the photoproducts may be a consequence of secondary thermal decomposition of the primary $ArSO_2NHO(H)$ photoproduct. Rate constants for thermal decomposition of $ArSO_2NHO(H)$ to $ArSO_2^-$ + HNO in CH_3CN/phosphate buffer, pH 7.0 solvent mixtures were therefore determined by UV-Vis spectroscopy (Figure 3.8, section 3.3.4) and are given in the last column of Table 3.7. The rate constant for thermal decomposition of $ArSO_2NHO(H)$ is independent of the components in the solvent mixture within experimental error. Given that it took ~5-7 h for collection of the NMR data at each solvent condition in the photodecomposition experiments and since the half-life for decomposition of the parent $ArSO_2NHO(H)$ is 40 min in CD_3CN/phosphate buffer pH 7.0 solvent mixtures, it was not possible to determine whether C-O/N-S concerted bond cleavage occurs in addition to C-O bond cleavage followed by decomposition of $ArSO_2NHO$- to the corresponding $ArSO_2^-$ with HNO release. As mentioned above, in pure CD_3CN, $ArSO_2NHOH$ is stable. In this solvent the small amount of $ArSO_2^-$ observed must arise from concerted C-O/N-S bond cleavage.

Table 3.7. Effect of solvent ratio on the photoproducts derived from the *N*-hydroxysulfonamide moiety and the observed rate constant for photodecomposition of **2-NPE-ON(H)-SO_2Ar** (1.0 mM).

Solvent ratio, % v/v (CD_3CN/phosphate buffer (30 mM), pH 7.0)	Percentage of Photoproducts			k_{obs} (min^{-1})	k_{obs} (min^{-1}) for thermal decomposition of $ArSO_2NHO(H)$ in (CH_3CN/phosphate buffer (30 mM), pH 7.0)
	$ArSO_2NHO(H)$ and $ArSO_2^-$ [a]	$ArSO_2NH_2$	Unknown species		
100/00	43[b]	45	12[c]	0.0312	No observed decomposition[b]
80/20	50	40	10[c]	0.0323	0.0172 ($t_{1/2}$ ~ 40 min)
60/40	85	10	4	0.0332	0.0183 ($t_{1/2}$ ~ 38 min)
40/60	83	14	3	0.0303	0.0175 ($t_{1/2}$ ~ 40 min)
10/90	85	11	4	0.0313	0.0193 ($t_{1/2}$ ~ 36 min)

[a] $ArSO_2NHO(H)$ is a reaction intermediate and decomposes further to give $ArSO_2^-$.

[b] In pure anhydrous CD_3CN, $ArSO_2NHOH$ is stable (~1% decomposition over 3 days) and in this solvent only $ArSO_2^-$ was observed.

[c] More than one species.

3.3.7 Effect of pH on the photoproducts

To obtain more information on factors which affect the mechanism of photodecomposition, the effect of pH of the aqueous component of the buffer on photoproducts were investigated. Walbert et al. reported that pH has a significant effect on the mechanism of decomposition reaction pathways for (2-nitrophenyl)ethyl-caged molecules.[124] β-Elimination of the leaving group to give 2-nitrostyrene was found to occur at higher pH values. Walbert et al. proposed that deprotonation of the monoprotonated aci-nitro intermediate to the aci-nitro anion occurs prior to β-elimination.

The effect of pH of the aqueous component of the solvent mixture on the mechanism of photodecomposition of **2-NPE-ON(H)-SO_2CF_3** was investigated in 10% v/v CD_3CN in aqueous solution. Prior to conducting these experiments, the thermal stability of **2-**

NPE-ON(H)-SO_2CF_3 was investigated. **2-NPE-ON(H)-SO_2CF_3** was not thermally stable at pH 1.0, decomposing to give $CF_3SO_2NH_2$ (90%) and a small amount of $CF_3SO_2^-$ (10%), with an estimated half-life of ~17 h (Figure 3.31). Further studies are needed to better understand thermal decomposition in acidic solution. One way to facilitate O-N cleavage is to further protonate the N, which is challenging in the presence of the strongly electron-withdrawing SO_2CF_3 group. At pH 12.0 **2-NPE-ON(H)-SO_2CF_3** thermally decomposes to give $CF_3SO_2NH_2$ (92%) and a small amount of $CF_3SO_2^-$ (8%), with an estimated half-life of ~16 h (Figure 3.32). Under these strongly basic conditions, predominant deprotonation of the β-methylene carbon with concomitant cleavage of the weak O-N bond and N-protonation via an E2-type mechanism would be expected, leading to $CF_3SO_2NH_2$ and *o*-nitrophenylethanal.[182]

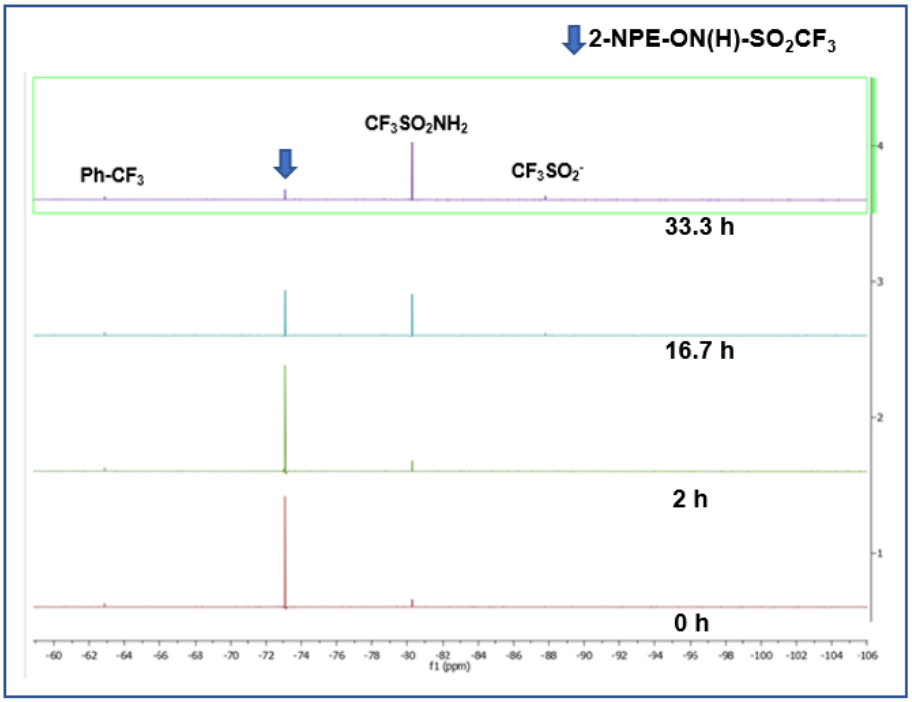

Figure 3.31. ^{19}F NMR spectra obtained for the thermal decomposition of **2-NPE-ON(H)-SO_2CF_3** (1.0 mM) in an anaerobic 90:10 v/v mixture of 0.10 M HCl (pH 1.0) and CD_3CN at 0, 2, 16.6 and 33.3 h. The half-life of the reaction is ~17 h.

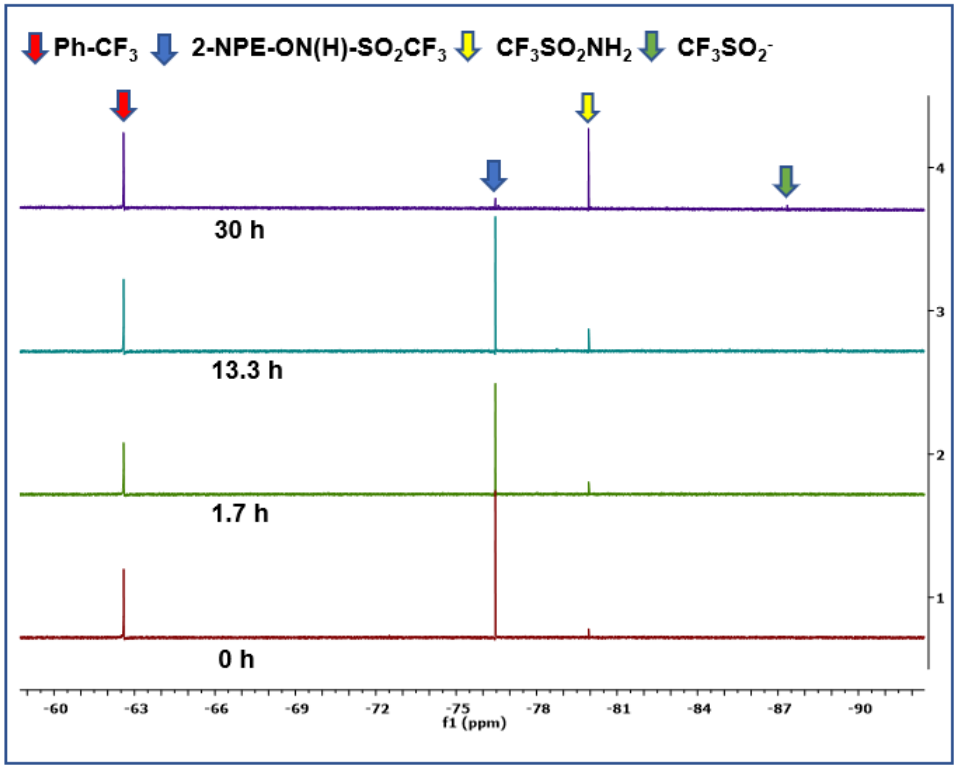

Figure 3.32. ^{19}F NMR spectra obtained for the thermal decomposition of **2-NPE-ON(H)-SO_2CF_3** (1.0 mM) in an anaerobic 90:10 v/v mixture of 0.010 M NaOH (pH 12.0) and CD_3CN at 0, 1.7, 13.3 and 30 h. The half-life of the reaction is ~16 h.

2-NPE-ON(H)-SO_2CF_3 was thermally stable (no observed decomposition) for at least 12 h when the pH of the aqueous component of the solvent mixture was in the pH 2-10 range. The major pathway for the photolysis of compound **2-NPE-ON(H)-SO_2CF_3** at pH 2.1 (Figure 3.33(a)) was C-O bond cleavage (75% CF_3SO_2NHOH). As indirect evidence for the correct assignment of the ^{19}F NMR peak to CF_3SO_2NHOH, the pH of a photolyzed sample of **2-NPE-ON(H)-SO_2CF_3** was increased from 2.1 to 5.0. As expected, $CF_3SO_2NHO(H)$ (pK_a ~ 5.6) [55] decomposed to give $CF_3SO_2^-$ (Figure 3.34). O-N bond cleavage also occurred as a minor pathway (23% $CF_3SO_2NH_2$). At -78.2 ppm an unknown photoproduct (~2%) was also observed. The ^{19}F NMR spectrum of an authentic sample of $CF_3SO_3^-$ (-80.2 ppm) recorded under the same solvent conditions showed that the unknown peak cannot be attributed to this anion.

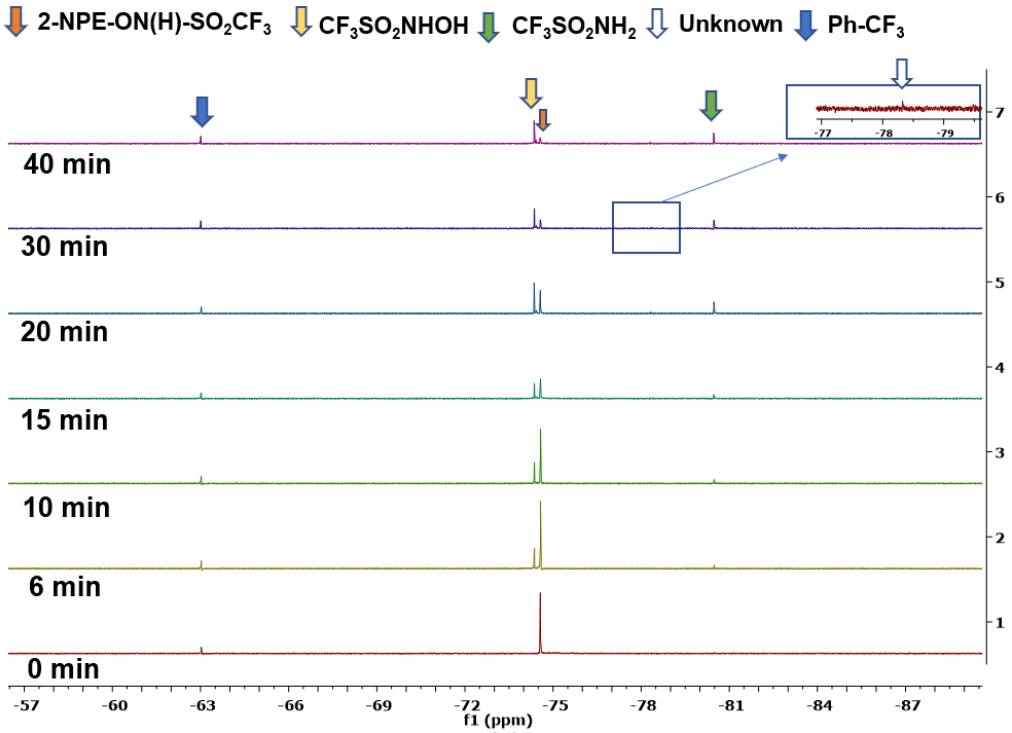

(a)

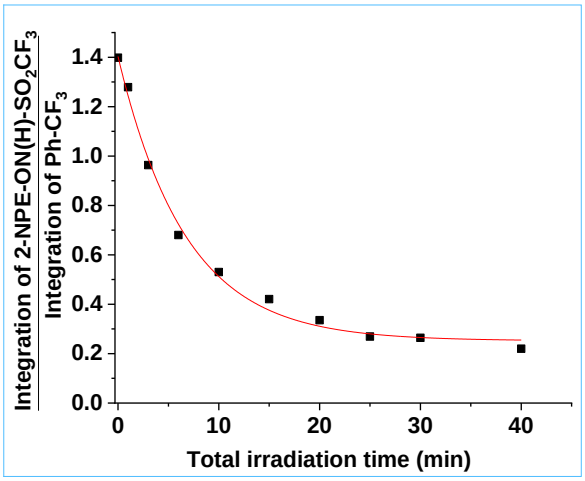

(b)

Figure 3.33. (a) ^{19}F NMR spectra as a function of total irradiation time for the photolysis of **2-NPE-ON(H)-SO_2CF_3** (1.0 mM) in a 10:90 v/v mixture of CD_3CN and phosphate buffer (30 mM, pH 2.1). (b) Ratio of the area of the CF_3 signal of **2-NPE-ON(H)-SO_2CF_3** and the Ph-CF_3 reference versus time. The best fit of the data to a first-order rate equation gives k_{obs} = 0.146 ± 0.001 min^{-1} ($t_{1/2}$ ~ 4.7 min).

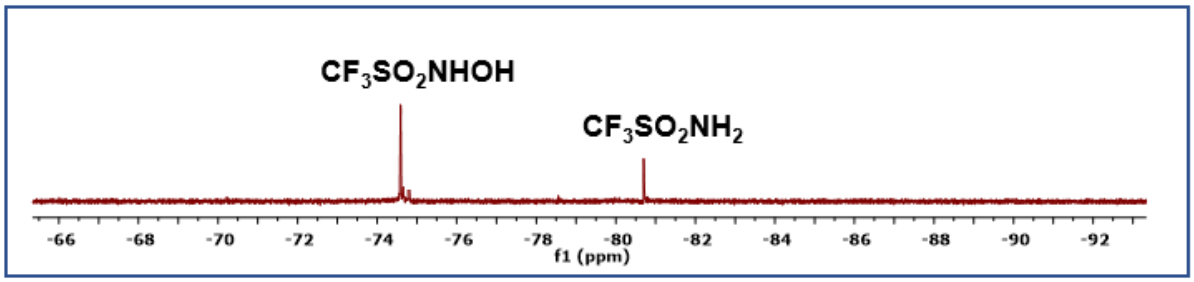

(a)

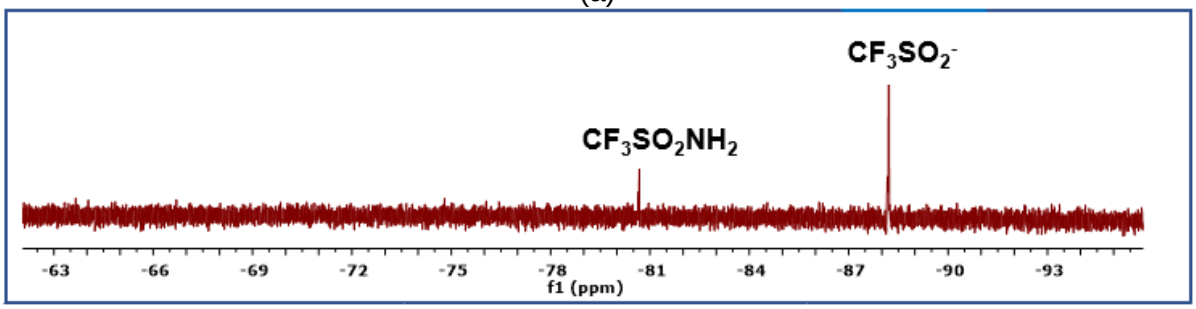

(b)

Figure 3.34. ^{19}F NMR spectrum obtained upon adjusting the pH of a photolyzed solution of **2-NPE-ON(H)-SO_2CF_3** at (a) pH 2.1 to (b) pH 5.0.

The photodecomposition of **2-NPE-ON(H)-SO_2CF_3** as a function of total irradiation time was also investigated using ^{19}F NMR spectroscopy in a 10:90 v/v mixture of CD_3CN and acetate buffer at pH 5.0 (Figure 3.35) and carbonate buffer at pH 10.0 (Figure 3.36). The area of the CF_3 peak as a function of irradiation time was plotted and fitted to a first-order equation at each pH condition, giving an observed rate constant for photodecomposition. At pH 5.0 the photoproducts were $CF_3SO_2NH_2$ (69%) and $CF_3SO_2^-$ (31%), k_{obs} = 0.138 ± 0.001 min^{-1} ($t_{1/2}$ = 5.0 min). At pH 10.0 the photoproducts were 70% $CF_3SO_2NH_2$ and 30% $CF_3SO_2^-$, with k_{obs} = 0.145 ± 0.001 min^{-1} ($t_{1/2}$ = 4.8 min). Data at pH 7.0 was presented earlier in section 3.3.5.

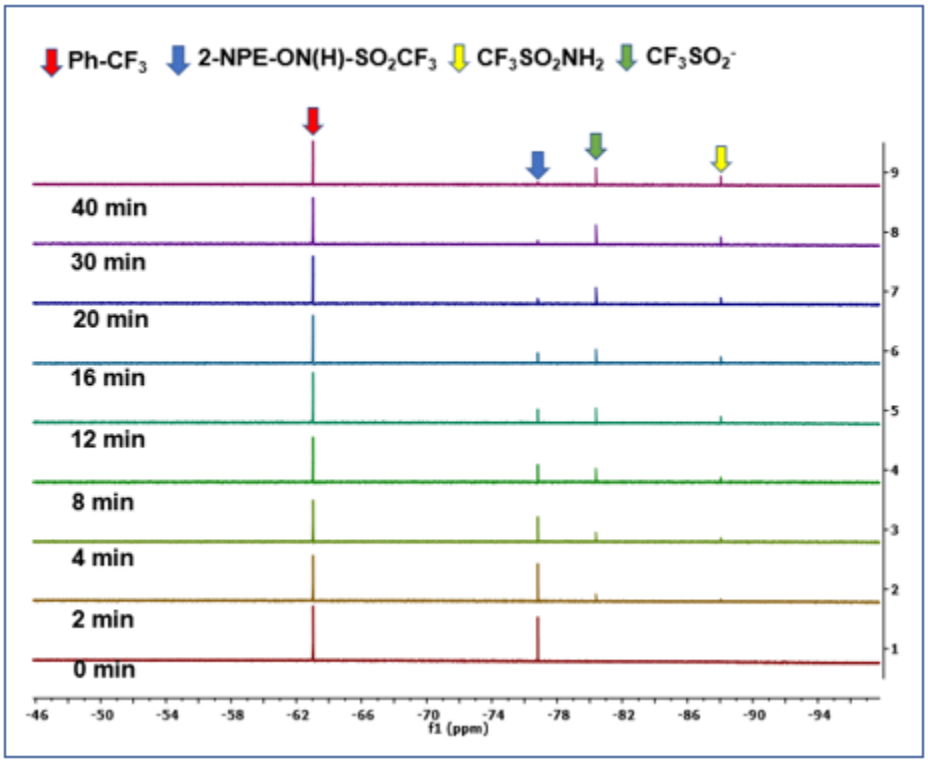

(a)

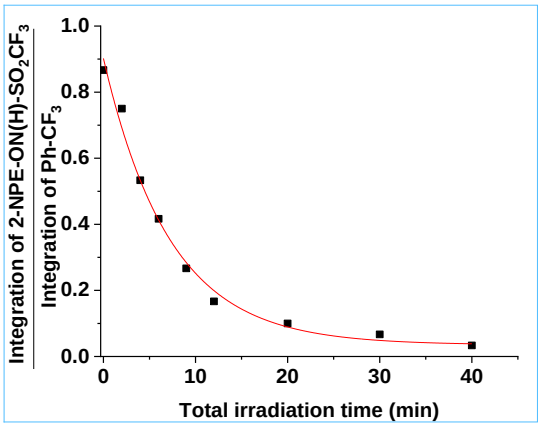

(b)

Figure 3.35. (a) ^{19}F NMR spectra as a function of total irradiation time for the photolysis of **2-NPE-ON(H)-SO_2CF_3** (1.0 mM) in a 10:90 v/v mixture of CD_3CN and acetate buffer (30 mM, pH 5.0). (b) Ratio of the area of the CF_3 signal of **2-NPE-ON(H)-SO_2CF_3** and the Ph-CF_3 reference versus time. The best fit of the data to a first-order equation gives k_{obs} = 0.138 ± 0.001 min^{-1} ($t_{1/2}$ = 5.0 min).

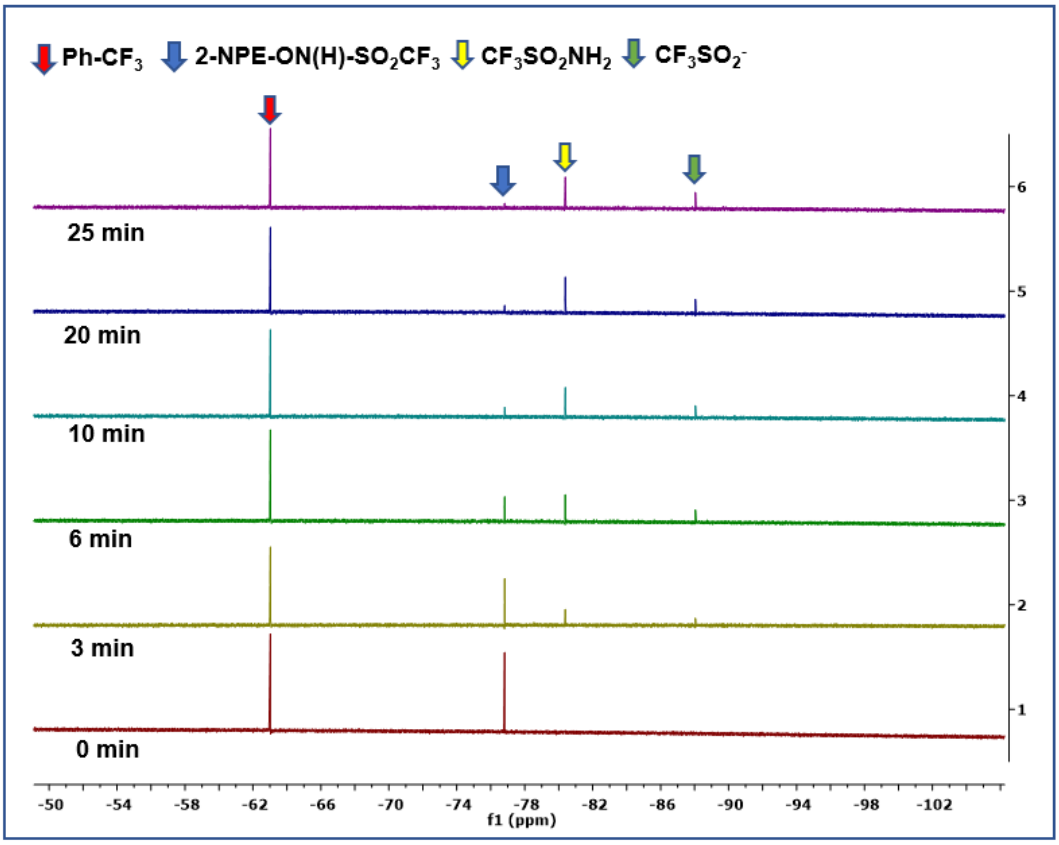

(a)

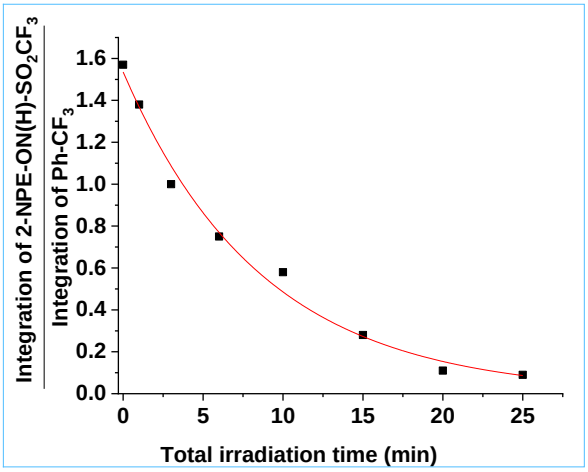

(b)

Figure 3.36. (a) ^{19}F NMR spectra as a function of total irradiation time for the photolysis of **2-NPE-ON(H)-SO_2CF_3** (1.0 mM) in a 90:10 v/v mixture of carbonate buffer (30 mM, pH 10.0) and CD_3CN. (b) Ratio of the area of the CF_3 signal of **2-NPE-ON(H)-SO_2CF_3** and the Ph-CF_3 reference versus time. The best fit of the data to a first-order equation gives k_{obs} = 0.145 ± 0.001 min^{-1} ($t_{1/2}$ = 4.8 min).

The results are summarized in Table 3.8. A significant increase in O-N bond cleavage was observed in the pH range 5.0–10.0, with ~70% $CF_3SO_2NH_2$ and ~30% $CF_3SO_2^-$. No $CF_3SO_2NHO(H)$ was observed during any of these experiments, consistent with $CF_3SO_2^-$ being generated as a result of concerted C-O/N-O bond cleavage rather than C-O bond cleavage. The last column of the Table 3.8 gives the observed rate constants

for the spontaneous (thermal) decomposition of $CF_3SO_2NHO(H)$ at each pH condition.[150] The value increases as pH increases.

Table 3.8. Effect of pH of the aqueous component of the solvent on the photoproducts and the observed rate constant for photodecomposition for **2-NPE-ON(H)-SO_2CF_3** (1.0 mM) in 10:90 v/v CD_3CN: aqueous buffer (30 mM).

pH	Percentage of Photoproducts			k_{obs} (min^{-1})	k_{obs} (min^{-1}) for spontaneous decomposition of $CF_3SO_2NHO(H)$[e]
	CF_3SO_2NHOH	$CF_3SO_2NH_2$	$CF_3SO_2^-$		
2.1[a,b]	75	23	00	0.146	1.4×10^{-3}
5.0[c]	00	69	31	0.138	5.0×10^{-3}
7.0[a]	00	67	33	0.138	2.8×10^{-2}
10.0[d]	00	70	30	0.145	5.8×10^{-2}

Aqueous component of solution: [a]phosphate buffer; [b]unknown species 2%, [c]acetate buffer; [d]carbonate buffer, [e] Aqueous conditions.[150]

The photoproducts obtained upon irradiation of **2-NPE-ON(H)-SO_2CH_3** were also investigated in 10% v/v CD_3CN in aqueous solution at different pH conditions using ^1H NMR spectroscopy. Prior to conducting these experiments, the thermal stability of **2-NPE-ON(H)-SO_2CH_3** was investigated. **2-NPE-ON(H)-SO_2CH_3** was found to be thermally stable in the pH range 3-12 in 10:90 v/v CH_3CN: aqueous solution for 12 h. Figure 3.37(a) shows ^1H NMR spectra as a function of total irradiation time for the **2-NPE-ON(H)-SO_2CH_3** at pH 3.1. From the data in the 3.20 to 2.30 ppm region the photoproducts were found to be CH_3SO_2NHOH (75%), $CH_3SO_2NH_2$ (15%) and $CH_3SO_2^-$ (10%). The integration area of the CH_3 peak of the reactant was plotted as a function of total irradiation time and the data fitted to first-order equation, giving k_{obs} = 0.061 ± 0.007 min^{-1} (Figure 3.37(b)).

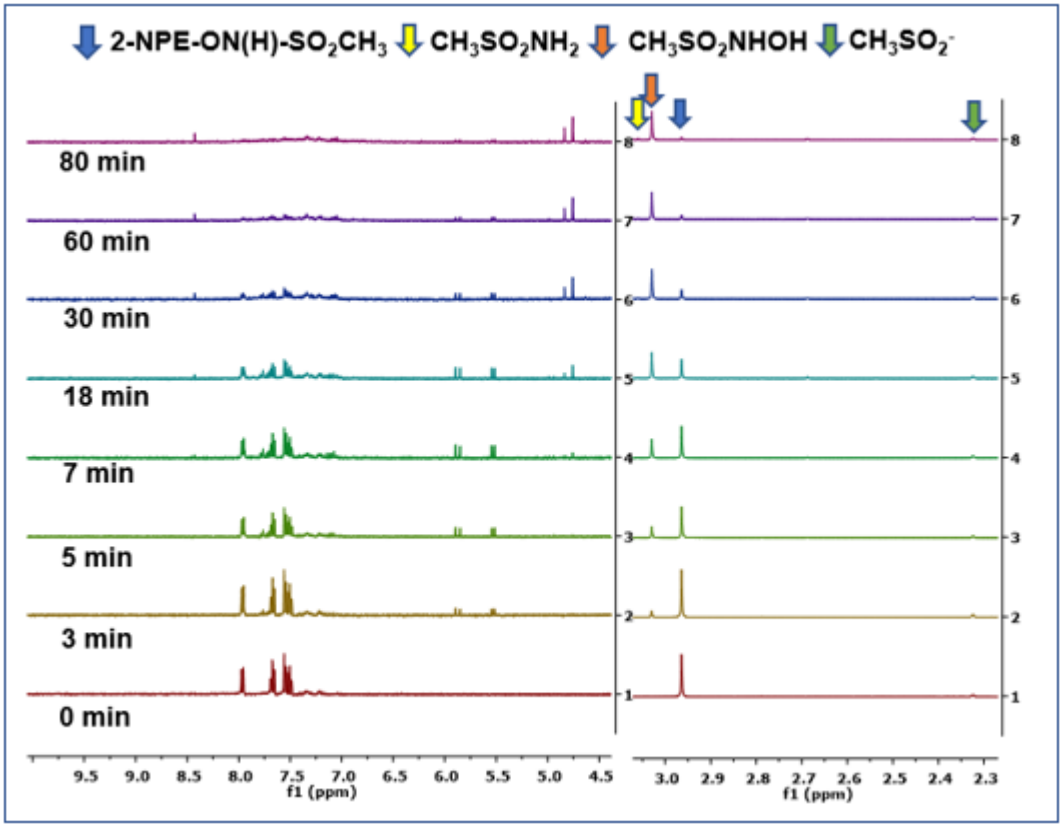

(a)

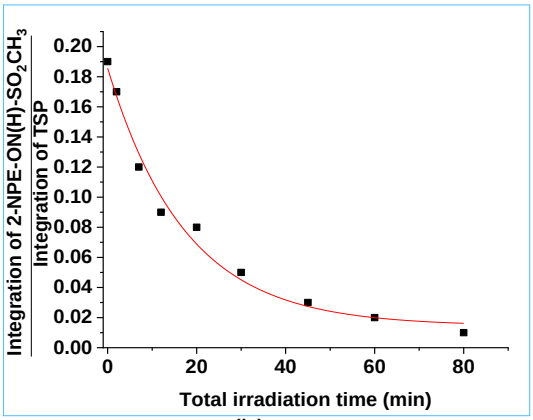

(b)

Figure 3.37. (a) ^{1}H NMR spectra as a function of total irradiation time for the photolysis of **2-NPE-ON(H)-SO$_2$CH$_3$** (1.0 mM) in a 90:10 v/v mixture of phosphate buffer (30 mM, pH 3.1) and CD_3CN. (b) Ratio of the area of the CH_3 signal of **2-NPE-ON(H)-SO$_2$CH$_3$** and the TSP reference versus time. The best fit of the data to a first-order equation gives k_{obs} = 0.061 ± 0.007 min^{-1} ($t_{1/2}$ = 11 min).

Steady state photolysis experiments for **2-NPE-ON(H)-SO$_2$CH$_3$** at pH 5.0 were also carried out. Figure 3.38(a) shows ^{1}H NMR spectra as a function of total irradiation time. The integration of the CH_3 peak of the reactant vs total irradiation time was fitted to first-order equation, giving k_{obs} = 0.059 ± 0.007 min^{-1} (Figure 3.38(b)). The percentage of each photoproducts was the same as at pH 3.0 within the experimental error.

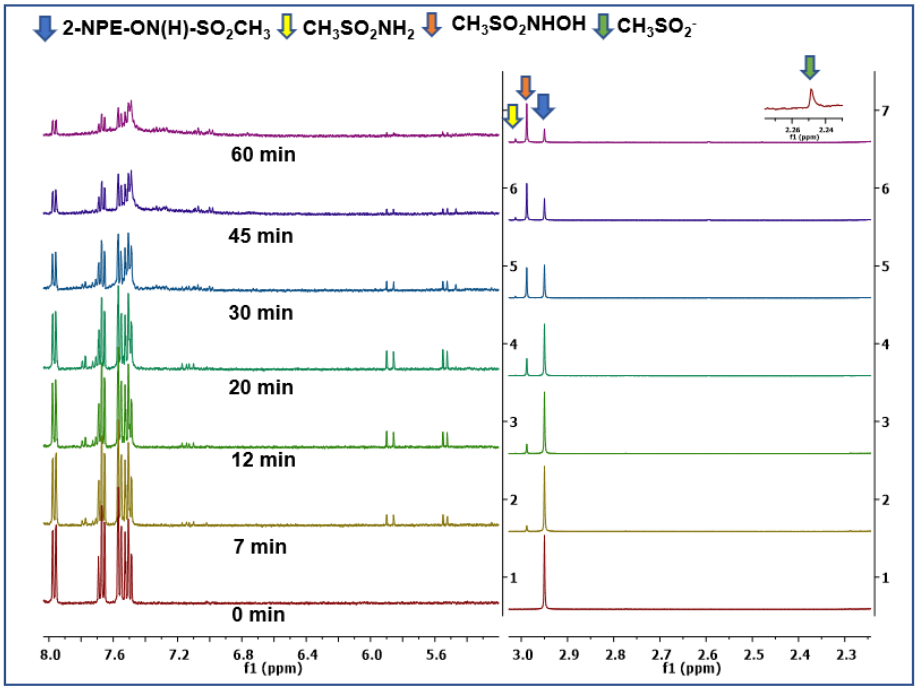

(a)

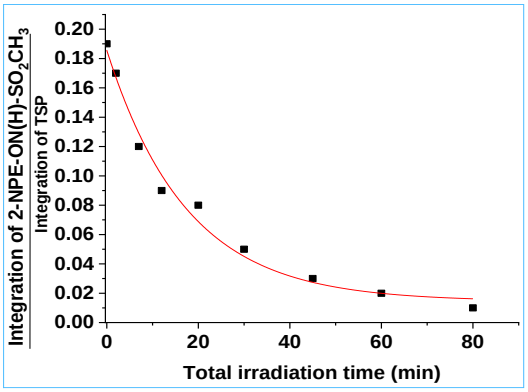

(b)

Figure 3.38. (a) ^{1}H NMR spectra as a function of total irradiation time for the photolysis of **2-NPE-ON(H)-SO$_2$CH$_3$** (1.0 mM) in a 90:10 v/v mixture of acetate buffer (30 mM, pH 5.0) and CD_3CN. (b) Ratio of the area of the CH_3 signal of **2-NPE-ON(H)-SO$_2$CH$_3$** and the TSP reference versus time. The best fit of the data to a first-order equation gives k_{obs} = 0.059 ± 0.007 min^{-1} ($t_{1/2}$ = 12 min).

Steady state photolysis experiments were carried out at higher pH conditions (pH 9.9 and 12.0). Figures 3.39(a) and 3.40(a) shows ^{1}H NMR spectra for the photodecomposition of **2-NPE-ON(H)-SO$_2$CH$_3$** as a function of total irradiation time at pH 9.9 and 12.0, respectively. The integration area of the CH_3 peak versus total irradiation time was fitted to a first-order equation, giving k_{obs} 0.048 ± 0.001 min^{-1} (pH 9.9, Figure 3.39(b)) and 0.049 ± 0.001 min^{-1} (pH 12.0, Figure 3.40(b)). The photoproducts observed were $CH_3SO_2NH_2$ (13%), CH_3SO_2NHOH (72%) and $CH_3SO_2^-$ (15%) at both pH conditions.

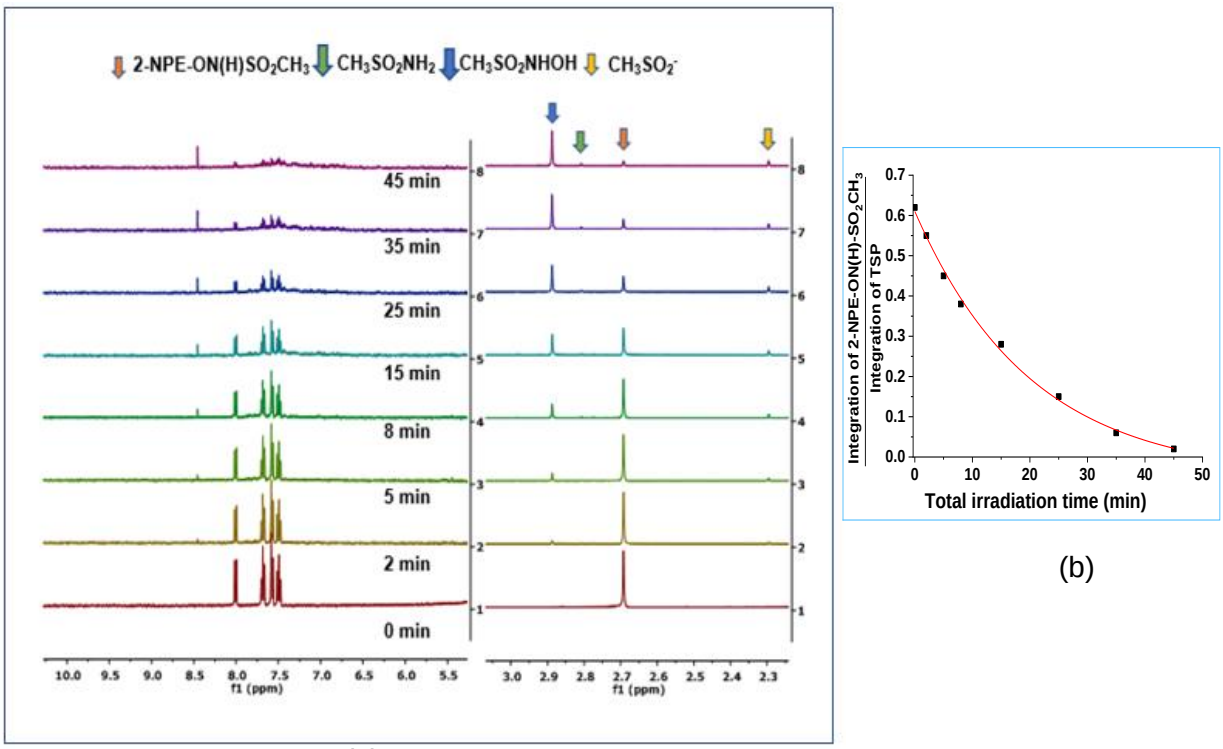

(a) (b)

Figure 3.39. (a) ^{1}H NMR spectra as a function of total irradiation time for the photolysis of **2-NPE-ON(H)-SO_2CH_3** (1.0 mM) in a 90:10 v/v mixture of carbonate buffer (30 mM, pH 9.9) and CD_3CN. (b) Ratio of the area of the CH_3 signal of **2-NPE-ON(H)-SO_2CH_3** and the TSP reference versus time. The best fit of the data to a first-order equation gives k_{obs} = 0.048 ± 0.001 min^{-1} ($t_{1/2}$ = 14 min).

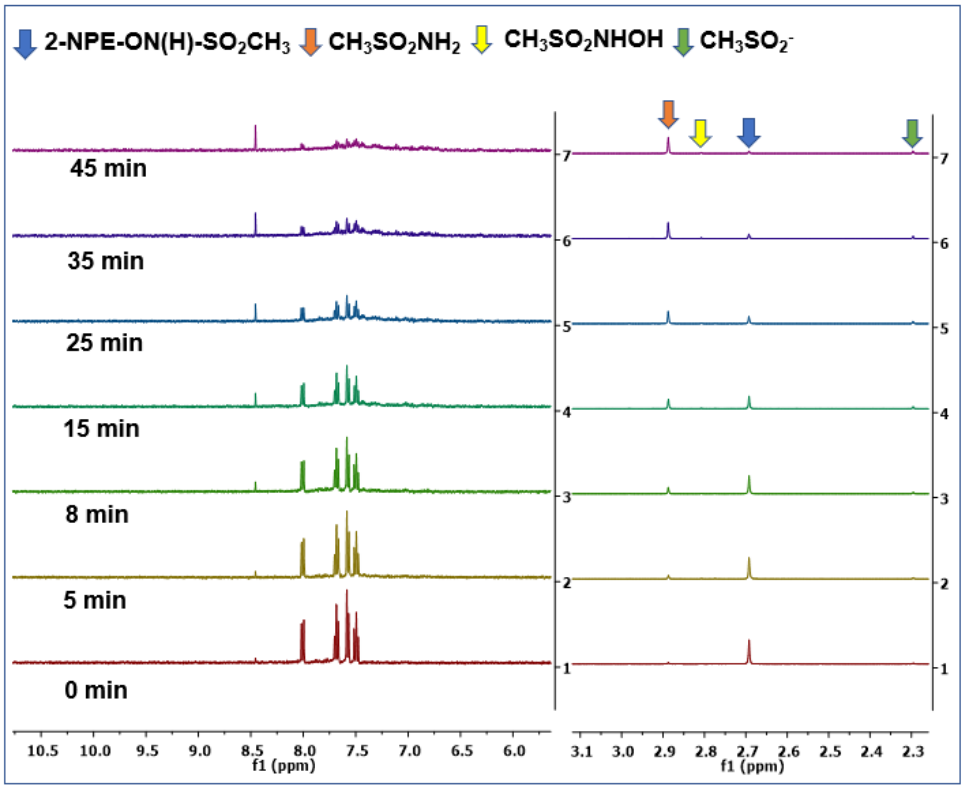

(a)

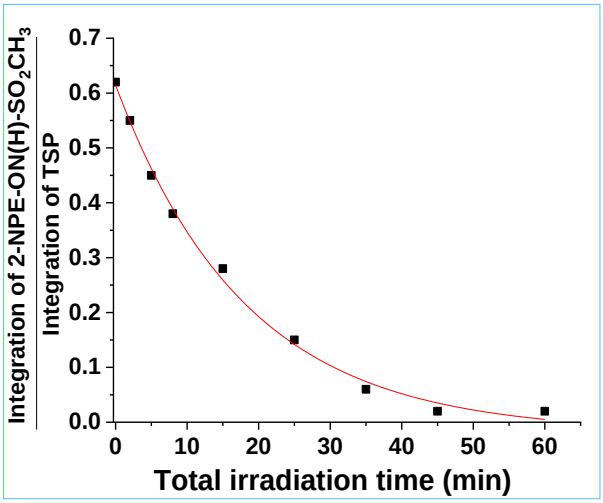

(b)

Figure 3.40. (a) ^{1}H NMR spectra as a function of total irradiation time for the photolysis of **2-NPE-ON(H)-SO_2CH_3** (1.0 mM) in a 90:10 v/v mixture of 0.010 M NaOH (pH 12.0) and CD_3CN. (b) Ratio of the area of the CH_3 signal of **2-NPE-ON(H)-SO_2CH_3** and the TSP reference versus time. The best fit of the data to a first-order equation gives k_{obs} = 0.049 ± 0.001 min^{-1} ($t_{1/2}$ = 14 min).

The effect of pH on the photoproducts obtained for the photodecomposition of **2-NPE-ON(H)-SO_2CH_3** is summarized in Table 3.9. At pH 3.0-7.0, C-O bond cleavage dominates (~83% CH_3SO_2NHOH), with ~9% N-O bond cleavage and ~8% concerted C-O/N-S bond cleavage. Under these conditions CH_3SO_2NHOH is thermally stable; hence in the pH 3.1-7.0 the photoproducts directly reflect the amount of C-O versus concerted C-O/N-S cleavage. At higher pH conditions O-N bond cleavage dominates (~72% $CH_3SO_2NH_2$ at pH 9.9 and pH 12.0). At pH 9.9 and 12.0 the $CH_3SO_2NHO(H)$ product generated from C-O bond cleavage decomposes during the timeframe of the photodecomposition experiment, decomposing to give $CH_3SO_2^-$ and HNO.[53] Observed rate constants for the thermal decomposition of $CH_3SO_2NHO(H)$ are given in the last column of Table 3.9. The two **2-NPE-ON(H)-SO_2CH_3** photolysis experiments at pH 9.9 and 12.0 took ~3 h each and $CH_3SO_2^-$ was observed even after short irradiation times (after 2 min irradiation at pH 12.0, Figure 3.40); hence some concerted C-O/N-S bond cleavage must occur as spontaneous decomposition of $CH_3SO_2NHO(H)$ is slow at pH 12.0, last column, Table 3.9 ($t_{1/2}$ ~ 80 min). At pH 9.9 and pH 12.0 there may be more C-O bond cleavage versus C-O/N-O concerted bond cleavage than the observed photoproduct percentages suggest, since $CH_3SO_2NHO(H)$ is not stable under these conditions.

Table 3.9. Effect of pH of the aqueous component of the solvent on the photoproducts and the observed rate constant for photodecomposition for **2-NPE-ON(H)-SO_2CH_3** (1.0 mM) in 10:90 v/v CD_3CN: aqueous buffer (30 mM).

pH	Percentage of Photoproducts			k_{obs} (min^{-1})	k_{obs} (min^{-1}) for spontaneous decomposition of CH_3SO_2NHOH[e]
	CH_3SO_2NHOH	$CH_3SO_2NH_2$	$CH_3SO_2^-$		
3.1[a]	75	15	10	0.0612	-
5.0[b]	82	10	8	0.0592	-
7.0[a]	85	7	8	0.0571	-
9.9[c]	13	72	15	0.0481	4.8×10^{-3}
12.0[d]	12	73	15	0.0493	8.5×10^{-3}

Aqueous component of solution: [a]phosphate buffer; [b]acetate buffer; [c]carbonate buffer; [d] 0.010 M NaOH. [e] From the PhD thesis of Sonya Adas.[53]

The photodecomposition of **2-NPE-ON(H)-SO_2Ar** (Ar = -Ph(2-$MeSO_2$)$SO_2NHO(H)$) was investigated in 10% v/v CD_3CN in aqueous solution at different pH conditions using ^1H NMR spectroscopy. Prior initiating these experiments, the thermal stability of this compound was investigated. In contrast to **2-NPE-ON(H)-SO_2CF_3** and **2-NPE-ON(H)-SO_2CH_3**, **2-NPE-ON(H)-SO_2Ar** is thermally stable at pH 1.0 in 10:90 v/v CH_3CN: aqueous solution (pH 1.0) for 12 h, Figure 3.41. Specifically, a solution of $ArSO_2NHOH$ was prepared in 10:90 v/v CH_3CN: aqueous solution, pH 3.0. The pH of the solution was then decreased to ~pH 1.0. The ^1H NMR spectrum was unchanged, confirming that the compound is stable at this pH. The pH of the solution was then increased back to pH 3.0 and the ^1H NMR spectrum re-recorded. There was no change in the ^1H NMR spectrum. At this pH condition the percentage of the

photoproducts $ArSO_2NHOH$ and $ArSO_2^-$ can be used to determine the relative amounts of the C-O versus concerted C-O/N-S bond cleavage processes.

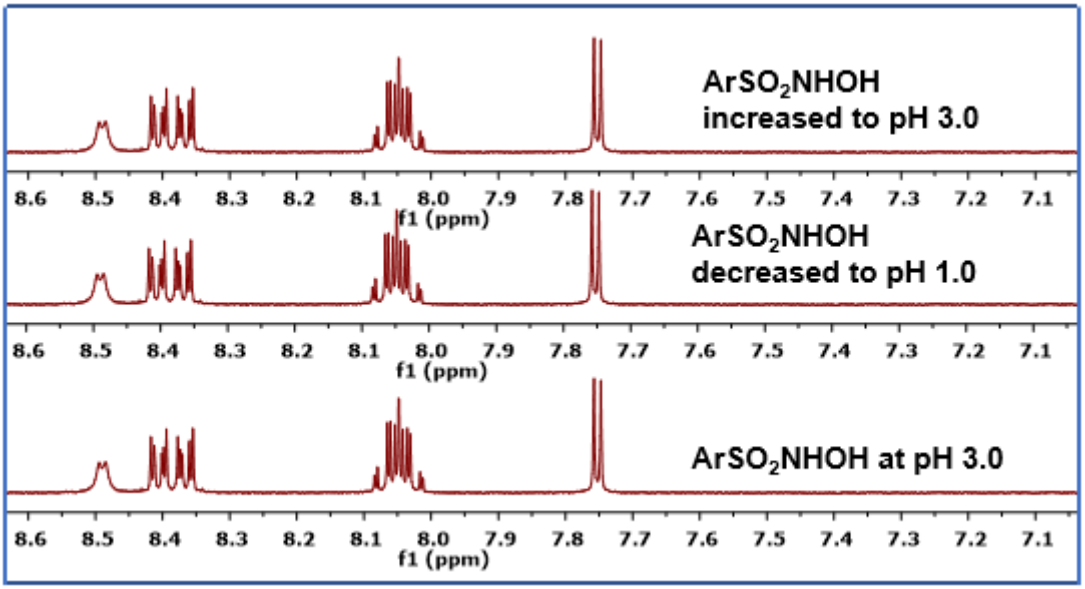

Figure 3.41. ^{1}H NMR spectrum of $ArSO_2NHOH$ in 10:90 v/v CH_3CN: aqueous solution where the pH of the aqueous component is pH 3.0 (lower spectrum), decreased to pH 1.0 and increased back to pH 3.0 (upper spectrum).

Figure 3.42(a) shows the ^{1}H NMR spectra obtained upon irradiation of **2-NPE-ON(H)-SO_2Ar** as a function of total irradiation time at pH 1.0. The integration area of the CH_3 peak was plotted as a function of total irradiation time and was fitted to first-order equation, giving k_{obs} = 0.030 ± 0.03 min^{-1} (Figure 3.42(b)). The percentage photoproducts were determined from the peak areas in the 3.20-3.70 ppm region. The photodecomposition primarily occurs by C-O bond cleavage (65% $ArSO_2NHOH$). Smaller amounts of the concerted C-O/N-S (21% $ArSO_2^-$) and O-N bond cleavage (10% $ArSO_2NH_2$) pathways also occur. At pH 1.0 $ArSO_2NHOH$ is stable. $ArSO_2^-$ therefore comes from concerted C-O/N-S bond cleavage.

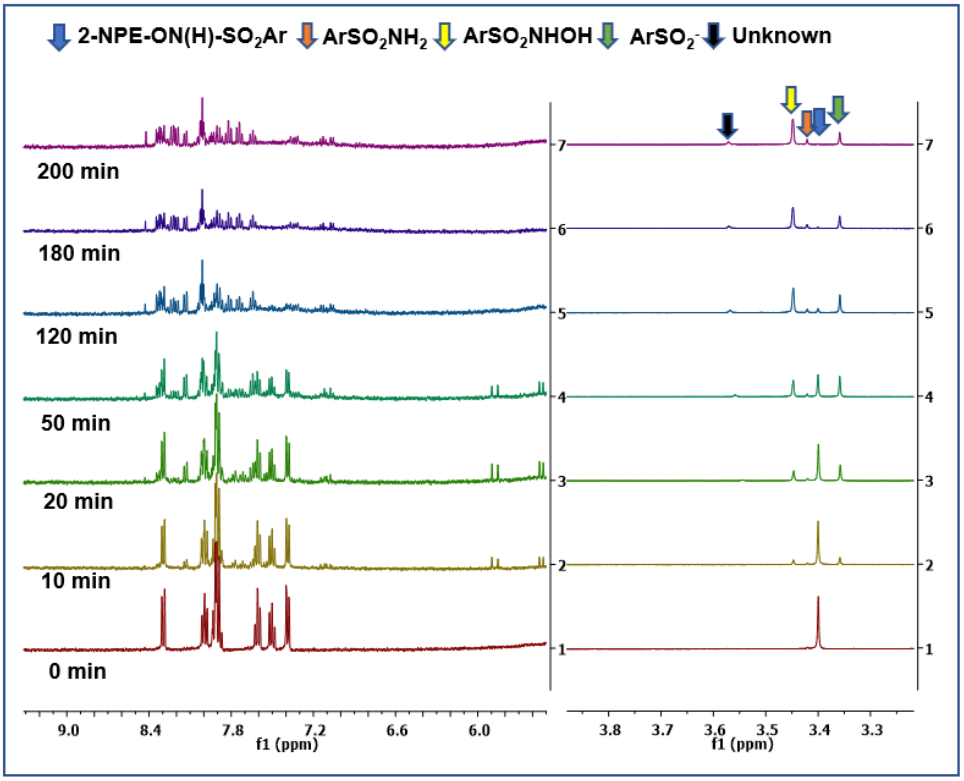

(a)

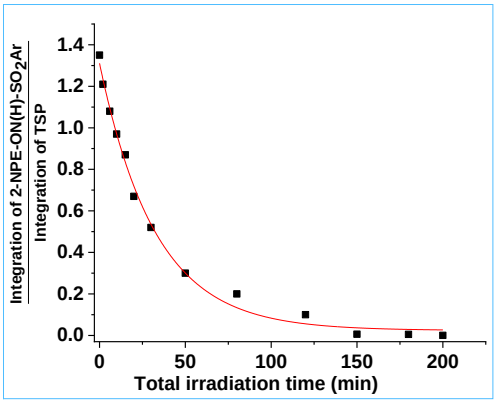

(b)

Figure 3.42. (a) ^{1}H NMR spectra as a function of total irradiation time for the photolysis of **2-NPE-ON(H)-SO$_2$Ar** (1.0 mM) in a 90:10 v/v mixture of 0.10 M HCl (pH 1.0) and CD_3CN. (b) Ratio of the area of the CH_3 signal of **2-NPE-ON(H)-SO$_2$Ar** and the TSP reference versus time. The best fit of the data to a first-order equation gives k_{obs} = 0.030 ± 0.03 min^{-1} ($t_{1/2}$ = 23 min).

Figure 3.43(a) and 3.44(a) show the ^{1}H NMR spectra as a function of total irradiation time at pH 3.1 and 5.0, respectively. The area of the CH_3 peak as a function of total irradiation time was fitted to first-order equation, giving k_{obs} = 0.026 ± 0.003 min^{-1} (pH 3.1, Figure 3.43(b)) and 0.030 ± 0.003 min^{-1} (pH 5.0, Figure 3.44(b)).

For pH ≥ 3.1 -Ph(2-MeSO$_2$)SO$_2$NHOH is not photostable, undergoing spontaneous (thermal) N-S bond cleavage to generate (2-MeSO$_2$)PhSO$_2^-$ and HNO. Rate constants

for thermal decomposition of -Ph(2-MeSO$_2$)SO$_2$NHO(H) are given in the last column of Table 3.10. The percentages of the photoproducts at pH 3.0 were 86% (ArSO$_2$NHOH + ArSO$_2^-$; Ar = -Ph(2-MeSO$_2$), 10% ArSO$_2$NH$_2$ and 4% of an unknown species. The percentages of photoproducts were the same at pH 5.0, but the percentage of ArSO$_2^-$ was slightly increased. This is most likely result of the increase in the rate of spontaneous decomposition of ArSO$_2$NHO(H) at higher pH conditions, Table 3.10, last column.

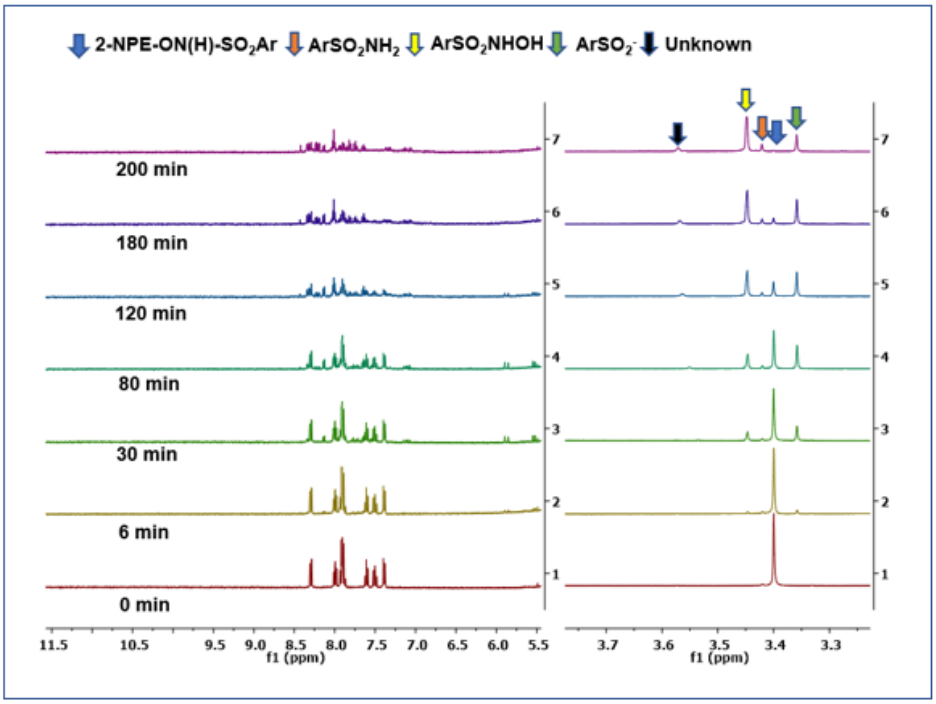

(a)

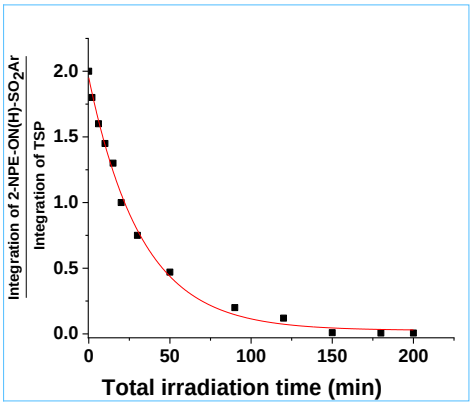

(b)

Figure 3.43. (a) ^{1}H NMR spectra as a function of total irradiation time for the photolysis of **2-NPE-ON(H)-SO$_2$Ar** (1.0 mM; Ar = -Ph(2-MeSO$_2$) in a 90:10 v/v mixture of phosphate buffer (30 mM, pH 3.1) and CD$_3$CN. (b) Ratio of the area of the CH$_3$ signal of **2-NPE-ON(H)-SO$_2$Ar** and the TSP reference versus time. The best fit of the data to a first-order equation gives k_{obs} = 0.026 ± 0.003 min^{-1} ($t_{1/2}$ = 26 min).

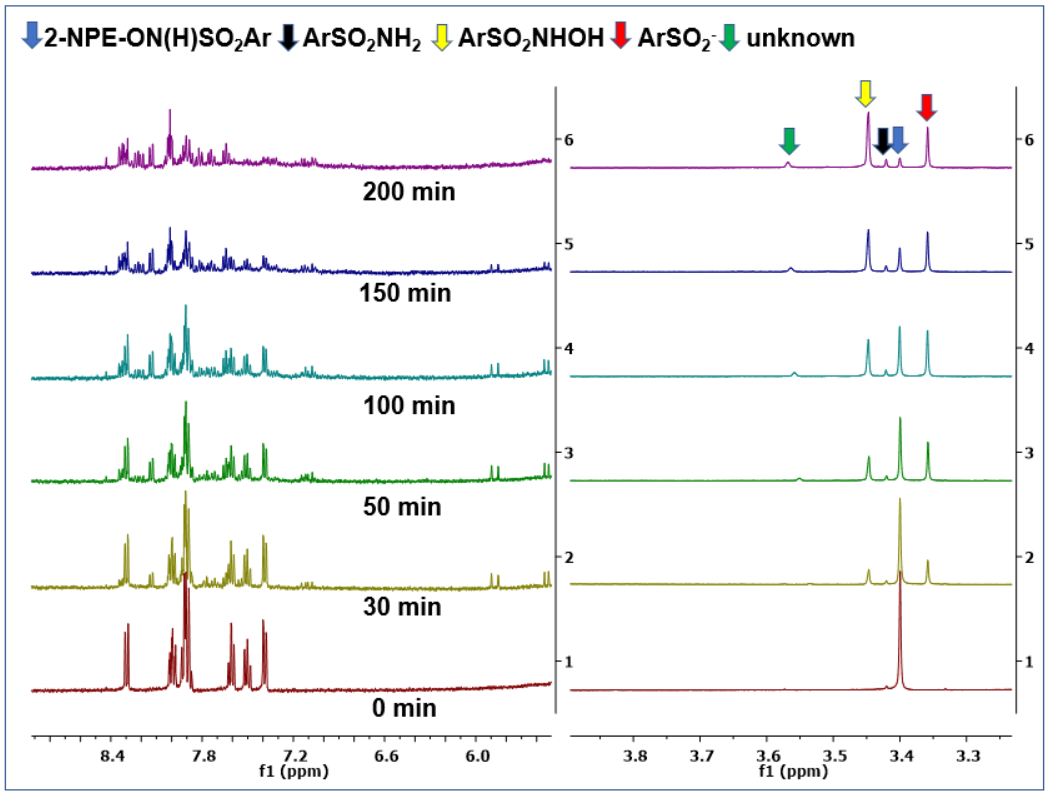

(a)

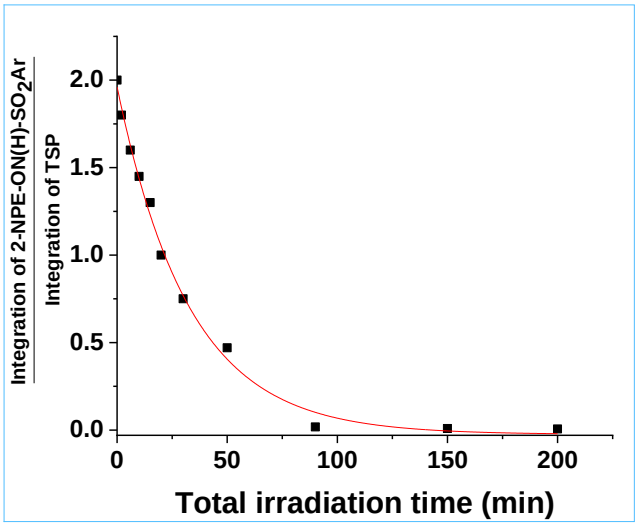

(b)

Figure 3.44. (a) ^{1}H NMR spectra of **2-NPE-ON(H)-SO$_2$Ar** (1.0 mM) as a function of total irradiation time in a 90:10 v/v mixture of acetate buffer (30 mM, pH 5.0) and CD_3CN. (b) Ratio of the area of the CH_3 signal of **2-NPE-ON(H)-SO$_2$Ar** and the TSP reference versus time. The best fit of the data to a first-order equation gives k_{obs} = 0.030 ± 0.003 min^{-1} ($t_{1/2}$ = 23 min).

Figure 3.45(a) and 3.46(a) show ^{1}H NMR spectra as a function of total irradiation time at pH 10.0 and 12.0, respectively. The integration of area of the CH_3 signal as a function of total irradiation time was fitted to first-order equation, giving k_{obs} = 0.026 ±

0.003 min^{-1} (pH 10.0, Figure 3.45(b)) and k_{obs} =0.264 ± 0.03 min^{-1} (pH 12.0, Figure 3.46(b)). At these pH conditions $ArSO_2^-$ was mainly observed. This is due to the rate of thermal decomposition of $ArSO_2NHOH$ to $ArSO_2^-$ increasing at these pH conditions.

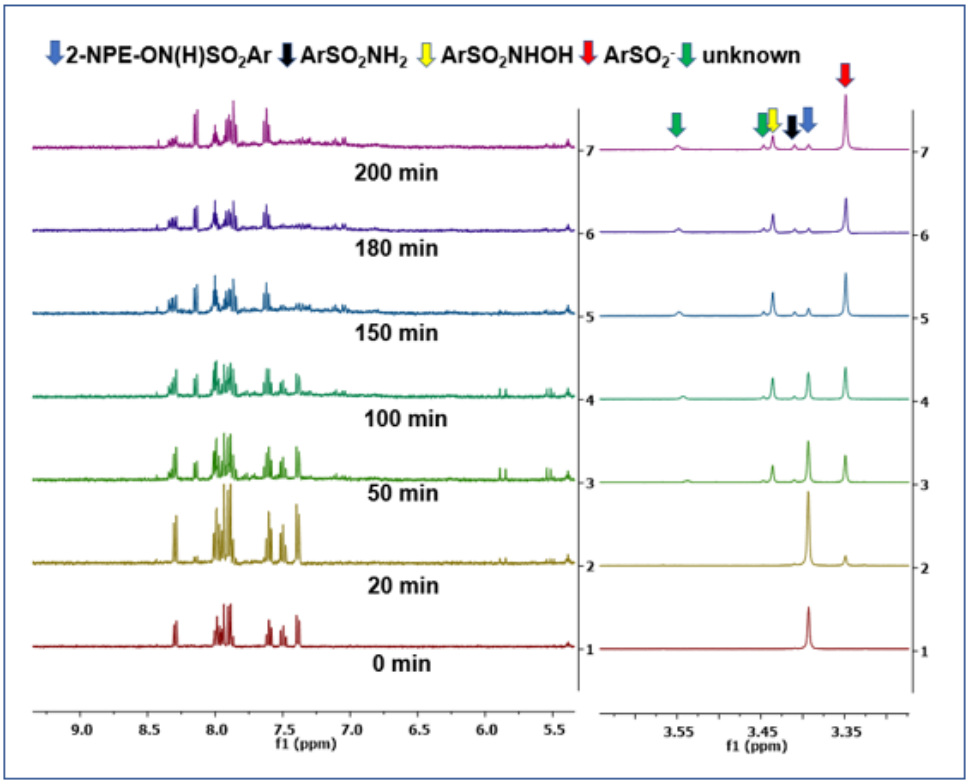

(a)

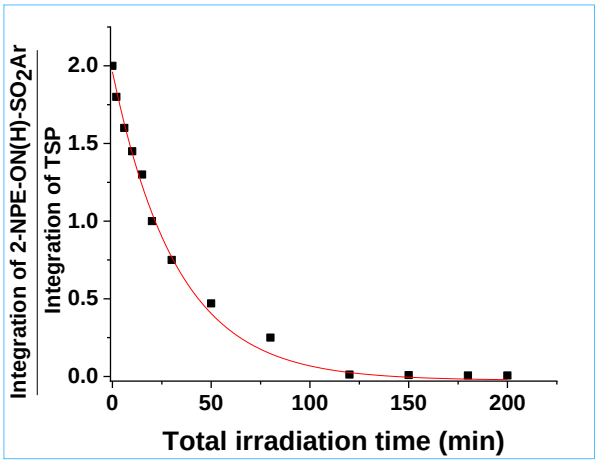

(b)

Figure 3.45. (a) ^{1}H NMR spectra as a function of total irradiation time for the photolysis of **2-NPE-ON(H)-SO_2Ar** (1.0 mM) in a 90:10 v/v mixture of carbonate buffer (30 mM, pH 10.0) and CD_3CN. (b) Ratio of the area of the CH_3 signal of **2-NPE-ON(H)-SO_2Ar** and the TSP reference versus time. The best fit of the data to a first-order equation gives k_{obs} = 0.030 ± 0.003 min^{-1} ($t_{1/2}$ = 23 min).

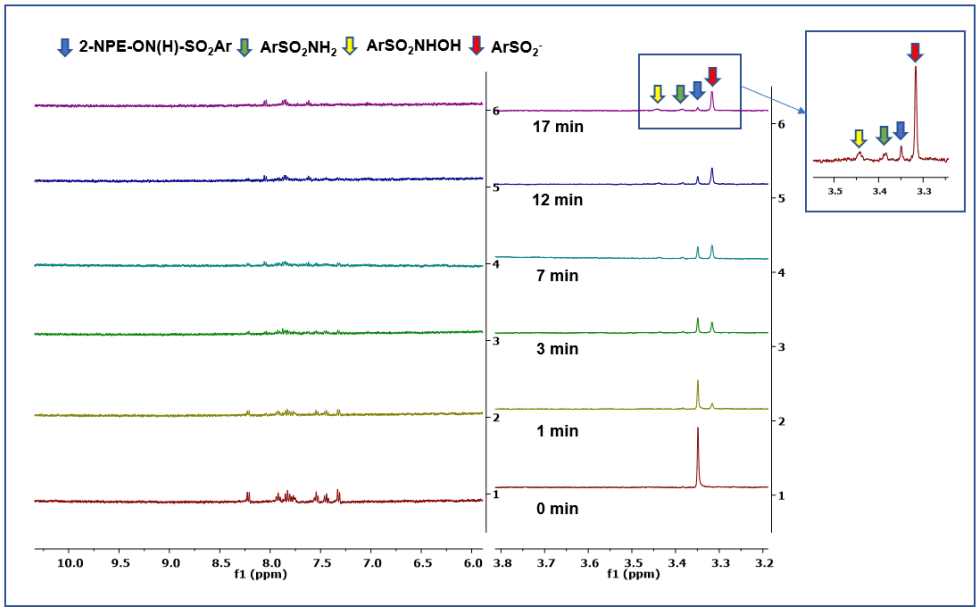

(a)

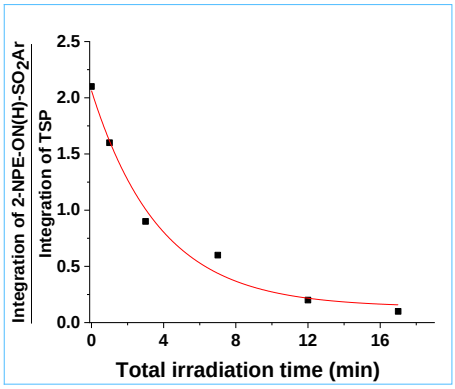

(b)

Figure 3.46. (a) ^{1}H NMR spectra as a function of total irradiation time for the photolysis of **2-NPE-ON(H)-SO$_2$Ar** (1.0 mM) in a 10:90 v/v mixture of NaOH (0.010 M, pH 12.0) and CD_3CN. (b) Ratio of the area of the CH_3 signal of **2-NPE-ON(H)-SO$_2$Ar** and the TSP reference versus time. The best fit of the data to a first-order equation gives k_{obs} = 0.264 ± 0.03 min^{-1} ($t_{1/2}$ = 2.6 min).

Observed rate constants for the spontaneous decomposition of ArSO$_2$NHOH in aqueous solution as a function of pH have not yet been reported. The spontaneous thermal decomposition of an authentic sample of ArSO$_2$NHOH was independently monitored by UV-Vis spectroscopy in aqueous solution at a range of pH conditions (pH 3.0-12.0, 30 mM buffer). The observed rate of decay of the absorbance at 272 nm versus time at each pH condition was fitted to a first-order equation, to give an observed rate constant (section 3.3.5), last column of Table 3.10.

The effect pH on the photoproducts is summarized in Table 3.10. As the pH increases, the rate of decomposition of ArSO$_2$NHOH to ArSO$_2^-$ and HNO increases. C-O bond cleavage dominates at low pH conditions. The pH 7.0 data is useful to assess whether

concerted C-O/N-S bond cleavage actually occurs, since significant amounts of $ArSO_2^-$ was observed in the product solution and the rate of spontaneous decomposition of $ArSO_2NHO(H)$ is not fast at this pH condition ($t_{1/2}$ ~50 min, Table 3.10, last column). After 10 min total irradiation time at pH 7.0 (Figure 3.17(a)), first data point), the ratio of $ArSO_2NHO(H)$:$ArSO_2^-$ was ~1:2. Given that the half-life for spontaneous decomposition of $ArSO_2NHO(H)$ is ~50 min at this pH condition and that the NMR and UV-Vis experiments were done under the same experimental conditions, the ratio of C-O and concerted C-O/N-S bond cleavage must also be ~1:2. Significant amounts of both elimination pathways are therefore occurring for this system. At higher pH conditions considerable $ArSO_2^-$ is found in the product solution (Figure 3.45-3.46). Given that each experiment takes ~5-7 h, where spontaneous decomposition of $ArSO_2NHO(H)$ can be rapid, the percentage of concerted C-O/N-S bond cleavage versus C-O bond cleavage may therefore be overestimated, especially at high pH values.

Table 3.10. Effect of the pH of the aqueous component of the solvent on the photoproducts and the observed rate constant for photodecomposition for **2-NPE-ON(H)-SO_2Ar** (1.0 mM) in 10:90 v/v CD_3CN: aqueous solution. Buffers (30 mM) were used in the pH 3.1-10.0 range.

pH	Percentage of Photoproducts			k_{obs} (min^{-1})[f]	k_{obs} (min^{-1}) for spontaneous decomposition of $ArSO_2NHO(H)$[f]
	$ArSO_2NHOH$ +$ArSO_2^-$	$ArSO_2NH_2$	Unknown species		
1.0[a]	86	10	4	0.0301	
3.1[b]	86	10	4	0.0264	4.3×10^{-3} ($t_{1/2}$ ~ 160 min)
5.0[c]	86	9	5	0.0296	4.8×10^{-3} ($t_{1/2}$ ~ 140 min)
7.0[b]	85	11	4	0.0298	1.4×10^{-2} ($t_{1/2}$ ~ 50 min)
10.0[d]	85	9	6	0.0302	3.4 ($t_{1/2}$ ~ 12 s)
12[e]	93	5	2	0.2642	3.8 ($t_{1/2}$ ~ 18 s)

Aqueous component of solution: [a]0.10 M HCl; [b]phosphate buffer; [c]acetate buffer; [d]carbonate buffer; [e]0.010 M NaOH. [f]Average value of two experiments. The percentage error is in each value is ~ 3%.

3.3.8 Effect of O_2

To probe the effect of oxygen on the mechanism of photodecomposition and on the quantum efficiency under steady state irradiation conditions, the rate of photodecomposition and the nature of the observed photoproducts were determined for one of the compounds, **2-NPE-ON(H)-SO_2CH_3**, under aerobic conditions. The ^1H NMR spectrum of the photoproduct solution (Figure 3.47) was identical to that observed under anaerobic conditions (Table 3.5). The percentage of the photoproducts under anaerobic conditions were 85% CH_3SO_2NHOH, 6% $CH_3SO_2NH_2$ and 9% $CH_3SO_2^-$, with an observed rate constant of k_{obs} = 0.053 ± 0.005 min^{-1}. The percentage of the photoproducts under aerobic conditions were 85% CH_3SO_2NHOH, 6% $CH_3SO_2NH_2$, 6% $CH_3SO_2^-$ and 3% $CH_3SO_3^-$, with an observed rate constant of k_{obs} = 0.052 ± 0.004 min^{-1}. In the presence of air $CH_3SO_2^-$ is easily oxidized to $CH_3SO_3^-$.

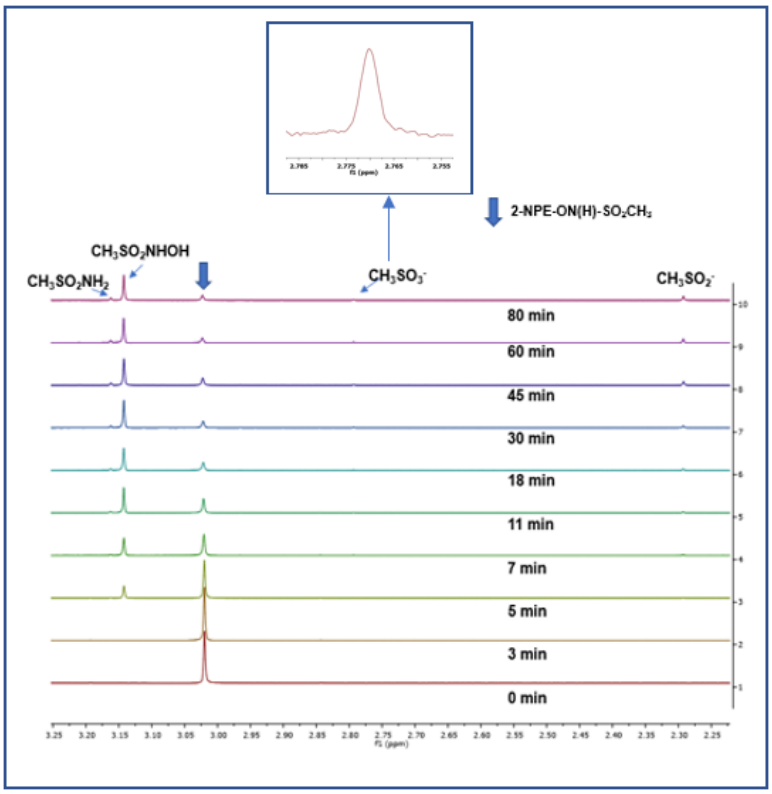

(a)

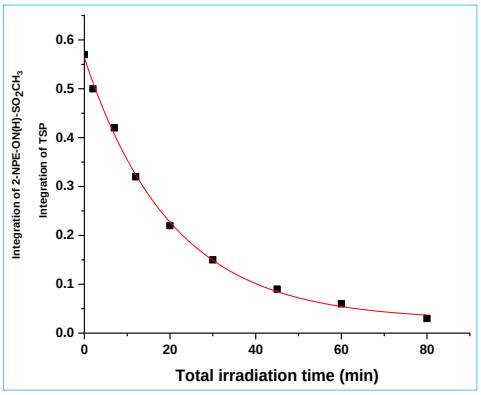

(b)

Figure 3.47. (a) ^{1}H NMR spectra as a function of total irradiation time for the photolysis of **2-NPE-ON(H)-SO$_2$CH$_3$** (1.0 mM) in a 90:10 v/v mixture of phosphate buffer (30 mM, pH 7.0) and CD_3CN under aerobic conditions. (b) Ratio of the area of the CH_3 signal of **2-NPE-ON(H)-SO$_2$CH$_3$** and the TSP reference versus time. The best fit of the data to a first-order equation gives k_{obs} = 0.052 ± 0.04 min^{-1} ($t_{1/2}$ = 13 min).

3.3.9 Determining the effect of the excitation wavelength on the photoproducts

McCulla et al. reported that the mechanism of photorelease of hydroxamic acid from 2-nitrobenzyl benzohydroxamate is dependent on the excitation wavelength.[113] To determine if this is also the case for **2-NPE-ON(H)-SO$_2$R** (note that **2-NPE-ON(H)-SO$_2$Ar** has two chromophores), the photoproducts from irradiation of these compounds at two different excitation wavelengths (264 and 330 nm) were determined (60:40 v/v CD_3CN: phosphate buffer (30 mM), pH 7.0)), using a xenon lamp in conjunction with a monochromator. The results are summarized in Table 3.11. The excitation wavelength did not have any effect on the observed photoproducts for all compounds. A similar result was found for 2-nitrobenzyl-caged *N*-hydroxysulfonamides.[150]

Table 3.11. Effect of excitation wavelength on the percentage of photoproducts of **2-NPE-ON(H)-SO_2R** (1.0 mM) in a mixture of phosphate buffer (30 mM, pH 7.0) and CD_3CN (40:60, v/v).

Compound	λ_{exc}	Photoproducts
2-NPE-ON(H)-SO_2CF_3	264	$CF_3SO_2NH_2$ (65%) and $CF_3SO_2^-$ (35%)
2-NPE-ON(H)-SO_2CF_3	330	$CF_3SO_2NH_2$ (65%) and $CF_3SO_2^-$ (35%)
2-NPE-ON(H)-SO_2CH_3	264	CH_3SO_2NHOH (85%), $CF_3SO_2NH_2$ (7%) and $CF_3SO_2^-$ (8%)
2-NPE-ON(H)-SO_2CH_3	330	CH_3SO_2NHOH (83%), $CF_3SO_2NH_2$ (9%) and $CF_3SO_2^-$ (8%)
2-NPE-ON(H)-SO_2Ar	272	$ArSO_2NHOH$ + $ArSO_2^-$ (88%), $ArSO_2NH_2$ (12%)
2-NPE-ON(H)-SO_2Ar	330	$ArSO_2NHOH$ + $ArSO_2^-$ (86%), $ArSO_2NH_2$ (14%)

3.3.10 Determination of the Photoproduct quantum yields (Φ)

The photoproduct quantum yields for compounds **2-NPE-ON(H)-SO_2R** were determined by actinometry, using *trans*-azobenzene as a reference compound ($\Phi_{(trans\text{-}cis)}$ = 0.14 at 313 nm; see Experimental section 3.2.6). The percentage of *trans*-azobenzene converted to *cis*-azobenzene upon irradiation was followed by UV-Vis spectroscopy, whereas the photodecomposition of **2-NPE-ON(H)-SO_2CF_3** was followed by ^{19}F NMR spectroscopy. The photodecomposition of **2-NPE-ON(H)-SO_2CH_3** and **2-NPE-ON(H)-SO_2Ar** were followed by ^1H NMR spectroscopy. The irradiation experiment for the *trans*-azobenzene actinometer was carried out on the same day as the irradiation experiments for **2-NPE-ON(H)-SO_2CF_3** and **2-NPE-ON(H)-SO_2CH_3**. The number of moles of product from the photolysis was plotted as a function of irradiation time to obtain a slope. The slope value for the azobenzene actinometer obtained was 4.28 ± 0.03 × 10^{-9} mol min^{-1} (Figure 3.48(a)). A separate irradiation experiment for the *trans*-azobenzene actinometer also carried out on the same day as the irradiation experiments for **2-NPE-ON(H)-SO_2Ar** using an identical experimental set up. The slope value for the azobenzene actinometer was 4.15 ± 0.03 × 10^{-9} mol min^{-1}. Slope values were therefore very similar on different days. Figure 3.49(a) shows the number of moles of product from the photolysis ($CF_3SO_2NH_2$ + $CF_3SO_2^-$) as a function of irradiation time for **2-NPE-ON(H)-SO_2CF_3**. The slope was (7.65 ± 0.02) × 10^{-9} mol min^{-1}. Figure 3.48(b) shows the number of moles of product from the photolysis ($CH_3SO_2NH_2$ + CH_3SO_2NHOH + $CH_3SO_2^-$) as a function of irradiation time

for **2-NPE-ON(H)-SO_2CH_3**. The slope was (5.00 ± 0.03) × 10^{-9} mol min^{-1}. Figure 3.48(c) shows the number of moles of product from the photolysis ($ArSO_2NH_2$ + $ArSO_2NHOH$ + $ArSO_2^-$) as a function of irradiation time for **2-NPE-ON(H)-SO_2Ar**. The slope was (9.73 ± 0.03) × 10^{-10} mol min^{-1}.

The photoproduct quantum yield was calculated using equation (3.5).

$$\phi\text{ (2-NPE-ON(H)-SO}_2\text{-R)} = \frac{\text{slope (2-NPE-ON(H)-SO}_2\text{-R) / Absorbance (2-NPE-ON(H)-SO}_2\text{-R)}}{\text{Slope (Azobenzene) / Absorbance (azobenzene)}} \times \phi\text{ (azobenzene)} \quad (3.5)$$

The absorbance of the solutions of **2-NPE-ON(H)-SO_2R** (1.00 mM) at the excitation wavelength were calculated using the molar extinction coefficient of each reactant at 313 nm (ε(**2-NPE-ON(H)-SO_2CF_3**) = (7.6 ± 0.2) × 10^2 M^{-1} cm^{-1}, ε(**2-NPE-ON(H)-SO_2CH_3**) = (7.3 ± 0.3) × 10^2 M^{-1} cm^{-1}, ε(**2-NPE-ON(H)-SO_2Ar**) = (7.0 ± 0.3) × 10^2 M^{-1} cm^{-1})). The photoproduct quantum yields were 0.47 ± 0.01 (**2-NPE-ON(H)-SO_2CF_3**), 0.32 ± 0.01 (**2-NPE-ON(H)-SO_2CH_3**) and 0.07 ± 0.01 (**2-NPE-ON(H)-SO_2Ar**). This data is in line with the observed rate constants for photodecomposition (0.080, 0.042 and 0.032 min^{-1} for **2-NPE-ON(H)-SO_2CF_3**, **2-NPE-ON(H)-SO_2CH_3**, and **2-NPE-ON(H)-SO_2Ar**, respectively). Reported photoproduct quantum yield values for (2-nitrophenyl)ethyl caged molecules range from 0.41-0.51.[124]

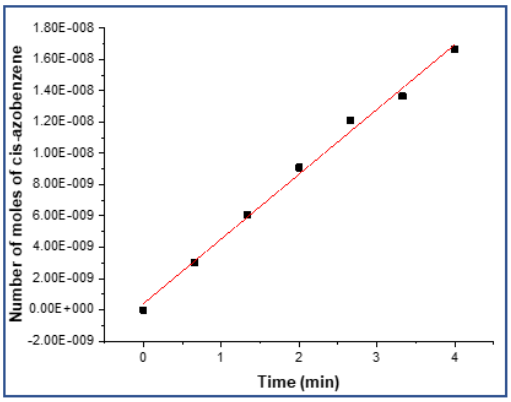

(a)

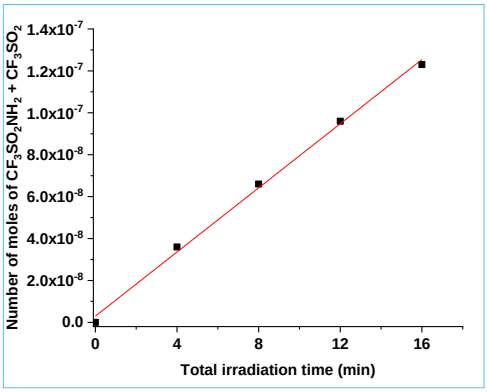

(b)

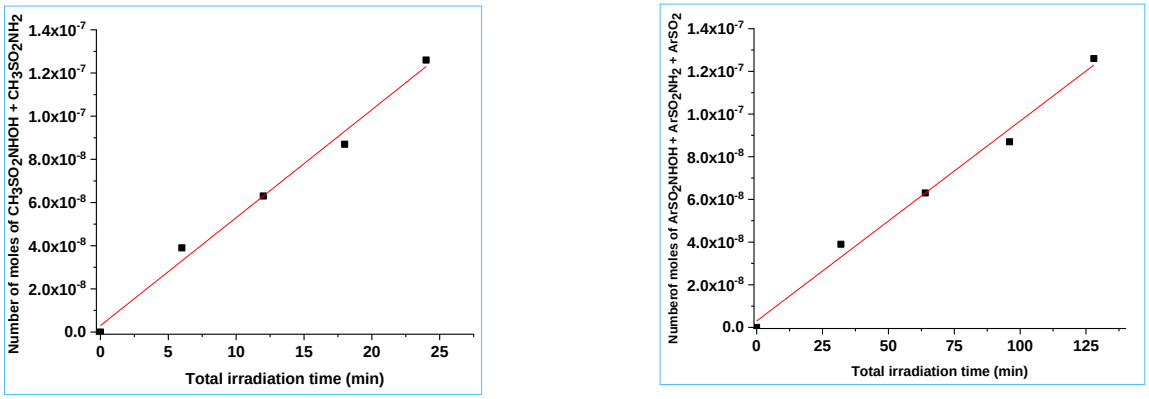

(c) (d)

Figure 3.48. (a) Plot of the number of moles of *cis*-azobenzene versus total irradiation time (min). The best fit of the data to straight line gives a slope of (4.28 ± 0.03) × 10^{-9} mol min^{-1} (b) Plot of the number of moles of the photoproduct $CF_3SO_2NH_2$ + $CF_3SO_2^-$ versus total irradiation time (min). The best fit of the data to a straight line gives a slope of (7.65 ± 0.02) × 10^{-9} mol min^{-1}. (c) Plot of the number of moles of the photoproducts ($CH_3SO_2NH_2$ + CH_3SO_2NHOH + $CH_3SO_2^-$) versus total irradiation time (min). The best fit of the data to a straight line gives a slope of (5.00 ± 0.03) × 10^{-9} mol min^{-1}. (d) Plot of the number of moles of the photoproducts ($ArSO_2NH_2$ + $ArSO_2NHOH$ + $ArSO_2^-$) versus total irradiation time (min). The best fit of the data to a straight line gives a slope of (9.73 ± 0.03) × 10^{-10} mol min^{-1}.

3.3.11 Evidence that photodecomposition proceeds through an aci-nitro intermediate for these systems

Flash photolysis studies were carried out to determine if photodecomposition proceeds via an aci-nitro intermediate. A short-lived aci-nitro species (µs time scale) has been observed by others for 2-NPE and 2-NO_2Bn systems. [98, 99, 101, 102, 159, 160]Figure 3.49 shows a transient absorption spectrum for **2-NPE-ON(H)-SO_2R** in CH_3CN in this time frame. The absorbance maximum (λ_{max}) in both spectra at 400 nm agrees with values reported by others for the monoprotonated aci-nitro species.[124] Importantly, in this solvent the three compounds undergo different amounts of C-O, C-O/N-S, and O-N bond cleavage (**2-NPE-ON(H)-SO_2CF_3** undergoes ~70% O-N bond cleavage and 30% concerted C-O/N-S bond cleavage; **2-NPE-ON(H)-SO_2CH_3** undergoes predominately C-O bond cleavage (85%); ~43% concerted C-O/N-S and ~45% O-N bond cleavage occurs for **2-NPE-ON(H)-SO_2Ar**); however in each case the monoprotonated aci-nitro species is observed. These data support the monoprotonated aci-nitro species being a common intermediate for all three pathways.

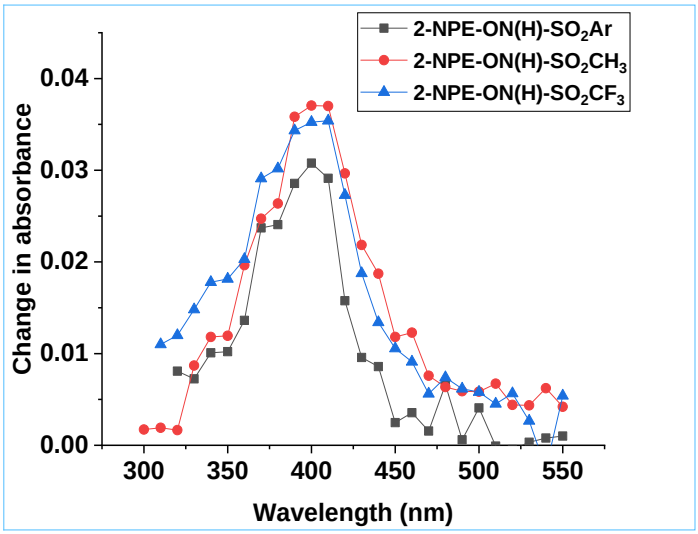

Figure 3.49. Change in absorbance versus wavelength upon photolysis of **2-NPE-ON(H)-SO_2R** (150 μM) in CH_3CN (λ_{exc} = 266 nm). Transient absorption spectra was obtained using an Applied Photophysics LKS80 laser flash photolysis spectrophotometer in conjunction with a Nd:YAG laser, with excitation at 266 nm. Data is shown at 2.2 × 10^{-5} s (**2-NPE-ON(H)-SO_2CF_3**), 2.5 × 10^{-5} s (**2-NPE-ON(H)-SO_2CH_3**) and 1.0 × 10^{-6} s (**2-NPE-ON(H)-SO_2Ar**). Note that the reactants do not absorb above 350 nm (Figure 3.2).

Transient absorption spectra (at 1.0 μs) of **2-NPE-ON(H)-SO_2CH_3** were also recorded as a function of solvent composition (CH_3CN and phosphate buffer (30 mM, pH 7.0)). The λ_{max} at 400 nm in CH_3CN shifts to 440 nm as the percentage of the aqueous component increases, Figure 3.50, in agreement with the wavelength maximum reported by others for the deprotonated form of the aci-nitro intermediate, equation (3.6).[124]

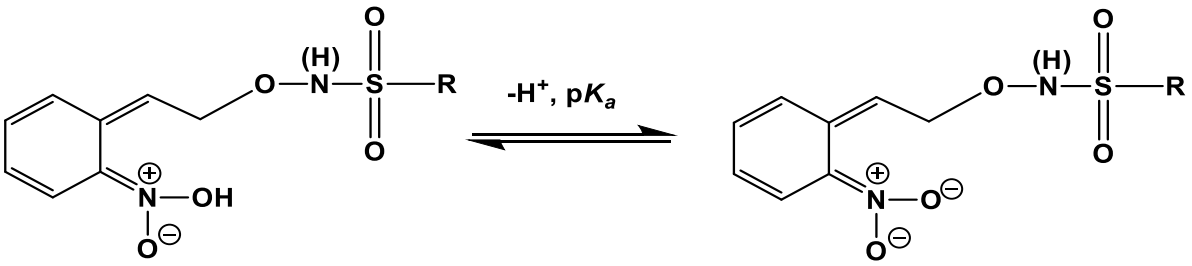

(3.6)

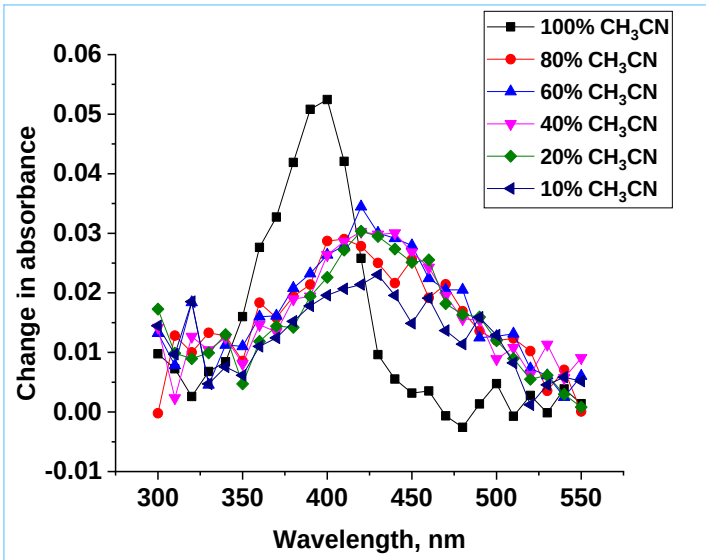

Figure 3.50. Transient absorption spectra of **2-NPE-ON(H)-SO_2CH_3** (150 μM) at 1.0 μs in different percentages of CH_3CN and phosphate buffer (30 mM, pH 7.0). The excitation wavelength was 266 nm.

A pK_a value in the ~4 range for deprotonation of the aci-nitro intermediate has been reported for 2-NPE-caged systems.[124] Interestingly, the photoproducts remained the same for **2-NPE-ON(H)-SO_2CH_3** in these solvent mixtures, Table 3.5. Walbert et al reported that only the deprotonated aci-nitro intermediate undergoes *β*-elimination.[124]

3.4 Discussion

Literature studies reveal that 2-NPE-caged compounds undergo C-O bond cleavage to release the leaving group and the byproduct 2-nitrostyrene.[45, 89, 123, 183] However, photo-uncaging of the newly developed 2-NPE derivatives **2-NPE-ON(H)-SO_2R** occurred via three pathways (see Scheme 3.1) that was dependent on the nature of the RSO_2 moiety.

For **2-NPE-ON(H)-SO_2CF_3** and **2-NPE-ON(H)-SO_2CH_3**, the observed photoproducts were independent of the composition of an CD_3CN/phosphate buffer, pH 7.0 solvent mixture, consistent with the initial events being intramolecular, with no solvent involvement. In related *N*-hydroxysulfonamide systems caged with 2-nitrobenzyl (2-NO_2Bn), (3-hydroxynaphthalen-2-yl)methyl (3,2-HNM) and (6-hydroxynaphthalen-2-yl)methyl (6,2-HNM) concomitant C-O and N-S bond cleavage results in the release of $CF_3SO_2^-$ and HNO, Figure 3.20.[76-78, 150] **2-NPE-ON(H)-SO_2CF_3** generated $CF_3SO_2NH_2$ as the major photolysis product (~70%) *via* photoinduced O-N bond cleavage, with smaller amounts of $CF_3SO_2^-$ (~30%). None of the corresponding parent

hydroxamic acid ($CF_3SO_2NHO(H)$) is observed in any of the ^{19}F NMR spectra collected during the photolysis of **2-NPE-ON(H)-SO_2CF_3**. Given that the half-life of $CF_3SO_2NHO(H)$ in pH 7.0 buffer solution is 13 min,[55] while the photodecomposition half-life of HNO donor **2-NPE-ON(H)-SO_2CF_3** under these conditions is shorter (8.7 min), some accumulation of $CF_3SO_2NHO(H)$ would be expected if it were formed as an intermediate. Thus, the data supports a mechanism for $CF_3SO_2^-$ release involving concomitant C-O and N-S bond cleavage from **2-NPE-ON(H)-SO_2CF_3**.

In contrast, photolysis of **2-NPE-ON(H)-SO_2CH_3** released mostly the parent HNO donor CH_3SO_2NHOH (MSHA, ~85%), presumably via photolytic C-O bond cleavage followed by protonation of the intermediate species $CH_3SO_2NHO^-$. A small amount of $CH_3SO_2NH_2$ (~7%) resulting from photoinduced O-N bond cleavage was also formed. CH_3SO_2-, (~8%; indicative of concomitant C-O/N-S bond cleavage and generation of HNO) was also observed. Given that MSHA is stable under neutral aqueous conditions (pH 7.0),[53] the formation of $CH_3SO_2^-$ can be assumed to proceed by a mechanism involving concomitant C-O/N-S bond cleavage.

2-NPE-ON(H)-SO_2Ar was found to show the highest selectivity for the HNO releasing pathway (diagnostic release of $ArSO_2^-$) in pure CD_3CN for the three 2-NPE derivatives. Interestingly, for **2-NPE-ON(H)-SO_2Ar** the percentage of photoinduced O-N bond cleavage decreased compared to the other two pathways when the percentage of phosphate buffer, pH 7.0 in the CD_3CN/phosphate buffer solvent mixture increased. Spontaneous decomposition of $ArSO_2NHO(H)$ unfortunately prevented quantification of the amounts of C-O versus concomitant C-O/N-S bond cleavage in the various solvent mixtures.

Several experimental observations provide support for the photodecomposition proceeding via a primary n-π* event centered on the NO_2 substituent (N=O) of the excited state of the parent molecule, resulting in H atom abstraction from the benzylic position to initially form a protonated (*Z*)-aci nitro intermediate. Importantly, the solvent ratio (CD_3CN and phosphate buffer, pH 7.0) had no effect on the photoproducts for **2-NPE-ON(H)-SO_2CF_3** and **2-NPE-ON(H)-SO_2CH_3**, consistent with the initial events being solvent-independent and a common intermediate for all three pathways. For a related system, experimental evidence was found for an additional minor primary event occurring at high excitation energies involving N-O bond homolysis;[113] however for our systems the photoproducts were unchanged when the excitation wavelength was altered. The presence or absence of the triplet excited state triplet quenchers

oxygen, *p*-terphenyl and cyclohexadiene did not affect the photoproducts or the observed rate constant of photodecomposition. These results suggest that the formation of the aci-nitro intermediate proceeds primarily through singlet excited state species. This contrasts with the previous work of Steiner et al who proposed the generation of an aci-nitro intermediate from analogous RC(O)O-NPE caged substrates via competing singlet and triplet excited state pathways.[124] McCulla et al also reported the operation of competing singlet and triplet excited state pathways in their related 2-nitrobenzyl-caged benzohydroxamic acid system.[113] Importantly, laser flash photolysis experiments provided support for formation of an aci-nitro intermediate regardless of the photoproducts.

The rate and mechanism of photodecomposition of HNO donors **2-NPE-ON(H)-SO_2R** depends on the nature of the sulfinate leaving group. From a comparison of the solvent dependence results for **2-NPE-ON(H)-SO_2CF_3** and **2-NPE-ON(H)-SO_2CH_3**, Tables 3.4 and 3.5, it is clear that the presence of the stronger electron-withdrawing group (**2-NPE-ON(H)-SO_2CF_3**: SO_2CF_3; **2-NPE-ON(H)-SO_2CH_3**: SO_2CH_3) favours the desired concomitant C-O/N-S bond cleavage versus C-O bond cleavage. For **2-NPE-ON(H)-SO_2CF_3** C-O/N-S bond cleavage is only observed upon deprotonation of the N(H) (pK_a = 3.77 ± 0.03), with C-O bond cleavage not occurring at these pH conditions. For **2-NPE-ON(H)-SO_2CH_3** deprotonation of the N(H) at high pH (pK_a = 10.06 ± 0.03) significantly decreases the amount of C-O bond cleavage at the expense of O-N bond cleavage. The amount of concomitant C-O/N-S bond cleavage increases from ~8% to 15%. Hence in both systems deprotonation of the N(H) disfavours simple C-O cleavage and instead favours both O-N bond cleavage and concomitant C-O/N-S bond cleavage. This is expected, as upon deprotonation of the N(H), expulsion of an unstable dianionic $RSO_2N^-O^-$ leaving group would be required.

For **2-NPE-ON(H)-SO_2Ar** in pure CD_3CN (SO_2Ar; Ar = -Ph(2-MeSO_2)), 43% C-O/N-S bond cleavage occurs. Currently, we have no definitive explanation for why O-N bond cleavage operates as the major pathway during the photolysis of **2-NPE-ON(H)-SO_2CF_3** (~70%) and is seen only as only a minor pathway in the photolysis of **2-NPE-ON(H)-SO_2Ar** (7%) and **2-NPE-ON(H)-SO_2CH_3** (10-45%). Similar competition from O-N bond cleavage was also observed with the analogous 2-nitrobenzyl-caged substrates, Chapter 2, but clearly a different mechanism must operate in the 2-NPE-caged systems. One possibility is presented in Scheme 3.2, where the *aci*-nitro

intermediate can either follow the usual elimination mechanism to afford the C-O bond cleavage products (Pathway 1a), undergo such an elimination in concert with N-S cleavage to release the sulfinate ion (Pathway 1b), or suffer competing removal of the allylic proton by the proximate oxyanion driven by cleavage of the weak O-N bond, to (ultimately) to generate the observed sulfonamide and aldehyde products (Pathway 2). The strongly electron-withdrawing trifluoromethanesulfonyl group in **2-NPE-ON(H)-SO_2CF_3** should enhance the acidity of the allyl proton and weaken the O-N bond, favouring Pathway 2, as was seen in these studies.

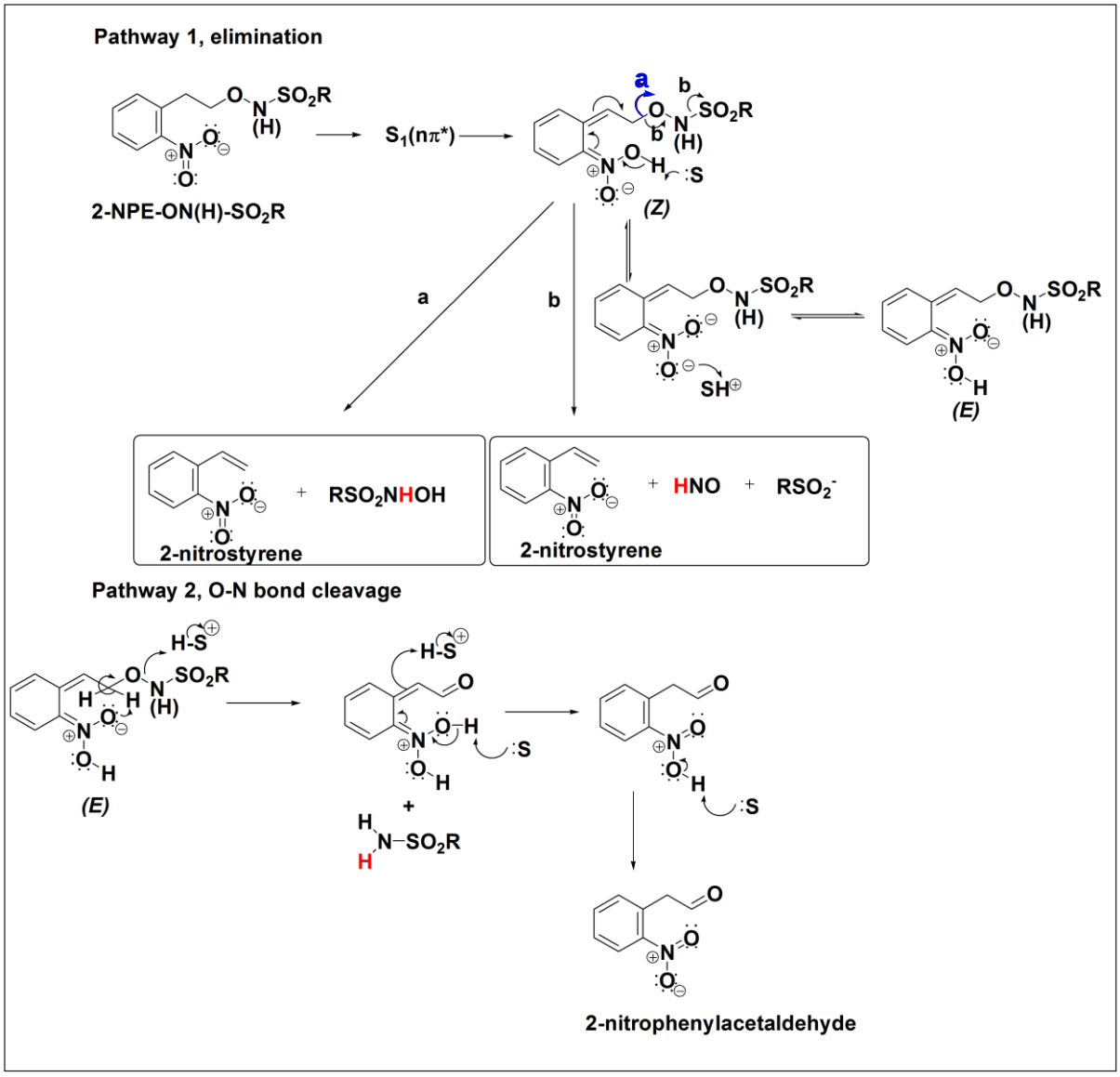

Scheme 3.2. Proposed mechanisms for photolysis of **2-NPE-ON(H)-SO_2R**.

The pH dependence data in Tables 3.8-3.10 also allows us to draw some important conclusions regarding factors determining which pathway dominates. Specifically,

from the data for **2-NPE-ON(H)-SO_2CF_3** in Table 3.8, it is clear that there is a complete switch in the photodecomposition mechanism from the C-O cleavage pathway dominating (~75%) with only minor competing O-N bond cleavage (23%) when the pH of the aqueous component is low (pH 2.1), to 70% O-N bond cleavage, and 30% concomitant C-O/N-S bond cleavage at pH ≥ 5. For **2-NPE-ON(H)-SO_2CF_3**, two pK_a values are found in this pH region - the pK_a of the aci nitro intermediate (pH = 3.7)[184] and the pK_a of the N(H) of the parent molecule (pK_a ~ 3.8 in D_2O; the pK_a values in H_2O are typically 0.05 – 0.6 lower than in D_2O;[176-178] that is, acids are stronger in H_2O versus D_2O). The pH dependence data for **2-NPE-ON(H)-SO_2CF_3** is therefore not conclusive with respect to which deprotonation process is responsible for the change in the ratios of the two decomposition pathways. However, for **2-NPE-ON(H)-SO_2CH_3** the switch in the major mechanism of photodecomposition occurs between pH 9.7 - 9.8 (Table 3.9); that is, in the region of pK_aN(H). From the chemical shift of the CH_3 of **2-NPE-ON(H)-SO_2CH_3**, the pK_aN(H) is estimated to be ~ 9.7 ± 0.1 in H_2O (8% v/v CD_3CN). This value is consistent with the more accurate pK_aN(H) ~ 10.2 in D_2O determined by NMR spectroscopy (the pK_a value is ~0.5 lower in H_2O). Hence deprotonation of the N(H) favours both O-N bond cleavage and concomitant C-O/N-S bond cleavage instead of C-O bond cleavage. Finally, laser flash photolysis data shows the presence of a monoprotonated aci-nitro species for **2-NPE-ON(H)-SO_2CH_3** in pure CH_3CN and the deprotonated anion of the aci-nitro species when a small amount of water is introduced. However, the photoproducts are unchanged. This is consistent with the protonation state of the aci-nitro species not affecting the mechanism by which **2-NPE-ON(H)-SO_2CH_3** decomposes, for all pathways. The pK_aN(H) is 9.95 for **2-NPE-ON(H)-SO_2Ar** and, once again it is deprotonation at this site, rather than at the aci-nitro intermediate (pK_a 3-4), that results in a significant change in the observed photoproducts, as seen for **2-NPE-ON(H)-SO_2CH_3**.

In summary, a novel family of photoactivatable *N*-hydroxysulfonamide derivatives **2-NPE-ON(H)-SO_2R** (R = CF_3, CH_3 and Ar) has been studied incorporating the (2-nitrophenyl)ethyl photoprotecting group. The photoproduct quantum yields were determined using actinometry. Steady state photolysis of these molecules showed three different photolytic pathways occurring. **2-NPE-ON(H)-SO_2CF_3** generated up to 30% $CF_3SO_2^-$ with 70% O-N bond cleavage. The highest amount of the HNO generating pathway (87%) was observed for **2-NPE-ON(H)-SO_2Ar**; however this

occurred via C-O bond cleavage followed by a second slower photodecomposition (8.6 min). **2-NPE-ON(H)-SO_2CH_3** decomposed predominantly via a C-O bond cleavage pathway. An undesired and unprecedented (with this PCG) photoinduced O-N bond cleavage to generate RSO_2NH_2 was observed as the major pathway (63%) for target **2-NPE-ON(H)-SO_2CF_3**, whereas this was seen only as a minor competing pathway for **2-NPE-ON(H)-SO_2CH_3** and **2-NPE-ON(H)-SO_2Ar**. The observed photoproducts were unchanged upon irradiation of **2-NPE-ON(H)-SO_2CF_3** and **2-NPE-ON(H)-SO_2CH_3** in solvent mixtures varying in the ratio of CD_3CN and phosphate buffer, pH 7.0. For **2-NPE-ON(H)-SO_2Ar** the percentage of the C-O/N-S bond cleavage increased with increase in the volumes of the aqueous pH 7.0 component in CD_3CN. The pK_a of the N(H) protons were determined using $^{19}F/^{1}H$ NMR spectroscopy. The pK_a of the N(H) protons played a key role in determining the photoproduct ratios. The aci-nitro intermediate was observed using laser flash photolysis. **2-NPE-ON(H)-SO_2CH_3** and **2-NPE-ON(H)-SO_2Ar** may find utility as photoprotected versions of the well-known HNO donor MSHA (**2-NPE-ON(H)-SO_2CH_3**) and the clinically promising HNO donor CXL-1020. The latter target may be of particular value, given the limited lifetime of CXL-1020 in aqueous solution. Photolysis would offer a spatiotemporally controlled mechanism for the release of this compound at a specific site in a biological setting.

Chapter 4: Studies of Photoactivatable *N*-Hydroxysulfonamide-caged HNO Donors incorporating the (6-bromo-7-hydroxycoumarin-4-yl)methyl Phototrigger

4.1 Introduction

In Chapters 2 and 3 the photodecomposition of 2-nitrobenzyl and 2-(nitrophenyl)ethyl -caged *N*-hydroxysulfonamides was investigated. Only a small amount of the HNO-generating pathway occurred for both systems. 2-nitrobenzyl (**2-NO_2Bn**) - caged *N*-hydroxysulfonamides mainly undergo O-N bond cleavage upon irradiation to instead generate a sulfonamide, with ~9% and ~7% of the desired HNO generating pathway occurring for **2-NO_2Bn-ON(H)-SO_2CF_3** and **4,5-$(MeO)_2$-2-NO_2Bn-ON(H)-SO_2CF_3**, respectively (Chapter 2). **2-NO_2Bn-ON(H)-SO_2CH_3** and **4,5-$(MeO)_2$-2-NO_2Bn-ON(H)-SO_2CH_3** decompose via O-N bond cleavage to generate $CH_3SO_2NH_2$. It was also shown that upon irradiation **2-NO_2Bn-OC(O)-ON(H)-SO_2CH_3** mainly underwent C-O bond cleavage to produce CH_3SO_2NHOH (Chapter 2). The 2-nitrophenylethyl photocaged *N*-hydroxysulfonamide **2-NPE-ON(H)-SO_2CF_3** released 30% $CF_3SO_2^-$ (and HNO) upon irradiation, via C-O/N-S bond cleavage (Chapter 3). **2-NPE-ON(H)-SO_2CH_3** and **2-NPE-ON(H)-SO_2Ar** (Ar = -Ph(2-$MeSO_2$)) instead primarily decomposed via C-O bond cleavage to produce CH_3SO_2NHOH or $ArSO_2NHOH$, respectively. $ArSO_2NHOH$ was unstable in most solvent conditions, decomposing further to give the sulfinate and HNO.

The (7-hydroxycoumarin-4-yl)methyl photocaging group has recently attracted increasing attention. Whereas 2-nitrobenzyl and 2-(nitrophenyl)ethyl - caged molecules photodecompose via a short lived (μs to ms) ground state aci-nitro intermediate upon irradiation prior to releasing the molecule of interest,[99, 121] for (7-hydroxycoumarin-4-yl)methyl derivatives rapid heterolytic bond cleavage occurs in the lowest singlet excited state of the system, generating a solvent-caged carbocation and releasing the molecule of interest. Nucleophilic attack at the reactive carbocation subsequently occurs, by the solvent in the absence of a stronger nucleophile. Another advantage of this photocage is that unlike the 2-nitrobenzyl and 2-nitrophenylethyl caged systems, (7-hydroxycoumarin-4-yl)methyl - caged compounds absorb in the visible region. This photocage also has enhanced water solubility.[71, 125-128]

In this chapter studies on the photodecomposition of (6-bromo-7-hydroxycoumarin-4-yl)methyl – caged *N*-hydroxysulfonamides of trifluoromethanesulfonylhydroxamic acid (**BHC-CF$_3$**) and methanesulfonylhydroxamic acid (**BHC-CH$_3$**) are presented. By replacing the o-nitrobenzyl and 2-nitrophenylethyl photocages with the (6-bromo-7-hydroxycoumarin-4-yl)methyl moiety, photodecomposition will not occur via an aci-nitro intermediate and O-N cleavage may be prevented. The structures of these potential HNO donor molecules are shown in Figure 4.1.

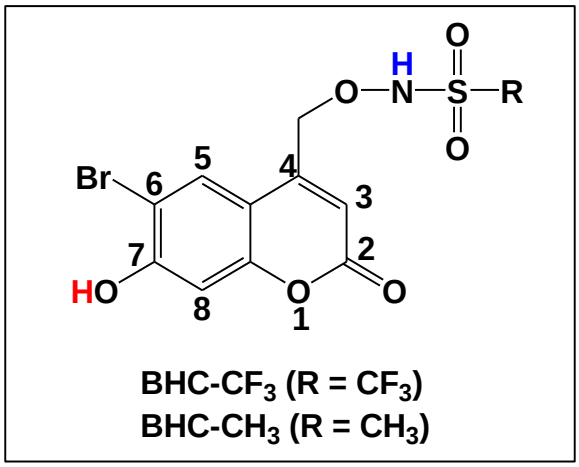

Figure 4.1. Structures of (6-bromo-7-hydroxycoumarin-4-yl)methyl – caged trifluoromethanesulfonylhydroxamic acid (**BHC-CF$_3$**) and methylsulfonylhydroxamic acid (**BHC-CH$_3$**).

4.2 Experimental section

4.2.1 Chemicals

(6-Bromo-7-hydroxycoumarin-4-yl)methyl trifluoromethanesulfonylhydroxamic acid (**BHC-CF$_3$**), (6-bromo-7-hydroxycoumarin-4-yl)methyl methylsulfonylhydroxamic acid (**BHC-CH$_3$**), (6-bromo-7-hydroxycoumarin-4-yl)methyl aldehyde (**BHC-CHO**), (6-bromo-7-hydroxy-4-hydroxymethyl coumarin (**BHC-OH**) and *(E)*-(6-bromo-7-hydroxycoumarin-4-aldoxime (***(E)*-BHC-Oxime**) were obtained from the lab of our collaborators at Kent State University, USA. The synthesis and characterization of these compounds was presented in the PhD dissertation of Mohammad Saifur Rahman.[152] The purity of each compound was checked before conducting photolysis experiments using ^{1}H and/ or ^{19}F NMR spectroscopy.

4.2.2 Instruments and methods

Details of the instruments used are given in Chapter 2, section 2.2.2.

4.2.3 Determination of the molar extinction coefficients

The molar extinction coefficients of **BHC-CF_3** and **BHC-CH_3** were determined using standard solutions of **BHC-CF_3** and **BHC-CH_3** (100, 150, 200, 250, 300, 350 and 400 µM) in a mixture of aerobic H_2O and CH_3CN (92:8; v/v). UV-Vis spectra were recorded at 25.0 ºC. Molar extinction coefficients of **BHC-CF_3** and **BHC-CH_3** were obtained from the plots of absorbance versus concentration, at wavelength maxima (370 nm and 366 nm for **BHC-CF_3** and **BHC-CH_3**, respectively).

4.2.4 Determination of pK_a

Experimental details for the determination of pK_a values using UV-Vis and NMR spectroscopy are given in section 3.2.4-3.2.5, Chapter 3. The solutions of **BHC-CF_3** and **BHC-CH_3** were prepared in the presence of red light to avoid photodecomposition.

4.2.5 Fluorescence spectroscopy

Emission spectra were recorded using a Varian Cary Eclipse Fluorescence Spectrophotometer. Solutions were flowed from a round bottom flask closed with a septum into the cuvette using a peristatic pump. The concentration of **BHC-CF_3** and **BHC-CH_3** was 6.61×10^{-5} M. UV-Vis spectra were recorded before and after fluorescence measurements, to check that the samples had not decomposed.

4.2.6 Photolysis experiments

Photolysis samples were prepared in an NMR tube (Wilmad, 535–JY–7) fitted with a J-Young air-tight cap inside the glove box under anaerobic conditions. Samples of **BHC-CF_3**/**BHC-CH_3** (1.0 mM) were irradiated using a Rayonet photoreactor (350 nm lamps, 4 W). $^{1}H/^{19}F$ NMR spectra were recorded after complete photodecomposition. The percentage of the photoproducts were determined by integrating peaks from the fully photolyzed $^{19}F/^{1}H$ NMR spectrum. The aromatic photoproducts were characterized for partially photolyzed solutions using ^{1}H NMR spectroscopy. Unless otherwise stated, all experiments were carried under anaerobic conditions. Occasionally samples were irradiated using a Xe lamp in conjunction with a monochromator. Internal or external standards (TSP or Ph-CF_3) were not used.

4.2.7 Photoproduct quantum yield

The photoproduct quantum yields were determined in CH_3OH as described in Chapter 2.3.15.

4.3 Results

4.3.1 UV-Vis spectrum of BHC-CF_3 and BHC-CH_3

The UV-Vis spectra of **BHC-CF_3** and **BHC-CH_3** are shown in Figure 4.2. The wavelength maxima of **BHC-CF_3** and **BHC-CH_3** (370 and 366 nm, respectively) can be assigned to a π-π* transition.[185] These wavelength maxima are lower in energy compared to 7-hydroxycoumarin (λ_{max} = 350 nm)[146] due to the presence of the 6-bromo substituent.[148] The molar extinction coefficients for **BHC-CF_3** and **BHC-CH_3** are (2.50 ± 0.03) × 10^4 (370 nm) and (1.42 ± 0.02) × 10^4 (366 nm) M^{-1} cm^{-1}, respectively. The plots are given in Figure A4.1, Appendix.

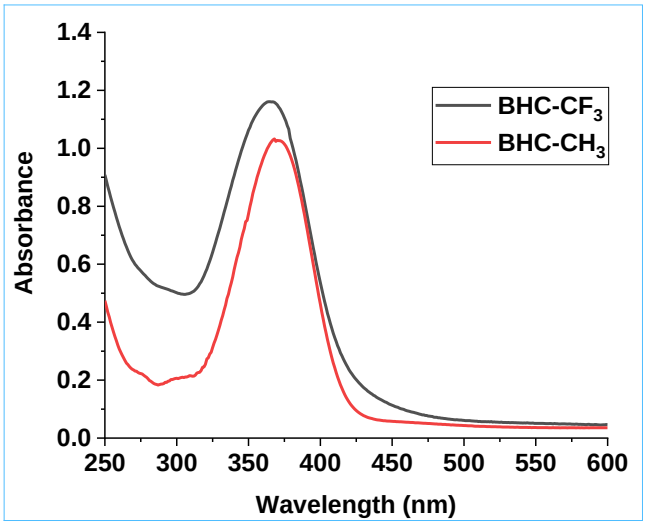

Figure 4.2. UV-Vis spectra of **BHC-CF_3** and **BHC-CH_3** (7.30 × 10^{-5} M) in a mixture of H_2O and CH_3CN (92:8, v/v) at 25.0 °C.

4.3.2 Photostability and thermal stability of BHC-CF_3 and BHC-CH_3

4.3.2.1 Photostability

BHC-CF_3 absorbs significantly in the visible region. The photostability of **BHC-CF_3** (1.0 mM) in CD_3CN was checked by recording the ^{19}F NMR spectrum ~10 min after preparing the sample and ~12 h later, in the presence of fluorescent light in the lab (Figure 4.3). This experiment was carried out under aerobic conditions. After 12 h, 58% **BHC-CF_3** had decomposed to give $CF_3SO_2NH_2$ (33%), $CF_3SO_2^-$ (17%) and $CF_3SO_3^-$ (8%).

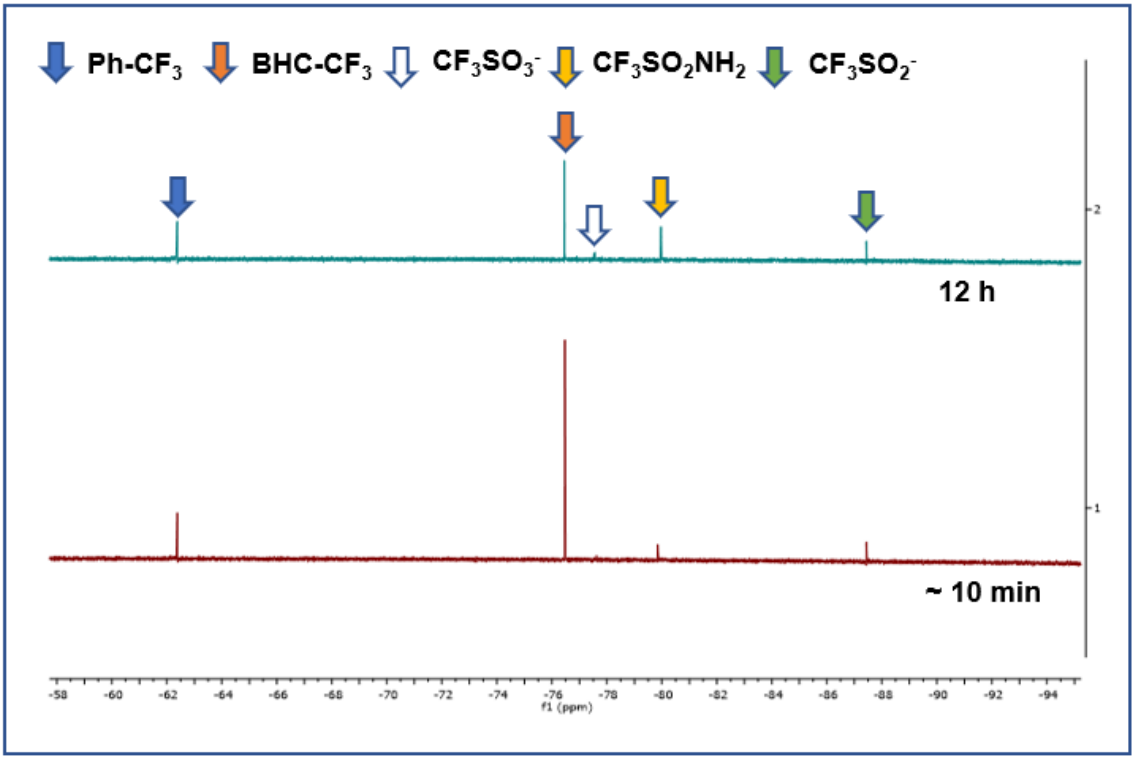

Figure 4.3. ^{19}F NMR spectra of **BHC-CF$_3$** (1.0 mM) in CD_3CN after ~10 min and 12 h following sample preparation under aerobic conditions. The solution was exposed to fluorescent light in the lab.

The photostability of **BHC-CH$_3$** was checked in the presence of the fluorescent light in the lab by recording the ^1H NMR spectrum immediately after sample preparation and also after 12 h. No photodecomposition was observed.

4.3.2.2 Thermal Stability

The thermal stability was checked under anerobic, dark conditions. The ^{19}F and/or ^1H NMR spectrum of **BHC-CF$_3$** and **BHC-CH$_3$** (1.0 mM) in CD_3CN was recorded ~10 min after preparing the sample and 8 days later. No detectable decomposition was observed after ~10 min for both **BHC-CF$_3$** and **BHC-CH$_3$**. After 8 days **BHC-CF$_3$** had decomposed to give 10% $CF_3SO_2NH_2$. The estimated half-life is ~40 days. No decomposition was observed for **BHC-CH$_3$** even after 8 days.

4.3.2.3 Stability of BHC-CF$_3$ in the presence of red light

BHC-CF$_3$ was found to be stable in the presence of red light ($\lambda \approx$ 620-680 nm, 40 Watts maximum). UV-Vis, ^{19}F and ^1H NMR spectra were recorded ~10 min after preparing a sample of **BHC-CF$_3$** in CH_3CN under right light conditions and again 240 min later (Figure 4.4 and Figure 4.5). Negligible decomposition was observed.

Therefore, all the photolysis experiments were carried in the presence of red light, including the sample preparation.

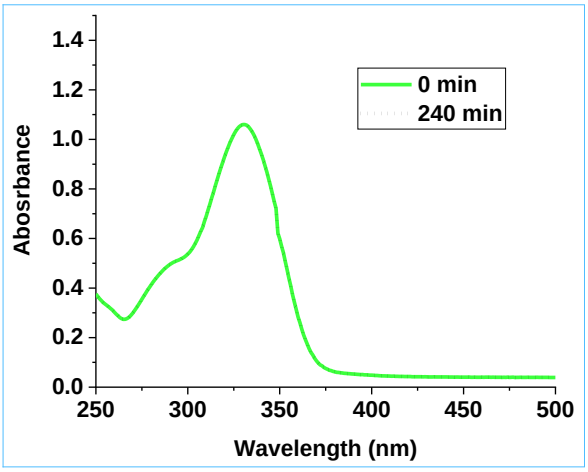

Figure 4.4. UV-Vis spectrum of **BHC-CF_3** (90 µM) in CH_3CN recorded after ~ 10 min and 240 min later. The sample was exposed to red light. There was no change in the UV-Vis spectra after irradiation. Spectra was recorded at 25 °C.

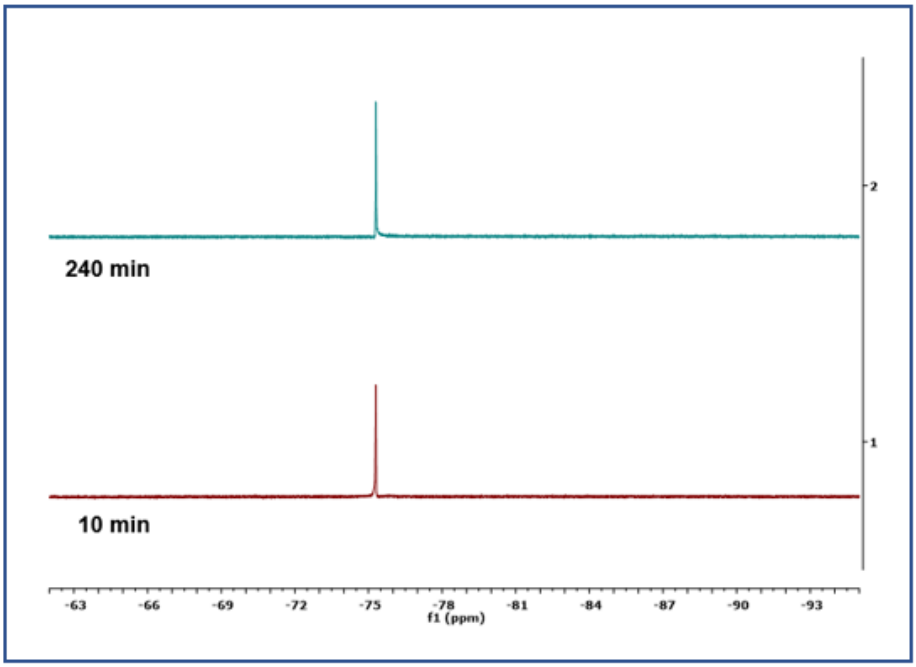

(a)

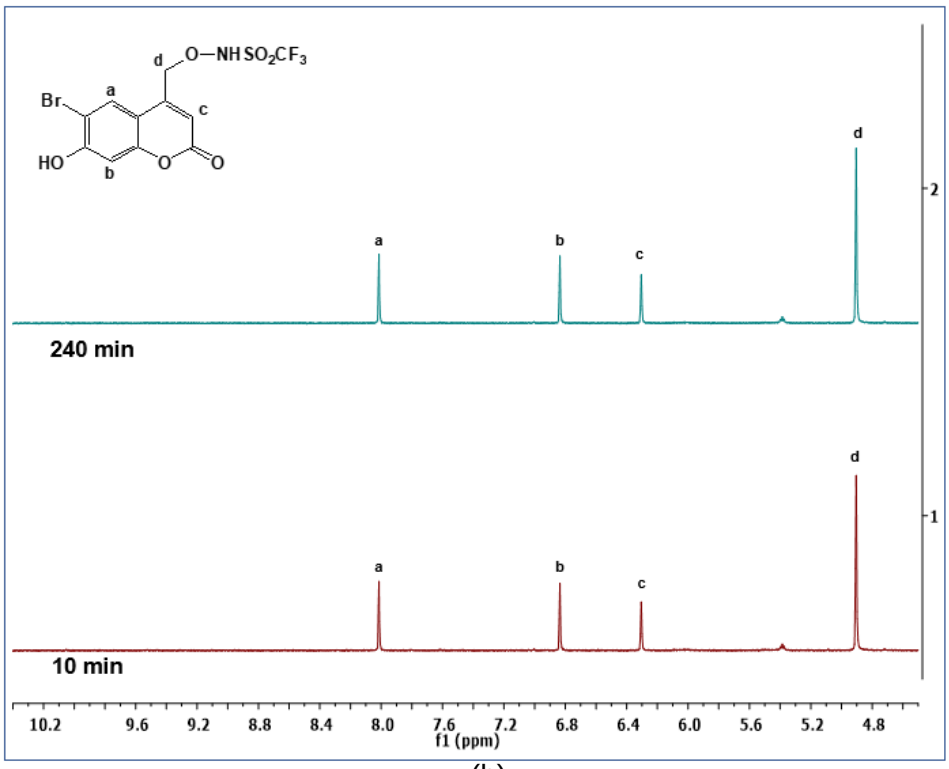

(b)

Figure 4.5. (a) ^{19}F and (b) ^{1}H NMR spectra of **BHC-CF$_3$** (1.0 mM) in CD_3CN recorded after ~10 min under red light conditions and again 240 min later. No decomposition occurred. The impurity at 5.37 ppm (^{1}H NMR) was from CD_3CN (solvent). The labelling scheme for aromatic protons of **BHC-CF$_3$** is also shown.

4.3.3 Characterisation of photoproducts in different solvent compositions

Possible pathways for photodecomposition of **BHC-CF$_3$** and **BHC-CH$_3$** are presented in Scheme 4.1. In Pathway 1 concerted C-O/N-S bond cleavage occurs, to generate a solvent caged reactive carbocation intermediate, HNO and the corresponding sulfinate. Previously *(E)*-6-hydroxynaphthalene-2-aldoxime was observed as a photoproduct upon the irradiation of (6-hydroxynaphthlen-2-yl)methyl (6,2-HNM) caged trifluoromethanesulfonyl hydroxamic acid from the reaction of the carbocation intermediate with HNO.[78] It was anticipated that this would also occur for the **BHC-CF$_3$** and **BHC-CH$_3$** systems The reaction of carbocation intermediate with solvent H_2O would instead generate **BHC-OH**. Competing C-O bond cleavage would generate the same carbocation intermediate and the parent anion of the *N*-hydroxysulfonamide, $CF_3SO_2NHO^-$ or $CH_3SO_2NHO^-$, Pathway 2. Once again the carbocation could react with H_2O to generate **BHC-OH**. O-N bond cleavage is also possible, with the generation of the corresponding sulfonamide and **BHC-CHO**, Pathway 3.

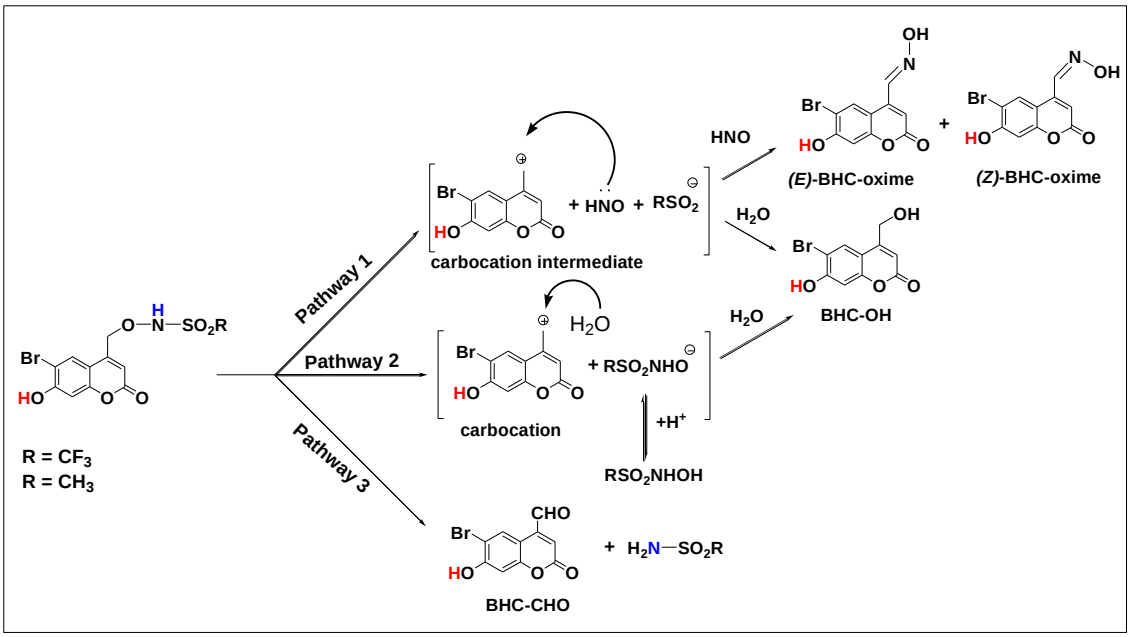

Scheme 4.1. Possible mechanisms for photodecomposition of **BHC-CH$_3$** and **BHC-CF$_3$**, via concomitant C-O/N-S bond cleavage (Pathway 1), C-O bond cleavage (Pathway 2), or O-N bond cleavage (Pathway 3).

The effect of the solvent composition (CD_3CN and phosphate buffer (30 mM), pH 7.0) on the photoproducts obtained upon irradiation of **BHC-CF$_3$** was investigated under anaerobic conditions. The samples were irradiated using a Rayonet photoreactor (350 nm bulbs). The percentage of the aliphatic photoproducts was calculated by integrating the peaks in the ^{19}F NMR spectrum of the photoproducts upon complete photodecomposition of **BHC-CF$_3$**. The aromatic photoproducts were characterized using ^{1}H NMR spectroscopy.

Initially, **BHC-CF$_3$** (1.0 mM) was irradiated in anhydrous CD_3CN. Figure 4.6(a) shows the ^{19}F NMR spectrum obtained upon completely photolyzing **BHC-CF$_3$**. The observed photoproducts were $CF_3SO_2^-$ (-88.6 ppm) and $CF_3SO_2NH_2$ (-80.7 ppm). The percentage of C-O/N-S and O-N bond cleavage was 82% ($CF_3SO_2^-$) and 18% ($CF_3SO_2NH_2$), respectively. There was no evidence for C-O bond cleavage occurring (CF_3SO_2NHOH was found at -74.1 ppm at this solvent, using an authentic sample of this compound). The half-life of decomposition of CF_3SO_2NHOH is ~13 min. The total time to fully photodecompose the sample is 3.6 min and running NMR is ~5 min.

The aromatic photoproducts of **BHC-CF$_3$** were characterized after partial decomposition using ^{1}H NMR spectroscopy, since some of the aromatic photoproducts are not photostable (see later). Figure 4.6(b) gives the ^{1}H NMR spectrum of a partially irradiated sample (0.40 min) of **BHC-CF$_3$**. The ^{1}H NMR spectra of authentic samples of **BHC-CHO** and a mixture of ***(E)*-BHC-oxime** and ***(Z)*-BHC-**

oxime are also given for comparison purposes. The chemical shifts at 8.61, 8.25, 6.95 and 6.32 ppm were assigned to ***(E)*-BHC-oxime** and 7.76, 7.65, 6.95 and 6.61 ppm were assigned to ***(Z)*-BHC-oxime**. The ^{1}H NMR peaks of **BHC-CHO** occur at 10.01, 8.67, 6.97 and 6.80 ppm. In addition, two unknown peaks (7.55, 5.45 ppm) were also observed. The structure and assignments for the photoproducts are shown in Figure 4.6(b).

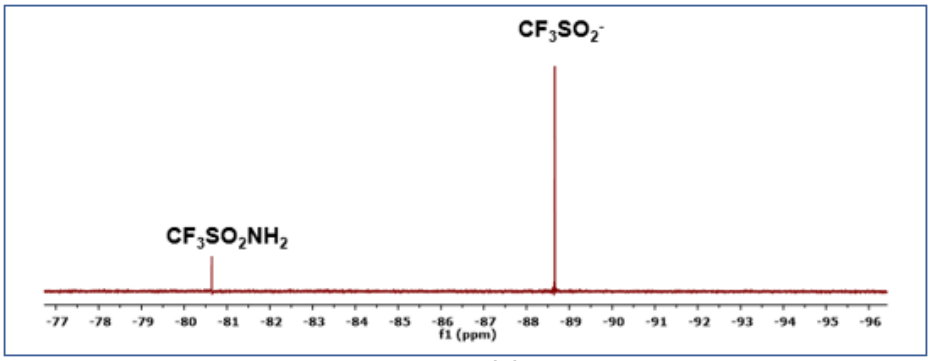

(a)

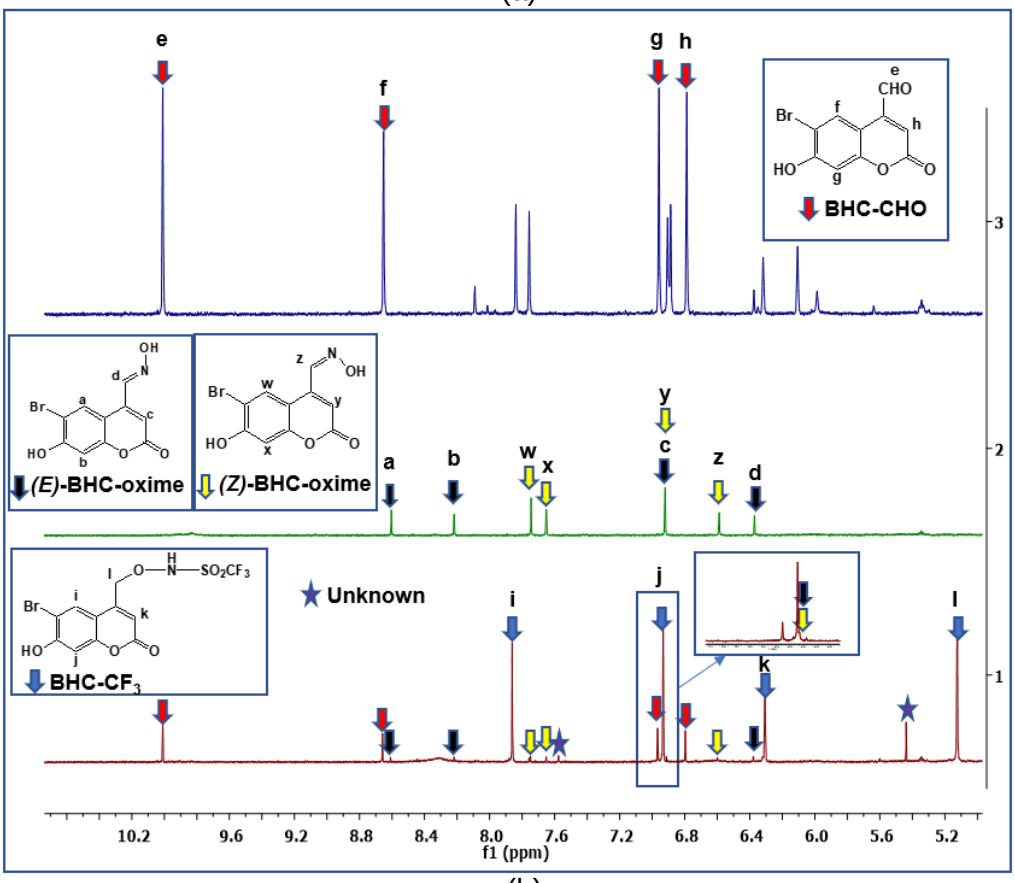

(b)

Figure 4.6. (a) ^{19}F NMR spectrum of **BHC-CF$_3$** (1.0 mM) after complete photodecomposition (3.6 min irradiation) in CD_3CN under anaerobic conditions. (b) Comparison of the ^{1}H NMR spectrum of an irradiated sample (0.40 min) of **BHC-CF$_3$** with authentic samples of a mixture of ***(E)*-BHC oxime** and ***(Z)*-BHC oxime,** and **BHC-CHO** in CD_3CN under anaerobic conditions. The impurity at 5.37 ppm was from the CD_3CN solvent.

***(E)*-BHC-oxime** was obtained as a pure compound. Our collaborators have shown that upon irradiation ***(E)*-BHC-oxime** isomerizes to ***(Z)*-BHC-oxime**, equation (4.1). Figure 4.7 shows the ^{1}H NMR spectrum of ***(E)*-BHC-oxime** before and after irradiation in CD_3CN using a Rayonet photoreactor (350 nm). Peaks at 8.63, 8.23, 6.91 and 6.36 ppm were assigned to ***(E)*-BHC-oxime**. After 0.40 min, additional peaks were appeared at 7.62, 7.71, 6.91, 6.55 ppm. These chemical shifts were assigned to ***(Z)*-BHC-oxime**. The photoconversion of ***(E)*-BHC-oxime** to ***(Z)*-BHC-oxime** was 50%.

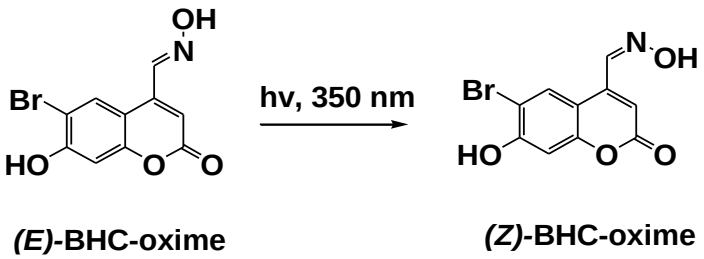

***(E)*-BHC-oxime** ***(Z)*-BHC-oxime**

(4.1)

Impure **BHC-CHO** (10.01, 8.67, 6.97 and 6.80 ppm) was used for identifying this compound in the photoproduct solutions, as all attempts to purify it were unsuccessful. A comparison of the ^{1}H NMR spectra of impure **BHC-CHO** and **BHC-OH** is shown in Figure 4.8. **BHC-CHO** contains 25% **BHC-OH** (7.78, 6.91, 6.33 and 4.70 ppm) and several peaks which could not be assigned were also observed at 7.82, 6.91 and 6.10 ppm. **BHC-OH** was not present in the photolyzed sample, Figure 4.6(b).

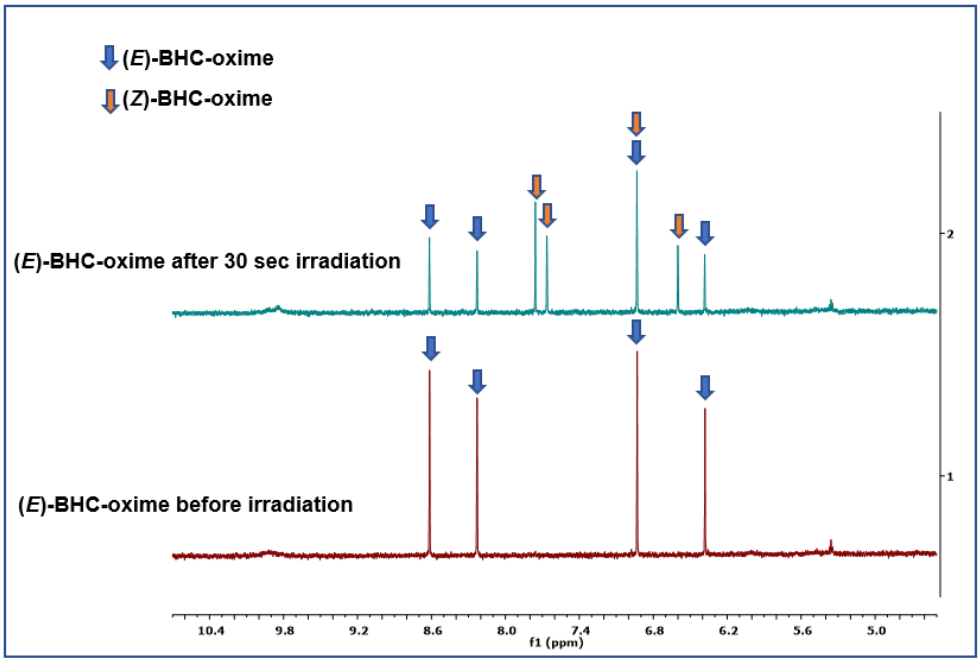

Figure 4.7. ^{1}H NMR spectra of ***(E)*-BHC-oxime** before irradiation and after 0.40 min irradiation in CD_3CN using a Rayonet photoreactor (350 nm). The impurity at 5.37 ppm was from the CD_3CN solvent.

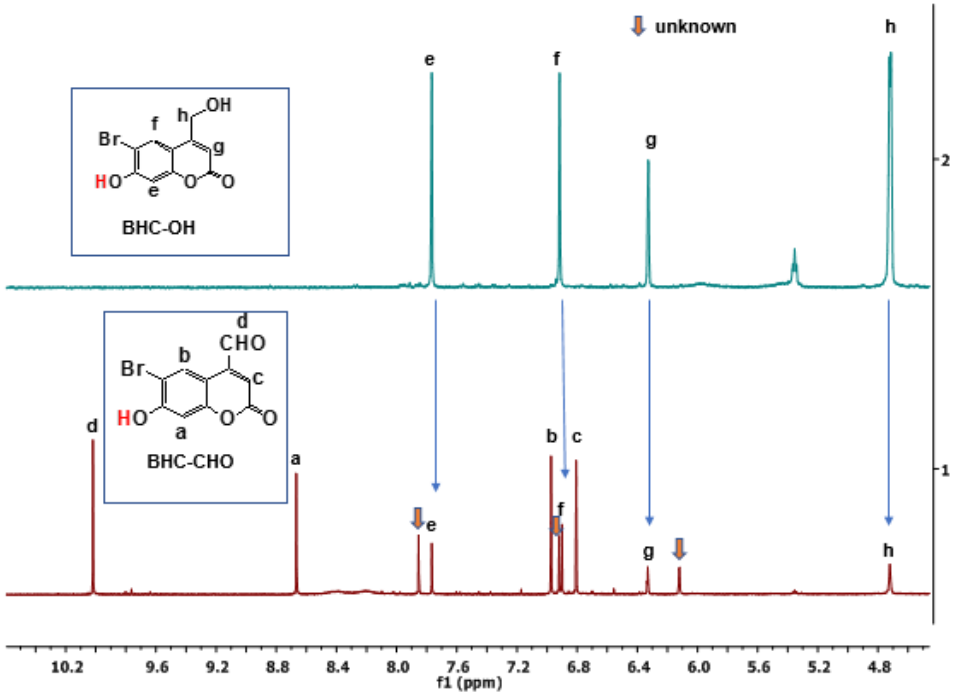

Figure 4.8. ^{1}H NMR spectra of impure **BHC-CHO** and **BHC-OH** in CD_3CN. The impurity at 5.37 ppm was from the CD_3CN solvent.

The ^{19}F NMR spectra of completely photodecomposed samples of **BHC-CF_3** in mixtures of phosphate buffer (30.0 mM, pH 7.0) and different volume percentages of CD_3CN (10:90, 40:60, 60:40 and 8:92 v/v) are shown in Figure 4.9, Figure 4.10(a), Figure 4.11 and Figure 4.12. The photoproducts $CF_3SO_2NH_2$ (O-N bond cleavage) and $CF_3SO_2^-$ (C-O/N-S bond cleavage) were observed at all volume percentages of CD_3CN. The photoproducts were assigned by recording the ^{19}F NMR spectrum in all solvent mixtures.

The aromatic photoproducts were characterized from a partial photolyzed sample (0.4 min irradiation) of **BHC-CF_3** in a mixture of phosphate buffer (pH 7.0, 30.0 mM) and CD_3CN (40:60, v/v), Figure 4.10(b). The chemical shifts at 8.28, 8.27, 6.63 and 6.57 ppm were assigned to ***(E)*-BHC-oxime**. The peaks at 7.73, 7.67, 6.63 and 6.59 ppm were assigned to ***(Z)*-BHC-oxime**. The peaks at 10.01, 8.47, 7.97 and 6.62 ppm were assigned to **BHC-CHO**. The peaks at 7.68, 6.45 and 6.22 ppm were assigned to **BHC-OH** and the remaining peak of **BHC-OH** overlaps with the HDO peak. These chemical shifts were assigned by recording the ^{1}H NMR spectra of all aromatic photoproducts in this solvent mixture.

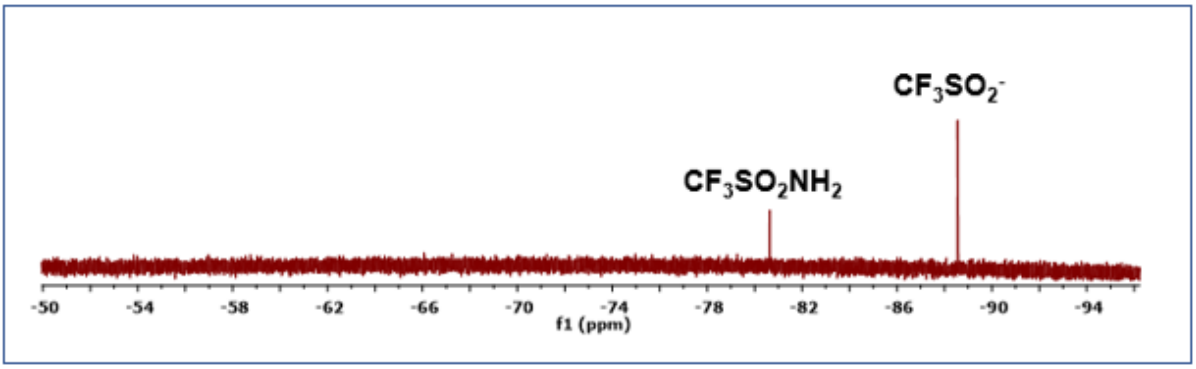

Figure 4.9. ^{19}F NMR spectrum of **BHC-CF$_3$** (1.0 mM) in a mixture of phosphate buffer (pH 7.0, 30.0 mM) and CD_3CN (10:90, v/v) after 3.6 min irradiation.

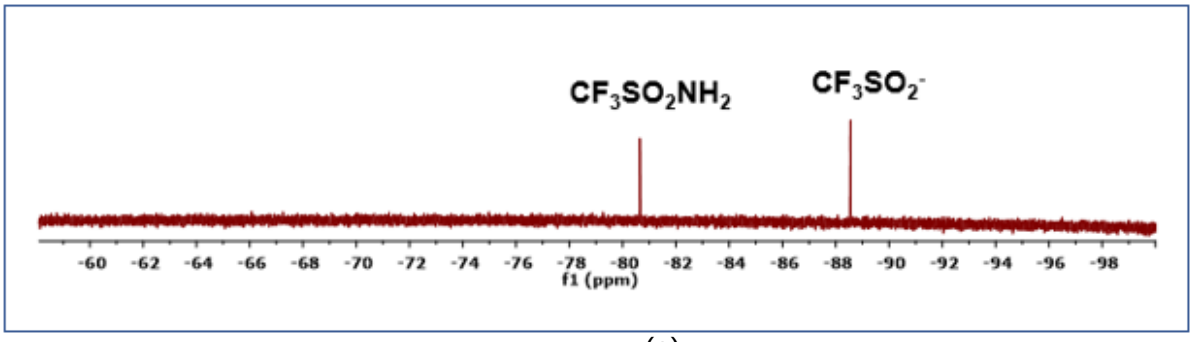

(a)

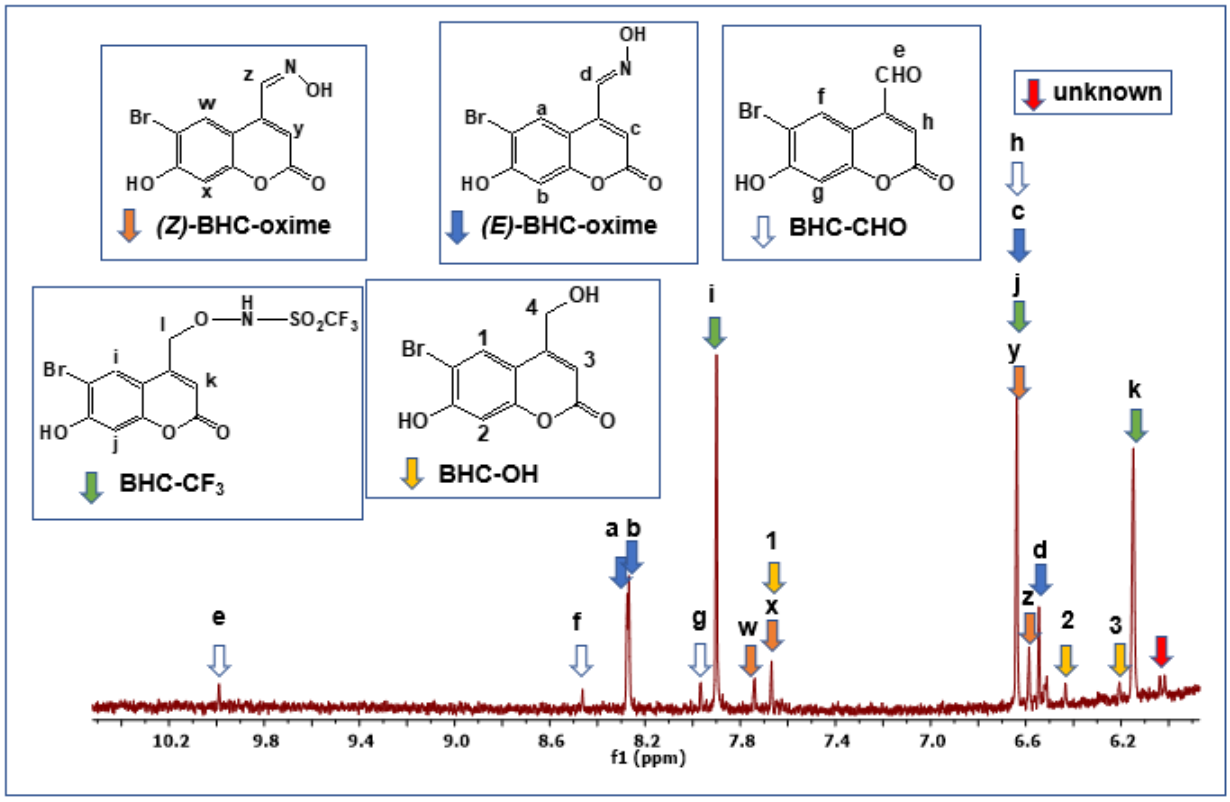

(b)

Figure 4.10. (a) ^{19}F NMR spectrum of **BHC-CF$_3$** (1.0 mM) in a mixture of phosphate buffer (pH 7.0, 30.0 mM) and CD_3CN (40:60, v/v) after 3.8 min irradiation. (b) ^{1}H NMR spectrum of a partially photolyzed solution of **BHC-CF$_3$** (1.0 mM) in a mixture of phosphate buffer (pH 7.0, 30.0 mM) and CD_3CN (40:60, v/v) after 0.40 min irradiation.

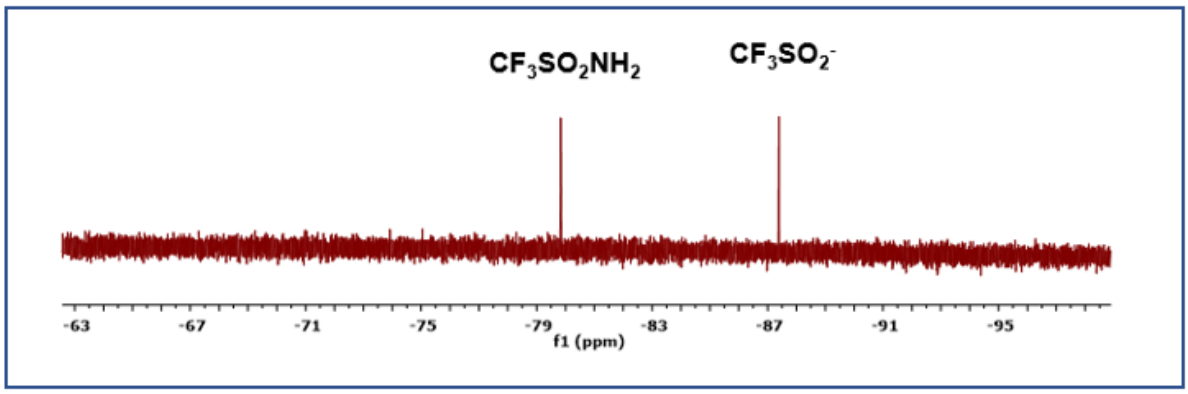

Figure 4.11. ^{19}F NMR spectrum of **BHC-CF_3** (1.0 mM) in a mixture of phosphate buffer (pH 7.0, 30.0 mM) and CD_3CN (60:40, v/v) after 3.8 min irradiation.

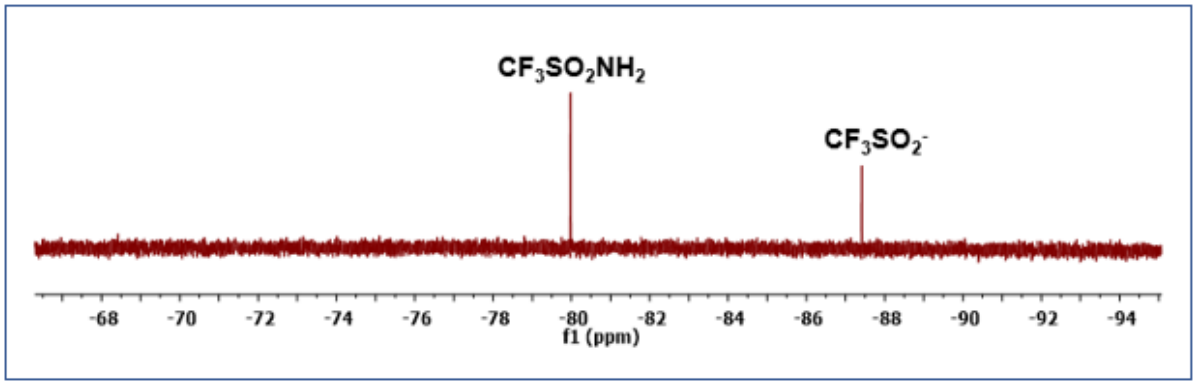

Figure 4.12. ^{19}F NMR spectrum of **BHC-CF_3** (1.0 mM) in a mixture of phosphate buffer (pH 7.0, 30.0 mM) and CD_3CN (92:8, v/v) after 3.8 min irradiation.

The effect of the solvent composition on the photoproducts for **BHC-CF_3** is summarized in Table 4.1. The percentage of the desired pathway which generates $CF_3SO_2^-$ and HNO by concomitant C-O/N-S bond cleavage increases as the volume percentage of CD_3CN in the CD_3CN/phosphate buffer (30 mM, pH 7.0) increases, with 82% $CF_3SO_2^-$ (and HNO) generated in pure CD_3CN.

Table 4.1. Effect of solvent ratio on the photoproducts derived from the *N*-hydroxysulfonamide moiety for photodecomposition of **BHC-CF_3** (1.0 mM).

Solvent ratio, % v/v (30 mM phosphate buffer, pH 7.0/CD_3CN)	Percentage of Photoproducts	
	$CF_3SO_2^-$	$CF_3SO_2NH_2$
00/100	82	18
10/90	75	25
40/60	60	40
60/40	45	55
90/10	30	70
92/8	25	75

The photoproducts obtained upon the irradiation of **BHC-CH_3** were also determined as a function of solvent composition in phosphate buffer (30 mM, pH 7.0)/CD_3CN solvent mixtures. **BHC-CH_3** solutions were irradiated using the Rayonet photoreactor (350 nm). The photoproducts were characterized by recording the ^{1}H NMR spectrum of fully and partially photodecomposed samples.

Figure 4.13(a) shows the ^{1}H NMR spectrum of a completely photodecomposed sample of **BHC-CH_3**. The peak at 3.05 ppm were assigned to $CH_3SO_2NH_2$ (82%), 2.94 ppm to CH_3SO_2NHOH (8%), 2.67 ppm to $CH_3SO_2^-$ (3%), and 2.17 ppm to $CH_3SO_3^-$ (3%) and 3.02 ppm to an unknown species (4%). These peaks were assigned by recording the ^{1}H NMR spectra of authentic samples of all compounds in the same solvent (spectra not shown).

In a separate experiment, **BHC-CH_3** was partially photolyzed to characterize the aromatic photoproducts. Partial photolysis was required due to the primary aromatic photoproducts undergoing secondary photolysis at longer irradiation times. Figure 4.13(b) shows the ^{1}H NMR spectrum of a partially irradiated (0.10 min) sample of **BHC-CH_3**. The peaks at 10.01, 8.67, 6.97 and 6.80 ppm can be assigned to **BHC-CHO**. The aromatic photoproduct **BHC-CHO** was assigned by comparing the ^{1}H NMR spectrum of an authentic sample of **BHC-CHO** with the partially photolyzed sample of **BHC-CH_3**. Two unknown peaks were also observed at 8.39 and 5.42 ppm. Upon further irradiation of the sample (total irradiation time 0.25 min), the peaks from **BHC-CHO** were no longer observed. The unknown peaks at 8.39 and 5.42 ppm became larger upon further irradiation and many additional peaks were also observed. There was no evidence for **(*E*)-BHC-oxime** or **(*Z*)-BHC-oxime or BHC-OH** in the irradiated samples, consistent with the low percentage of sulfinate upon complete photodecomposition (6% $CH_3SO_2^-$ + $CH_3SO_3^-$). That is, Pathway C (O-N bond cleavage, Scheme 4.1) dominates, with the expected photoproducts $CH_3O_2NH_2$ (82%) and **BHC-CHO** observed by ^{1}H NMR spectroscopy.

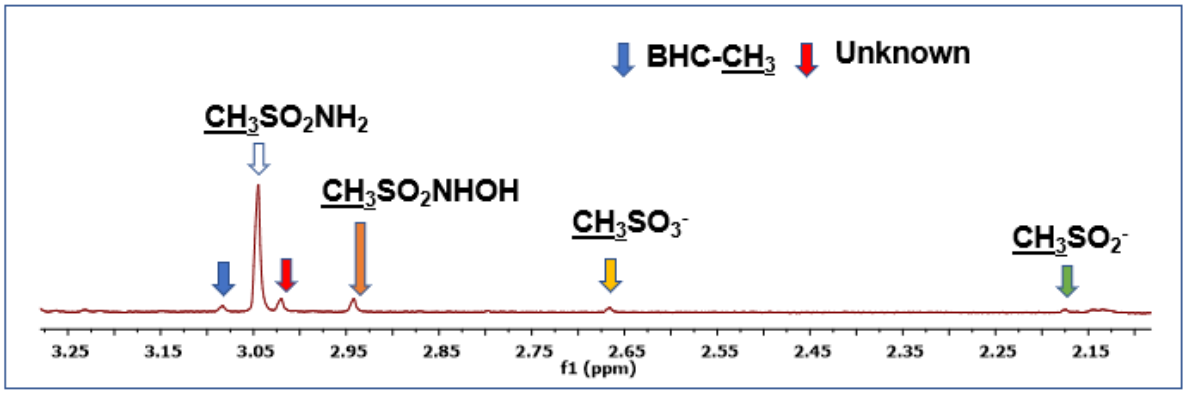

(a)

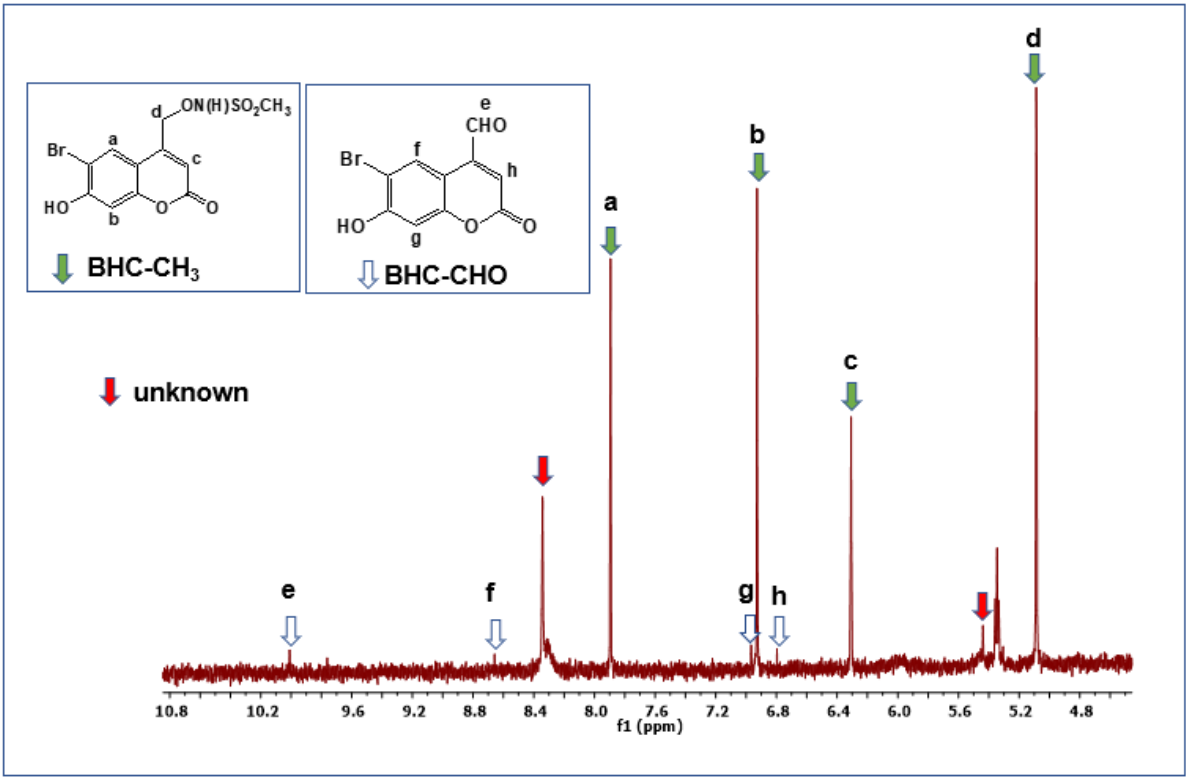

(b)

Figure 4.13. (a) ^{1}H NMR spectrum upon complete photodecomposition of **BHC-CH$_3$** (1.0 mM) recorded after 5 min irradiation in CD_3CN. (b) ^{1}H NMR spectrum of **BHC-CH$_3$** (1.0 mM) after partial irradiation (0.10 min) in CD_3CN. The peak at 5.37 ppm is from the CD_3CN solvent and the peaks at 8.39 and 5.42 ppm could not be assigned.

The aliphatic photoproducts were also characterized using ^{1}H NMR spectroscopy in a fully photodecomposed sample of **BHC-CH$_3$** in a mixture of phosphate buffer (pH 7.0, 30.0 mM) and CD_3CN (60:40, v/v) (Figure 4.14(a)). The photoproducts were $CH_3SO_2NH_2$ (3.05 ppm, 77%), CH_3SO_2NHOH (2.94 ppm, 7%), $CH_3SO_2^-$ (2.17 ppm, 2%) and $CH_3SO_3^-$ (2.17 ppm, 7%) and an unknown species (3.04 ppm, 7%). The ^{1}H NMR spectrum of a partially photodecomposed sample was also recorded, to characterize the aromatic photoproducts, Figure 4.14(b). The aromatic photoproducts

were found to be **BHC-CHO** (10.01, 8.47, 7.98 and 6.62 ppm) and **BHC-OH** (7.69, 6.46, 6.22 and 4.75 ppm). The peaks at 6.17, 6.04, 5.46 and 5.24 ppm could not be assigned. A similar experiment was carried out in a mixture of phosphate buffer (pH 7.0, 30.0 mM) and CD_3CN (9:10, v/v). The detailed analysis of the photoproducts is discussed in section 4.3.13.

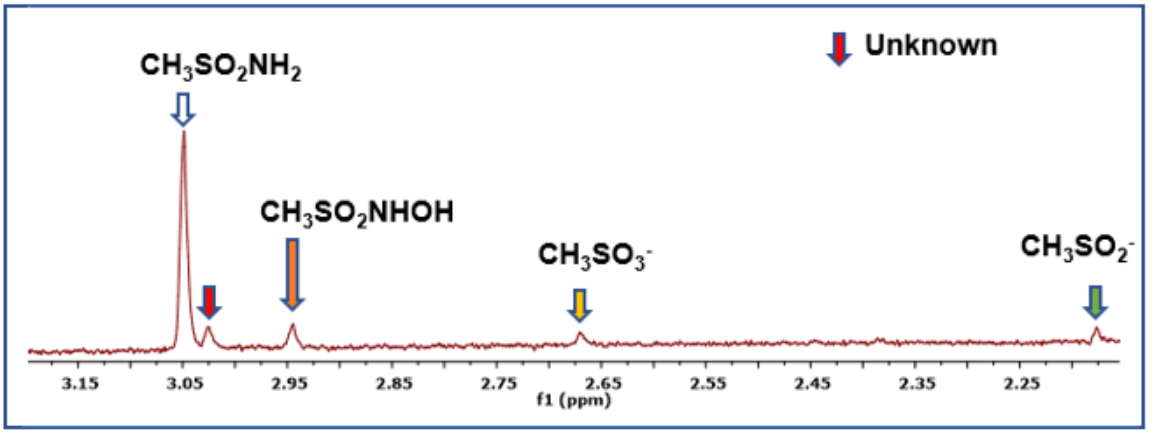

(a)

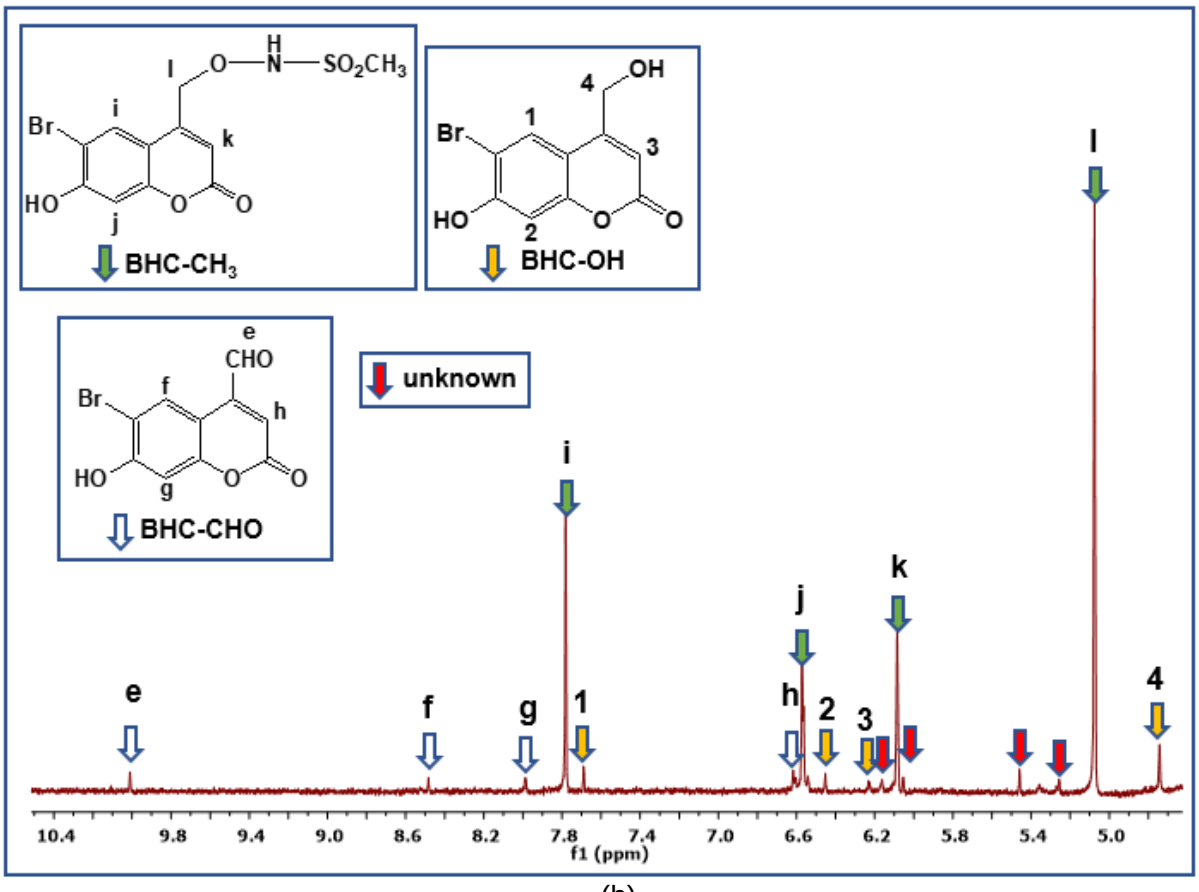

(b)

Figure 4.14. (a) ^{1}H NMR spectrum of **BHC-CH$_3$** (1.0 mM) recorded after complete photodecomposition in a mixture of phosphate buffer (pH 7.0, 30.0 mM) and CD_3CN (60:40, v/v). (b) ^{1}H NMR spectrum of partially irradiated sample of **BHC-CH$_3$** after 0.20 min.

Table 4.2 summarizes the effect of the solvent composition on the observed photoproducts. The solvent composition does not affect the observed photoproducts with the major photoproduct being $CH_3SO_2NH_2$ (~80%, O-N bond cleavage). Smaller amounts of CH_3SO_2NHOH (~7%), $CH_3SO_2^-$ (2%), $CH_3SO_3^-$ (7%) and an unknown species were also observed.

Table 4.2. Effect of solvent ratio on the photoproducts derived from the *N*-hydroxysulfonamide moiety for photodecomposition of **BHC-CH$_3$** (1.0 mM).

Solvent ratio, % v/v (30 mM phosphate buffer, pH 7.0/ CD_3CN)	Percentage of Photoproducts				
	$CH_3SO_2NH_2$	CH_3SO_2NHOH	$CH_3SO_2^-$	$CH_3SO_3^-$	unknown
00/100	82	8	3	3	4
60/40	77	7	2	7	7
90/10	79	5	2	9	5

4.3.4 Effect of O_2

To probe the effect of oxygen on the mechanism of photodecomposition, the observed photoproducts were determined for **BHC-CF$_3$** (1.00 mM) in a mixture of phosphate buffer (pH 7.0, 30.0 mM) and CD_3CN (60:40, v/v) under aerobic conditions (Figure 4.15). The photoproducts were $CF_3SO_3^-$ (45%) and $CF_3SO_2NH_2$ (55%). $CF_3SO_2^-$ was fully oxidized to $CF_3SO_3^-$ in the presence of air. The percentages of the photoproducts were identical to those observed under anaerobic conditions within experimental error (45% $CF_3SO_2^-$ and 55% $CF_3SO_2NH_2$, Figure 4.11). Therefore, no effect of O_2 was observed on the photoproducts obtained upon irradiation of **BHC-CF$_3$**.

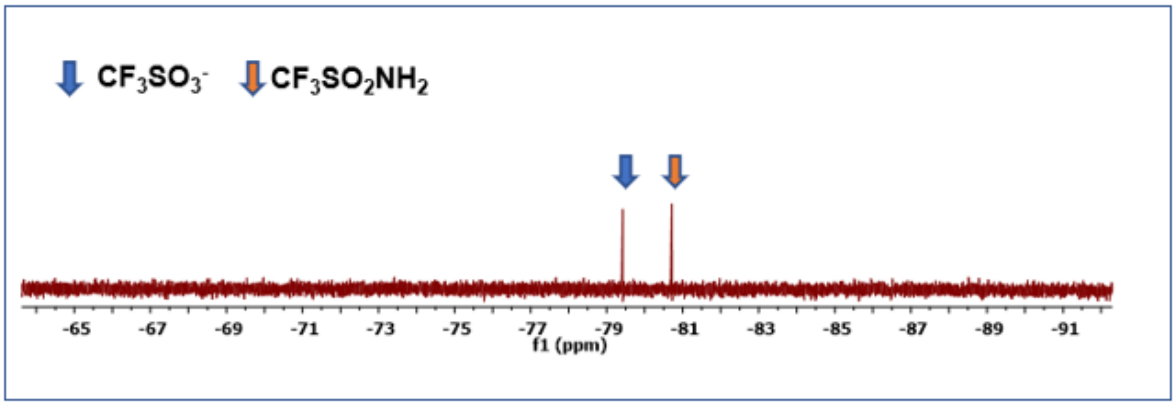

Figure 4.15. ^{19}F NMR spectrum of fully photodecomposed **BHC-CF$_3$** (1.0 mM) in an aerobic mixture of phosphate buffer (pH 7.0, 30.0 mM) and CD_3CN (60:40, v/v) after 3.8 min irradiation.

4.3.5 Photostability of the primary aromatic photoproducts

4.3.5.1 BHC-OH and BHC-CHO

The photostability of **BHC-OH** and **BHC-CHO** was investigated in CD_3CN. Figure 4.16 and Figure 4.17 shows the ^1H NMR spectra of **BHC-OH** and **BHC-CHO** in CD_3CN before and after irradiation. **BHC-OH** (7.73, 6.89 and 6.31 ppm) was found to be photostable. After irradiation, there was no change in the NMR spectrum. **BHC-CHO** was not pure, as discussed earlier. The sample of **BHC-CHO** used contains 25% **BHC-OH** (7.73, 6.89 and 6.31 ppm) and three unknown peaks (7.82, 6.91 and 6.10 ppm). Both **BHC-CHO** and **BHC-OH** were found to be photostable.

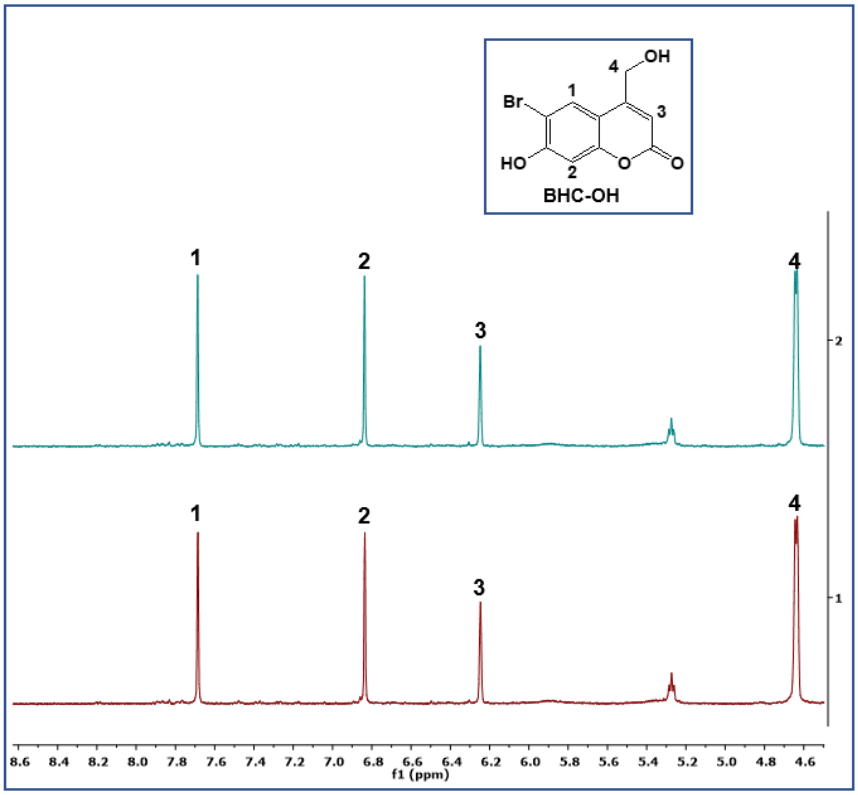

Figure 4.16. ^1H NMR spectra of **BHC-OH** before irradiation and after 0.20 min irradiation in CD_3CN using a Rayonet photoreactor (350 nm). The impurity at 5.27 ppm was from the CD_3CN.

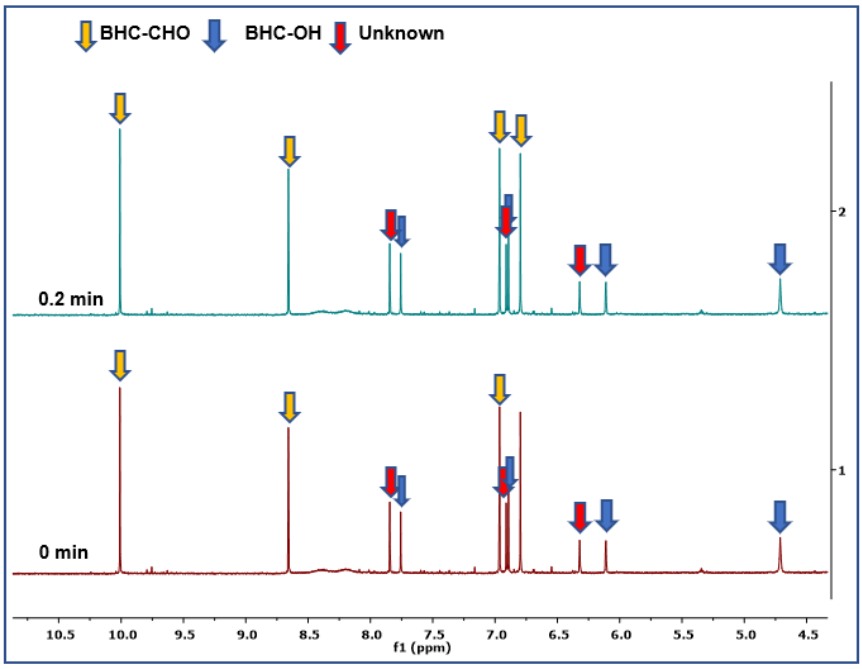

Figure 4.17. ^{1}H NMR spectra of **BHC-CHO** before irradiation and after 0.20 min irradiation in CD_3CN using a Rayonet photoreactor (350 nm). The impurity at 5.27 ppm was from the CD_3CN.

4.3.6 Determining the ground state pK_a for BHC-CF_3 and BHC-CH_3

The ground state pK_a for each BHC-caged molecule was determined to understand the role of the protonation state of the ground state molecule on the mechanism of photodecomposition. It was previously reported that the pK_a values for the N(H) of the structurally related **2-NPE-ON(H)-SO_2CF_3** and 6-hydroxynaphthalen-2-yl)methyl-photocaged *N*-hydroxysulfonamide (6,2-HNM-ON(H)-SO_2CF_3) were 3.77 ± 0.03 (in D_2O with 5% v/v CH_3CN, I = 1.0 M, $NaCF_3SO_3$, section 3.3.3, Chapter 3) and 4.4 ± 0.1 (aqueous solution), respectively.[78] The pK_a value for the -N(H) in **2-NPE-ON(H)-SO_2CH_3** was 10.06 ± 0.03 (in D_2O with 5% v/v CH_3CN, I = 1.0 M, $NaCF_3SO_3$, section 3.3.3, Chapter 3). The pK_a of **BHC-OH** and the 7-hydroxy substituent of (6-bromo-7-hydroxycoumarin-4-yl)methyl acetate was reported to be 6.2 (in aqueous solution)[139] and 5.88 (10:90 v/v DMSO: H_2O).[148] Deprotonation of both the N(H) and O(H) of **BHC-CF_3** and **BHC-CH_3** would also be expected to occur in aqueous solution.

4.3.7 Determining the ground state pK_a values of BHC-CF_3 using NMR spectroscopy

A control experiment was conducted to check that **BHC-CF_3** does not decompose during the pK_a determination experiments. **BHC-CF_3** was dissolved in a mixture of CH_3CN and D_2O (8:92 v/v CH_3CN: D_2O). The pD was adjusted to 2.35 and the ^{1}H

NMR spectrum was recorded. The pD was increased to pD 5.70 (adjusted by adding a small volume of NaOH dissolved in D_2O) and the ^1H NMR spectrum was again recorded. The solution was then adjusted back to pD 2.25 (addition of a small volume of 40% HCl in D_2O) and the ^1H NMR spectrum recorded for the last time. The chemical shifts of **BHC-CF$_3$** were identical within experimental error to their original values, and no decomposition was observed (spectra not shown). This experiment was conducted under red light conditions.

The ^{19}F and ^1H NMR spectra of **BHC-CF$_3$** were recorded in D_2O with the pD of the aqueous component of the solvent mixture varying from pD 2.03-11.23, to obtain an estimate of pK_a (see experimental section 4.2.4). A small amount of CH_3CN (8% v/v CH_3CN) was required to ensure that the compound was fully dissolved. The chemical shifts at pD < 2.03 and pD > 11.22 were not obtained since **BHC-CF$_3$** is not stable at these pD conditions. Selected ^{19}F NMR spectra are shown in Figure 4.18. The chemical shift of the -CF_3 signal moves upfield from -74.4 to -77.0 ppm as pD is increased from 2.40 to 5.05. The chemical shift of this signal is essentially unchanged from pD 5.05 to 11.22 (≤ 0.2 ppm, Table 4.3). A plot of the observed chemical shift, δ_{obs} versus pD is shown in Figure 4.19 for the entire data. Fitting the data to equation (4.2).

$$\delta_{obs} = \frac{\delta_{HA} + \delta_{A^-}(10^{pD-pKa})}{1 + (10^{pD-pKa})} \qquad (4.2)$$

where δ_{obs} = observed chemical shift (ppm), δ_{HA} = the chemical shift (ppm) of the acid and δ_{A^-} = the chemical shift (ppm) of the conjugate base gives a pK_a value of 3.42 ± 0.02.

This pK_a value is assigned to the -N(H) proton of the *N*-hydroxysulfonamide, based on its value and the large change in the chemical shift of the CF_3 peak. The chemical shift of the CF_3 signal of **BHC-CF$_3$** moves upfield upon deprotonation of the N(H) proton, as the CF_3 experiences more electron density. The pK_a value of 3.42 ± 0.02 is similar to that observed for 6,2-HNM-ON(H)-SO_2CF_3 (4.4 ± 0.1 in aqueous solution)[78] and **2-NPE-ON(H)-SO$_2$CF$_3$** (3.77 ± 0.03 (in D_2O with 5% v/v CH_3CN, I = 1.0 M, $NaCF_3SO_3$, section 3.3.6.1, Chapter 3). ^1H NMR spectroscopy was not useful for determining this pK_a value. The BHC-$\underline{CH_2}$-ON(H)-SO_2CF_3 peak overlapped with the HDO peak from the aqueous component of the solvent mixture.

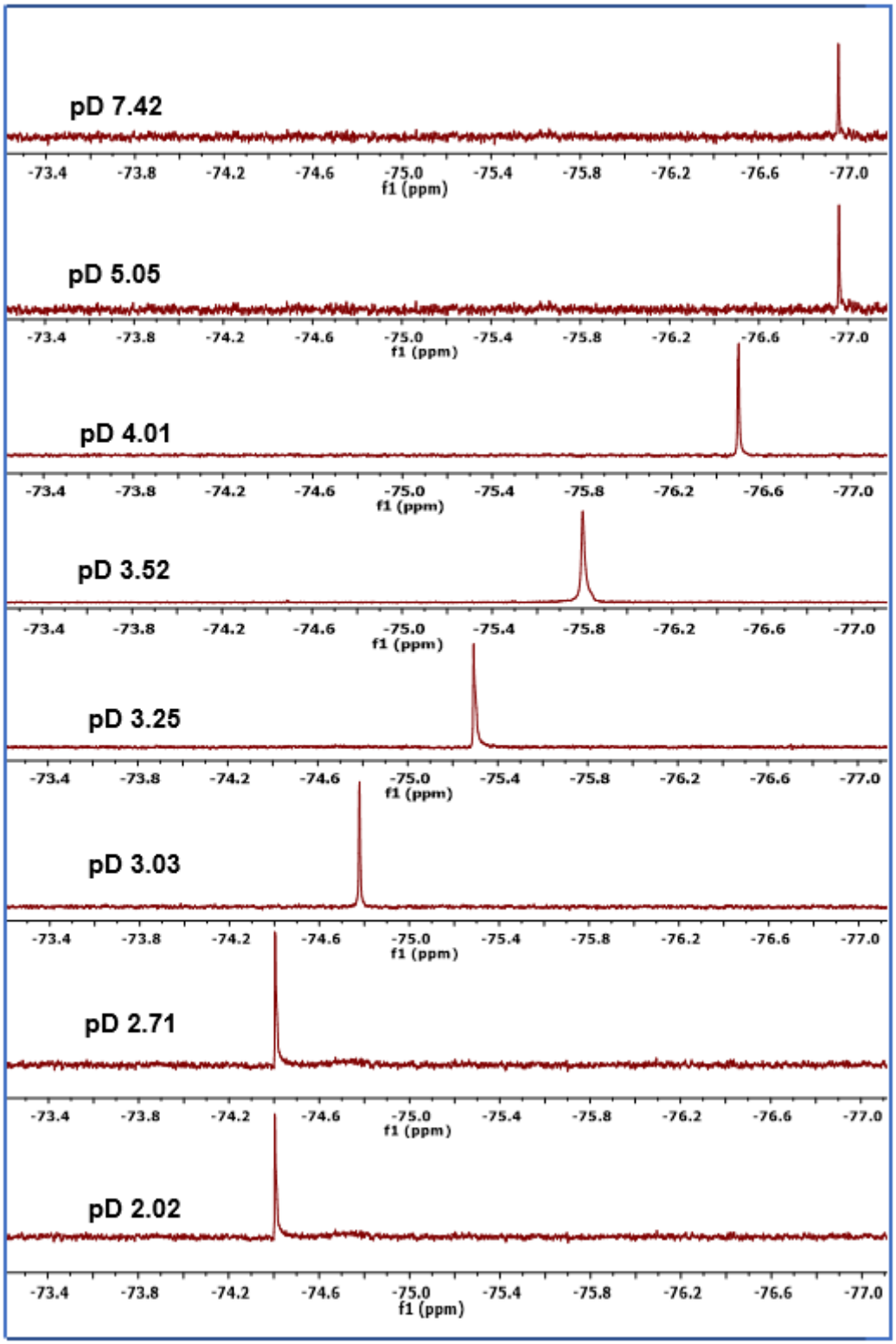

Figure 4.18. Selected ^{19}F NMR spectra of **BHC-CF_3** as a function of pD, in D_2O with 8% v/v CH_3CN, I = 1.0 M, $NaCF_3SO_3$. The spectra are referenced to **Ph-CF_3** (-62.9 ppm).

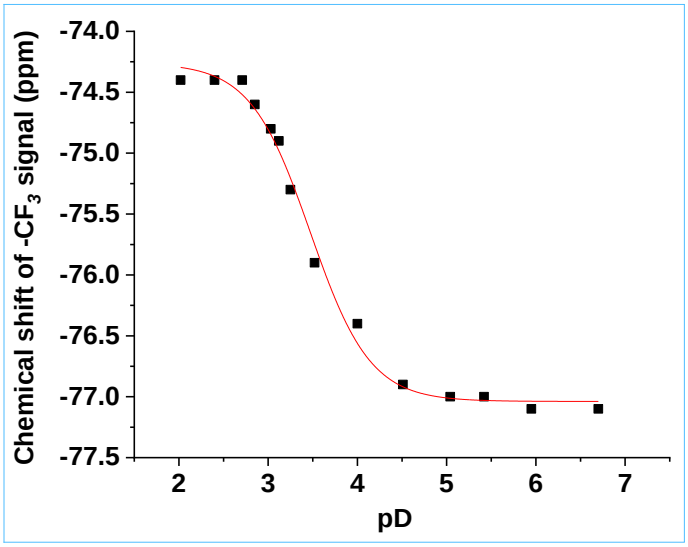

Figure 4.19. Plot of chemical shift of the CF_3 peak of **BHC-CF₃** versus pD. Data were fitted to equation (4.2), giving pK_a = 3.42 ± 0.02, δ_{HA}= -77.0 ± 0.1 ppm and δ_{A^-} = -74.7 ± 0.1 ppm.

The pK_a for deprotonation of the 7-hydroxy substituent of **BHC-CF₃** was determined by recording ^{1}H NMR spectra from pD 4.90 to 9.43. The assignments of the aromatic protons are shown in Figure 4.20. The chemical shifts were unchanged (<0.01 ppm) (Table 4.3) from 2.02 to 4.92 ppm. The chemical shift of protons **a**, **b** and **c** of **BHC-CF₃** progressively decreased from 7.92 to 7.77 ppm, 6.77 to 6.48 ppm and 6.26 to 6.03 ppm, respectively, as the pD was increased from 4.90 to 9.43. Selected ^{1}H NMR spectra are shown in Figure 4.21. Deprotonation of -O(H) resulted in an upfield shift of chemical shifts **a**, **b** and **c**, due to protons **a**, **b** and **c** experiencing more electron density with increasing pD. The chemical shift of proton **d** overlapped with the HDO peak of aqueous component. The chemical shifts of protons **a, b** and **c** were plotted as a function of pD. Data were fitted to equation (4.2), giving pK_a = 6.35 ± 0.03 (proton **a**), pK_a = 6.28 ± 0.03 (proton **b**) and pK_a = 6.32 ± 0.03 (proton **c**) (Figure 4.22). The overall change in the chemical shift was 0.16, 0.29 and 0.23 ppm for protons **a**, **b** and **c,** respectively. The average pK_a value is 6.31 ± 0.03, which is similar to the value reported for the 7-hydroxy substituent of (6-bromo-7-hydroxycoumarin-4-yl)methanol (pK_a 6.2, in H_2O). Essentially no change in the CF_3 shift was observed upon deprotonating the 7-hydroxy substituent because the CF_3 moiety is at some distance from the site of deprotonation.

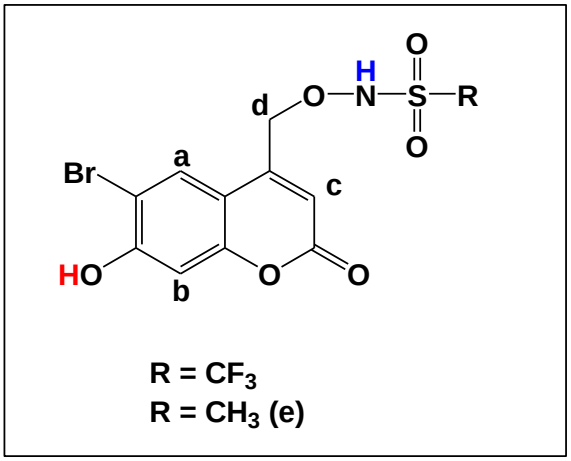

Figure 4.20. Structure of the **BHC-CF_3** and **BHC-CH_3** with proton labelling scheme.

Table 4.3. ^{19}F and ^{1}H NMR chemical shifts as a function of pD for **BHC-CF_3** in a mixture of CH_3CN and D_2O (8:92 v/v CH_3CN: D_2O) (25° C).

pD	Chemical shift (ppm) of -CF_3 signal	Chemical shift (ppm) of aromatic protons		
		Proton **a**	Proton **b**	Proton **c**
2.02	-74.4	7.92	6.77	6.26
2.40	-74.4	7.92	6.77	6.26
2.71	-74.4	7.92	6.77	6.26
2.85	-74.6	7.92	6.78	6.26
3.03	-74.8	7.92	6.77	6.26
3.12	-74.9	7.93	6.77	6.26
3.25	-75.3	7.92	6.77	6.26
3.52	-75.9	7.92	6.77	6.26
4.01	-76.4	7.92	6.77	6.26
4.51	-76.9	7.93	6.77	6.27
4.90	-76.9	7.92	6.77	6.26
5.05	-76.9	7.92	6.77	6.26
5.42	-77.0	7.91	6.69	6.22
5.95	-77.0	7.88	6.66	6.17
6.32	-77.0	7.84	6.59	6.14
6.70	-77.0	7.82	6.54	6.09
7.42	-76.9	7.80	6.50	6.06
8.20	-77.0	7.78	6.48	6.04
9.43	-77.0	7.77	6.48	6.03
10.42	-77.0	7.77	6.48	6.03

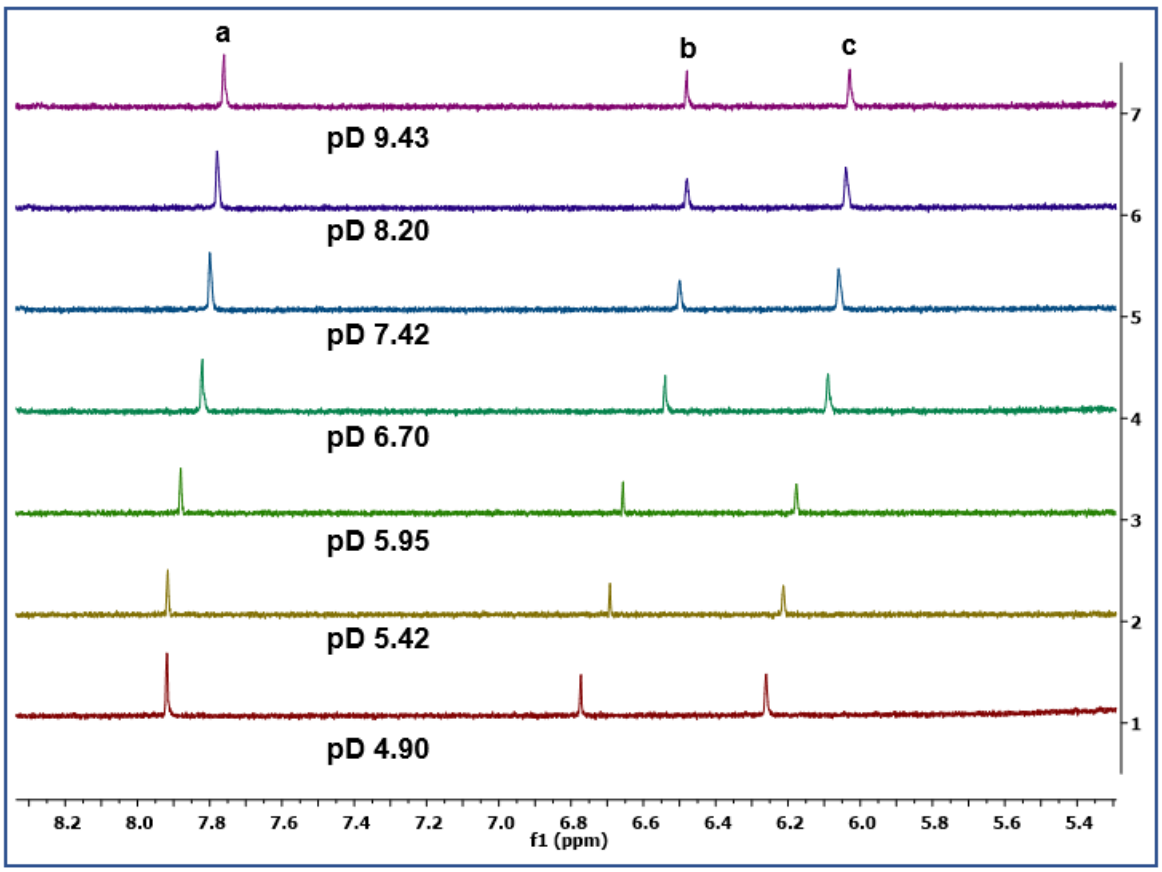

Figure 4.21. Selected ^{1}H NMR spectra for **BHC-CF$_3$** as a function of pD, in D_2O with 8% v/v CH_3CN, I = 1.0 M, $NaCF_3SO_3$. TSP (0.00 ppm) was used as an external reference.

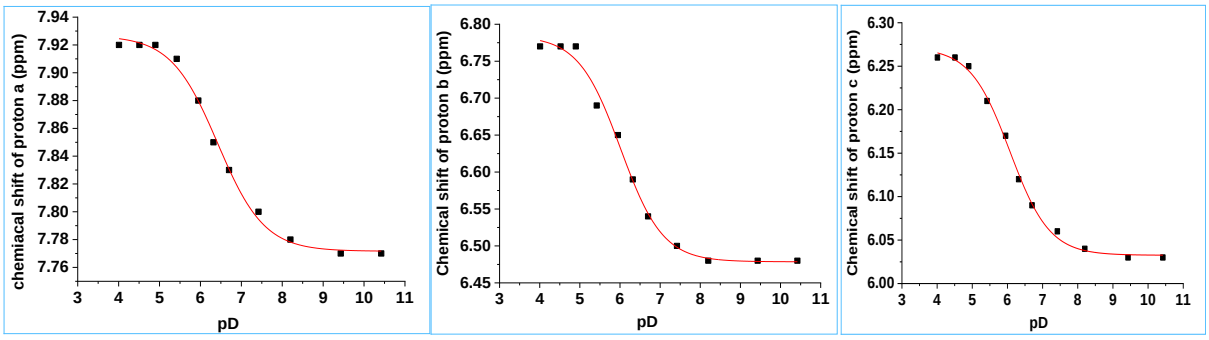

(a) (b) (c)

Figure 4.22. (a) Plot of chemical shift of proton **a** vs pD. Data were fitted to equation (4.2), giving pK_a = 6.35 ± 0.03, δ_{HA}= 7.92 ± 0.01 ppm and δ_{A^-} = 7.77 ± 0.01 ppm. (b) Plot of chemical shift of proton **b** vs pD. Data were fitted to equation (4.2), giving pK_a = 6.28 ± 0.03, δ_{HA}= 6.77 ± 0.01 ppm and δ_{A^-} = 6.47 ± 0.01 ppm. (c) Plot of chemical shift of proton **c** vs pD. Data were fitted to equation (4.2), giving pK_a = 6.32 ± 0.03, δ_{HA}= 6.26 ± 0.01 ppm and δ_{A^-} = 6.04 ± 0.01 ppm.

4.3.8 Determining the ground state pK_a value of BHC-CF$_3$ using UV-Vis spectroscopy

The ground state pK_a for the 7-hydroxy substituent of **BHC-CF$_3$** was also determined using UV-Vis spectroscopy. Significant changes in the UV-Vis spectra were only observed upon deprotonation of the O(H) and not the N(H) since the O(H) is an aromatic substituent and the N(H) is not conjugated into the arene chromophore. As the O(H) site deprotonates, the wavelength maximum shifts from 330 nm to 365 nm, Figure 4.23(a).

Prior to carrying out a UV-Vis titration experiment, a control experiment was conducted to ensure that **BHC-CF$_3$** does not decompose during the pK_a determination experiments using UV-Vis spectroscopy. The UV-Vis spectrum of **BHC-CF$_3$** was recorded in a mixture of CH_3CN and H_2O (8:92 v/v; CH_3CN: H_2O) at pH 2.01. The solution was increased to pH 9.01 (by adding a small volume of aqueous NaOH) and the UV-Vis spectrum was recorded again. The solution was then adjusted back to pH 2.10 (addition of a small volume of aqueous HCl). The final absorbance spectrum of **BHC-CF$_3$** was identical to the original UV-Vis spectrum recorded within experimental error, and no decomposition was observed (spectra not shown). This is in agreement with the control experiments conducted using ^{19}F NMR spectroscopy (see section 4.3.6.1).

BHC-CF$_3$ (3.5×10^{-5} M) was dissolved in a mixture of CH_3CN and H_2O (8:92 v/v CH_3CN: H_2O). The solution (30 mL) was circulated using a peristaltic pump through a 1 cm path length quartz flow-through cell at 25.0 °C. A small volume of acid (~1 M HCl; negligible change in total volume of the solution) was added to the solution (3.5×10^{-5} M, 30 mL). UV-Vis spectra were recorded after the pH stabilized in the reservoir flask. The spectra are shown in Figure 4.23(a). The observed absorbance, A_{obs} at 367 nm, was plotted as a function of pH, Figure 4.23(b) and the data fitted to equation (4.3) (see equation (A1), Appendix for a derivation of this equation).

$$A_{obs} = \frac{A_{HA} + A_{A^-}(10^{pH-pKa})}{1 + (10^{pH-pKa})} \qquad (4.3)$$

A_{HA} = the absorbance of the conjugate acid and A_{A^-} = the absorbance of the conjugate base. Fitting the data to equation (4.3) gives $pK_a = 6.35 \pm 0.03$ (Figure 4.23(b)).

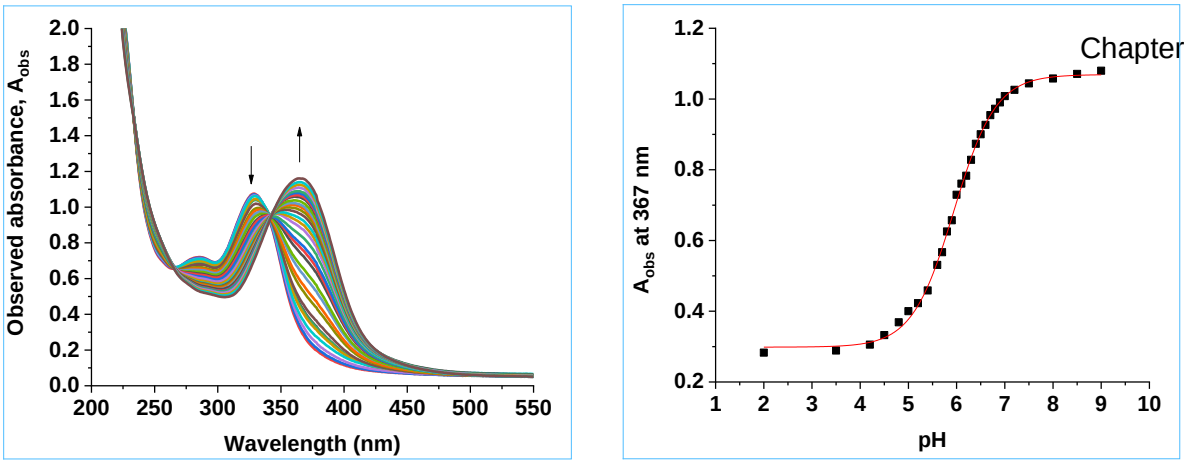

(a) (b)

Figure 4.23. (a) UV-Vis spectra of **BHC-CF$_3$** as a function of pH from pH 2.0 to 9.5 (8:92 v/v CH_3CN: H_2O). (b) Plot of absorbance at 367 nm versus pH. The data has been fitted to equation (4.3), giving pK_{a2} = 6.35 ± 0.03, A_{HA}= 1.08 ± 0.03 ppm and A_{A^-} = 0.30 ± 0.03.

The pK_a of the O(H) of **BHC-CF$_3$** determined by ^{1}H NMR spectroscopy was 6.31 ± 0.03. This study was conducted in D_2O with 8% v/v CH_3CN, I = 1.0 M, $NaCF_3SO_3$. The value obtained by UV-Vis spectroscopy was 6.35 ± 0.03, in 8:92 v/v, CH_3CN: H_2O. The pK_a values in H_2O are typically 0.05 – 0.6 lower than in D_2O[176-178]; that is, acids are stronger in H_2O versus D_2O. The differences in ionic strength will also have an effect on the pK_a value.

4.3.9 Determining the ground state pK_a values for BHC-CH_3 using NMR spectroscopy

A control experiment was conducted to check that **BHC-CH$_3$** does not decompose during an NMR titration experiment. The ^{1}H NMR spectrum of **BHC-CH$_3$** (1.0 mM) was recorded in 8:92 v/v CH_3CN: D_2O. The pD was then increased to 11.03 and the ^{1}H NMR spectrum again recorded, with no observed decomposition. The pD was decreased back to pD 2.52. The ^{1}H NMR spectrum showed that no decomposition had occurred (spectra not shown). At pD values lower than 2.5 or higher than 11.0, **BHC-CH$_3$** was thermally unstable.

^{1}H NMR spectra of **BHC-CH$_3$** were recorded with the pD of the aqueous component of the D_2O/CH_3CN (8% v/v CH_3CN, I = 1.0 M, $NaCF_3SO_3$) solvent mixture varying from pD 2.52-11.03. Selected ^{1}H NMR spectra are shown in Figure 4.24 and the chemical shifts are summarized in Table 4.4. The chemical shifts of proton **a**, **b** and **c** of **BHC-CH$_3$** move downfield from 8.02 ppm to 7.94 ppm, 6.94 ppm to 6.63 ppm and 6.39 ppm to 6.19 ppm respectively, as the pD was increased from 4.90 to 10.42. The chemical

shift moves downfield due to increase in electron density on the aromatic ring upon deprotonation of the O(H) substituent.

The chemical shift of protons **a**, **b** and **c** were plotted as a function of pD (Figure 4.25 (a-c)). Fitting the data to equation (4.2) gave pK_a (proton **a**) = 6.28 ± 0.03, pK_a (proton **b**) = 6.42 ± 0.03, pK_a (proton **c**) = 6.38 ± 0.03 (I = 1.0 M, $NaCF_3SO_3$). The average pK_a value was found to be 6.40 ± 0.03 (protons **b** and **c**). The pK_a of 6-bromo-7-hydroxycoumarin is 6.63 ± 0.03 (see later). This pK_a value is therefore assigned to deprotonation of the OH substituent of **BHC-CH$_3$**. Protons **a-c** are aromatic protons, so their chemical shifts change upon deprotonation of the OH substituent on the aromatic ring. The chemical shift of protons **a**, **b** and **c** were unchanged from 2.52 to 4.90 (< 0.01 ppm) and from 10.30 to 11.03 ppm (Table 4.4). The change in the chemical shifts for protons sites **a**, **b** and **c** are 0.07, 0.31 and 0.18, respectively. Proton **e** (the CH_3 group) is 6 bonds away from the aromatic group, so its chemical shift is unchanged (pD 2.52-pD 9.75).

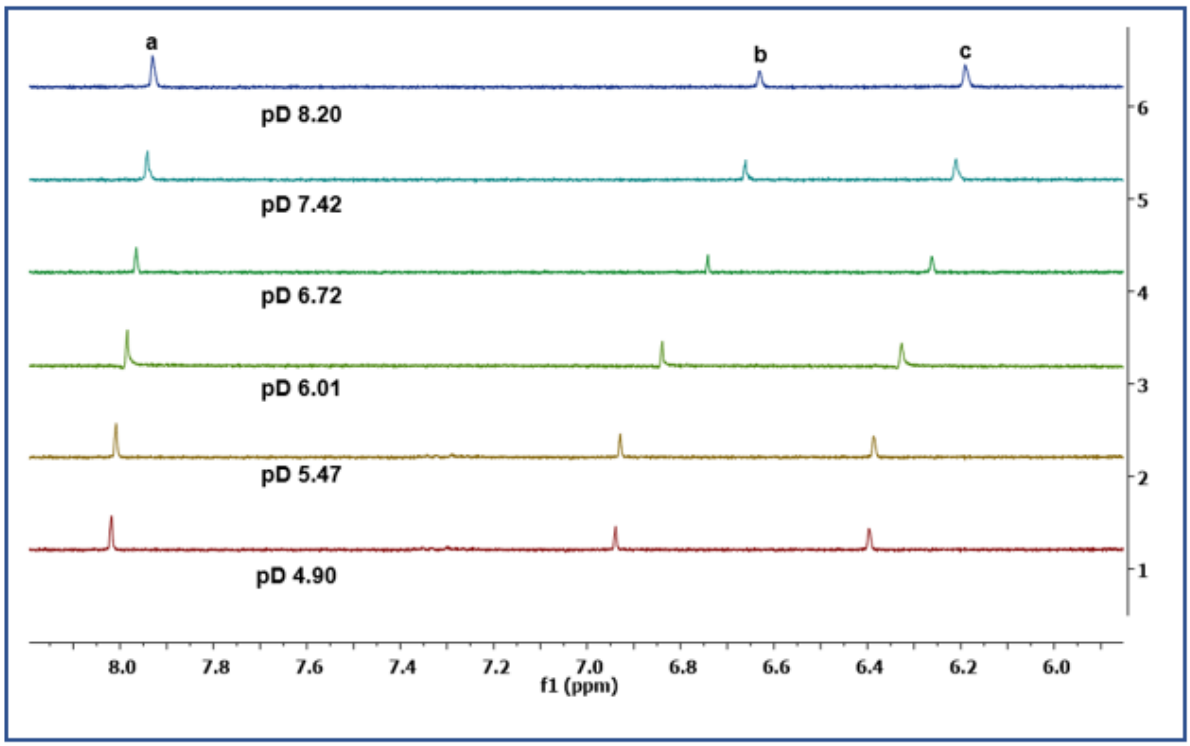

Figure 4.24. Selected ^{1}H NMR chemical shifts (ppm) of **BHC-CH$_3$** as a function of pD, in D_2O with 8% v/v CH_3CN, I = 1.0 M, $NaCF_3SO_3$. TSP (0.00 ppm) was used as an external reference.

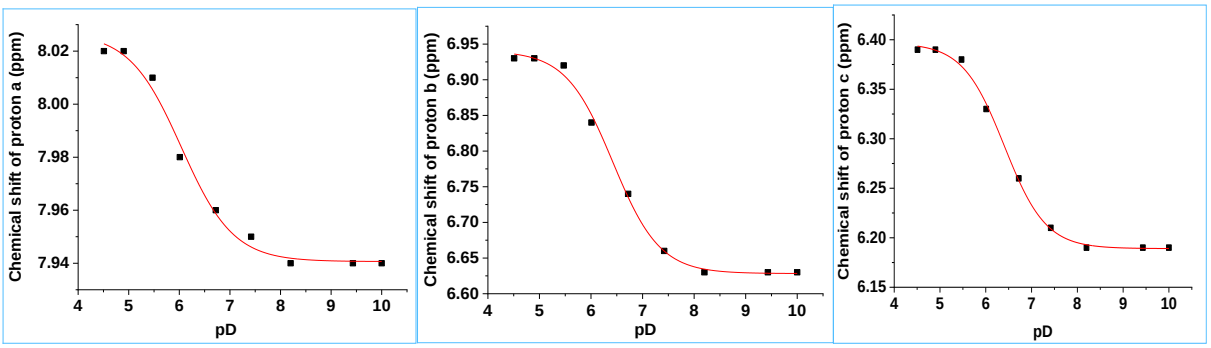

(a) (b) (c)

Figure 4.25. (a) Plot of chemical shift of proton **a** vs pD, Data were fitted to equation (4.2), giving pK_a = 6.28 ± 0.01, δ_{HA}= 8.02 ± 0.01 ppm and δ_{A^-} = 7.94 ± 0.01 ppm. (b) Plot of chemical shift of proton **b** versus pD. Data were fitted to equation (4.2), giving pK_a = 6.42 ± 0.03, δ_{HA}= 6.94 ± 0.01 ppm and δ_{A^-} = 6.63 ± 0.01 ppm. (c) Plot of chemical shift of proton **c** versus pD. Data were fitted to equation (4.2), giving pK_a = 6.38 ± 0.03, δ_{HA}= 6.39 ± 0.01 ppm and δ_{A^-} = 6.18 ± 0.01 ppm.

Table 4.4. ^{1}H NMR chemical shift for protons **a**-**c** and **e** (see Figure 4.20 for labelling scheme) as a function of pD for **BHC-CH_3** in D_2O with 8% v/v CH_3CN, I = 1.0 M, $NaCF_3SO_3$. Proton **d** overlapped with the HDO peak (25° C).

pD	Proton **a**	Proton **b**	Proton **c**	Proton **e**
2.52	8.02	6.94	6.39	3.22
3.08	8.02	6.94	6.39	3.22
3.52	8.02	6.94	6.39	3.22
4.20	8.02	6.94	6.39	3.21
4.51	8.02	6.93	6.39	3.22
4.90	8.02	6.94	6.39	3.22
5.47	8.01	6.92	6.38	3.22
6.01	7.98	6.84	6.33	3.22
6.72	7.96	6.74	6.26	3.22
7.42	7.95	6.66	6.21	3.21
8.20	7.94	6.63	6.19	3.22
8.75	7.94	6.63	6.19	3.22
9.25	7.94	6.63	6.19	3.22
9.62	7.94	6.62	6.18	3.22
9.75	7.95	6.63	6.19	3.21
9.95	7.94	6.63	6.18	3.15
10.08	7.94	6.63	6.19	3.08
10.18	7.95	6.62	6.18	2.95
10.30	7.94	6.63	6.19	2.88
10.50	7.94	6.63	6.19	2.88
11.03	7.95	6.63	6.19	2.88

The chemical shift of the CH_3 (**e**) proton signal moved upfield from 3.19 ppm to 2.86 ppm as pD of the solution was increased from 9.62 to 10.50 shown in Figure 4.26 (^{1}H NMR spectra). Proton **e** is adjacent to the N(H) moiety of the *N*-hydroxysulfonamide of **BHC-CH$_3$**, hence the change in the chemical shift is attributed to deprotonation of this site. The chemical shift of the proton **e** was plotted as a function of pD (Figure 4.27). Fitting the data to equation (4.2) gives pK_a = 10.11 ± 0.03. Like **BHC-CF$_3$**, the BHC-$\underline{CH_2}$-ON(H)-SO_2CH_3 peak overlapped with the HDO peak from the solvent, so proton **d** could not be used to determine the pK_a of the N(H) proton of **BHC-CH$_3$**.

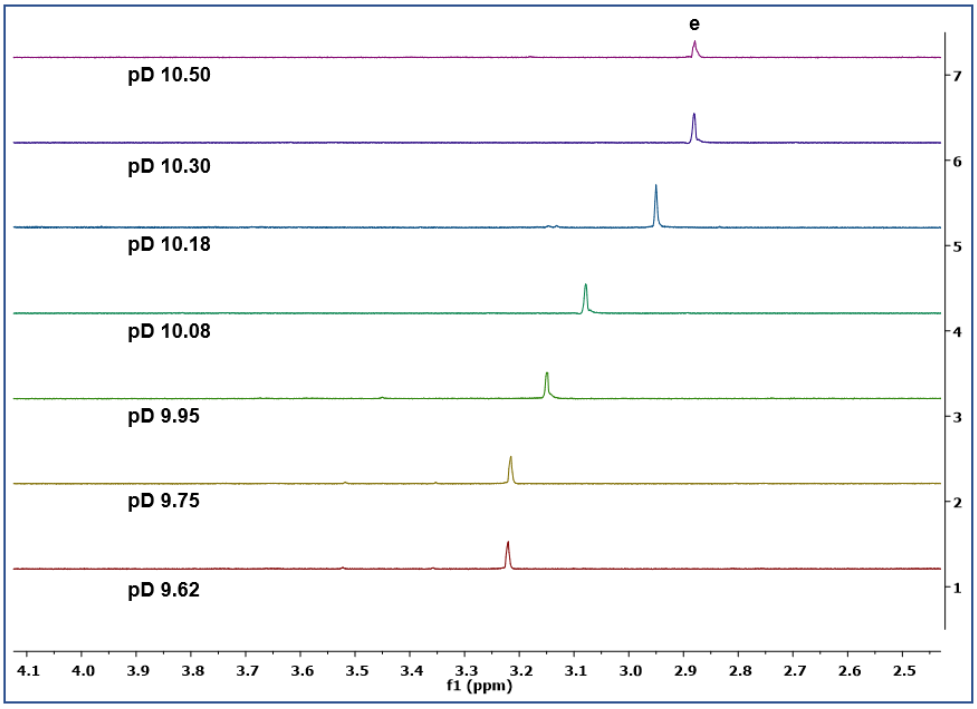

Figure 4.26. ^{1}H NMR spectra showing the chemical shift of the CH_3 (**e**) proton of **BHC-CH$_3$** as a function of pD, in D_2O with 8% v/v CH_3CN, I = 1.0 M, $NaCF_3SO_3$.

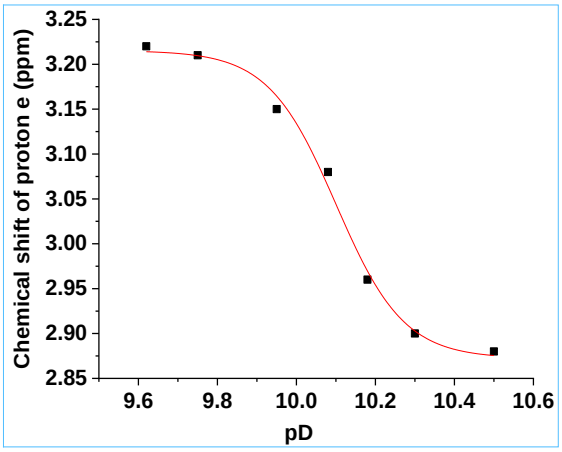

Figure 4.27. ^{1}H NMR chemical shift (ppm) for the CH_3 proton (proton **e**) of **BHC-CH$_3$** as a function of pD, in D_2O with 8% v/v CH_3CN, I = 1.0 M, $NaCF_3SO_3$. Data were fitted to equation (4.2), giving pK_a = 10.11 ± 0.03, δ_{HA}= 3.22 ± 0.01 ppm and δ_{A^-} = 2.87 ± 0.01 ppm.

4.3.10 Determining the ground state pK_a value of BHC-CH_3 using UV-Vis spectroscopy

A UV-Vis spectroscopic titration experiment for **BHC-CH_3** was carried out to determine the pK_a value. Only deprotonation of the O(H) substituent can be determined using this method, as found for **BHC-CF_3** (see section 4.3.8).

A UV-Vis spectrophotometric titration of **BHC-CH_3** (3.1×10^{-5} M, in 8:92 v/v CH_3CN: H_2O, 30 mL) was conducted using the same flow set up. The absorbance at 370 nm was plotted as a function of pH (Figure 4.28(a)). Data were fitted to equation (4.3), giving pK_a = 6.47 ± 0.03 (8:92 v/v CH_3CN: H_2O, Figure 4.28(b)). The pK_a of deprotonation of O(H) from NMR spectroscopy data was 6.40 ± 0.03 (in D_2O with 8% v/v CH_3CN, I = 1.0 M, $NaCF_3SO_3$, section 4.3.7). The pK_a values in H_2O are typically 0.05 – 0.6 lower than in D_2O;[176-178] that is, acids are stronger in H_2O versus D_2O.

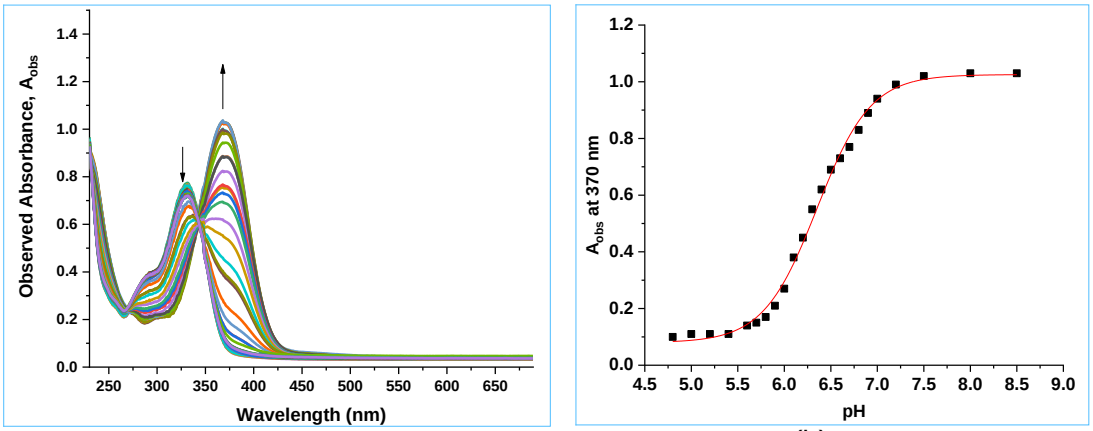

(a) (b)

Figure 4.28. (a) UV-Vis spectra of **BHC-CH_3** as a function of pH from pH 4.4-8.7 (8:92 v/v CH_3CN: H_2O). (b) Plot of absorbance at 367 nm versus pH. The data has been fitted to equation (4.3), giving pK_{a2} = 6.47 ± 0.03, A_{HA}= 1.03 ± 0.03 ppm and A_{A^-} = 0.10 ± 0.03.

To summarize, two pK_a values were determined for both **BHC-CF_3** and **BHC-CH_3** by NMR and UV-Vis spectroscopy. For **BHC-CF_3**, the N(H) site deprotonates first followed by the O(H) site. For **BHC-CH_3**, the O(H) site instead deprotonates first followed by the N(H) site. Deprotonation sites for **BHC-CF_3** and **BHC-CH_3** are shown in Scheme 4.2.

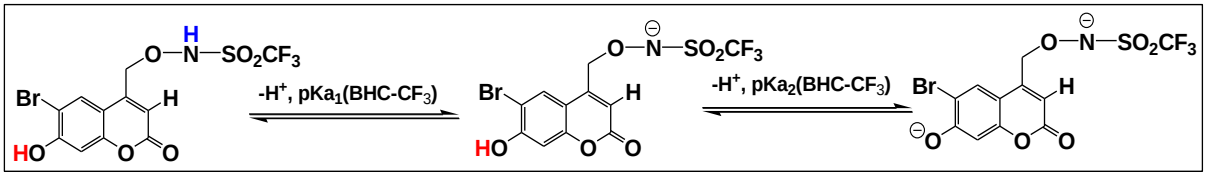

(a)

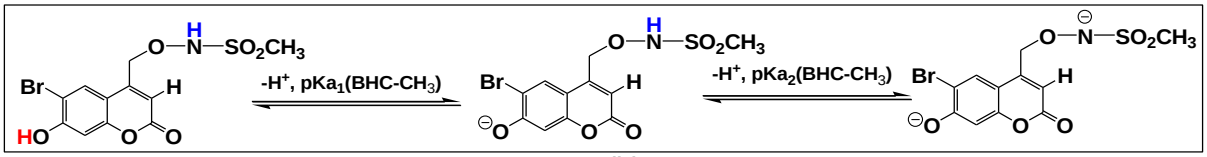

(b)

Scheme 4.2. Ground state ionization equilibria of (a) **BHC-CF$_3$**, pK_{a1} =3.42 ± 0.02 (in D_2O with 8% v/v CH_3CN, I = 1.0 M, $NaCF_3SO_3$, ^{19}F NMR spectroscopy), pK_{a2} = 6.31 ± 0.03 (in D_2O with 8% v/v CH_3CN, I = 1.0 M, $NaCF_3SO_3$, ^1H NMR spectroscopy) and 6.35 ± 0.03 (in 8:92 v/v, CH_3CN: H_2O, UV-Vis spectroscopy). (b) **BHC-CH$_3$**, pKa_1 = 6.40 ± 0.03 (in D_2O with 8% v/v CH_3CN, I = 1.0 M, $NaCF_3SO_3$, ^1H NMR spectroscopy) and pKa_1 = 6.47 ± 0.03 (in 8:92 v/v, CH_3CN: H_2O, UV-Vis spectroscopy), pK_{a2} = 10.11 ± 0.03 (in D_2O with 8% v/v CH_3CN, I = 1.0 M, $NaCF_3SO_3$, ^1H NMR spectroscopy).

4.3.11 Determining the pK_a of 6-bromo-7-hydroxy-4-methylcoumarin

A pK_a titration experiment was conducted for 6-bromo-7-hydroxy-4-methylcoumarin (equation (4.4)), so this value could be compared to the pK_a for the 7-hydroxy substituent of **BHC-CF$_3$** and **BHC-CH$_3$**.

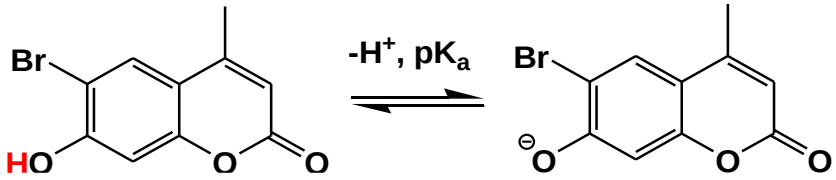

(4.4)

A UV-Vis spectroscopic titration of 6-bromo-7-hydroxy-4-methylcoumarin (110 µM, 30 mL solution) was conducted in a mixture of 8:92 v/v CH_3CN: H_2O, using the flow set up. The absorbance at 367 nm was plotted as a function of pH (Figure 4.29(a)). Data were fitted to equation (4.3), giving pK_a = 6.91 ± 0.03 (Figure 4.29(b)). The pK_a for deprotonation of the 7-hydroxy substituent of each compound in the same solvent mixture (8:92 v/v CH_3CN: H_2O) follow the order **BHC-CF$_3$** (6.35 ± 0.03) > **BHC- CH$_3$** (6.47 ± 0.03) > 6-bromo-7-hydroxy-4-methylcoumarin (6.91 ± 0.03), which follows the order expected based on the electron withdrawing abilities of the substituent at the 4-position of the 6-bromo-7-hydroxycoumarin. Interestingly, the order is not affected by the protonation state of the N(H) proton, presumably because this is located at some distance from the aromatic group.

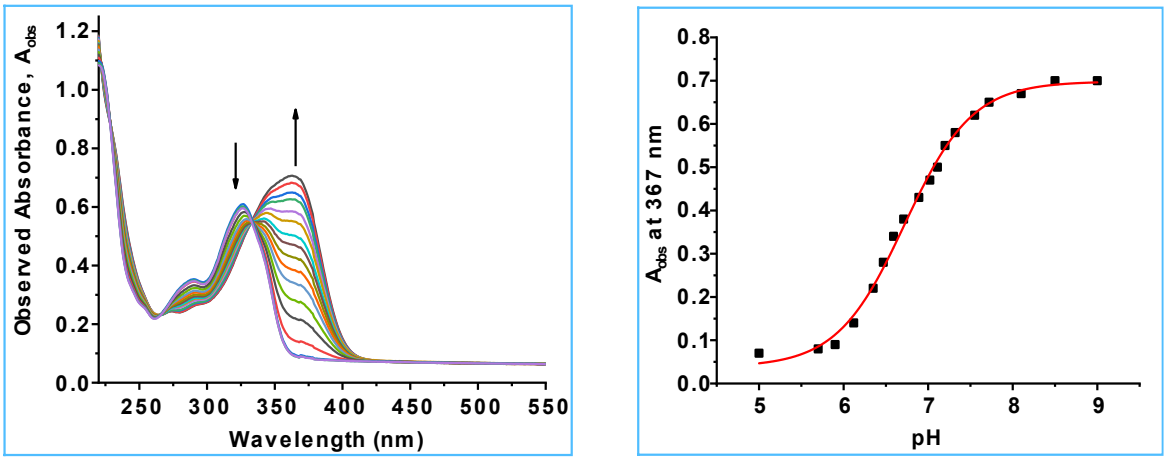

(a) (b)

Figure 4.29. (a) UV-Vis spectra of 6-bromo-7-hydroxy-4-methylcoumarin (110 µM) as a function of pH from pH 4.4-8.7 (8:92 v/v; CH_3CN: H_2O). (b) Plot of absorbance at 367 nm versus pH. The data has been fitted to equation (4.3), giving pK_a = 6.91 ± 0.03, A_{HA}= 0.71 ± 0.03 ppm and A_{A^-} = 0.05 ± 0.03.

4.3.12 Determining the ground state pK_a of *(E)*-BHC-oxime using UV-Vis spectroscopy

A UV-Vis spectrophotometric titration of ***(E)*-BHC-oxime** (4.2 x 10^{-5} M, 30 mL) was carried out in a mixture of CH_3CN and H_2O (8:92 v/v CH_3CN: H_2O) using a flow set up to determine the pK_a value of the 7-hydroxy substituent of this compound, as described in section 4.3.7. UV-Vis spectra were recorded from pH 2.0-9.5 (Figure 4.30(a)). The absorbance at 403 nm was plotted as a function of pH and the data were fitted to equation (4.3), giving pK_a = 6.42 ± 0.03 (Figure 4.30(b)). The ground state pK_a of O(H) is shown in equation (4.5).

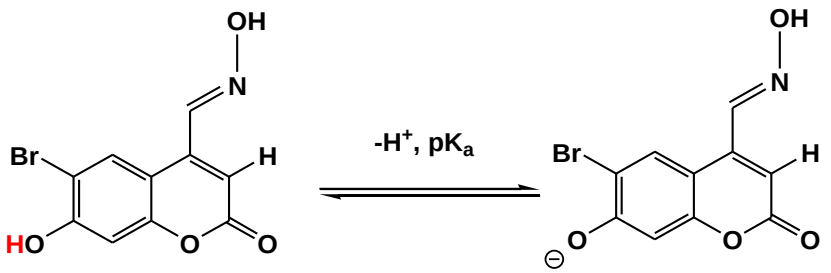

(4.5)

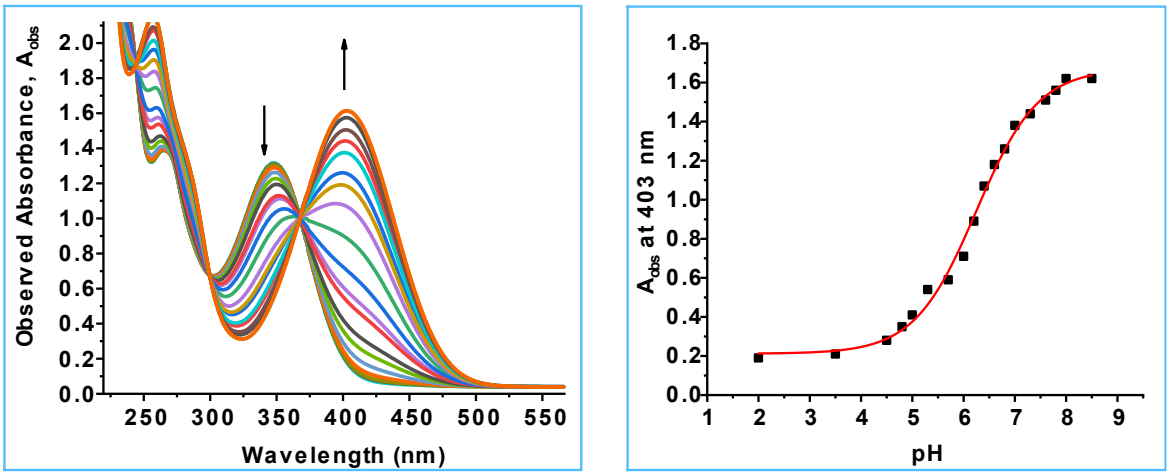

(a) (b)

Figure 4.30. (a) UV-Vis spectra of ***(E)*-BHC-oxime** as a function of pH, from pH 2.02-9.56. (b) Plot of absorbance at 403 nm versus pH. The best fit of the data to equation (4.3) gives pK_a = 6.42 ± 0.03, A_{HA}= 1.67 ± 0.03 ppm and A_{A^-} = 0.21 ± 0.03.

4.3.13 Effect of pH on the photoproducts

The effect of the pH of the aqueous component of a solvent mixture on the photoproducts obtained after irradiation of **BHC-CF_3** was investigated in 10% v/v CD_3CN in aqueous solution. All the experiments were carried out under red-light conditions. Prior to doing these experiments the stability of the **BHC-CF_3** in the presence of the red light was checked at pH 2.1, 5.0, 7.0 and 10.0 using ^1H and ^{19}F NMR spectroscopy. **BHC-CF_3** (1.0 mM) was found to be photostable for at least 210 min in the presence of the red light, by ^1H and ^{19}F NMR spectroscopy.

Figure 4.31(a) shows ^{19}F NMR spectra of **BHC-CF_3** recorded before and after 1.0 and 3.0 min total irradiation in a solution of 10:90 v/v CD_3CN: phosphate buffer, pH 2.1. The solutions were irradiated using a Rayonet photoreactor (350 nm). Only O-N bond cleavage ($CF_3SO_2NH_2$ observed at -80.2 ppm) occurred. There was no evidence for C-O or C-O/N-S bond cleavage (CF_3SO_2NHOH at -73.1 ppm and $CF_3SO_2^-$ at -88.9 ppm) in this solvent mixture.

To characterize the aromatic photoproducts, the ^1H NMR spectrum of a partially decomposed sample (1.0 min irradiation) was recorded, Figure 4.31(b). The chemical shifts at 10.01, 8.66, 8.11 and 7.00 ppm were assigned to **BHC-CHO**. The ^1H NMR spectrum of authentic **BHC-CHO** at pH 2.1 in the same solvent mixture was recorded to confirm this. An unknown peak at 6.87 ppm was observed. To check whether this unknown peak originated from the photodecomposition of **BHC-CHO**, the ^1H NMR

spectrum of **BHC-CHO** was recorded after irradiation for 1.0 min. **BHC-CHO** was found to be photostable within this timeframe. So this unknown peak does not arise from photodecomposition of **BHC-CHO**.

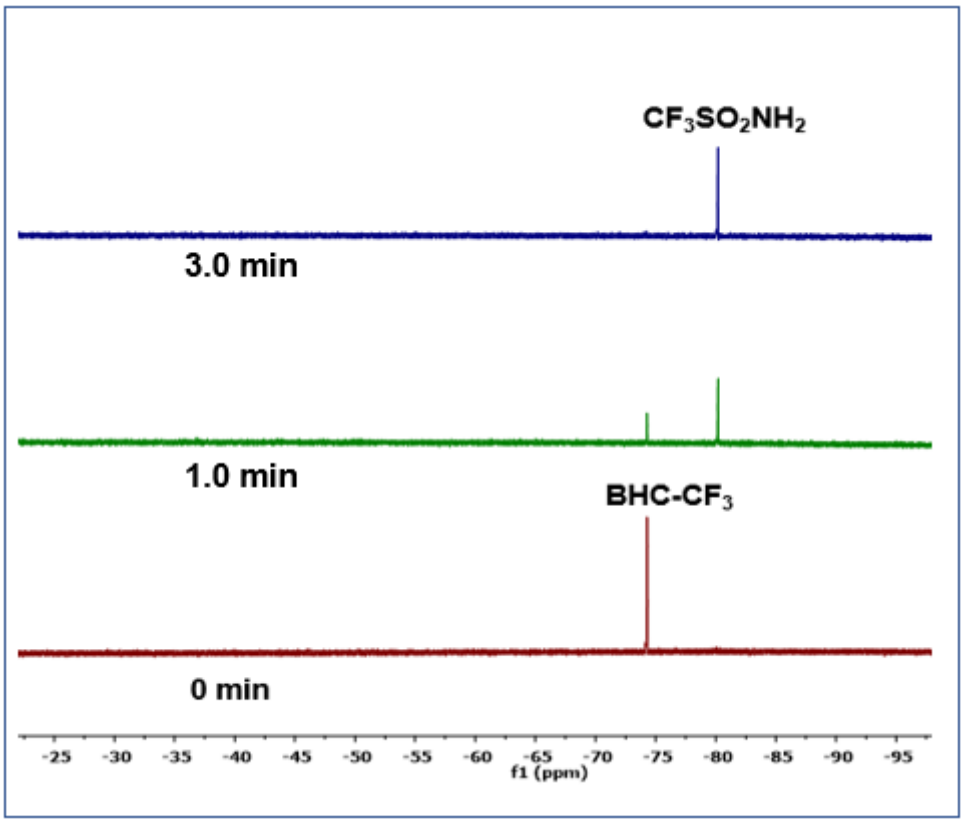

(a)

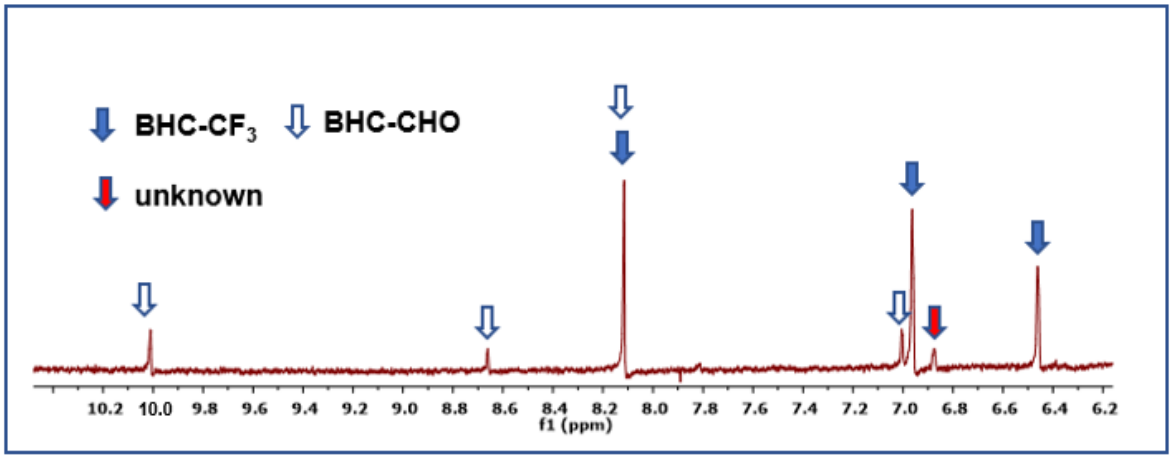

(b)

Figure 4.31. (a) ^{19}F NMR spectra for the photodecomposition of **BHC-CF$_3$** (1.0 mM) in 10:90 v/v CD_3CN: phosphate buffer (30 mM, pH 2.1) before irradiation, after 1.0 min and 3.0 min total irradiation (350 nm). (b) ^{1}H NMR spectrum of the same sample after 1.0 min irradiation. Approximately 30% decomposition has occurred.

(a)

Photolysis experiments were also conducted at pH 5.0, 7.0 and 10.0. Figure 4.32(a), Figure 4.33(a) and Figure 4.34(a) show the ^{19}F NMR spectra of fully photodecomposed samples of **BHC-CF_3** at pH 5.0, 7.0 and 10.0 (10:90 v/v CD_3CN: 30 mM acetate buffer (pH 5.0), 30 mM phosphate buffer (pH 7.0) or 30 mM carbonate buffer (pH 10.0)). The fluorinated photoproducts were found to be $CF_3SO_2^-$ (-88.2 ppm) and $CF_3SO_2NH_2$ (-80.2 ppm) at all these pH conditions. The percentage of the photoproduct $CF_3SO_2NH_2$ at pH 5.0, 7.0 and 10.0 was 70%, 68% and 72%, respectively. The percentages of each photoproduct are therefore unaffected by the increase in the pH of the aqueous component of the 10:90 v/v CD_3CN: aqueous buffer mixture.

In separate experiments, the aromatic photoproducts were characterized by recording the ^1H NMR spectrum after 0.40 min irradiation (~15% conversion) at pH 5.0, 7.0 and 10.0 (Figure 4.32(b), Figure 4.33(b) and Figure 4.34(b)); 10:90 v/v CD_3CN: aqueous buffer, 30 mM; acetate (pH 5.0), phosphate (pH 7.0) or carbonate (pH 10.0) buffer. ^1H NMR spectra of authentic samples of the aromatic photoproducts **BHC-CHO**, **BHC-OH**, ***(E)*-BHC-oxime** and ***(Z)*-BHC-oxime** were also recorded at these pH conditions, to enable the assignments of the peaks. The chemical shifts of these compounds at pH 5.0, 7.0 and 10.0 are summarized in Table 4.5 and 4.6. Separate samples of **BHC-CHO** and **BHC-OH** were also photolyzed for 0.40 min to check whether the unknown peaks appeared from the photodecomposition of these photoproducts.

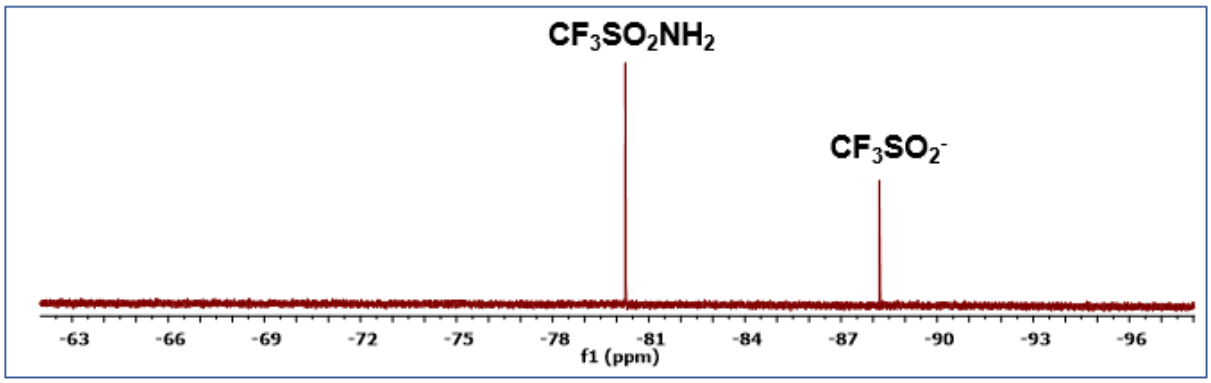

(a)

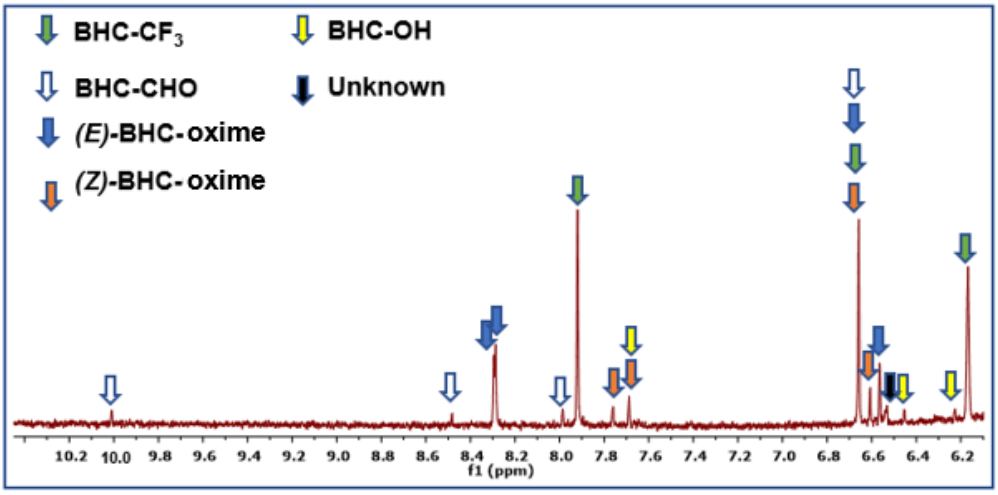

(b)

Figure 4.32. (a) ^{19}F NMR spectrum of **BHC-CF$_3$** (1.0 mM) in a mixture of acetate buffer (pH 5.0, 30.0 mM) and CD_3CN (90:10 v/v) after 3.0 min irradiation. (b) ^{1}H NMR spectrum of the same solution after irradiating for 0.40 min.

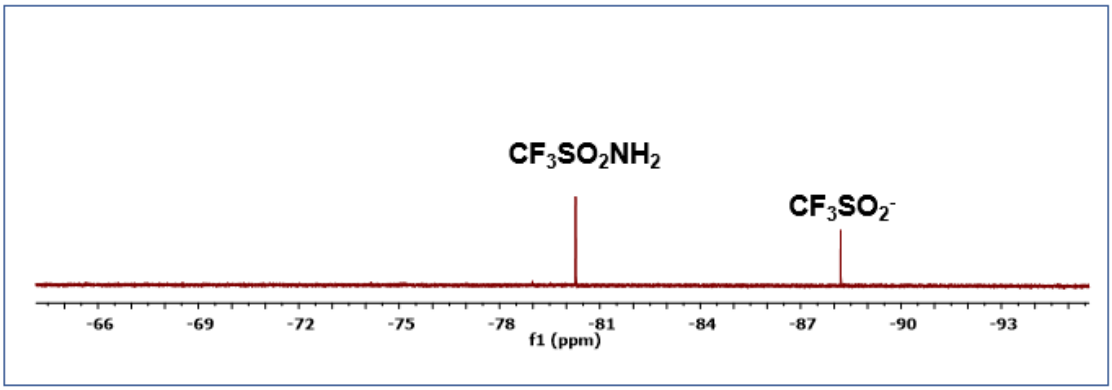

(a)

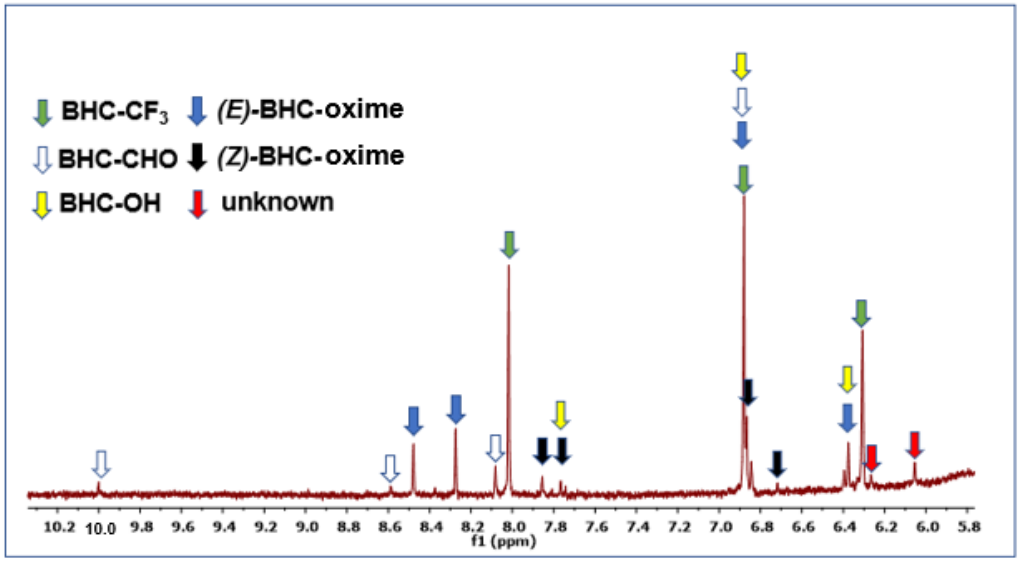

(b)

Figure 4.33. (a) ^{19}F NMR spectrum of **BHC-CF$_3$** (1.0 mM) in a mixture of phosphate buffer (pH 7.0, 30.0 mM) and CD_3CN (90:10 v/v) after 3.8 min irradiation. (b) ^{1}H NMR spectrum of the same solution after irradiating for 0.40 min.

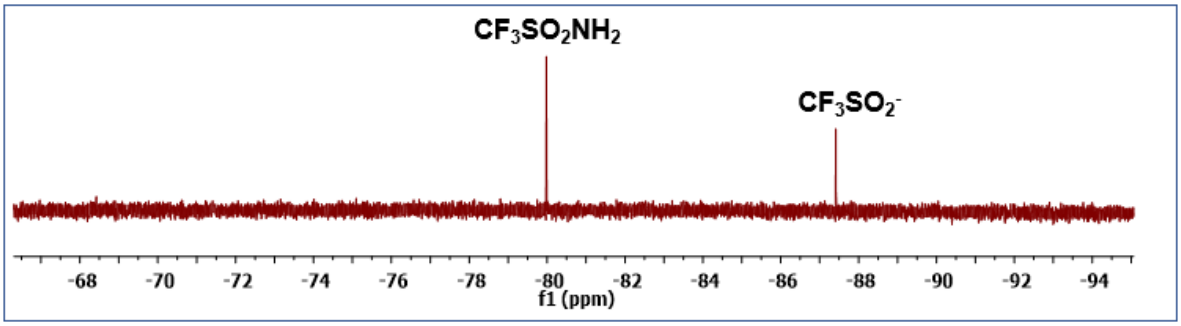

(a)

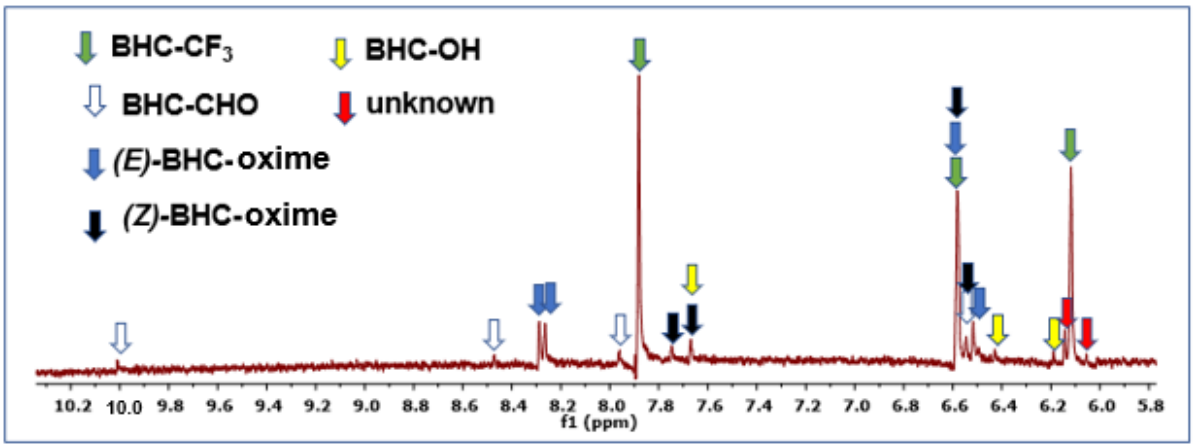

(b)

Figure 4.34. (a) ^{19}F NMR spectrum of **BHC-CF$_3$** (1.0 mM) in a mixture of carbonate buffer (pH 10.0, 30.0 mM) and CD_3CN (90:10, v/v) after 3.5 min irradiation. (b) ^{1}H NMR spectrum of the same solution after irradiating for 0.40 min.

Table 4.5. Chemical shifts of **(*E*)-BHC-oxime and (*Z*)-BHC-oxime** in 10:90 v/v CD_3CN: aqueous buffer (30 mM; acetate buffer (pH 5.0), phosphate buffer (pH 7.0) and carbonate buffer (pH 10.0)). The labelling scheme is also shown.

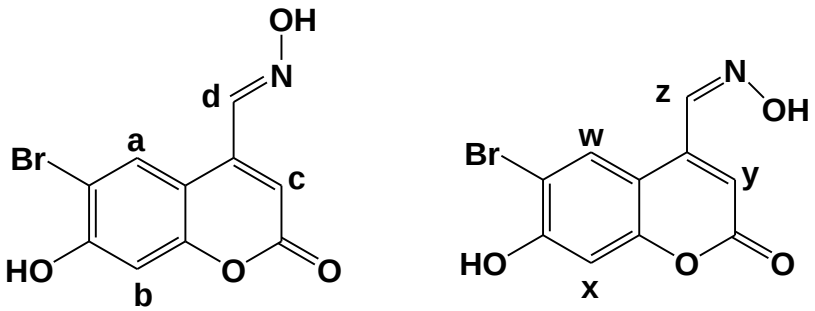

pH	Chemical shifts (ppm) of Photoproducts							
	(*E*)-BHC-oxime protons				**(Z)-BHC-oxime** protons			
	a	**b**	**c**	**D**	**W**	**x**	**y**	**Z**
5.0	8.48	8.27	6.88	6.38	7.85	7.76	6.88	6.71
7.0	8.28	8.27	6.63	6.57	7.73	7.67	6.63	6.59
10.0	8.28	8.26	6.59	5.53	7.74	7.66	6.58	6.54

Table 4.6. Chemical shifts of **BHC-CHO** and **BHC-OH** in 10:90 v/v CD_3CN: aqueous buffer (30 mM; acetate buffer (pH 5.0), phosphate buffer (pH 7.0) and carbonate buffer (pH 10.0)). The labelling scheme is also shown.

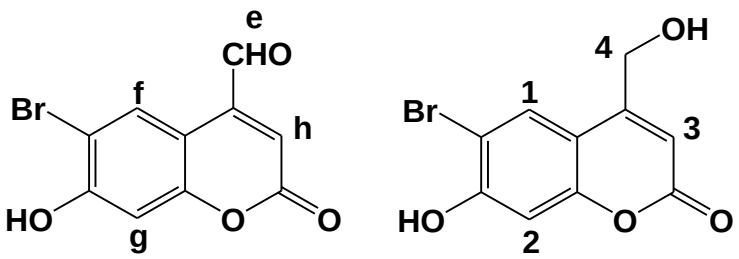

pH	Chemical shifts (ppm) of Photoproducts							
	BHC-CHO proton positions				**BHC-OH** proton positions			
	e	**f**	**g**	**H**	**1**	**2**	**3**	**4**
5.0	10.01	8.58	8.07	6.88	7.76	6.88	6.38	-
7.0	10.04	8.47	7.97	6.62	7.68	6.45	6.22	-
10.0	10.00	8.47	7.96	6.54	7.66	6.45	6.18	-

The results are summarized in Table 4.7. At pH 2.1, only $CF_3SO_2NH_2$ (O-N bond cleavage) was observed. At pH 5.0, the percentage of the O-N bond cleavage decreases to 70% and $CF_3SO_2^-$ is observed, indicating that concomitant C-O/N-S bond cleavage has occurred in addition to O-N bond cleavage. At pH 7.0 and 10.0 the percentages of the photoproducts remain the same as those observed at pH 5.0, within experimental error.

Table 4.7. Effect of the pH of the aqueous component of the solvent on the photoproducts derived from *N*-hydroxysulfonamide moiety for photodecomposition for **BHC-CF_3** (1.0 mM) in 10:90 v/v CD_3CN: aqueous buffer (30 mM).

pH	Percentages of photoproducts	
	$CF_3SO_2^-$	$CF_3SO_2NH_2$
2.1[a]	00	100
5.0[b]	30	70
7.0[c]	32	68
10.0[d]	28	72

Aqueous buffer: [a,c]phosphate buffer, [b]acetate buffer, [d]carbonate buffer.

The effect of the pH on the photoproducts obtained upon irradiating **BHC-CH_3** was determined under anaerobic conditions in 10% v/v CD_3CN in aqueous buffered solution. The photoproducts generated at pH 2.5, 5.0, 7.0, 10.0 and 10.7 were characterized using ^{1}H NMR spectroscopy. A Rayonet photoreactor (350 nm) was used to irradiate the samples. The percentage of the photoproducts were calculated by integrating the methyl peak of each compounds ($CH_3SO_2NH_2$, CH_3SO_2NHOH, $CH_3SO_2^-$ or $CH_3SO_3^-$) from the fully decomposed ^{1}H NMR spectrum. The aromatic photoproducts were characterized using partially photolyzed (15%) samples, since numerous secondary photoproducts are obtained at longer irradiation times.

Figure 4.35(a) shows the ^{1}H NMR spectrum in the 2.15-3.25 ppm region after irradiating a solution of **BHC-CH_3** in 90:10 v/v phosphate buffer, pH 2.5:CD_3CN. The percentages of $CH_3SO_2NH_2$, CH_3SO_2NHOH, $CH_3SO_2^-$ and $CH_3SO_3^-$ are 78%, 8%, 2% and 6%, respectively. Hence the main mechanism of photoproducts is via O-N bond cleavage. A small amount of unknown species was also observed (6%).

Figure 4.35(b) shows the aromatic region of the ^{1}H NMR spectrum. Peaks at 10.01, 8.49, 8.00 and 6.62 ppm were assigned to **BHC-CHO**. Peaks at 7.69, 6.45 and 6.23 ppm were assigned to **BHC-OH**. Two unassigned peaks were observed at 6.18 and 6.05 ppm.

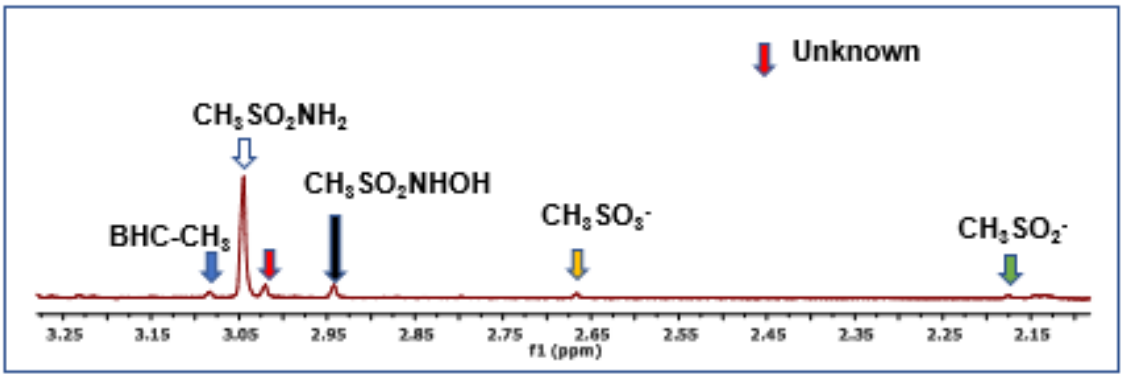

(a)

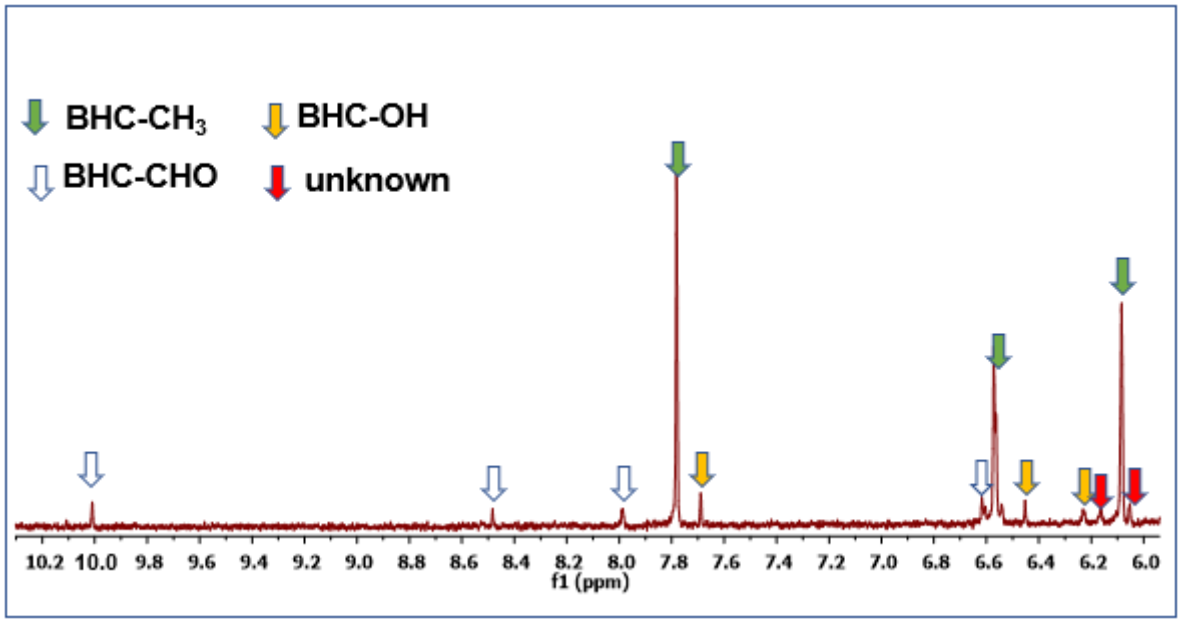

(b)

Figure 4.35. (a) ^{1}H NMR spectrum in the 2.15-3.25 ppm region for a solution of **BHC-CH$_3$** (1.0 mM) in a mixture of phosphate buffer (pH 2.5, 30.0 mM) and CD_3CN (90:10, v/v) after 3.0 min irradiation. (b) The aromatic region of the ^{1}H NMR spectrum for same solution after 0.20 min.

Figure 4.36(a) shows the ^{1}H NMR spectrum of **BHC-CH$_3$** in 10:90 v/v CD_3CN: acetate buffer (30 mM, pH 5.0). The ^{1}H NMR spectra of the expected aliphatic photoproducts were also recorded in the same solvent, to aid assignment of the peaks. The chemical shift at 3.07 ppm was assigned to $CH_3SO_2NH_2$ (78%), 2.97 ppm to CH_3SO_2NHOH (8%), 2.71 ppm to $CH_3SO_3^-$ (5%) and 2.19 ppm to $CH_3SO_2^-$ (2%). Three small unknown peaks were also observed at 2.80 (2%), 3.01 (1%) and 3.08 ppm (4%). To characterize the aromatic photoproducts, the ^{1}H NMR spectrum of a partially photolyzed sample was recorded after 0.20 min irradiation (Figure 4.36(b)) in a separate experiment. The chemical shifts of the observed aromatic photoproducts are summarized earlier in Table 4.6. ^{1}H NMR spectra of authentic samples of each compound were recorded in the same solvent mixture, to aid in the assignments of the peaks. Both **BHC-CHO** and **BHC-OH** were observed in the partially photolyzed solution, arising a result of O-N bond cleavage and the elimination pathways, respectively, Scheme 4.1.

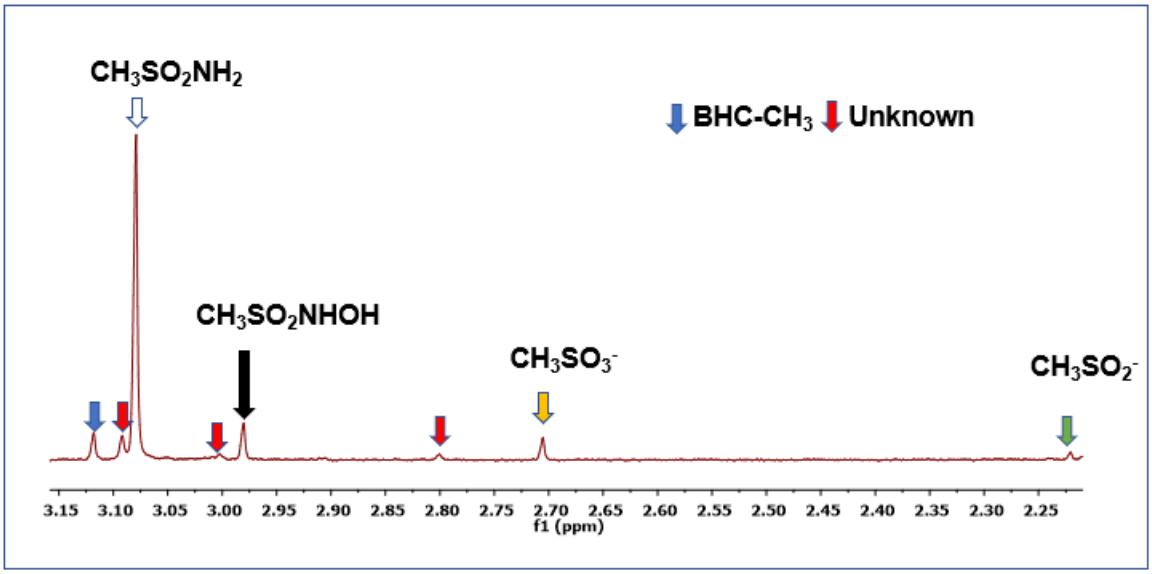

(a)

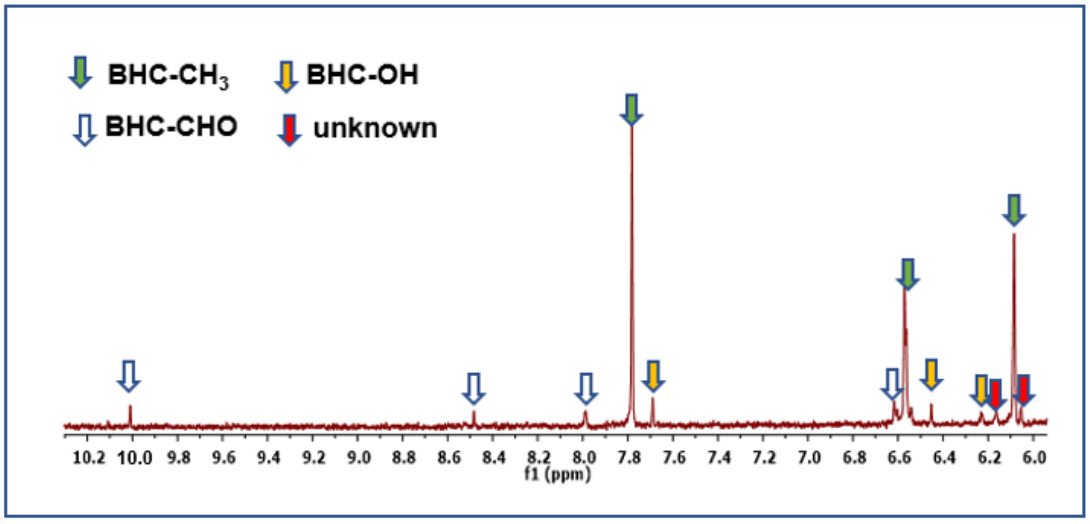

(b)

Figure 4.36. (a) ^{1}H NMR spectrum for a solution of **BHC-CH_3** (1.0 mM) in a mixture of acetate buffer (pH 5.0, 30.0 mM) and CD_3CN (90:10, v/v) after 3.0 min irradiation. (b) The aromatic region of the ^{1}H NMR spectrum for same solution after 0.20 min.

Aliphatic photoproducts were characterized by recording the ^{1}H NMR spectrum of a fully photodecomposed sample of **BHC-CH_3** at pH 7.0 Figure 4.37(a). The chemical shift at 3.05 ppm was assigned to $CH_3SO_2NH_2$ (81%), 2.95 ppm to CH_3SO_2NHOH (11%), 2.68 ppm to $CH_3SO_3^-$ (4%) and 2.19 ppm to $CH_3SO_2^-$ (4%).

The aromatic photoproducts were characterized at pH 7.0 using a partially irradiated sample of ^{1}H NMR spectroscopy (Figure 4.37(b)). The chemical shifts of all photoproducts are listed in Table 4.6.

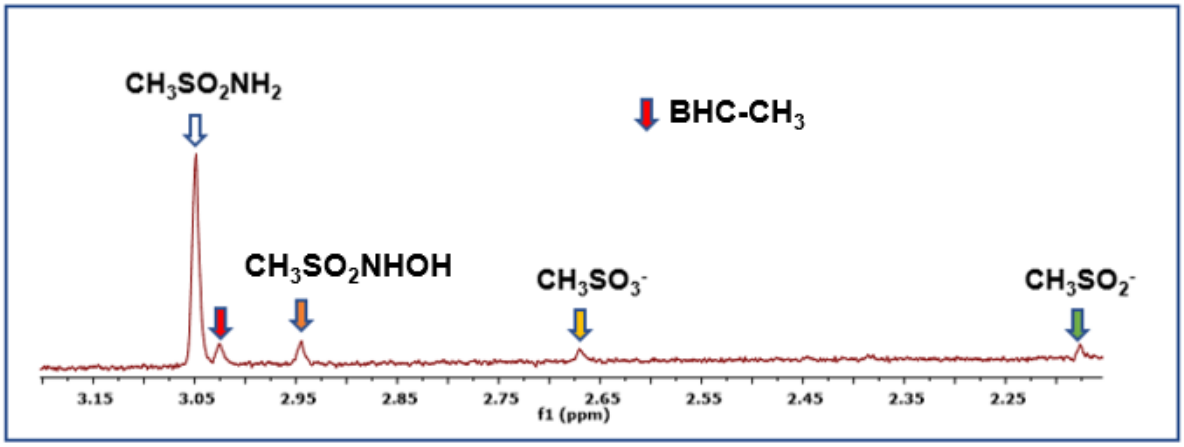

(a)

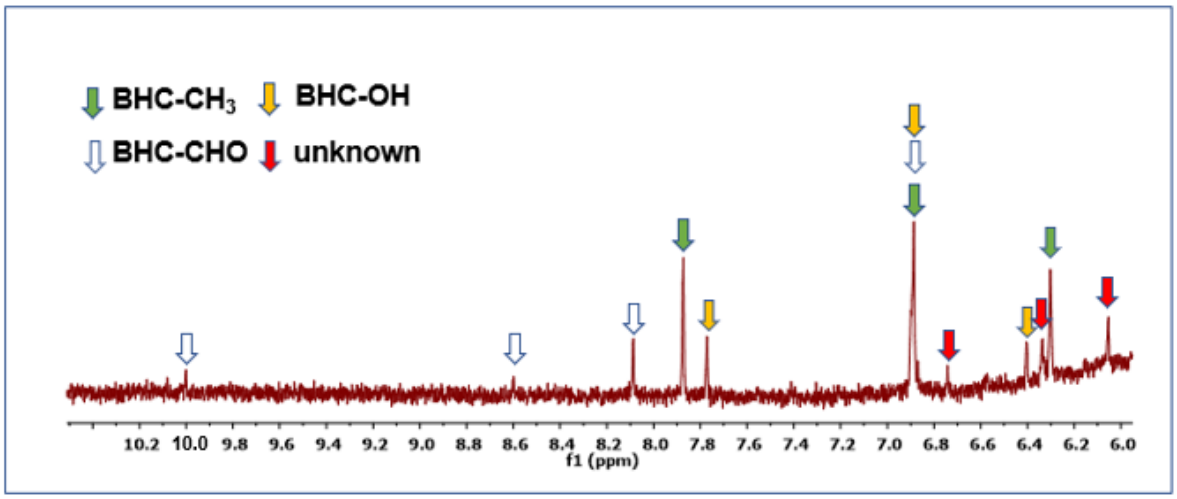

(b)

Figure 4.37. (a) ^{1}H NMR spectrum in the 2.15-3.15 ppm region for a solution of **BHC-CH$_3$** (1.0 mM) in a mixture of phosphate buffer (pH 7.0, 30.0 mM) and CD_3CN (90:10, v/v) after 5.0 min irradiation. (b) The aromatic region of ^{1}H NMR spectrum for the same solution after 0.20 min irradiation.

The aliphatic photoproducts at pH 10.0 were characterized using ^{1}H NMR spectroscopy. Figure 4.38(a) shows the ^{1}H NMR spectrum of a fully photodecomposed sample. The chemical shift at 3.07 ppm was assigned to $CH_3SO_2NH_2$ (40%), 2.94 ppm to CH_3SO_2NHOH (4%), 2.67 ppm to $CH_3SO_2^-$ (48%) and 2.17 ppm to $CH_3SO_3^-$ (8%). The aromatic photoproducts were also characterized by recording the ^{1}H NMR spectrum of partially photolyzed (0.20 min irradiation) samples and comparing with the authentic standards (Figure 4.38(b)). The chemical shifts of all products are listed in the Table 4.6. The aliphatic photoproducts were also characterized at pH 10.7 (spectra not shown).

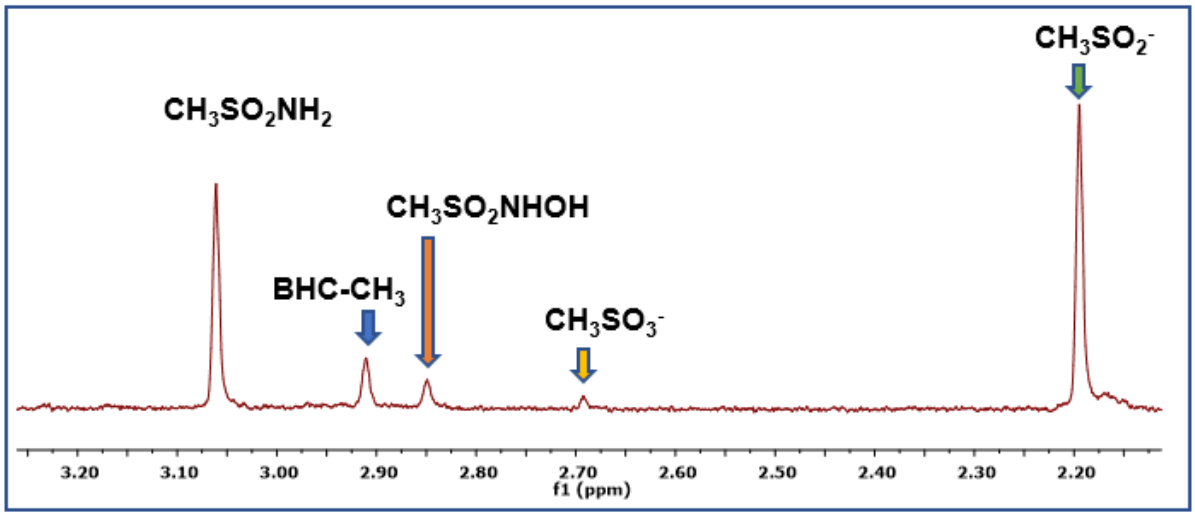

(a)

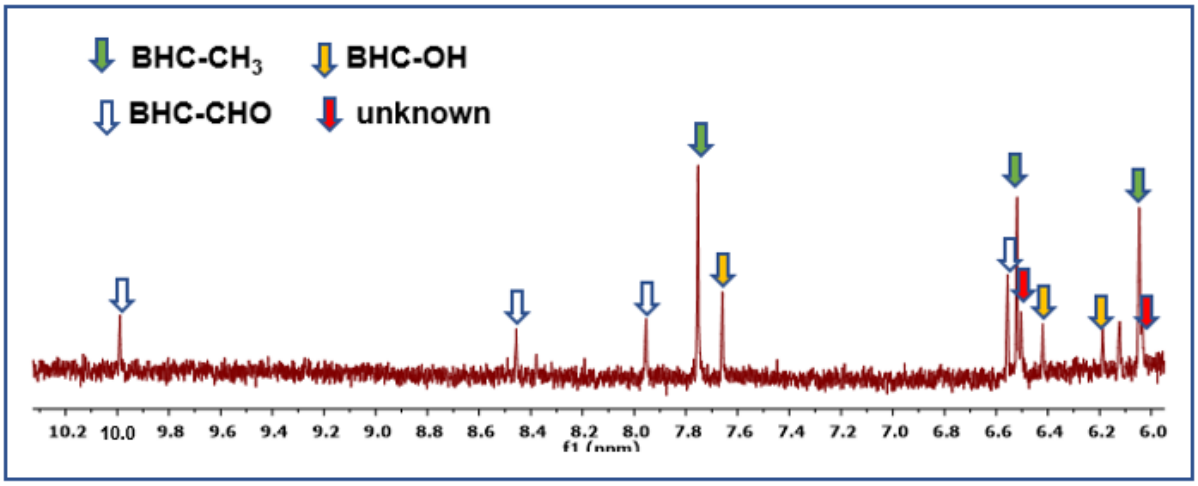

(b)

Figure 4.38. (a) ^{1}H NMR spectrum in the 2.20-3.20 ppm region for a solution of **BHC-CH$_3$** (1.0 mM) in a mixture of carbonate buffer (pH 10.0, 30.0 mM) and CD_3CN (90:10, v/v) after 5 min irradiation. (b) The aromatic region of ^{1}H NMR spectrum for the same solution after 0.20 min irradiation.

Table 4.8 summarizes the percentages of the aliphatic photoproducts obtained in aqueous buffer/CD_3CN solvent mixtures (90% v/v aqueous buffer/10% CD_3CN). The percentage of each photoproduct is unchanged from pH 2.1 to pH 7.0 within experimental error, with O-N bond cleavage (80%) dominating from pH 2.1 to pH 7.0, to give $CF_3SO_2NH_2$ and **BHC-CHO**. At pH 10.0 and 10.7 both O-N bond cleavage (40% $CH_3SO_2NH_2$) and concomitant C-O/N-S bond cleavage (54% $CF_3SO_2^-$) bond cleavage pathways are important. The amount of C-O bond cleavage is almost pH independent within experimental error.

Table 4.8. Effect of the pH of the aqueous component of the solvent on the photoproducts derived from the *N*-hydroxysulfonamide for photodecomposition for **BHC-CH_3** (1.0 mM) in 10:90 v/v CD_3CN: aqueous buffer (30 mM).

pH	Percentage of Photoproducts				
	$CH_3SO_2NH_2$	CH_3SO_2NHOH	$CH_3SO_2^-$	$CH_3SO_3^-$	Unknown
2.1[a]	78	8	2	6	6
5.0[b]	78	8	2	5	7
7.0[c]	81	11	4	4	0
10.0[d]	40	4	48	8	0
10.7[e]	39	5	54	2	0

Aqueous component of solution: [a,c]phosphate buffer, [b]acetate buffer; [d,e]carbonate buffer.

4.3.14 Emission spectra of BHC-CF_3, BHC-CH_3 and 6-bromo-7-hydroxy-4-methylcoumarin

The isosbestic wavelength for **BHC-CF_3** was determined prior to recording emission spectra, by recording the UV-Vis spectra of **BHC-CF_3** at pH 1.98, pH 6.30 and pH 11.23 (Figure 4.39(a)) using a flow set up (section 4.3.7). The pH was adjusted using a small volume of 0.1 M aqueous NaOH or aqueous HCl. Deprotonation of the 6-hydroxy group changes the wavelength maximum from 330 nm to 370 nm and an isosbestic point was observed at 342 nm. Similarly, the isosbestic wavelengths of **BHC-CH_3** and 6-bromo-7-hydroxy-4-methylcoumarin were found to be 341 and 333 nm, respectively, by recording the UV-Vis spectra (Figure 4.39(b) and (c)).

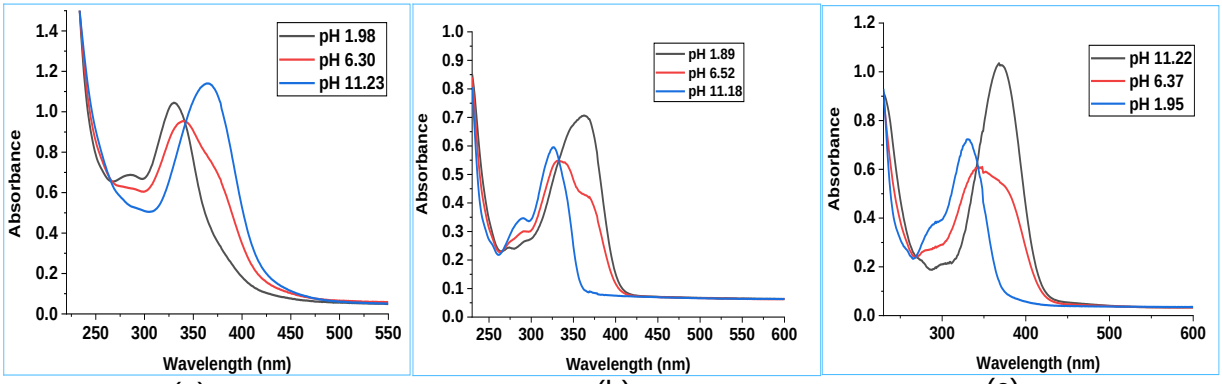

(a) (b) (c)

Figure 4.39. UV-Vis spectra of (a) **BHC-CF_3** at pH 1.98, 6.30 and 11.23. (b) **BHC-CH_3** at pH 1.89, 6.52 and 11.18 and (c) 6-bromo-7-hydroxy-4-methylcoumarin at pH 1.95, 6.37 and 11.22. The spectra were recorded in 8:92 v/v CH_3CN: H_2O.

An aqueous solution of **BHC-CF_3**, **BHC-CH_3** or 6-bromo-7-hydroxy-4-methylcoumarin (1.05×10^{-6} M, 8:92 v/v CH_3CN: H_2O) was circulated using a peristaltic pump through a 1 cm path length quartz flow-through cell at 25.0 °C. These experiments were carried out under red light conditions to avoid photodecomposition. ^1H and ^{19}F NMR spectra were recorded before starting and at the end of the experiment to ensure that the compounds had not decomposed. The effect of changing the pH on the emission spectrum was determined by adding a small volume of acid (~0.10 M aqueous HCl; negligible change in total volume of the solution) to each solution (30 mL). The emission intensity was recorded from pH 1.98 to 11.23 (**BHC-CF_3**), pH 1.98 to 11.18 (**BHC-CH_3**) and pH 1.95 to 11.22 (6-bromo-7-hydroxy-4-methylcoumarin), at the isosbestic point. The entire experiment was finished in ~3.5 h for each compound.

The excited state pK_a, pK_a^* for the 7-hydroxy substituent of 7-hydroxy-4-methylcoumarin was reported to be 0.9.[171, 186] To the best of our knowledge pK_a^* values of 6-bromo-7-hydroxy-4-methylcoumarin or other bromomethylcoumarins have not yet been reported. At pH 2.1 only N-O bond cleavage occurs, whereas at pH 5.0, 7.0 and 10.0, 30% C-O/N-S bond cleavage and 70% N-O bond cleavage occurs for **BHC-CF_3**. The emission spectra of **BHC-CF_3** were recorded at pH 1.98, 6.30 and 11.28 (Figure 4.40(a)). There was essentially no change in the emission intensity at any pH conditions, consistent with the same singlet excited state species at all pH conditions. **BHC-CF_3** was not thermally stable below pH 1.42 so the value of pK_a* could not be experimentally determined.

For **BHC-CH_3**, the percentage of C-O/N-S bond cleavage increases from 4% (at pH 2.5 – 7.0) to 50% at pH 10.0. Figure 4.40(b) shows the emission spectra of **BHC-CH_3** recorded at pH 1.95, 6.37 and 11.22. Once again there is very little change in the emission spectrum. The emission spectra of 6-bromo-7-hydroxycoumarin also showed no change at pH 1.89, 6.52 and 11.18 (Figure 4.40(c)). These results are consistent with no changes in the singlet excited state species at all pH conditions.

For the related 6-hydroxynaphthalen-2-yl -caged $ON(H)SO_2CF_3$ (**6,2-HNM-CF_3**), it was observed that the intensity of the emission spectrum was highly dependent on whether the HNO-generating pathway was occurring, with a significant drop in the emission intensity in the pH region where concerted C-O/N-S bond cleavage is favourable (pH ~ 5-9).[75] We are currently unable to explain the differences between the emission intensities of this system and **BHC-CF_3**, **BHC-CH_3** and 6-bromo-7-hydroxy-4-methylcoumarin. One factor that could potentially contribute to these

differences is that the experiments for **6,2-HNM-CF$_3$** were carried out in 80:20 v/v $CH_3CN:H_2O$, whereas the emission spectra experiments for **BHC-CF$_3$**, **BHC-CH$_3$** and 7-hydroxy-4-methylcoumarin were recorded in 8:92 v/v $CH_3CN:H_2O$. In 80:20 v/v $CH_3CN:H_2O$ deprotonation is much less favourable from the thermodynamic perspective in addition to being slower to occur. To obtain further insight on this, the emission spectra for **6,2-HNM-CF$_3$** could be recorded in 8:92 v/v $CH_3CN:H_2O$.

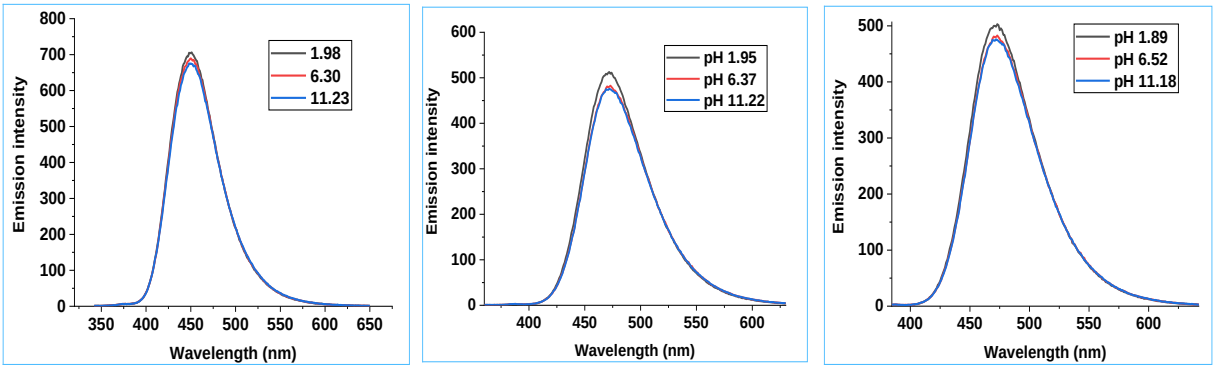

(a) (b) (c)

Figure 4.40. Emission spectra of (a) **BHC-CF$_3$** at pH 1.98, 6.30 and 11.23 (λ_{exc} = 342 nm), (b) **BHC-CH$_3$** at pH 1.95, 6.37 and 11.22 (λ_{exc} = 341 nm) and (c) 6-bromo-7-hydroxy-4-methylcoumarin at pH 1.89, 6.52 and 11.18 (λ_{exc} = 330 nm). The spectra were recorded in 8:92 v/v CH_3CN: H_2O.

4.3.15 Effect of the excitation wavelength on the photoproducts

The photoproducts obtained upon irradiation of **BHC-CF$_3$** (1.0 mM) at two different excitation wavelengths (355 and 270 nm) were investigated in a mixture of phosphate buffer (30 mM, pH 7.0) and CD_3CN (40:60, v/v), using a xenon lamp in conjunction with a monochromator. The excitation wavelength did not have any effect on the observed photoproducts (Table 4.9). This is consistent with a π-π* transition occurring for this system regardless of the excitation wavelength.

Table 4.9. Effect of excitation wavelength on the photoproducts derived from *N*-hydroxysulfonamide upon irradiation of **BHC-CF$_3$** or **BHC-CH$_3$** (1.0 mM) in a mixture of phosphate buffer (30 mM, pH 7.0) and CD_3CN (40:60, v/v).

compound	λ_{exc}	Photoproducts
BHC-CF$_3$	270	$CF_3SO_2NH_2$ (40%) and $CF_3SO_2^-$ (60%)
BHC-CF$_3$	355	$CF_3SO_2NH_2$ (38%) and $CF_3SO_2^-$ (62%)
BHC-CH$_3$	270	CH_3SO_2NHOH (7%), $CF_3SO_2NH_2$ (78%), $CH_3SO_2^-$ (4%), $CH_3SO_3^-$ (3%) and unknown (8%)
BHC-CH$_3$	355	CH_3SO_2NHOH (8%), $CF_3SO_2NH_2$ (77%), $CH_3SO_2^-$ (3%), $CH_3SO_3^-$ (5%) and unknown (7%)

4.3.16 Effect of triplet quenchers on the photoproducts

Steady state photolysis experiments were carried out in the presence of the triplet quenchers p-terphenyl and cyclohexadiene.[113] Photolysing **BHC-CH_3** in the presence of 20 mol equivalent *p*-terphenyl or 20 mol equivalent cyclohexadiene under aerobic conditions in a mixture of phosphate buffer (30 mM, pH 7.0) and CD_3CN (40:60, v/v) gave CH_3SO_2NHOH (7%), $CF_3SO_2NH_2$ (78%), $CH_3SO_2^-$ (4%), $CH_3SO_2^-$ (3%) and 8% of an unknown species. Under anaerobic conditions the photoproducts were $CH_3SO_2NH_2$ (77%), CH_3SO_2NHOH (7%), $CH_3SO_2^-$ (2%), $CH_3SO_3^-$ (7%) and an unknown species (7%). The presence of the triplet quenchers oxygen, *p*-terpene or cyclohexadiene had no effect on the photoproducts and hence the mechanism of photodecomposition (Pathways 1-3, Scheme 4.1).

4.3.17 Photoproduct quantum yield

The photoproduct quantum yields for **BHC-CF_3** and **BHC-CH_3** at 313 nm were determined by actinometry, using the isomerisation of *trans*-azobenzene to its *cis* isomer as a reference compound (Φ = 0.14 at 313 nm; see section 2.3.13, Chapter 2). The percentage of *trans*-azobenzene (6.61×10^{-5} M) converted to *cis*-azobenzene upon irradiation was followed by UV-Vis spectroscopy, whereas the photodecomposition of **BHC-CF_3** (1.00 mM) and **BHC-CH_3** (1.00 mM) was followed by ^{19}F or ^{1}H NMR spectroscopy. All the experiments were carried on the same day. Figure 4.41(a) shows a plot of the number of moles of *cis*-azobenzene as a function of total irradiation time. The slope is $4.15 \pm 0.03 \times 10^{-9}$ mol min^{-1}. Figure 4.41(b) and Figure 4.41(c) give plots of the total number of moles of photoproduct as a function of total irradiation time for **BHC-CF_3** and **BHC-CH_3**, respectively. The slope values for **BHC-CF_3** and **BHC-CH_3** are $(7.62 \pm 0.02) \times 10^{-9}$ mol min^{-1} and $(5.12 \pm 0.03) \times 10^{-9}$ mol min^{-1}, respectively. The slopes were substituted into equation (4.6) to obtain photoproduct quantum yields.

$$\phi\,(\text{BHC-CF}_3 \text{ or BHC-CH}_3) = \frac{\text{slope (BHC-CF}_3 \text{ or BHC-CH}_3) \,/\, \text{Absorbance (BHC-CF}_3 \text{ or BHC-CH}_3)}{\text{Slope (reference)} \,/\, \text{Absorbance (reference)}} \times \phi\,(\text{reference}) \quad (4.6)$$

The absorbance of the solutions of **2-NPE-ON(H)-SO_2R** (1.00 mM) at the excitation wavelength were calculated using the molar extinction coefficient of each reactant at 313 nm and were $(7.50 \pm 0.04) \times 10^3$ M^{-1} cm^{-1} (**BHC-CF_3**) and $(2.40 \pm 0.03) \times 10^3$ M^{-1}

cm^{-1} (**BHC-CH_3**). The photoproduct quantum yields were 0.45 ± 0.01 **(BHC-CF_3)** and 0.22 ± 0.01 **(BHC-CH_3)**. The photoproduct quantum yield is clearly affected by the alkyl group of the sulfonamide. The quantum yields for 2-nitrobenzyl caged N-hydroxysulfonamides are **2-NO_2Bn-ON(H)SO_2CF_3** 0.67 ± 0.03, **2-NO_2Bn-ON(H)SO_2CH_3** 0.77 ± 0.03, **4,5-$(MeO)_2$-2-NO_2Bn-ON(H)SO_2CF_3** 0.46 ± 0.02, **4,5-$(MeO)_2$-2-NO_2Bn-ON(H)SO_2CH_3** 0.27 ± 0.01 and **2-NO_2Bn-OC(O)ON(H)SO_2CH_3** 0.23 ± 0.01. The quantum yields for the 2-nitrophenylethyl caged compounds are **2-NPE-ON(H)-SO_2CF_3** 0.47 ± 0.01, **2-NPE-ON(H)-SO_2CH_3** 0.32 ± 0.01 and **2-NPE-ON(H)-SO_2Ar** 0.07 ± 0.01. The quantum yield for (6-bromo-7-hydroxycoumarin-4-yl)methyl acetate was found to be 0.13 (350 nm, aqueous solution).[148]

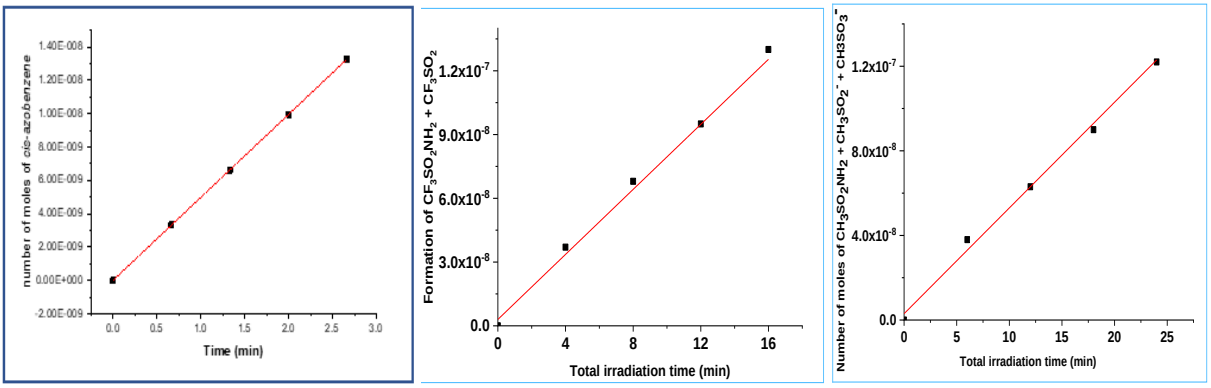

(a) (b) (c)

Figure 4.41. (a) Plot of the number of moles of *cis*-azobenzene vs total irradiation time (min). The slope was (4.38 ± 0.03) × 10^{-9} mol min^{-1}, and the absorbance of *trans*-azobenzene before irradiation was 1.32. (b) Plot of the number of moles of the photoproduct $CF_3SO_2NH_2$ + $CF_3SO_2^-$ versus total irradiation time (min) obtained from the photolysis of **BHC-CF_3** (1.00 mM, 313 nm) in CD_3OD. The best fit of the data to a straight line gives a slope of (7.62 ± 0.02) × 10^{-9} mol min^{-1}. (c) Plot of the number of moles of the photoproducts ($CH_3SO_2NH_2$ + CH_3SO_2NHOH) versus total irradiation time (min) obtained from the photolysis of **BHC-CF_3** (1.00 mM, 313 nm) in CD_3OD. The best fit of the data to a straight line gives a slope of (5.12 ± 0.03) × 10^{-9} mol min^{-1}.

4.4 Discussion

In this chapter the mechanisms of the photodecomposition of two compounds, **BHC-CF_3** and **BHC-CH_3**, were investigated. Studies by others of molecules photocaged with the (6-bromo-7-hydroxycoumarin-4-yl)methyl moiety have shown that for these systems, upon π-π* excitation, internal conversion to the lowest energy singlet excited state occurs, followed by rapid heterolytic C-O bond cleavage to release the molecule of interest and generate a carbocation intermediate.[128, 136, 187, 188] The carbocation then reacts with nucleophiles including solvent H_2O or CH_3OH.[152]

For both systems, the photoproduct percentages were not affected by the excitation wavelength selected using a Xe lamp in conjunction with a monochromator (270 or 355 nm Table 3.11), consistent with π-π^* excitation occurring regardless of the excitation wavelength. The triplet state quenchers oxygen (aerobic versus anaerobic conditions), p-terphenyl and cyclohexadiene had no effect on the observed percentages of the photoproducts, which indicates no involvement of triplet excited state species in the bond cleavage events leading to the primary photoproducts. Hence both **BHC-CF_3** and **BHC-CH_3** undergo bond cleavage from singlet excited state species. The photoproduct quantum yields of both systems were also determined. The photoproduct quantum yields values for **BHC-CF_3** and **BHC-CH_3** were extremely good (0.45 ± 0.01 and 0.22 ± 0.01, respectively, at 313 nm in CH_3OH). The quantum yield of 6-bromo-7-hydroxy-4-methylcoumarin was reported to be 0.13 (350 nm, aqueous solution).[148]

The pK_a of the O(H) of the coumarin photocage and N(H) of the *N*-hydroxysulfonamide moiety played a crucial role in determining the mechanism of photodecomposition for the analogous (6-hydroxynapthalen-2-yl)methyl (6,2-HNM) photocaged N-hydroxytrifluoromethanesulfonamide system (**6,2-HNM-CF_3)**.[75] This latter molecule also generates a carbocation, HNO and $CF_3SO_2^-$ upon rapid concomitant C-O/N-S heterolytic bond cleavage in the lowest singlet excited state of this system.[75] The ground state pK_a values for the N(H) and O(H) protons of **BHC-CF_3** and **BHC-CH_3** were therefore determined using a combination of ^{19}F NMR spectroscopy, ^1H NMR spectroscopy and UV-vis spectroscopy titration experiments. The pK_a values for the N(H) proton of **BHC-CF_3** was 3.42 ± 0.02 (8:92 v/v CH_3CN: D_2O, I = 1.0 M, $NaCF_3SO_3$), which is similar to the pK_a value of the -N(H) proton of **2-NPE-ON(H)-SO_2CF_3** (3.77 ± 0.03, in D_2O with 5% v/v CH_3CN, I = 1.0 M, $NaCF_3SO_3$, section 3.3.3, Chapter 3) and (6-hydroxynaphthalen-2-yl)methyl-photocaged *N*-hydroxysulfonamide (4.4 ± 0.1, in aqueous solution).[78] The pK_a of the O(H) of the coumarin photocage of **BHC-CF_3** was 6.31 ± 0.03 (8:92 v/v CH_3CN: D_2O, I = 1.0 M, $NaCF_3SO_3$; ^1H NMR spectroscopy) and 6.35 ± 0.03 (in 8:92 v/v CH_3CN: H_2O); UV-Vis spectroscopy). The pK_a values in H_2O are typically 0.05 – 0.6 lower than in D_2O,[176-178] It was observed that acids are stronger in H_2O. These values are in agreement with the value predicted earlier in the PhD thesis of our US collaborator.[152] pK_a values of 6.2 (aqueous solution) and 5.88 (10:90 v/v DMSO: H_2O) have been reported by others for **BHC-OH** and (6-bromo-7-

hydroxycoumarin-4-yl)methyl acetate, respectively.[139] The pK_a of 6-bromo-7-hydroxy-4-methylcoumarin was also determined in this chapter, and found to be 6.91 ± 0.03 (8:92 v/v CH_3CN: H_2O; UV-vis spectroscopy). The electron withdrawing $-ON^-SO_2CF_3$ moiety of **BHC-CF$_3$** decreases the pK_a of the O(H) proton compared with 6-bromo-7-hydroxy-4-methylcoumarin. Despite the deprotonation of the N(H) of $-ON^-SO_2CF_3$, this group still behaves as an electron withdrawing group.

The pK_a values were also determined for **BHC-CH$_3$**. The pK_a of the N(H) of **BHC-CH$_3$** is 10.11 ± 0.03 (8:92 v/v CH_3CN: D_2O, I = 1.0 M, $NaCF_3SO_3$, ^1H NMR spectroscopy) and is, as expected, similar to **2-NPE-ON(H)-SO$_2$CH$_3$** (pK_a 10.06 ± 0.03; 8:92 v/v CH_3CN: D_2O, I = 1.0 M, $NaCF_3SO_3$, section 3.3.3, Chapter 3). The pK_a of the O(H) was found to be 6.47 ± 0.03 for **BHC-CH$_3$** (8:92 v/v CH_3CN: H_2O) using UV-Vis spectroscopy. The pK_a of the O(H) in these systems therefore follows the order **BHC-CF$_3$** (6.35 ± 0.03) < **BHC-CH$_3$** (6.47 ± 0.03) < 6-bromo-7-hydroxy-4-methyl coumarin (6.91 ± 0.03). This order parallels the electron withdrawing ability of the 4-substituent of the coumarin. The deprotonation of the N(H) of **BHC-CF$_3$** does not affect this order (the electron-withdrawing abilities are expected to be significantly reduced upon deprotonation of the N(H)), despite the N(H) being protonated for **BHC-CH$_3$.**

The dependence of solvent on the photoproducts and hence the mechanisms of photodecomposition of **BHC-CF$_3$** was investigated, by varying volume percentages of phosphate buffer (pH 7.0) and CD_3CN. **BHC-CF$_3$** was not photostable under ambient light conditions (fluorescent lights and daylight in the laboratory), so experiments were carried out under red light conditions. Steady state analysis of the photoproducts showed that two pathways for decomposition occur - concomitant C-O/N-S bond cleavage or O-N bond cleavage, Pathways 1 and 3, Scheme 4.1. The aromatic photoproducts observed in partially photolyzed solutions were **BHC-OH** and ***(E)*-** and ***(Z)*-BHC-Oximes** from C-O/N-S bond cleavage, Pathway 1 and **BHC-CHO** from N-O bond cleavage, Pathway 3. These species decompose at longer irradiation times. Our collaborators also demonstrated that HNO is released for this system using an established phosphine trapping agent, which reacts with HNO to produce the characteristic phosphine ylide; hence not all the released NO^- upon C-O/N-S bond cleavage is trapped by the carbocation intermediate.[152] In pure CD_3CN, ~80% C-O/N-S bond cleavage occurs (~80% $CF_3SO_2^-$), with ~20% O-N bond cleavage (~20% $CF_3SO_2NH_2$ generated, Table 4.1). Importantly, our collaborators observed only C-

O/N-S bond cleavage in CD_3CN.[152] Our experiment was performed multiple times with dry reagents (**BHC-CF_3** dried under vacuum using a Schlenkline, an ampule of dry CD_3CN purchased, and the solution prepared in a glovebox). Our collaborators are currently repeating this experiment. The amount of C-O/N-S bond cleavage progressively decreases from 80% (pure CD_3CN) to 25% in 90:10 v/v phosphate buffer (pH 7.0): CD_3CN, Table 4.1. A similar trend is reported in the PhD thesis of our US collaborator.[152] Hence increasing the volume percentage of H_2O in the solvent mixture results in a decrease in the desired HNO-releasing pathway. This results parallels what was observed for the **6,2-HNM-CF_3** system. For this latter system 98% concomitant C-O/N-S bond cleavage was observed for 5:95 v/v phosphate buffer (pH 7.0) : CD_3CN, which progressively decreased to ~54% in 95:5 v/v phosphate buffer (pH 7.0): CD_3CN, at the expense of O-N bond cleavage.[78] There is, however, one important difference between these two systems. Only O-N bond cleavage occurs for **6,2-HNM-CF_3** in pure CD_3CN, whereas ~80% C-O/C-S bond cleavage occurs for **BHC-CF_3** in this solvent. For **6,2-HNM-CF_3** it was proposed that the addition of a trace amount of water was required for C-O/N-S bond cleavage since the N(H) of the *N*-hydroxysulfonamide of the reactant must be deprotonated.[76] DFT calculations are currently underway and the preliminary results also suggest that deprotonation of the N(H) of the reactant is required for HNO generation. One important difference between the two systems is the excited state pK_a* for the O(H), with the value anticipated to be lower for (6-bromo-7-hydroxycoumarin-4-yl)methyl – caged molecules (pK_a* for O(H) = 0.9 for 7-hydroxy-4-methylcoumarin compared with **6,2-HNM-CF_3** (pK_a* for O(H) ~ 3.4 ± 0.4)).[186, 75]

The effect of pH on the photoproducts and hence the mechanism of photodecomposition was also studied for **BHC-CF_3**, in 90:10 % v/v mixtures of aqueous buffer:CD_3CN. When the pH of the aqueous component was pH 2.1, only O-N bond cleavage (100% $CF_3SO_2NH_2$) was observed. However, at pH 5.0, 7.0 and 10.0, ~30% $CF_3SO_2^-$ and 70% $CF_3SO_2NH_2$ was observed at all pH conditions, Scheme 4.3.

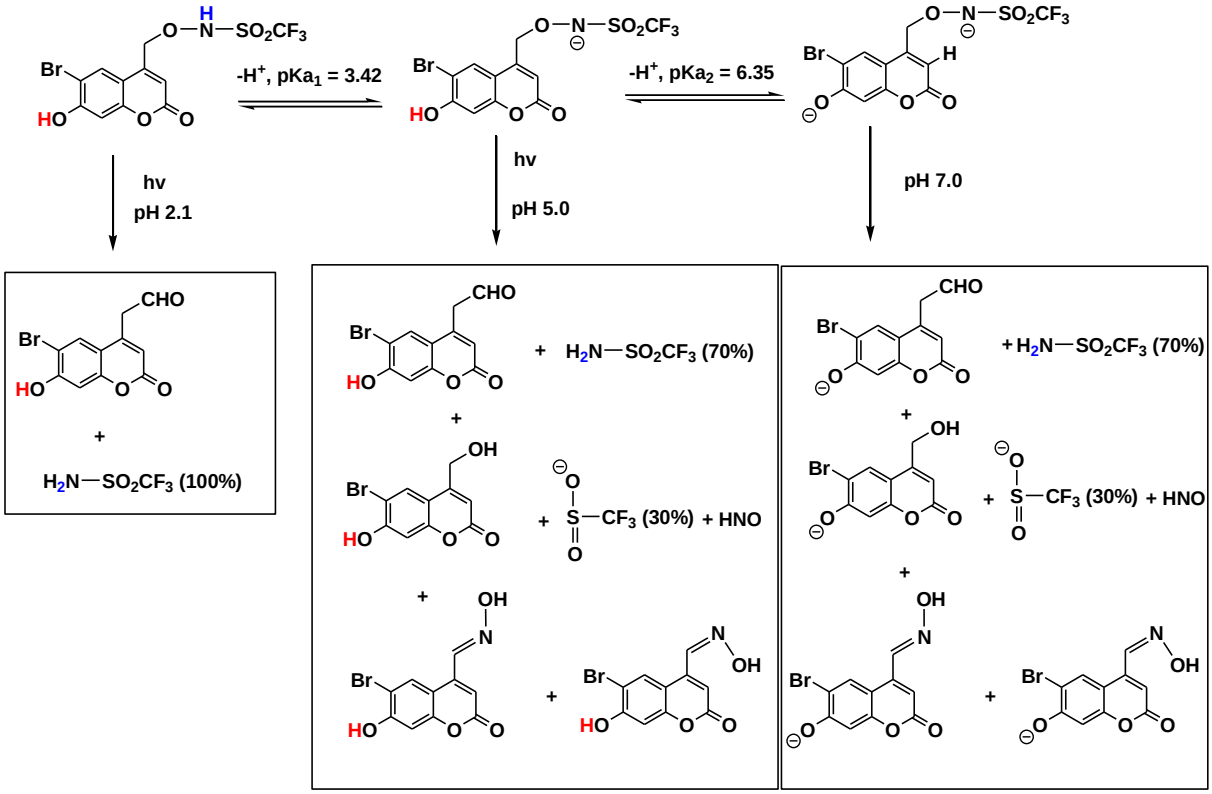

Scheme 4.3. Observed photoproducts for **BHC-CF$_3$** as a function of pH (in 10:90 v/v CD_3CN: phosphate buffer).

This is consistent with deprotonation of the N(H) of **BHC-CF$_3$** being essential for concomitant C-O/N-S bond cleavage (pK_a 3.42 ± 0.02 in 8:92 v/v CH_3CN: D_2O, I = 1.0 M, $NaCF_3SO_3$). A similar observation was made for the **6,2-HNM-CF$_3$** system – that is, deprotonation of the N(H) proton is essential for C-O/N-S bond cleavage to occur.[75] Interestingly, deprotonation of the 6-hydroxy substituent of **BHC-CF$_3$** (6.35 ± 0.03 in 8:92 v/v CH_3CN: H_2O) had no effect on the percentages of the observed photoproducts in 92:8 v/v mixtures of aqueous buffer:CD_3CN. However, since bond cleavage occurs in the excited state molecule and that deprotonation is rapid since 92% of the solvent is H_2O, the pK_a* values for these two sites is most likely more relevant for this system. Given that the N(H) is some distance from the chromophore and that bond conjugation does not extend to this site, pK_a(NH) is probably not that different from the ground state pK_a(NH). However this will not be the case for the 6-hydroxy substituent of the coumarin, as it is well-known that the pK_a of aromatic OH groups can drop several orders of magnitude upon excitation of the molecule.[186] pK_a* values of 0.9 have been reported for the 7-hydroxy substituent of 7-hydroxy-4-methylcoumarin.[186] Hence it is likely that this site is deprotonated at even the lowest pH condition (pH 2.1) of this

study. Unfortunately, a fluorescence titration experiment could not be conducted to obtain an estimate of pK_a^* for the O(H) substituent of the singlet excited state of **BHC-CF_3**, since the compound was not stable at pH values less than 0.9. Importantly, unpublished data from our collaborators shows that replacing the OH substituent of both **6,2-HNM-CF_3** and **BHC-CF_3** with a non-ionisable group (the methoxymethyl ether (MOM) protecting group) does lower the amount of O-N bond cleavage system.[152] Note that a base-catalyzed (hydroxide) deprotonation is unlikely to occur in the pH 5-10 range, given that the percentage of $CF_3SO_2NH_2$ does not change when the pH of the aqueous component is increased. However, studies at higher pH for the related **2-NPE** system showed that thermal base-catalyzed deprotonation of the methylene carbon is possible for these systems and will result in O-N bond cleavage (section 3.3.7). Therefore, if the pH of the aqueous component is high enough, it is anticipated that base-catalyzed deprotonation leading to increased O-N bond cleavage will also occur for this system. We therefore hypothesize that the main role of H_2O is to promote H_2O-assisted deprotonation of the methylene carbon in the excited state species and to protonate the N centre, leading to O-N bond cleavage and generation of RSO_2NH_2. The presence of the strongly electron withdrawing $CF_3SO_2N(H)O$- group will assist in weakening the C-H methylene bond.

Examination of the results for the related **BHC-CH_3** system revealed some key differences. Firstly, unlike the **BHC-CF_3** system, increasing the volume percentage of aqueous phosphate buffer (pH 7.0) in CD_3CN/phosphate buffer mixtures had no significant effect on the photoproduct percentages, Table 4.2. For this system 80% $CH_3SO_2NH_2$ was observed regardless of the solvent, with ~6% C-O bond cleavage (CH_3SO_2NHOH) and ~3% C-O/N-S bond cleavage ($CH_3SO_2^-$ and its oxidized product, $CH_3SO_3^-$). These results are consistent with the results presented in the PhD thesis of our collaborator.[152] Others have reported that $CH_3SO_3^-$ can be formed from the reaction of $CH_3SO_2^-$ with the hydroxyl radical.[158] Trace amounts of the hydroxyl radical are generated upon photolysis of aqueous solutions. Importantly, the pK_a of the N(H) of **BHC-CH_3** was 10.11 ± 0.03 (in D_2O with 8% v/v CH_3CN, I = 1.0 M, $NaCF_3SO_3$); hence generation of HNO via C-O/N-S bond cleavage is not favorable since this site is protonated regardless of the solvent composition. This conclusion is supported by the results obtained upon varying the pH of the aqueous component for 92:8 v/v aqueous solution: CD_3CN mixtures, Table 4.7. Specifically, while the amount of the HNO generation pathway remained low when the pH of the aqueous component was

pH 5.0 and 7.0 (2% $CH_3SO_2^-$, 6% $CH_3SO_3^-$, 6% CH_3SO_2NHOH, 78% $CH_3SO_2NH_2$, and 6% of an unknown species), at pH 10.0 and 10.7 the percentage of C-O/N-S bond cleavage increased 15-fold (51% $CH_3SO_2^-$, 2% $CH_3SO_3^-$, 5% CH_3SO_2NHOH and 40% $CH_3SO_2NH_2$), consistent with deprotonation of the N(H) of the sulfonamide playing a key role in determining the major mechanisms of photodecomposition for **BHC-CH$_3$**. Note that the percentage of C-O/N-S bond cleavage is even higher for **BHC-CH$_3$** than that observed for **BHC-CF$_3$** in the same solvent mixture (55% $CH_3SO_2^-$ versus 30% $CF_3SO_2^-$ in 92:8 % v/v pH 10.0 buffer: CD_3CN; Tables 4.6 and 4.7). Hence it is clear that the electron-withdrawing CF_3 of the latter molecule promotes O-N bond cleavage, presumably by the ability of a good leaving group to accelerate the reaction.

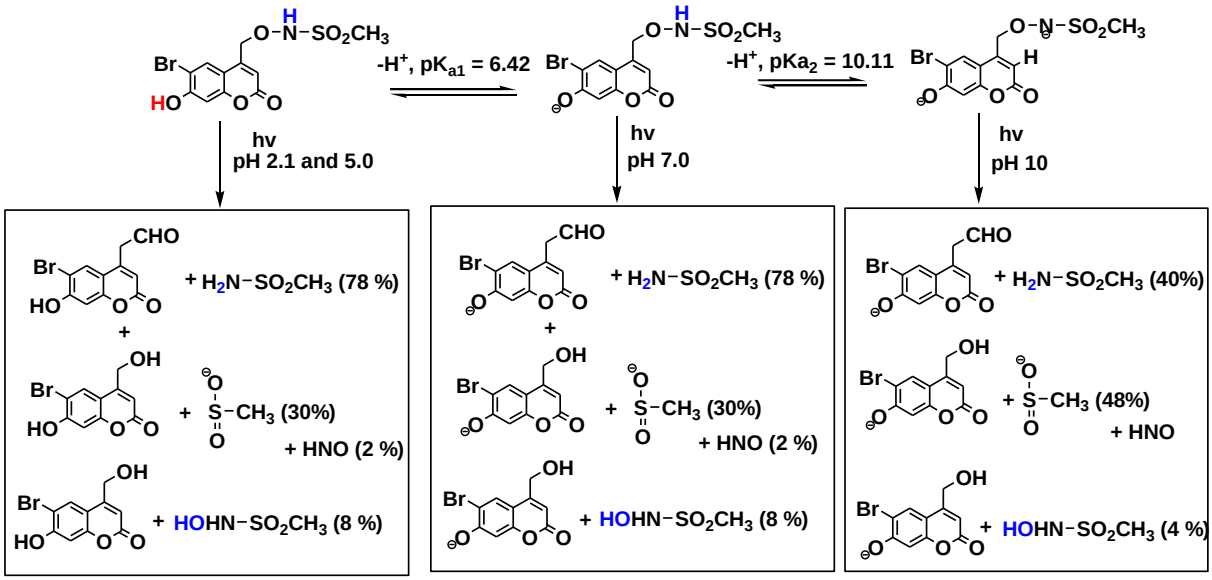

Scheme 4.4. Observed photoproducts for **BHC-CH$_3$** as a function of pH (in 10:90 v/v CD_3CN: phosphate buffer).

Nakagawa et al. recently reported the synthesis of (7-diethylaminocoumarin-4-yl)methyl photocaged derivatives of the Piloty's acid derivatives (2-Br)$PhSO_2NHOH$ and (2-NO_2)$PhSO_2NHOH$.[80] These molecules also absorb in the visible region (~400 nm). HNO generation was confirmed indirectly for the latter compound by GC-MS analysis via observation of N_2O formation from the dimerization of HNO and the sulfinamide and disulfide products formed from the reaction of HNO with the thiol N-acetylcysteine. Both compounds also caused an enhancement in fluorescence upon binding to an HNO-specific fluorescence probe. The corresponding oxime compound was also observed upon irradiation of the photocaged 2-nitro derivative of Piloty's acid and the authors speculated that the HNO generating pathway proceeds via C-O bond

cleavage to generate the carbocation intermediate and the anion of the parent *N*-hydroxysulfonamide. The latter molecule would then decompose further to generate HNO and the sulfinate product. Alternatively, subsequent nucleophilic attack of the N lone pair of the anion of the *N*-hydroxysulfonic acid was proposed, to give the oxime product via a nitroso compound which subsequently tautomerizes. The possible role of the protonation state of the N(H) was not investigated and there was no experimental evidence for C-O bond cleavage to give the anion of the parent *N*-hydroxysulfonic acid in addition to the carbocation. Based on our results we think that deprotonation of the N(H) will also be required for HNO generation for these two systems, and that the HNO generating pathway instead involves concomitant C-O/N-S bond cleavage. It is likely that NO^- is released in the solvent cage and is then trapped before it can escape the solvent cage.

To summarize, the mechanisms of photodecomposition of two novel (6-bromo-7-hydroxy-coumarin-4-yl)methyl caged *N*-hydroxysulfonamides has been investigated. The pK_a values for the N(H) and O(H) sites were determined for the ground state molecules by UV-vis and/or NMR spectroscopy titration experiments. The release of HNO from these molecules depends on the pH of the aqueous component of the system, with deprotonation of the N(H) proton required for efficient concerted C-O/N-S bond cleavage to give a carbocation, NO^- and a sulfinate. The protonation state of the O(H) does not have any effect on the observed photoproducts. In the absence of a species that reacts rapidly with (H)NO, this species reacts with the carbocation intermediate to ultimately generate **(*E*)-BHC-oxime** and **(*Z*)-BHC-oxime**. O-N Bond cleavage competes with the desired HNO generating pathway and becomes more favourable when the volume percentage of water in acetonitrile/water solvent mixtures is increased. The role of the water is to promote water-assisted deprotonation of the methylene carbon, and may even occur in the excited state molecule, so the O-N bond cleavage pathway occurs via a E1cB elimination mechanism. Alternatively the water also solvates the developing anionic leaving group, stabilizing the transition state required for O-N bond cleavage occurring via a E2 mechanism.

Only C-O/N-S and O-N bond cleavage are observed for **BHC-CF_3**, whereas small amount of C-O bond cleavage is also observed for **BHC-CH_3**. From a comparison of the photoproducts at pH conditions where the N(H) is deprotonated for both systems, it is clear that the presence of the electron withdrawing CF_3 moiety of **BHC-CF_3** promotes undesired O-N bond cleavage compared with the **BHC-CH_3** system,

presumably by lowering the pK_a of the methylene proton resulting in O-N bond cleavage. Finally, it is likely that bond cleavage occurs in the singlet excited state as observed for a closely related (6-hydroxynapthalen-2-yl)methyl - photocaged system,[75] since triplet quenchers had no effect on the observed photoproducts.

Chapter 5: Conclusions and Future directions

There is increasing interest in HNO from both a biological and therapeutic perspective. Given that this molecule is unstable in addition to reacting rapidly with numerous biomolecules, the development of compounds which rapidly and cleanly generate HNO upon light activation in aqueous solution would be very valuable research tools to scientists working in this exciting new field.

In Chapter 2 the photodecomposition of a new class of photocaged *N*-hydroxysulfonamides incorporating the well-established 2-nitrobenzyl (2-NO_2Bn) photoprotecting group, including a derivative incorporating an additional carbonate linker, is presented. The desired concerted C-O/N-S pathway to release HNO and $CF_3SO_2^-$ was a minor pathway (8 ± 1%) for **2-NO_2Bn-ON(H)SO_2CF_3** and the corresponding 2-nitro-4,5-dimethoxybenzyl analogue, with the major photodecomposition pathway being photoinduced O-N bond cleavage to generate sulfonamide, $CF_3SO_2NH_2$, Table 5.1. Only O-N bond cleavage was observed for **2-NO_2Bn-ON(H)SO_2CH_3** and the corresponding 2-nitro-4,5-dimethoxybenzyl analogue. The presence or absence of methoxy groups on the 2-nitrophenyl ring had minimal influence on the observed photoproducts. The effect of the composition of the solvent (CD_3CN and aqueous phosphate buffer, pH 7.0) and the pH of the aqueous component (10:90 v/v CD_3CN: buffer) also had no effect on the photoproduct percentages for **2-NO_2Bn-ON(H)SO_2CH_3** (Tables 5.1 and 5.2), consistent with a mechanism involving a Norrish type II 1,5 hydrogen atom abstraction occurring in the excited state to give a ground state *(Z)*-aci-nitro intermediate. Evidence for formation of an aci-nitro intermediate was obtained by laser flash photolysis. The presence or absence of air (O_2) had no effect on the photoproduct percentages. A mechanism was proposed in which the *(Z)*-aci-nitro intermediate either undergoes O-N bond cleavage to generate the sulfonamide and 2-nitrobenzaldehyde or instead isomerises to the *(E)* isomer (ON(H)SO_2CF_3 derivatives only), followed by cyclization and ultimately C-O/N-S bond cleavage to generate HNO and $CF_3SO_2^-$. For **2-NO_2Bn-OC(O)-ON(H)-SO_2CH_3** three decomposition pathways occurred, with the major decomposition pathway being C-O bond cleavage to generate the parent sulfohydroxamic acid $MeSO_2NHOH$ via the *(E)*-aci-nitro intermediate (60:40 v/v CD_3CN:phosphate buffer, Table 5.1).

In Chapter 3 the photodecomposition of a second new class of photocaged *N*-hydroxysulfonamides incorporating the (2-nitrophenyl)ethyl (2-NPE) photoprotecting group is presented, with the $ON(H)SO_2CF_3$, $ON(H)SO_2CH_3$ and $ON(H)SO_2$-2-$(MeSO_2)Ph$ head groups. The photoproduct percentages were independent of the solvent composition (CD_3CN and phosphate buffer, pH 7.0 solvent mixtures) for **2-NPE-ON(H)-SO_2CF_3** and **2-NPE-ON(H)-SO_2CH_3** (Table 5.1). Approximately ~30% of the desired concerted C-O/N-S pathway to release HNO and $CF_3SO_2^-$ was observed for **2-NPE-ON(H)-SO_2CF_3**, with ~70% O-N bond cleavage. For **2-NPE-ON(H)-SO_2CH_3** C-O bond cleavage dominated (85%), with ~7% O-N bond cleavage and ~8% concerted C-O/N-S bond cleavage to release HNO and $CH_3SO_2^-$. All three decomposition pathways were also observed for **2-NPE-ON(H)-SO_2Ar** (Ar = 2-$(MeSO_2)Ph$); however spontaneous thermal decomposition of the $ArSO_2NHO(H)$ product of C-O bond cleavage meant that it was not possible to determine the percentages of C-O versus C-O/N-S bond cleavage except in pure CD_3CN for this compound (Table 5.1).

The dependence of the photoproducts on the pH of the aqueous component of the buffer in 10% v/v aqueous buffer mixtures was determined. Whereas the percentage of photoproducts did not change for **2-NPE-ON(H)-SO_2CF_3** (pH 5.0, 7.0, 10.0, Table 5.2), for **2-NPE-ON(H)-SO_2CH_3** the photoproduct percentages switched from ~83% CH_3SO_2NHOH, 9% $CH_3SO_2NH_2$ and 8% $CH_3SO_2^-$ at pH 5.0 and 7.0 to 13% CH_3SO_2NHOH, 72% $CH_3SO_2NH_2$ and 15% $CH_3SO_2^-$ at pH 9.9 and 12.0 (Table 5.2). Separate experiments were carried out to determine the ground state pK_a for the N(H) of the N-hydroxysulfonamide moiety of each compound, using NMR and/or UV-vis spectroscopy. The pK_a of the N(H) of **2-NPE-ON(H)-SO_2CF_3** was 3.77 ± 0.03 (in D_2O with 5% v/v CH_3CN, I = 1.0 M, $NaCF_3SO_3$), whereas the pK_a of the N(H) of **2-NPE-ON(H)-SO_2CH_3** was 10.06 ± 0.03 (in D_2O with 5% v/v CH_3CN, I = 1.0 M, $NaCF_3SO_3$). Hence in both systems deprotonation of the N(H) disfavours C-O bond cleavage and instead favours concerted C-O/N-S bond cleavage, as expected, since upon deprotonation of the N(H), expulsion of an unstable dianionic $RSO_2N^-O^-$ leaving group would be required. Deprotonation of the N(H) also favours O-N bond cleavage, due to the enhanced acidity of the allyl proton, with deprotonation at this site required for O-N bond cleavage. The photoproduct percentages were unaltered upon the addition of triplet quenchers. The experimental data are consistent with a Norrish type II 1,5

hydrogen atom abstraction occurring in the singlet excited state, to give a *(Z)*-aci-nitro intermediate. Evidence for formation of an aci-nitro intermediate was obtained by laser flash photolysis. The *(Z)*-aci-nitro intermediate either undergoes heterolytic C-O bond cleavage to release $RSO_2NHO(H)$, concerted C-O/N-S bond cleavage to generate RSO_2^- and HNO, or instead isomerises to the *(E)* isomer, cyclizes, and ultimately generates RSO_2NH_2 upon O-N bond cleavage.

In Chapter 4 the photodecomposition of two *N*-hydroxysulfonamides photocaged by the (6-bromo-7-hydroxycoumarin-4-yl)methyl moiety is presented, with the $ON(H)SO_2CF_3$ and $ON(H)SO_2CH_3$ head groups. Excellent photoproduct quantum yields were obtained for both systems. For **BHC-CF_3** the photoproduct percentages were dependent of the solvent composition (CD_3CN and phosphate buffer, pH 7.0 solvent mixtures, Table 5.1), with 82% of the desired concerted C-O/N-S pathway to release HNO and $CF_3SO_2^-$ in pure CD_3CN. The percentage of concerted C-O/N-S bond cleavage decreased to 25% in 8% CD_3CN in phosphate buffer, pH 7.0, at the expense of increased O-N bond cleavage to generate $CF_3SO_2NH_2$. Interestingly, for **BHC-CH_3** the photoproduct percentages were unchanged upon the addition of phosphate buffer, pH 7.0 to CD_3CN, with mainly O-N bond cleavage occurring, Table 5.1.

The ground state pK_a values of the OH and NH of both compounds were determined by NMR and/or UV-vis spectroscopy. The effect of varying the pH of the aqueous component of a water/CD_3CN solvent mixture was also investigated. For **BHC-CF_3** only O-N bond cleavage was observed at pH 2.1 (Table 5.2), whereas upon deprotonation of the N(H) (pH $\geq$5.0) the percentage of O-N bond cleavage decreased to ~70%, with ~30% C-O/N-S bond cleavage. For **BHC-CH_3** 8% C-O/N-S bond cleavage was observed at pH 2.1 - 7.0, whereas at pH 10.0 the percentage of C-O/N-S bond cleavage dramatically increased to 56% (Table 5.2). Hence deprotonation of the N(H) of the compound results in concerted C-O/N-S bond cleavage (pK_a of the N(H) of **BHC-CH_3** = 10.11 ± 0.03 (D_2O with 8% v/v CH_3CN)), at the expense of C-O bond cleavage, presumably once again because of the requirement for expulsion of an unstable dianionic $RSO_2N^-O^-$ leaving group for C-O bond cleavage.

Table 5.1. Effect of solvent ratio on the photoproducts derived from the *N*-hydroxysulfonamide for photodecomposition of the various compounds (1.0 mM) in CD_3CN: aqueous phosphate buffer (pH 7.0, 5 or 30 mM).

PPG	R	Solvent ratio (CD_3CN/phosphate buffer pH 7.0)	Effect of solvent on photoproducts		
			RSO_2NH_2	**RSO_2NHOH**	**RSO_2^-**
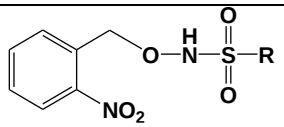 **2-NO_2Bn-ON(H)-SO_2R**	**CF_3**	60/40	91	0	9
	CH_3	100/00	100	0	0
		80/20	100	0	0
		60/40	100	0	0
		10/90	100	0	0
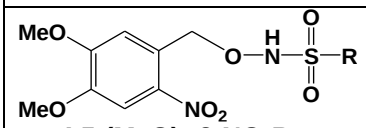 **4,5-(MeO)$_2$-2-NO_2Bn-ON(H)-SO_2R**	**CF_3**	60/40	93	0	7
	CH_3	60/40	100	0	0
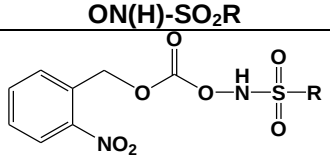 **2-NO_2Bn-OC(O)-ON(H)-SO_2R**	**CH_3**	60/40	12	71	17[a]
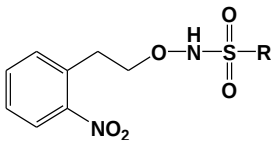 **2-NPE-ON(H)-SO_2R**	**CF_3**	100/00	72	0	28
		80/20	70	0	30
		60/40	67	0	33
		40/60	70	0	30
		10/90	72	0	28
	CH_3	100/00	7	85	8
		80/20	7	85	8
		60/40	8	85	7
		40/60	7	85	8
		10/90	6	85	9
	Ar[b]	100/00	45	0	43[c]
		80/20	40	50[c,d]	
		60/40	10	85[c,d]	
		40/60	14	83[c,d]	
		10/90	11	85[c,d]	
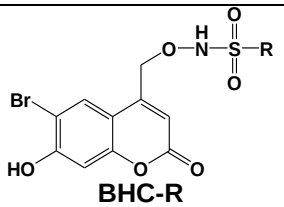 **BHC-R**	**CF_3**	100/00	18	0	82
		90/10	25	0	75
		60/40	40	0	60
		40/60	55	0	45
		10/90	70	0	30
		8/92	75	0	25
	CH_3	100/00	82	8	6[a,c]
		40/60	77	7	9[a,c]
		10/90	79	5	11[a,c]

[a]$CH_3SO_2^-$ + $CH_3SO_3^-$. [c]Small amount of one or more unknown species.

b 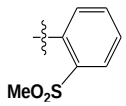 [d]$ArSO_2NHOH + ArSO_2^-$. $ArSO_2NHOH$ decomposes further to give $ArSO_2^-$.

Table 5.2. Effect of pH of the aqueous component of the solvent on the photoproducts derived from the *N*-hydroxysulfonamide for photodecomposition of the various compounds (1.0 mM) in 10:90 v/v CD_3CN: aqueous solution (0, 5 or 30 mM buffer).

PPG	R	pH[b]	Effect of pH on photoproducts		
			RSO_2NH_2	**RSO_2NHOH**	**RSO_2^-**
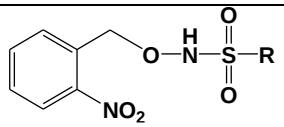 **2-NO_2Bn-ON(H)-SO_2R**	**CH_3**	1.0	100	0	0
		7.0	100	0	0
		12.0	100	0	0
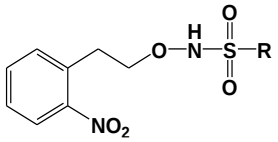 **2-NPE-ON(H)-SO_2R**	**CF_3**	2.1	23	75	0[c]
		5.0	69	0	31
		7.0	67	0	33
		10.0	70	0	30
	CH_3	3.1	15	75	10
		5.0	10	82	8
		7.0	7	85	8
		9.9	72	13	15
		12.0	73	12	15
	Ar[a]	1.0	10	86[c,d]	
		3.1	10	86[c,d]	
		5.0	9	86[c,d]	
		7.0	11	85[c,d]	
		10.0	9	85[c,d]	
		12.0	5	93[c,d]	
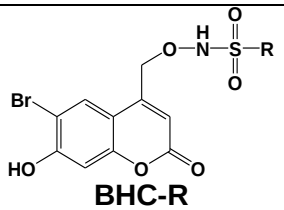 **BHC-R**	**CF_3**	2.1	100	0	0
		5.0	70	0	30
		7.0	68	0	32
		10.0	72	0	28
	CH_3	2.1	78	8	8[c,e]
		5.0	78	8	7[c,e]
		7.0	81	11	8[e]
		10.0	40	4	56[e]
		10.7	39	5	56[e]

a 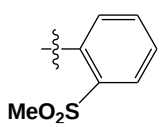

[b] In 10:90 v/v CD_3CN: buffer; phosphate buffer at pH 2.1, 3.1 and 7.0, acetate buffer at pH 5.0, carbonate buffer at pH 9.9, 10.0, and 10.7, 0.10 M HCl at pH 1.0 and 0.10 M NaOH at pH 12.0.

[c] Small amount of one or more unknown species.

[d] $ArSO_2NHOH$ + $ArSO_2^-$. $ArSO_2NHOH$ decomposes further to give $ArSO_2^-$.

[e] $CH_3SO_2^-$ + $CH_3SO_3^-$.

However more O-N bond cleavage is observed for **BHC-CF_3** compared with **BHC-CH_3**, consistent with the increased acidity of the methylene protons as a result of the stronger electron-withdrawing group for the former compound. The protonation state of the OH and the presence of triplet state quenchers did not affect the photoproduct percentages.

From the experimental data it is proposed that heterolytic O-N, C-O and/or C-O/N-S bond cleavage occur in the singlet excited state molecule. Concerted heterolytic C-O/N-S bond cleavage generates a solvent-caged carbocation and $^1NO^-$. The carbocation reacts rapidly with nucleophiles, including solvent and (H)NO, with the latter reaction ultimately generating an oxime. Increasing the aqueous component of CD_3CN/aqueous buffer mixtures and promotes solvent-assisted deprotonation of a methylene proton which results in undesired O-N bond cleavage.

There are a number of similarities between these three systems. Firstly, heterolytic bond cleavage occurs for all systems. Secondly, deprotonation of the N(H) of the N-hydroxysulfonamide moiety results in a switch from C-O bond cleavage to concerted C-O/N-S bond cleavage, since expulsion of the dianion RSO_2NO^{2-} is not favourable. For the -CF_3 systems this pK_a is < 4, hence the HNO generating pathway was observed rather than C-O bond cleavage under almost all experimental conditions except in strongly acidic solutions. However, for the -CH_3 and Piloty's acid analogues this pK_a is considerably higher (~ 10), so C-O bond cleavage is observed except at highly alkaline pH conditions. Thirdly, deprotonation of the N(H) for the -CF_3 systems in particular can result in increased O-N bond cleavage, since deprotonation of the methylene proton is required for O-N bond cleavage for the 2-NO_2Bn and BHC systems. Deprotonation of the N(H) is expected to decrease the electron withdrawing properties of the N-hydroxysulfonamide, but it appears that -$ON^-SO_2CF_3$ is also a good electron withdrawing group which increases the acidity of the methylene protons for these two systems compared with the corresponding -$ON^-SO_2CH_3$ analogues.

A range of additional experiments would provide additional information on these systems. Although it was not realized earlier on in this research, the pK_a for the N(H) of the 2-nitroBn caged compounds is likely to also affect the mechanism of photodecomposition, and could also be investigated for these systems. Investigating

the rate of decay of the aci-nitro intermediate formed for the 2-nitro and (2-nitrophenyl) ethyl systems as a function of the pH in aqueous buffer mixtures could provide more detailed information on the role of the protonation state in the bond cleavage pathways. Transient absorption and IR spectroscopy measurements would be useful here. Femtosecond time resolved absorption experiments and time resolved fluorescence experiments (coumarinylmethyl systems) could also be carried out, to provide further information on the excited state events. Finally, DFT calculations are urgently needed, to obtain a better understanding of the factors which determine which bond cleavage pathway dominates. This is now underway, in collaboration with a group in Hong Kong. DFT calculations will help us to rationalize the effect of the protonation state of the molecules on the energies and bond lengths of the ground state species and singlet excited states and to determine whether the bond cleavage is likely to be homolytic followed by rapid electron transfer or heterolytic (by calculating energies of species, including the intermediate when homolysis occurs). Calculations can also be used to simulate spectra of short-lived intermediates; however for this to be useful the intermediates need to be spectroscopically distinguishable from other species.

Other systems have recently been synthesized in the labs of our US collaborators or are currently being synthesized. Based on the results presented in this thesis and in the thesis of Dr Ruth Cink, the (6-bromo-7-hydroxycoumarin-4-yl)methyl and (6-hydroxynapthalen-2-yl)methyl caged *N*-hydroxysulfonamides appear to be the most promising photoactive HNO donors. A major problem in both these systems is that a solvent caged carbocation, $^{1}NO^{-}$ (and sulfinate) are formed upon C-O/N-S bond cleavage. Nucleophilic attack by NO^{-} on the carbocation results in an oxime product rather than HNO being generated. To prevent oxime formation, the synthesis of new systems is currently underway where intramolecular carbocation trapping will prevent oxime formation. The synthesis of analogues with one or two substituents at the benzylic carbon is also underway, since deprotonation at this carbon is required for O-N bond cleavage and substituents at this site will affect the stability of the ground and excited state molecules. For the (6-hydroxynapthalen-2-yl)methyl caged N-hydroxysulfonamides, preliminary results in our collaborators' labs show that substituting the OH on the naphthalene ring for a methoxy substituent further promotes the HNO-releasing pathways. Detailed mechanistic studies on all these systems will provide valuable information on the key factors which determine the fate of systems

caged with these chromophores upon irradiation. This will assist us and others interested in the rationale design of photocaged molecules - an exciting field of importance to both chemistry and biology.

Glossary

Abs	Absorbance
AS	Angeli's Salt
DMSO	Dimethyl sulfoxide
EtOH	Ethanol
GC-MS	Gas Chromatography-Mass Spectrometry
HNM	(Hydroxynaphthenyl)methyl
IC	Internal Conversion
ISC	Intersystem Crossing
LC-HRMS	Liquid Chromatography-High Resolution Mass Spectrometry
LFP	Laser Flash Photolysis
MO	Molecular Orbital
MS	Mass Spectrum
Nd: YAG	Neodymium-Doped Yttrium Aluminium Garnet
NMR	Nuclear Magnetic Resonance
Ns	Nanosecond
PA	Piloty's Acid
Ps	Picosecond
S	Singlet State
T	Triplet State
TSP	3-(Trimethylsilyl)propionic-2,2,3,3-d4 acid sodium salt
UV-Vis	Ultraviolet-Visible
E	Molar Extinction Coefficient
λ_{max}	Wavelength at Maximum Absorbance
Ms	Microsecond
Φ	Photoproduct Quantum Yield

Appendix

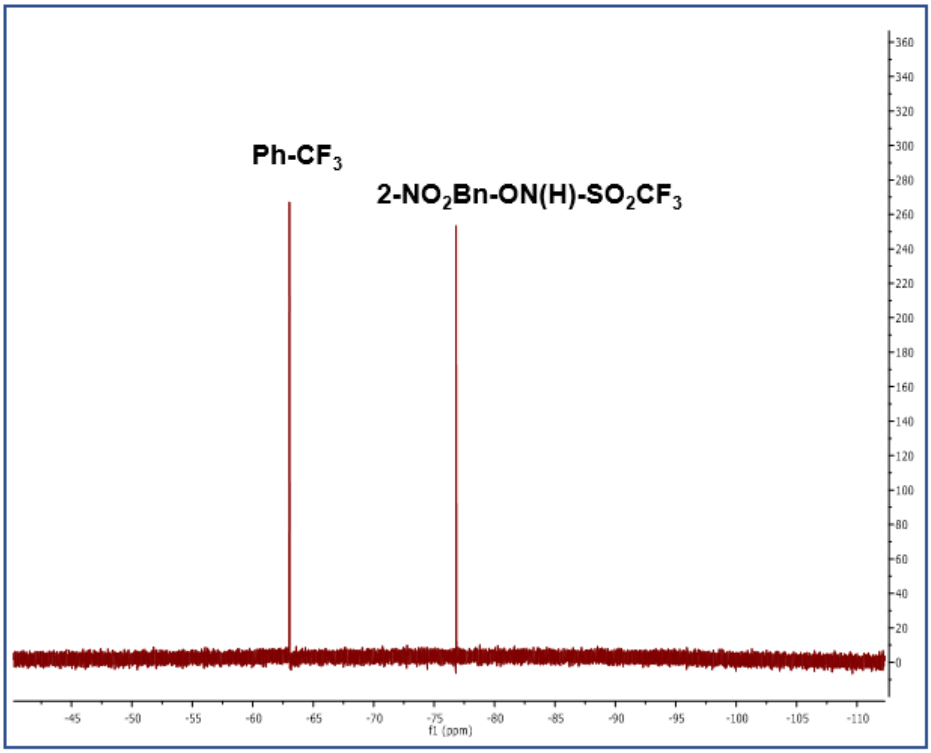

(a)

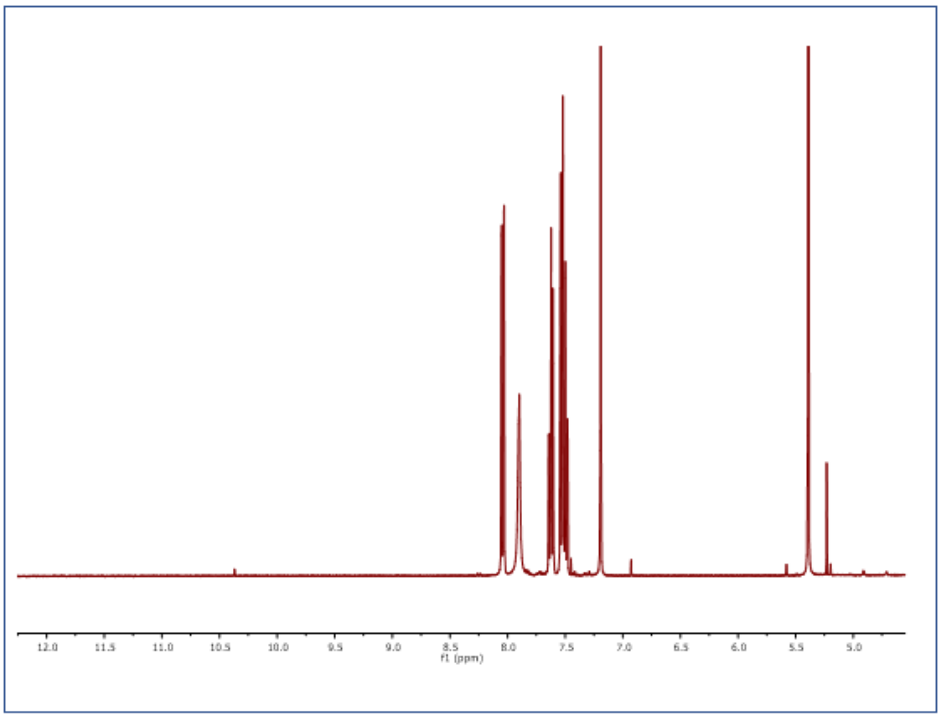

(b)

Figure A2.1. (a) ^{19}F NMR spectrum of **2-NO_2Bn-ON(H)SO_2CF_3** (-76.8 ppm). Ph-CF_3 (-62.9 ppm) was used as an external reference. (b) ^{1}H NMR spectrum in $CDCl_3$ after column chromatography. δ 8.13 (dd, *J* = 8.0, 1.2 Hz, 1H), 7.83-7.78 (m, 2 H), 7.69 (td, *J* = 8.0, 2.0 Hz, 1 H), 5.48 (s, 2 H), 3.47 (s, 6 H).

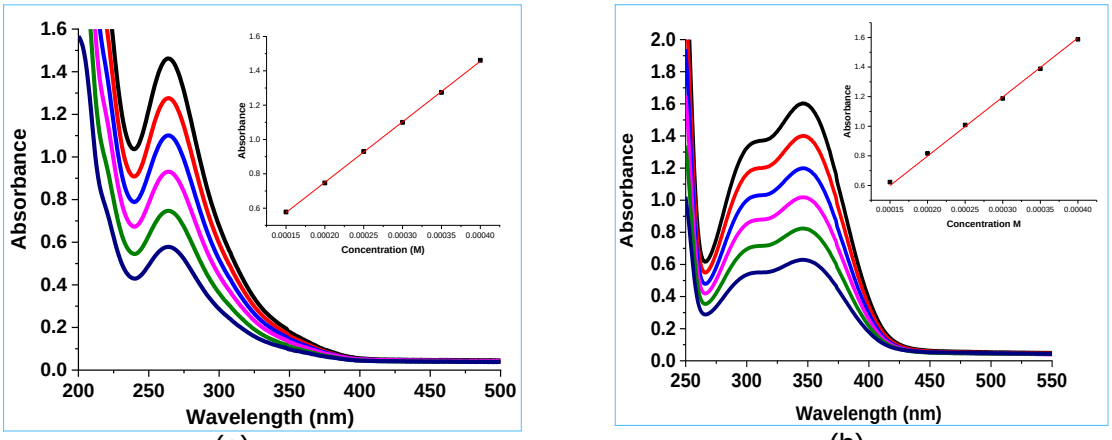

(a) (b)

Figure A2.2. UV-Vis spectra of (a) **2-NO_2Bn-ON(H)-SO_2CF_3** and (b) **4,5-$(MeO)_2$-2-NO_2Bn-ON(H)-SO_2CF_3** in a mixture of H_2O and CH_3CN (92%:8%, v/v) at a range of concentrations (150, 200, 250, 300, 350 and 400 µM). Inset: Plot of absorbance at 264 nm versus concentration of (a) **2-NO_2Bn-ON(H)-SO_2CF_3** and (b) **4,5-$(MeO)_2$-2-NO_2Bn-ON(H)-SO_2CF_3.** The best fit of the data to a line passing through the origin gives ε(**2-NO_2Bn-ON(H)SO_2CF_3**) = (3.68 ± 0.02) × 10^3 M^{-1} cm^{-1} and ε(**4,5-$(MeO)_2$-2-NO_2Bn-ON(H)SO_2CF_3**)= (3.99 ± 0.02) × 10^3 M^{-1} cm^{-1}.

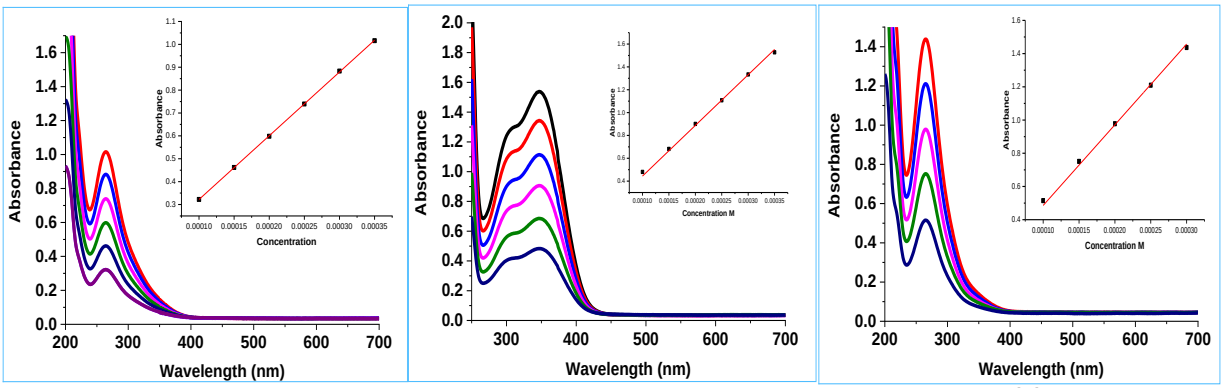

(a) (b) (c)

Figure A2.3. UV-Vis spectra of (a) **2-NO_2Bn-ON(H)-SO_2CH_3** (b) **4,5-$(MeO)_2$-2-NO_2Bn-ON(H)-SO_2CH_3** and (c) **2-NO_2Bn-OC(O)-ON(H)-SO_2CH_3** in a mixture of H_2O and CH_3CN (92%:8%, v/v) at a range of concentrations (100, 150, 200, 250, 300, and 350 µM). Inset: Plot of absorbance at 264 nm versus concentration of **2-NO_2Bn-ON(H)-SO_2CH_3**, **4,5-$(MeO)_2$-2-NO_2Bn-ON(H)-SO_2CH_3** and **2-NO_2Bn-OC(O)-ON(H)-SO_2CH_3**. The best fit of the data to a line passing through the origin gives ε(**2-NO_2Bn-ON(H)-SO_2CH_3**) = (2.95 ± 0.02) × 10^3 M^{-1} cm^{-1}, ε(**4,5-$(MeO)_2$-2-NO_2Bn-ON(H)SO_2CH_3**) = (4.44 ± 0.04) × 10^3 M^{-1} cm^{-1}) and ε(**2-NO_2Bn-OC(O)-ON(H)-SO_2CH_3**) = (4.86 ± 0.03) × 10^3 M^{-1} cm^{-1}).

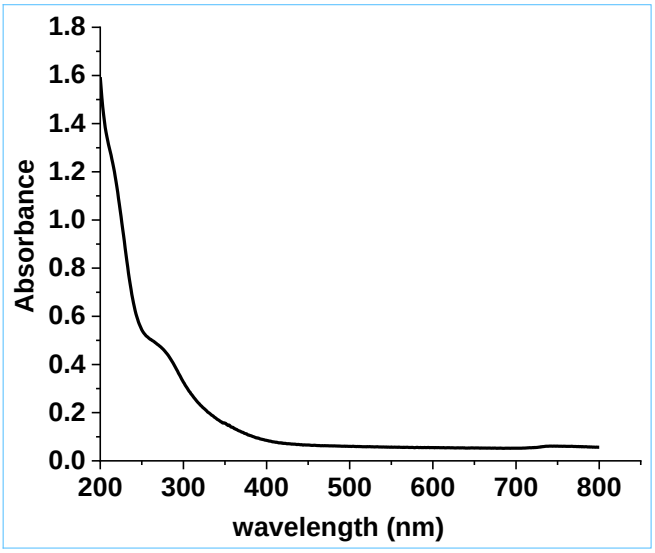

Figure A2.4. UV-Vis spectrum of potassium ferrioxalate in H_2O at 25°C.

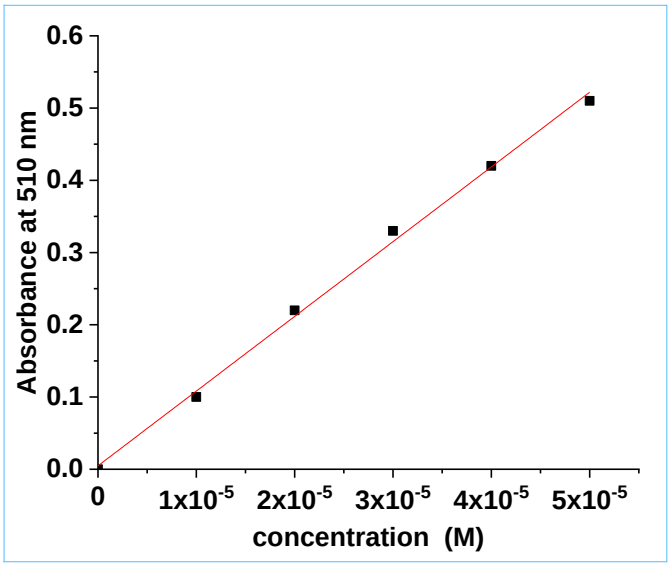

Figure A2.5. Plot of absorbance at 510 nm versus concentration of $[Fe(phen)_3]^{2+}$. The molar extinction coefficient (slope) is $(1.03 \pm 0.02) \times 10^4$ M^{-1} cm^{-1}.

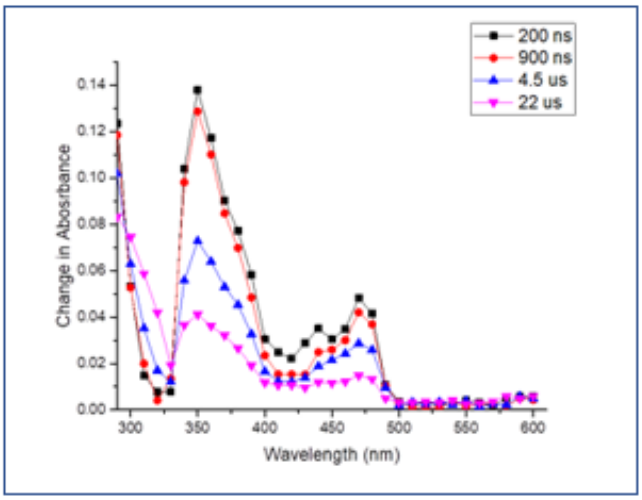

Figure A2.6. Transient absorption spectral changes of 2-naphthol (150 μM) *tris*(bipyridine)ruthenium(II) chloride [$Ru(bipy)_3Cl_2$] in oxygenated MeCN. The data were collected at 370 nm after photoexcitation at 355 nm. 1.0 mm slit width after sample, primary monochromator; 2.5 mm slit width, secondary monochromator.

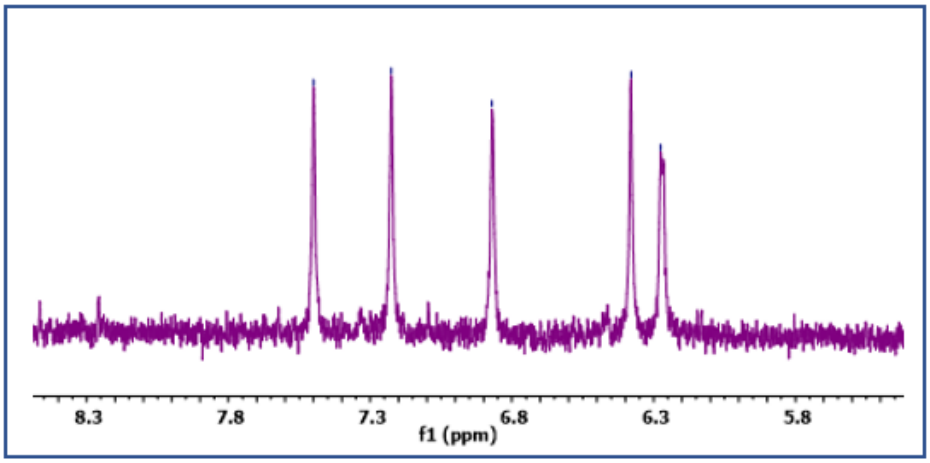

Figure A2.7. ^{1}H NMR spectrum of the aromatic region of NOCbl dissolved in TES buffer (0.010M, pD 7.4) in D_2O: chemical shifts 7.42, 7.21 ,6.82, 6.35, 6.26 (d) ppm.

A1.1 Determining the stoichiometry of the reaction between hydroxocobalamin and CF_3SO_2NHOH

Prior to the stochiometric experiment the concentration of HOCbl and CF_3SO_2NHOH were determined from UV-Vis and ^{19}F NMR spectroscopy. A solution was prepared by diluting a stock solution of HOCbl•HCl (~5 ×10^{-4} M, 0.28 mL) in carbonate buffer (0.30 M, 2.72 mL). The UV-Vis spectrum was recorded immediately (Figure A2.8), and the average absorbance value at 475 nm was 0.320 (two separate experiments; ε_{475nm}= 6.99 × 10^3 M^{-1} cm^{-1}), giving a concentration of (4.6 ± 0.1) × 10^{-5} M (2% error).

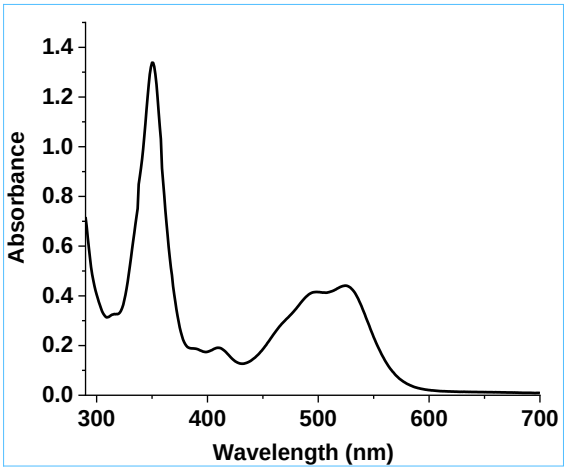

Figure A2.8. UV−Vis spectrum of HOCbl (4.6 ± 0.1) $\times 10^{-5}$ M at pH 9.96 under anaerobic conditions.

An anerobic sample of CF_3SO_2NHOH (1 mM) was obtained from our collaborator's lab at Kent State University. It was stored in the glove box for ~10 months. A sample (~1 mM, 440 µL) in CD_3OD and α,α,α-trifluorotoluene, Ph-CF_3 (10.0 µL, 52.75 mM) in CD_3OD were transferred to an NMR tube fitted with a J-Young airtight cap. The ^{19}F NMR spectrum was recorded immediately as shown in Figure A2.9. By integrating the peaks of CF_3SO_2NHOH and Ph-CF_3, the concentration of the CF_3SO_2NHOH stock solution was found to be 1.03 ± 0.05 mM (~5% error). A correction was made for ~8% $CF_3SO_2^-$ impurity in the stock CF_3SO_2NHOH solution.

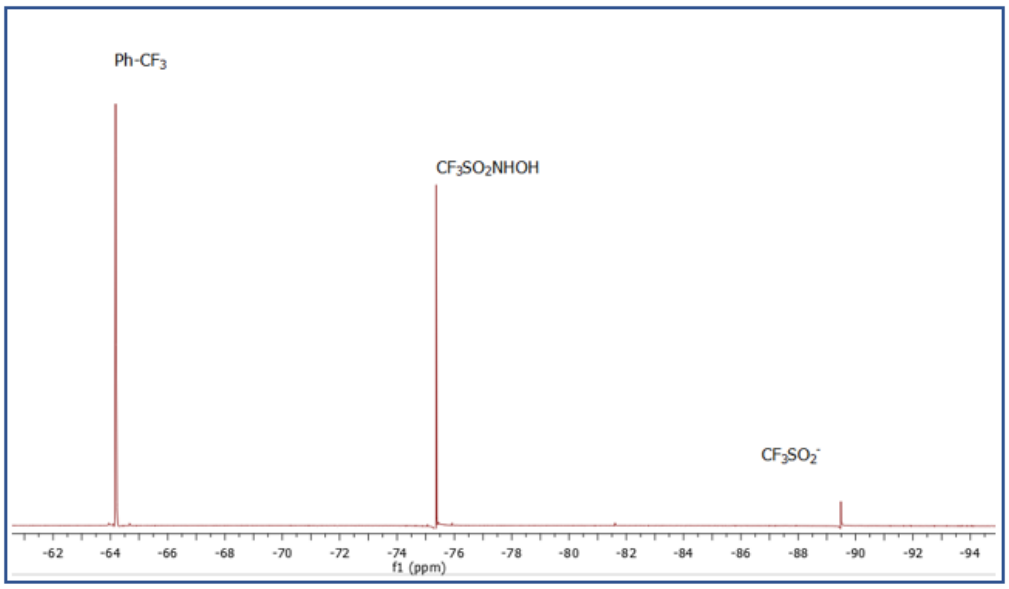

Figure A2.9. ^{19}F NMR spectrum of CF_3SO_2NHOH in methanol (Ph-CF_3 as a standard).

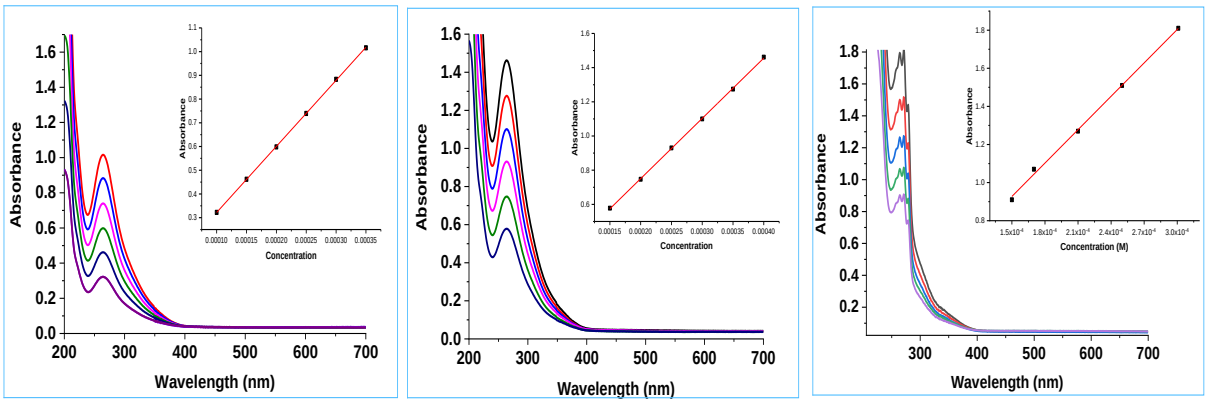

(a) (b) (c)

Figure A3.1.UV-Vis spectrum of (a) **2-NPE-ON(H)-SO_2CF_3** (100, 150, 200, 250, 300 and 350 µM), (b) **2-NPE-ON(H)-SO_2CH_3** (150, 200, 250, 300, 350 and 400 µM) and (c) **2-NPE-ON(H)-SO_2Ar** (150, 200, 250, 300, 350 and 400 µM) in a mixture of water and CH_3CN (92:8 v/v) at a range of concentrations at 25.0 °C. Inset: Plot of absorbance at 264 nm versus concentration of **2-NPE-ON(H)-SO_2CF_3.** The best fit of the data to a line passing through the origin gives a molar extinction coefficient, $\varepsilon = (2.87 \pm 0.01) \times 10^3$ M^{-1} cm^{-1}, $\varepsilon = (4.17 \pm 0.01) \times 10^3$ M^{-1} cm^{-1} and $\varepsilon = (6.06 \pm 0.03) \times 10^3$ M^{-1} cm^{-1}.

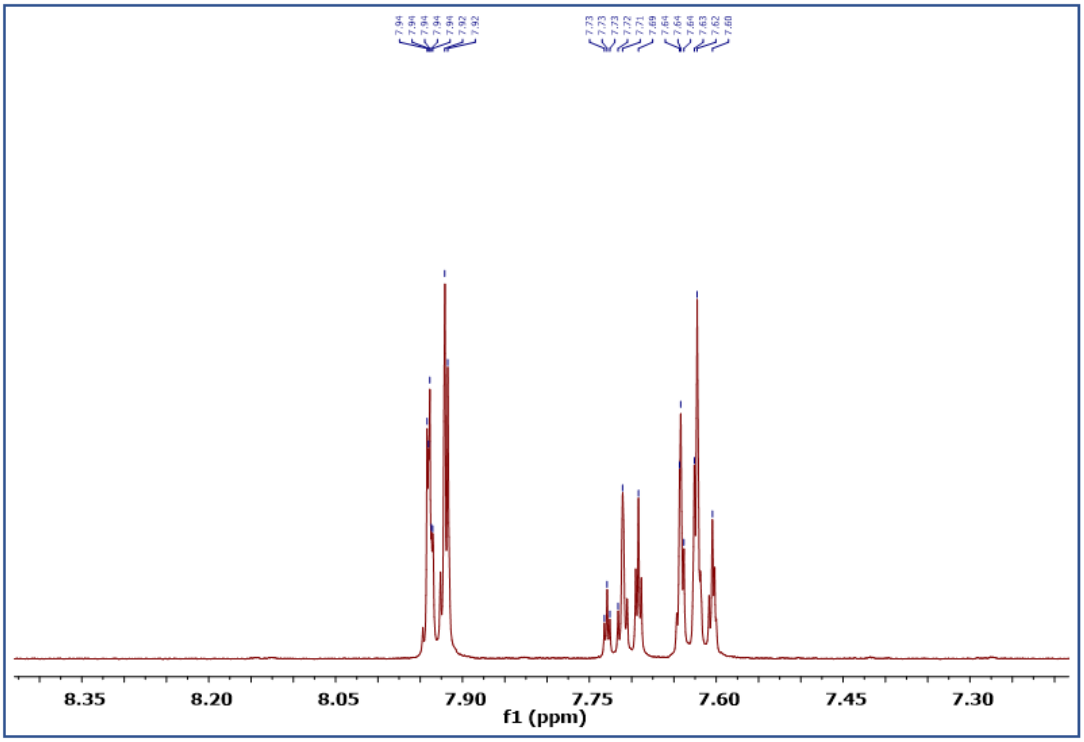

Figure A3.2. ^1H NMR spectrum of Piloty's acid in acetone-d_6 (δ = 7.94, 7.93, 7.92, 7.73, 7.72, 7.69, 7.64, 7.62, 7.60 ppm).

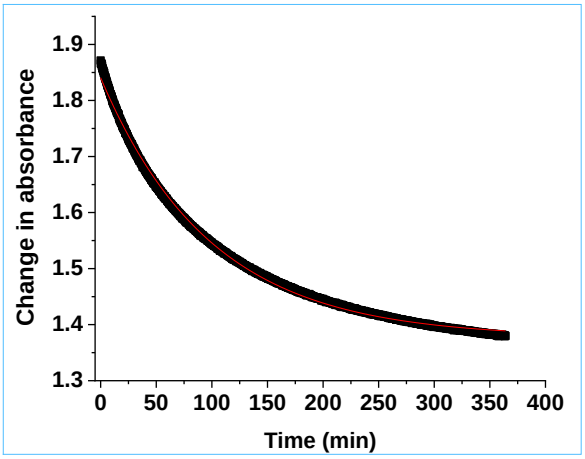
Change in absorbance
1.9
1.8
1.7
1.6
1.5
1.4
1.3
0 50 100 150 200 250 300 350 400
Time (min)

(a)

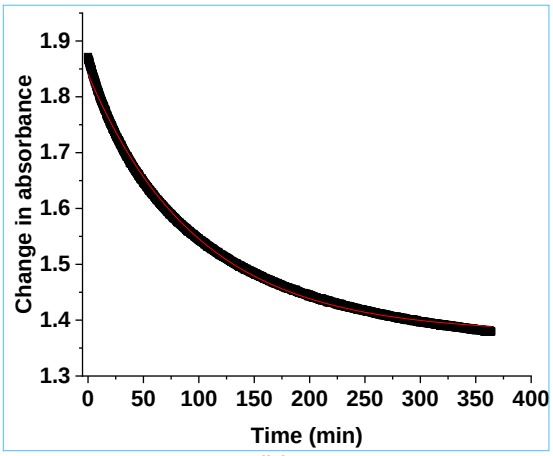
Change in absorbance
1.9
1.8
1.7
1.6
1.5
1.4
1.3
0 50 100 150 200 250 300 350 400
Time (min)

(b)

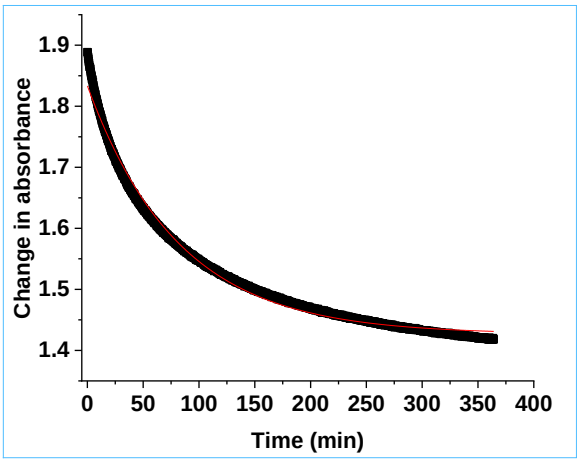
Change in absorbance
1.9
1.8
1.7
1.6
1.5
1.4
0 50 100 150 200 250 300 350 400
Time (min)

(c)

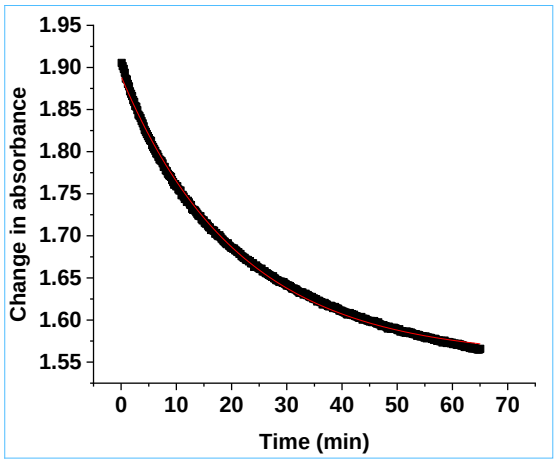
Change in absorbance
1.95
1.90
1.85
1.80
1.75
1.70
1.65
1.60
1.55
0 10 20 30 40 50 60 70
Time (min)

(d)

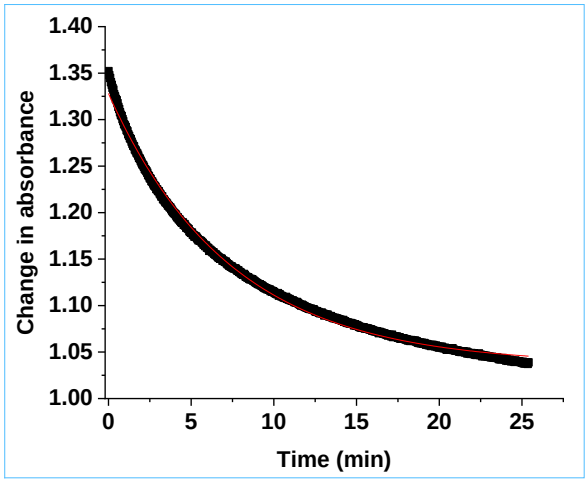
Change in absorbance
1.40
1.35
1.30
1.25
1.20
1.15
1.10
1.05
1.00
0 5 10 15 20 25
Time (min)

(e)

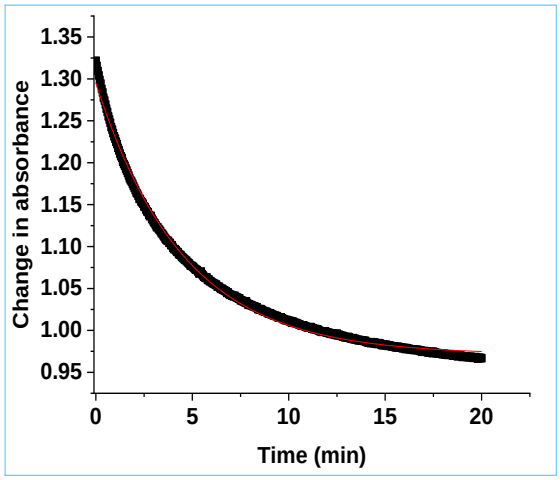
Change in absorbance
1.35
1.30
1.25
1.20
1.15
1.10
1.05
1.00
0.95
0 5 10 15 20
Time (min)

(f)

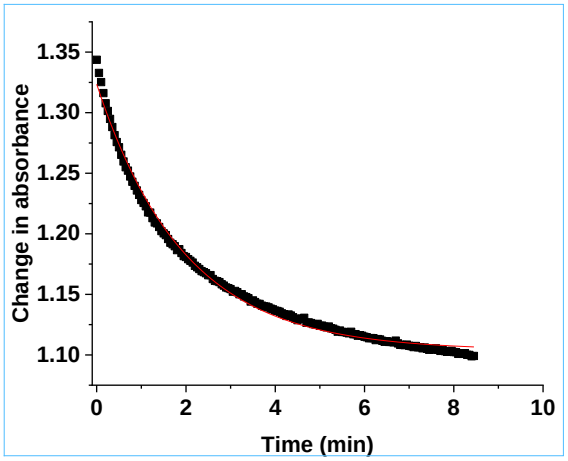

(g)

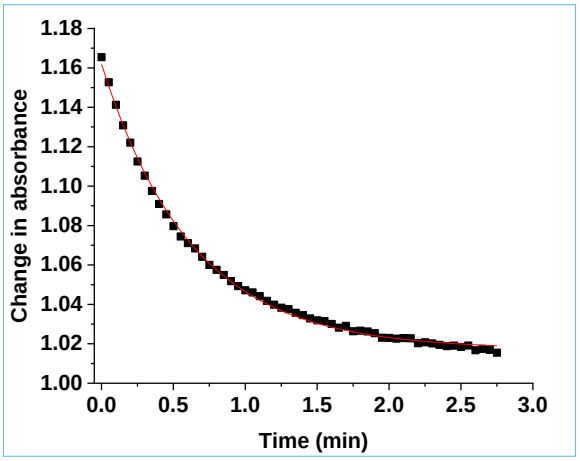

(h)

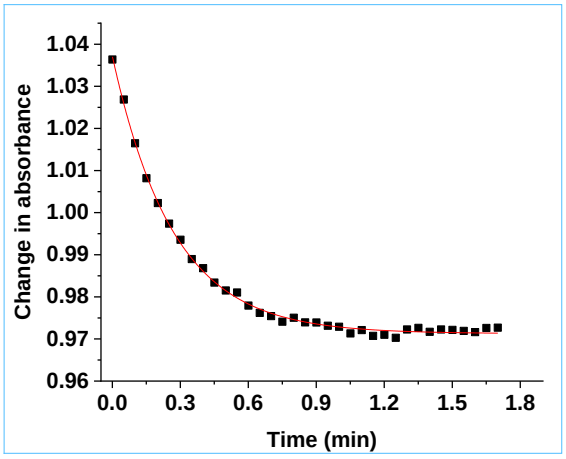

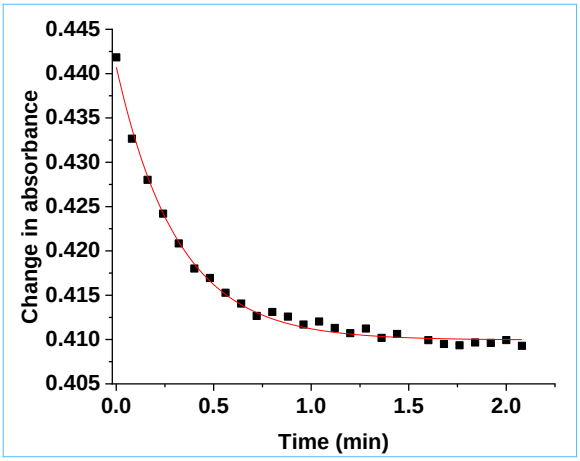

(j)

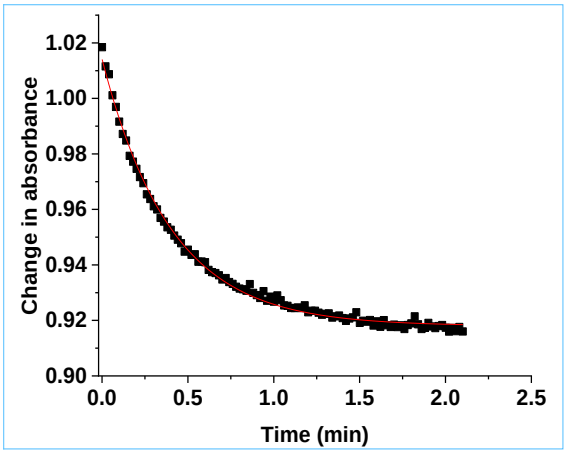

(k)

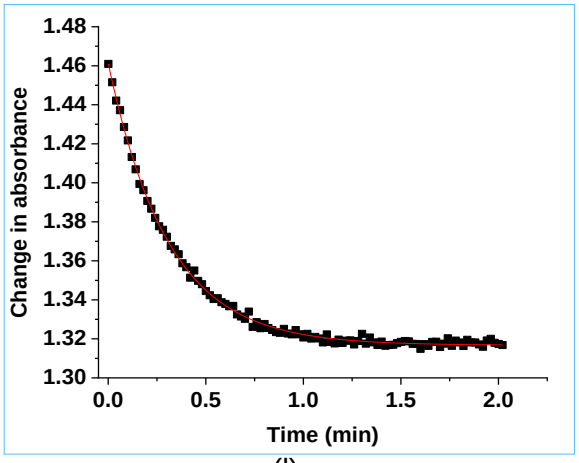

(l)

Figure A3.3. Plots of absorbance at 272 nm versus time for the spontaneous decomposition of 2-(SO_2Me)$PhSO_2NHOH$ at (a) pH 3.0 (b) pH 5.0 (c) pH 6.5 (d) pH 7.0 (e) pH 7.5 (f) pH 8.0 (g) pH 8.5 (h) pH 9.0 (i) pH 9.5 (j) pH 9.75 (k) 10.5 (l) pH 11.0. The best fit of the data to a first-order equation gave k_{obs} = (a) pH 3.0 - (4.30 ± 0.07) × 10^{-3} (b) pH 5.0 - (4.87 ± 0.08) × 10^{-3} (c) pH 6.5 – (1.01 ± 0.07) × 10^{-2} min^{-1} (d) pH 7.0 - (4.62 ± 0.03) × 10^{-2} min^{-1} (e) pH 7.5 – (1.40 ± 0.02) × 10^{-1} min^{-1} (f) pH 8.0 – (2.22 ± 0.04) × 10^{-2} min^{-1} (g) pH 8.5 – (5.10 ± 0.09) × 10^{-1} min^{-1} (h) pH 9.0 – 1.59 ± 0.04 min^{-1} (i) pH 9.5 – 2.51 ± 0.03 (j) pH 9.75- 3.27 ± 0.05 (k) pH 10.5 – 3.71 ± 0.07 (l) pH 11.0 – 3.68 ± 0.05.

Table A3.1. Effect of solvent ratio on the photoproducts and observed rate constant for photodecomposition of **2-NPE-ON(H)-SO_2CF_3** (1.0 mM). Two separate experiments were carried out. The percentages of products were determined by integration of the ^{19}F NMR spectra after complete photolysis.

Solvent ratio, % v/v (CD_3CN/30 mM phosphate buffer, pH 7.0)	Percentage of Photoproducts		k_{obs} (min^{-1})
	$CF_3SO_2NH_2$	$CF_3SO_2^-$	
100/00	72	28	0.142 ± 0.011
80/20	70	30	0.138 ± 0.012
60/40	67	33	0.135 ± 0.013
40/60	70	30	0.137 ± 0.011
10/90	72	28	0.142 ± 0.012

Solvent ratio, % v/v (CD_3CN/30 mM phosphate buffer, pH 7.0)	Percentage of Photoproducts		k_{obs} (min^{-1})
	$CF_3SO_2NH_2$	$CF_3SO_2^-$	
100/00	72	33	0.139 ± 0.011
80/20	70	30	0.135 ± 0.011
60/40	67	33	0.133 ± 0.011
40/60	70	30	0.135 ± 0.011
10/90	72	28	0.136 ± 0.011

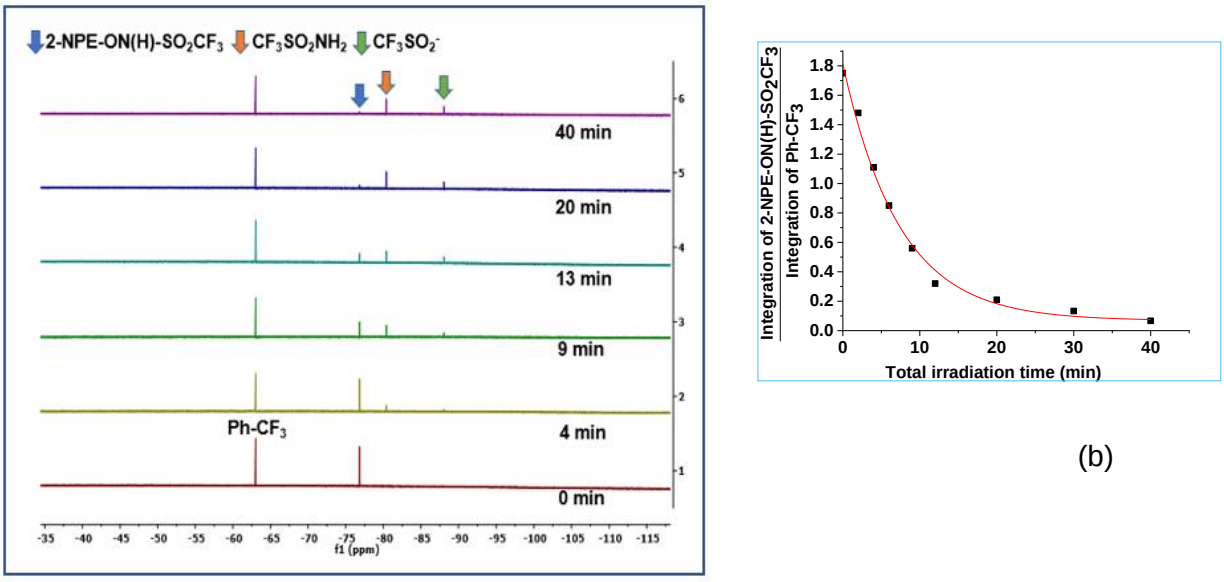

(a) (b)

Figure A3.4. (a) Stack of ^{19}F NMR spectra for the photolysis of **2-NPE-ON(H)-SO_2CF_3** (1.0 mM) in a 60:40 mixture of CD_3CN and phosphate buffer (30.0 mM, pH 7.0). (b Ratio of the area of the CF_3 signal of **2-NPE-ON(H)-SO_2CF_3** and the **Ph-CF_3** reference versus time. The best fit of the data to a first-order rate equation gives k_{obs} = 0.134 ± 0.001 min^{-1} ($t_{1/2}$ ~ 4.9 min).

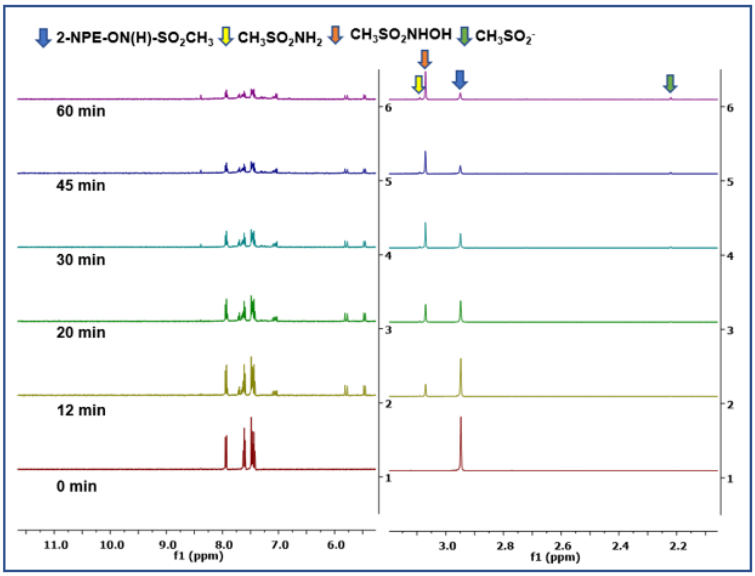

(a)

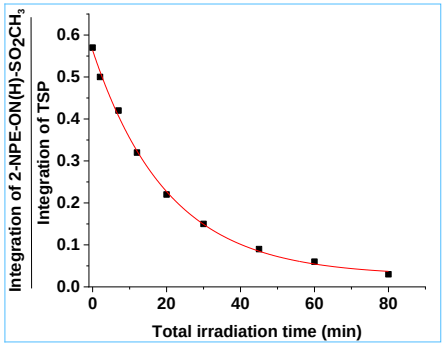

(b)

Figure A3.5. (a) Stack of ^{1}H NMR spectra for the photolysis of **2-NPE-ON(H)-SO$_2$CH$_3$** (1.0 mM) in in a mixture of phosphate buffer (pH 7.0, 30.0 mM) and CD_3CN (60:40). (b Ratio of the area of the CH_3 signal of **2-NPE-ON(H)-SO$_2$CH$_3$** and the **TSP** reference versus time. The best fit of the data to a first-order rate equation gives k_{obs} = 0.056 ± 0.005 min^{-1} ($t_{1/2}$ ~ 12 min).

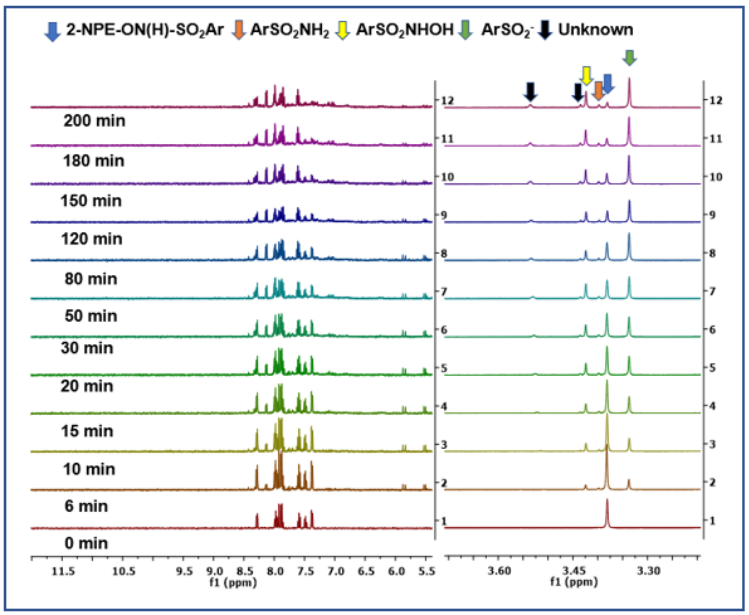

(a)

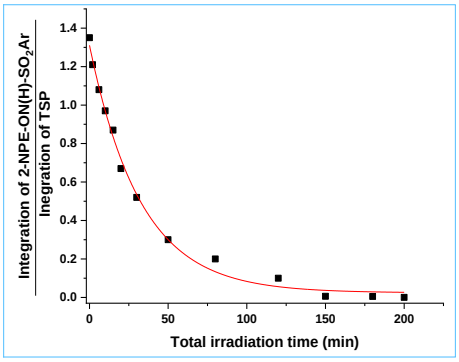

(b)

Figure A3.6. (a) ^{1}H NMR spectra for the photolysis of **2-NPE-ON(H)-SO$_2$Ar** (1.0 mM) in a mixture of phosphate buffer (pH 7.0, 30.0 mM) and CD_3CN (40:60). (b) Ratio of the area of the CH_3 signal of **2-NPE-ON(H)-SO$_2$CH$_3$** and the **TSP** reference versus time. The best fit of the data to a first-order rate equation gives k_{obs} = 0.033 ± 0.006 min^{-1} ($t_{1/2}$ ~ 21 min).

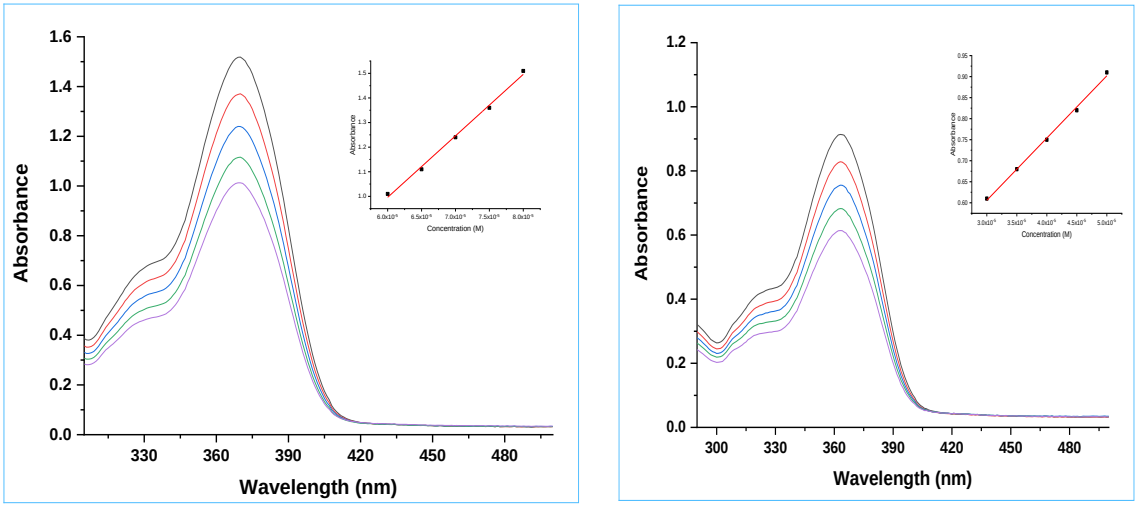

(a) (b)

Figure A4.1. UV-vis spectrum of (a) **BHC-CF_3** (600, 650, 700, 750 and 800 µM) and (b) **BHC-CH_3** (300, 350, 400, 450 and 500 µM) in a mixture of water and CH_3CN (92:8 v/v) at a range of concentrations at 25.0 °C. Inset: Plot of absorbance at 370 nm versus concentration**.** The best fit of the data to a line passing through the origin gives a molar extinction coefficient, $\varepsilon_{370\ nm}$ = (2.50 ± 0.03) × 10^4 M^{-1} cm^{-1}, $\varepsilon_{366\ nm}$ = (1.42 ± 0.02) × 10^4 M^{-1} cm^{-1}.

Equation A4.1. Relationship between observed absorbance and the ratio of acid and conjugate base

$$A_{obs} = fraction_{HA}\ A_{HA} + fraction_{A^-}\ A_{A^-}$$

$$A_{obs} = \frac{[HA]}{[HA] + [A^-]}\ A_{HA} + \frac{[A^-]}{[HA] + [A^-]}\ A_{A^-}$$

$$\frac{[A^-]}{[HA]} = \frac{A_{obs} - A_{HA}}{A_{A^-} - A_{obs}}$$

Substituting into the Henderson-Hasselbalch equation:

$$pH = pK_a + \log \frac{[A^-]}{[HA]}$$

$$pH = pK_a + \log \frac{A_{obs} - A_{HA}}{A_{A^-} - A_{obs}}$$

$$A_{obs} = \frac{A_{HA} + A_{A^-}(10^{pH-pKa})}{1 + (10^{pH-pKa})}$$

A_{HA} and A_{A^-} are the absorbances of the acid and its conjugate base, respectively.

Similarly, for the NMR titration data, the relationship between the observed chemical shift δ_{obs} and δ_{HA} and δ_{A^-} is

$$\delta_{obs} = \frac{\delta_{HA} + \delta_{A^-} (10^{pD-pKa})}{1 + (10^{pD-pKa})}$$

δ_{HA} and δ_{A^-} are chemical shifts of the acid and its conjugate base, respectively.

For the UV-Vis spectroscopic titration data, the values of k_{obs} were plotted as a function of pH and the data fitted to

$$k_{obs} = \frac{k \times 10^{pH-pKa}}{1 + 10^{pH-pKa}}$$

The rate constants k_{obs} and k are the observed rate constant and the second-order rate constant, respectively.

References

1. Doctorovich, F.; Bikiel, D.; Pellegrino, J.; Suarez, S. A.; Larsen, A.; Marti, M. A., Nitroxyl (azanone) trapping by metalloporphyrins. *Coordination Chemistry Reviews* **2011,** *255* (23-24), 2764-2784.
2. Shafirovich, V.; Lymar, S. V., Nitroxyl and its anion in aqueous solutions: Spin states, protic equilibria, and reactivities toward oxygen and nitric oxide. *Proceedings of the National Academy of Sciences of the United States of America* **2002,** *99* (11), 7340-7345.
3. Paolocci, N.; Jackson, M. I.; Lopez, B. E.; Miranda, K.; Tocchetti, C. G.; Wink, D. A.; Hobbs, A. J.; Fukuto, J. M., The pharmacology of nitroxyl (HNO) and its therapeutic potential: Not just the janus face of NO. *Pharmacology & Therapeutics* **2007,** *113* (2), 442-458.
4. Miranda, K. M.; Katori, T.; de Holding, C. L. T.; Thomas, L.; Ridnour, L. A.; McLendon, W. J.; Cologna, S. M.; Dutton, A. S.; Champion, H. C.; Mancardi, D.; Tocchetti, C. G.; Saavedra, J. E.; Keefer, L. K.; Houk, K. N.; Fukuto, J. M.; Kass, D. A.; Paolocci, N.; Wink, D. A., Comparison of the NO and HNO donating properties of diazeniumdiolates: Primary amine adducts release HNO in vivo. *Journal of Medicinal Chemistry* **2005,** *48* (26), 8220-8228.
5. Fehling, C.; Friedrichs, G., Dimerization of HNO in Aqueous Solution: An Interplay of Solvation Effects, Fast Acid-Base Equilibria, and Intramolecular Hydrogen Bonding? *Journal of the American Chemical Society* **2011,** *133* (44), 17912-17922.
6. Ferrer-Sueta, G.; Campolo, N.; Trujillo, M.; Bartesaghi, S.; Carballal, S. n.; Romero, N.; Alvarez, B.; Radi, R., Biochemistry of peroxynitrite and protein tyrosine nitration. *Chemical reviews* **2018,** *118* (3), 1338-1408.
7. Miao, Z. R.; King, S. B., Recent advances in the chemical biology of nitroxyl (HNO) detection and generation. *Nitric Oxide-Biology and Chemistry* **2016,** *57*, 1-14.
8. Moncada, S.; Higgs, E., Endogenous nitric oxide: physiology, pathology and clinical relevance. *European Journal of Clinical Investigation* **1991,** *21* (4), 361-374.
9. Sharpe, M. A.; Cooper, C. E., Reactions of nitric oxide with mitochondrial cytochrome c: a novel mechanism for the formation of nitroxyl anion and peroxynitrite. *Biochemical Journal* **1998,** *332*, 9-19.
10. Wong, P. S.-Y.; Hyun, J.; Fukuto, J. M.; Shirota, F. N.; DeMaster, E. G.; Shoeman, D. W.; Nagasawa, H. T., Reaction between S-nitrosothiols and thiols: generation of nitroxyl (HNO) and subsequent chemistry. *Biochemistry* **1998,** *37* (16), 5362-5371.
11. Shoman, M. E.; Aly, O. M., Nitroxyl (HNO): A Reduced Form of Nitric Oxide with Distinct Chemical, Pharmacological, and Therapeutic Properties. *Oxidative Medicine and Cellular Longevity* **2016**, 15.
12. Irvine, J. C.; Ritchie, R. H.; Favaloro, J. L.; Andrews, K. L.; Widdop, R. E.; Kemp-Harper, B. K., Nitroxyl (HNO): the Cinderella of the nitric oxide story. *Trends in Pharmacological Sciences* **2008,** *29* (12), 601-608.
13. Flores-Santana, W.; Salmon, D. J.; Donzelli, S.; Switzer, C. H.; Basudhar, D.; Ridnour, L.; Cheng, R.; Glynn, S. A.; Paolocci, N.; Fukuto, J. M.; Miranda, K. M.; Wink, D. A., The Specificity of Nitroxyl Chemistry Is Unique Among Nitrogen Oxides in Biological Systems. *Antioxidants & Redox Signaling* **2011,** *14* (9), 1659-1674.
14. Ivanovic-Burmazovic, I.; Filipovic, M. R., Saying NO to H_2S: A Story of HNO, HSNO, and $SSNO^-$. *Inorganic Chemistry* **2019,** *58* (7), 4039-4051.
15. Miljkovic, J. L.; Filipovic, M. R., HNO/Thiol Biology as a Therapeutic Target. In *Redox-Active Therapeutics*, Springer: 2016; pp 335-375.
16. Stamler, J. S., Redox signaling: nitrosylation and related target interactions of nitric oxide. *Cell* **1994,** *78* (6), 931-936.
17. Shoeman, D. W.; Shirota, F. N.; DeMaster, E. G.; Nagasawa, H. T., Reaction of nitroxyl, an aldehyde dehydrogenase inhibitor, with N-acetyl-L-cysteine. *Alcohol* **2000,** *20* (1), 55-59.

18. Miranda, K. M., The chemistry of nitroxyl (HNO) and implications in biology. *Coordination Chemistry Reviews* **2005,** *249* (3-4), 433-455.
19. DeMaster, E. G.; Redfern, B.; Nagasawa, H. T., Mechanisms of inhibition of aldehyde dehydrogenase by nitroxyl, the active metabolite of the alcohol deterrent agent cyanamide. *Biochemical Pharmacology* **1998,** *55* (12), 2007-2015.
20. Edenberg, H. J., The genetics of alcohol metabolism: role of alcohol dehydrogenase and aldehyde dehydrogenase variants. *Alcohol Research & Health* **2007,** *30* (1), 5.
21. Lee, M. J.; Nagasawa, H. T.; Elberling, J. A.; DeMaster, E. G., Prodrugs of nitroxyl as inhibitors of aldehyde dehydrogenase. *Journal of Medicinal Chemistry* **1992,** *35* (20), 3648-3652.
22. Dux, M.; Will, C.; Vogler, B.; Filipovic, M. R.; Messlinger, K., Meningeal blood flow is controlled by H2S-NO crosstalk activating a HNO-TRPA1-CGRP signalling pathway. *British Journal of Pharmacology* **2016,** *173* (3), 431-445.
23. Cowart, D.; Aranda, J.; Haas, G.; Neutel, J.; Smith, W.; Mazhari, R.; Kalish, V.; Colucci, W., A phase I/IIA first in man safety and tolerability study of a novel HNO donor, CXL-1020, in patients with stable congestive heart failure. *Journal of the American College of Cardiology* **2011,** *57* (14S), E299-E299.
24. Subedi, H.; Brasch, N. E., Studies on the Reaction of Reduced Vitamin B-12 Derivatives with the Nitrosyl Hydride (HNO) Donor Angeli's Salt: HNO Oxidizes the Transition-Metal Center of Cob(I)alamin. *European Journal of Inorganic Chemistry* **2015,** (23), 3825-3834.
25. Subedi, H.; Brasch, N. E., Mechanistic studies of the reactions of the reduced vitamin B-12 derivatives with the HNO donor Piloty's acid: further evidence for oxidation of cob(I)alamin by (H)NO. *Dalton Transactions* **2016,** *45* (1), 352-360.
26. Subedi, H.; Hassanin, H. A.; Brasch, N. E., Kinetic and Mechanistic Studies on the Reaction of the Vitamin B-12 Complex Aquacobalamin with the HNO Donor Angeli's Salt: Angeli's Salt and HNO React with Aquacobalamin. *Inorganic Chemistry* **2014,** *53* (3), 1570-1577.
27. Doctorovich, F.; Farmer, P. J.; Marti, M. A., *The chemistry and biology of nitroxyl (HNO)*. Elsevier: 2016.
28. Doyle, M. P.; Mahapatro, S. N.; Broene, R. D.; Guy, J. K., Oxidation and reduction of hemoproteins by trioxodinitrate (II). The role of nitrosyl hydride and nitrite. *Journal of the American Chemical Society* **1988,** *110* (2), 593-599.
29. Bartberger, M. D.; Fukuto, J. M.; Houk, K., On the acidity and reactivity of HNO in aqueous solution and biological systems. *Proceedings of the National Academy of Sciences of the United States of America* **2001,** *98* (5), 2194-2198.
30. Miranda, K. M.; Paolocci, N.; Katori, T.; Thomas, D. D.; Ford, E.; Bartberger, M. D.; Espey, M. G.; Kass, D. A.; Feelisch, M.; Fukuto, J. M.; Wink, D. A., A biochemical rationale for the discrete behavior of nitroxyl and nitric oxide in the cardiovascular system. *Proceedings of the National Academy of Sciences of the United States of America* **2003,** *100* (16), 9196-9201.
31. Hadimani, M. B.; Mukherjee, R.; Banerjee, R.; Shoman, M. E.; Aly, O. M.; King, S. B., Ring expansions of acyloxy nitroso compounds. *Tetrahedron Letters* **2015,** *56* (43), 5870-5873.
32. Reisz, J. A.; Zink, C. N.; King, S. B., Rapid and Selective Nitroxyl (HNO) Trapping by Phosphines: Kinetics and New Aqueous Ligations for HNO Detection and Quantitation. *Journal of the American Chemical Society* **2011,** *133* (30), 11675-11685.
33. An, W.; Ryan, L. S.; Reeves, A. G.; Bruemmer, K. J.; Mouhaffel, L.; Gerberich, J. L.; Winters, A.; Mason, R. P.; Lippert, A. R., A Chemiluminescent Probe for HNO Quantification and Real-Time Monitoring in Living Cells. *Angewandte Chemie* **2019,** *131* (5), 1375-1379.
34. Kawai, K.; Ieda, N.; Aizawa, K.; Suzuki, T.; Miyata, N.; Nakagawa, H., A reductant-resistant and metal-free fluorescent probe for nitroxyl applicable to living cells. *Journal of the American Chemical Society* **2013,** *135* (34), 12690-12696.
35. Reisz, J. A.; Klorig, E. B.; Wright, M. W.; King, S. B., Reductive phosphine-mediated ligation of nitroxyl (HNO). *Organic Letters* **2009,** *11* (13), 2719-2721.

36. Smulik-Izydorczyk, R.; Dębowska, K.; Pięta, J.; Michalski, R.; Marcinek, A.; Sikora, A., Fluorescent probes for the detection of nitroxyl (HNO). *Free Radical Biology and Medicine* **2018,** *128*, 69-83.
37. Guthrie, D. A.; Nourian, S.; Takahashi, C. G.; Toscano, J. P., Curtailing the Hydroxylaminobarbituric Acid-Hydantoin Rearrangement To Favor HNO Generation. *Journal of Organic Chemistry* **2015,** *80* (3), 1349-1356.
38. Bonner, F. T.; Ravid, B., Thermal decomposition of oxyhyponitrite (sodium trioxodinitrate(II)) in aqueous solution. *Inorganic Chemistry* **1975,** *14* (3), 558-563.
39. Maragos, C. M.; Morley, D.; Wink, D. A.; Dunams, T. M.; Saavedra, J. E.; Hoffman, A.; Bove, A. A.; Isaac, L.; Hrabie, J. A.; Keefer, L. K., Complexes of ·NO with nucleophiles as agents for the controlled biological release of nitric oxide. Vasorelaxant effects. *Journal of Medicinal Chemistry* **1991,** *34* (11), 3242-3247.
40. Bonner, F. T.; Ko, Y. H., Kinetic, isotopic, and nitrogen-15 NMR study of N-hydroxybenzenesulfonamide decomposition: an nitrosyl hydride (HNO) source reaction. *Inorganic Chemistry* **1992,** *31* (12), 2514-2519.
41. Seel, F.; Bliefert, C., Decomposition mechanism of sodium salt of benzene sulfhydroxamic acid in aqueous-solution. *Zeitschrift fur Anorganische und Allgemeine Chemie* **1972,** *394* (1-2), 187-&.
42. Switzer, C. H.; Flores-Santana, W.; Mancardi, D.; Donzelli, S.; Basudhar, D.; Ridnour, L. A.; Miranda, K. M.; Fukuto, J. M.; Paolocci, N.; Wink, D. A., The emergence of nitroxyl (HNO) as a pharmacological agent. *Biochimica et Biophysica Acta (BBA)-Bioenergetics* **2009,** *1787* (7), 835-840.
43. Zeng, B. B.; Huang, J. M.; Wright, M. W.; King, S. B., Nitroxyl (HNO) release from new functionalized N-hydroxyurea-derived acyl nitroso-9,10-dimethylanthracene cycloadducts. *Bioorganic & Medicinal Chemistry Letters* **2004,** *14* (22), 5565-5568.
44. Sha, X.; Isbell, T. S.; Patel, R. P.; Day, C. S.; King, S. B., Hydrolysis of acyloxy nitroso compounds yields nitroxyl (HNO). *Journal of the American Chemical Society* **2006,** *128* (30), 9687-9692.
45. Adachi, Y.; Nakagawa, H.; Matsuo, K.; Suzuki, T.; Miyata, N., Photoactivatable HNO-releasing compounds using the retro-Diels-Alder reaction. *Chemical Communications* **2008,** (41), 5149-5151.
46. Matsuo, K.; Nakagawa, H.; Adachi, Y.; Kameda, E.; Tsumoto, H.; Suzuki, T.; Miyata, N., Alternative photoinduced release of HNO or NO from an acyl nitroso compound, depending on environmental polarity. *Chemical Communications* **2010,** *46* (21), 3788-3790.
47. Walter, M. R.; Dzul, S. P.; Rodrigues, A. V.; Stemmler, T. L.; Telser, J.; Conradie, J.; Ghosh, A.; Harrop, T. C., Synthesis of Co-II-NO- Complexes and Their Reactivity as a Source of Nitroxyl. *Journal of the American Chemical Society* **2016,** *138* (38), 12459-12471.
48. Hughes, M. N.; Wimbledon, P. E., The chemistry of trioxodinitrates. Part I. Decomposition of sodium trioxodinitrate (Angeli's salt) in aqueous solution. *Journal of the Chemical Society-Dalton Transactions* **1976,** (8), 703-707.
49. Hughes, M. N.; Cammack, R., Synthesis, chemistry, and applications of nitroxyl ion releasers sodium trioxodinitrate or Angeli's salt and Piloty's acid. *Methods in Enzymology* **1999,** *301*, 279-287.
50. Fukuto, J. M.; Jackson, M. I.; Kaludercic, N.; Paolocci, N., Examining nitroxyl in biological systems. *Methods in Enzymology* **2008,** *440*, 411-431.
51. Porcheddu, A.; De Luca, L.; Giacomelli, G., A Straightforward Route to Piloty's Acid Derivatives: A Class of Potential Nitroxyl-Generating Prodrugs. *Synlett* **2009,** (13), 2149-2153.
52. Smulik-Izydorczyk, R.; Rostkowski, M.; Gerbich, A.; Jarmoc, D.; Adamus, J.; Leszczyńska, A.; Michalski, R.; Marcinek, A.; Kramkowski, K.; Sikora, A., Decomposition of Piloty's acid derivatives–Toward the understanding of factors controlling HNO release. *Archives of Biochemistry and Biophysics* **2019,** *661*, 132-144.
53. Adas, S. K. Part 1 Synthesis and Structural Investigation of Group 11 1, 3-Dicyclohexyl-2, 2-diethylguanidinate Complexes. Part 2 Synthesis and Kinetic Studies of N-Hydroxysulfonamide

Nitrosyl Hydride Donor Molecules and their Reactions with Cob (III) alamin. Kent State University, USA, 2016.
54. Conway, T. T.; DeMaster, E. G.; Lee, M. J. C.; Nagasawa, H. T., Prodrugs of nitroxyl and nitrosobenzene as cascade latentiated inhibitors of aldehyde dehydrogenase. *Journal of Medicinal Chemistry* **1998,** *41* (15), 2903-2909.
55. Adas, S. K.; Bharadwaj, V.; Zhou, Y.; Zhang, J.; Seed, A. J.; Brasch, N. E.; Sampson, P., Synthesis and HNO Donating Properties of the Piloty's Acid Analogue Trifluoromethanesulphonylhydroxamic Acid: Evidence for Quantitative Release of HNO at Neutral pH Conditions. *Chemistry–A European Journal* **2018,** *24* (29), 7330-7334.
56. Bobko, A. A.; Khramtsov, V. V., Mechanistic studies of oxidative decomposition of Angeli's salt and PAPA NONOate. *Nitric Oxide-Biology and Chemistry* **2014,** *40*, 92-98.
57. Stoyanovsky, D. A.; Tyurina, Y. Y.; Tyurin, V. A.; Anand, D.; Mandavia, D. N.; Gius, D.; Ivanova, J.; Pitt, B.; Billiar, T. R.; Kagan, V. E., Thioredoxin and lipoic acid catalyze the denitrosation of low molecular weight and protein S-nitrosothiols. *Journal of the American Chemical Society* **2005,** *127* (45), 15815-15823.
58. Nagasawa, H. T.; Demaster, E. G.; Redfern, B.; Shirota, F. N.; Goon, J. W., Evidence for nitroxyl in the catalase-mediated bioactivation of the alcohol deterrent agent cyanamide. *Journal of Medicinal Chemistry* **1990,** *33* (12), 3120-3122.
59. Guthrie, D. A.; Kim, N. Y.; Siegler, M. A.; Moore, C. D.; Toscano, J. P., Development of N-Substituted Hydroxylamines as Efficient Nitroxyl (HNO) Donors. *Journal of the American Chemical Society* **2012,** *134* (4), 1962-1965.
60. DuMond, J. F.; Wright, M. W.; King, S. B., Water soluble acyloxy nitroso compounds: HNO release and reactions with heme and thiol containing proteins. *Journal of Inorganic Biochemistry* **2013,** *118*, 140-147.
61. Mohamed, H. A.; Abdel-Aziz, M.; Abuo-Rahma, G. E.-D. A.; King, S. B., New acyloxy nitroso compounds with improved water solubility and nitroxyl (HNO) release kinetics and inhibitors of platelet aggregation. *Bioorganic & Medicinal Chemistry* **2015,** *23* (17), 6069-6077.
62. Trabelsi, T.; Linguerri, R.; Ben Yaghlane, S.; Jaidane, N. E.; Al-Mogren, M. M.; Francisco, J. S.; Hochlaf, M., On the role of HNS and HSN as light-sensitive NO-donors for delivery in biological media. *Journal of Chemical Physics* **2015,** *143* (13), 7.
63. Rhine, M. A.; Rodrigues, A. V.; Urbauer, R. J. B.; Urbauer, J. L.; Stemmler, T. L.; Harrop, T. C., Proton-Induced Reactivity of NO- from a $\{CoNO\}^8$ Complex. *Journal of the American Chemical Society* **2014,** *136* (36), 12560-12563.
64. Tseng, Y. T.; Chen, C. H.; Lin, J. Y.; Li, B. H.; Lu, Y. H.; Lin, C. H.; Chen, H. T.; Weng, T. C.; Sokaras, D.; Chen, H. Y.; Soo, Y. L.; Lu, T. T., To Transfer or Not to Transfer? Development of a Dinitrosyl Iron Complex as a Nitroxyl Donor for the Nitroxylation of an Fe(III) Porphyrin Center. *Chemistry-a European Journal* **2015,** *21* (49), 17570-17573.
65. Silva Sousa, E. H.; Ridnour, L. A.; Gouveia Jr, F. n. S.; Silva da Silva, C. D.; Wink, D. A.; de França Lopes, L. G.; Sadler, P. J., Thiol-activated HNO release from a ruthenium antiangiogenesis complex and HIF-1α inhibition for cancer therapy. *ACS Chemical Biology* **2016,** *11* (7), 2057-2065.
66. Truzzi, D. R.; Franco, D. W., *trans*-$Ru(NO)(NH_3)P(O^-)(OEt)_2^{2+}$: A new and robust NO/ HNO-donor in aqueous media. *Inorganica Chimica Acta* **2014,** *421*, 74-79.
67. Montenegro, A. C.; Bari, S. E.; Olabe, J. A., Reactivity of iron(II)-bound nitrosyl hydride (HNO, nitroxyl) in aqueous solution. *Journal of Inorganic Biochemistry* **2013,** *118*, 108-114.
68. Fukuto, J. M.; Cisneros, C. J.; Kinkade, R. L., A comparison of the chemistry associated with the biological signaling and actions of nitroxyl (HNO) and nitric oxide (NO). *Journal of Inorganic Biochemistry* **2013,** *118*, 201-208.
69. Pierri, A. E.; Muizzi, D. A.; Ostrowski, A. D.; Ford, P. C., Photo-controlled release of NO and CO with inorganic and organometallic complexes. *Luminescent and Photoactive Transition Metal Complexes as Biomolecular Probes and Cellular Reagents* **2014**, 1-45.

70. Evans, A. S.; Cohen, A. D.; Gurard-Levin, Z. A.; Kebede, N.; Celius, T. C.; Miceli, A. P.; Toscano, J. P., Photogeneration and reactivity of acyl nitroso compounds. *Canadian Journal of Chemistry* **2011,** *89* (2), 130-138.
71. Cohen, A. D.; Zeng, B.-B.; King, S. B.; Toscano, J. P., Direct observation of an acyl nitroso species in solution by time-resolved IR spectrocopy. *Journal of the American Chemical Society* **2003,** *125* (6), 1444-1445.
72. Quadrelli, P.; Caramella, P., Synthesis and synthetic applications of 1,2,4-oxadiazole-4-oxides. *Current Organic Chemistry* **2007,** *11* (11), 959-986.
73. Nakagawa, H., Controlled release of HNO from chemical donors for biological applications. *Journal of Inorganic Biochemistry* **2013,** *118*, 187-190.
74. Lymar, S. V.; Shafirovich, V., Photoinduced release of nitroxyl and nitric oxide from diazeniumdiolates. *Journal of Physical Chemistry B* **2007,** *111* (24), 6861-6867.
75. Cink, R. B.; Zhou, Y.; Du, L.; Rahman, M. S.; Phillips, D. L.; Simpson, M. C.; Seed, A. J.; Sampson, P.; Brasch, N. E., Mechanistic Insights into the Rapid Generation of Nitroxyl from a Photocaged N-Hydroxysulfonamide Incorporating the (6-Hydroxynaphthalen-2-yl)methyl Chromophore *The Journal of Organic Chemistry* **2021**.
76. Zhou, Y.; Cink, R. B.; Dassanayake, R. S.; Seed, A. J.; Brasch, N. E.; Sampson, P., Rapid photoactivated generation of nitroxyl (HNO) under neutral pH conditions. *Angewandte Chemie* **2016,** *128* (42), 13423-13426.
77. Zhou, Y.; Cink, R. B.; Fejedelem, Z. A.; Cather Simpson, M.; Seed, A. J.; Sampson, P.; Brasch, N. E., Development of Photoactivatable Nitroxyl (HNO) Donors Incorporating the (3-Hydroxy-2-naphthalenyl) methyl Phototrigger. *European Journal of Organic Chemistry* **2018,** *2018* (15), 1745-1755.
78. Zhou, Y.; Cink, R. B.; Seed, A. J.; Simpson, M. C.; Sampson, P.; Brasch, N. E., Stoichiometric nitroxyl photorelease using the (6-hydroxy-2-naphthalenyl) methyl phototrigger. *Organic Letters* **2019,** *21* (4), 1054-1057.
79. Kulikov, A.; Arumugam, S.; Popik, V. V., Photolabile protection of alcohols, phenols, and carboxylic acids with 3-hydroxy-2-naphthalenemethanol. *Journal of Organic Chemistry* **2008,** *73* (19), 7611-7615.
80. Kawaguchi, M.; Tani, T.; Hombu, R.; Ieda, N.; Nakagawa, H., Development and cellular application of visible-light-controllable HNO releasers based on caged Piloty's acid. *Chemical Communications* **2018,** *54* (73), 10371-10374.
81. Levine, R. D., *Molecular reaction dynamics and chemical reactivity*. Oxford University Press, USA: 1987.
82. Logan, S., Does a photochemical reaction have a reaction order? *Journal of Chemical Education* **1997,** *74* (11), 1303.
83. Kuhn, H.; Braslavsky, S.; Schmidt, R., Chemical actinometry (IUPAC technical report). *Pure and Applied Chemistry* **2004,** *76* (12), 2105-2146.
84. Ladányi, V.; Dvořák, P.; Al Anshori, J.; Vetráková, Ľ.; Wirz, J.; Heger, D., Azobenzene photoisomerization quantum yields in methanol redetermined. *Photochemical & Photobiological Sciences* **2017,** *16* (12), 1757-1761.
85. Siampiringue, N.; Guyot, G.; Monti, S.; Bortolus, P., The cis→ trans photoisomerization of azobenzene: an experimental re-examination. *Journal of Photochemistry* **1987,** *37* (1), 185-188.
86. Turro, N. J.; Ramamurthy, V.; Ramamurthy, V.; Scaiano, J. C., *Principles of molecular photochemistry: an introduction*. University Science books: 2009.
87. Atkins, P.; De Paula, J., Atkins' physical chemistry. Oxford University Press, Oxford: 2006.
88. Hansen, M. J.; Velema, W. A.; Lerch, M. M.; Szymanski, W.; Feringa, B. L., Wavelength-selective cleavage of photoprotecting groups: strategies and applications in dynamic systems. *Chemical Society Reviews* **2015,** *44* (11), 3358-3377.

89. Klán, P.; Šolomek, T. s.; Bochet, C. G.; Blanc, A.; Givens, R.; Rubina, M.; Popik, V.; Kostikov, A.; Wirz, J., Photoremovable protecting groups in chemistry and biology: reaction mechanisms and efficacy. *Chemical Reviews* **2013,** *113* (1), 119-191.
90. Ma, C.; Kwok, W. M.; Chan, W. S.; Du, Y.; Kan, J. T. W.; Toy, P. H.; Phillips, D. L., Ultrafast time-resolved transient absorption and resonance Raman spectroscopy study of the photodeprotection and rearrangement reactions of *p*-hydroxyphenacyl caged phosphates. *Journal of the American Chemical Society* **2006,** *128* (8), 2558-2570.
91. Abou Nakad, E.; Bolze, F.; Specht, A., o-Nitrobenzyl photoremovable groups with fluorescence uncaging reporting properties. *Organic & Biomolecular Chemistry* **2018,** *16* (33), 6115-6122.
92. Tebikachew, B. E.; Börjesson, K.; Kann, N.; Moth-Poulsen, K., Release of Terminal Alkynes via Tandem Photodeprotection and Decarboxylation of o-Nitrobenzyl Arylpropiolates in a Flow Microchannel Reactor. *Bioconjugate Chemistry* **2018,** *29* (4), 1178-1185.
93. Tso, K. K.-S.; Leung, K.-K.; Liu, H.-W.; Lo, K. K.-W., Photoactivatable cytotoxic agents derived from mitochondria-targeting luminescent iridium (iii) poly (ethylene glycol) complexes modified with a nitrobenzyl linkage. *Chemical Communications* **2016,** *52* (24), 4557-4560.
94. Ellis-Davies, G. C. R.; Barsotti, R. J., Tuning caged calcium: Photolabile analogues of EGTA with improved optical and chelation properties. *Cell Calcium* **2006,** *39* (1), 75-83.
95. Stutz, A.; Pitsch, S., Automated RNA-synthesis with photocleavable sugar and nucleobase protecting groups. *Synlett* **1999**, 930-934.
96. Chalmers, S.; Caldwell, S. T.; Quin, C.; Prime, T. A.; James, A. M.; Cairns, A. G.; Murphy, M. P.; McCarron, J. G.; Hartley, R. C., Selective Uncoupling of Individual Mitochondria within a Cell Using a Mitochondria-Targeted Photoactivated Protonophore. *Journal of the American Chemical Society* **2012,** *134* (2), 758-761.
97. Pirrung, M. C., How to make a DNA chip. *Angewandte Chemie-International Edition* **2002,** *41* (8), 1277-+.
98. Corrie, J. E. T.; Munasinghe, V. R. N.; Trentham, D. R.; Barth, A., Studies of decarboxylation in photolysis of alpha-carboxy-2-nitrobenzyl (CNB) caged compounds. *Photochemical & Photobiological Sciences* **2008,** *7* (1), 84-97.
99. Abbruzzetti, S.; Carcelli, M.; Rogolino, D.; Viappiani, C., Deprotonation yields, p K a, and aci-nitro decay rates in some substituted o-nitrobenzaldehydes. *Photochemical & Photobiological Sciences* **2003,** *2* (7), 796-800.
100. George, M. V.; Scaiano, J. C., Photochemistry of o-nitrobenzaldehyde and related studies. *Journal of Physical Chemistry* **1980,** *84* (5), 492-495.
101. Il'ichev, Y. V.; Schworer, M. A.; Wirz, J., Photochemical reaction mechanisms of 2-nitrobenzyl compounds: Methyl ethers and caged ATP. *Journal of the American Chemical Society* **2004,** *126* (14), 4581-4595.
102. Corrie, J. E.; Barth, A.; Munasinghe, V. R. N.; Trentham, D. R.; Hutter, M. C., Photolytic cleavage of 1-(2-nitrophenyl) ethyl ethers involves two parallel pathways and product release is rate-limited by decomposition of a common hemiacetal intermediate. *Journal of the American Chemical Society* **2003,** *125* (28), 8546-8554.
103. Schwörer, M.; Wirz, J., Photochemical reaction mechanisms of 2-nitrobenzyl compounds in solution, I. 2-Nitrotoluene: thermodynamic and kinetic parameters of the aci-nitro tautomer. *Helvetica Chimica Acta* **2001,** *84* (6), 1441-1458.
104. Hellrung, B.; Kamdzhilov, Y.; Schworer, M.; Wirz, J., Photorelease of alcohols from 2-nitrobenzyl ethers proceeds via hemiacetals and may be further retarded by buffers intercepting the primary aci-nitro intermediates. *Journal of the American Chemical Society* **2005,** *127* (25), 8934-8935.
105. Walker, J. W.; Reid, G. P.; McCray, J. A.; Trentham, D. R., Photolabile 1-(2-nitrophenyl)ethyl phosphate esters of adenine nucleotide analogs. Synthesis and mechanism of photolysis. *Journal of the American Chemical Society* **1988,** *110* (21), 7170-7177.

106. Heinz, B.; Schmierer, T.; Laimgruber, S.; Gilch, P., Excited state processes of nitrobenzaldehydes probed by ultrafast fluorescence and absorption spectroscopy. *Journal of Photochemistry and Photobiology A-Chemistry* **2008,** *199* (2-3), 274-281.
107. Laimgruber, S.; Schachenmayr, H.; Schmidt, B.; Zinth, W.; Gilch, P., A femtosecond stimulated raman spectrograph for the near ultraviolet. *Applied Physics B-Lasers and Optics* **2006,** *85* (4), 557-564.
108. Laimgruber, S.; Schmierer, T.; Gilch, P.; Kiewisch, K.; Neugebauer, J., The ketene intermediate in the photochemistry of ortho-nitrobenzaldehyde. *Physical Chemistry Chemical Physics* **2008,** *10* (26), 3872-3882.
109. Leyva, V.; Corral, I.; Schmierer, T.; Gilch, P.; Gonzalez, L., A comparative analysis of the UV/Vis absorption spectra of nitrobenzaldehydes. *Physical Chemistry Chemical Physics* **2011,** *13* (10), 4269-4278.
110. Leyva, V.; Corral, I.; Schmierer, T.; Heinz, B.; Feixas, F.; Migani, A.; Blancafort, L.; Gilch, P.; Gonzalez, L., Electronic states of o-nitrobenzaldehyde: A combined experimental and theoretical study. *Journal of Physical Chemistry A* **2008,** *112* (23), 5046-5053.
111. Schmierer, T.; Laimgruber, S.; Haiser, K.; Kiewisch, K.; Neugebauer, J.; Gilch, P., Femtosecond spectroscopy on the photochemistry of ortho-nitrotoluene. *Physical Chemistry Chemical Physics* **2010,** *12* (48), 15653-15664.
112. Schmierer, T.; Ryseck, G.; Villnow, T.; Regner, N.; Gilch, P., Kasha or state selective behavior in the photochemistry of ortho-nitrobenzaldehyde? *Photochemical & Photobiological Sciences* **2012,** *11* (8), 1313-1321.
113. Grither, W. R.; Korang, J.; Sauer, J. P.; Sherman, M. P.; Vanegas, P. L.; Zhang, M.; McCulla, R. D., The effect of nitro substitution on the photochemistry of benzyl benozhydroxamate: Photoinduced release of benzohydroxamic acid. *Journal of Photochemistry and Photobiology A: Chemistry* **2012,** *227* (1), 1-10.
114. Leonidova, A.; Mari, C.; Aebersold, C.; Gasser, G., Selective photorelease of an organometallic-containing enzyme inhibitor. *Organometallics* **2016,** *35* (6), 851-854.
115. Parasar, B.; Chang, P. V., Chemical optogenetic modulation of inflammation and immunity. *Chemical Science* **2017,** *8* (2), 1450-1453.
116. Seven, I.; Weinrich, T.; Gränz, M.; Grünewald, C.; Brüß, S.; Krstić, I.; Prisner, T. F.; Heckel, A.; Göbel, M. W., Photolabile protecting groups for nitroxide spin labels. *European Journal of Organic Chemistry* **2014,** *2014* (19), 4037-4043.
117. McCune, C. D.; Chan, S. J.; Beio, M. L.; Shen, W.; Chung, W. J.; Szczesniak, L. M.; Chai, C.; Koh, S. Q.; Wong, P. T.-H.; Berkowitz, D. B., "Zipped synthesis" by cross-metathesis provides a cystathionine β-synthase inhibitor that attenuates cellular H_2S levels and reduces neuronal infarction in a rat ischemic stroke model. *ACS Central Science* **2016,** *2* (4), 242-252.
118. Qvortrup, K.; Nielsen, T. E., In-Bead Screening of Hydroxamic Acids for the Identification of HDAC Inhibitors. *Angewandte Chemie* **2016,** *128* (14), 4548-4551.
119. Qvortrup, K.; Petersen, R. G.; Dohn, A. O.; Møller, K. B.; Nielsen, T. E., Solvent-Controlled Chemoselectivity in the Photolytic Release of Hydroxamic Acids and Carboxamides from Solid Support. *Organic Letters* **2017,** *19* (12), 3263-3266.
120. Kohl-Landgraf, J. r.; Buhr, F.; Lefrancois, D.; Mewes, J.-M.; Schwalbe, H.; Dreuw, A.; Wachtveitl, J., Mechanism of the photoinduced uncaging reaction of puromycin protected by a 6-nitroveratryloxycarbonyl group. *Journal of the American Chemical Society* **2014,** *136* (9), 3430-3438.
121. Olejniczak, J.; Chan, M.; Almutairi, A., Light-triggered intramolecular cyclization in poly (lactic-co-glycolic acid)-based polymers for controlled degradation. *Macromolecules* **2015,** *48* (10), 3166-3172.
122. Papageorgiou, G.; Corrie, J. E., Synthesis and properties of carbamoyl derivatives of photolabile benzoins. *Tetrahedron* **1997,** *53* (11), 3917-3932.
123. Wang, P., Photolabile protecting groups: structure and reactivity. *Asian Journal of Organic Chemistry* **2013,** *2* (6), 452-464.

124. Walbert, S.; Pfleiderer, W.; Steiner, U. E., Photolabile protecting groups for nucleosides: Mechanistic studies of the 2-(2-nitrophenyl) ethyl group. *Helvetica Chimica Acta* **2001,** *84* (6), 1601-1611.
125. Dore, T. M.; Wilson, H. C., Chromophores for the delivery of bioactive molecules with two-photon excitation. In *Photosensitive Molecules for Controlling Biological Function*, Springer: 2011; pp 57-92.
126. Hagen, V.; Kilic, F.; Schaal, J.; Dekowski, B.; Schmidt, R.; Kotzur, N., [8-[Bis (carboxymethyl) aminomethyl]-6-bromo-7-hydroxycoumarin-4-yl] methyl Moieties as Photoremovable Protecting Groups for Compounds with COOH, NH2, OH, and C. O Functions. *The Journal of Organic Chemistry* **2010,** *75* (9), 2790-2797.
127. Schmidt, R.; Geissler, D.; Hagen, V.; Bendig, J., Kinetics Study of the Photocleavage of (Coumarin-4-yl)methyl Esters. *The Journal of Physical Chemistry A* **2005,** *109* (23), 5000-5004.
128. Schmidt, R.; Geissler, D.; Hagen, V.; Bendig, J., Mechanism of photocleavage of (coumarin-4-yl) methyl esters. *The Journal of Physical Chemistry A* **2007,** *111* (26), 5768-5774.
129. Kim, Y. A.; Ramirez, D. M. C.; Costain, W. J.; Johnston, L. J.; Bittman, R., A new tool to assess ceramide bioactivity: 6-bromo-7-hydroxycoumarinyl-caged ceramide. *Chemical Communications* **2011,** *47* (32), 9236-9238.
130. Nomura, W.; Narumi, T.; Ohashi, N.; Serizawa, Y.; Lewin, N. E.; Blumberg, P. M.; Furuta, T.; Tamamura, H., Synthetic Caged DAG-lactones for Photochemically Controlled Activation of Protein Kinase C. *ChemBioChem* **2011,** *12* (4), 535-539.
131. Wosnick, J. H.; Shoichet, M. S., Three-dimensional chemical patterning of transparent hydrogels. *Chemistry of Materials* **2008,** *20* (1), 55-60.
132. Wylie, R. G.; Shoichet, M. S., Two-photon micropatterning of amines within an agarose hydrogel. *Journal of Materials Chemistry* **2008,** *18* (23), 2716-2721.
133. Soares, A. M. S.; Costa, S. P. G.; Goncalves, M. S. T., 2-Oxo-2H-benzo[h]benzopyran as a new light sensitive protecting group for neurotransmitter amino acids. *Amino Acids* **2010,** *39* (1), 121-133.
134. Suzuki, A. Z.; Watanabe, T.; Kawamoto, M.; Nishiyama, K.; Yamashita, H.; Ishii, M.; Iwamura, M.; Furuta, T., Coumarin-4-ylmethoxycarbonyls as phototriggers for alcohols and phenols. *Organic Letters* **2003,** *5* (25), 4867-4870.
135. Senda, N.; Momotake, A.; Nishimura, Y.; Arai, T., Synthesis and photochemical properties of a new water-soluble coumarin, designed as a chromophore for highly water-soluble and photolabile protecting group. *Bulletin of the Chemical Society of Japan* **2006,** *79* (11), 1753-1757.
136. Schade, B.; Hagen, V.; Schmidt, R.; Herbrich, R.; Krause, E.; Eckardt, T.; Bendig, J., Deactivation behavior and excited-state properties of (coumarin-4-yl) methyl derivatives. 1. Photocleavage of (7-methoxycoumarin-4-yl) methyl-caged acids with fluorescence enhancement. *The Journal of Organic Chemistry* **1999,** *64* (25), 9109-9117.
137. Kotzur, N.; Briand, B. t.; Beyermann, M.; Hagen, V., Wavelength-selective photoactivatable protecting groups for thiols. *Journal of the American Chemical Society* **2009,** *131* (46), 16927-16931.
138. Fonseca, A. S.; Gonçalves, M. S. T.; Costa, S. P., Photocleavage studies of fluorescent amino acid conjugates bearing different types of linkages. *Tetrahedron* **2007,** *63* (6), 1353-1359.
139. Furuta, T.; Takeuchi, H.; Isozaki, M.; Takahashi, Y.; Kanehara, M.; Sugimoto, M.; Watanabe, T.; Noguchi, K.; Dore, T. M.; Kurahashi, T., Bhc-cNMPs as either water-soluble or membrane-permeant photoreleasable cyclic nucleotides for both one-and two-photon excitation. *ChemBioChem* **2004,** *5* (8), 1119-1128.
140. Pocker, Y.; Davison, B.; Deits, T., Decarboxylation of monosubstituted derivatives of carbonic acid. Comparative studies of water-and acid-catalyzed decarboxylation of sodium alkyl carbonates in water and water-d_2. *Journal of the American Chemical Society* **1978,** *100* (11), 3564-3567.
141. Rossi, F. M.; Kao, J. P., Nmoc-DBHQ, a new caged molecule for modulating sarcoplasmic/endoplasmic reticulum Ca2+ ATPase activity with light flashes. *Journal of Biological Chemistry* **1997,** *272* (6), 3266-3271.

142. Perrin, D. D.; Dempsey, B.; Serjeant, E. P., *pKa prediction for organic acids and bases*. Springer: 1981; Vol. 1.
143. Johnson, S.; Morrison, D. L., Kinetics and mechanism of decarboxylation of N-arylcarbamates. Evidence for kinetically important zwitterionic carbamic acid species of short lifetime. *Journal of the American Chemical Society* **1972,** *94* (4), 1323-1334.
144. Oshima, T.; Ueno, S.-y.; Nagai, T., Acid-catalyzed hydrolysis of cyclic benzophenone acetals. Effects of ring size and ring substituent. *Heterocycles* **1995,** *40* (2), 607-17.
145. Piloto, A. M.; Rovira, D.; Costa, S. P.; Gonçalves, M. S. T., Oxobenzo [f] benzopyrans as new fluorescent photolabile protecting groups for the carboxylic function. *Tetrahedron* **2006,** *62* (51), 11955-11962.
146. Nowak, P. M.; Sagan, F.; Mitoraj, M. P., Origin of Remarkably Different Acidity of Hydroxycoumarins· Joint Experimental and Theoretical Studies. *The Journal of Physical Chemistry B* **2017,** *121* (17), 4554-4561.
147. Furuta, T.; Wang, S. S.-H.; Dantzker, J. L.; Dore, T. M.; Bybee, W. J.; Callaway, E. M.; Denk, W.; Tsien, R. Y., Brominated 7-hydroxycoumarin-4-ylmethyls: photolabile protecting groups with biologically useful cross-sections for two photon photolysis. *Proceedings of the National Academy of Sciences of the United States of America* **1999,** *96* (4), 1193-1200.
148. Narumi, T.; Takano, H.; Ohashi, N.; Suzuki, A.; Furuta, T.; Tamamura, H., Isostere-based design of 8-azacoumarin-type photolabile protecting groups: A hydrophilicity-increasing strategy for coumarin-4-ylmethyls. *Organic Letters* **2014,** *16* (4), 1184-1187.
149. Takano, H.; Narumi, T.; Nomura, W.; Furuta, T.; Tamamura, H., Utilization of the Heavy Atom Effect for the Development of a Photosensitive 8-Azacoumarin-Type Photolabile Protecting Group. *Organic Letters* **2015,** *17* (21), 5372-5375.
150. Zhou, Y.; Bharadwaj, V.; Rahman, M. S.; Sampson, P.; Brasch, N. E.; Seed, A. J., Synthesis and photochemical studies of 2-nitrobenzyl-caged N-hydroxysulfonamides. *Journal of Photochemistry and Photobiology A: Chemistry* **2019,** *384*, 112033.
151. Romero, M. A.; Basílio, N.; Moro, A. J.; Domingues, M.; González-Delgado, J. A.; Arteaga, J. F.; Pischel, U., Photocaged Competitor Guests: A General Approach Toward Light-Activated Cargo Release From Cucurbiturils. *Chemistry–A European Journal* **2017,** *23* (53), 13105-13111.
152. Rahman, M. S. Synthesis and photochemical studies of new photoactivatable nitroxyl (HNO)-releasing compounds. Kent State University, 2019.
153. Olmsted, J., Preparation and analysis of potassium tris (oxalato) ferrate (III) trihydrate: A general chemistry experiment. *Journal of Chemical Education* **1984,** *61* (12), 1098.
154. Pozdnyakov, I. P.; Kel, O. V.; Plyusnin, V. F.; Grivin, V. P.; Bazhin, N. M., New insight into photochemistry of ferrioxalate. *The Journal of Physical Chemistry A* **2008,** *112* (36), 8316-8322.
155. Hannibal, L.; Smith, C. A.; Jacobsen, D. W.; Brasch, N. E., Nitroxylcob (III) alamin: Synthesis and X-ray Structural Characterization. *Angewandte Chemie* **2007,** *119* (27), 5232-5235.
156. Cink, R. Mechanistic Studies on the Decomposition of Photoactive Nitrosyl Hydride (HNO) Precursors. Auckland University of Technology, 2019.
157. Šolomek, T.; Bochet, C. G.; Bally, T., The Primary steps in excited-state hydrogen transfer: the phototautomerization of o-nitrobenzyl derivatives. *Chemistry–A European Journal* **2014,** *20* (26), 8062-8067.
158. Flyunt, R.; Makogon, O.; Schuchmann, M. N.; Asmus, K.-D.; von Sonntag, C., OH-Radical-induced oxidation of methanesulfinic acid. The reactions of the methanesulfonyl radical in the absence and presence of dioxygen. *Journal of the Chemical Society, Perkin Transactions 2* **2001,** (5), 787-792.
159. Barth, A.; Corrie, J. E. T.; Gradwell, M. J.; Maeda, Y.; Mantele, W.; Meier, T.; Trentham, D. R., Time-resolved infrared spectroscopy of intermediates and products from photolysis of 1-(2-nitrophenyl)ethyl phosphates: Reaction of the 2-nitrosoacetophenone byproduct with thiols. *Journal of the American Chemical Society* **1997,** *119* (18), 4149-4159.

160. Carcelli, M.; Pelagatti, P.; Viappiani, C., Determination of the pKa of the Aci-Nitro Intermediate in o-Nitrobenzyl Systems. *Israel Journal of Chemistry* **1998,** *38* (3), 213-221.
161. Zheng, D.; Birke, R. L., Spectroscopic evidence for nitric oxide binding with cob (II) alamin. *Journal of the American Chemical Society* **2001,** *123* (19), 4637-4638.
162. Confer, A. M.; Vilbert, A. C.; Dey, A.; Lancaster, K. M.; Goldberg, D. P., Mononuclear, Nonheme Fe^{II}–Piloty's Acid ($PhSO_2NHOH$) Adduct: An Intermediate in the Production of {FeNO}$^{7/8}$ Complexes from Piloty's Acid. *Journal of the American Chemical Society* **2019**.
163. Suarez, S. A.; Neuman, N. I.; Munoz, M.; Alvarez, L.; Bikiel, D. E.; Brondino, C. D.; Ivanovic-Burmazovic, I.; Miljkovic, J. L.; Filipovic, M. R.; Marti, M. A.; Doctorovich, F., Nitric Oxide Is Reduced to HNO by Proton-Coupled Nucleophilic Attack by Ascorbate, Tyrosine, and Other Alcohols. A New Route to HNO in Biological Media? *Journal of the American Chemical Society* **2015,** *137* (14), 4720-4727.
164. Bunyan, P.; Cadogan, J., 7. The reactivity of organophosphorus compounds. Part XIV. Deoxygenation of aromatic C-nitroso-compounds by triethyl phosphite and triphenylphosphine: a new cyclisation reaction. *Journal of the Chemical Society* **1963**, 42-49.
165. Cadogan, J., Reduction of nitro-and nitroso-compounds by tervalent phosphorus reagents. *Quarterly Reviews, Chemical Society* **1968,** *22* (2), 222-251.
166. Zepp, R. G., Quantum yields for reaction of pollutants in dilute aqueous solution. *Environmental Science & Technology* **1978,** *12* (3), 327-329.
167. Šolomek, T.; Mercier, S.; Bally, T.; Bochet, C. G., Photolysis of ortho-nitrobenzylic derivatives: the importance of the leaving group. *Photochemical & Photobiological Sciences* **2012,** *11* (3), 548-555.
168. Aqil, M.; Deliu, Z.; Elseth, K. M.; Shen, G.; Xue, J. P.; Radosevich, J. A., Part II-mechanism of adaptation: A549 cells adapt to high concentration of nitric oxide through bypass of cell cycle checkpoints. *Tumor Biology* **2014,** *35* (3), 2417-2425.
169. Lipczynska-Kochany, E., Photochemistry of hydroxamic acids and derivatives. *Chemical Reviews* **1991,** *91* (4), 477-491.
170. Johnson, J. E.; Arfan, M.; Hodzi, R.; Caswell, L. R.; Rasmussen, S., Mechanisms of photoelimination reactions of alkyl benzohydroxamates. *Photochemistry and Photobiology* **1990,** *51* (2), 139-144.
171. Trepka, R.; Belisle, J.; Harrington, J., Acidites and partition coefficients of fluoromethanesulfonamides. *The Journal of Organic Chemistry* **1974,** *39* (8), 1094-1098.
172. Bordwell, F. G., Equilibrium acidities in dimethyl sulfoxide solution. *Accounts of Chemical Research* **1988,** *21* (12), 456-463.
173. Branch, G.; Clayton, J., The strength of acetamide as an acid. *Journal of the American Chemical Society* **1928,** *50* (6), 1680-1686.
174. Glasoe, P. K.; Long, F., Use of glass electrodes to measure acidities in deuterium oxide1, 2. *The Journal of Physical Chemistry* **1960,** *64* (1), 188-190.
175. Foti, M.; Ingold, K.; Lusztyk, J., The surprisingly high reactivity of phenoxyl radicals. *Journal of the American Chemical Society* **1994,** *116* (21), 9440-9447.
176. Krężel, A.; Bal, W., A formula for correlating pKa values determined in D_2O and H_2O. *Journal of Inorganic Biochemistry* **2004,** *98* (1), 161-166.
177. Mora-Diez, N.; Egorova, Y.; Plommer, H.; Tremaine, P. R., Theoretical study of deuterium isotope effects on acid–base equilibria under ambient and hydrothermal conditions. *RSC Advances* **2015,** *5* (12), 9097-9109.
178. Rubinson, K. A., Practical corrections for p (H, D) measurements in mixed H_2O/D_2O biological buffers. *Analytical Methods* **2017,** *9* (18), 2744-2750.
179. Seebach, D.; Beck, A. K.; Bichsel, H. U.; Pichota, A.; Sparr, C.; Wünsch, R.; Schweizer, W. B., Preparation and Characterization of New C2-and C1-Symmetric Nitrogen, Oxygen, Phosphorous, and Sulfur Derivatives and Analogs of TADDOL. Part III: Some New Chiral Brønsted Acids for

Organocatalysis and pKa Values in MeO-$(CH_2)_2$-OH/H_2O–A Survey. *Helvetica Chimica Acta* **2012,** *95* (8), 1303-1324.
180. Seel, F.; Bliefert, C., Über die Bildung von HNO durch thermische Zersetzung des Natriumsalzes der Benzolsulfhydroxamsäure. *Zeitschrift für Anorganische und Allgemeine Chemie* **1974,** *406* (2-3), 277-281.
181. Cordonier, C. E.; Nakamura, A.; Shimada, K.; Fujishima, A., Enhanced photoefficiency in positive-tone direct patterning of metal complexes for forming patterned indium tin oxide films. *Thin Solid Films* **2012,** *520* (18), 5867-5876.
182. Canham, S. M.; France, D. J.; Overman, L. E., Total synthesis of (+)-sieboldine A: Evolution of a pinacol-terminated cyclization strategy. *The Journal of Organic Chemistry* **2013,** *78* (1), 9-34.
183. Kretschy, N.; Holik, A. K.; Somoza, V.; Stengele, K. P.; Somoza, M. M., Next-Generation o-Nitrobenzyl Photolabile Groups for Light-Directed Chemistry and Microarray Synthesis. *Angewandte Chemie International Edition* **2015,** *54* (29), 8555-8559.
184. Wettermark, G.; Black, E.; Dogliotti, L., Reactions of photochemically formed transients from 2-nitrotoluene. *Photochemistry and Photobiology* **1965,** *4* (2), 229-239.
185. Herzig, L.-M.; Elamri, I.; Schwalbe, H.; Wachtveitl, J., Light-induced antibiotic release from a coumarin-caged compound on the ultrafast timescale. *Physical Chemistry Chemical Physics* **2017,** *19* (22), 14835-14844.
186. Schulman, S. G.; Rosenberg, L. S., Tautomerization kinetics of 7-hydroxy-4-methylcoumarin in the lowest excited singlet state. *Journal of Physical Chemistry* **1979,** *83* (4), 447-451.
187. Schmidt, R.; Geissler, D.; Hagen, V.; Bendig, J., Kinetics Study of the Photocleavage of (Coumarin-4-yl) methyl Esters. *The Journal of Physical Chemistry A* **2005,** *109* (23), 5000-5004.
188. Wong, P. T.; Choi, S. K., Mechanisms of drug release in nanotherapeutic delivery systems. *Chemical Reviews* **2015,** *115* (9), 3388-3432.